

Autoimmune and autoinflammatory diseases: from genes to metabolites in the discovery of predictive, diagnostic and therapeutic targets

Edited by

Evangelia Sarandi, Dimitris Tsoukalas, Vassileios Fragoulakis
and Aristidis M. Tsatsakis

Published in

Frontiers in Molecular Biosciences



FRONTIERS EBOOK COPYRIGHT STATEMENT

The copyright in the text of individual articles in this ebook is the property of their respective authors or their respective institutions or funders. The copyright in graphics and images within each article may be subject to copyright of other parties. In both cases this is subject to a license granted to Frontiers.

The compilation of articles constituting this ebook is the property of Frontiers.

Each article within this ebook, and the ebook itself, are published under the most recent version of the Creative Commons CC-BY licence. The version current at the date of publication of this ebook is CC-BY 4.0. If the CC-BY licence is updated, the licence granted by Frontiers is automatically updated to the new version.

When exercising any right under the CC-BY licence, Frontiers must be attributed as the original publisher of the article or ebook, as applicable.

Authors have the responsibility of ensuring that any graphics or other materials which are the property of others may be included in the CC-BY licence, but this should be checked before relying on the CC-BY licence to reproduce those materials. Any copyright notices relating to those materials must be complied with.

Copyright and source acknowledgement notices may not be removed and must be displayed in any copy, derivative work or partial copy which includes the elements in question.

All copyright, and all rights therein, are protected by national and international copyright laws. The above represents a summary only. For further information please read Frontiers' Conditions for Website Use and Copyright Statement, and the applicable CC-BY licence.

ISSN 1664-8714
ISBN 978-2-8325-5964-2
DOI 10.3389/978-2-8325-5964-2

About Frontiers

Frontiers is more than just an open access publisher of scholarly articles: it is a pioneering approach to the world of academia, radically improving the way scholarly research is managed. The grand vision of Frontiers is a world where all people have an equal opportunity to seek, share and generate knowledge. Frontiers provides immediate and permanent online open access to all its publications, but this alone is not enough to realize our grand goals.

Frontiers journal series

The Frontiers journal series is a multi-tier and interdisciplinary set of open-access, online journals, promising a paradigm shift from the current review, selection and dissemination processes in academic publishing. All Frontiers journals are driven by researchers for researchers; therefore, they constitute a service to the scholarly community. At the same time, the *Frontiers journal series* operates on a revolutionary invention, the tiered publishing system, initially addressing specific communities of scholars, and gradually climbing up to broader public understanding, thus serving the interests of the lay society, too.

Dedication to quality

Each Frontiers article is a landmark of the highest quality, thanks to genuinely collaborative interactions between authors and review editors, who include some of the world's best academicians. Research must be certified by peers before entering a stream of knowledge that may eventually reach the public - and shape society; therefore, Frontiers only applies the most rigorous and unbiased reviews. Frontiers revolutionizes research publishing by freely delivering the most outstanding research, evaluated with no bias from both the academic and social point of view. By applying the most advanced information technologies, Frontiers is catapulting scholarly publishing into a new generation.

What are Frontiers Research Topics?

Frontiers Research Topics are very popular trademarks of the *Frontiers journals series*: they are collections of at least ten articles, all centered on a particular subject. With their unique mix of varied contributions from Original Research to Review Articles, Frontiers Research Topics unify the most influential researchers, the latest key findings and historical advances in a hot research area.

Find out more on how to host your own Frontiers Research Topic or contribute to one as an author by contacting the Frontiers editorial office: frontiersin.org/about/contact

Autoimmune and autoinflammatory diseases: from genes to metabolites in the discovery of predictive, diagnostic and therapeutic targets

Topic editors

Evangelia Sarandi — University of Crete, Greece

Dimitris Tsoukalas — Metabolomic Medicine, Greece

Vassileios Fragoulakis — The Golden Helix Foundation, United Kingdom

Aristidis M. Tsatsakis — University of Crete, Greece

Citation

Sarandi, E., Tsoukalas, D., Fragoulakis, V., Tsatsakis, A. M., eds. (2025). *Autoimmune and autoinflammatory diseases: from genes to metabolites in the discovery of predictive, diagnostic and therapeutic targets*. Lausanne: Frontiers Media SA.
doi: 10.3389/978-2-8325-5964-2

Dr. Tsoukalas is the scientific director of Metabolomic medicine and Dr. Sarandi works as a molecular biologist at Metabolomic Medicine. All other Topic Editors declare no competing interests.

Table of contents

05	N-3 Polyunsaturated Fatty Acid Dehydrogenase Fat-1 Regulates Mitochondrial Energy Metabolism by Altering DNA Methylation in Isolated Cells of Transgenic Cattle Xueqiao Wang, Lin Zhu, Zhuqing Wei, Mingjuan Gu, Miaomiao Yang, Xinyu Zhou, Chunling Bai, Guanghua Su, Xuefei Liu, Lei Yang and Guangpeng Li
16	Toward Personalized Interventions for Psoriasis Vulgaris: Molecular Subtyping of Patients by Using a Metabolomics Approach Dan Dai, Chunyan He, Shuo Wang, Mei Wang, Na Guo and Ping Song
30	Cuproptosis-related gene identification and immune infiltration analysis in systemic lupus erythematosus Wuquan Li, Xiaoran Guan, Yong Wang, Yan Lv, Yuyong Wu, Min Yu and Yeying Sun
43	Identification of key signaling pathways and hub genes related to immune infiltration in Kawasaki disease with resistance to intravenous immunoglobulin based on weighted gene co-expression network analysis Yue Wang, Yinyin Cao, Yang Li, Meifen Yuan, Jin Xu and Jian Li
59	Psoriasis immunometabolism: progress on metabolic biomarkers and targeted therapy Evangelia Sarandi, Sabine Krueger-Krasagakis, Dimitris Tsoukalas, Polytimi Sidiropoulou, George Evangelou, Maria Sifaki, Gottfried Rudofsky, Nikolaos Drakoulis and Aristidis Tsatsakis
73	Unveiling the key genes, environmental toxins, and drug exposures in modulating the severity of ulcerative colitis: a comprehensive analysis Yao Wang, Hao Zhuang, Xiao-han Jiang, Rui-han Zou, Hai-yang Wang and Zhi-ning Fan
112	Clinical application of serum biomarkers for detecting and monitoring of chronic plaque psoriasis Criselda Jean G. Cruz and Chao-Chun Yang
120	Identification of immunological characterization and Anoikis-related molecular clusters in rheumatoid arthritis Jianan Zhao, Kai Wei, Yiming Shi, Ping Jiang, Lingxia Xu, Cen Chang, Linshuai Xu, Yixin Zheng, Yu Shan, Jia Liu, Li Li, Shicheng Guo, Steven J. Schrod, Rongsheng Wang and Dongyi He
136	An IL-17A-centric response to Epstein-Barr virus DNA mediated by dendritic Cell-T cell interactions Marwa Shehab, Hadi Hussein, Sukayna Fadlallah and Elias A. Rahal

- 149 **Inflammatory bowel disease and rheumatoid arthritis share a common genetic structure**
Guoling Cao, Qinghua Luo, Yunxiang Wu and Guanghua Chen
- 162 **The harmful effect of ankylosing spondylitis on diabetes mellitus: new evidence from the Mendelian randomization analysis**
Zheng Ren, Liang He, Jing Wang, Li Shu, Chenyang Li and Yuan Ma



N-3 Polyunsaturated Fatty Acid Dehydrogenase Fat-1 Regulates Mitochondrial Energy Metabolism by Altering DNA Methylation in Isolated Cells of Transgenic Cattle

OPEN ACCESS

Edited by:

Jin Ye,
University of Texas Southwestern
Medical Center, United States

Reviewed by:

Jing Tian,
University of Texas Southwestern
Medical Center, United States
Guosheng Liang,
University of Texas Southwestern
Medical Center, United States

*Correspondence:

Guangpeng Li
gpl@imu.edu.cn
Lei Yang
mrknowall@126.com

[†]These authors have contributed
equally to this work

Specialty section:

This article was submitted to
Cellular Biochemistry,
a section of the journal
Frontiers in Molecular Biosciences

Received: 20 January 2022

Accepted: 04 March 2022

Published: 19 April 2022

Citation:

Wang X, Zhu L, Wei Z, Gu M, Yang M,
Zhou X, Bai C, Su G, Liu X, Yang L and
Li G (2022) N-3 Polyunsaturated Fatty
Acid Dehydrogenase Fat-1 Regulates
Mitochondrial Energy Metabolism by
Altering DNA Methylation in Isolated
Cells of Transgenic Cattle.
Front. Mol. Biosci. 9:857491.
doi: 10.3389/fmolb.2022.857491

Xueqiao Wang^{1,2†}, Lin Zhu^{1,2†}, Zhuoying Wei^{1,2}, Mingjuan Gu^{1,2}, Miaomiao Yang^{1,2},
Xinyu Zhou^{1,2}, Chunling Bai^{1,2}, Guanghua Su^{1,2}, Xuefei Liu^{1,2}, Lei Yang^{1,2*} and
Guangpeng Li^{1,2*}

¹State Key Laboratory of Reproductive Regulation and Breeding of Grassland Livestock, Inner Mongolia University, Hohhot, China, ²School of Life Science, Inner Mongolia University, Hohhot, China

The fatty acid dehydrogenase *fat-1* gene, derived from *Caenorhabditis elegans*, encodes n-3 polyunsaturated fatty acid dehydrogenase ($\Delta 15$ desaturase) and catalyzes the 18–20-carbon n-6 polyunsaturated fatty acids (n-6 PUFA) to generate corresponding n-3 polyunsaturated fatty acids (n-3 PUFA). Subsequently, *fat-1* can influence the n-6: n-3 PUFA ratio in *fat-1* transgenic cells. This study aimed to explore which processes of energy metabolism are affected exogenous *fat-1* transgene and the relationship between these effects and DNA methylation. Compared with the wild-type group, the n-3 PUFA content in *fat-1* transgenic bovine fetal fibroblasts was significantly increased, and the n-6 PUFA content and the n-6: n-3 PUFA ratio decreased. In the context of energy metabolism, the increase of exogenous *fat-1* transgene decreased ATP synthesis by 39% and reduced the activity and expression of key rate-limiting enzymes in glycolysis, the tricarboxylic acid cycle, and oxidative phosphorylation, thus weakening the cells' capacity for ATP production. DNA methylation sequencing indicated that this inhibition of gene expression may be due to altered DNA methylation that regulates cell energy metabolism. Exogenous *fat-1* transgenic cells showed changes in the degree of methylation in the promoter region of genes related to energy metabolism rate-limiting enzymes. We suggest that alters the balance of n-6/n-3 PUFA could regulate altered DNA methylation that affect mitochondrial energy metabolism.

Keywords: *fat-1*, metabolism, rate-limiting enzyme, ATP, DNA methylation

Abbreviations: FT, *fat-1* transgenic; WT, Wild-type; PUFA, Polyunsaturated fatty acid; TCA cycle, Tricarboxylic acid cycle; OXPHOS, Oxidative phosphorylation; GLUT4, The glucose transporter 4; PPAR γ , Peroxisome proliferator activation receptor γ ; bEFs: Bovine fetal fibroblast cells; GC-MS, Gas Chromatography-Mass Spectrometer; RIPA, Radio Immunoprecipitation Assay; MeDIP, Methylated DNA immunoprecipitation; HK, hexokinase; PFK, Phosphofructokinase; PK, Pyruvate kinase; FDP, Fructose 1, 6-diphosphate; PA, Pyruvate; CA, Citric acid; ICDHm: Mitochondrial isocitrate dehydrogenase; MDHm, Mitochondrial malate dehydrogenase; α -KGDH, α -ketoglutarate; SDH, Succinate dehydrogenase.

INTRODUCTION

In mammals, the n-3 polyunsaturated fatty acid (PUFA) α -linolenic acid and n-6 PUFA linoleic acid cannot be synthesized *de novo* and are thus considered “essential dietary fatty acids”. Once ingested, these PUFA are then catalyzed by desaturase and elongase enzymes (Wallis et al., 2002; Mokoena et al., 2020). The n-3 desaturase gene (*fat-1*) encodes n-3 fatty acid desaturase in the *Caenorhabditis elegans* genome (Spychalla et al., 1997; Wang et al., 2006), catalyzes n-6 PUFA to yield corresponding n-3 PUFA and subsequently influences the *in vivo* ratio of n-6 PUFA to n-3 PUFA (Mokoena et al., 2020). In lipid and fatty acid metabolism, PUFA can not only inhibit fat cell differentiation but also promote fatty acid oxidation (Kim and Voy, 2021). Additionally, PUFA can be used to treat non-alcoholic steatohepatitis by targeting the metabolism of liver to encourage mitochondrial β -oxidation (Okada et al., 2018). Another study showed that the synergistic effect of n-3 PUFA and squalene, a polyunsaturated hydrocarbon to maintain the antioxidant status of mitochondria. Squalene and n-3 PUFA work to regulate the activity of mitochondrial energy metabolism-related enzymes, thereby resisting reactive oxygen species in the liver mitochondria of older rats (Obulesu et al., 2014). In mammals, *fat-1* transgenic with not only have anti-arrhythmic effects (Kang, 2005), anti-tumor effects (Nowak et al., 2007), immune effects (Yamashita et al., 2013), and anti-inflammatory effects (Tomio et al., 2013) but also increased cholesterol metabolism (Kim et al., 2012) and nerve damage repair (Gladman et al., 2012). In livestock animals (e.g., sheep and cows), we produced *fat-1* genetically modified animals and found that this increase in endogenous n-3 PUFA caused by *fat-1* transgene not only changed the metabolic pathways of transgenic animals, but also changed the intestinal flora to benefit animal health (Duan et al., 2012; Wu et al., 2012; Liu et al., 2015).

The impact of changes in PUFA on metabolism has been examined in several previous studies, and its impact in the field of epigenetics has also received extensive attention. Daily supplementation of docosahexaenoic acid (DHA) for pregnant women at 18–22 weeks of gestation has increased global methylation levels (Lee et al., 2013). The maternal intake of n-3 PUFA during pregnancy may influence the DNA methylation status of the offspring as well (Bianchi et al., 2019). Other studies have shown significant changes in DNA methylation in skeletal muscle after bariatric surgery (Barres et al., 2013). Additionally, DNA methylation alters the expression of different genes involved in energy metabolism, such as insulin genes in glucose homeostasis (Kuroda et al., 2009), the glucose transporter 4 (GLUT4)-encoding gene (Yokomori et al., 1999), and the peroxisome proliferator activation receptor γ gene (PPAR γ) (Fujiki et al., 2009). Real-time quantitative polymerase chain reaction (RT-qPCR) results have shown that the expressions of four oxidative phosphorylation (OXPHOS)-related genes were significantly downregulated in islet cells from patients with abnormal glucose metabolism (Olsson et al., 2011). In skeletal muscle, DNA methylations in genes of *NDUFA5*, *COX11*, and *ATP6V1H* significantly affected transcriptions of

these genes (Ling et al., 2007; Ronn et al., 2008; Ronn et al., 2009). Interestingly, in gastric cancer cells, DNA methylation also affects PUFA biosynthesis (Lee et al., 2020). These studies indicate that DNA methylation plays an important role in energy metabolism regulation, whether in fat cells, muscle cells, or pancreatic islet cells. However, the degree and direction of DNA methylation varies in different cells.

The effect of exogenous gene transfer on DNA methylation has been studied before (Fang et al., 2014). In this study, bovine fetal fibroblasts (bEFs) isolated from *fat-1* transgenic (FT) and wild-type, (WT) cattle were used to detect the activity, expression, and product content of rate-limiting enzymes associated with energy metabolism. Specifically, the methylation pattern in promoter regions of rate-limiting enzyme-encoding genes were analyzed to determine the effects exogenous *fat-1* transgene may exert on bovine metabolism.

MATERIALS AND METHODS

Ethics Statement

All experimental procedures in this study were consistent with the National Research Council Guide for the Care and Use of Laboratory Animals. All protocols were approved by the Institutional Animal Care and Use Committee at Inner Mongolia University.

Animals

Three *fat-1* transgenic cattle fetuses (FT_1, FT_2 and FT_3) and three wild-type Luxi cattle fetuses (WT_1, WT_2 and WT_3) at 50–60 days were obtained from Shengmu Experimental Base (Holinger District, Hohhot). The fetuses were rinsed with normal saline, placed in phosphate-buffered saline (PBS) containing dual antibodies (15140-122, Gibco, United States), placed in an icebox, and brought back to the laboratory for analysis.

Cell Isolation and Culture

The head, limbs, internal organs, and bones of the fetus were removed and discarded. The remaining tissues were rinsed three times with PBS and then once with 75% ethanol for 15 s and transferred back to PBS. Then, the samples were sectioned into 1–3-mm slices and placed in Petri dishes. collagenase IV at a concentration of 1 mg/ml was added; cultures were maintained at 38.5°C with 5% CO₂ for 2–3 h. After the tissues were dissolved, the mixtures were centrifuged at 1,500 rpm/min for 5 min. The cell pellet was collected, resuspended in DMEM F12 (11330107, Gibco, United States) supplemented with 20% FBS (10099141, Gibco, United States), and cultured in 60-mm dishes at 38.5°C with 5% CO₂. bEFs were passaged when they reached 90% confluence.

Fatty Acid Gas Chromatography

Fatty acids were analyzed from bEFs when they reached 80% confluency. Briefly, bEFs were collected using 0.05% trypsin (25300062, Gibco, United States). Digested cells were placed into PBS-containing centrifuge tubes and centrifuged at

1,500 rpm for 5 min. Next, 1 ml 2.5% H₂SO₄/methanol solution was added to the isolated supernatant, which was then incubated in an 80°C water bath for 90 min. The solution was allowed to cool to room temperature before 1.5 ml 0.9% NaCl solution and 1 ml n-hexane was added. The solution was vigorously mixed for 5 min and then centrifuged at 1,500 rpm for 5 min. The organic phase was transferred to a new centrifuge tube. Saturated KOH-methanol solution was added, vigorously mixed for 5 min, and centrifuged at 1,500 rpm for 10 min. The upper liquid was collected into gas chromatography–mass spectrometry (GC-MS) sample vials for fatty acid analysis. The gas chromatographic conditions were as follows: carrier gas helium, chromatographic column HP-88, constant linear velocity 20.0 cm/s, separation ratio 20.0%, injection volume 1 µL, heating program 60°C for 1 min, 40°C/min heating to 140°C, maintained at 140°C for 10 min, increased to 240°C at 4°C/min, and maintained at 240°C for 15 min.

RNA-Seq of bEFs

Total RNA of bEFs was extracted using Trizol reagent (15596026, Invitrogen, United States). Poly (A) RNA was purified from total RNA (5 µg) by poly-T oligo-attached magnetic beads and then broken into small fragments. The spliced RNA fragments were reverse-transcribed to construct the final cDNA library. Paired-end sequencing was performed in LC Science using an HiSeq 4000 (Illumina, United States). The read values of the samples were aligned with the UCSC (<http://genome.ucsc.edu/>) reference genome using the HISAT package. This package initially removed a portion of the reads based on the quality information accompanying each read value, and then mapped the reads to the reference genome. All the transcripts in the samples were combined to reconstruct a comprehensive transcriptome using Perl Scripts. StringTie and edgeR were used to estimate expression levels of all transcripts. The differentially expressed mRNAs and genes with log₂ (fold change) > 1 or log₂ (fold change) < –1 and with statistical significance (*p* value < 0.05) were screened using R.

Metabolic Substrates and Enzymes Assays

The activity of key restriction enzymes and substrate contents in glycolysis, TCA cycle, and OXPHOS were measured using commercial kits following the manufacturer's instructions. The following commercial kits, all obtained from Comibio Biotechnology, China: the content of ATP (ATP-1-Y), glucose (PT-1-Y), FDP (FDP-1-G), PA (PA-1-Y), CA (CA-1-Y), NADH (NAD-1-Y) and the activity of HK (HK-1-Y), PFK (PFK-1-Y), PK (PK-1-Y), ICDHm (ICDHm-1-Y), α-KGDH (KGDH-1-Y), SDH (SDH-1-Y), MDHm (MDHm-1-Y), mitochondrial complex I (FHTA-1-Y), complex III (FHTC-1-Y), complex IV (FHTD-1-Y), complex V (FHTE-1-Y). Briefly, 10⁷ cells were placed in a homogenizing tube containing 1 ml kit extract with ~15 ceramic beads. The solution was homogenized at a low temperature with a homogenizer (Bertin, France). The supernatant was then added to a 96-well plate along with other reagents, as instructed. The absorbance was recorded with a microplate spectrophotometer (Thermo, United States) to calculate the enzyme activity or metabolite concentration.

Real-Time Quantitative PCR Assay

Total RNA was isolated from tissues using the RNAiso Plus kit (9109, Takara, Japan) according to the manufacturer's instructions. Briefly, RNA was then reverse-transcribed into cDNA using a cDNA reverse transcription kit (RR036A, Takara, Japan). RT-qPCR was performed using a real-time PCR detection system (7500, ABI, United States). The reaction mixture (20 µL) contained 1 µL cDNA, 0.5 µL of each primer, and 10 µL TB Green Supermix (RR820A, Takara, Japan). The primers used are listed in **Supplementary Table S1**. The protocol was as follows: initial denaturation step at 95°C for 30 s and then 40 cycles of [95°C for 15 s, 60°C for 30 s]. Relative abundance was quantified using the 2^{–ΔΔC_t} method. *RPLP0* was used as a housekeeping gene.

Genome-wide DNA Methylation Analysis

Total DNA was extracted using a QIAamp Fast DNA Tissue Kit (51404, Qiagen, Germany) following the manufacturer's protocol and quantified using a spectrophotometer and the A260/A280 ratio. DNA samples were fragmented using sonication and subjected to bisulfite conversion. The Accel-NGS Methyl-Seq DNA Library Kit (Swift, MI, United States) was utilized for attaching adapters to single-stranded DNA fragments. Briefly, the Adaptase step is a highly efficient, proprietary reaction that simultaneously performs end repair, tailing of 3' ends, and ligation of the first truncated adapter complement to 3' ends. The Extension step incorporates the truncated adapter 1 by a primer extension reaction. The Ligation step is used to add the second truncated adapter to the bottom strand only. The Indexing PCR step increases the yield and incorporates full-length adapters. Bead-based Solid Phase Reverse Immobilization (SPRI) clean-ups are used to remove both oligonucleotides and small fragments, as well as to change enzymatic buffer composition. Finally, the pair-end 2 150 bp sequencing was performed in LC Science using an HiSeq 4000 (Illumina, United States).

5-mC and 5-hmC Quantitative Assays

DNA methylation and hydroxymethylation were quantified using the MethylFlash methylated and hydroxymethylated colorimetric DNA quantification kits (P-1034; P-1036; Epigentek, United States), respectively, according to the manufacturer's instructions. The percentage of methylated DNA was proportional to the optical density intensity measured. All samples were obtained in triplicates.

Western Blot Assay

BEFs were rinsed with PBS and lysed in 150 µL of ice-cold Radio Immunoprecipitation Assay buffer. Proteins were extracted from tissues with cell lysis buffer, boiled for 5 min, and stored at –80°C. Samples were separated using a 10% sodium dodecyl sulfate-polyacrylamide gel electrophoresis (SDS-PAGE), and then electrically transferred to polyvinylidene fluoride membranes blocked with 5% nonfat dry milk in TBS-Tween 20 (blocking buffer) for 1 h. The membrane was subsequently incubated with the following antibodies, all obtained from Santa Cruz Biotechnology, United States

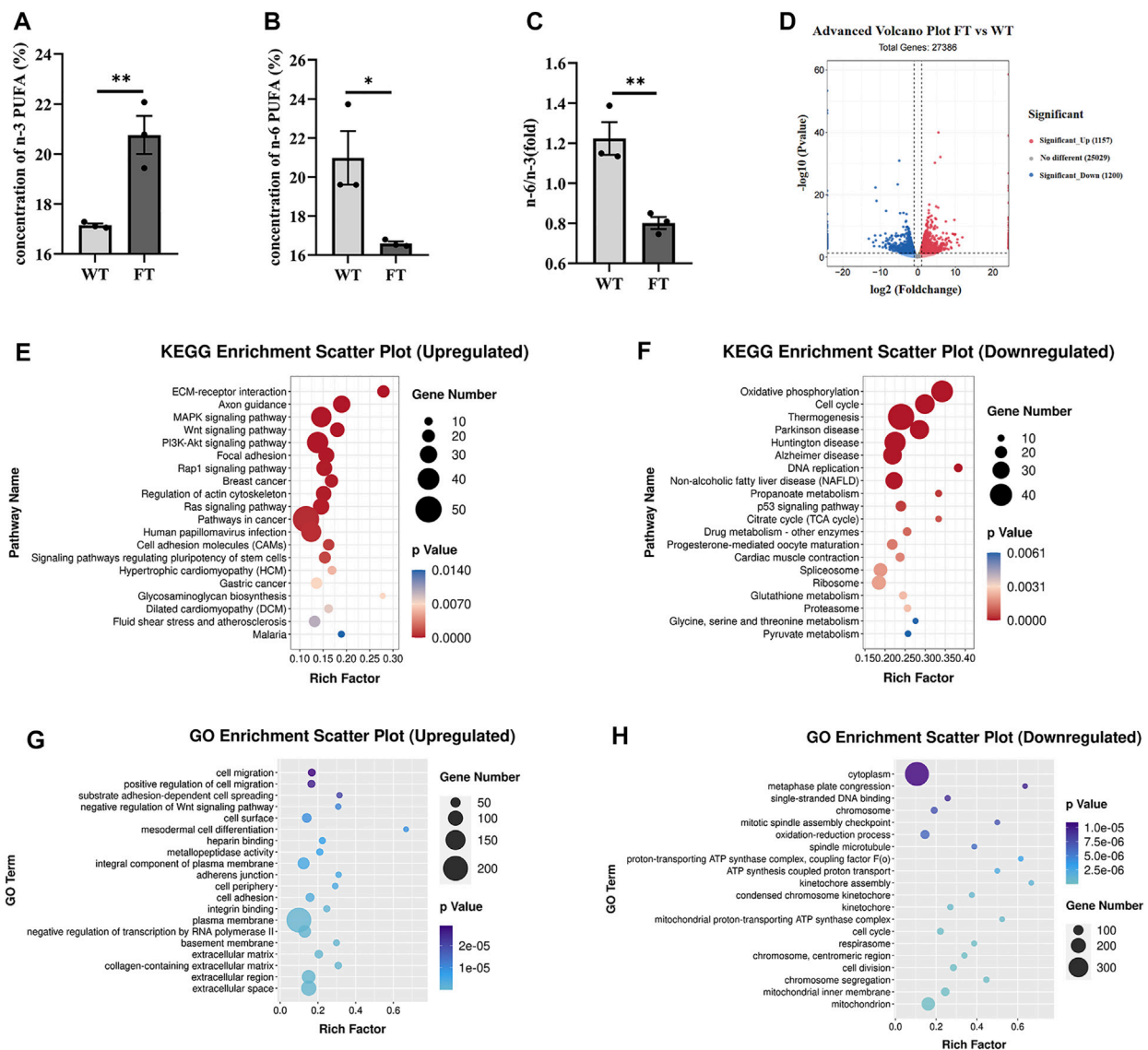


FIGURE 1 | Exogenous *fat-1* gene affects ATP synthesis in bovine fetal fibroblasts (bEFs). **(A,B)** Percent total of n-3 PUFA and percent total of n-6 PUFA by Gas Chromatography-Mass Spectrometer (GC-MC). N-3 PUFA (sum of C18:3n3, C20:3n3, C20:5n3 C22:6n3 and C18:2n6t), N-6 PUFA (sum of C18:2n6c, C18:3n6, C20:3n6 and C20:4n6). ($n = 3$) **(C)** The ratio of n-6 PUFA to n-3 PUFA was statistically lower in FT. ($n = 3$) **(D)** Differential expression genes between fat-1 and control fibroblasts. Significant_Up: significantly upregulated genes; No different: no significant differences in gene expression; Significant_down: significantly downregulated genes. ($n = 3$) **(E)** KEGG pathway upregulating enrichment. **(F)** KEGG pathway downregulating enrichment. **(G)** GO upregulated enrichment analysis of differential genes. **(H)** GO upregulated enrichment analysis of differential genes. Each dot represents an independent experiment, 0001 Each dot represents an independent experiment **(A–C)**. All data are presented as mean \pm SEM. Compared with the WT group, * $p < 0.05$, ** $p < 0.01$, *** $p < 0.001$, **** $p < 0.0001$; t-tests were used to calculate the p -values.

unless otherwise stated: anti-DNMT1 (1:500; sc-271729), anti-DNMT3a (1:500; sc-373905), anti-DNMT3b (1:500; sc-393279), anti-TET1 (1:500; sc-293186) and anti-TET2 (1:1,000; ab94580; Abcam, United States) and anti-TET3 (1:1,000; ab139311; Abcam, United States) or with a polyclonal antibody against α -Tubulin (11224-AP, proteinch, China) at 1:1,000 in TBST at 4°C overnight. Membranes were then washed three times and incubated with a horseradish peroxidase-conjugated goat anti-mouse and anti-rabbit secondary antibody at 1:5,000 in blocking buffer.

Prediction of CpG Islands

The CpG islands and CpG sites in the promoters of *PKM*, *PFKM*, *IDH2*, *MDH2*, *NDUFS1* and *ATP5F1C* were examined using MethPrimer software online (<http://www.urogene.org/cgi-bin/methprimer/methprimer.cgi>).

MeDIP Assay

The MeDIP analysis was performed according to the manufacturer's instructions (ab117133; Abcam, United States). Sonication of total genomic DNA (three pulses for 10–12 s at level

2 with 30–40 s intervals between pulses while resting on ice) produced DNA fragments between 200 bp and 1,000 bp in length. Single-stranded DNA was produced by heating and denaturing 1 µg of DNA. Then, 1 µL of anti-5mC antibody (or normal mouse IgG for a negative control) was added to induce immunoprecipitation at room temperature for 2 h. Proteinase K was added and the mixture incubated at 65°C for 1 h to release mDNA from the DNA/antibody complex. Finally, the mDNA was captured, eluted, and detected by real-time quantitative PCR. The qPCR primers are listed in **Supplementary Table S2**.

Statistical Analysis

GraphPad Prism 8.0 software was used for statistical analyses. The fatty acid contents of each tissue and the enzymatic activities and mRNA expressions in each group of cells were expressed as mean ± SEM. The mean of *fat-1* transgenic and wild-type cattle samples was compared by one-way analysis of variance (ANOVA). $p < 0.05$ was considered statistically significant.

RESULTS

Exogenous *Fat-1* Transgene Affected ATP Synthesis Pathway

Both DNA and mRNA of exogenous *fat-1* gene were significantly expressed in the transgenic bEFs, but not detected in WT cells (**Supplementary Figure S1**). n-3 PUFA were quantified using gas chromatography; % total n-3 PUFA (sum of C18:3n3, C20:3n3, C20:5n3 and C22:6n3) were significantly increased in FT groups in comparison to WT groups (17.149 ± 0.070 vs. 20.764 ± 0.761 , $p = 0.009$, **Figure 1A**), while % total n-6 PUFA (sum of C18:2n6t, C18:2n6c, C18:3n6, C20:3n6 and C20:4n6) were significantly reduced in FT cells (20.976 ± 1.377 vs. 16.591 ± 0.102 , $p = 0.034$, **Figure 1B**). Subsequently, the n-6/n-3 ratio was significantly lower in the FT group (**Figure 1C**). These results suggest the exogenous *fat-1* gene impacts n-6 and n-3 PUFA synthesis and subsequently alters the balance of n-6/n-3 PUFA.

RNA-seq analysis was performed on FT and WT cells. Out of a total of 27,386 differential genes, 1,157 genes were significantly up-regulated, and 1,200 genes were significantly down-regulated (**Figure 1D**). The KEGG pathway identified ECM-receptor interaction, axon guidance, and MAPK signaling pathways were significantly upregulated (**Figure 1E**). Among the pathways identified by the KEGG pathway that were significantly downregulated included OXPHOS, thermogenesis, and the TCA cycle (**Figure 1F**). GO enrichment analysis suggested the upregulated genes were mainly related to cell migration, positive regulation of cell migration, and substrate adhesion-dependent cell spreading (**Figure 1G**). Downregulated genes identified included enriched cytoplasm, oxidation-reduction process, single-stranded DNA binding. However, many genes related to ATP synthesis, oxidation-reduction process, and the proton-transporting ATP synthase complex were also downregulated (**Figure 1H**). These results suggest that the transgenic *fat-1* gene not only changes the fatty acid

composition to decreased the ratio of n-6: n-3 PUFA, but also regulates and influences energy metabolism, possibly through the ATP synthesis pathway.

Exogenous *Fat-1* Transgene Inhibited Energy Metabolism and Reduced ATP Production

ATP levels in FT and WT cells decreased by approximately 39% (30.101 ± 0.599 vs. 18.318 ± 0.762 nmol/min/ 10^7 cells, $p < 0.0001$, **Figure 2A**), while glucose content increased by 47% (10.265 ± 1.633 vs. 19.347 ± 3.207 µmol/ 10^7 cells, $p = 0.032$, **Figure 2A**). The activity of key glycolytic rate-limiting enzymes hexokinase (HK), phosphofructokinase (PFK) and pyruvate kinase (PK) in FT cells were significantly lower than those in WT cells (**Figure 2B**). The catalytic product of PFK, fructose-1,6-diphosphate (FDP) was also significantly reduced (0.700 ± 0.011 vs. 0.528 ± 0.021 mg/ 10^7 cells, $p < 0.0001$, **Figure 2A**). Pyruvate (PA), a product of PK, was also significantly lower in FT cells (1.897 ± 0.039 vs. 1.673 ± 0.046 µg/ 10^7 cell, $p = 0.004$, **Figure 2A**). RT-qPCR further confirmed that the mRNA expression levels of *HK1*, *PFKM*, and *PKM* subunits were significantly down-regulated (**Figure 2C**).

Detection of citric acid (CA) and NADH, products of the TCA cycle, were significantly lower in FT cells (0.425 ± 0.008 vs. 0.387 ± 0.002 nmol/ 10^7 cells, $p = 0.0009$ and 1.151 ± 0.104 vs. 0.620 ± 0.056 nmol/ 10^7 cells, $p = 0.001$, **Figure 2A**). In FT cells, the activity of mitochondrial isocitrate dehydrogenase (ICDHm) and mitochondrial malate dehydrogenase (MDHm), key rate-limiting enzymes in the TCA cycle, were significantly reduced in FT cells when compared to WT (**Figure 2D**). RT-qPCR results also confirmed that *IDH2* of ICDHm and *MDH2* were significantly downregulated (**Figure 2E**). There was no significant difference between the activity of α-ketoglutarate (α-KGDH) (**Figure 2D**) and the expression of *OGDH* encoding it (**Figure 2E**). Although there was no significant change in succinate dehydrogenase (SDH) activity (**Figure 2D**), the expressions of *SDHA*, *SDHB* and *SDHD* were downregulated to varying degrees (**Figure 2E**).

NADH dehydrogenase (complex I), pigment reductase (complex III), cytochrome oxidase (complex IV), and ATP synthase (complex V) participate in OXPHOS. Subsequently, these enzymes were examined and found (with the exception of complex IV) to be significantly downregulated (**Figure 2F**), which was additionally confirmed by RT-qPCR (**Figure 2G**).

Genome-wide DNA Methylation Is Elevated in *Fat-1* Transgenic bEFs

Previous studies have shown exogenous addition of n-3 PUFA increased the overall degree of DNA methylation in adipocytes (Perfilyev et al., 2017). Therefore, we performed global methylation on FT cells compared to WT cells. Higher levels of % total DNA methylation was observed in FT cells in comparison to WT (**Figures 3A,B**), although levels of 5-hmc methylation was not statistically significant. Genome-wide DNA-methylation analysis also identified differences between the two

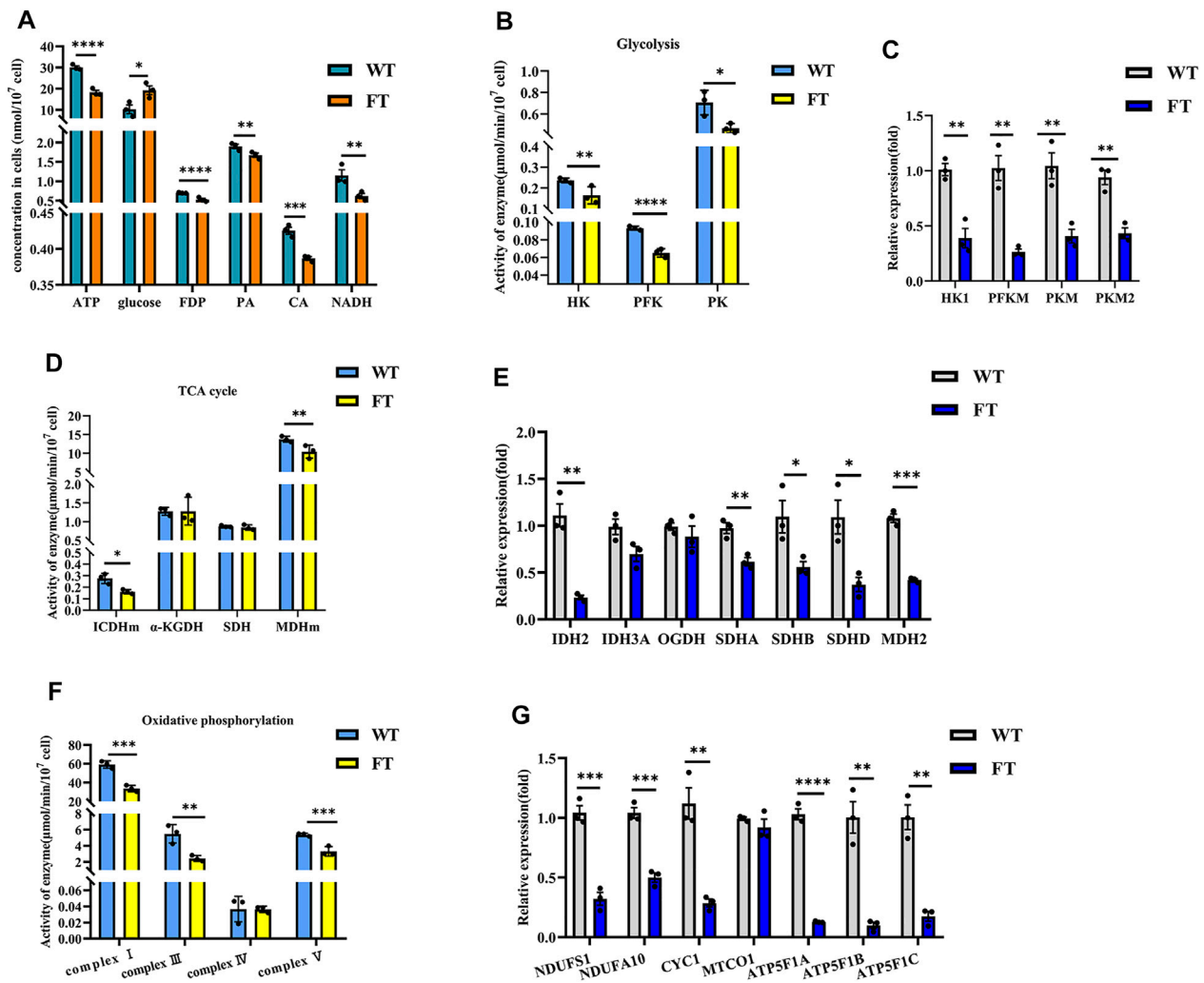


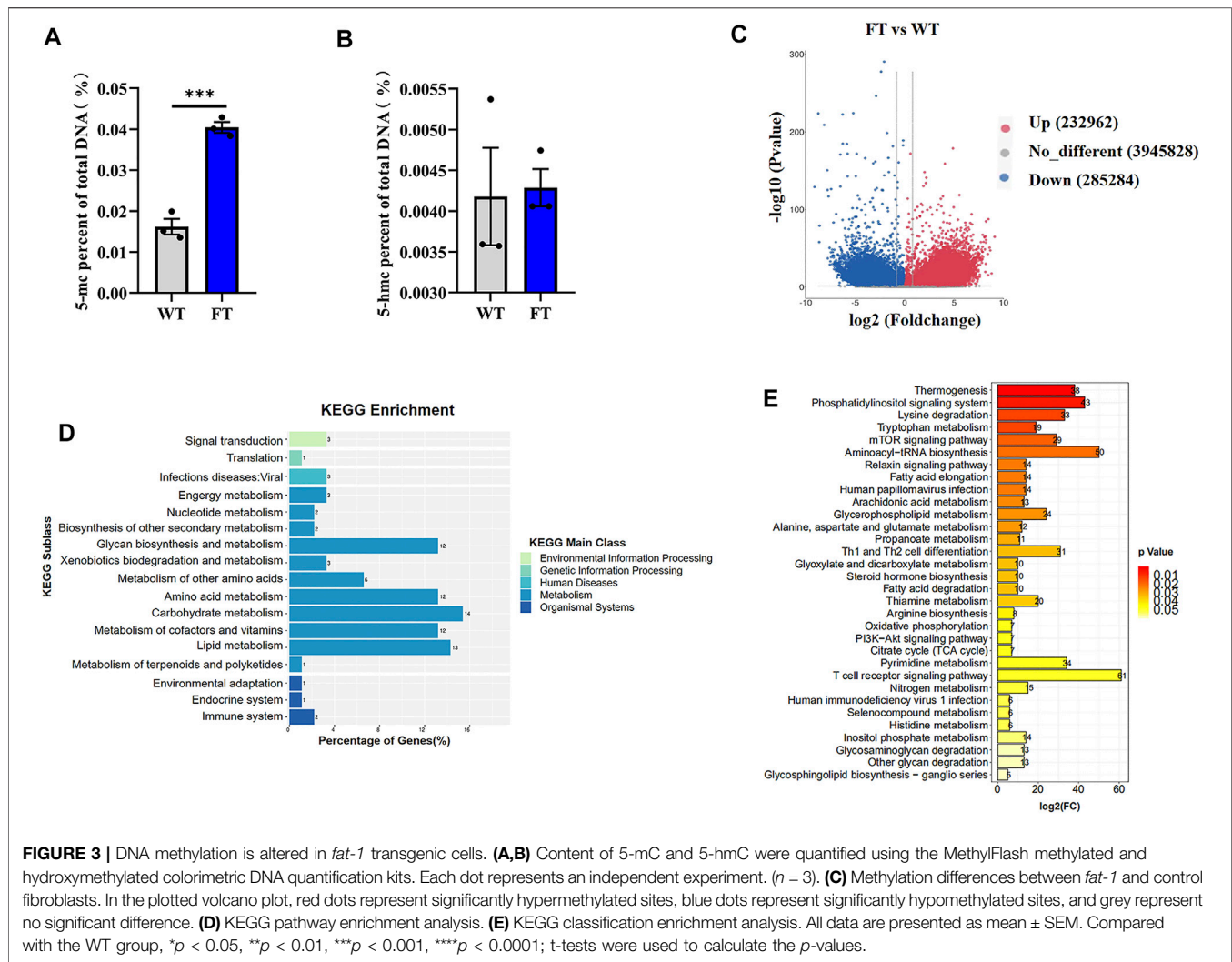
FIGURE 2 | Exogenous *fat-1* gene is effect on bEFs energy metabolism pathway of cattle. **(A)** Energy metabolism related product contents ($n = 3$). **(B,D,F)** Activity for key rate-limiting enzymes involved in glycolysis **(B)** and TCA cycle **(D)** and OXPHOS **(F)** pathway. ($n = 3$). **(C, (E,G))** Expression of mRNA for key rate-limiting enzymes involved in glycolysis **(C)** and TCA cycle **(E)** and OXPHOS **(G)** pathway by RT-qPCR in FT and WT bEFs. ($n = 3$) All assays involving enzyme activity and metabolite contents were statistically calculated by calculating the absorbance in microplate spectrophotometer. Each dot represents an independent experiment. All data are presented as mean \pm SEM. Compared with the WT group, $*p < 0.05$, $**p < 0.01$, $***p < 0.001$, $****p < 0.0001$; t-tests were used to calculate the p -values.

groups (Figure 3C). KEGG analysis revealed that approximately 80% of the differential genes were enriched in metabolic pathways, and significant changes occurred in DNA methylation of genes related to thermogenesis, fatty acid elongation, TCA cycle, and OXPHOS between FT and WT cells (Figures 3D,E).

DNA Methylation in the Promoter Region of Rate-Limiting Enzymes Are Elevated in *Fat-1* Transgenic bEFs

Methylation of genes associated with the key limiting enzymes in glycolysis, TCA cycle, and OXPHOS were all significantly increased in FT cells compared with WT cells (Figure 4A). *PFKM* and *PKM* in glycolysis, *IDH2* and *MDH2* in the TCA cycle, and *NDUFS1* and *ATP5F1* in

OXPHOS were all hypermethylated at their promoters' CpG island in FT cells (Figures 4A–C), correlating to *fat-1* transgene. This suggests balance of n-6: n-3 PUFA ratios could play a role in energy metabolism-associated gene expression. We then analyzed activity of the methylases DNMT1, DNMT3A, DNMT3B, TET1, TET2, and TET3. As expected, expression of DNMT1 and DNMT3B increased, expression of TET2 and TET3 significantly decreased, and expression DNMT3A and TET1 did not change (Figures 4D–F). These results further suggest that exogenous *fat-1* transgene in the FT group can influence hypermethylation of genes related to energy metabolic rate-limiting enzymes by upregulating the methyltransferases DNMT1 and DNMT3B and downregulating TET2 and TET3 to reduce the demethylation of genes encoding these enzymes.



DISCUSSION

As an n-3 PUFA desaturase, *fat-1* transgenes have been shown to significantly alter ratio of n-6: n-3 PUFA by converting n-6 PUFA to n-3 PUFA in mice (Kang, 2007), pigs (Pan et al., 2010; Tang et al., 2014; Liu et al., 2016), cows (Wu et al., 2012), sheep (Duan et al., 2012), and zebrafish (Sun et al., 2020). A similar phenomenon was also observed in this study. This study focused on the n-3 PUFA dehydrogenase gene *fat-1*, which affects the substrates of n-3 PUFA and n-6 PUFA, thereby affecting the ratio of n-6: n-3 PUFA, as to which changes in the effects of two fatty acids on energy metabolism will be studied in the future. Exactly which of the two fatty acids plays a greater role cannot be determined. Interestingly, Previous studies have shown that fish oil supplementation, rich in n-3 PUFA, can increase glucose production in human liver cells (Aggarwal et al., 2018). Furthermore, n-3 PUFA participate in the metabolic pathways of mitochondrial respiration and energy production. In diabetic patients, n-3 PUFA can improve impaired energy metabolism. Long-term supplementation of

n-3 PUFA in diabetic patients has been associated with improved energy metabolism in the brain and myocardium mitochondria, suggesting n-3 PUFA supplementation can prevent cardiovascular or neurological complications in the later stage of diabetes (Ochoa et al., 2005; Carvalho-Silva et al., 2019). In this way, changes in n-3 PUFA content may have more effects on the body. Studies have shown that *fat-1* transgenes regulate energy metabolism by downregulating the ratio of n-6: n-3 PUFA (Hagopian et al., 2010; Sun et al., 2020). Moreover, PUFA act as a substrate for energy metabolism and signaling molecules, which can also regulate gene expression (Jump, 2004; Jump et al., 2008). Romanatto et al. found that *fat-1* mouse tissues was associated with better glucose homeostasis (Romanatto et al., 2014). The complete oxidative decomposition of glucoses starts during glycolysis, in which HK, PFK, and PK are the key rate-limiting enzymes. The activity of these enzymes affected the rate and direction of glycolysis (Tappy et al., 2006). In this study, glucose content and the activity and expressions of HK, PFK and PK of *fat-1* transgenic cells were significantly decreased when compared to the control group. FDP, catalytic product of PFK

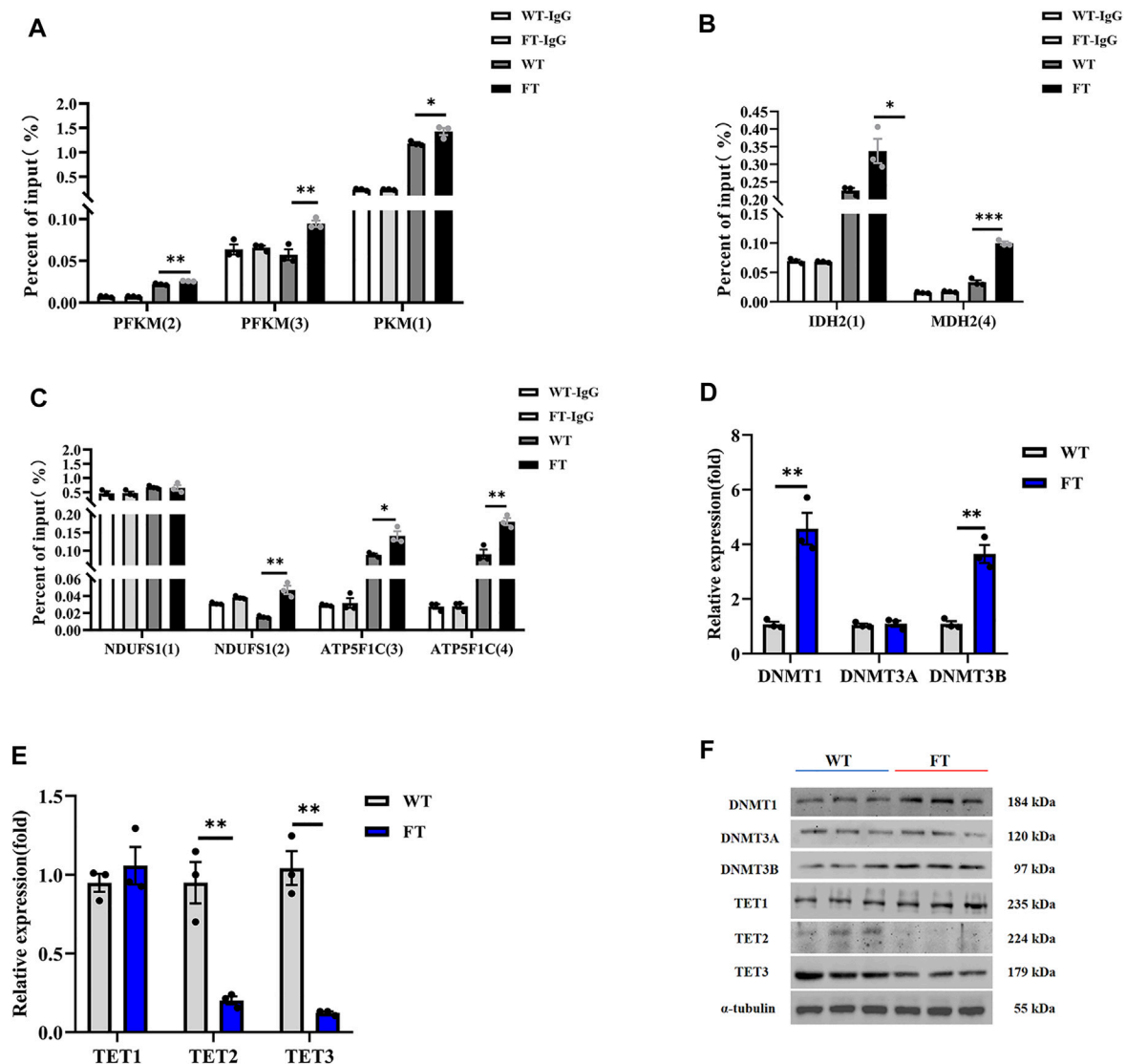


FIGURE 4 | Effect of DNA methylation on rate-limiting enzymes related to energy metabolism. **(A–C)** Methylation levels in promoters of genes associated with rate-limiting enzymes in glycolysis **(A)**, TCA cycle **(B)**, and OXPHOS **(C)** ($n = 3$). The CpG island was predicted in the promoter region of the gene, and then the predicted CpG island was detected by Methylated DNA immunoprecipitation (MeDIP) by RT-qPCR. Location of CpG island was shown in **Supplementary Figure S2**. **(D,E)** Expression of mRNA for methyltransferases and demethyltransferases by RT-qPCR in WT and FT bEfs. ($n = 3$). **(F)** Expression of protein for methyltransferases and demethyltransferases by immunoprecipitation in WT and FT bEfs. Western blots obtained by immunoblotting antibodies directed against DNMT1, DNMT3A, DNMT3B, TET1, TET2 and TET3. WT (blue line) vs. FT (red line). indicates the location of Island, please refer to **Supplementary Figure S2** for detailed location. e.g., PFK (2) means PFK (Island 2). Each dot represents an independent experiment. All data are presented as mean \pm SEM. Compared with the WT group, * $p < 0.05$, ** $p < 0.01$, *** $p < 0.001$, **** $p < 0.0001$; t-tests were used to calculate the p -values.

(Pinheiro et al., 2010) and PA, the final product of glycolysis, was also significantly reduced in FT cells. These results suggest that the change of n-6: n-3 PUFA ratios could inhibit glucose utilization during glycolysis in FT bEfs.

Obulesu et al. reported dietary supplementation with squalene and PUFA significantly attenuated age-associated inhibition on mitochondrial TCA cycle enzyme activity, including ICDHm, α -KGDH, SDH, MDH, and mitochondrial complex I, which maintained hepatic energy status at near normal levels (Obulesu et al., 2014). In *fat-1* transgenic mice, activity of

complex I was weakened, and the products of the TCA cycle also decreased (Sun et al., 2020). The present data indicated that, in the *fat-1* transgene cells, products from glycolysis (glucose, PA and CA), the key limiting enzymes in TCA cycle (IDHm, SDH, and MDHm), and key enzymes in OXPHOS were all downregulated. These results indicated that three main processes of energy metabolisms, glycolysis, the TCA cycle and OXPHOS were all inhibited in FT cells, suggesting *fat-1* transgene attenuates energy metabolism by weakening the activity of the key-limiting enzymes related to metabolism.

The methylation mark 5mC is often associated with gene repression within gene promoters (Laird, 2010; Pawson, 2004). In this study, 5mC was significantly increased in exogenous *fat-1* transgenic bEFs, indicating increased genome-wide methylation levels, which may be the reason for the down-regulation of the gene expression of key rate-limiting enzymes in energy metabolism. In cancer cells, α -ketoglutarate increases the content of 5hmC and down-regulates the content of 5mC (Lin et al., 2015). Our results show that there is no significant difference in the content of 5hmC. Changes, which led us to notice that in **Figure 2D**, the activity of α -ketoglutarate dehydrogenase did not differ between the two groups. This data may be related to 5hmC. Since this study focuses more on the fact that the exogenous *fat-1* transgene inhibits the expression of key rate-limiting enzymes in energy metabolism through DNA methylation, for demethylation-related 5hmC or 5fC or 5caC, we will in follow-up research. In a study of *fat-1* transgenic sheep, we reported that hypermethylation of the expression vector promoter region resulted in silencing of the target genes (Duan et al., 2012). We further found in transgenic sheep that exogenous *fat-1* expression was influenced by the methylation status of 721-1346nt, regulated by the methylation level of CAG promoters 101, 108 and 115nt, and maintained by DNMT1 for hypermethylation (Yang et al., 2017). Dietary fat quality impacts genome-wide DNA methylation patterns, as demonstrated in a cross-sectional study of Greek preadolescents (Voisin et al., 2015). In addition, mice fed with α -linolenic acid had 1–2% higher average methylation levels of fatty acid dehydrogenase 2 promoter in liver tissue (Niculescu et al., 2013). *In vitro*, following treatment of HT29/219 cancer cells with 100 μ M DHA and EPA for 6 days, the overall methylation levels was significantly increased, particularly from higher expression of DNMTs (Sarabi and Naghibalhossaini, 2018). Other studies have compared PUFA intake and genome-wide methylation and found increasing levels of dietary PUFA was associated with an increase in DNA methylation (Aslibekyan et al., 2014; Gonzalez-Becerra et al., 2019). In this study, the *fat-1* transgene decreased the ratio of n-6: n-3 PUFA and increased the overall degree of genome-wide methylation. Methylation of important rate-limiting enzymes involved in glycolysis, the TCA cycle and OXPHOS, which are involved in ATP production synthesis, were significantly increased in FT cells, suggesting that energy metabolism and ATP production were reduced. Compared with WT group, expressions of DNA methyltransferase DNMT1 and DNMT3B was significantly upregulated in FT cells, while expressions of demethylases TET2 and TET3 were significantly decreased. Our results suggest that changes in DNA methylation of the rate-limiting enzymes related to energy metabolism could be caused by DNA methyltransferase. Further studies will investigate how *fat-1* regulates DNA methylation through methyltransferase.

CONCLUSION

In conclusion, the change of n-6: n-3 PUFA ratios in *fat-1* transgenic cells lead to an increase in the methyltransferases

DNMT1 and DNMT3B and a decrease in the demethylases TET2 and TET3. Therefore, glycolysis, the TCA cycle, and OXPHOS are impacted by *fat-1* transgene and gene methylation.

DATA AVAILABILITY STATEMENT

The original contributions presented in the study are publicly available. This data can be found here: <https://www.ncbi.nlm.nih.gov/geo/>, GSE189689; GSE190293.

ETHICS STATEMENT

The animal study was reviewed and approved by Institutional Animal Care and Use Committee at Inner Mongolia University.

AUTHOR CONTRIBUTIONS

GL and LY conceptualized and designed the experiment; GL and XW were responsible for data management; XW prepared the first draft manuscript; XW, ZW, LZ processing methods and research investigations; MG conducted gas chromatography analysis; MY, XZ, conducted RNA-seq analysis; CB and GS conducted MeDIP analysis, and XL manuscript was reviewed and edited. All authors have read and approved the final manuscript.

FUNDING

This study was supported by the Genetically Modified Organisms Breeding Major Projects (2016ZX08007-002), the opening project of State Key Laboratory of R2BGL (to LY), the Inner Mongolia University Chief Scientist Program (to GL and LY), the Inner Mongolia Autonomous Region Basic Research Project (to LY and GL), the Major Science and Technology projects of Inner Mongolia Autonomous Region (application no. 2021ZD0009-01), the key projects of Revitalizing Inner Mongolia Autonomous Region Through Science and Technology (KJXM2020002-03).

ACKNOWLEDGMENTS

We thank Ying Zhang and Yunxi Wu for their technical support.

SUPPLEMENTARY MATERIAL

The Supplementary Material for this article can be found online at: <https://www.frontiersin.org/articles/10.3389/fmolb.2022.857491/full#supplementary-material>

REFERENCES

- Aggarwal, H., Nair, J., Sharma, P., Sehgal, R., Naeem, U., Rajora, P., et al. (2018). Aegle Marmelos Differentially Affects Hepatic Markers of Glycolysis, Insulin Signalling Pathway, Hypoxia, and Inflammation in HepG2 Cells Grown in Fructose versus Glucose-Rich Environment. *Mol. Cel Biochem* 438, 1–16. doi:10.1007/s11010-017-3108-8
- Aslibekyan, S., Wiener, H. W., Havel, P. J., Stanhope, K. L., O'Brien, D. M., Hopkins, S. E., et al. (2014). DNA Methylation Patterns Are Associated with N-3 Fatty Acid Intake in Yup'ik People. *J. Nutr.* 144, 425–430. doi:10.3945/jn.113.187203
- Barres, R., Kirchner, H., Rasmussen, M., Yan, J., Kantor, F. R., Krook, A., et al. (2013). Weight Loss after Gastric Bypass Surgery in Human Obesity Remodels Promoter Methylation. *Cel Rep.* 3, 1020–1027. doi:10.1016/j.celrep.2013.03.018
- Bianchi, M., Alisi, A., Fabrizi, M., Vallone, C., Ravà, L., Giannico, R., et al. (2019). Maternal Intake of N-3 Polyunsaturated Fatty Acids during Pregnancy Is Associated with Differential Methylation Profiles in Cord Blood white Cells. *Front. Genet.* 10, 1050. doi:10.3389/fgene.2019.01050
- Carvalho-Silva, M., Gomes, L. M., Gomes, M. L., Ferreira, B. K., Schuck, P. F., Ferreira, G. C., et al. (2019). Omega-3 Fatty Acid Supplementation Can Prevent Changes in Mitochondrial Energy Metabolism and Oxidative Stress Caused by Chronic Administration of L-Tyrosine in the Brain of Rats. *Metab. Brain Dis.* 34, 1207–1219. doi:10.1007/s11011-019-00411-6
- Duan, B., Cheng, L., Gao, Y., Yin, F. X., Su, G. H., Shen, Q. Y., et al. (2012). Silencing of Fat-1 Transgene Expression in Sheep May Result from Hypermethylation of its Driven Cytomegalovirus (CMV) Promoter. *Theriogenology* 78, 793–802. doi:10.1016/j.theriogenology.2012.03.027
- Fang, Y., Fu, X., Li, J., Du, B., Zhang, J., Zhang, X., et al. (2014). Effects of the TLR4 Transgene on Reproductive Traits and DNA Methylation Pattern of Oocytes in Ewes. *Front. Agr. Sci. Eng.* 1, 314–320. doi:10.15302/j-fase-2014038
- Fujiki, K., Kano, F., Shiota, K., and Murata, M. (2009). Expression of the Peroxisome Proliferator Activated Receptor γ Gene Is Repressed by DNA Methylation in Visceral Adipose Tissue of Mouse Models of Diabetes. *BMC Biol.* 7, 38. doi:10.1186/1741-7007-7-38
- Gladman, S. J., Huang, W., Lim, S.-N., Dyall, S. C., Boddy, S., Kang, J. X., et al. (2012). Improved Outcome after Peripheral Nerve Injury in Mice with Increased Levels of Endogenous omega-3 Polyunsaturated Fatty Acids. *J. Neurosci.* 32, 563–571. doi:10.1523/jneurosci.3371-11.2012
- González-Becerra, K., Ramos-Lopez, O., Barrón-Cabrera, E., Riezu-Boj, J. I., Milagro, F. I., Martínez-López, E., et al. (2019). Fatty Acids, Epigenetic Mechanisms and Chronic Diseases: a Systematic Review. *Lipids Health Dis.* 18, 178. doi:10.1186/s12944-019-1120-6
- Hagopian, K., Weber, K. L., Hwee, D. T., Van Eenennaam, A. L., López-Lluch, G., Villalba, J. M., et al. (2010). Complex I-Associated Hydrogen Peroxide Production Is Decreased and Electron Transport Chain Enzyme Activities Are Altered in N-3 Enriched Fat-1 Mice. *PLoS One* 5, e12696. doi:10.1371/journal.pone.0012696
- Jump, D. B., Botolin, D., Wang, Y., Xu, J., Demeure, O., and Christian, B. (2008). Docosahexaenoic Acid (DHA) and Hepatic Gene Transcription. *Chem. Phys. Lipids* 153, 3–13. doi:10.1016/j.chemphyslip.2008.02.007
- Jump, D. B. (2004). Fatty Acid Regulation of Gene Transcription. *Crit. Rev. Clin. Lab. Sci.* 41, 41–78. doi:10.1080/10408360490278341
- Kang, J. X. (2007). Fat-1 Transgenic Mice: a New Model for omega-3 Research. *Prostaglandins, Leukot. Essent. Fatty Acids* 77, 263–267. doi:10.1016/j.plefa.2007.10.010
- Kang, J. X. (2005). From Fat to Fat-1: a Tale of omega-3 Fatty Acids. *J. Membr. Biol.* 206, 165–172. doi:10.1007/s00232-005-0790-3
- Kim, E.-H., Bae, J.-S., Hahm, K. B., and Cha, J.-Y. (2012). Endogenously Synthesized N-3 Polyunsaturated Fatty Acids in Fat-1 Mice Ameliorate High-Fat Diet-Induced Non-alcoholic Fatty Liver Disease. *Biochem. Pharmacol.* 84, 1359–1365. doi:10.1016/j.bcp.2012.08.029
- Kim, M., and Voy, B. H. (2021). Fighting Fat with Fat: N-3 Polyunsaturated Fatty Acids and Adipose Deposition in Broiler Chickens. *Front. Physiol.* 12, 755317. doi:10.3389/fphys.2021.755317
- Kuroda, A., Rauch, T. A., Todorov, I., Ku, H. T., Al-Abdullah, I. H., Kandeel, F., et al. (2009). Insulin Gene Expression Is Regulated by DNA Methylation. *PLoS One* 4, e6953. doi:10.1371/journal.pone.0006953
- Laird, P. W. (2010). Principles and Challenges of Genome-wide DNA Methylation Analysis. *Nat. Rev. Genet.* 11, 191–203. doi:10.1038/nrg2732
- Lee, H.-S., Barraza-Villarreal, A., Hernandez-Vargas, H., Sly, P. D., Biessy, C., Ramakrishnan, U., et al. (2013). Modulation of DNA Methylation States and Infant Immune System by Dietary Supplementation with ω -3 PUFA during Pregnancy in an Intervention Study. *Am. J. Clin. Nutr.* 98, 480–487. doi:10.3945/ajcn.112.052241
- Lee, J.-Y., Nam, M., Son, H. Y., Hyun, K., Jang, S. Y., Kim, J. W., et al. (2020). Polyunsaturated Fatty Acid Biosynthesis Pathway Determines Ferroptosis Sensitivity in Gastric Cancer. *Proc. Natl. Acad. Sci. U.S.A.* 117, 32433–32442. doi:10.1073/pnas.2006828117
- Lin, A.-P., Abbas, S., Kim, S.-W., Ortega, M., Bouamar, H., Escobedo, Y., et al. (2015). D2HGDH Regulates Alpha-Ketoglutarate Levels and Dioxygenase Function by Modulating IDH2. *Nat. Commun.* 6, 7768. doi:10.1038/ncomms8768
- Ling, C., Poulsen, P., Simonsson, S., Rönn, T., Holmkvist, J., Almgren, P., et al. (2007). Genetic and Epigenetic Factors Are Associated with Expression of Respiratory Chain Component NDUFB6 in Human Skeletal Muscle. *J. Clin. Invest.* 117, 3427–3435. doi:10.1172/jci30938
- Liu, X., Bai, C., Ding, X., Wei, Z., Guo, H., and Li, G. (2015). Microarray Analysis of the Gene Expression Profile and Lipid Metabolism in Fat-1 Transgenic Cattle. *PLoS One* 10, e0138874. doi:10.1371/journal.pone.0138874
- Liu, X., Pang, D., Yuan, T., Li, Z., Li, Z., Zhang, M., et al. (2016). N-3 Polyunsaturated Fatty Acids Attenuates Triglyceride and Inflammatory Factors Level in Hfat-1 Transgenic Pigs. *Lipids Health Dis.* 15, 89. doi:10.1186/s12944-016-0259-7
- Mokoena, N. Z., Sebolai, O. M., Albertyn, J., and Pohl, C. H. (2020). Synthesis and Function of Fatty Acids and Oxylipins, with a Focus on *Caenorhabditis elegans*. *Prostaglandins & Other Lipid Mediators* 148, 106426. doi:10.1016/j.prostaglandins.2020.106426
- Niculescu, M. D., Lupu, D. S., and Craciunescu, C. N. (2013). Perinatal Manipulation of α -linolenic Acid Intake Induces Epigenetic Changes in Maternal and Offspring Livers. *FASEB j.* 27, 350–358. doi:10.1096/fj.12-210724
- Nowak, J., Weylandt, K. H., Habbel, P., Wang, J., Dignass, A., Glickman, J. N., et al. (2007). Colitis-Associated Colon Tumorigenesis is Suppressed in Transgenic Mice Rich in Endogenous n-3 Fatty Acids. *Carcinogenesis* 28, 1991–1995. doi:10.1093/carcin/bgm166
- Obulesu, T., Mathew, S., Lakshmanan, P. T., Krishna, G., Lakra, W. S., and Anandan, R. (2014). Salubrious Effects of Dietary Supplementation of Squalene and N-3 Polyunsaturated Fatty Acid Concentrate on Mitochondrial Function in Young and Aged Rats. *Fish. Technol.* 51, 98–101. <http://hdl.handle.net/123456789/1811>. <http://210.212.228.207/handle/123456789/1811>
- Ochoa, J. J., Quiles, J. L., Huertas, J. R., and Mataix, J. (2005). Coenzyme Q10 Protects from Aging-Related Oxidative Stress and Improves Mitochondrial Function in Heart of Rats Fed a Polyunsaturated Fatty Acid (PUFA)-rich Diet. *Journals Gerontol. Ser. A: Biol. Sci. Med. Sci.* 60, 970–975. doi:10.1093/gerona/60.8.970
- Okada, L. S. D. R., Oliveira, C. P., Stefano, J. T., Nogueira, M. A., Silva, I. D. C. G. D., Cordeiro, F. B., et al. (2018). Omega-3 PUFA Modulate Lipogenesis, ER Stress, and Mitochondrial Dysfunction Markers in NASH - Proteomic and Lipidomic Insight. *Clin. Nutr.* 37, 1474–1484. doi:10.1016/j.clnu.2017.08.031
- Olsson, A. H., Yang, B. T., Hall, E., Taneera, J., Salehi, A., Dekker Nitert, M., et al. (2011). Decreased Expression of Genes Involved in Oxidative Phosphorylation in Human Pancreatic Islets from Patients with Type 2 Diabetes. *Eur. J. Endocrinol.* 165, 589–595. doi:10.1530/eje-11-0282
- Pan, D., Zhang, L., Zhou, Y., Feng, C., Long, C., Liu, X., et al. (2010). Efficient Production of omega-3 Fatty Acid Desaturase (sFat-1)-Transgenic Pigs by Somatic Cell Nuclear Transfer. *Sci. China Life Sci.* 53, 517–523. doi:10.1007/s11427-010-0080-x
- Pawson, T. (2004). Specificity in Signal Transduction. *Cell* 116, 191–203. doi:10.1016/s0092-8674(03)01077-8
- Perfilyev, A., Dahlman, I., Gillberg, L., Rosqvist, F., Iggman, D., Volkov, P., et al. (2017). Impact of Polyunsaturated and Saturated Fat Overfeeding on the DNA-Methylation Pattern in Human Adipose Tissue: a Randomized Controlled Trial. *Am. J. Clin. Nutr.* 105, 991–1000. doi:10.3945/ajcn.116.143164

- Pinheiro, C. H. d. J., Silveira, L. R., Nachbar, R. T., Vitzel, K. F., and Curi, R. (2010). Regulation of Glycolysis and Expression of Glucose Metabolism-Related Genes by Reactive Oxygen Species in Contracting Skeletal Muscle Cells. *Free Radic. Biol. Med.* 48, 953–960. doi:10.1016/j.freeradbiomed.2010.01.016
- Romanatto, T., Fiamoncini, J., Wang, B., Curi, R., and Kang, J. X. (2014). Elevated Tissue omega-3 Fatty Acid Status Prevents Age-Related Glucose Intolerance in Fat-1 Transgenic Mice. *Biochim. Biophys. Acta (Bba) - Mol. Basis Dis.* 1842, 186–191. doi:10.1016/j.bbadis.2013.10.017
- Rønn, T., Poulsen, P., Hansson, O., Holmkvist, J., Almgren, P., Nilsson, P., et al. (2008). Age Influences DNA Methylation and Gene Expression of COX7A1 in Human Skeletal Muscle. *Diabetologia* 51, 1159–1168. doi:10.1007/s00125-008-1018-8
- Rönn, T., Poulsen, P., Tuomi, T., Isomaa, B., Groop, L., Vaag, A., et al. (2009). Genetic Variation in ATP5O Is Associated with Skeletal Muscle ATP5O mRNA Expression and Glucose Uptake in Young Twins. *PLoS One* 4, e4793. doi:10.1371/journal.pone.0004793
- Sarabi, M. M., and Naghibalhossaini, F. (2018). The Impact of Polyunsaturated Fatty Acids on DNA Methylation and Expression of DNMTs in Human Colorectal Cancer Cells. *Biomed. Pharmacother.* 101, 94–99. doi:10.1016/j.biopha.2018.02.077
- Spychalla, J. P., Kinney, A. J., and Browse, J. (1997). Identification of an Animal -3 Fatty Acid Desaturase by Heterologous Expression in Arabidopsis. *Proc. Natl. Acad. Sci.* 94, 1142–1147. doi:10.1073/pnas.94.4.1142
- Sun, S., Castro, F., Monroig, Ó., Cao, X., and Gao, J. (2020). fat-1 Transgenic Zebrafish Are Protected from Abnormal Lipid Deposition Induced by High-Vegetable Oil Feeding. *Appl. Microbiol. Biotechnol.* 104, 7355–7365. doi:10.1007/s00253-020-10774-x
- Tang, M., Qian, L., Jiang, S., Zhang, J., Song, P., Chen, Y., et al. (2014). Functional and Safety Evaluation of Transgenic Pork Rich in omega-3 Fatty Acids. *Transgenic Res.* 23, 557–571. doi:10.1007/s11248-014-9796-x
- Tappy, L., Berger, M. M., Schwarz, J.-M., Schneider, P., Kim, S., Revelly, J.-P., et al. (2006). Metabolic Effects of Parenteral Nutrition Enriched with N-3 Polyunsaturated Fatty Acids in Critically Ill Patients. *Clin. Nutr.* 25, 588–595. doi:10.1016/j.clnu.2006.03.008
- Tomio, K., Kawana, K., Taguchi, A., Isobe, Y., Iwamoto, R., Yamashita, A., et al. (2013). Omega-3 Polyunsaturated Fatty Acids Suppress the Cystic Lesion Formation of Peritoneal Endometriosis in Transgenic Mouse Models. *PLoS One* 8, e73085. doi:10.1371/journal.pone.0073085
- Voisin, S., Almén, M. S., Moschonis, G., Chrousos, G. P., Manios, Y., Schiöth, H. B., et al. (2015). Dietary Fat Quality Impacts Genome-wide DNA Methylation Patterns in a Cross-Sectional Study of Greek Preadolescents. *Eur. J. Hum. Genet.* 23, 654–662. doi:10.1038/ejhg.2014.139
- Wallis, J. G., Watts, J. L., and Browse, J. (2002). Polyunsaturated Fatty Acid Synthesis: what Will They Think of Next? *Trends Biochem. Sci.* 27, 467–473. doi:10.1016/s0968-0004(02)02168-0
- Wang, J.-W., Jiang, Y.-N., Huang, C.-Y., Huang, P.-Y., Huang, M.-C., Cheng, W. T.-K., et al. (2006). Proliferin Enhances Microvilli Formation and Cell Growth of Neuroblastoma Cells. *Neurosci. Res.* 56, 80–90. doi:10.1016/j.neures.2006.05.011
- Wu, X., Ouyang, H., Duan, B., Pang, D., Zhang, L., Yuan, T., et al. (2012). Production of Cloned Transgenic Cow Expressing omega-3 Fatty Acids. *Transgenic Res.* 21, 537–543. doi:10.1007/s11248-011-9554-2
- Yamashita, A., Kawana, K., Tomio, K., Taguchi, A., Isobe, Y., Iwamoto, R., et al. (2013). Increased Tissue Levels of omega-3 Polyunsaturated Fatty Acids Prevents Pathological Preterm Birth. *Sci. Rep.* 3, 3113. doi:10.1038/srep03113
- Yang, C., Shang, X., Cheng, L., Yang, L., Liu, X., Bai, C., et al. (2017). DNMT 1 Maintains Hypermethylation of CAG Promoter Specific Region and Prevents Expression of Exogenous Gene in Fat-1 Transgenic Sheep. *PLoS One* 12, e0171442. doi:10.1371/journal.pone.0171442
- Yokomori, N., Tawata, M., and Onaya, T. (1999). DNA Demethylation during the Differentiation of 3T3-L1 Cells Affects the Expression of the Mouse GLUT4 Gene. *Diabetes* 48, 685–690. doi:10.2337/diabetes.48.4.685

Conflict of Interest: The authors declare that the research was conducted in the absence of any commercial or financial relationships that could be construed as a potential conflict of interest.

Publisher's Note: All claims expressed in this article are solely those of the authors and do not necessarily represent those of their affiliated organizations, or those of the publisher, the editors and the reviewers. Any product that may be evaluated in this article, or claim that may be made by its manufacturer, is not guaranteed or endorsed by the publisher.

Copyright © 2022 Wang, Zhu, Wei, Gu, Yang, Zhou, Bai, Su, Liu, Yang and Li. This is an open-access article distributed under the terms of the Creative Commons Attribution License (CC BY). The use, distribution or reproduction in other forums is permitted, provided the original author(s) and the copyright owner(s) are credited and that the original publication in this journal is cited, in accordance with accepted academic practice. No use, distribution or reproduction is permitted which does not comply with these terms.



Toward Personalized Interventions for Psoriasis Vulgaris: Molecular Subtyping of Patients by Using a Metabolomics Approach

Dan Dai¹, Chunyan He², Shuo Wang³, Mei Wang^{4,5*}, Na Guo^{6*} and Ping Song^{1*}

¹Department of Dermatology, Guang'anmen Hospital, China Academy of Chinese Medical Sciences, Beijing, China, ²Department of Dermatology, Hubei Provincial Hospital of TCM, Wuhan, China, ³Department of Oncology, Guang'anmen Hospital, China Academy of Chinese Medical Sciences, Beijing, China, ⁴Leiden University-European Center for Chinese Medicine and Natural Compounds, Institute of Biology Leiden, Leiden University, Leiden, Netherlands, ⁵SU BioMedicine, BioPartner Center 3, Leiden, Netherlands, ⁶Experimental Research Center, China Academy of Chinese Medical Sciences, Beijing, China

OPEN ACCESS

Edited by:

Christopher Staley,
University of Minnesota Health Twin
Cities, United States

Reviewed by:

Jie Zheng,
Shanghai Jiao Tong University, China
Claudio Luchinat,
University of Florence, Italy

*Correspondence:

Mei Wang
m.wang@biology.leidenuniv.nl
Na Guo
guona5246@126.com
Ping Song
songping_cacms@163.com

Specialty section:

This article was submitted to
Metabolomics,
a section of the journal
Frontiers in Molecular Biosciences

Received: 20 May 2022

Accepted: 15 June 2022

Published: 19 July 2022

Citation:

Dai D, He C, Wang S, Wang M, Guo N
and Song P (2022) Toward
Personalized Interventions for Psoriasis
Vulgaris: Molecular Subtyping of
Patients by Using a
Metabolomics Approach.
Front. Mol. Biosci. 9:945917.
doi: 10.3389/fmolb.2022.945917

Aim: Psoriasis vulgaris (PV) is a complicated autoimmune disease characterized by erythema of the skin and a lack of available cures. PV is associated with an increased risk of metabolic syndrome and cardiovascular disease, which are both mediated by the interaction between systemic inflammation and aberrant metabolism. However, whether there are differences in the lipid metabolism between different levels of severity of PV remains elusive. Hence, we explored the molecular evidence for the subtyping of PV according to alterations in lipid metabolism using serum metabolomics, with the idea that such subtyping may contribute to the development of personalized treatment.

Methods: Patients with PV were recruited at a dermatology clinic and classified based on the presence of metabolic comorbidities and their Psoriasis Area and Severity Index (PASI) from January 2019 to November 2019. Age- and sex-matched healthy controls were recruited from the preventive health department of the same institution for comparison. We performed targeted metabolomic analyses of serum samples and determined the correlation between metabolite composition and PASI scores.

Results: A total of 123 participants, 88 patients with PV and 35 healthy subjects, were enrolled in this study. The patients with PV were assigned to a “PVM group” (PV with metabolic comorbidities) or a “PV group” (PV without metabolic comorbidities) and further subdivided into a “mild PV” (MP, PASI <10) and a “severe PV” (SP, PASI ≥10) groups. Compared with the matched healthy controls, levels of 27 metabolites in the MP subgroup and 28 metabolites in the SP subgroup were found to be altered. Among these, SM (d16:0/17:1) and SM (d19:1/20:0) were positively correlated with the PASI in the MP subgroup,

Abbreviation: BMI, body mass index; Cer, ceramide; CV, coefficient of variation; FFA, free fatty acid; HC, healthy control; HC-MP, healthy controls matched with mild psoriasis vulgaris; HC-SP, healthy controls matched with severe psoriasis vulgaris; HDL-C, high-density lipoprotein cholesterol; LDL-C, low-density lipoprotein cholesterol; LPC, lysophosphatidylcholine; LPE, lysophosphatidylethanolamine; MP, mild psoriasis vulgaris; PASI, Psoriasis Area and Severity Index; PC, phosphatidylcholine; PE, phosphatidylethanolamine; PLS-DA, partial least squares discriminant analysis; PV, psoriasis vulgaris; PVM, psoriasis vulgaris with metabolic diseases; QC, quality control; SM, sphingomyelin; SP, severe psoriasis vulgaris; UPLC-MS/MS, ultra-performance liquid chromatography–tandem mass spectrometry; VIP, variables of importance in projection.

while Cer (d18:1/18:0), PC (18:0/22:4), and PC (20:0/22:4) were positively correlated with the PASI in the SP subgroup. In the PVM group, levels of 17 metabolites were increased, especially ceramides and phosphatidylcholine, compared with matched patients from the PV group. In addition, the correlation analysis indicated that Cer (d18:1/18:0) and SM (d16:1/16:1) were not only correlated with PASI but also has strongly positive correlations with biochemical indicators.

Conclusion: The results of this study indicate that patients with PV at different severity levels have distinct metabolic profiles, and that metabolic disorders complicate the disease development. These findings will help us understand the pathological progression and establish strategies for the precision treatment of PV.

Keywords: psoriasis vulgaris, metabolomics, lipid metabolites, severity biomarkers, metabolic diseases, molecular subtyping

BACKGROUND

Psoriasis is a chronic, relapsing, immunoinflammatory skin disease that affects nearly 125 million of the global population (Takeshita et al., 2017). Psoriasis vulgaris (PV), also known as “plaque-type psoriasis,” accounts for approximately 90% of all cases (Boehncke and Schön, 2015) and has a multifactorial etiology, including polygenetic disorders, environmental factors, inflammation, and mental health (e.g., depression) (Kamiya et al., 2019). PV progression has been reported to be closely associated with metabolic disorders, such as obesity, diabetes, hypertension, and cardiovascular disease (Elmets et al., 2019; Kim et al., 2019), which may be attributed to the interplay between inflammation and metabolic dysfunction (Dutkiewicz et al., 2016; Kang et al., 2017). Aberrations in lipid expression and metabolism, as well as in receptors, enzymes, and lipid transport proteins, are frequently observed in patients with psoriasis. Such lipid abnormalities exacerbate psoriatic lesions and increase the risk of developing hyperlipidemia, metabolic syndrome, and cardiovascular disorders (Jia et al., 2018; Cai et al., 2021; Nowowiejska et al., 2021). Moreover, the drugs used in psoriasis therapy may have an impact on the patient’s lipid profile (Cao et al., 2021); therefore, monitoring the lipid profile is of great importance not only to disease development but also for possible adverse response caused by treatments. A high-fat diet rich in saturated fatty acids not only induces obesity but also exacerbates psoriasiform dermatitis (Herbert et al., 2018). A large clinical observation sample also highlighted the link between lipid metabolites and cardiovascular events in patients with PV (Colaco et al., 2021). The treatments of PV involve a variety of medications such as interleukins, nonsteroidal anti-inflammatory drugs, lithium, interferons, beta-blockers, antimalarial medications, calcium channel blockers, terbinafine (Jain, 2017), lipid-lowering medications (James, 2005), and contentious TNF inhibitors such as infliximab or adalimumab (Guerra and Gisbert, 2013). Untargeted metabolomics data revealed that interleukin-17A monoclonal antibody (ixekizumab) treatment improves

lipids metabolism and has the potential to reduce the cardiovascular risk in patients with psoriasis (Cao et al., 2021). Therefore, developing a personalized intervention strategy using an advanced technology platform will be cost-effective and increase the quality of life of patients. For this purpose, we first aimed to stratify patients with PV into subtypes. The inherent relationship between PV and metabolic diseases sheds lights on new intervention strategies.

Metabolomics approaches enable us to decode the complex perturbations between individual genetic inheritance and dynamic environments by combining high-throughput analysis technology combined with pattern recognition and expert systems (Donnelly et al., 2019). Such methods have been applied to capture the overall metabolic trajectory of patients with PV by profiling small molecular metabolites (Kamleh et al., 2015; Alonso et al., 2016; Ottas et al., 2017). As the molecular mechanisms underlying PV pathogenesis are not fully understood, it is difficult to identify a conclusive method for PV treatment (Raychaudhuri et al., 2014). The application of metabolomics is of great importance in exploring pathological features for successful clinical management and individualized medicine (Tarentini et al., 2021). Kang et al. (2017) identified hypoxanthine, ornithine, azelaic acid, and crotonic acid as candidate biomarkers for patients with psoriasis in an untargeted serum metabolomics study. Kamleh et al. (2015) revealed that PV has specific metabolic profiles at different degrees of severity, and that the severity-associated metabolic perturbations may stem from keratinocyte hyperproliferation, active collagen synthesis, or the incidence of cachexia. However, whether differences in lipid metabolism can indeed be observed in different severities of PV remains largely unknown.

Here, we therefore recruited patients with PV as well as healthy controls (HCs) and further subclassified the patients by the presence of metabolic comorbidities and their Psoriasis Area and Severity Index (PASI). A targeted lipidomics approach based on ultra-performance liquid chromatography–tandem mass spectrometry (UPLC-MS/MS) was applied to characterize lipid biomarkers for PV subtyping and examine distinct metabolic signatures.

MATERIALS AND METHODS

Participant Selection

Patients with PV and HC participants were recruited at Guang'anmen Hospital, China Academy of Chinese Medical Sciences (Beijing, China). We posted recruitment advertisements on the hospital's websites and notice boards, providing a brief overview of the study's goals, the medical assessments participants were to undergo, the eligibility criteria, and instructions on how to get involved. Patients were enrolled based on the following criteria: 1) aged 18–65 years, 2) diagnosis of PV, and 3) provision of a signed informed consent form. The following participants were excluded: 1) those who underwent systemic treatment within 4 weeks; 2) those with a diagnosis of pustular psoriasis, psoriatic arthritis, or erythrodermic psoriasis; 3) those with severe cardiovascular or cerebrovascular disease, abnormal liver or renal function, cancer, or psychosis disorders; and 4) pregnant or lactating women. None of the participants had dietary restrictions. Enrolled patients with PV were assigned to either the “PVM group” (PV with metabolic diseases) or the “PV group” (PV without metabolic diseases) and further subdivided into the “mild PV” (MP, PASI <10) and the “severe PV” (SP, PASI ≥10) groups. Healthy individuals without a history of psoriasis, chronic inflammatory systemic diseases, or obesity-related metabolic diseases served as the HC group and were age- and sex-matched to the MP and SP subgroups. Participants' eligibility was examined by two dermatology physicians at the dermatological clinic of our institution, both deemed them fit for this study. Written informed consent was obtained from all participants. Serum samples were collected and analyzed from each recruited participant to obtain lipid biomarkers for PV subtyping. The recruitment process began in January 2019 and was completed in November 2019.

Chemicals and Materials

We purchased internal standards for ceramide (Cer (d18:1/17:0)), phosphatidylethanolamine (PE [12:0/13:0]), sphingomyelin (SM [d18:1/12:0]), and phosphatidylcholine (PC (19:0/19:0)) from Avanti Polar Lipids (Alabaster, AL, United States). Free fatty acid (FFA C19:0) was sourced from Larodan (Stockholm, Sweden). MS-grade isopropanol, acetonitrile, methanol, and formic acid were purchased from Fisher Scientific (Waltham, MA, United States). Ultra-pure water was obtained from a Milli-Q water purification system and used throughout the experiments (Millipore, Bedford, MA, United States). All other reagents and chemicals used were of analytical grade and commercially available.

Sample Preparation

Following collection, whole blood samples were centrifuged for 10 min at 3,000 rpm in a refrigerated centrifuge (4°C), after which the supernatants were aliquoted into 1.5-ml Eppendorf tubes and stored at –80°C until the subsequent metabolomic analysis. Standard stock solutions were prepared by dissolving the compounds in methanol to a concentration of 1 mg/ml and stored below –20°C.

For the targeted lipid and fatty acid analyses, 10 µl of serum was added to 150 µl of cold methanol containing a mixture of the following internal standards: FFA C19:0 (200 ng/ml), SM (d18:1/12:0) (40 ng/ml), PC (19:0/19:0) (30 ng/ml), Cer (d18:1/17:0) (200 ng/ml), and PE (12:0/13:0) (100 ng/ml). The samples were mixed for 30 s, after which 500 µl of methyl tert-butyl ether was added, and the samples were incubated under gentle agitation for 20 min at room temperature to extract the full lipids. After the addition of 125 µl of water, the samples were shaken and centrifuged for 10 min at 13,200 rpm at 4°C. The upper lipid extracts of 100 µl were transferred into a new centrifuge tube, vacuum-dried, and resuspended in a 200 µl solution of acetonitrile/isopropanol/water (65:30:5, v/v/v). The samples were again vortexed for 1 min and centrifuged as described previously, and the supernatants were instantly analyzed using UPLC-MS/MS.

To validate the stability of the LC-MS system, pooled quality control (QC) samples were prepared by mixing 1 ml of each serum sample prepared as described previously.

UPLC-MS/MS Conditions

The UPLC and MS systems were controlled using MassLynx Mass Spectrometry Software (v4.1) (Waters Corp., MA, United States). All chromatographic separations were performed using an Acquity UPLC BEH C8 Column (1.7 µm, 100 × 2.1 mm²; Waters Corp.). The mobile phase consisted of 5 mM ammonium formate in acetonitrile/water (6:4, v/v; mobile phase A) and 5 mM ammonium formate in isopropanol/acetonitrile (9:1, v/v; mobile phase B). The column was maintained at 55°C, and the flow rate was set at 0.26 ml/min. The linear elution gradient settings are shown in **Supplementary Table S1**. An injection volume of 1 µl was applied in the positive ion mode and a 2 µl volume in the negative ion mode. During the mass spectrometer (Xevo TQ-S; Waters Corp.) operation, we applied multiple reaction monitoring in the positive and negative ion modes. The TargetLynx Application Manager (Waters Corp.) was used to process the data.

System Stability

To guarantee the stability of the LC-MS system throughout our analyses, we evaluated the pooled QC samples in both the positive and the negative ion modes. The retention time and intensity measurements suggested that the stability and repeatability of the measurements was satisfactory and high, respectively, throughout for the experiment. The bulk of the coefficient of variation (CV) values belonging to the internal standard peak area for the targeted lipid and fatty acid tests fell below 15%.

Data Analysis

Raw data from the UPLC-MS/MS analysis were first imported into Progenesis QI Software (v2.3; Waters Corp.). Baseline filtering, peak identification, integration, retention time correction, and peak alignment were then performed to optimize the setting parameters. All chromatographic peaks were confirmed manually by careful investigation to verify the accuracy of the results, and a data matrix was obtained, including information such as mass-to-charge ratio (m/z),

TABLE 1 | Demographics of the study cohort.

Comparison 1			
Characteristic	MP patient (n = 31)	HC-MP subject (n = 31)	p-value
Age (years)	19–62, 33.45 ± 11.38	19–58, 34.84 ± 10.74	0.667
Female	14	18	0.309
PASI	6.08 ± 2.52	NA	NA
Duration of psoriasis (years)	9.81 ± 7.01	NA	NA
Family history	11	NA	NA
BMI (kg/m ²)	23.23 ± 2.98	22.35 ± 2.66	0.383
Total cholesterol (mmol/L)	4.53 ± 0.63	4.77 ± 0.79	0.252
Triglyceride (mmol/L)	1.37 ± 0.77	0.91 ± 0.26	0.071
LDL cholesterol (mmol/L)	2.76 ± 0.43	2.94 ± 0.58	0.203
HDL cholesterol (mmol/L)	1.29 ± 0.26	1.43 ± 0.28	0.063
Comparison 2			
Characteristic	SP patient (n = 32)	HC-SP subject (n = 32)	p-value
Age (years)	19–57, 36.03 ± 10.16	19–58, 36.25 ± 11.38	0.92
Female	13	19	0.134
PASI	17.69 ± 6.41	NA	NA
Duration of psoriasis (years)	13.07 ± 8.26	NA	NA
Family history	9	NA	NA
BMI (kg/m ²)	23.33 ± 3.99	22.34 ± 2.60	0.243
Total cholesterol (mmol/L)	4.68 ± 0.90	4.79 ± 0.82	0.665
Triglyceride (mmol/L)	1.23 ± 0.56	0.94 ± 0.26	0.059
LDL cholesterol (mmol/L)	2.92 ± 0.72	2.97 ± 0.58	0.812
HDL cholesterol (mmol/L)	1.27 ± 0.30	1.41 ± 0.26	0.066
Comparison 3			
Characteristic	MP patient (n = 31)	SP patient (n = 32)	p-value
Age (years)	19–62, 33.45 ± 11.38	19–57, 36.03 ± 10.16	0.346
Female	14	13	0.716
PASI	6.08 ± 2.52	17.69 ± 6.41	0
Duration of psoriasis (years)	9.81 ± 7.01	13.07 ± 8.26	0.097
Family history	11	9	0.53
BMI (kg/m ²)	23.23 ± 2.98	23.33 ± 3.99	0.91
Total cholesterol (mmol/L)	4.53 ± 0.63	4.68 ± 0.90	0.488
Triglyceride (mmol/L)	1.37 ± 0.77	1.23 ± 0.56	0.741
LDL cholesterol (mmol/L)	2.76 ± 0.43	2.92 ± 0.72	0.339
HDL cholesterol (mmol/L)	1.29 ± 0.26	1.27 ± 0.30	0.766
Comparison 4			
Characteristic	PVM patient (n = 25)	PV patient (n = 25)	p-value
Age (years)	26–65, 45.04 ± 9.34	24–57, 42.60 ± 8.22	0.332
Female	9	9	1
PASI	18.99 ± 14.62	15.62 ± 8.74	0.816
Duration of psoriasis (years)	15.83 ± 10.76	14.48 ± 8.23	0.621
Family history	7	7	1
BMI (kg/m ²)	27.29 ± 3.75	23.91 ± 3.28	0.002
Total cholesterol (mmol/L)	5.49 ± 1.13	5.06 ± 0.77	0.165
Triglyceride (mmol/L)	2.85 ± 1.27	1.43 ± 0.64	0
LDL cholesterol (mmol/L)	3.56 ± 0.88	3.13 ± 0.64	0.084
HDL cholesterol (mmol/L)	1.15 ± 0.19	1.29 ± 0.34	0.107

BMI, body mass index; HDL-C, high-density lipoprotein cholesterol; HC-MP, healthy controls matched with mild psoriasis vulgaris; HC-SP, healthy controls matched with severe psoriasis vulgaris; LDL-C, low-density lipoprotein cholesterol; MP, mild psoriasis vulgaris (PASI <10); PASI, Psoriasis Area and Severity Index; PVM, psoriasis vulgaris with metabolic diseases; PV, psoriasis vulgaris without metabolic diseases; SP, severe psoriasis vulgaris (PASI ≥10).

retention time, and peak area (intensity). The data matrix obtained was exported to SIMCA software (v14.1; Umetrics, Umeå, Sweden) for partial least squares discriminant analysis (PLS-DA). The R^2 and Q^2 statistics were used to assess the

quality of the PLS-DA model, whereas its reliability was determined using a permutation test, because of the model's potential to overestimate the separation performance. All statistical tests were performed using SPSS (v25.0; SPSS Inc.,

TABLE 2 | Metabolic disorder in sub-population of PV.

Patient	PASI <10	PASI ≥10
No. of PV patient	38	50
No. of PVM patient	7 (18.42%)	18 (36%)

IL, United States). The non-parametric Student's *t*-test, Kruskal–Wallis test, and chi-square test were used to compare the data, as appropriate. The *p*-values of <0.05 were considered significant, and no corrections were performed for multiple testing as the study was exploratory. The variables of importance in projection (VIP) analysis following PLS-DA modeling and a Student's *t*-test analysis were applied to identify biomarkers (VIP >1, *p* < 0.05). Spearman's correlation coefficients were calculated to study the associations between the expression of metabolites, PASI, and biochemical indicators using the ggplot2 package (v3.3.5) in R (<https://www.R-project.org>).

RESULTS

Participant Baseline Characteristics

In total, 123 participants, including 88 patients with PV and 35 HCs, were enrolled in this study. The PV group consisted of 63 patients, and the PVM group consisted of 25; the patients in

the PV group were further subdivided into 31 in the MP subgroup and 32 in the SP subgroup. We performed four pairwise comparisons, one between the MP subgroup and matched HCs (MP vs. HC-MP; 31 vs. 31), one between the SP subgroup and matched HCs (SP vs. HC-SP; 32 vs. 32), one between both subgroups (MP vs. SP; 31 vs. 32), and one between the PVM group and matched patients from the PV group (PVM vs. PV, 25 vs. 25). The HC-MP and HC-SP subgroups were based on the same 25 shared healthy subjects. The characteristics of the study cohorts are shown in **Table 1**, and the metabolic complications of the patients in the PVM group are illustrated in **Supplementary Table S2**. Among the 38 patients with PV whose PASI was <10, we identified 7 (18.42%) patients with metabolic disorders, while of the 50 patients with PV whose PASI was ≥10, 18 (36%) had metabolic disorders (**Table 2**). These data demonstrated a significant increase in metabolic disorders in patients with severe PV, suggesting that dysfunctions in lipid metabolism may contribute to the progression of PV.

Targeted Metabolomic Analysis

In our targeted metabolomics analysis, we focused on the expressions of specific lipids and fatty acids in the different groups. During the UPLC-MS/MS analysis, QC samples were regularly run to ensure the reproducibility of the results, and the majority of the CV values corresponding to the internal standard peak area were <15%, which is consistent with good stability and reliability. In total, 25 FFAs and 131 lipid metabolites were

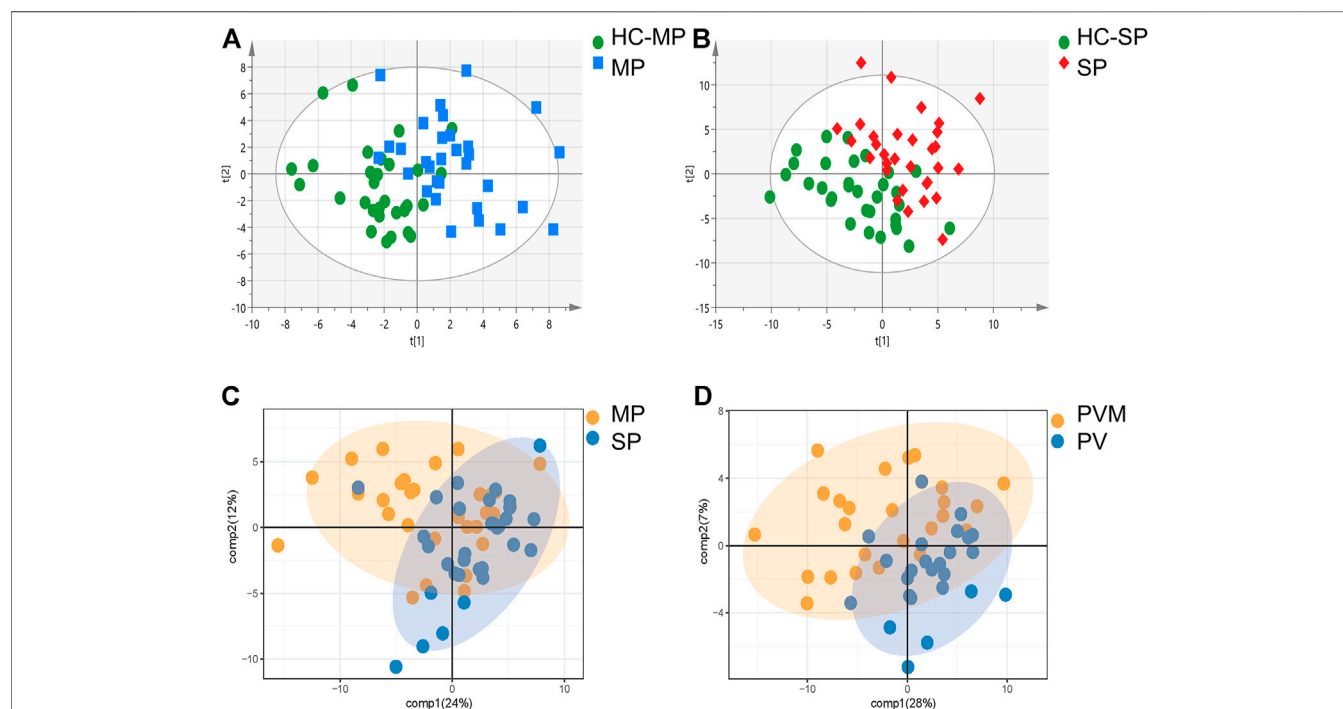


FIGURE 1 | Comparison of metabolites using PLS-DA models. **(A)** PLS-DA model of the MP and HC-MP subgroups. **(B)** PLS-DA model of the SP and HC-SP subgroups. **(C)** PLS-DA model of the MP and SP subgroups. **(D)** PLS-DA model of the PVM and PV groups. HC-MP, healthy controls matched to the group with mild psoriasis vulgaris; HC-SP, healthy controls matched to the group with severe psoriasis vulgaris; MP, mild psoriasis vulgaris; PLS-DA, partial least squares discriminant analysis; PV, psoriasis vulgaris without metabolic diseases; PVM, psoriasis vulgaris with metabolic diseases; SP, severe psoriasis vulgaris.

TABLE 3 | Significantly altered lipids between different groups.

Lipid	MP vs. HC-MP	SP vs. HC-SP	SP vs. MP	PVM vs. PV
Cer	–	✓	–	✓
FFA	✓	✓	–	✓
LPC	✓	✓	✓	✓
LPE	–	✓	–	–
PC	✓	✓	✓	✓
PE	✓	✓	–	✓
SM	✓	✓	✓	–

Cer, ceramide; FFA, free fatty acid; LPC, lysophosphatidylcholine; LPE, lysophosphatidylethanolamine; PC, phosphatidylcholine; PE, phosphatidylethanolamine; SM, sphingomyelin.

detected. Relevant information on precursor ions, product ions, and collisions for all the lipid and fatty acid samples is provided in **Supplementary Table S3**.

Serum Metabolic Profiling Identifies Patients With PV at Different Severity Levels

The PLS-DA analysis was performed to investigate the metabolic differences among the groups and subgroups (**Figure 1**). Permutation tests (200 permutations) were performed to verify the PLS-DA models. Both the permuted R^2 and Q^2 values were significantly lower than the corresponding original values (see **Supplementary Figure S1**), suggesting good compatibility of the data and predictive ability of the model. Compared with the matched HC-MP and HC-SP control groups, participants in the MP and SP subgroups exhibited a significantly distinctive metabolic signature, suggesting dysfunctional lipid metabolism in patients with PV (**Figures 1A,B**). Although the MP subgroup coincided with the SP group, PC, LPC, and SM showed alterations between the two (**Figure 1C**). A clear distinction was also observed between the PVM group and matched patients in the PV group, with differences in Cer, FFA, LPC, PC, and PE between the two groups (**Figure 1D**). This finding suggests an overlap of PV and metabolic disorders (**Table 3**).

Altered Metabolites in Patients With PV at Different Severity Levels

Our univariate statistical analysis revealed significant differences in lipid and fatty acid levels among the groups and subgroups (**Table 4**). The MP subgroup exhibited higher levels of three types of PE, six types of PC, and FA 16:2, and lower levels of five types of PC, four types of LPC, seven types of SM, and PE (18:2/16:1) than the HC-MP subgroup (**Figure 2A**). In the comparison between the SP and HC-SP subgroups, the levels of two types of PC, two types of Cer, PE (18:2/16:0), and FA 16:2 were elevated in the SP subgroup, while the levels of two types of LPC, ten types of SM, nine types of PC, and lysophosphatidylethanolamine 20:2 (LPE 20:2) were reduced (**Figure 2B**). The lower levels of PC, LPC, and SM observed in the SP subgroup distinguished it from the MP subgroup (**Figure 2C**). As for the comparison between the PVM and PV groups, levels of six types of Cer, two types of FFA, seven types of PC, LPC 20:2, and PE (22:5/16:0) were all

significantly high in the PVM group (**Figure 2D**), indicating that the disorder in lipid metabolism served a critical role in metabolic complications of psoriasis.

Associations Between the Altered Metabolites and the Metabolic Signatures of Severity

Spearman's correlation was applied to explore the associations between all the measured metabolites and the patient's PASI scores (**Supplementary Table S4**). SM (d16:1/16:1) and LPE 20:4 were negatively correlated with PASI, whereas a positive correlation was observed between Cer (d18:1/18:0) and the PASI. The correlation analysis between all the measured metabolites and biochemical indicators including cholesterol, triglyceride, high-density lipoprotein cholesterol (HDL-C), and low-density lipoprotein cholesterol (LDL-C) was also performed to enrich the significance of the harvested lipid biomarkers (**Supplementary Table S5**). Surprisingly, Cer (d18:1/18:0) and SM (d16:1/16:1) were not only correlated with PASI but also strongly correlated with biochemical indicators. Cer (d18:1/18:0) was strongly positively correlated with cholesterol, triglyceride, and LDL-C, whereas SM (d16:1/16:1) had the strongly positive correlations with cholesterol, HDL-C, and LDL-C. Furthermore, we observed positive correlations (all values of $p < 0.05$) among most of the altered metabolites (**Figure 3**). SM and PC, and PC and PE showed a strong correlation within the altered metabolites in the MP subgroup (**Figure 3A**). In the SP subgroup, a strong correlation between SM and PC, and PC and LPC was observed in the altered metabolites (**Figure 3B**). This observation indicates that the progression of PV symptoms may be associated with an alteration of lipid metabolism. Moreover, we also found a strong correlation between PC and FFA, and PE and Cer in the PVM group (**Figure 3E**). To further investigate the severity biomarkers of PV, we conducted Spearman's correlation analysis between the PASI scores and the altered metabolites (MP vs. HC-MP and SP vs. HC-SP). The results show that SM (d19:1/20:0) and SM (d16:1/17:0) in the MP subgroup were positively correlated with the PASI scores (**Figure 4A**). In addition, PC (18:0/22:4), PC (20:0/22:4), and Cer (d18:1/18:0) in the SP subgroup were positively correlated with the PASI scores (**Figure 4B**). There was no metabolite that strongly was correlated with the PASI in both the MP and the SP subgroups.

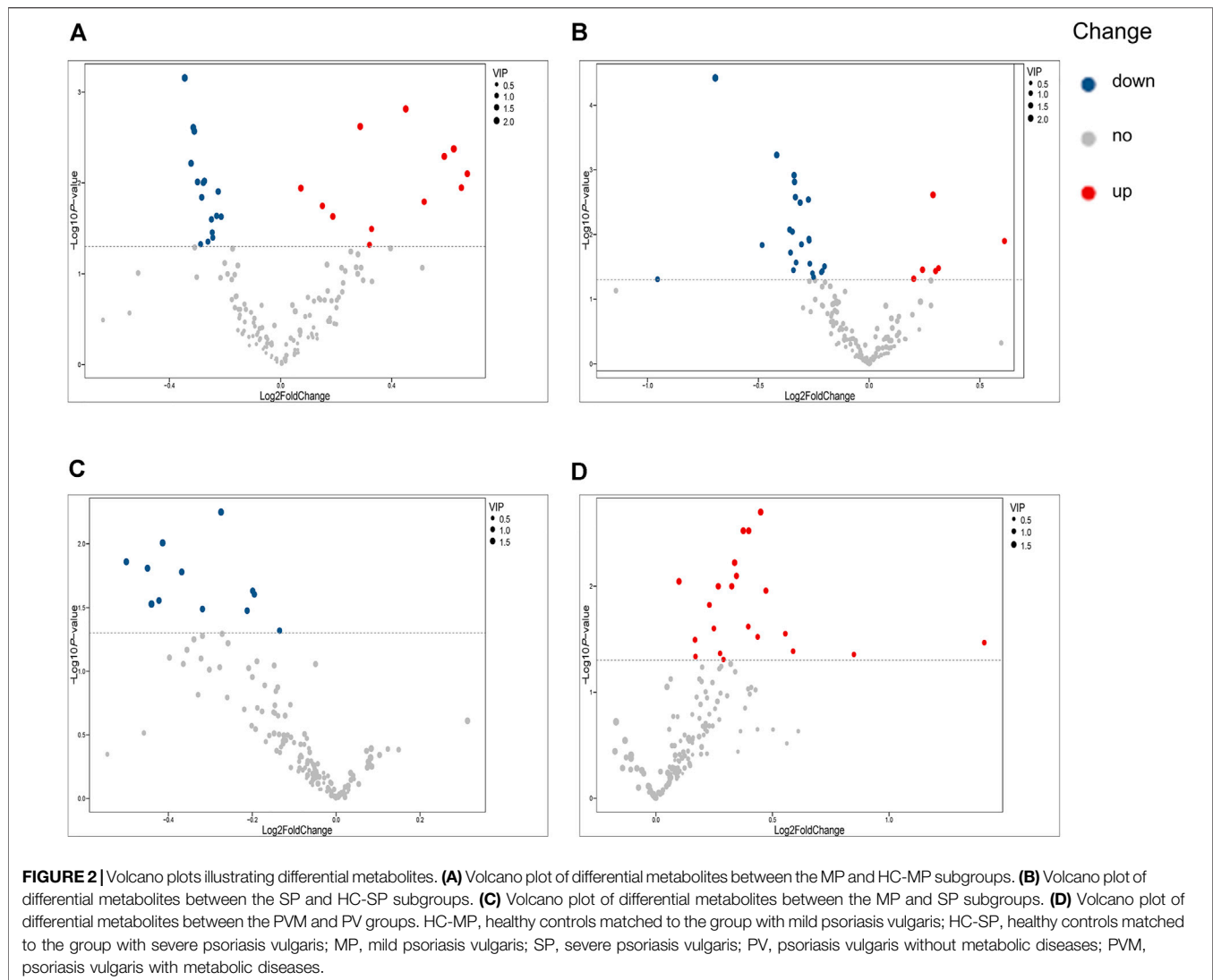
DISCUSSION

Based on the idea that subtyping of PV may contribute to the development of personalized treatment, we explored the molecular evidence for alterations in lipid metabolism at different severity levels of the disease using serum metabolomics. The identified metabolic disorders related to the progress of PV are summarized in **Figure 5** excessive hydrolysis causes the accumulation of PC and subsequently lipids droplet formates, which may be an important factor that contributes to disease progression. Using the targeted UPLC-MS/MS-based lipidomics platform to characterize the

TABLE 4 | Expression trends of metabolites altered between different groups.

Metabolite	MP vs. HC-MP	SP vs. HC-SP	SP vs. MP	PVM vs. PV
Cer (d18:1/16:0)	–	–	–	–
Cer (d18:1/18:0)	–	Δ↑	–	–
Cer (d18:1/24:1)	–	Δ↑	–	*↑
Cer (d18:1/25:0)	–	–	–	Δ↑
Cer (d18:1/22:0)	–	–	–	*↑
Cer (d18:1/22:2)	–	–	–	*↑
Cer (d18:1/24:0)	–	–	–	*↑
Cer (d18:2/22:0)	–	–	–	Δ↑
FA 16:2	*↑	Δ↑	–	–
FA 19:0	–	–	–	Δ↑
FA 24:0	–	–	–	Δ↑
LPC 17:0	Δ↓	–	–	–
LPC 20:0	Δ↓	–	–	–
LPC 20:2	–	–	–	Δ↑
LPC 20:3	–	–	Δ↓	–
LPC 20:5	–	Δ↓	Δ↓	–
LPC 21:0	Δ↓	–	–	–
LPC 22:0	Δ↓	–	–	–
LPC 22:6	–	Δ↓	–	–
LPE 20:2	–	Δ↓	–	–
PC (10:0/19:1)	Δ↓	*↓	–	–
PC (16:1/16:0)	Δ↑	–	Δ↓	–
PC (16:0/17:1)	–	–	Δ↓	–
PC (14:0/18:2)	–	–	–	*↑
PC (18:0/16:0)	–	–	–	Δ↑
PC (15:1/18:2)	Δ↓	Δ↓	–	–
PC (16:1/18:2)	–	–	Δ↓	Δ↑
PC (18:3/16:0)	–	–	Δ↓	–
PC (20:4/14:0)	–	–	Δ↓	Δ↑
PC (18:1/17:0)	–	Δ↓	–	–
PC (18:2/17:0)	–	Δ↓	–	–
PC (18:2/19:1)	–	–	–	Δ↑
PC (17:1/18:2)	–	–	Δ↓	–
PC (18:0/18:1)	Δ↑	–	Δ↓	–
PC (20:4/16:1)	–	Δ↓	Δ↓	–
PC (20:4/17:0)	–	*↓	–	–
PC (15:0/22:6)	Δ↓	Δ↓	–	–
PC (18:0/20:2)	Δ↑	–	–	Δ↑
PC (18:0/20:5)	–	–	Δ↓	–
PC (18:0/22:4)	Δ↑	Δ↑	–	–
PC (18:0/22:5)	Δ↑	–	–	–
PC (20:4/20:4)	Δ↓	Δ↓	–	–
PC (20:4/22:6)	Δ↓	Δ↓	–	–
PC (20:0/18:0)	–	–	–	*↑
PC (20:0/22:4)	Δ↑	Δ↑	–	–
PE (12:0/13:0)	–	–	–	–
PE (16:0/16:0)	–	–	–	–
PE (16:0/18:1)	*↑	–	–	–
PE (18:2/16:0)	Δ↑	Δ↑	–	–
PE (18:2/16:1)	Δ↓	–	–	–
PE (18:0/22:5)	Δ↑	–	–	–
PE (22:5/16:0)	–	–	–	Δ↑
SM (d16:0/15:1)	–	#↓	–	–
SM (d16:1/16:0)	–	Δ↓	Δ↓	–
SM (d16:1/17:0)	*↓	*↓	–	–
SM (d18:1/15:1)	Δ↓	*↓	–	–
SM (d18:1/17:0)	Δ↓	Δ↓	–	–
SM (d18:1/17:1)	*↓	*↓	–	–
SM (d18:1/19:0)	–	–	–	–
SM (d18:1/19:1)	Δ↓	Δ↓	–	–
SM (d19:1/20:0)	Δ↓	*↓	–	–
SM (d20:0/22:6)	–	Δ↓	–	–
SM (d17:1/26:1)	–	Δ↓	–	–
SM (d16:0/22:3)	–	–	–	–
SM (d16:0/17:0)	Δ↓	–	–	–

Δ, $p < 0.05$; *, $p < 0.01$; and #, $p < 0.001$



serum samples of patients, we inspected the pathological mechanism underlying PV that is closely associated with complex lipid metabolism dysfunction and thereby identified a set of PV's lipid biomarkers. The correlation analysis indicated that Cer (d18:1/18:0) and SM (d16:1/16:1) were not only correlated with PASI but also has strongly positive correlations with biochemical indicators in our analysis. Positive correlations were observed among the most altered metabolites. Among the altered metabolites in the MP subgroup, SM and PC levels showed a strong correlation. A strong correlation between SM and PC, and PC and LPC was observed for the altered metabolites in the SP subgroup. We focused on the biomarkers associated with the severity of PV and found that in the MP subgroup, SM (d16:0/17:1) and SM (d19:1/20:0) were positively correlated with the PASI, whereas in the SP subgroup, PC (18:0/22:4), PC (20:0/22:4), and Cer (d18:1/18:0) were positively correlated with PASI scores. These results suggest that SM disorders

dominated the lipid abnormalities in the MP subgroup, while Cer and PC disorders were predominant in the SP subgroup. In addition, we found more patients with severe PV complicated by metabolic diseases than patients with mild PV, suggesting that dysfunction in lipid metabolism may contribute to the progression of PV. Cer, FFA, PC, LPC, and PE levels were significantly higher in patients with PV complicated by metabolic diseases than in those without metabolic diseases. Although the pathogenesis of metabolic complications of PV is unclear, it has been linked to lipid accumulation caused by dysfunctional lipid metabolism. Our findings thus offer novel insights into the metabolic nature of PV. The metabolic biomarkers we suggest for the subtyping of PV may assist practitioners in identifying potentially important risk factors in the future and support the development of precision medicine treatment for PV.

SM is primarily produced in the Golgi apparatus and transferred to all other cellular membranes (Campelo et al.,

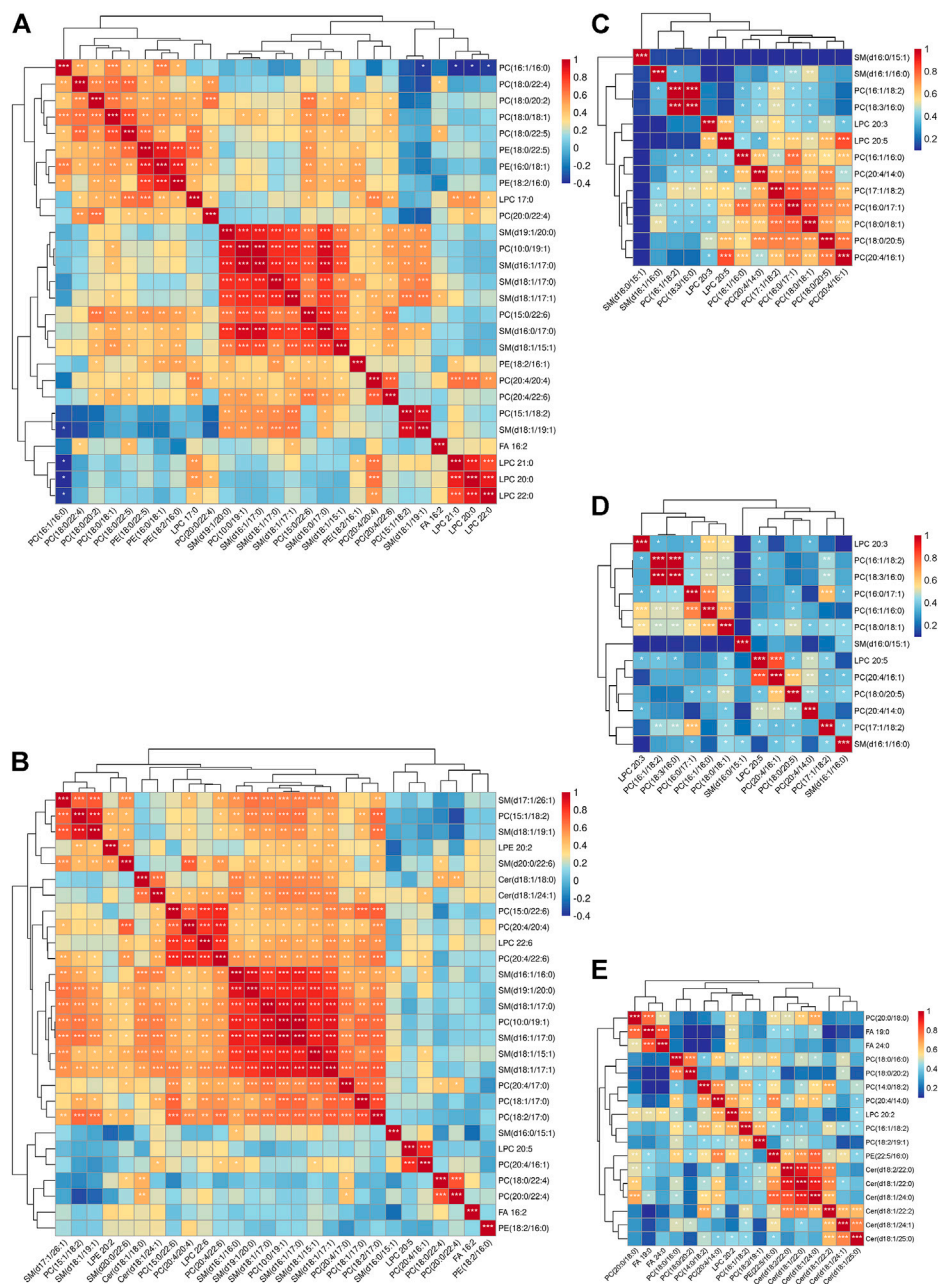


FIGURE 3 | Heatmaps illustrating Spearman's correlations between the altered metabolites. **(A)** Correlation heatmap of altered metabolites (MP vs. HC-MP) in the MP subgroup. **(B)** Correlation heatmap of altered metabolites (SP vs. HC-SP) in the SP subgroup. **(C)** Correlation heatmap of altered metabolites (MP vs. SP) in the MP subgroup. **(D)** Correlation heatmap of altered metabolites (MP vs. SP) in the SP subgroup. **(E)** Correlation heatmap of altered metabolites (PVM vs. PV) in the PVM group. Correlation analysis performed with Spearman's correlation coefficient, * $p < 0.05$, ** $p < 0.01$, and *** $p < 0.001$. HC-MP, healthy controls matched to the group with mild psoriasis vulgaris; HC-SP, healthy controls matched to the group with severe psoriasis vulgaris; MP, mild psoriasis vulgaris; SP, severe psoriasis vulgaris; PV, psoriasis vulgaris without metabolic diseases; PVM, psoriasis vulgaris with metabolic diseases.

2017). Sphingomyelinase catalyzes the hydrolysis of the phosphodiester bond of sphingomyelin and yields Cer and PC after stimulation by TNF- α or IL-1 β (Sindhu et al., 2021). In our sample, SM disorders dominated the lipid abnormalities observed in the MP subgroup and thus provide possible treatment targets for MP. Our results indicate that SM was reduced in patients in

the MP subgroup compared to HCs. Among all the measured lipid metabolites, SM (d16:1/16:1) is negatively correlated with PASI and had strongly positive correlations with cholesterol, HDL-C, and LDL-C. SMs are the most abundant surface components of plasma lipoproteins including LDL and HDL, and abnormal SM metabolism dysfunction impairs the structure

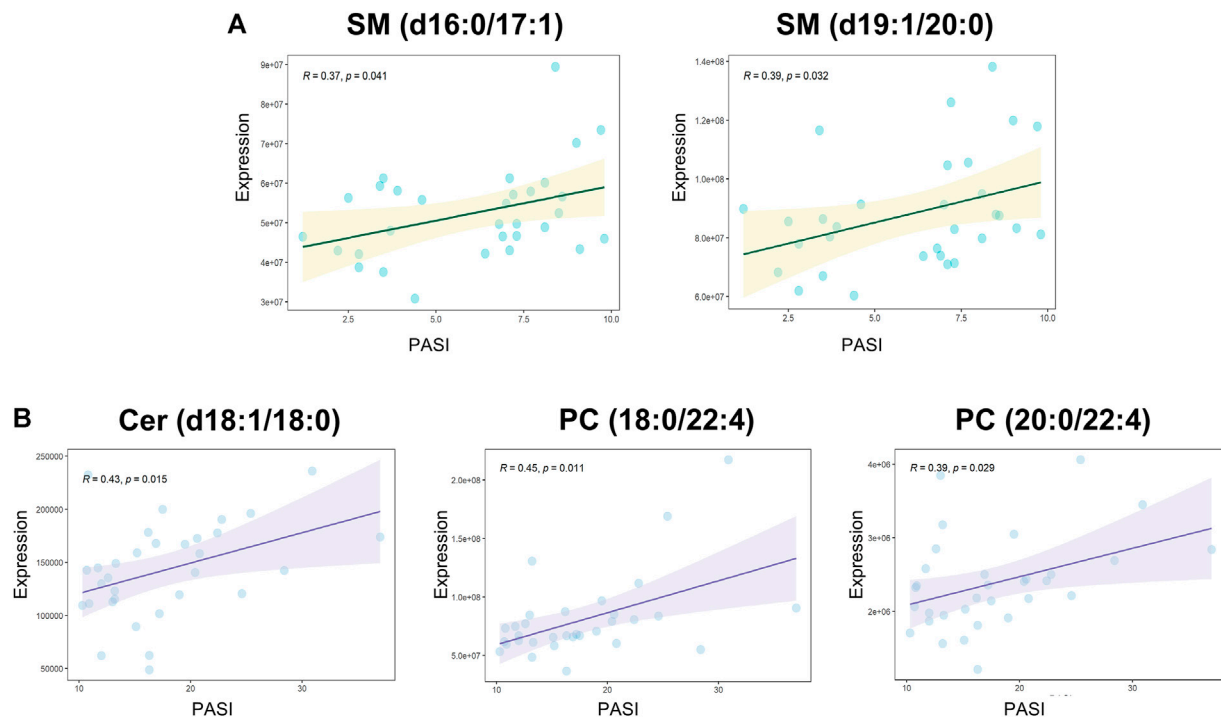


FIGURE 4 | Spearman's correlations between altered metabolites and the PASI. **(A)** Correlation analyses between PASI and altered metabolites (MP vs. HC-MP) in the MP subgroup: SM (d16:1/17:0): $R = 0.37, p = 0.041$; SM (d19:1/20:0): $R = 0.39, p = 0.032$. **(B)** Positive correlations between PASI and altered metabolites (SP vs. HC-SP) in the SP subgroup: Cer (d18:1/18:0): $R = 0.42, p = 0.015$; PC (18:0/22:4): $R = 0.45, p = 0.01$; and PC (20:0/22:4): $R = 0.39, p = 0.029$. PASI, Psoriasis Area and Severity Index; HC-MP, healthy controls matched to the group with mild psoriasis vulgaris; HC-SP, healthy controls matched to the group with severe psoriasis vulgaris; MP, mild psoriasis vulgaris; SP, severe psoriasis vulgaris.

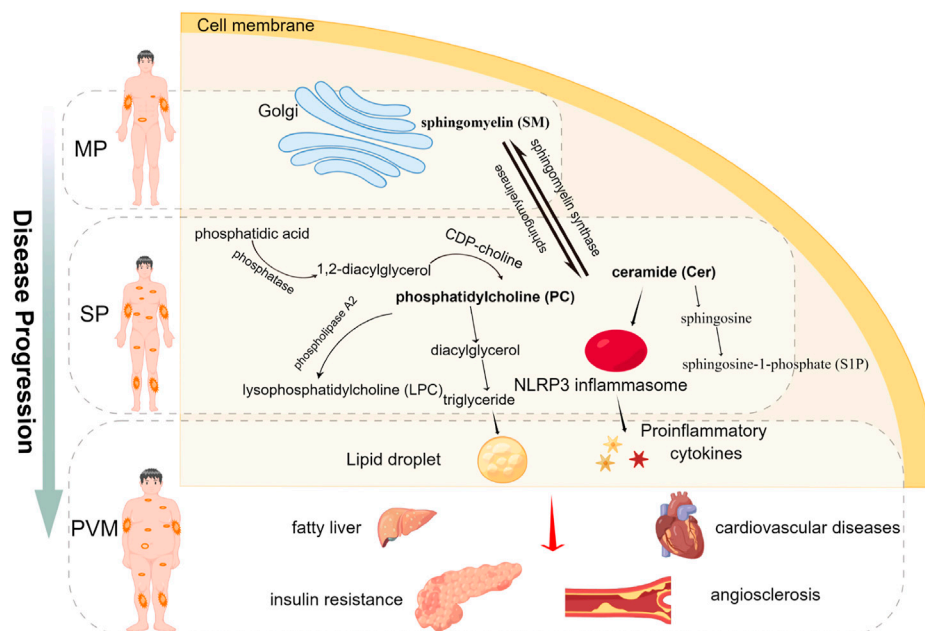


FIGURE 5 | Graphical abstract showing the major findings of the study.

and biofunctions of LDL and HDL (Iqbal et al., 2017; Tsuji et al., 2021). Reduced SM levels may contribute to disease progression, as it has been reported that SM supplements appear to protect against aberrant lipid metabolism, intestinal dysbiosis, and inflammation (Norris et al., 2017; Norris et al., 2019). The SM derivative sphingosine-1-phosphate (S1P) activates differentiation and inhibits keratinocyte proliferation (Jeon et al., 2020). S1P receptor agonists have been found to alleviate psoriasis-like dermatitis in mice (Liu et al., 2021). Moreover, controversially, a high-fat diet can induce sphingomyelin accumulation in the liver (Chocian et al., 2010). The lack of sphingomyelinase promotes sphingomyelin accumulation and causes defective cholesterol trafficking and efflux, which may occur in diabetes and atherosclerotic heart disease (Leventhal et al., 2001; Summers, 2006). The seemingly opposite functions of SM may thus explain why SM is deficient in MP but positively correlated with the PASI.

Cer and PC were found to be related to lipid metabolism dysfunction in the SP subgroup. Cer is the key precursors for the synthesis of other sphingolipids, and the decreased SM and elevated Cer values suggest excessive hydrolysis or impaired synthesis of SM in this group. Different Cer species have specific and sometimes opposing biological functions (Gomez-Larrauri et al., 2020). Cer promotes the NLRP3 inflammasome, which increases IL-1 β levels (Vandanmagsar et al., 2011) and enhances TNF- α , MCP-1, and IL-6 production in adipocytes (Samad et al., 2006). High concentrations of Cer in the white adipose tissue exacerbate chronic inflammation and insulin resistance (Kolak et al., 2007; Chaurasia et al., 2016), which is an independent risk factor for cardiovascular death in patients with stable coronary artery disease (Laaksonen et al., 2016). However, the overall serum content of Cer was reported to be lower in psoriatic patients (Myśliwiec et al., 2017), which is not in line with our results. Cer deficiency in the stratum corneum has also been found to lead to the dry desquamation of the skin (Bocheńska and Gabig-Cimińska, 2020). The correlation analysis highlighted that the expression of Cer (18:1/18:0) was strongly positively correlated with PASI not only in an early stage of PV such as SP group but also in all enrolled patients with PV, which can be considered a severity biomarker for clinical reference.

PC plays a role in regulating blood lipoprotein homeostasis. Impaired hepatic PC biosynthesis significantly reduces the concentrations of circulating very low-density lipoproteins as well as high-density lipoproteins (HDLs) (da Silva et al., 2020; Sprenger et al., 2021). HDL not only eliminates excess cholesterol but also has anti-inflammatory and antioxidant properties (Kuai et al., 2016). The phospholipid composition determines HDL function and secretion. The composition of HDL phosphatidylcholine affects the hepatic absorption of HDL lipid cargo (Kadowaki et al., 1993). In our sample, some kinds of PC were downregulated, while some were upregulated in patients with PV serum, which is consistent with the results of previous studies (Zeng et al., 2017; Li et al., 2020). Downregulated PC was also found in patients with PV (Łuczaj et al., 2020), potentially due to the excessive proliferation of keratinocytes during the progression of PV. Dietary PC supplementation substantially ameliorates lipid transportation dysfunction and

atherosclerosis (Aldana-Hernández et al., 2021). Excess PC may be catabolized and promote triglyceride synthesis and triglyceride-mediated steatosis (Martínez-Uña et al., 2013), which increases the risk of obesity-related diseases in patients with PV. The positive correlation between triglyceride and PC in our experiment also supported this conclusion. The significantly high triglyceride levels observed in our comparison of the PV and PVM groups may have been a result of PC accumulation. PC disorders dominated the lipid abnormalities observed in the SP subgroup, which suggests the need for attention to lipoprotein functions when it comes to the development of targeted preventive treatment for PV.

LPC is generated from PC through the hydrolysis of phospholipase A2 and is the core component of oxidatively damaged low-density lipoprotein (Shoda et al., 1997; Ohigashi et al., 2019). Thus, the altered PC and LPC levels we observed in the SP subgroup were strongly correlated. Increasing evidence indicates that LPC levels are elevated in inflammation-related diseases, including psoriasis (Zeng et al., 2017; Li et al., 2020). Nevertheless, in the current study, the entire PC composition was decreased. LPC usually has a bidirectional effect on inflammation regulation, resulting in various functions in the progression of inflammatory diseases (Liu et al., 2020). LPC with polyunsaturated acyls can curtail inflammation induced by saturated LPC by acting as an anti-inflammatory lipid mediator (Hung et al., 2012). Moreover, LPC can reinforce the immunosuppressive function of regulatory T cells by increasing the production of TGF- β and Foxp3 via the G2A-JNK pathway (Hasegawa et al., 2011).

The top three metabolic comorbidities in the PVM group were hyperlipidemia (48%), hypercholesterolemia (28%), and hyperlipidemia and hypertension (12%), which were presented with serum accumulation of Cer, PC, LPC, FFA, and PE. Elevated PC levels promote triglyceride synthesis and triglyceride-mediated steatosis (Łuczaj et al., 2020). In addition to the routine synthesis pathway (CDP-choline pathway) (Kennedy and Weiss, 1956), the liver possesses a unique PC synthesis pathway that involves three consecutive methylations of the ethanolamine moiety of PE catalyzed by PE methyltransferase and accounts for approximately 30% of hepatic PC synthesis (Sundler and Akesson, 1975). Abnormal cellular PC/PE molar ratios in diverse tissues have been associated with disease progression and alterations in energy metabolism (van der Veen et al., 2017). Ottas et al. (2017) found that PE levels are high in the serum of patients with psoriasis. This finding is consistent with our observations. Increased PE fraction breakdown could release arachidonic acid, which would be accompanied by lower quantities of bile acids in the serum of patients with psoriasis, as well as poorer antioxidant indicators, such as glutathione (Sorokin et al., 2018; Miura et al., 2021). We also found higher Cer levels in patients with only PV than HCs, but their levels were still lower than those of patients with PV and metabolic diseases, suggesting that Cer may contribute to metabolic and inflammatory responses. Circulating FFAs are the primary energy source for almost all tissues and are obtained mostly from adipose tissue lipolysis, and elevated saturated fatty acids levels exacerbate early psoriatic skin

inflammation (Herbert et al., 2018). Fatty acid synthesis appears to drive the formation of Th17 cells (Young et al., 2017; Nicholas et al., 2019). Polyunsaturated fatty acids can induce thrombosis and proinflammation, resulting in an increased prevalence of atherosclerosis, obesity, and diabetes (Simopoulos, 2013; Kromhout and de Goede, 2014; Simopoulos, 2016).

This study has some limitations. The reported lipids could not be identified with high certainty using MS/MS because of poor lipid abundance, ion suppression, and co-elution. Moreover, the correlations obtained in the current study were retrieved from cross-sectional data; thus, the identified biomarkers need to be verified in a large independent cohort before being applied in clinical practice. Future work should focus on a detailed understanding of the intricate mechanisms governing the interaction between systemic inflammation and abnormal lipid metabolic responses.

CONCLUSION

Classification into molecular subtypes enables the identification of potential therapeutic targets that are specific to complex and refractory diseases, such as PV. We validated the subtypes of PV with different lipid metabolic profiles and identified their molecular biomarkers related to disease progression. Our findings therefore contribute to the understanding of the pathogenesis and development of novel strategies for precision treatment of PV.

DATA AVAILABILITY STATEMENT

The raw data supporting the conclusion of this article will be made available by the authors, without undue reservation.

ETHICS STATEMENT

The studies involving human participants were reviewed and approved by the Ethics Committee of the Guang'anmen Hospital,

China Academy of Chinese Medical Sciences. The patients/participants provided their written informed consent to participate in this study.

AUTHOR CONTRIBUTIONS

PS, NG, and MW conceived the study, designed the experiments, interpreted the results, and reviewed the manuscript. DD wrote the manuscript. DD and CH collected clinical samples and information. CH performed the targeted metabolomics experiment. SW performed the targeted metabolomics analysis. All authors read and approved the final manuscript.

FUNDING

The laboratory of the authors benefits from ongoing support from the Scientific and Technological Innovation Project of China Academy of Chinese Medical Sciences (CI2021A02301), National Natural Science Foundation of China (82074448), and the Fundamental Research Funds for the Central Public Welfare Research Institutes (JBGS2021002).

ACKNOWLEDGMENTS

The authors thank the patients, their families, and the investigators who participated in this study for their support and valuable input. Also, the authors thank the Figdraw (<https://www.figdraw.com/>) for assistance regarding illustrations.

SUPPLEMENTARY MATERIAL

The Supplementary Material for this article can be found online at: <https://www.frontiersin.org/articles/10.3389/fmolb.2022.945917/full#supplementary-material>

REFERENCES

- Aldana-Hernández, P., Azarcocoy-Barrera, J., van der Veen, J. N., Leonard, K.-A., Zhao, Y.-Y., Nelson, R., et al. (2021). Dietary Phosphatidylcholine Supplementation Reduces Atherosclerosis in Ldlr Male Mice2. *J. Nutr. Biochem.* 92, 108617. doi:10.1016/j.jnutbio.2021.108617
- Alonso, A., Julià, A., Julià, A., Vinaixa, M., Domènech, E., Fernández-Nebro, A., et al. (2016). Urine Metabolome Profiling of Immune-Mediated Inflammatory Diseases. *BMC Med.* 14 (1), 133. doi:10.1186/s12916-016-0681-8
- Bocheńska, K., and Gabig-Cimińska, M. (2020). Unbalanced Sphingolipid Metabolism and its Implications for the Pathogenesis of Psoriasis. *Molecules* 25 (5). doi:10.3390/molecules25051130
- Boehncke, W.-H., and Schön, M. P. (2015). Psoriasis. *Lancet* 386 (9997), 983–994. doi:10.1016/s0140-6736(14)61909-7
- Cai, J., Cui, L., Wang, Y., Li, Y., Zhang, X., and Shi, Y. (2021). Cardiometabolic Comorbidities in Patients with Psoriasis: Focusing on Risk, Biological Therapy, and Pathogenesis. *Front. Pharmacol.* 12, 774808. doi:10.3389/fphar.2021.774808
- Campelo, F., van Galen, J., Turacchio, G., Parashuraman, S., Kozlov, M. M., García-Parajo, M. F., et al. (2017). Sphingomyelin Metabolism Controls the Shape and Function of the Golgi Cisternae. *Elife* 6. doi:10.7554/eLife.24603
- Cao, H., Su, S., Yang, Q., Le, Y., Chen, L., Hu, M., et al. (2021). Metabolic Profiling Reveals interleukin-17A Monoclonal Antibody Treatment Ameliorate Lipids Metabolism with the Potentiality to Reduce Cardiovascular Risk in Psoriasis Patients. *Lipids Health Dis.* 20 (1), 16. doi:10.1186/s12944-021-01441-9
- Chaurasia, B., Kaddai, V. A., Lancaster, G. I., Henstridge, D. C., Sriram, S., Galam, D. L. A., et al. (2016). Adipocyte Ceramides Regulate Subcutaneous Adipose Browning, Inflammation, and Metabolism. *Cell. Metab.* 24 (6), 820–834. doi:10.1016/j.cmet.2016.10.002
- Chocian, G., Chabowski, A., Zendzian-Piotrowska, M., Harasim, E., Łukaszuk, B., and Górski, J. (2010). High Fat Diet Induces Ceramide and Sphingomyelin Formation in Rat's Liver Nuclei. *Mol. Cell. Biochem.* 340 (1-2), 125–131. doi:10.1007/s11010-010-0409-6
- Colaco, K., Lee, K. A., Akhtari, S., Winer, R., Welsh, P., Sattar, N., et al. (2021). Targeted Metabolomic Profiling and Prediction of Cardiovascular Events: a Prospective Study of Patients with Psoriatic Arthritis and Psoriasis. *Ann. Rheum. Dis.* doi:10.1136/annrheumdis-2021-220168

- da Silva, M. T., Mujica-Coopman, M. F., Figueiredo, A. C. C., Hampel, D., Vieira, L. S., Farias, D. R., et al. (2020). Maternal Plasma Folate Concentration Is Positively Associated with Serum Total Cholesterol and Low-Density Lipoprotein across the Three Trimesters of Pregnancy. *Sci. Rep.* 10 (1), 20141. doi:10.1038/s41598-020-77231-7
- Donnelly, D., 3rd, Aung, P. P., and Jour, G. (2019). The "OMICs" Facet of Melanoma: Heterogeneity of Genomic, Proteomic and Metabolomic Biomarkers. *Seminars Cancer Biol.* 59, 165–174. doi:10.1016/j.semcancer.2019.06.014
- Dutkiewicz, E. P., Hsieh, K.-T., Wang, Y.-S., Chiu, H.-Y., and Urban, P. L. (2016). Hydrogel Micropatch and Mass Spectrometry-Assisted Screening for Psoriasis-Related Skin Metabolites. *Clin. Chem.* 62 (8), 1120–1128. doi:10.1373/clinchem.2016.256396
- Elmets, C. A., Leonardi, C. L., Davis, D. M. R., Gelfand, J. M., Lichten, J., Mehta, N. N., et al. (2019). Joint AAD-NPF Guidelines of Care for the Management and Treatment of Psoriasis with Awareness and Attention to Comorbidities. *J. Am. Acad. Dermatol.* 80 (4), 1073–1113. doi:10.1016/j.jaad.2018.11.058
- Gomez-Larrauri, A., Presa, N., Dominguez-Herrera, A., Ouro, A., Trueba, M., and Gomez-Muñoz, A. (2020). Role of Bioactive Sphingolipids in Physiology and Pathology. *Essays Biochem.* 64 (3), 579–589. doi:10.1042/ebc20190091
- Guerra, I., and Gisbert, J. P. (2013). Onset of Psoriasis in Patients with Inflammatory Bowel Disease Treated with Anti-TNF Agents. *Expert Rev. Gastroenterology Hepatology* 7 (1), 41–48. doi:10.1586/egh.12.64
- Hasegawa, H., Lei, J., Matsumoto, T., Onishi, S., Suemori, K., and Yasukawa, M. (2011). Lysophosphatidylcholine Enhances the Suppressive Function of Human Naturally Occurring Regulatory T Cells through TGF- β Production. *Biochem. Biophysical Res. Commun.* 415 (3), 526–531. doi:10.1016/j.bbrc.2011.10.119
- Herbert, D., Franz, S., Popkova, Y., Anderegg, U., Schiller, J., Schwede, K., et al. (2018). High-Fat Diet Exacerbates Early Psoriatic Skin Inflammation Independent of Obesity: Saturated Fatty Acids as Key Players. *J. Investigative Dermatology* 138 (9), 1999–2009. doi:10.1016/j.jid.2018.03.1522
- Hung, N. D., Sok, D.-E., and Kim, M. R. (2012). Prevention of 1-palmitoyl Lysophosphatidylcholine-Induced Inflammation by Polyunsaturated Acyl Lysophosphatidylcholine. *Inflamm. Res.* 61 (5), 473–483. doi:10.1007/s00011-012-0434-x
- Iqbal, J., Walsh, M. T., Hammad, S. M., and Hussain, M. M. (2017). Sphingolipids and Lipoproteins in Health and Metabolic Disorders. *Trends Endocrinol. Metabolism* 28 (7), 506–518. doi:10.1016/j.tem.2017.03.005
- Jain, S. (2017). *Dermatology: Illustrated Study Guide and Comprehensive Board Review*. 2nd ed. Switzerland: Springer Cham, 83–87.
- James, W. D. (2005). *Andrews' Diseases of the Skin: Clinical Dermatology*. 10th ed. USA: Saunders, 191–197.
- Jeon, S., Song, J., Lee, D., Kim, G.-T., Park, S.-H., Shin, D.-Y., et al. (2020). Inhibition of Sphingosine 1-phosphate Lyase Activates Human Keratinocyte Differentiation and Attenuates Psoriasis in Mice. *J. Lipid Res.* 61 (1), 20–32. doi:10.1194/jlr.ra119000254
- Jia, Y., Gan, Y., He, C., Chen, Z., and Zhou, C. (2018). The Mechanism of Skin Lipids Influencing Skin Status. *J. Dermatological Sci.* 89 (2), 112–119. doi:10.1016/j.jdermsci.2017.11.006
- Kadowaki, H., Patton, G., and Robins, S. (1993). Effect of Phosphatidylcholine Molecular Species on the Uptake of HDL Triglycerides and Cholesteryl Esters by the Liver. *J. Lipid Res.* 34 (2), 180–189. doi:10.1016/s0022-2275(20)40745-x
- Kamiya, K., Kishimoto, M., Sugai, J., Komine, M., and Ohtsuki, M. (2019). Risk Factors for the Development of Psoriasis. *Int. J. Mol. Sci.* 20 (18). doi:10.3390/ijms20184347
- Kamleh, M. A., Snowden, S. G., Grapov, D., Blackburn, G. J., Watson, D. G., Xu, N., et al. (2015). LC-MS Metabolomics of Psoriasis Patients Reveals Disease Severity-dependent Increases in Circulating Amino Acids that Are Ameliorated by Anti-TNF α Treatment. *J. Proteome Res.* 14 (1), 557–566. doi:10.1021/pr500782g
- Kang, H., Li, X., Zhou, Q., Quan, C., Xue, F., Zheng, J., et al. (2017). Exploration of Candidate Biomarkers for Human Psoriasis Based on Gas Chromatography-Mass Spectrometry Serum Metabolomics. *Br. J. Dermatol.* 176 (3), 713–722. doi:10.1111/bjd.15008
- Kennedy, E. P., and Weiss, S. B. (1956). The Function of Cytidine Coenzymes in the Biosynthesis of Phospholipides. *J. Biol. Chem.* 222 (1), 193–214. doi:10.1016/s0021-9258(19)50785-2
- Kim, H.-N., Han, K., Park, Y.-G., and Lee, J. H. (2019). Metabolic Syndrome Is Associated with an Increased Risk of Psoriasis: A Nationwide Population-Based Study. *Metabolism* 99, 19–24. doi:10.1016/j.metabol.2019.07.001
- Kolak, M., Westerbacka, J., Velagapudi, V. R., Wa'gsäter, D., Yetukuri, L., Makkonen, J., et al. (2007). Adipose Tissue Inflammation and Increased Ceramide Content Characterize Subjects with High Liver Fat Content Independent of Obesity. *Diabetes* 56 (8), 1960–1968. doi:10.2337/db07-0111
- Kromhout, D., and de Goede, J. (2014). Update on Cardiometabolic Health Effects of ω -3 Fatty Acids. *Curr. Opin. Lipidol.* 25 (1), 85–90. doi:10.1097/mol.0000000000000041
- Kuai, R., Li, D., Chen, Y. E., Moon, J. J., and Schwendeman, A. (2016). High-Density Lipoproteins: Nature's Multifunctional Nanoparticles. *ACS Nano* 10 (3), 3015–3041. doi:10.1021/acsnano.5b07522
- Laaksonen, R., Ekroos, K., Sysi-Aho, M., Hilvo, M., Viikari-Juntura, T., Kauhanen, D., et al. (2016). Plasma Ceramides Predict Cardiovascular Death in Patients with Stable Coronary Artery Disease and Acute Coronary Syndromes beyond LDL-Cholesterol. *Eur. Heart J.* 37 (25), 1967–1976. doi:10.1093/eurheartj/ehw148
- Leventhal, A. R., Chen, W., Tall, A. R., and Tabas, I. (2001). Acid Sphingomyelinase-Deficient Macrophages Have Defective Cholesterol Trafficking and Efflux. *J. Biol. Chem.* 276 (48), 44976–44983. doi:10.1074/jbc.m106455200
- Li, L., Yao, D.-n., Lu, Y., Deng, J.-w., Wei, J.-a., Yan, Y.-h., et al. (2020). Metabonomics Study on Serum Characteristic Metabolites of Psoriasis Vulgaris Patients with Blood-Stasis Syndrome. *Front. Pharmacol.* 11, 558731. doi:10.3389/fphar.2020.558731
- Liu, L., Wang, J., Li, H.-j., Zhang, S., Jin, M.-z., Chen, S.-t., et al. (2021). Sphingosine-1-Phosphate and its Signal Modulators Alleviate Psoriasis-like Dermatitis: Preclinical and Clinical Evidence and Possible Mechanisms. *Front. Immunol.* 12, 759276. doi:10.3389/fimmu.2021.759276
- Liu, P., Zhu, W., Chen, C., Yan, B., Zhu, L., Chen, X., et al. (2020). The Mechanisms of Lysophosphatidylcholine in the Development of Diseases. *Life Sci.* 247, 117443. doi:10.1016/j.lfs.2020.117443
- Łuczaj, W., Dobrzyńska, I., Wroński, A., Domingues, M. R., Domingues, P., and Skrzydlewska, E. (2020). Cannabidiol-Mediated Changes to the Phospholipid Profile of UVB-Irradiated Keratinocytes from Psoriatic Patients. *Int. J. Mol. Sci.* 21 (18)6592. doi:10.3390/ijms21186592
- Martínez-Uña, M., Varela-Rey, M., Cano, A., Fernández-Ares, L., Beraza, N., Aurrekoetxea, I., et al. (2013). Excess S-Adenosylmethionine Reroutes Phosphatidylethanolamine towards Phosphatidylcholine and Triglyceride Synthesis. *Hepatology* 58 (4), 1296–1305. doi:10.1002/hep.26399
- Miura, H., Mizuguchi, H., Amano-Iwashita, M., Maeda-Kogure, R., Negishi, A., Sakai, A., et al. (2021). Clofibrate Acid Increases Molecular Species of Phosphatidylethanolamine Containing Arachidonic Acid for Biogenesis of Peroxisomal Membranes in Peroxisome Proliferation in the Liver. *Biochimica Biophysica Acta (BBA) - Mol. Cell. Biol. Lipids* 1866 (8), 158963. doi:10.1016/j.bbalip.2021.158963
- Myśliwiec, H., Baran, A., Harasim-Symor, E., Choromańska, B., Myśliwiec, P., Milewska, A. J., et al. (2017). Increase in Circulating Sphingosine-1-Phosphate and Decrease in Ceramide Levels in Psoriatic Patients. *Arch. Dermatol. Res.* 309 (2), 79–86. doi:10.1007/s00403-016-1709-9
- Nicholas, D. A., Proctor, E. A., Agrawal, M., Belkina, A. C., Van Nostrand, S. C., Panneerselam-Bharath, L., et al. (2019). Fatty Acid Metabolites Combine with Reduced β Oxidation to Activate Th17 Inflammation in Human Type 2 Diabetes. *Cell. Metab.* 30 (3), 447–461.e5. doi:10.1016/j.cmet.2019.07.004
- Norris, G. H., Milard, M., Michalski, M.-C., and Blesso, C. N. (2019). Protective Properties of Milk Sphingomyelin against Dysfunctional Lipid Metabolism, Gut Dysbiosis, and Inflammation. *J. Nutr. Biochem.* 73, 108224. doi:10.1016/j.jnutbio.2019.108224
- Norris, G. H., Porter, C. M., Jiang, C., Millar, C. L., and Blesso, C. N. (2017). Dietary Sphingomyelin Attenuates Hepatic Steatosis and Adipose Tissue Inflammation in High-Fat-Diet-Induced Obese Mice. *J. Nutr. Biochem.* 40, 36–43. doi:10.1016/j.jnutbio.2016.09.017
- Nowowiejska, J., Baran, A., and Flisiak, I. (2021). Aberrations in Lipid Expression and Metabolism in Psoriasis. *Int. J. Mol. Sci.* 22 (12). doi:10.3390/ijms22126561
- Ohigashi, T., Kanno, K., Sugiyama, A., Nguyen, P. T., Kishikawa, N., Otani, Y., et al. (2019). Protective Effect of Phosphatidylcholine on Lysophosphatidylcholine-induced Cellular Senescence in Cholangiocyte. *J. Hepatobiliary Pancreat. Sci.* 26 (12), 568–577. doi:10.1002/jhbp.684

- Ottas, A., Fishman, D., Okas, T.-L., Kingo, K., and Soomets, U. (2017). The Metabolic Analysis of Psoriasis Identifies the Associated Metabolites while Providing Computational Models for the Monitoring of the Disease. *Arch. Dermatol. Res.* 309 (7), 519–528. doi:10.1007/s00403-017-1760-1
- Raychaudhuri, S. K., Maverakis, E., and Raychaudhuri, S. P. (2014). Diagnosis and Classification of Psoriasis. *Autoimmun. Rev.* 13 (4–5), 490–495. doi:10.1016/j.autrev.2014.01.008
- Samad, F., Hester, K. D., Yang, G., Hannun, Y. A., and Bielawski, J. (2006). Altered Adipose and Plasma Sphingolipid Metabolism in Obesity. *Diabetes* 55 (9), 2579–2587. doi:10.2337/db06-0330
- Shoda, J., Ueda, T., Ikegami, T., Matsuzaki, Y., Satoh, S., Kano, M., et al. (1997). Increased Biliary Group II Phospholipase A2 and Altered Gallbladder Bile in Patients with Multiple Cholesterol Stones. *Gastroenterology* 112 (6), 2036–2047. doi:10.1053/gast.1997.v112.pm9178697
- Simopoulos, A. (2016). An Increase in the Omega-6/Omega-3 Fatty Acid Ratio Increases the Risk for Obesity. *Nutrients* 8 (3), 128. doi:10.3390/nu8030128
- Simopoulos, A. (2013). Dietary Omega-3 Fatty Acid Deficiency and High Fructose Intake in the Development of Metabolic Syndrome, Brain Metabolic Abnormalities, and Non-alcoholic Fatty Liver Disease. *Nutrients* 5 (8), 2901–2923. doi:10.3390/nu5082901
- Sindhu, S., Leung, Y. H., Arefanian, H., Madiraju, S. R. M., Al-Mulla, F., Ahmad, R., et al. (2021). Neutral Sphingomyelinase-2 and Cardiometabolic Diseases. *Obes. Rev.* 22 (8), e13248. doi:10.1111/obr.13248
- Sorokin, A. V., Domenichiello, A. F., Dey, A. K., Yuan, Z.-X., Goyal, A., Rose, S. M., et al. (2018). Bioactive Lipid Mediator Profiles in Human Psoriasis Skin and Blood. *J. Investigative Dermatology* 138 (7), 1518–1528. doi:10.1016/j.jid.2018.02.003
- Sprenger, R. R., Hermansson, M., Neess, D., Becciolini, L. S., Sørensen, S. B., Fagerberg, R., et al. (2021). Lipid Molecular Timeline Profiling Reveals Diurnal Crosstalk between the Liver and Circulation. *Cell. Rep.* 34 (5), 108710. doi:10.1016/j.celrep.2021.108710
- Summers, S. (2006). Ceramides in Insulin Resistance and Lipotoxicity. *Prog. Lipid Res.* 45 (1), 42–72. doi:10.1016/j.plipres.2005.11.002
- Sundler, R., and Akesson, B. (1975). Regulation of Phospholipid Biosynthesis in Isolated Rat Hepatocytes. Effect of Different Substrates. *J. Biol. Chem.* 250 (9), 3359–3367. doi:10.1016/s0021-9258(19)41523-8
- Takeshita, J., Grewal, S., Langan, S. M., Mehta, N. N., Ogdie, A., Van Voorhees, A. S., et al. (2017). Psoriasis and Comorbid Diseases. *J. Am. Acad. Dermatology* 76 (3), 377–390. doi:10.1016/j.jaad.2016.07.064
- Tarentini, E., Odorici, G., Righi, V., Paganelli, A., Giacomelli, L., Mirisola, V., et al. (2021). Integrated Metabolomic Analysis and Cytokine Profiling Define Clusters of Immuno-Metabolic Correlation in New-Onset Psoriasis. *Sci. Rep.* 11 (1), 10472. doi:10.1038/s41598-021-89925-7
- Tsuji, T., Yuri, T., Terada, T., and Morita, S.-y. (2021). Application of Enzymatic Fluorometric Assays to Quantify Phosphatidylcholine, Phosphatidylethanolamine and Sphingomyelin in Human Plasma Lipoproteins. *Chem. Phys. Lipids* 238, 105102. doi:10.1016/j.chemphyslip.2021.105102
- van der Veen, J. N., Kennelly, J. P., Wan, S., Vance, J. E., Vance, D. E., and Jacobs, R. L. (2017). The Critical Role of Phosphatidylcholine and Phosphatidylethanolamine Metabolism in Health and Disease. *Biochim. Biophys. Acta Biomembr.* 1859 (9 Pt B), 1558–1572. doi:10.1016/j.bbmem.2017.04.006
- Vandanmagsar, B., Youm, Y.-H., Ravussin, A., Galgani, J. E., Stadler, K., Mynatt, R. L., et al. (2011). The NLRP3 Inflammasome Instigates Obesity-Induced Inflammation and Insulin Resistance. *Nat. Med.* 17 (2), 179–188. doi:10.1038/nm.2279
- Young, K. E., Flaherty, S., Woodman, K. M., Sharma-Walia, N., and Reynolds, J. M. (2017). Fatty Acid Synthase Regulates the Pathogenicity of Th17 Cells. *J. Leukoc. Biol.* 102 (5), 1229–1235. doi:10.1189/jlb.3ab0417-159rr
- Zeng, C., Wen, B., Hou, G., Lei, L., Mei, Z., Jia, X., et al. (2017). Lipidomics Profiling Reveals the Role of Glycerophospholipid Metabolism in Psoriasis. *Gigascience* 6 (10), 1–11. doi:10.1093/gigascience/gix087

Conflict of Interest: MW was employed by SU BioMedicine, BioPartner Center 3, Leiden, Netherlands.

The remaining authors declare that the research was conducted in the absence of any commercial or financial relationships that could be construed as a potential conflict of interest.

Publisher's Note: All claims expressed in this article are solely those of the authors and do not necessarily represent those of their affiliated organizations or those of the publisher, the editors, and the reviewers. Any product that may be evaluated in this article, or claim that may be made by its manufacturer, is not guaranteed or endorsed by the publisher.

Copyright © 2022 Dai, He, Wang, Wang, Guo and Song. This is an open-access article distributed under the terms of the Creative Commons Attribution License (CC BY). The use, distribution or reproduction in other forums is permitted, provided the original author(s) and the copyright owner(s) are credited and that the original publication in this journal is cited, in accordance with accepted academic practice. No use, distribution or reproduction is permitted which does not comply with these terms.



OPEN ACCESS

EDITED BY
Evangelia Sarandi,
University of Crete, Greece

REVIEWED BY
Uma Sriram,
Temple University, United States
Prathyusha Bachali,
AMPEL BioSolutions, United States

*CORRESPONDENCE
Yeying Sun
✉ sunyy21cn@gmail.com

RECEIVED 17 February 2023

ACCEPTED 17 May 2023

PUBLISHED 29 May 2023

CITATION

Li W, Guan X, Wang Y, Lv Y, Wu Y, Yu M
and Sun Y (2023) Cuproptosis-related gene
identification and immune infiltration
analysis in systemic lupus erythematosus.
Front. Immunol. 14:1157196.
doi: 10.3389/fimmu.2023.1157196

COPYRIGHT

© 2023 Li, Guan, Wang, Lv, Wu, Yu and Sun.
This is an open-access article distributed
under the terms of the [Creative Commons
Attribution License \(CC BY\)](#). The use,
distribution or reproduction in other
forums is permitted, provided the original
author(s) and the copyright owner(s) are
credited and that the original publication in
this journal is cited, in accordance with
accepted academic practice. No use,
distribution or reproduction is permitted
which does not comply with these terms.

Cuproptosis-related gene identification and immune infiltration analysis in systemic lupus erythematosus

Wuquan Li¹, Xiaoran Guan¹, Yong Wang¹, Yan Lv², Yuyong Wu¹,
Min Yu¹ and Yeying Sun^{1*}

¹College of Pharmacy, Binzhou Medical University, Yantai, China, ²College of Life Science, Yantai University, Yantai, China

Background: Systemic lupus erythematosus (SLE) is an autoimmune disease characterized by loss of tolerance to self-antigen, autoantibody production, and abnormal immune response. Cuproptosis is a recently reported cell death form correlated with the initiation and development of multiple diseases. This study intended to probe cuproptosis-related molecular clusters in SLE and constructed a predictive model.

Methods: We analyzed the expression profile and immune features of cuproptosis-related genes (CRGs) in SLE based on GSE61635 and GSE50772 datasets and identified core module genes associated with SLE occurrence using the weighted correlation network analysis (WGCNA). We selected the optimal machine-learning model by comparing the random forest (RF) model, support vector machine (SVM) model, generalized linear model (GLM), and the extreme gradient boosting (XGB) model. The predictive performance of the model was validated by nomogram, calibration curve, decision curve analysis (DCA), and external dataset GSE72326. Subsequently, a CeRNA network based on 5 core diagnostic markers was established. Drugs targeting core diagnostic markers were acquired using the CTD database, and Autodock vina software was employed to perform molecular docking.

Results: Blue module genes identified using WGCNA were highly related to SLE initiation. Among the four machine-learning models, the SVM model presented the best discriminative performance with relatively low residual and root-mean-square error (RMSE) and high area under the curve (AUC = 0.998). An SVM model was constructed based on 5 genes and performed favorably in the GSE72326 dataset for validation (AUC = 0.943). The nomogram, calibration curve, and DCA validated the predictive accuracy of the model for SLE as well. The CeRNA regulatory network includes 166 nodes (5 core diagnostic markers, 61 miRNAs, and 100 lncRNAs) and 175 lines. Drug detection showed that D00156 (Benzo (a) pyrene), D016604 (Aflatoxin B1), D014212 (Tretinoin), and D009532 (Nickel) could simultaneously act on the 5 core diagnostic markers.

Conclusion: We revealed the correlation between CRGs and immune cell infiltration in SLE patients. The SVM model using 5 genes was selected as the

optimal machine learning model to accurately evaluate SLE patients. A CeRNA network based on 5 core diagnostic markers was constructed. Drugs targeting core diagnostic markers were retrieved with molecular docking performed.

KEYWORDS

systemic lupus erythematosus, WGCNA, machine learning, immune infiltration, biomarker

1 Introduction

Systemic lupus erythematosus (SLE) is an autoimmune disease (1) (AID) featuring loss of tolerance to self-antigen, autoantibody production, and abnormal immune response. It affects multiple organs, such as skin, joints, kidneys, lungs, and hearts (2), severely interrupting work, normal routine, and physical and mental health. The pathogenesis of SLE is not clear. Genetic and environmental factors and viral infection are considered possible pathogenic factors (3–5). So far, specific drugs for SLE are very scarce, and SLE patients are still treated with traditional anti-inflammatory drugs, immunoregulatory drugs, and corticosteroids, often accompanied by adverse events (AE). Therefore, investigating molecular characteristics and mechanisms of SLE has substantial implications for providing new strategies for SLE diagnosis and treatment.

Copper serves as a cofactor in many enzymes and has important physiological functions in vital activities (6). Normal cells have a quite low copper concentration, and they prevent the accumulation of free intracellular copper ions mainly by active transport mechanisms, thereby sustaining copper homeostasis (7, 8). Copper imbalance leads to oxidative stress (9), aberrant autophagy (10), etc., thereby inducing various copper/copper ion-associated diseases. Cuproptosis is a copper-dependent programmed cell death form, and its mechanism is different from apoptosis, pyroptosis, necrosis, and autophagy. In cuproptosis, copper directly binds with lipoylated proteins in the tricarboxylic acid (TCA) cycle, leading to lipoylated protein aggregation and following iron-sulfur cluster loss, inducing proteotoxic stress and eventually cell death (11). Research showed that ferroptosis in neutrophils leads to the occurrence of SLE, and the mechanism is by promoting cAMP response element modulator CREM binding with glutathione peroxidase 4 (GPX4) promoter to downregulate GPX4 expression (12). The significance of copper homeostasis in immune infiltration has been reported in relevant studies recently. It was reported that copper chelation in macrophages can eliminate lysyl oxidase-like 4-mediated programmed death-ligand 1 presentation, thereby suppressing cell immune escape (13). However, currently, cuproptosis's role in the initiation and development of SLE is still not clear. Hence, elucidating cuproptosis's role in SLE has considerable implications.

Machine learning is being widely applied in the medical field, particularly in disease diagnosis, prediction, and treatment. With its high efficiency in thousands of types of diseases, machine learning can be divided into three main types: supervised learning (14), semi-supervised learning (15), and unsupervised learning (16) each being

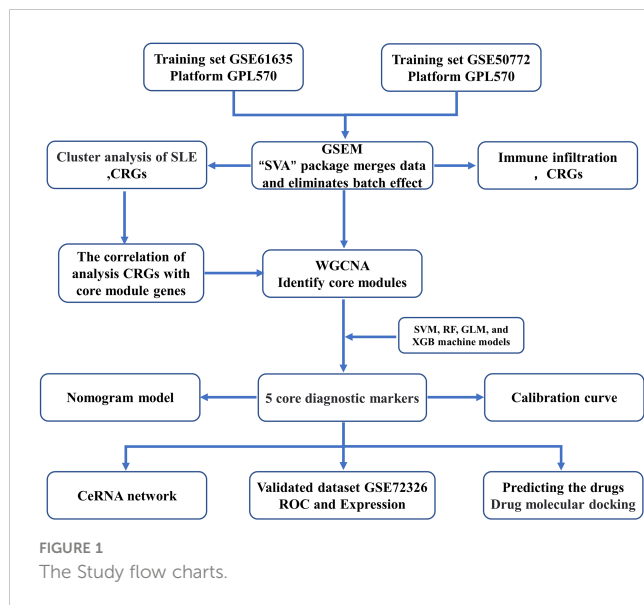
used to train artificial intelligence models with different types of data in different circumstances. Among these, the prediction of disease biomarkers is one important application of machine learning in disease prediction, which can provide doctors with more accurate diagnostics and treatment decisions, ultimately increasing the cure rate and prognosis of the disease. The future of medicine will place increasing emphasis on machine learning. For instance, it could be used to quickly and accurately detect lung cancer in chest CT scans, improving patient survival rates (17). Machine learning can also predict the risk of heart disease in electrocardiograms (18), detect early retinal lesions using semi-supervised learning techniques (19), and assist in diagnosing Alzheimer's disease (20). By incorporating machine learning, we can gain better insight into the underlying mechanisms of diseases and provide potential targets for future treatments. However, machine learning is just a tool, and we still need to combine it with practical disease research to effectively address specific problems.

In this study, we analyzed differentially expressed cuproptosis-related genes (CRGs) between healthy people and SLE patients using the Gene Expression Omnibus (GEO) database and conducted a bioinformatics analysis of immune characteristics. Based on the CRG expression profile, we assigned SLE patients to two cuproptosis-related clusters and further compared the CRGs of the two clusters. Subsequently, we identified key modules associated with SLE initiation using the weighted gene co-expression network analysis (WGCNA) algorithm. Furthermore, we constructed a predictive model that can reveal the prognoses of patients with different molecular clusters by comparing multiple machine-learning methods. Nomogram, calibration curve, decision curve analysis (DCA), and an external dataset were adopted to verify the performance of the predictive model. Additionally, we established a competing endogenous RNA (CeRNA) regulation network, and selected drugs that act on key biomarkers using the CTD database, which were used as candidate drugs for SLE.

2 Materials and methods

2.1 Data acquisition and preprocessing

The flow chart of this study is shown in **Figure 1**. The GSE61635 (21), GSE50772 (22), and GSE72326 (23) datasets were retrieved from the GEO database (**Table 1**), and CRGs (11) were collected from published studies. GSE61635 and GSE50772 were merged as



one dataset (GSEM) serving as the training cohort since the two datasets were obtained from the same platform, and the GSE72326 dataset was used as the validation cohort. The raw data were normalized and annotated with background subtracted, and batch effects from the merged dataset were removed using the “SVA” package.

2.2 WGCNA

WGCNA was performed using the R “WGCN” package (24). The optimal value of the weighting parameter in the adjacent function was obtained using the pickSoftThreshold function and served as soft-thresholding power for following network construction (25). Subsequently, weighted adjacency matrices were established, and gene modules were created by hierarchical clustering based on a 1-TOM dissimilarity matrix (26). Each module was assigned a unique color identifier, and the module eigengene represents the expression profile of the entire module. Module–disease state relationships represent module significance (MS), and gene significance describes a gene’s correlation with a phenotype.

2.3 Predictive model construction based on multiple machine-learning methods

Machine-learning predictive models include the support vector machine (SVM) model, random forest (RF) model, generalized linear model (GLM), and extreme gradient boosting (XGB) model. The SVM algorithm seeks the separating hyperplane that yields the maximal margin to discriminate positive instances from negative instances (27). The RF is an ensemble learning method yielding several independent decision trees to predict classification or regression (28). The GLM is an extension of the multiple linear regression model, and it can flexibly assess the relationship between normally-distributed dependent characteristics and continuous or categorical independent characteristics (29). XGB is a collection of gradient-boosted trees that can carefully compare and analyze complexity and classification error (30). The four machine learning models were explained using the “DALEX” package, and residual distribution and feature importance among the models were visualized. The AUC of the ROC curve was visualized using the “pROC” R package. Eventually, we confirmed the optimal machine learning model and selected the top 5 factors as SLE-related key predictors.

2.4 Nomogram construction and validation

A nomogram was established to evaluate SLE occurrence in clusters using the “RMS” R package. Each predictor contributes to a score, and the “total score” represents the sum of the score of the above predictors. The calibration curve and DCA were adopted to evaluate the predictive performance of the nomogram.

2.5 Immune cell infiltration analysis

The CIBERSORT algorithm (<https://cibersort.stanford.edu/>) was performed to estimate the relative abundance of 22 kinds of immune cells for each sample using the LM22 signature matrix and gene expression data. CIBERSORT uses Monte Carlo sampling to obtain a p-value for the deconvolution of each sample. Only samples with $P < 0.05$ were considered to have accurate immune cell fractions, and the sum of the 22 immune cell compositions in each sample was 1 (31).

TABLE 1 Basic Information of Gene Expression Profiling.

GEO ID	Platform	Samples	Number of Controls	Number of Cases	Country	Year	Author
Training set							
GSE61635	GPL570	110	30	80	USA	2015	Greidinger EL
GSE50772	GPL570	81	20	61	USA	2015	Kennedy WP
Validation set							
GSE72326	GPL10558	177	20	157	USA	2022	Chiche L
CRGs	NFE2L2, NLRP3, ATP7B, SLC31A1, FDX1, LIAS, LIPT1, DLD, DLAT, PDHA1, PDHB, MTF1, GLS, CDKN2A, DBT, DLST						Tsvetkov

2.6 lncRNA-miRNA-mRNA CeRNA network construction

miRNA-miRNA interactions were predicted using TargetScan (<http://www.targetscan.org>), miRDB (<http://www.mirdb.org/>), and miRanda (<http://www.microrna.org/>) databases, and miRNA-lncRNAs were predicted using the SpongeScan database (<http://spongescan.rc.ufl.edu/>). Based on lncRNA-miRNA-mRNA interactions, a ceRNA network was constructed using Cytoscape software (3.8.2).

2.7 Identification of candidate small-molecule drugs

Drugs corresponding to those diagnostic biomarkers were retrieved using the CTD database (<http://ctdbase.org/>) to confirm

potential SLE drugs. Drug-gene network was constructed and visualized. Molecular docking was performed between selected drugs and sites of key biomarkers using Autodock vina software V1.1.2, and the results were visualized using Pymol V3.9.2.

3 Results

3.1 CRG expression and immune infiltration analysis in SLE patients

We evaluated the expression profile of 17 CRGs in SLE and normal Control samples using the merged dataset GSEM to investigate CRGs' biological functions in SLE patients. SLE samples presented higher expression of NFE2L2, NLRP3, ATP7A, MTF1, and CDKN2A genes and lower expression of LIAS, LIPT1, DLD, DLAT, PDHA1, PDHB, GLS, DBT, and DLST genes versus the Control group (Figures 2A, B). Subsequently, we conducted

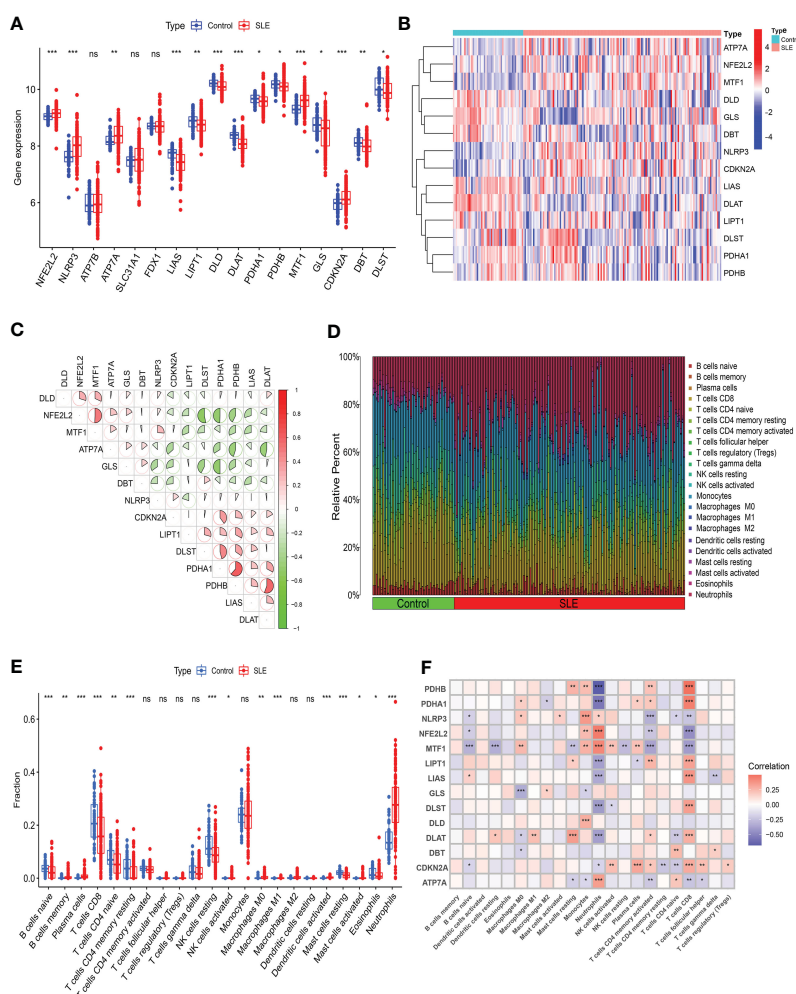


FIGURE 2

Identification of the expression of CRGs and Immune infiltration analysis in SLE. (A) Boxplots showed the expression of 14 CRGs between SLE and Control. (B) The expression patterns of 14 CRGs were presented in the heatmap. (C) The correlation of CRGs. (D) The relative abundance of immune cells between SLE and Control. (E) Boxplots showed the difference of Immune infiltration in SLE and Control. (F) The correlation analysis between 14 CRGs and immune cells. (* $p \leq 0.05$, ** $p \leq 0.01$, *** $p \leq 0.001$, ns, no significance).

correlation analysis for differentially expressed CRGs (Figure 2C) to probe CRGs' role in SLE development. Notably, some CRGs like PDHB and PDHA1 exhibited synergistic effects ($R = 0.62$). Meanwhile, NFE2L2 and DLST displayed significant antagonistic effects ($R = 0.53$). Moreover, we performed an immune infiltration analysis to illustrate the difference in immune systems between the normal Control group and SLE patients. The CIBERSORT algorithm revealed a significant distinction in the proportions of 22 kinds of immune cells between the Control and SLE groups such as neutrophils, plasma cells, CD8⁺ T cells, naive CD8⁺ lymphocytes, M1 macrophages, activated dendritic cells (DC), resting mast cells, etc. (Figures 2D, E), suggesting that immune system alteration might be the primary cause of SLE occurrence. Additionally, correlation analysis demonstrated that neutrophils and CD8⁺ T cells were correlated with cuproptosis (Figure 2F).

3.2 Identification of SLE cuproptosis cluster

To understand the expression patterns of CRGs in SLE, we conducted a consensus clustering analysis with the expression of the 14 CRGs, and the consensus index fluctuated within a minimal range of 0.2-0.6 (Figures 3A, B, Figure S1). When $k = 2-9$, the area under the CDF curve is presented as the difference between two CDF curves (k and $k-1$) (Figure 3C). Furthermore, only when $k = 2$, the consistency score of all subtypes was > 0.9 (Figure 3D). Combining the consensus matrix heatmap, we divided 141 patients into two clusters, including Cluster 1 ($n = 98$) and Cluster 2 ($n = 43$) (Figure 3E). Patients were clustered by t-distributed stochastic neighbor embedding (t-SNE), showing a significant difference between the two clusters (Figure 3F). We generally evaluated the expression difference in 14 CRGs between Clusters 1 and 2 to

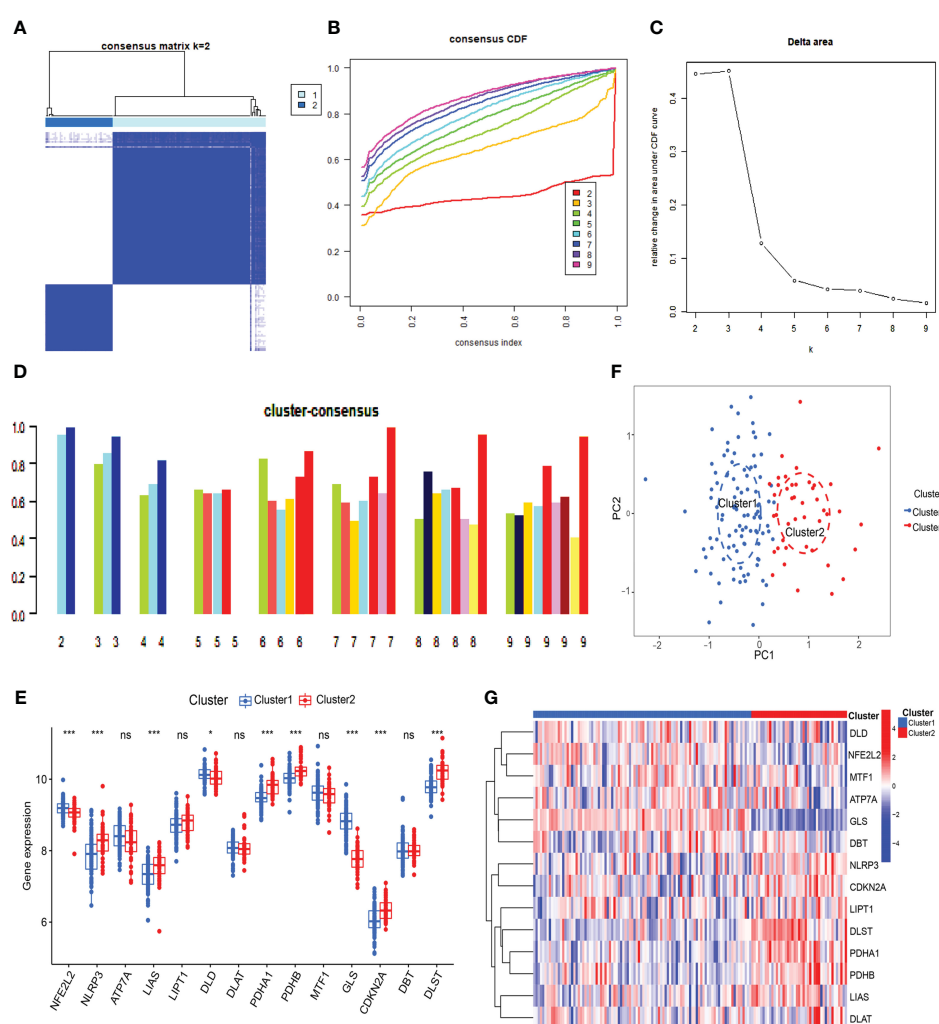


FIGURE 3

Identification of cuproptosis-related molecular clusters in SLE. (A) Consensus clustering matrix when $k=2$. (B, C) Representative cumulative distribution function (CDF) curves (B), CDF delta area curves (C), the score of consensus clustering (D). (E) T-SNE visualizes the distribution of two subtypes. (F) Boxplots showed the expression of 14 CRGs between two cuproptosis clusters. (G) The expression patterns of 14 CRGs were presented in the heatmap. (* $p \leq 0.05$, *** $p \leq 0.001$, ns, no significance).

investigate the molecular characteristics of clusters. Distinct CRG expression patterns were observed between two Clusters. Cluster 1 showed high expression of FDX1, DLD, DLAT, PDHA1, PDHB, and GLS, while Cluster 2 showed enhanced expression of LIPT1, MTF1, CDKN2A, and SLC31A1 (Figure 3G). Next, our analysis focused on the immune cell infiltration differences between the two groups, revealing distinct levels of four immune cells. T cells CD8 and M0 macrophages were found to be higher in cluster 2, while neutrophils and M2 macrophages were lower (Figures S2, 3). Further analysis using GSVA revealed functional differences in cluster-specific DEGs between the two clusters. Cluster 1 showed up-regulation in Glycine serine and threonine metabolism, Cysteine and methionine metabolism, and Pathogenic *Escherichia coli* infection signal activity, whereas cluster 2 showed enhancement in inflammation, metabolism, immune response, and TGF- β signal activity (Figure S4). Additionally, the functional enrichment results revealed that cluster 1 was significantly associated with positive regulation of ATPase

complex of proton transport, mitosis, vitamin D metabolism, and smooth muscle cell apoptosis. In contrast, H3K9me2 demethylase activity, aminophospholipid transferase activity, regulation of RNA binding, and negative regulation of cytoplasmic translation were enriched in cluster 2 (Figure S5).

3.3 Weighted co-expression network construction and core module selection

Co-expression network and module were constructed for the Control and SLE groups using the WGCNA algorithm to identify SLE-related core gene modules. We calculated the variance of gene expression in the GSEM dataset and selected the top 25% of genes with the highest variance for further analysis. When Soft was set to 7, scale-free $R^2 = 0.9$, and co-expression modules were identified (Figure 4A). Altogether 9 co-expression modules with different

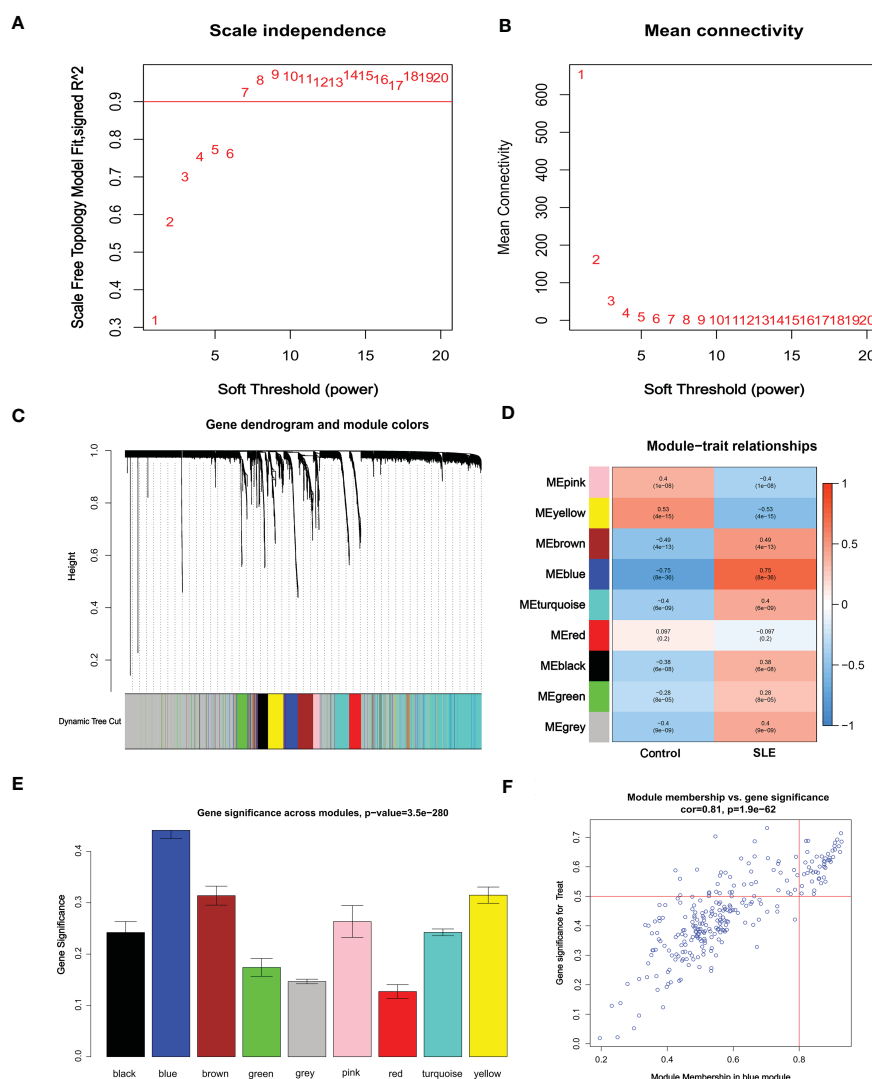


FIGURE 4

Identification of weighted gene co-expression network modules associated with SLE in GSEM. (A, B) Soft threshold selection. (C) Dynamic shearing tree merging similar module genes. (D) Correlation analysis between module eigengenes and clinical status. (E) The correlation between genes and traits between modules. (F) The correlation between module membership and genetic importance. cor represents the correlation between GS and MM.

colors were obtained using the dynamic cut-tree algorithm, and TOM Heatmap was generated (Figures 4B–D). Subsequently, genes were consecutively applied in 9 color modules with module-clinical characteristics (Control and SLE) co-expression similarity and adjacency analyzed. The blue module presented the strongest correlation with SLE, including 263 genes (Figure 4E, Table S1). We also observed the correlation between modules and module-related genes (Figure 4F, Table S2).

3.4 Machine learning model construction and evaluation

To further identify critical markers with high diagnostic value, we established 4 machine-learning models based on the blue core module expression profile, including SVM, RF, GLM, and XGB models. The 4 models were explained using the “DALEX” package, and residuals from each model in the training cohort were plotted. The SVM model had a relatively low residual (Figures 5A, B). The top 10 important variables of each model were obtained according to root-mean-square error (RMSE) (Figure 5C). Moreover, ROC curves of the 5-fold cross-validation were plotted to appraise the

diagnostic performance of the 4 machine learning algorithms in the training cohort. SVM model had the highest AUC (SVM, AUC = 0.998; RF, AUC = 0.976; XGB, AUC = 0.960; GLM, AUC = 0.943, Figure 5D). Combining those results, the SVM model had the best performance in distinguishing patients from different clusters. The top 5 variables (IFIT3, PLSCR1, CCR1, IL1RN, and ETV7) were selected from the SVM model as critical predictive markers for the following analysis.

A nomogram was constructed to assess the predictive efficiency of the SVM model using 141 SLE cases to predict the risk of cuproptosis aggregation (Figure 6A). The predictive efficiency of the nomogram was assessed using the calibration curve and DCA. According to the calibration curve, in the SLE cluster, the error between the actual risk and the predicted risk was very small (Figure 6B). DCA revealed that the nomogram had high accuracy that can provide evidence for clinical decisions (Figure 6C). Subsequently, we validated the predictive capability of the 5 core markers using the validation cohort GSE72326. The ROC curve revealed that the predictive model with 5 core markers had a favorable performance with an AUC of 0.943 (Figure 6D), suggesting that our diagnostic model can effectively discriminate SLE patients from normal cases. Meanwhile, the diagnostic value of

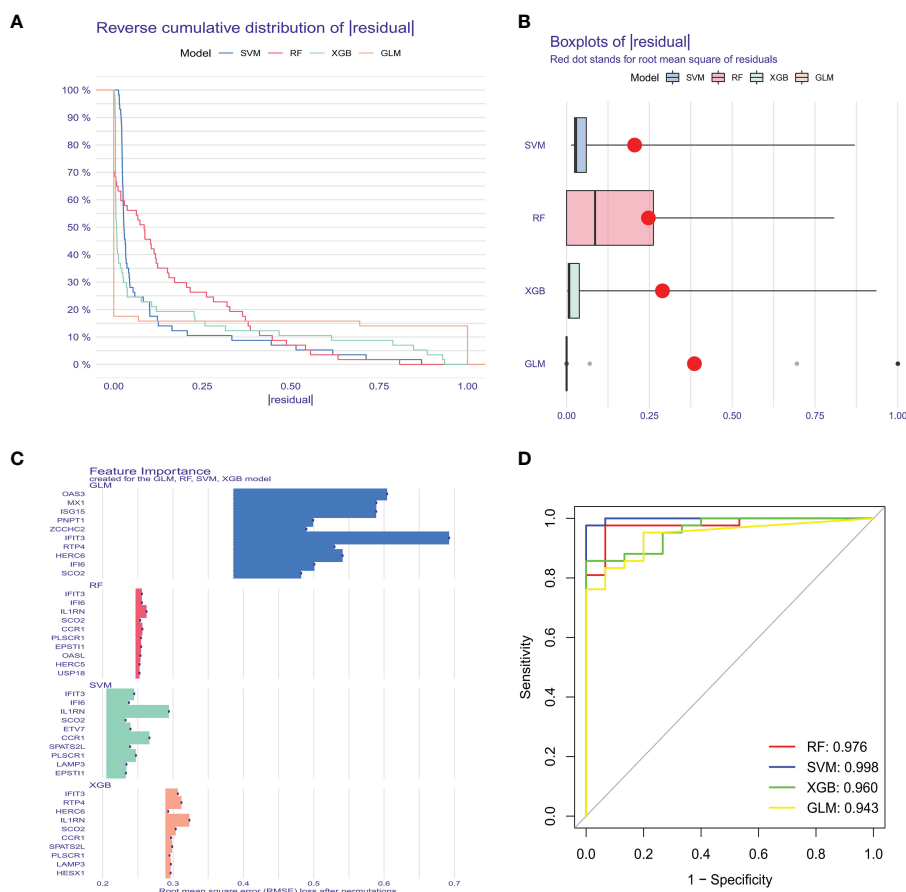


FIGURE 5

Construction and evaluation of SVM, RF, GLM, and XGB machine models. (A) Cumulative residual distribution of each machine learning model. (B) Boxplots showed the residuals of each machine learning model. Red dot represented the root mean square of residuals (RMSE). (C) The important features in SVM, RF, GLM, and XGB machine models. (D) ROC analysis of four machine learning models based on 5-fold cross-validation in the testing cohort.

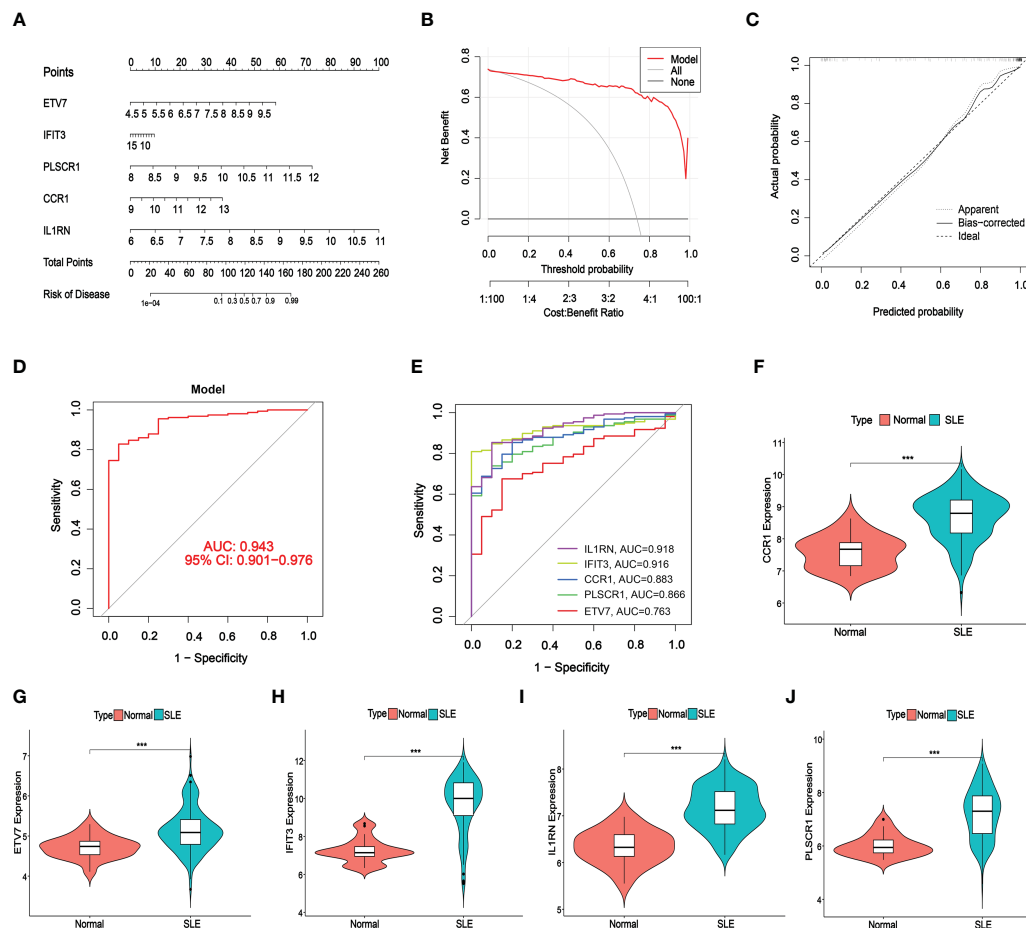


FIGURE 6

Validation of the 5-gene-based SVW model. (A) Construction of a nomogram for predicting the risk of SLE clusters based on the 5-gene-based SVW model. (B, C) Construction of calibration curve (B) and DCA (C) for assessing the predictive efficiency of the nomogram model. (D, E) ROC analysis of the 5-gene-based SVW model based on 5-fold cross-validation in GSE72326. (F–J) The expression levels of 5-genes were verified with validated dataset GSE72326. (***) $p \leq 0.001$.

single markers was verified as well, and IL1RN had the highest AUC (AUC = 0.918, Figure 6E). The expression of the 5 core diagnostic markers was all upregulated in SLE patients (Figures 6F–J).

3.5 CeRNA network establishment of core diagnostic markers

A CeRNA sponge was constructed using miRanda, targetScan, miRDB, and Spongescan databases with 5 core diagnostic markers. The CeRNA network contains 166 nodes (5 core diagnostic markers, 61 miRNAs, and 100 lncRNAs) and 175 lines (Figure 7). Eventually, 47 lncRNAs can competitively bind with IL1RN regulated by hsa-miR-650, hsa-miR-515-5p, hsa-miR-377-3p, hsa-miR-185-3p, and hsa-miR-1205, among which lncRNA SNHG14 can simultaneously target hsa-miR-515-5p and hsa-miR-185-3p. 23 lncRNA can target IFIT3 regulated by hsa-miR-876-3p, hsa-miR-127-5p, hsa-miR-34a-3p, hsa-miR-143-3p, hsa-miR-1207-5p, and hsa-miR-876-5p. Additionally, 19 lncRNA can regulate CCR1

expression by competitively binding with hsa-miR-149-3p. In the ceRNA network of PLSCR1, LINC00662 can bind with hsa-miR-28-3p and hsa-miR-708-3p to regulate PLSCR1. 8 lncRNAs competing with hsa-miR-342-5p to regulate ETV7 expression.

3.6 Prediction of targeted drugs for core diagnostic markers

We further predicted drugs of the 5 core diagnostic markers using the CTD database, extracted drug-marker interactions, and constructed a drug-marker network containing 226 knots and 319 edges, in which 5 core diagnostic markers and 221 drugs were included. The results were visualized using the Cytoscape software (Figure 8A, Table S3). Drug detection showed that D00156 (Benzo (a) pyrene), D016604 (Aflatoxin B1), D014212 (Tretinoin), and D009532 (Nickel) could simultaneously act on the 5 core diagnostic markers. And a molecular docking was performed between drugs and predicted molecular targets (Figures 8B–E, Figure S7, Table S4).

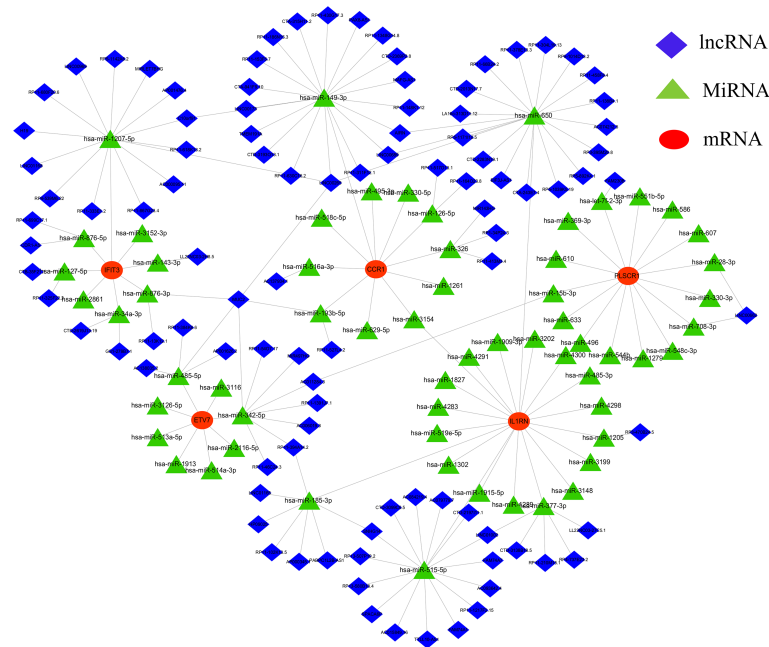


FIGURE 7
lncRNA-miRNA-mRNA regulatory network. The red represent the mRNAs, the green represent the miRNAs and the blue represent the lncRNAs.

4 Discussion

At present, the pathogenesis of SLE has not been fully elucidated. It is widely accepted that SLE develops on a specific genetic background and epigenetic modifications upset the immune system balance, leading to aberrant immune cell proliferation, massive production of autoantibodies, and eventually multiple organ damage (32, 33). However, a single causal gene has not been identified. Conversely, currently, mounting studies reported that multigenic interactions were closely related to SLE initiation and multi-organ involvement (34, 35). Therefore, searching for core molecular clusters is crucial to instruct SLE diagnosis and individualized treatment. Cuproptosis is a newly reported copper-dependent cell death form, mainly manifesting mitochondrial aggregase lipoylation, and is closely associated with disease progression (36). However, the specific mechanism and regulatory role of cuproptosis in various diseases have not been further delved into. Hence, we endeavored to elucidate the role of CRGs in SLE phenotype and immune microenvironment. In this study, we analyzed the expression profile of CRGs in the peripheral whole blood of SLE patients. The aberrant gene expression level in SLE patients was higher than in normal individuals, suggesting that CRGs play a significant role in SLE initiation. The correlation among CRGs was calculated to reveal the relationship between CRGs and SLE. Significant synergistic or antagonistic effects were identified among CRGs. Meanwhile, differentiation was observed in immune cell abundance between the control group and SLE patients. SLE patients exhibited a higher infiltration level of neutrophils, memory B cells, plasma cells, and activated DC. Neutrophils play a pathogenic role in multiple AIDs, including SLE (37). Neutrophils can induce plasmacytoid dendritic cells

(pDC) to generate interferon (IFN), thereby advancing disease progression (38). Furthermore, the complex genetic background of SLE patients could provide multiple amplification steps for the perpetuation and subsequent pathogenicity of neutrophil-pDC interactions (39). ISG15 in neutrophils may also induce the production of Th1 lymphocytes with pro-inflammatory properties (40). Moreover, by applying unsupervised clustering analysis, we confirmed two distinct clusters based on CRG expression to illustrate the different regulatory patterns of SLE patients. These results demonstrated that CRGs might be the key factors that regulate SLE occurrence and immune infiltration status.

Machine learning is a multidisciplinary discipline, and modeling using the machine learning method can explore the underlying value of data. Additionally, machine learning plays an indispensable role in effectively utilizing data and supporting clinical decisions. In this study, we compared the predictive performance of the 4 machine learning methods (SVM, RF, GLM, and XGB), and constructed a predictive model based on SVM (best performance, AUC = 0.998), suggesting that the SVM model had favorable performance when predicting SLE. An SVM model was established using the 5 important factors (IFIT3, PLSCR1, CCR1, IL1RN, and ETV7). Research showed that IFIT3 belongs to the interferon-induced protein family and is an anti-viral protein (41). IFIT3 can block the synthesis of type I IFN and other inflammatory cytokines via the cGAS/STING pathway (42). PLSCR1 shows increased expression in multiple systemic AIDs, such as primary antiphospholipid syndrome, rheumatoid arthritis, idiopathic inflammatory myopathies, and SLE (43, 44). A correlation was identified between PLSCR1 expression and type I interferon-stimulated genes (45), and PLSCR1 is highly expressed in neutrophils, DC, and macrophages (46). CCR1 is a member of

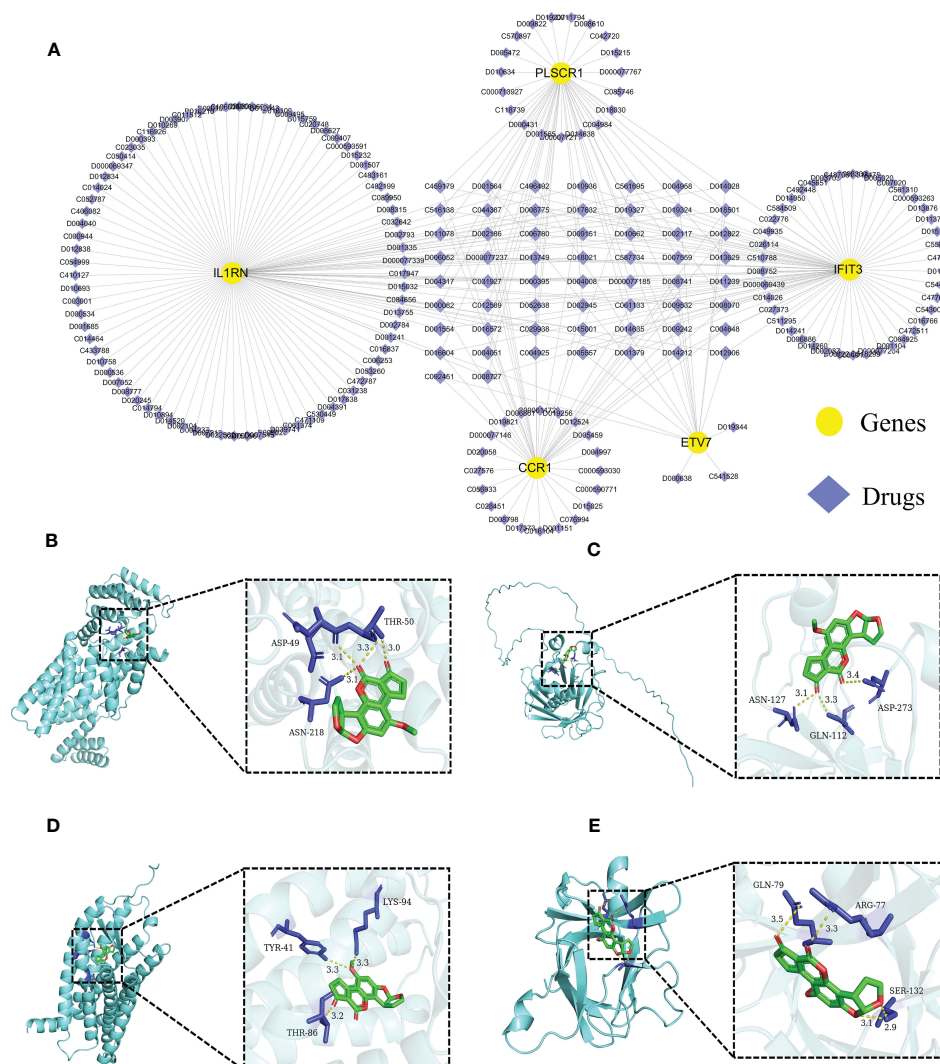


FIGURE 8
Predicting the drugs targeting the diagnostic biomarkers. (A) Drug-gene network. (B–E) Molecular docking analysis. Aflatoxin B1 was docked with IFIT3, PLSCR1, CCR1, and IL1RN.

the β -chemokine receptor family and can interact with numerous ligands, such as CCL5, and suppressing CCR1 could improve lupus nephritis progression in New Zealand black/white mice (47). IL1RN is a natural IL-1 inhibitor that can regulate multiple IL-1-related immune and inflammatory responses. IL1RN polymorphism is a factor that affects SLE severity, and IL1RN might be a potential biomarker for SLE (48). Transcription factor ETV7 exhibited elevated expression in SLE (49), which might be induced by IFN- α/γ (50, 51). The SVM model accurately predicted SLE in the validation cohort (AUC = 0.943), providing new insights for SLE diagnosis. More importantly, a nomogram was plotted based on IFIT3, PLSCR1, CCR1, IL1RN, and ETV7 for diagnosing SLE subtypes. The nomogram displayed significant predictive value, suggesting that the model has clinical utility.

In addition, we constructed a CeRNA network using the 5 core diagnostic markers to explore the regulatory mechanism of the core markers. MicroRNA (miRNA) is one of the major epigenetic regulators of SLE-related genes. Remarkable research progress has

been made in miRNA-based biomarkers and therapies (52). The CeRNA network illustrated that lncRNA SNHG14 could simultaneously interact with hsa-miR-515-5p and hsa-miR-185-3p, lncRNA SNHG14 could participate in the production of proinflammatory cytokines in rheumatoid arthritis by regulating the MINK1/JNK pathway (53). It was reported that hsa-miR-515-5p regulated WISP1 expression, inhibited the TLR4/JNK signaling pathway, and reduced apoptosis in fibroblast-like synoviocytes (RAFLS) of rheumatoid arthritis (54). The hsa-miR-185-3p modulating transcription factor Foxo1 plays a foremost role in AIDs and can serve as a diagnostic marker of SLE (55–57). We also predicted diagnostic markers-associated drugs using the CTD database, constructed the drug-gene network, and predicted targets of action by constructing molecular docking models. This offered a reference for devising new protocols or investigating potential pathogenic factors for SLE (58). For instance, tretinoin simultaneously targets 5 core diagnostic markers and is a reactive derivative of vitamin A, which can regulate cellular proliferation,

differentiation, and maturation (59). Previous studies have indicated that the imbalance of Th17/Treg cells was closely related to the pathogenesis and disease activity of SLE (60). Tretinoin can regulate the balance of Th17/Treg cells by downregulating IL-6Ra expression, which affects the binding of IL-6 to IL-6Ra and gp130, leading to the recruitment of STAT3 and promotion of its phosphorylation to induce ROR γ t expression, and ultimately inhibits Th17 cell differentiation and promotes Treg cell proliferation (61, 62). Tretinoin is a potent inhibitor of Pin1, effectively blocking the TLR-7/TLR-9/Pin1/IRAK-1/IRF-7 signaling pathway by inhibiting and degrading activated Pin1, making it an attractive candidate for treating SLE, as Pin1 plays a key role in preventing the progression of the disease (63). Although the potential therapeutic effects of tretinoin are still being explored in this field, it has gained increasing attention, and more research can be carried out to explore its potential therapeutic effects and bring more medical progress.

Nevertheless, there are some limitations to this study. First, this current study is based on bioinformatics, and additional clinical data and experiments are required to verify CRG expression levels. Second, more detailed clinical characteristics are required to identify the performance of the predictive model, and more SLE samples are required to demonstrate the accuracy of the CRG-based model. The correlation between CRGs and immune response needs to be further explored.

Data availability statement

The original contributions presented in the study are included in the article/Supplementary Material. Further inquiries can be directed to the corresponding author.

Author contributions

WL and YS conceived the project and designed the study. YoW and XG analyzed the data and wrote the manuscript. YL and YuW

interpreted the data and provided practical resources. MY revised the paper. All authors contributed to the article and approved the submitted version.

Funding

This work was supported by Provincial Natural Science Foundation of Shandong Province (Grant No. ZR2021MH082). This work was also supported by the National Natural Science Foundation of China (Grant No.81801192 and 91639102) and the funding of Taishan Scholars of Shan-dong Province to Binzhou Medical University.

Conflict of interest

The authors declare that the research was conducted in the absence of any commercial or financial relationships that could be construed as a potential conflict of interest.

Publisher's note

All claims expressed in this article are solely those of the authors and do not necessarily represent those of their affiliated organizations, or those of the publisher, the editors and the reviewers. Any product that may be evaluated in this article, or claim that may be made by its manufacturer, is not guaranteed or endorsed by the publisher.

Supplementary material

The Supplementary Material for this article can be found online at: <https://www.frontiersin.org/articles/10.3389/fimmu.2023.1157196/full#supplementary-material>

References

1. Tsokos GC, Lo MS, Reis PC, Sullivan KE. New insights into the immunopathogenesis of systemic lupus erythematosus. *Nat Rev Rheumatol* (2016) 12(12):716–30. doi: 10.1038/nrrheum.2016.186
2. Hermansen ML, Lindhardsen J, Torp-Pedersen C, Faurschou M, Jacobsen S. The risk of cardiovascular morbidity and cardiovascular mortality in systemic lupus erythematosus and lupus nephritis: a Danish nationwide population-based cohort study. *Rheumatol (Oxford)* (2017) 56(5):709–15. doi: 10.1093/rheumatology/kew475
3. Grammatikos AP, Kyttaris VC, Kis-Toth K, Fitzgerald LM, Devlin A, Finnell MD, et al. A T cell gene expression panel for the diagnosis and monitoring of disease activity in patients with systemic lupus erythematosus. *Clin Immunol* (2014) 150(2):192–200. doi: 10.1016/j.clim.2013.12.002
4. Kang SC, Hwang SJ, Chang YS, Chou CT, Tsai CY. Characteristics of comorbidities and costs among patients who died from systemic lupus erythematosus in Taiwan. *Arch Med Sci* (2012) 8(4):690–6. doi: 10.5114/aoms.2012.30293
5. Wakeland EK, Liu K, Graham RR, Behrens TW. Delineating the genetic basis of systemic lupus erythematosus. *Immunity* (2001) 15(3):397–408. doi: 10.1016/S1074-7613(01)00201-1
6. Kim BE, Nevitt T, Thiele DJ. Mechanisms for copper acquisition, distribution and regulation. *Nat Chem Biol* (2008) 4(3):176–85. doi: 10.1038/nchembio.72
7. Ge EJ, Bush AI, Casini A, Cobine PA, Cross JR, DeNicola GM, et al. Connecting copper and cancer: from transition metal signalling to metalloplasia. *Nat Rev Cancer* (2022) 22(2):102–13. doi: 10.1038/s41568-021-00417-2
8. Lutsenko S. Human copper homeostasis: a network of interconnected pathways. *Curr Opin Chem Biol* (2010) 14(2):211–7. doi: 10.1016/j.cbpa.2010.01.003
9. Guo HR, Wang YQ, Cui HM, Ouyang YJ, Yang TY, Liu CY, et al. Copper induces spleen damage through modulation of oxidative stress, apoptosis, DNA damage, and inflammation. *Biol Trace Elem Res* (2022) 200(2):669–77. doi: 10.1007/s12011-021-02672-8
10. Jian Z, Guo H, Liu H, Cui H, Fang J, Zuo Z, et al. Oxidative stress, apoptosis and inflammatory responses involved in copper-induced pulmonary toxicity in mice. *Aging (Albany NY)* (2020) 12(17):16867–86. doi: 10.18632/aging.103585
11. Tsvetkov P, Coy S, Petrova B, Dreishpoon M, Verma A, Abdusamad M, et al. Copper induces cell death by targeting lipoylated TCA cycle proteins. *Science* (2022) 375(6586):1254–61. doi: 10.1126/science.abf0529
12. Li P, Jiang M, Li K, Li H, Zhou Y, Xiao X, et al. Glutathione peroxidase 4-regulated neutrophil ferroptosis induces systemic autoimmunity. *Nat Immunol* (2021) 22(9):1107–17. doi: 10.1038/s41590-021-00993-3

13. Tan HY, Wang N, Zhang C, Chan YT, Yuen MF, Feng Y. Lysyl oxidase-like 4 fosters an immunosuppressive microenvironment during hepatocarcinogenesis. *Hepatology* (2021) 73(6):2326–41. doi: 10.1002/hep.31600
14. Goodfellow I, Bengio Y, Courville A. *Deep learning*. MIT press (2016).
15. Oliver A, Odena A, Raffel CA, Cubuk ED, Goodfellow IJ. Realistic evaluation of deep semi-supervised learning algorithms. *32nd Conference on Neural Information Processing Systems* (2018). doi: 10.48550/arXiv.1804.09170
16. Hinton GE, Osindero S, Teh YW. A fast learning algorithm for deep belief nets. *Neural Comput* (2006) 18(7):1527–54. doi: 10.1162/neco.2006.18.7.1527
17. Li X, Guo F, Zhou Z, Zhang F, Wang Q, Peng Z, et al. [Performance of deep-learning-based artificial intelligence on detection of pulmonary nodules in chest CT]. *Zhongguo fei ai za zhi = Chin J Lung Cancer* (2019) 22(6):336–40. doi: 10.3779/j.issn.1009-3419.2019.06.02
18. Feeny AK, Chung MK, Madabhushi A, Attia ZI, Cikes M, Firouzian M, et al. Artificial intelligence and machine learning in arrhythmias and cardiac electrophysiology. *Circ Arrhythm Electrophysiol* (2020) 13(8):e007952. doi: 10.1161/CIRCEP.119.007952
19. Schlegl T, Seebock P, Waldstein SM, Schmidt-Erfurth U, Langs G. (2017). Unsupervised anomaly detection with generative adversarial networks to guide marker discovery. Information processing in medical imaging, in: *25th International Conference, IPMI 2017*, Boone, NC, USA, June 25–30, 2017. pp. 146–57. Proceedings, Springer. doi: 10.48550/arXiv.1703.05921
20. Choi H, Jin KHALzheimer's Disease Neuroimaging Initiative. Predicting cognitive decline with deep learning of brain metabolism and amyloid imaging. *Behav Brain Res* (2018) 344:103–9. doi: 10.1016/j.bbr.2018.02.017
21. Carpintero MF, Martinez L, Fernandez I, Romero AC, Mejia C, Zang YJ, et al. Diagnosis and risk stratification in patients with anti-RNP autoimmunity. *Lupus* (2015) 24(10):1057–66. doi: 10.1177/0961203315575586
22. Kennedy WP, Maciura R, Wolslegel K, Tew W, Abbas AR, Chaivorapol C, et al. Association of the interferon signature metric with serological disease manifestations but not global activity scores in multiple cohorts of patients with SLE. *Lupus Sci Med* (2015) 2(1):e000080. doi: 10.1136/lupus-2014-000080
23. Chiche L, Jourde-Chiche N, Whalen E, Presnell S, Gersuk V, Dang K, et al. Modular transcriptional repertoire analyses of adults with systemic lupus erythematosus reveal distinct type I and type II interferon signatures. *Arthritis Rheumatol (Hoboken N.J.)* (2014) 66(6):1583–95. doi: 10.1002/art.38628
24. Langfelder P, Horvath S. WGCNA: an R package for weighted correlation network analysis. *BMC Bioinf* (2008) 9:559. doi: 10.1186/1471-2105-9-559
25. Wang FZ, Wang B, Long JB, Wang FM, Wu P. Identification of candidate target genes for endometrial cancer, such as ANO1, using weighted gene co-expression network analysis. *Exp Ther Med* (2019) 17(1):298–306. doi: 10.3892/etm.2018.6965
26. Ravasz E, Somera AL, Mongru DA, Oltvai ZN, Barabasi AL. Hierarchical organization of modularity in metabolic networks. *Science* (2002) 297(5586):1551–5. doi: 10.1126/science.1073374
27. Gold C, Sollich P. Model selection for support vector machine classification. *Neurocomputing* (2003) 55(1):221–49. doi: 10.1016/S0925-2312(03)00375-8
28. Rigatti SJ. Random forest. *J Insur Med* (2017) 47(1):31–9. doi: 10.17849/in-sm-47-01-31-39.1
29. Nelder JA, Wedderburn RWM. Generalized linear models. *J R Stat Soc* (1972) 135(3):370–84. doi: 10.2307/2344614
30. Chen T, He T, Benesty M, Khotilovich V, Tang Y, Cho H, et al. Xgboost: extreme gradient boosting. *The annals of statistics* (2015) 1(4):1–4.
31. Newman AM, Liu CL, Green MR, Gentles AJ, Feng W, Xu Y, et al. Robust enumeration of cell subsets from tissue expression profiles. *Nat Methods* (2015) 12(5):453–7. doi: 10.1038/nmeth.3337
32. Bakshi J, Segura BT, Wincup C, Rahman A. Unmet needs in the pathogenesis and treatment of systemic lupus erythematosus. *Clin Rev Allergy Immunol* (2018) 55(3):352–67. doi: 10.1007/s12016-017-8640-5
33. Gordon C, Amisssah-Arthur MB, Gayed M, Brown S, Bruce IN, D'Cruz D, et al. The British society for rheumatology guideline for the management of systemic lupus erythematosus in adults. *Rheumatol (Oxford)* (2018) 57(1):e1–e45. doi: 10.1093/rheumatology/kex286
34. Zakharova MY, Belyanina TA, Sokolov AV, Kiselev IS, Mamedov AE. The contribution of major histocompatibility complex class II genes to an association with autoimmune diseases. *Acta Naturae* (2019) 11(4):4–12. doi: 10.32607/20758251-2019-11-4-4-12
35. Luque A, Serrano I, Ripoll E, Malta C, Goma M, Blom AM, et al. Noncanonical immunomodulatory activity of complement regulator C4BP(beta-) limits the development of lupus nephritis. *Kidney Int* (2020) 97(3):551–66. doi: 10.1016/j.kint.2019.10.016
36. Tang D, Chen X, Kroemer G. Cuproptosis: a copper-triggered modality of mitochondrial cell death. *Cell Res* (2022) 32(5):417–8. doi: 10.1038/s41422-022-00653-7
37. Papayannopoulos V. Neutrophil extracellular traps in immunity and disease. *Nat Rev Immunol* (2018) 18(2):134–47. doi: 10.1038/nri.2017.105
38. Chasset F, Arnaud L. Targeting interferons and their pathways in systemic lupus erythematosus. *Autoimmun Rev* (2018) 17(1):44–52. doi: 10.1016/j.autrev.2017.11.009
39. Moser KL, Kelly JA, Lessard CJ, Harley JB. Recent insights into the genetic basis of systemic lupus erythematosus. *Genes Immun* (2009) 10(5):373–9. doi: 10.1038/gene.2009.39
40. Carrillo-Vazquez DA, Jardon-Valadez E, Torres-Ruiz J, Juarez-Vega G, Maravillas-Montero JL, Meza-Sanchez DE, et al. Conformational changes in myeloperoxidase induced by ubiquitin and NETs containing free ISG15 from systemic lupus erythematosus patients promote a pro-inflammatory cytokine response in CD4(+) T cells. *J Transl Med* (2020) 18(1):429. doi: 10.1186/s12967-020-02604-5
41. Fleith RC, Mears HV, Leong XY, Sanford TJ, Emmott E, Graham SC, et al. IFIT3 and IFIT2/3 promote IFIT1-mediated translation inhibition by enhancing binding to non-self RNA. *Nucleic Acids Res* (2018) 46(10):5269–85. doi: 10.1093/nar/gky191
42. Wang JH, Dai M, Cui YG, Hou GJ, Deng J, Gao X, et al. Association of abnormal elevations in IFIT3 with overactive cyclic GMP-AMP Synthase/Stimulator of interferon genes signaling in human systemic lupus erythematosus monocytes. *Arthritis Rheumatol* (2018) 70(12):2036–45. doi: 10.1002/art.40576
43. Bernalles I, Fullaondo A, Marin-Vidal MJ, Ucar E, Martinez-Taboada V, Lopez-Hoyos M, et al. Innate immune response gene expression profiles characterize primary antiphospholipid syndrome. *Genes Immun* (2008) 9(1):38–46. doi: 10.1038/sj.gene.6364443
44. O'Hanlon TP, Rider LG, Gan L, Fannin R, Paules RS, Umbach DM, et al. Gene expression profiles from discordant monozygotic twins suggest that molecular pathways are shared among multiple systemic autoimmune diseases. *Arthritis Res Ther* (2011) 13(2):R69. doi: 10.1186/ar3330
45. Deng Y, Zheng Y, Li D, Hong Q, Zhang M, Li Q, et al. Expression characteristics of interferon-stimulated genes and possible regulatory mechanisms in lupus patients using transcriptomics analyses. *EBioMedicine* (2021) 70:103477. doi: 10.1016/j.ebiom.2021.103477
46. Bing PF, Xia W, Wang L, Zhang YH, Lei SF, Deng FY. Common marker genes identified from various sample types for systemic lupus erythematosus. *PloS One* (2016) 11(6):e0156234. doi: 10.1371/journal.pone.0156234
47. Bignon A, Gaudin F, Hemon P, Tharinger H, Mayol K, Walzer T, et al. CCR1 inhibition ameliorates the progression of lupus nephritis in NZB/W mice. *J Immunol* (2014) 192(3):886–96. doi: 10.4049/jimmunol.1300123
48. Tsai LJ, Lan JL, Lin CY, Hsiao SH, Tsai LM, Tsai JJ. The different expression patterns of interleukin-1 receptor antagonist in systemic lupus erythematosus. *Tissue Antigens* (2006) 68(6):493–501. doi: 10.1111/j.1399-0039.2006.00704.x
49. Idborg H, Zandian A, Sandberg AS, Nilsson B, Elvin K, Truedsson L, et al. Two subgroups in systemic lupus erythematosus with features of antiphospholipid or sjogren's syndrome differ in molecular signatures and treatment perspectives. *Arthritis Res Ther* (2019) 21:62. doi: 10.1186/s13075-019-1836-8
50. Irudayam JJ, Contreras D, Spurka L, Subramanian A, Allen J, Ren S, et al. Characterization of type I interferon pathway during hepatic differentiation of human pluripotent stem cells and hepatitis C virus infection. *Stem Cell Res* (2015) 15(2):354–64. doi: 10.1016/j.scr.2015.08.003
51. Minutti CM, Garcia-Fojeda B, Saenz A, de Las Casas-Engel M, Guillaumat-Prats R, de Lorenzo A, et al. Surfactant protein A prevents IFN-gamma/IFN-gamma receptor interaction and attenuates classical activation of human alveolar macrophages. *J Immunol* (2016) 197(2):590–8. doi: 10.4049/jimmunol.1501032
52. Hong SM, Liu C, Yin Z, Wu L, Qu B, Shen N. MicroRNAs in systemic lupus erythematosus: a perspective on the path from biological discoveries to clinical practice. *Curr Rheumatol Rep* (2020) 22(6):17. doi: 10.1007/s11926-020-00895-7
53. Zhang J, Lei H, Li X. LncRNA SNHG14 contributes to proinflammatory cytokine production in rheumatoid arthritis via the regulation of the miR-17-5p/MINK1-JNK pathway. *Environ Toxicol* (2021) 36(12):2484–92. doi: 10.1002/tox.23361
54. Cai D, Hong S, Yang J, San P. The effects of microRNA-515-5p on the toll-like receptor 4 (TLR4)/JNK signaling pathway and WNT1-Inducible-Signaling pathway protein 1 (WISP-1) expression in rheumatoid arthritis fibroblast-like synovial (RAFLS) cells following treatment with receptor activator of nuclear factor-kappa-B ligand (RANKL). *Med Sci Monit* (2020) 26:e920611. doi: 10.12659/MSM.920611
55. Zhou SL, Zhang J, Luan PF, Ma ZB, Dang J, Zhu H, et al. miR-183-5p is a potential molecular marker of systemic lupus erythematosus (vol 2021, 5547635, 2021). *J Immunol Res* (2021) 2021:5547635. doi: 10.1155/2021/5547635
56. Wan C, Ping CY, Shang XY, Tian JT, Zhao SH, Li L, et al. MicroRNA 182 inhibits CD4(+)CD25(+)Foxp3(+) treg differentiation in experimental autoimmune encephalomyelitis. *Clin Immunol* (2016) 173:109–16. doi: 10.1016/j.clim.2016.09.008
57. Yang X, He QY, Guo ZZ, Xiong F, Li Y, Pan Y, et al. MicroRNA-425 facilitates pathogenic Th17 cell differentiation by targeting forkhead box O1 (Foxo1) and is associated with inflammatory bowel disease. *Biochem Bioph Res Co* (2018) 496(2):352–8. doi: 10.1016/j.bbrc.2018.01.055
58. Chu Y, Zhao C, Zhang B, Wang X, Wang Y, An J, et al. Restoring T-helper 17 cell/regulatory T-cell balance and decreasing disease activity by rapamycin and all-trans retinoic acid in patients with systemic lupus erythematosus. *Lupus* (2019) 28(12):1397–406. doi: 10.1177/0961203319877239
59. Cassani B, Villablanca EJ, De Calisto J, Wang S, Mora JR. Vitamin A and immune regulation: role of retinoic acid in gut-associated dendritic cell education, immune protection and tolerance. *Mol Aspects Med* (2012) 33(1):63–76. doi: 10.1016/j.mam.2011.11.001

60. Ma J, Yu J, Tao X, Cai L, Wang J, Zheng SG. The imbalance between regulatory and IL-17-secreting CD4+ T cells in lupus patients. *Clin Rheumatol* (2010) 29:1251–8. doi: 10.1007/s10067-010-1510-7
61. Wang X, Wang W, Xu J, Wu S, Le Q. All-trans retinoid acid promotes allogeneic corneal graft survival in mice by regulating treg-Th17 balance in the presence of TGF- β . *BMC Immunol* (2015) 16(1):1–13. doi: 10.1186/s12865-015-0082-3
62. Ivanov II, Zhou L, Littman DR. Transcriptional regulation of Th17 cell differentiation. In: *Seminars in immunology*. Elsevier (2007). p. 409–17. doi: 10.1016/j.smim.2007.10.011
63. Wei S, Yoshida N, Finn G, Kozono S, Nechama M, Kyttaris VC, et al. Rheumatology, Pin1-targeted therapy for systemic lupus erythematosus. *Arthritis Rheumatol* (2016) 68(10):2503–13. doi: 10.1002/art.39741



OPEN ACCESS

EDITED BY

Evangelia Sarandi,
University of Crete, Greece

REVIEWED BY

Kazuma Sakamoto,
Nagoya University, Japan
Tusharkanti Ghosh,
University of Colorado Anschutz Medical
Campus, United States

*CORRESPONDENCE

Jin Xu,
✉ xujinekjy@163.com
Jian Li,
✉ lijianjuliale@126.com

RECEIVED 08 March 2023

ACCEPTED 15 May 2023

PUBLISHED 30 May 2023

CITATION

Wang Y, Cao Y, Li Y, Yuan M, Xu J and Li J
(2023), Identification of key signaling
pathways and hub genes related to
immune infiltration in Kawasaki disease
with resistance to intravenous
immunoglobulin based on weighted
gene co-expression network analysis.
Front. Mol. Biosci. 10:1182512.
doi: 10.3389/fmolb.2023.1182512

COPYRIGHT

© 2023 Wang, Cao, Li, Yuan, Xu and Li.
This is an open-access article distributed
under the terms of the [Creative
Commons Attribution License \(CC BY\)](#).
The use, distribution or reproduction in
other forums is permitted, provided the
original author(s) and the copyright
owner(s) are credited and that the original
publication in this journal is cited, in
accordance with accepted academic
practice. No use, distribution or
reproduction is permitted which does not
comply with these terms.

Identification of key signaling pathways and hub genes related to immune infiltration in Kawasaki disease with resistance to intravenous immunoglobulin based on weighted gene co-expression network analysis

Yue Wang¹, Yinyin Cao², Yang Li¹, Meifen Yuan¹, Jin Xu^{1*} and
Jian Li^{1*}

¹Clinical Laboratory Center, Children's Hospital of Fudan University, National Children's Medical Center, Shanghai, China, ²Cardiovascular Center, Children's Hospital of Fudan University, National Children's Medical Center, Shanghai, China

Background: Kawasaki disease (KD) is an acute vasculitis, that is, the leading cause of acquired heart disease in children, with approximately 10%–20% of patients with KD suffering intravenous immunoglobulin (IVIG) resistance. Although the underlying mechanism of this phenomenon remains unclear, recent studies have revealed that immune cell infiltration may associate with its occurrence.

Methods: In this study, we downloaded the expression profiles from the GSE48498 and GSE16797 datasets in the Gene Expression Omnibus database, analyzed differentially expressed genes (DEGs), and intersected the DEGs with the immune-related genes downloaded from the ImmPort database to obtain differentially expressed immune-related genes (DEIGs). Then CIBERSORT algorithm was used to calculate the immune cell compositions, followed by the WGCNA analysis to identify the module genes associated with immune cell infiltration. Next, we took the intersection of the selected module genes and DEIGs, then performed GO and KEGG enrichment analysis. Moreover, ROC curve validation, Spearman analysis with immune cells, TF, and miRNA regulation network, and potential drug prediction were implemented for the finally obtained hub genes.

Results: The CIBERSORT algorithm showed that neutrophil expression was significantly higher in IVIG-resistant patients compared to IVIG-responsive patients. Next, we got differentially expressed neutrophil-related genes by intersecting DEIGs with neutrophil-related module genes obtained by WGCNA, for further analysis. Enrichment analysis revealed that these genes were associated with immune pathways, such as cytokine-cytokine receptor interaction and neutrophil extracellular trap formation. Then we combined the PPI network in the STRING database with the MCODE plugin in Cytoscape and identified 6 hub genes (TLR8, AQP9, CXCR1, FPR2, HCK, and IL1R2), which had good diagnostic performance in IVIG resistance according to ROC analysis. Furthermore, Spearman's correlation analysis confirmed that these genes were closely

related to neutrophils. Finally, TFs, miRNAs, and potential drugs targeting the hub genes were predicted, and TF-, miRNA-, and drug-gene networks were constructed.

Conclusion: This study found that the 6 hub genes (TLR8, AQP9, CXCR1, FPR2, HCK, and IL1R2) were significantly associated with neutrophil cell infiltration, which played an important role in IVIG resistance. In a word, this work rendered potential diagnostic biomarkers and prospective therapeutic targets for IVIG-resistant patients.

KEYWORDS

IVIG-resistance, intravenous immunoglobulin, Kawasaki disease, weighted gene coexpression network analysis, immune infiltration, neutrophil

1 Introduction

Kawasaki disease (KD), also known as mucocutaneous lymph node syndrome, is an acute febrile systemic vasculitis that mainly occurs in children under five (Agarwal and Agrawal, 2017). The pathogenesis of KD remains unknown, but an immune-mediated inflammatory cascade triggered by an unknown stimulus in genetically susceptible children is believed to be one of the major mechanisms (Rife and Gedalia, 2020). The most severe complication of KD is the occurrence of coronary artery lesions, such as coronary artery aneurysms, which is the most common cause of acquired heart disease among children in developed countries (Hedrich et al., 2018). Early use of high-dose intravenous immunoglobulin (IVIG) is well-accepted as the standard treatment for KD (Fukui et al., 2021). The risk of coronary artery aneurysms will be reduced five-fold if IVIG is used within 10 days of fever onset (Newburger et al., 2016). However, up to 20% of KD patients are IVIG-resistant and have a persistent or recrudescence fever at least 36 h after the end of the initial IVIG infusion (Kaya Akca et al., 2022). These patients have a higher risk of developing coronary artery lesions, compared to IVIG responders (Song, 2019). Therefore, it is crucial to explore new biomarkers to predict KD patients' treatment response, which can improve the prediction of prognosis and guide clinical decision-making.

In recent years, to better understand the mechanisms underlying IVIG resistance in KD and identify new treatment options, numerous studies have focused on the relationship between immunity and IVIG resistance. For instance, one study involving T cells has suggested that excessive CD8⁺ T cell activation and the imbalance between CD8⁺ T cell activation and inhibition contribute to the pathogenesis of KD. While IVIG can inhibit CD8⁺ T cell activation, excessive activation of these cells may lead to IVIG resistance (Ye et al., 2016). Additionally, research involving neutrophils has found that IVIG-resistant patients have a higher percentage of neutrophils and higher neutrophil-to-lymphocyte ratios than IVIG-responsive patients at IVIG administration (Sato et al., 2013; Lee and Song, 2016; Han et al., 2022). These studies provide new insights into the importance of immune regulation in IVIG resistance.

Weighted gene co-expression network analysis (WGCNA) is a systems biology approach that studies patterns of gene co-expression and constructs co-expression network models based on gene expression profiles. This method has been widely used to investigate the pathogenesis of many diseases, including KD (Wang T et al., 2022). In this study, we used WGCNA to identify module genes highly associated with immune cell infiltration, to better

understand the development of IVIG resistance, and make it possible to design early diagnosis and therapeutic procedures for IVIG resistance. The workflow diagram of this study was displayed in Figure 1.

2 Materials and methods

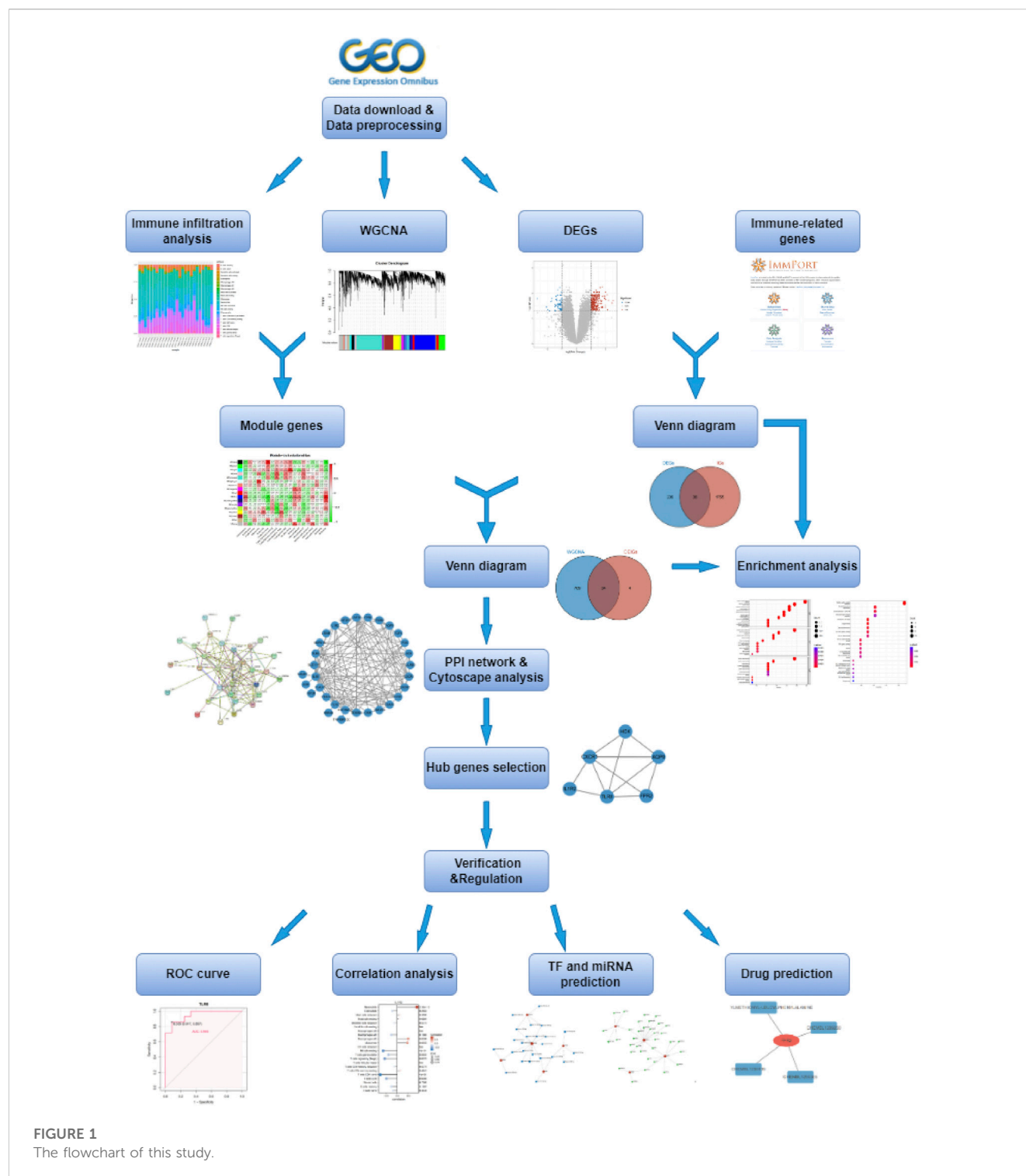
2.1 Data acquisition

This study utilized two datasets, namely GSE48498 and GSE16797, obtained from the Gene Expression Omnibus (GEO) database (<http://www.ncbi.nlm.nih.gov/geo>) (Ogihara et al., 2009; Ogihara et al., 2014). Both datasets were derived from the same platform GPL570, which was important for merging the data and performing subsequent integrated analysis. Then a total of 26 KD patients were included in this study, of which 14 patients were resistant to IVIG treatment and 12 patients were responsive to IVIG treatment (Table 1). Additionally, 2483 immune-related genes (IGs) data were retrieved from the ImmPort database (<https://immport.niaid.nih.gov>), which would be used in our study (Bhattacharya et al., 2018).

2.2 Data preprocessing and screening of differentially expressed genes

After the raw data of the GSE48498 and GSE16797 were read by the “Affy” package of Bioconductor (<http://www.bioconductor.org/packages/release/bioc/html/affy.html>) in R software, they were performed with background correction, normalization, and probe summarization using robust multi-array average (RMA) algorithm (Gautier et al., 2004; Harbron et al., 2007). In addition, the batch effect was eliminated by utilizing the combat function of the R software package “SVA” (Leek et al., 2012). The effect of data correction was demonstrated using two-dimensional PCA cluster plots before and after data correction respectively (Metsalu and Vilo, 2015).

Next, the differentially expressed genes (DEGs) between the IVIG-resistant group and the IVIG-responsive group were identified using the “Limma” package in R software (Diboun et al., 2006). The filter criteria for DEGs were set as $|\log_2 \text{fold change (FC)}| > 1$ and adjusted p -value < 0.05 . The volcano plot and heatmap were drawn using the “ggplot2” package in R software to visualize the DEGs. Differentially expressed immune-related genes (DEIGs) were



obtained by taking the intersection of DEGs and IGs using the “VennDiagram” R package (Chen and Boutros, 2011).

2.3 GO and KEGG enrichment analysis

Gene Ontology (GO) annotation and Kyoto Encyclopedia of Genes and Genomes (KEGG) enrichment analysis were performed using the “clusterProfiler” R package to reveal the potential biological

functions and pathway mechanisms of genes (Yu et al., 2012). Adjusted $p < 0.05$ was considered statistically significant in this study.

2.4 Immune infiltration analysis

A bioinformatics algorithm called CIBERSORT (<https://cibersortx.stanford.edu/>) was used to measure the infiltration status of immune cells to quantify the relative proportions of infiltrating immune cells

TABLE 1 IVIG-resistant and IVIG-responsive KD patients.

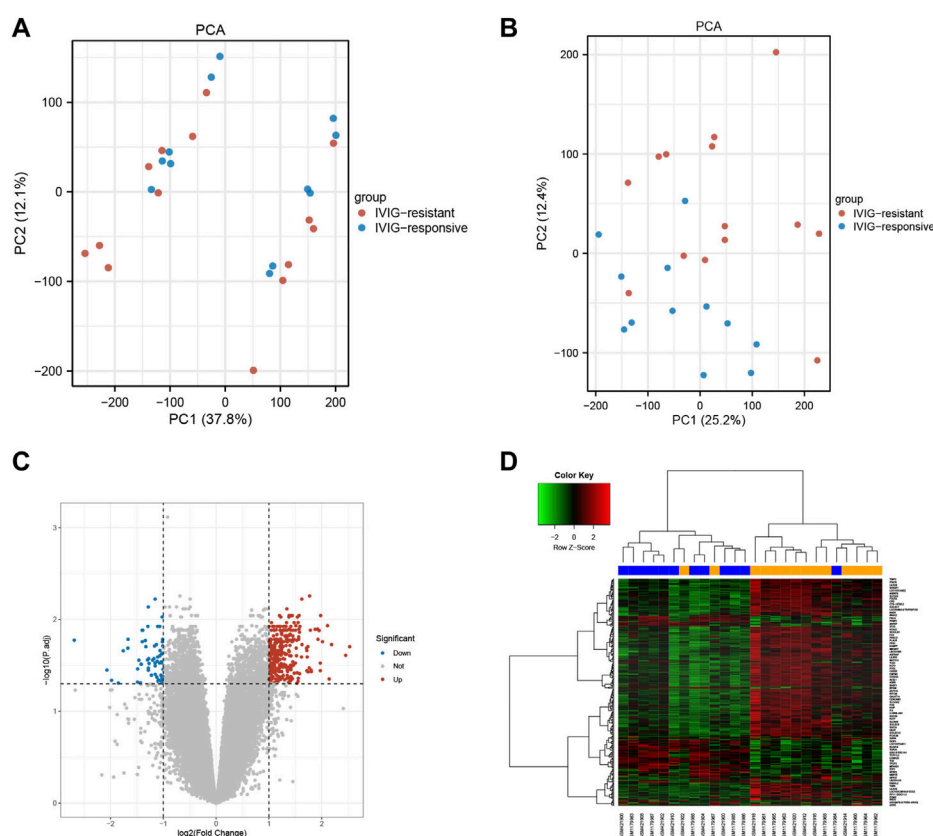
Platform	Datasets	Total samples	Intravenous immunoglobulin G (IVIG)	
			Groups	Samples
GPL570	GSE48498	28	IVIG-resistant	GSM1179961
				GSM1179962
				GSM1179963
				GSM1179964
				GSM1179965
				GSM1179966
				GSM1179967
				GSM1179968
			IVIG-responsive	GSM1179983
				GSM1179984
				GSM1179985
				GSM1179986
				GSM1179987
				GSM1179988
	GSE16797	34	IVIG-responsive	GSM421900
				GSM421902
				GSM421904
				GSM421906
				GSM421908
				GSM421910
			IVIG-resistant	GSM421912
				GSM421914
				GSM421916
				GSM421918
				GSM421920
				GSM421922

from the gene expression profiles of our samples (Newman et al., 2015). A standard set of 22 kinds of immune cell subsets (IM22) having 1,000 permutations were utilized to assess the predicted abundance level of immune cells. To visualize the results of the CIBERSORT algorithm, we used the “pheatmap” package to generate a heatmap about the proportion of 22 infiltrating immune cells in each sample, and the “ggboxplot” package to obtain a boxplot to show the differences in each infiltrating immune cell between the IVIG-resistant group and IVIG-responsive group, respectively.

2.5 Construction of weighted gene Co-expression network

A gene co-expression network was constructed using the WGCNA method, which was implemented with the R-based

package “WGCNA” (Langfelder and Horvath, 2008). First, we selected the top 5000 genes based on variance from the gene expression data for analysis, then performed hierarchical clustering analysis to detect and remove outlier samples. In order to construct a scale-free network, the optimal soft-thresholding power was identified and the adjacency matrix was transformed into a topological overlap matrix (TOM) (Shuai, et al., 2021). Subsequently, the hierarchical cluster tree was cut into gene modules using the dynamic tree cut algorithm, with a minimum module size of 30 genes. Then, the heatmap was plotted to reflect the relationships between each module and 18 subtypes of immune infiltrating cells, and the module with a high correlation coefficient was selected. Finally, the R package “Venndiagram” was used to take the intersection of these genes in the selected module and DEIGs, and the obtained genes were used for subsequent analysis.

**FIGURE 2**

The effects of data processing and the recognition of differences express genes. (A) PCA diagram before data processing. (B) PCA diagram after data processing. (C) The volcano plot of DEGs. The upregulated genes were marked in red dots, while the downregulated genes were marked in blue dots. (D) The heatmap of DEGs. The upregulated genes were represented by red, and the downregulated genes were represented by green.

2.6 Construction of protein-protein interaction network and identification of hub genes

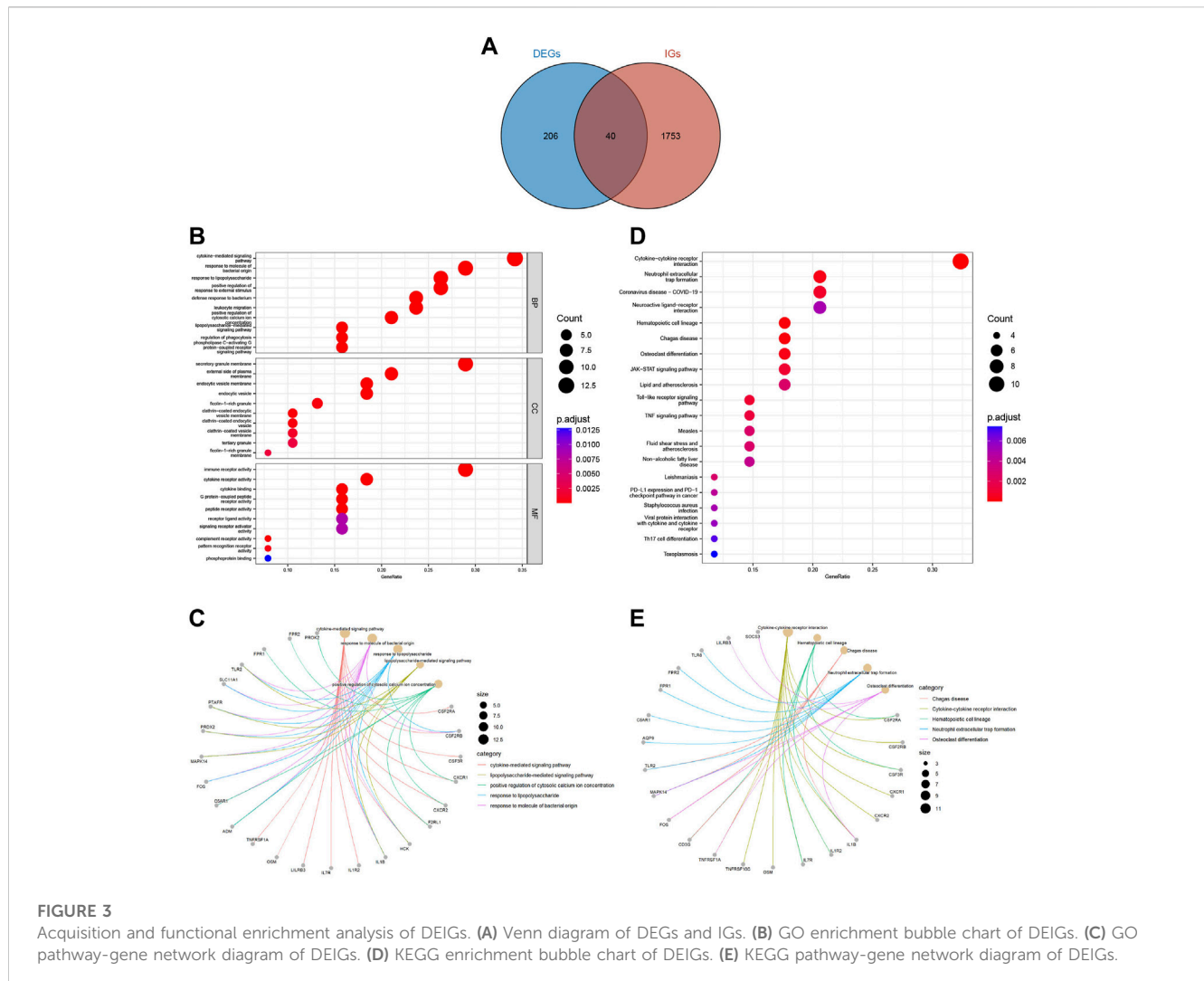
The above-obtained genes were subjected to protein-protein interaction (PPI) network analysis using the Search Tool for the Retrieval of Interacting Genes/Proteins (STRING, <https://string-db.org/>) database (Szkarczyk et al., 2017). Moreover, Cytoscape is an open-source software project for integrating biomolecular interaction networks, which is one of the most powerful network biology analyses and visualization tools when applied in conjunction with large databases of protein-protein, protein-DNA, and genetic interactions (Shannon et al., 2003). Thus, we visualized the PPI network through Cytoscape software. Additionally, the Cytoscape plugin Molecular Complex Detection (MCODE), an app for clustering a given network based on its topology to find densely connected regions (Bandettini et al., 2012), was utilized to identify clusters of genes that were highly connected across the entire PPI network, which ultimately led to the determination of hub genes.

2.7 ROC curve analysis

Receiver operating characteristic (ROC) curves are standard statistical tools for the analysis of disease markers and the area under a ROC curve (AUC) is a popular measure of diagnostic accuracy that is independent of the proportion of diseased subjects in the analyzed sample (Parodi et al., 2022). We separately performed ROC curve analysis on each screened hub gene to verify its accuracy in GSE48498 and GSE16797 two datasets. ROC curve analysis was executed with the R package “pROC” (Robin et al., 2011). The AUC value was calculated to evaluate the predictive utility of these hub genes. When the $AUC > 0.7$, the hub gene was considered to have good sensitivity for IVIG resistance diagnosis.

2.8 Correlation analysis between diagnostic genes and infiltrating immune cells

Immune infiltration analysis was performed using the CIBERSORT algorithm. Subsequently, Spearman correlation



analysis was employed to examine the relationship between diagnostic gene expression and immune cell infiltration (Pripp, 2018). To illustrate these relationships more intuitively, lollipop plots were created using the “ggplot2” package for visualization.

2.9 Construction of potential TF-, MiRNA-, and drug-diagnostic gene regulatory network

NetworkAnalyst (<http://www.networkanalyst.ca/>) is a comprehensive web-based tool that integrates all three steps of biological network analysis - identification of genes or proteins of interest, network construction, and network analysis and visualization - and is designed to allow researchers to perform a variety of common and complex meta-analyses of gene expression data through an intuitive web interface (Zhou et al., 2019). To identify possible transcription factors (TFs) and miRNA regulating diagnostic genes, we used NetworkAnalyst online database integrating TF database ENCODE (<https://www.encodeproject.org/>) and miRNA database miRTarBase (<https://mirtarbase.cuhk.edu.cn/>) (ENCODE Project Consortium, 2011; Huang et al., 2022). What's more, the Drug-Gene Interaction

Database (DGIdb; <https://www.dgiddb.org/>) integrates, organizes, and presents information on drug-gene interactions and genetic drug-forming properties from papers, databases, and web resources (Cotto et al., 2018). And the DGIdb online database was used to predict the potential targeted drugs that interacted with the diagnostic genes, then the drug-gene interaction network was visualized in the Cytoscape software.

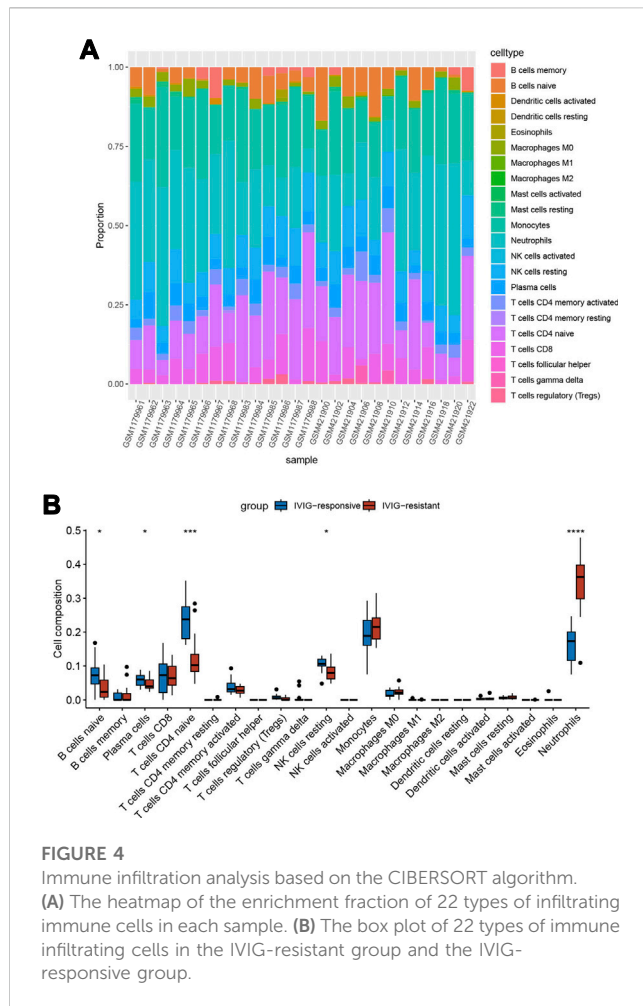
2.10 Statistical analysis

All statistical analyses in our study were performed with the R software (version 4.2.2, <https://www.r-project.org/>). Unless otherwise specified, the *p*-value for statistical significance was set at 0.05.

3 Results

3.1 Identification of DEGs

The selected samples from the GSE48498 and GSE16797 datasets were subjected to background correction,



normalization, and batch removal. The sample distributions before and after the removal of batch effects were visualized in two-dimensional PCA cluster diagrams (Figures 2A, B). All samples in Figure 2A were divided into two distinct clusters, however, Figure 2B showed that after processing, the samples in the two datasets were more evenly mixed, indicating a significant effect of batch removal and more reliable integrated data. Differential gene expression analysis was performed using the processed data, and a total of 246 DEGs were obtained ($|\log_2 \text{FC}| > 1$ and adjusted $p < 0.05$), of which 189 DEGs were upregulated and 57 were downregulated (Supplementary Table S1). The volcano plot and heatmap of DEGs were shown respectively in Figures 2C, D.

3.2 Functional enrichment analysis of DEIGs

We downloaded 2483 IGs from the ImmPort database and obtained 40 differentially expressed immune-related genes (DEIGs) through an intersection with 246 DEGs (Supplementary Table S2). A Venn diagram was used to show the intersection between the IGs and DEGs (Figure 3A). GO analysis of DEIGs indicated that, for the biological process (BP), these genes were mainly involved in cytokine-mediated signaling

pathways, response to bacterial-origin molecules, and response to lipopolysaccharides. In terms of cellular component (CC), DEIGs may play critical roles in secretory granule membranes, plasma membrane outer and inner vesicle membranes. Regarding molecular function (MF), DEIGs were found to have crucial roles in immune receptor activity, cytokine receptor activity, and cytokine binding (Figures 3B, C). In addition, KEGG pathway enrichment analysis revealed that DEIGs were mainly enriched in cytokine-cytokine receptor interactions, neutrophil extracellular trap (NET) formation, and coronavirus disease - COVID-19 (Figures 3D, E).

3.3 Immune infiltration analysis

To explore the immune microenvironment of IVIG-resistant patients, we estimated the relative abundance of 22 types of immune cells using the CIBERSORT algorithm. Figure 4A showed the composition of the 22 types of immune infiltration cells in each sample. Figure 4B compared the infiltration differences of 22 types of immune cells between the IVIG-resistant group and the IVIG-responsive group. The results indicated that naïve CD4 T cells and neutrophils were significantly different between the two groups, with the most significant difference observed in neutrophil infiltration.

3.4 Construction of weighted gene Co-expression network

In Figure 5A, the sample clustering tree showed that one outlier was removed, and 25 samples were retained, of which 13 belonged to the IVIG-resistant group and 12 belonged to the IVIG-responsive group. We then selected the optimal soft-thresholding power of 16 to ensure that our gene distribution conformed to a scale-free network (Figure 5B). Next, WGCNA analysis yielded the gene dendrogram and module colors and identified 17 modules in this study (Figure 5C). After analyzing the correlation of each module with the 22 infiltrating immune cells, the blue module was found to possess the highest positive correlation with neutrophils and presented the highest score of total scores in the plot of the module-trait relationship (Figure 5D). Figure 5E illustrated the significant correlation ($\text{cor} = 0.84$, $P < 1e-200$) between gene significance (GS) and module membership (MM) in the blue module, indicating that the genes highly associated with neutrophils were also important elements in this blue module, thus they were suitable for further analysis.

3.5 Functional enrichment analysis of DENGs

A total of 743 genes were contained in the blue module (Supplementary Table S3). Through the intersection between genes in the blue module and DEIGs, we identified 34 differentially expressed neutrophil-related genes (DENGs) (Figure 6A). GO and KEGG analyses were performed to

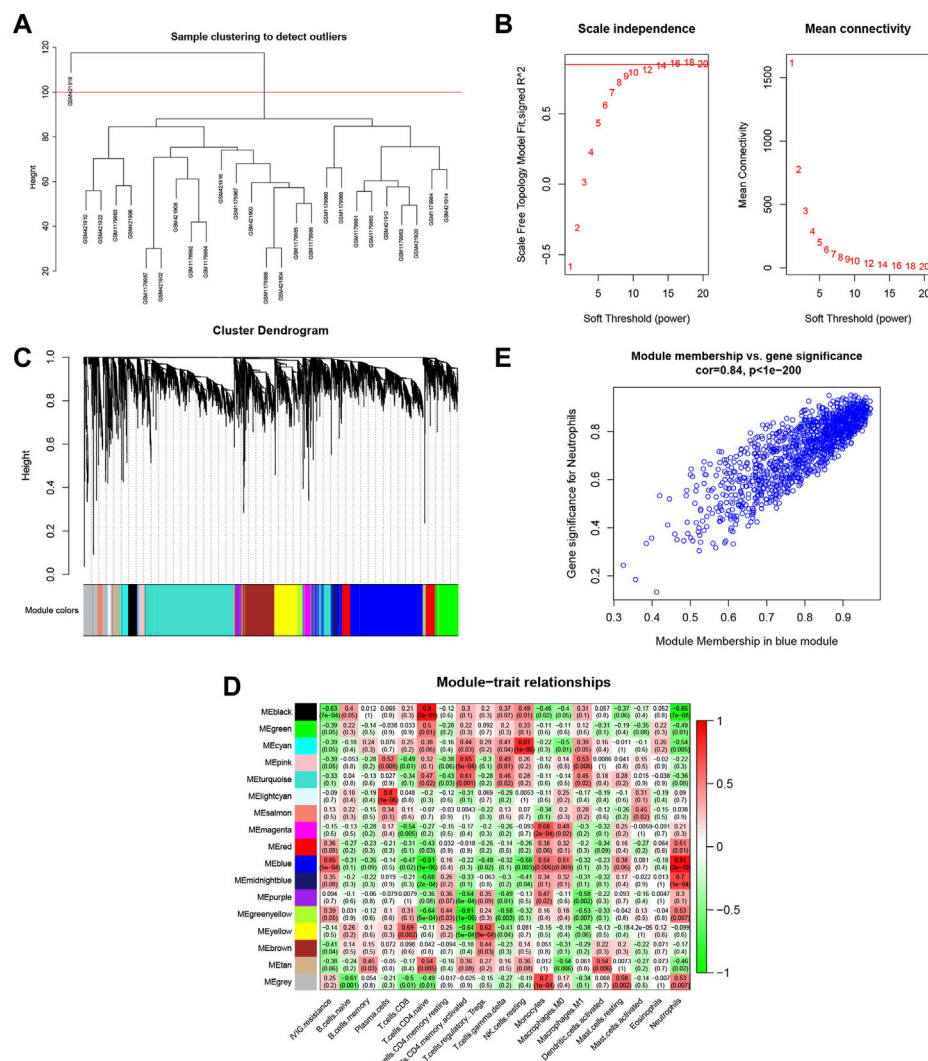


FIGURE 5

Identification of the gene modules related to infiltrating immune cells by WGCNA. (A) Sample clustering of WGCNA to detect abnormal samples. (B) Selection of soft-thresholding power. The left panel displayed the change of the fitting index of different soft-thresholding powers; the right panel displayed the mean connectivity corresponding to different soft-thresholding powers. (C) Hierarchical clustering dendrogram of identified co-expressed genes. Different colors reflected the corresponding modules, and the gray module indicated that the genes were not assigned to any module. (D) The heatmap of the relationship between each gene module and each immune cell. The red represented a positive correlation, while the green represented a negative correlation. (E) Scatterplot of gene significance (GS) for neutrophil vs. module membership (MM) in the blue modules.

explore relevant molecular biological functions and pathways of these 34 DENGs. GO analysis showed that the BPs of these genes were mainly involved in cytokine-mediated signaling pathways, response to bacterial-origin molecules, and positive regulation of cytosolic calcium ion concentration (Figures 6B, C). The CCs of these genes were mostly in the area of secretory granule membrane, lactotransferrin-1-containing granule, and endocytic vesicle membrane (Figures 6D, E). The MFs of these genes were significantly enriched in immune receptor activity, cytokine receptor activity, and cytokine binding (Figures 6F, G). KEGG analysis indicated that the 34 DENGs were significantly related to immune pathways, such as cytokine-cytokine receptor

interaction, neutrophil extracellular trap formation, and coronavirus disease - COVID-19 (Figure 6H).

3.6 Construction of protein-protein interaction network and identification of hub genes

A protein-protein interaction (PPI) network of the obtained DENGs was constructed by the STRING database (Figure 7A). We visualized the PPI network through Cytoscape software and identified hub genes in the PPI network using the MCODE

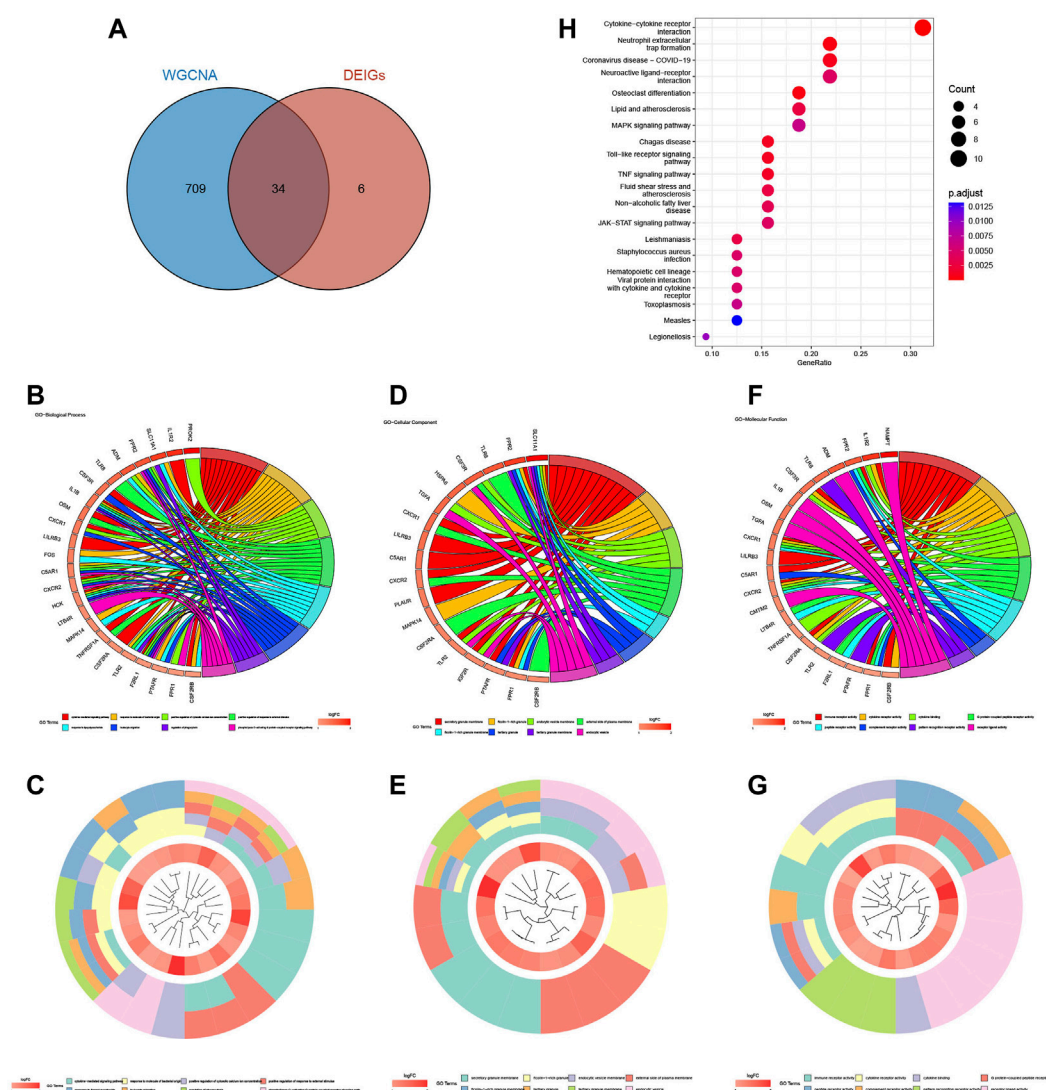


FIGURE 6

Acquisition and enrichment analysis of DEGs. (A) Venn diagram of the blue module genes and DEGs. (B, C) GO chord diagram and GO cluster diagram of BP of DEGs. (D, E) GO chord diagram and GO cluster diagram of CC of DEGs. (F, G) GO chord diagram and GO cluster diagram of MF of DEGs. (H) The KEGG enrichment bubble chart of DEGs.

plugin (Figures 7B, C). Finally, six hub genes were identified, namely TLR8, CXCR1, HCK, AQP9, FPR2, and IL1R2.

3.7 ROC curve analysis

The diagnostic performance of the identified hub genes for IVIG resistance was evaluated by ROC curve analysis in GSE48498 and GSE16797 two datasets separately (Figures 8A, B). We considered an AUC > 0.7 as the screening criterion for hub genes. As a result, in the GSE48498 dataset, six hub genes had AUC > 0.7, with TLR8, AQP9, CXCR1, and FPR2 having AUC > 0.9. In the GSE16797 dataset, six hub genes also had AUC > 0.7, with only TLR8 and HCK having AUC > 0.9. Altogether these results suggested that six hub genes were able to distinguish IVIG-resistant from IVIG-responsive patients after KD patients were treated with IVIG in both

datasets, so we believed that they could have good diagnostic value and were considered as potential biomarkers for the diagnosis of IVIG resistance.

3.8 Correlation analysis between diagnostic genes and immune cells

For the purpose of better understanding the role of six diagnostic genes in immune infiltration, we performed Spearman's correlation analysis to determine the correlation of hub genes with infiltrating immune cells. The results showed that six diagnostic genes, including TLR8, AQP9, CXCR1, FPR2, HCK, and IL1R2, were significantly positively correlated with neutrophil infiltration, which could confirm that they were screened from the blue module related to neutrophils. In addition, these diagnostic genes

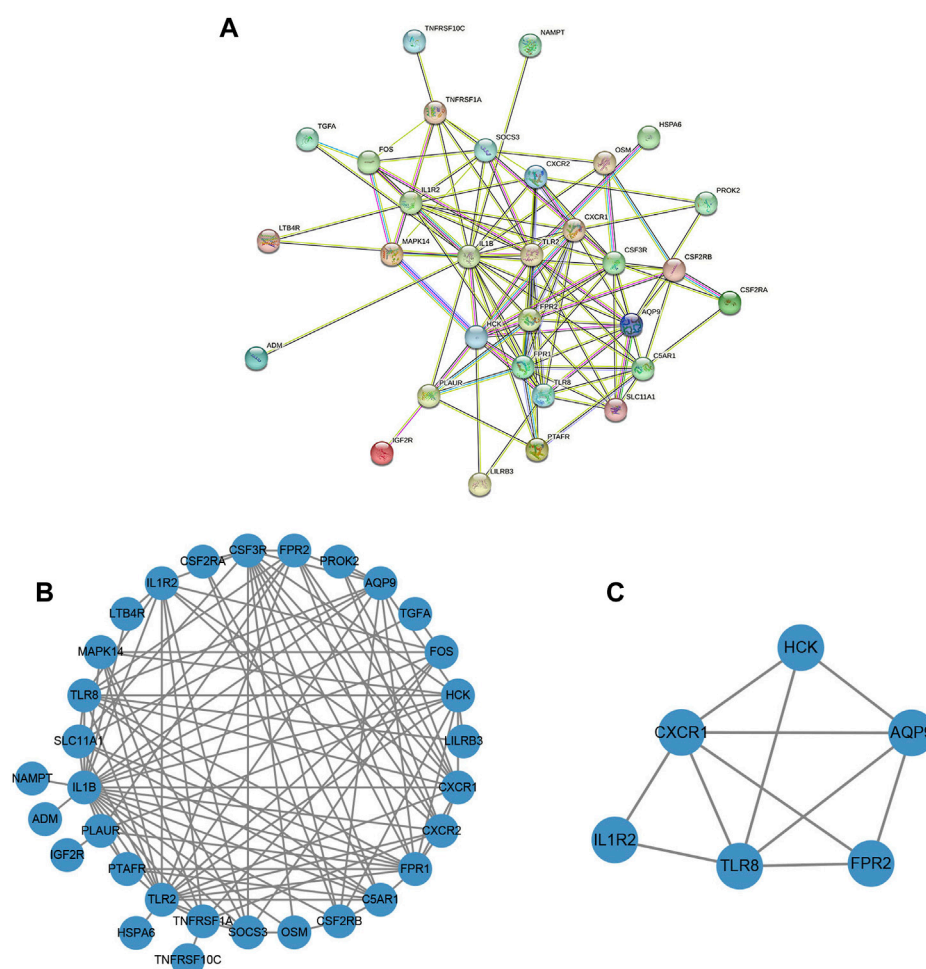


FIGURE 7

The construction of the PPI network and the identification of the hub genes. (A) PPI network based on the STRING database. (B) The PPI network was visualized by Cytoscape software. (C) Screening of clusters of genes that were highly connected using the MCODE algorithm.

were negatively correlated with the immune infiltration of naïve CD4 T cells, resting NK cells, and regulatory T cell (Figure 9).

mechanisms of these diagnostic genes and provided clues for further research.

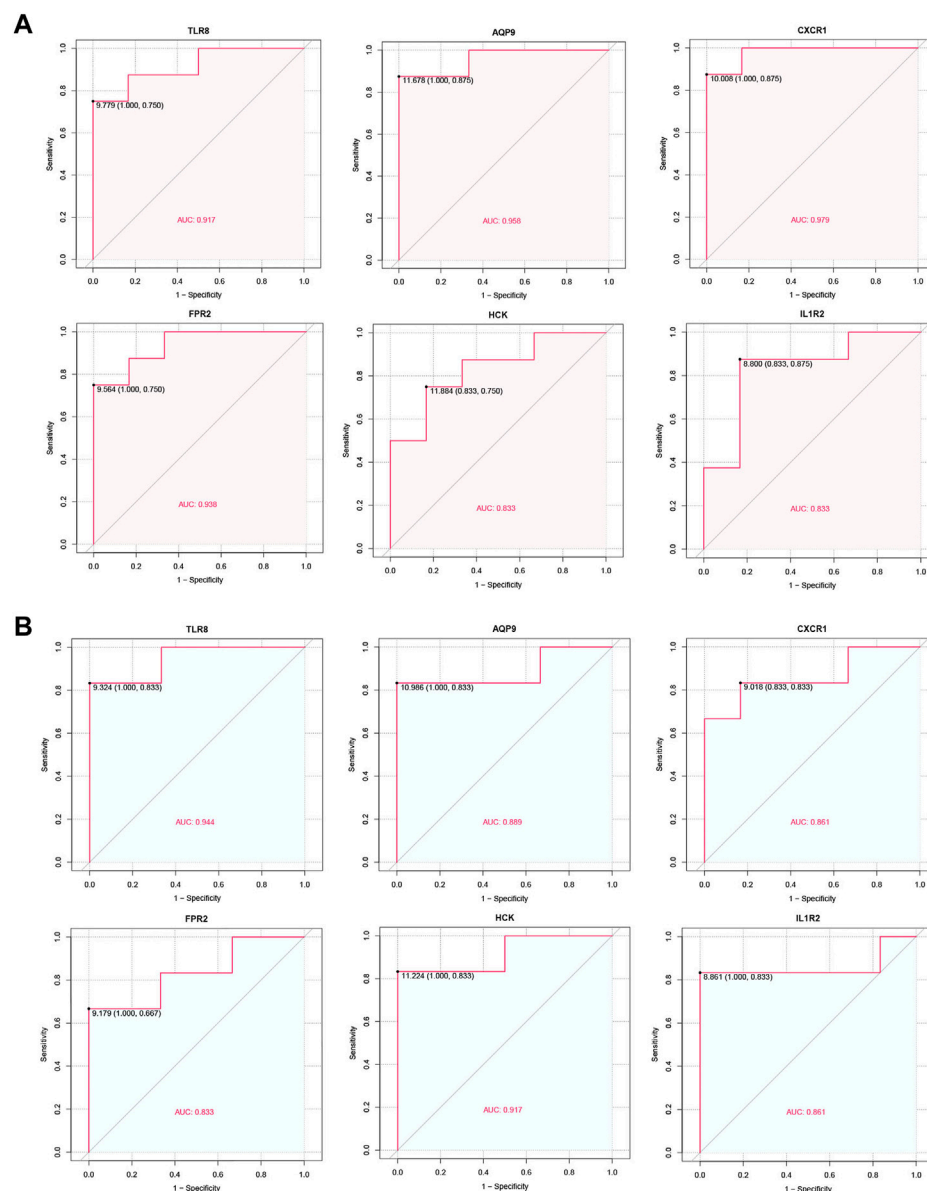
3.9 Prediction of key TF-, MiRNA-, and drug-diagnostic gene regulatory network

We used the NetworkAnalyst database to predict the TFs that may regulate diagnostic genes and generated a TF-diagnostic gene network (Figure 10A). The network consisted of 4 diagnostic genes and 34 TFs. Then the NetworkAnalyst database was used to predict related miRNAs and formed a regulatory network diagram (Figure 10B). This regulatory network diagram contained 5 diagnostic genes and 24 miRNAs, the most abundant of which were regulating IL1R2.

Finally, the DGIdb database was utilized and made it possible to search for potential drugs that might treat IVIG resistance. We found 36 potential therapeutic drugs and 11 of them were approved (Figure 10C; Supplementary Table S4). These results helped to deepen our understanding of the regulatory and intervention

4 Discussion

Kawasaki disease is an acute self-limiting febrile illness of unknown etiology that primarily affects children under 5 years of age (McCrindle et al., 2017). Prompt treatment of KD patients with IVIG has been shown to reduce the incidence of coronary artery aneurysms from 25% to less than 5% (Altammar and Lang, 2018). However, approximately 10%–20% of KD patients experience persistent or recurrent fever after standard treatment with IVIG and aspirin (Tremoulet et al., 2008; Tremoulet et al., 2014). Patients with IVIG resistance are at higher risk of developing coronary artery aneurysms (Hamada et al., 2019). Risk factors associated with IVIG resistance include male sex, young age, high C-reactive protein levels, high neutrophil count, and early presentation, among others (Lo and Newburger, 2018). Although there are currently some risk scoring systems that can predict the responsiveness of

**FIGURE 8**

ROC curve of the hub genes. (A) ROC curve of hub genes in the GSE48498. (B) ROC curve of hub genes in the GSE16797.

IVIG, they are not so accurate enough that no scoring systems are universally accepted (Wang et al., 2019). Recent studies have shown that immune cell infiltration is one of the important factors in the development of IVIG resistance in KD, but only a few studies have linked IVIG responsiveness to biomarkers related to the level of immune cell infiltration (Wu et al., 2020). Therefore, we aimed to explore the immunogenetic mechanisms of IVIG resistance in KD to screen for potential diagnostic indicators and signaling pathways in those patients. This study will help to better understand the pathogenesis and treatment of IVIG resistance and ultimately provide patients with more optimal treatment options.

This study explored the differences in immune cell infiltration between IVIG-resistant and IVIG-responsive patients by the CIBERSORT algorithm and found that neutrophil infiltration had

significant differences in the degree of infiltration. Similar results were reported in previous studies, indicating the important role of neutrophils in the pathogenesis of IVIG resistance. Studies showed that compared to IVIG-responsive patients, IVIG-resistant patients had a higher proportion of neutrophils, a higher neutrophil-to-lymphocyte ratio (NLR), and NLR was also considered to be a reliable predictor for IVIG resistance (Ha et al., 2020; Y. Chen et al., 2019; Liu and Wu, 2022). It could be seen that infiltrating immune cells were closely related to IVIG resistance, and the role of neutrophils was indispensable in the mechanism.

Next, the gene module with the highest score in the module-trait relationship diagram was screened through WGCNA analysis, which was the most correlated with neutrophil expression. By intersecting the module genes with the DEIGs, 34 DENGs were obtained. KEGG

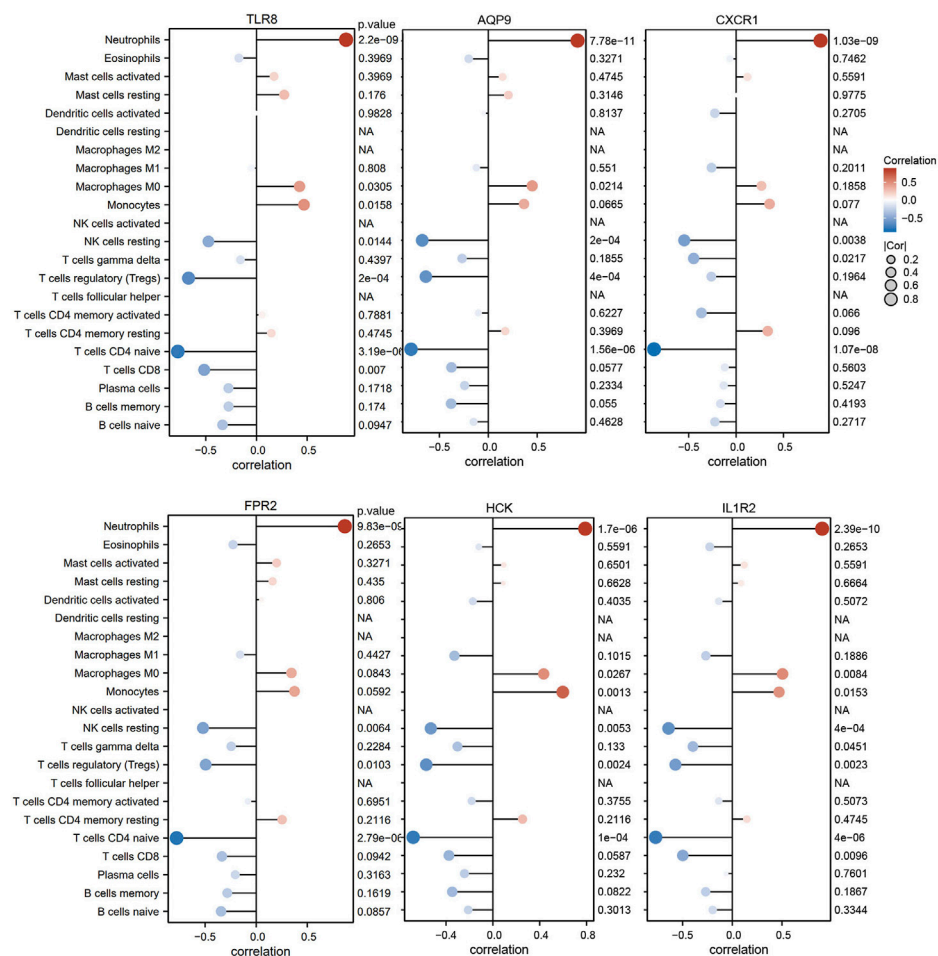


FIGURE 9

The correlation between diagnostic genes and infiltrating immune cells.

enrichment analysis showed that they were mainly concentrated in pathways such as cytokine-cytokine receptor interaction, neutrophil extracellular trap formation, and coronavirus disease - COVID-19, indicating their important biological functions in immune response and regulation. It is noteworthy that neutrophils contribute to pathogen clearance by forming neutrophil extracellular traps (NETs) in a process known as NETosis, but the excessive release of NETs has been reported to be involved in the pathogenesis of various diseases, including vasculitis, by inducing tissue injury (Grayson and Kaplan, 2016). In KD patients, neutrophils increase from the acute phase and decrease in the recovery phase; studies have shown that NET formation is enhanced in acute KD patients compared to recovery-phase KD patients and healthy controls (Yoshida et al., 2020). In addition, it has been found that neutrophils are significantly increased in the acute phase of KD patients, and are prone to forming NETs, which can significantly promote the activation of PI3K/Akt and NF- κ B signaling pathways in peripheral blood mononuclear cells (PBMCs) of KD patients, leading to upregulation of HIF-1 α and VEGF expression and triggering more severe inflammatory responses (Jing et al., 2020). This indicates that NETs are one of the mechanisms of Kawasaki disease, however, whether NETs can distinguish between IVIG-resistant and IVIG-responsive patients has not been proven by

previous research. Our data analysis results showed that the expression of neutrophils in the two groups of patients is significantly different, and the enriched pathway of differentially expressed genes contained NETs. Therefore, we believed that NET formation was expected to be an important mechanism of IVIG resistance. In addition, the pathway of coronavirus disease - COVID-19 is also closely related to neutrophils. It is reported that the number of neutrophils is considered as a clinical marker related to acute respiratory distress syndrome in COVID-19 patients (Oishi et al., 2022). Moreover, one study has also demonstrated that similar neutrophilic dysregulation occurs in severe COVID-19 and KD two pronounced hyperinflammatory states, which plays a crucial role in the overactivation and defective aging program of granulocytes (Chen K D et al., 2022). In short, based on the results of the KEGG enrichment analysis, we could conclude that these genes were more likely to be involved in neutrophil-related biological activities.

Finally, six hub genes, including TLR8, AQP9, CXCR1, FPR2, HCK, and IL1R2, were identified from the 34 DENGs by the MCODE algorithm. These hub genes may serve as diagnostic biomarkers for distinguishing IVIG-resistant patients from IVIG-responsive patients based on ROC curve analysis. Further investigation was conducted to explore the functions of each hub

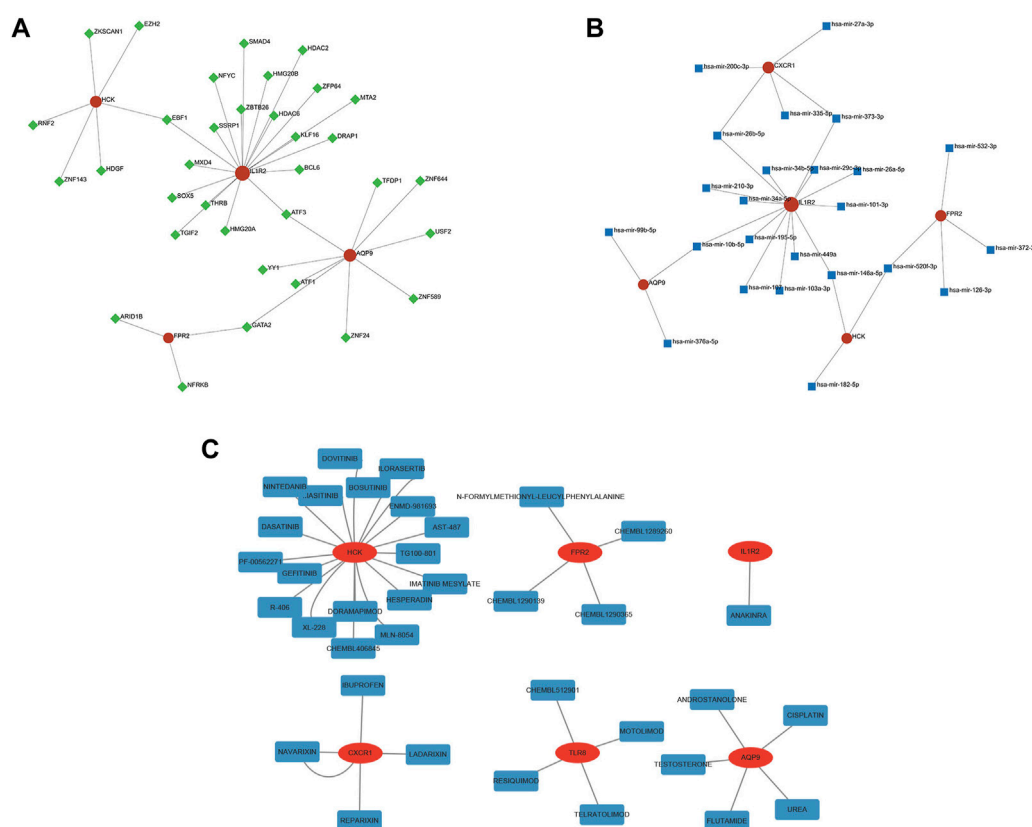


FIGURE 10

TF-, miRNA-, and drug-gene network of the diagnostic genes. (A) The TF network of HCK, IL1R2, AQP9, and FPR2. (B) The miRNA network of CXCR1, HCK, IL1R2, AQP9, and FPR2. (C) The drug-gene network of six diagnostic genes.

gene. TLR8, a member of the Toll-like receptor (TLR) family, is an intracellular type I transmembrane protein primarily expressed in human monocytes, macrophages, and neutrophils (Cai and Hu, 2022). Studies have indicated that TLR8 expression increases as a marker of M2 macrophages during the acute phase of KD (Guo et al., 2020). Aquaporins (AQPs) are transmembrane channels essential for water, energy, and redox homeostasis, with proven involvement in various pathophysiological conditions. AQP9 has been reported to be upregulated in patients with systemic inflammatory response syndrome compared to healthy individuals, and this is attributed to the functional impact of AQP9 on F-actin polymerization, leading to changes in the morphology and function of neutrophils (da Silva et al., 2022). CXC chemokine receptor-1 (CXCR1) is a representative chemokine receptor that initiates the neutrophil-mediated immune response pathway through its association with its homologous chemokine interleukin-8 (IL-8 or CXCL8) and can control the migration of neutrophils to infected tissues (Kharche et al., 2021). The formyl peptide receptors (FPRs) are G protein-coupled receptors, and formyl peptides act on FPR1 and FPR2, transducing chemotactic signals in phagocytes, and mediating host-defense as well as inflammatory responses including cell adhesion, directed migration, granule release, and superoxide production (He and Ye, 2017). It has been shown that the expression of FPR2 in the KD group is significantly higher than that in the healthy control

group, and the increase in FPR2 levels may be involved in the regulation of the *in vivo* balance of the immune system (Wang Y et al., 2022). Hematopoietic cell kinase (HCK) is a member of the Src family of non-receptor tyrosine kinases, which plays a critical role in neutrophil phagocytosis (Cheng et al., 2022). Studies have shown that HCK is a significantly upregulated hub gene in KD, but its specific mechanism of action is not yet clear (Cai and Hu, 2022). Interleukin-1 receptor type II (IL1R2) is a member of the interleukin-1 (IL-1) receptor family and is abnormally expressed in many inflammatory diseases (Chen Q et al., 2022). Studies have shown that IL1R2 is upregulated in IVIG-resistant KD, which is consistent with our research conclusion (Geng et al., 2020). Seen from the above gene functions, they are all related to the body's immune response and are highly correlated with neutrophils. This was also confirmed by Spearman's correlation analysis in our study.

What's more, we predicted the TFs and miRNAs that regulate the hub genes through the NetworkAnalyst database, then searched for potential therapeutic drugs by the DGIdb database, to further explore the regulatory mechanisms and intervention methods of these hub genes. Because these results were derived from continuously updated resources from papers, databases, and web resources that can provide directions for further research, the reliability of some of these predicted molecules will require experimental proof.

Despite yielding interesting results, there are some limitations in our study. Firstly, this study covered a relatively small sample size, and a larger sample cohort is needed to confirm the research results. Secondly, the lack of experimental validation may affect the accuracy of the study, so further experiments are needed to verify the biological mechanisms and treatment response. In addition, since our study only analyzed samples of KD patients who developed resistance or response to IVIG after use, it cannot be inferred that these genes can be used as diagnostic genes for IVIG resistance before treatment. Therefore, adopting KD patient samples that have already been diagnosed with IVIG resistance or response and analyzing their genes before IVIG use may help to identify IVIG resistance earlier and improve treatment plans as soon as possible.

All in all, the results of this study suggest new clues for the potential pathogenesis of IVIG resistance and provide valuable insights into the diagnosis and treatment of IVIG resistance. Previous studies have shown that the percentage of neutrophils in leukocytes, percentage of polymorphonuclear neutrophils, peripheral blood neutrophil-to-lymphocyte ratio, and neutrophil activation rate are higher in the IVIG-resistant group relative to the IVIG-responsive group (Sato et al., 2013; Kawamura et al., 2016; Kim, Song, and Kim, 2018; Ko et al., 2019). Our study found that immune pathways involved in hub genes, such as the formation of neutrophil extracellular traps, were more likely to result in IVIG resistance. And these hub genes, TLR8, AQP9, CXCR1, FPR2, HCK, and IL1R2, verified to be more or less associated with neutrophils, were possible to lead to IVIG resistance in KD. Therefore, our results corroborated previous literature and no longer stopped at clinical indicators, but explored more deeply at the genetic level. We believed that they may serve in the future as a more in-depth complement to the diagnostic model of IVIG resistance clinical indicators and important therapeutic targets that may help to reduce the incidence of coronary artery abnormalities and to improve the quality of life of KD patients.

5 Conclusion

In this study, we investigated potential signaling pathways and hub genes associated with immune infiltration involved in IVIG resistance, and the final identified hub genes included TLR8, AQP9, CXCR1, FPR2, HCK, and IL1R2. Additionally, we found that these signaling pathways and hub genes were closely related to neutrophils, which was confirmed by previous studies and Spearman's correlation analysis in our study. And six hub genes were validated that they could serve as reliable diagnostic biomarkers for IVIG resistance. Finally, their related TFs, miRNAs, and targeted drugs were predicted, which would provide new ideas and methods for further understanding the mechanism of IVIG resistance and help develop treatment strategies.

References

- Agarwal, S., and Agrawal, D. K. (2017). Kawasaki disease: Etiopathogenesis and novel treatment strategies. *Expert Rev. Clin. Immunol.* 13, 247–258. doi:10.1080/1744666X.2017.1232165
- Altammar, F., and Lang, B. (2018). Kawasaki disease in the neonate: Case report and literature review. *Pediatr. Rheumatol. Online J.* 16, 43. doi:10.1186/s12969-018-0263-8

Data availability statement

The original contributions presented in the study are included in the article/[Supplementary Material](#), further inquiries can be directed to the corresponding authors.

Author contributions

JL and JX designed the research. YW, YC, YL, and MY extracted the data from the databases. YW, YC, YL, and MY analysed the data. YW drafted the manuscript. JL and JX revised the manuscript. All authors contributed to the article and approved the submitted version.

Funding

This study was supported by the Natural Science Foundation of China (82271174) and the scientific research project of the Shanghai Municipal Health Commission (20204Y0100).

Acknowledgments

We would like to thank the GEO database for the availability of the data.

Conflict of interest

The authors declare that the research was conducted in the absence of any commercial or financial relationships that could be construed as a potential conflict of interest.

Publisher's note

All claims expressed in this article are solely those of the authors and do not necessarily represent those of their affiliated organizations, or those of the publisher, the editors and the reviewers. Any product that may be evaluated in this article, or claim that may be made by its manufacturer, is not guaranteed or endorsed by the publisher.

Supplementary material

The Supplementary Material for this article can be found online at: <https://www.frontiersin.org/articles/10.3389/fmolb.2023.1182512/full#supplementary-material>

- Bandettini, W. P., Kellman, P., Mancini, C., Booker, O. J., Vasu, S., Leung, S. W., et al. (2012). MultiContrast delayed enhancement (MCOE) improves detection of subendocardial myocardial infarction by late gadolinium enhancement cardiovascular magnetic resonance: A clinical validation study. *J. Cardiovasc. Magn. Reson.* 14 (1), 83. doi:10.1186/1532-429X-14-83
- Bhattacharya, S., Dunn, P., Thomas, C. G., Smith, B., Schaefer, H., Chen, J., et al. (2018). ImmPort, toward repurposing of open access immunological assay data for translational and clinical research. *Sci. Data* 5, 180015. doi:10.1038/sdata.2018.15
- Cai, Y., and Hu, W. (2022). Identifying differentially expressed genes and miRNAs in Kawasaki disease by bioinformatics analysis. *Sci. Rep.* 12, 21879. doi:10.1038/s41598-022-26608-x
- Chen, H., and Boutros, P. C. (2011). VennDiagram: A package for the generation of highly-customizable Venn and euler diagrams in R. *BMC Bioinforma.* 12, 35. doi:10.1186/1471-2105-12-35
- Chen, K. D., Huang, Y. H., Wu, W. S., Chang, L. S., Chu, C. L., and Kuo, H. C. (2022). Comparable bidirectional neutrophil immune dysregulation between Kawasaki disease and severe COVID-19. *Front. Immunol.* 13, 995886. doi:10.3389/fimmu.2022.995886
- Chen, Q. Q., Li, Z., Wang, M., and Li, G. (2022). Over-expression of IL1R2 in PBMCs of patients with coronary artery disease and its clinical significance. *Anatol. J. Cardiol.* 26, 710–716. doi:10.5152/AnatolJCardiol.2022.1241
- Chen, Y., Hua, Y., Zhang, C., Chen, S., Zhang, Q., Liao, Y., et al. (2019). Neutrophil-to-Lymphocyte ratio predicts intravenous immunoglobulin-resistance in infants under 12-months old with Kawasaki disease. *Front. Pediatr.* 7, 81. doi:10.3389/fped.2019.00081
- Cheng, F., Li, Q., Wang, J., Wang, L., Li, W., and Zeng, F. (2022). HCK is a potential prognostic biomarker that correlates with immune cell infiltration in acute myeloid leukemia. *Dis. Markers* 2022, 3199589. doi:10.1155/2022/3199589
- Cotto, K. C., Wagner, A. H., Feng, Y. Y., Kiwala, S., Coffman, A. C., Spies, G., et al. (2018). DGIdb 3.0: A redesign and expansion of the drug-gene interaction database. *Nucleic Acids Res.* 46, D1068–D1073. doi:10.1093/nar/gkx1143
- da Silva, I. V., Garra, S., Calamita, G., and Soveral, G. (2022). The multifaceted role of aquaporin-9 in Health and its potential as a clinical biomarker. *Biomolecules* 12, 897. doi:10.3390/biom12070897
- Diboun, I., Wernisch, L., Orengo, C. A., and Koltzenburg, M. (2006). Microarray analysis after RNA amplification can detect pronounced differences in gene expression using limma. *BMC Genomics* 7, 252. doi:10.1186/1471-2164-7-252
- ENCODE Project Consortium (2011). A user's guide to the encyclopedia of DNA elements (ENCODE). *PLoS Biol.* 9, e1001046. doi:10.1371/journal.pbio.1001046
- Fukui, S., Seki, M., Minami, T., Kotani, K., Oka, K., Yokomizo, A., et al. (2021). Efficacy and safety associated with the infusion speed of intravenous immunoglobulin for the treatment of Kawasaki disease: A randomized controlled trial. *Pediatr. Rheumatol. Online J.* 19, 107. doi:10.1186/s12969-021-00601-6
- Gautier, L., Cope, L., Bolstad, B. M., and Irizarry, R. A. (2004). affy-analysis of Affymetrix GeneChip data at the probe level. *Bioinformatics* 20, 307–315. doi:10.1093/bioinformatics/btg405
- Geng, Z., Liu, J., Hu, J., Wang, Y., Tao, Y., Zheng, F., et al. (2020). Crucial transcripts predict response to initial immunoglobulin treatment in acute Kawasaki disease. *Sci. Rep.* 10, 17860. doi:10.1038/s41598-020-75039-z
- Grayson, P. C., and Kaplan, M. J. (2016). At the Bench: Neutrophil extracellular traps (NETs) highlight novel aspects of innate immune system involvement in autoimmune diseases. *J. Leukoc. Biol.* 99, 253–264. doi:10.1189/jlb.5BT0615-247R
- Guo, M. M. H., Chang, L. S., Huang, Y. H., Wang, F. S., and Kuo, H. C. (2020). Epigenetic regulation of macrophage marker expression profiles in Kawasaki disease. *Front. Pediatr.* 8, 129. doi:10.3389/fped.2020.00129
- Ha, K. S., Lee, J., and Lee, K. C. (2020). Prediction of intravenous immunoglobulin resistance in patients with Kawasaki disease according to the duration of illness prior to treatment. *Eur. J. Pediatr.* 179, 257–264. doi:10.1007/s00431-019-03474-w
- Hamada, H., Suzuki, H., Onouchi, Y., Ebata, R., Terai, M., Fuse, S., et al. (2019). Efficacy of primary treatment with immunoglobulin plus ciclosporin for prevention of coronary artery abnormalities in patients with Kawasaki disease predicted to be at increased risk of non-response to intravenous immunoglobulin (KAICA): A randomised controlled, open-label, blinded-endpoints, phase 3 trial. *Lancet* 393, 1128–1137. doi:10.1016/S0140-6736(18)32003-8
- Han, S. B., Suh, W., and Rhim, J. W. (2022). High-concentration intravenous immunoglobulin may influence the course of fever and rate of reported treatment resistance in children with Kawasaki disease: A single-center retrospective analysis. *Paediatr. Drugs* 24, 689–697. doi:10.1007/s40272-022-00537-8
- Harbron, C., Chang, K. M., and South, M. C. (2007). RefPlus: an R package extending the RMA Algorithm. *Bioinformatics* 23, 2493–2494. doi:10.1093/bioinformatics/btm357
- He, H. Q., and Ye, R. D. (2017). The formyl peptide receptors: Diversity of ligands and mechanism for recognition. *Molecules* 22, 455. doi:10.3390/molecules22030455
- Hedrich, C. M., Schnabel, A., and Hospach, T. (2018). Kawasaki disease. *Front. Pediatr.* 6, 198. doi:10.3389/fped.2018.00198
- Huang, H. Y., Lin, Y. C., Cui, S., Huang, Y., Tang, Y., Xu, J., et al. (2022). miRTarBase update 2022: an informative resource for experimentally validated miRNA-target interactions. *Nucleic Acids Res.* 50, D222–D230. doi:10.1093/nar/gkab1079
- Jing, Y., Ding, M., Fu, J., Xiao, Y., Chen, X., and Zhang, Q. (2020). Neutrophil extracellular trap from Kawasaki disease alter the biologic responses of PBMC. *Biosci. Rep.* 40, BSR20200928. doi:10.1042/BSR20200928
- Kawamura, Y., Takeshita, S., Kanai, T., Yoshida, Y., and Nonoyama, S. (2016). The combined usefulness of the neutrophil-to-lymphocyte and platelet-to-lymphocyte ratios in predicting intravenous immunoglobulin resistance with Kawasaki disease. *J. Pediatr.* 178, 281–284. doi:10.1016/j.jpeds.2016.07.035
- Kaya Akca, U., Arslanoglu Aydin, E., Aykan, H. H., Serin, O., Sag, E., Demir, S., et al. (2022). Comparison of IVIG resistance predictive models in Kawasaki disease. *Pediatr. Res.* 91, 621–626. doi:10.1038/s41390-021-01459-w
- Kharche, S., Joshi, M., Chattopadhyay, A., and Sengupta, D. (2021). Conformational plasticity and dynamic interactions of the N-terminal domain of the chemokine receptor CXCR1. *PLoS Comput. Biol.* 17, e1008593. doi:10.1371/journal.pcbi.1008593
- Kim, M. K., Song, M. S., and Kim, G. B. (2018). Factors predicting resistance to intravenous immunoglobulin treatment and coronary artery lesion in patients with Kawasaki disease: Analysis of the Korean nationwide multicenter survey from 2012 to 2014. *Korean Circ. J.* 48 (1), 71–79. doi:10.4070/kcj.2017.0136
- Ko, T. M., Chang, J. S., Chen, S. P., Liu, Y. M., Chang, C. J., Tsai, F. J., et al. (2019). Genome-wide transcriptome analysis to further understand neutrophil activation and lncRNA transcript profiles in Kawasaki disease. *Sci. Rep.* 9 (1), 328. doi:10.1038/s41598-018-36520-y
- Langfelder, P., and Horvath, S. (2008). Wgcna: an R package for weighted correlation network analysis. *BMC Bioinforma.* 9, 559. doi:10.1186/1471-2105-9-559
- Lee, H. Y., and Song, M. S. (2016). Predictive factors of resistance to intravenous immunoglobulin and coronary artery lesions in Kawasaki disease. *Korean J. Pediatr.* 59, 477–482. doi:10.3345/kjp.2016.59.12.477
- Leek, J. T., Johnson, W. E., Parker, H. S., Jaffe, A. E., and Storey, J. D. (2012). The sva package for removing batch effects and other unwanted variation in high-throughput experiments. *Bioinformatics* 28, 882–883. doi:10.1093/bioinformatics/bts034
- Liu, C., and Wu, J. (2022). Value of blood inflammatory markers for predicting intravenous immunoglobulin resistance in Kawasaki disease: A systematic review and meta-analysis. *Front. Pediatr.* 10, 969502. doi:10.3389/fped.2022.969502
- Lo, M. S., and Newburger, J. W. (2018). Role of intravenous immunoglobulin in the treatment of Kawasaki disease. *Int. J. Rheum. Dis.* 21, 64–69. doi:10.1111/1756-185X.13220
- McCordle, B. W., Rowley, A. H., Newburger, J. W., Burns, J. C., Bolger, A. F., Gewitz, M., et al. (2017). Diagnosis, treatment, and long-term management of Kawasaki disease: A scientific statement for Health professionals from the American heart association. *Circulation* 135, e927–e999. doi:10.1161/CIR.0000000000000484
- Metsalu, T., and Vilo, J. (2015). ClustVis: A web tool for visualizing clustering of multivariate data using principal component analysis and heatmap. *Nucleic Acids Res.* 43, W566–W570. doi:10.1093/nar/gkv468
- Newburger, J. W., Takahashi, M., and Burns, J. C. D. (2016). Kawasaki disease. *J. Am. Coll. Cardiol.* 67, 1738–1749. doi:10.1016/j.jacc.2015.12.073
- Newman, A. M., Liu, C. L., Green, M. R., Gentles, A. J., Feng, W., Xu, Y., et al. (2015). Robust enumeration of cell subsets from tissue expression profiles. *Nat. Methods* 12, 453–457. doi:10.1038/nmeth.3337
- Ogihara, Y., Ogata, S., Nomoto, K., Ebata, T., Sato, K., Kokubo, K., et al. (2009). Clinical score and transcript abundance patterns identify Kawasaki disease patients who may benefit from addition of methylprednisolone. *Pediatr. Res.* 66, 577–584. doi:10.1203/PDR.0b013e3181baa3c2
- Ogihara, Y., Ogata, S., Nomoto, K., Ebata, T., Sato, K., Kokubo, K., et al. (2014). Transcriptional regulation by infliximab therapy in Kawasaki disease patients with immunoglobulin resistance. *Pediatr. Res.* 76, 287–293. doi:10.1038/pr.2014.92
- Oishi, K., Horiuchi, S., Frere, J., Schwartz, R. E., and tenOever, B. R. (2022). A diminished immune response underlies age-related SARS-CoV-2 pathologies. *Cell Rep.* 39, 111002. doi:10.1016/j.celrep.2022.111002
- Parodi, S., Verda, D., Bagnasco, F., and Muselli, M. (2022). The clinical meaning of the area under a receiver operating characteristic curve for the evaluation of the performance of disease markers. *Epidemiol. Health* 44, e2022088. doi:10.4178/epih.e2022088
- Pripp, A. H. (2018). Pearson's or Spearman's correlation coefficients. *Tidsskr. Nor. Lægeforen* 138. doi:10.4045/tidsskr.18.0042
- Rife, E., and Gedalia, A. (2020). Kawasaki disease: An update. *Curr. Rheumatol. Rep.* 22, 75. doi:10.1007/s11926-020-00941-4
- Robin, X., Turck, N., Hainard, A., Tiberti, N., Lisacek, F., Sanchez, J. C., et al. (2011). pROC: an open-source package for R and S+ to analyze and compare ROC curves. *BMC Bioinforma.* 12, 77. doi:10.1186/1471-2105-12-77
- Sato, S., Kawashima, H., Kashiwagi, Y., and Hoshika, A. (2013). Inflammatory cytokines as predictors of resistance to intravenous immunoglobulin therapy in Kawasaki disease patients. *Int. J. Rheum. Dis.* 16, 168–172. doi:10.1111/1756-185X.12082

- Shannon, P., Markiel, A., Ozier, O., Baliga, N. S., Wang, J. T., Ramage, D., et al. (2003). Cytoscape: A software environment for integrated models of biomolecular interaction networks. *Genome Res.* 13, 2498–2504. doi:10.1101/gr.1239303
- Shuai, M., He, D., and Chen, X. (2021). Optimizing weighted gene co-expression network analysis with a multi-threaded calculation of the topological overlap matrix. *Stat. Appl. Genet. Mol. Biol.* 20, 145–153. doi:10.1515/sagmb-2021-0025
- Song, M. S. (2019). Predictors and management of intravenous immunoglobulin-resistant Kawasaki disease. *Korean J. Pediatr.* 62, 119–123. doi:10.3345/kjp.2019.00150
- Szklarczyk, D., Morris, J. H., Cook, H., Kuhn, M., Wyder, S., Simonovic, M., et al. (2017). The STRING database in 2017: Quality-controlled protein-protein association networks, made broadly accessible. *Nucleic Acids Res.* 45, D362–D368. doi:10.1093/nar/gkw937
- Tremoulet, A. H., Best, B. M., Song, S., Wang, S., Corinaldesi, E., Eichenfield, J. R., et al. (2008). Resistance to intravenous immunoglobulin in children with Kawasaki disease. *J. Pediatr.* 153, 117–121. doi:10.1016/j.jpeds.2007.12.021
- Tremoulet, A. H., Jain, S., Jaggi, P., Jimenez-Fernandez, S., Pancheri, J. M., Sun, X., et al. (2014). Infliximab for intensification of primary therapy for Kawasaki disease: A phase 3 randomised, double-blind, placebo-controlled trial. *Lancet* 383, 1731–1738. doi:10.1016/S0140-6736(13)62298-9
- Wang, H., Shang, J., Tong, M., Song, Y., and Ruan, L. (2019). Evaluation of left ventricular function in immunoglobulin-resistant children with Kawasaki disease: A two-dimensional speckle tracking echocardiography study. *Clin. Cardiol.* 42, 753–759. doi:10.1002/clc.23213
- Wang, T., Liu, G., Guo, X., and Ji, W. (2022). Single-cell analysis reveals the role of the neuropeptide receptor FPR2 in monocytes in Kawasaki disease: A bioinformatic study. *Dis. Markers* 2022, 1666240. doi:10.1155/2022/1666240
- Wang, Y., Zhou, W., Chen, Y., He, D., Qin, Z., Wang, Z., et al. (2022). Identification of susceptibility modules and hub genes of osteoarthritis by WGCNA analysis. *Front. Genet.* 13, 1036156. doi:10.3389/fgene.2022.1036156
- Wu, G., Yue, P., Ma, F., Zhang, Y., Zheng, X., and Li, Y. (2020). Neutrophil-to-lymphocyte ratio as a biomarker for predicting the intravenous immunoglobulin-resistant Kawasaki disease. *Med. Baltim.* 99, e18535. doi:10.1097/MD.00000000000018535
- Ye, Q., Gong, F. Q., Shang, S. Q., and Hu, J. (2016). Intravenous immunoglobulin treatment responsiveness depends on the degree of CD8+ T cell activation in Kawasaki disease. *Clin. Immunol.* 171, 25–31. doi:10.1016/j.clim.2016.08.012
- Yoshida, Y., Takeshita, S., Kawamura, Y., Kanai, T., Tsujita, Y., and Nonoyama, S. (2020). Enhanced formation of neutrophil extracellular traps in Kawasaki disease. *Pediatr. Res.* 87, 998–1004. doi:10.1038/s41390-019-0710-3
- Yu, G., Wang, L. G., Han, Y., and He, Q. Y. (2012). clusterProfiler: an R package for comparing biological themes among gene clusters. *OMICS* 16, 284–287. doi:10.1089/omi.2011.0118
- Zhou, G., Soufan, O., Ewald, J., Hancock, R. E. W., Basu, N., and Xia, J. (2019). NetworkAnalyst 3.0: A visual analytics platform for comprehensive gene expression profiling and meta-analysis. *Nucleic Acids Res.* 47, W234–W241–W241. doi:10.1093/nar/gkz240



OPEN ACCESS

EDITED BY

Alexander V. Glushakov,
University of Virginia, United States

REVIEWED BY

Kunju Zhu,
University of Pittsburgh, United States
Liang Yang,
Yanan University, China

*CORRESPONDENCE

Aristidis Tsatsakis,
✉ tsatsaka@uoc.gr
Evangelia Sarandi,
✉ esarandi6@hotmail.com

RECEIVED 07 April 2023

ACCEPTED 05 June 2023

PUBLISHED 19 June 2023

CITATION

Sarandi E, Krueger-Krasagakis S,
Tsoukalas D, Sidiropoulou P,
Evangelou G, Sifaki M, Rudofsky G,
Drakoulis N and Tsatsakis A (2023),
Psoriasis immunometabolism: progress
on metabolic biomarkers and
targeted therapy.
Front. Mol. Biosci. 10:1201912.
doi: 10.3389/fmolb.2023.1201912

COPYRIGHT

© 2023 Sarandi, Krueger-Krasagakis,
Tsoukalas, Sidiropoulou, Evangelou,
Sifaki, Rudofsky, Drakoulis and Tsatsakis.
This is an open-access article distributed
under the terms of the [Creative
Commons Attribution License \(CC BY\)](#).
The use, distribution or reproduction in
other forums is permitted, provided the
original author(s) and the copyright
owner(s) are credited and that the original
publication in this journal is cited, in
accordance with accepted academic
practice. No use, distribution or
reproduction is permitted which does not
comply with these terms.

Psoriasis immunometabolism: progress on metabolic biomarkers and targeted therapy

Evangelia Sarandi^{1,2*}, Sabine Krueger-Krasagakis³,
Dimitris Tsoukalas^{2,4}, Polytimi Sidiropoulou^{5,6},
George Evangelou³, Maria Sifaki⁶, Gottfried Rudofsky⁷,
Nikolaos Drakoulis⁶ and Aristidis Tsatsakis^{1*}

¹Laboratory of Toxicology and Forensic Sciences, Medical School, University of Crete, Heraklion, Greece,

²Metabolomic Medicine, Health Clinics for Autoimmune and Chronic Diseases, Athens, Greece,

³Dermatology Department, University Hospital of Heraklion, Heraklion, Greece, ⁴European Institute of
Molecular Medicine, Rome, Italy, ⁵1st Department of Dermatology-Venereology, Faculty of Medicine, "A.
Sygros" Hospital, National and Kapodistrian University of Athens, Athens, Greece, ⁶Research Group of
Clinical Pharmacology and Pharmacogenomics, Faculty of Pharmacy, School of Health Sciences, National
and Kapodistrian University of Athens, Athens, Greece, ⁷Clinic of Endocrinology and Metabolic Disorders,
Cantonal Hospital Olten, Olten, Switzerland

Psoriasis is a common inflammatory disease that affects mainly the skin. However, the moderate to severe forms have been associated with several comorbidities, such as psoriatic arthritis, Crohn's disease, metabolic syndrome and cardiovascular disease. Keratinocytes and T helper cells are the dominant cell types involved in psoriasis development via a complex crosstalk between epithelial cells, peripheral immune cells and immune cells residing in the skin. Immunometabolism has emerged as a potent mechanism elucidating the aetiopathogenesis of psoriasis, offering novel specific targets to diagnose and treat psoriasis early. The present article discusses the metabolic reprogramming of activated T cells, tissue-resident memory T cells and keratinocytes in psoriatic skin, presenting associated metabolic biomarkers and therapeutic targets. In psoriatic phenotype, keratinocytes and activated T cells are glycolysis dependent and are characterized by disruptions in the TCA cycle, the amino acid metabolism and the fatty acid metabolism. Upregulation of the mammalian target of rapamycin (mTOR) results in hyperproliferation and cytokine secretion by immune cells and keratinocytes. Metabolic reprogramming through the inhibition of affected metabolic pathways and the dietary restoration of metabolic imbalances may thus present a potent therapeutic opportunity to achieve long-term management of psoriasis and improved quality of life with minimum adverse effects.

KEYWORDS

psoriasis, T cell, keratinocyte, glycolysis, lipid metabolism, TCA, biomarkers, metabolic targets

1 Introduction

Plaque-type psoriasis is a common immune-mediated inflammatory skin disease involving skin-homing pathogenic T cells, dendritic cells, keratinocytes and their cytokines in its complex pathogenesis. An imbalance between Th1/Th17 axes seems to be a common feature in the psoriatic cascade through the secretion of pro-inflammatory cytokines that promote keratinocyte proliferation (Vollmer et al., 1994; Lowes et al., 2008; Hu et al., 2021). In synergy with Th1 and Th17, the IL-22-secreting T cells have been

identified as indispensable contributors to the development of psoriatic lesions along with IL-23-producing myeloid cells (Schön and Erpenbeck, 2018). In addition, psoriatic lesions are characterized by impaired regulation of excess immune response due to functional defects of regulatory T cells (Tregs) (Sugiyama et al., 2005). Keratinocytes are appreciated as initiators of the immune response through the production of autoantigens and in the establishment of the disease through the crosstalk with adaptive immunity cells that aggravates the cytokine milieu and intensifies chronic inflammation (Lande et al., 2007; Hawkes et al., 2017; Zhou et al., 2022).

Epidemiological data on psoriasis are scarce, considering that only 19% of the countries worldwide have available data. However, it is estimated that psoriasis prevalence ranges from 0.11% in East Asia to 3.61% in Denmark and 3% in the United States, collectively affecting over 125 million people worldwide (Parisi et al., 2020; Armstrong et al., 2021; National Psoriasis Foundation, 2022). Psoriasis is characterized by increased comorbidities, such as psoriatic arthritis, Crohn's disease and cardiometabolic diseases (Takeshita et al., 2017) and significant quality of life compromise (Stern et al., 2004). Several studies have indicated that metabolic complications implicate a higher risk of developing psoriasis and directly correlate with disease severity and worse therapeutic outcomes (Polic et al., 2018; Hao et al., 2021; Lee et al., 2021). Since different subsets of helper cells have been considered key players in psoriasis' immunological pathways, interest has increasingly been focused on elucidating the impact of metabolism on the immune system's function of psoriasis patients.

In this sense, the evolving field of immunometabolism, linking immunology and metabolism, could provide critical points for investigating how metabolic cellular reactions and processes may control immunity and inflammation, offering novel tools for monitoring and managing immune-mediated diseases, including psoriasis.

Given that emerging evidence suggests targeting specific metabolic events as a strategy to limit cutaneous inflammation, this review will first focus on the potential mechanisms underlying the association between the metabolic reprogramming of the critical cell players and inflammatory skin responses of psoriasis. Potential metabolic biomarkers and therapeutic anti-psoriatic approaches integrating immune/metabolic responses from the published literature are also summarized.

2 Pathogenetic mechanism of psoriasis

Psoriasis is widely regarded as a multifactorial immune-related disease triggered by environmental factors in the background of genetic predisposition. Although the precise pathogenetic mechanisms have yet to be deciphered, psoriasis seems to be controlled by endogenous and exogenous factors.

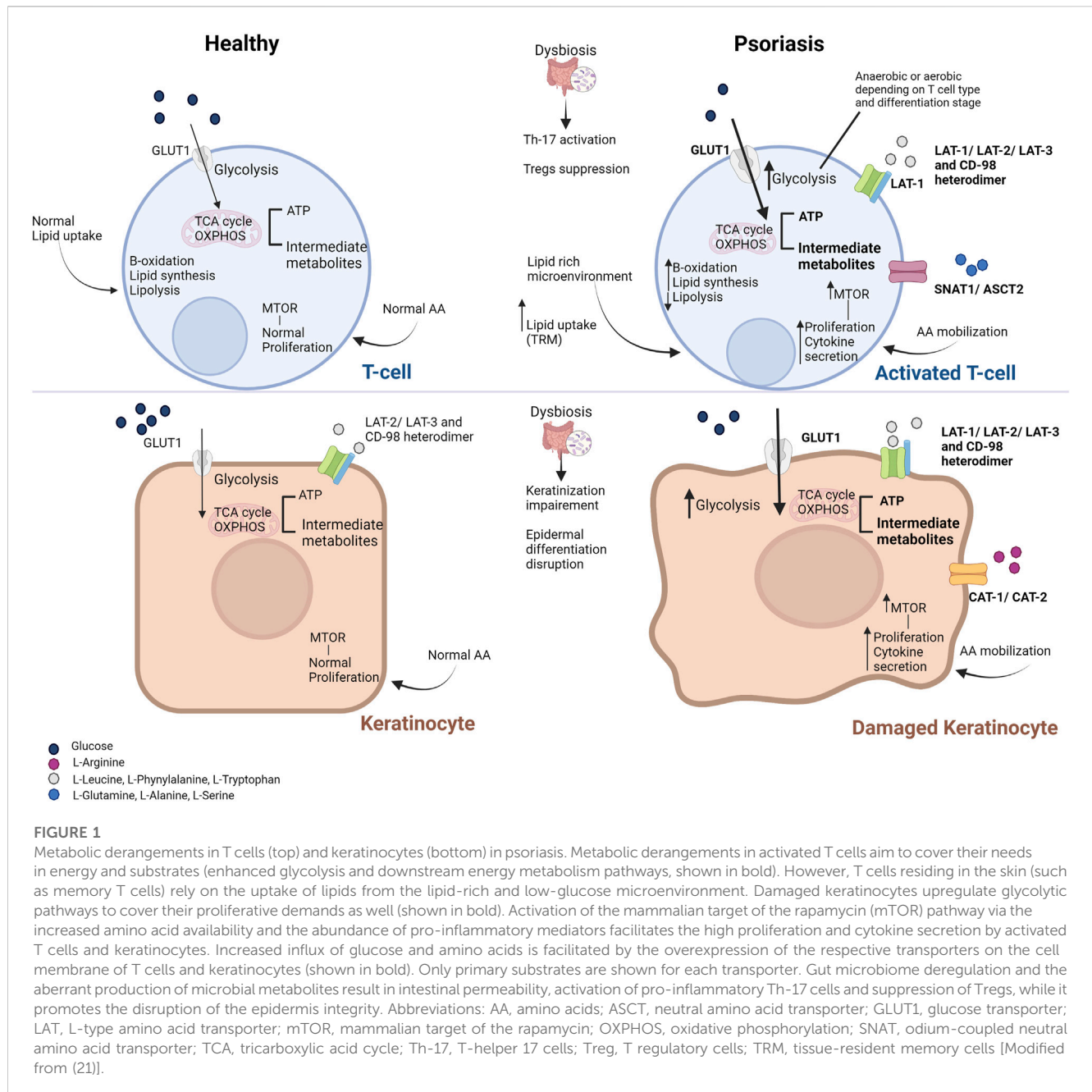
The genetic basis of psoriasis has been supported by family and twin studies suggesting a higher incidence of psoriasis within families and in monozygotic twins than in dizygotic twins. Genome-wide association studies have indicated thirteen different genetic regions, known as Psoriasis Susceptibility (PSORS)1-13, contributing to disease susceptibility. The PSORS1, located within the Major Histocompatibility Complex

(MHC) on chromosome 6p21, is the primary locus for psoriasis susceptibility. The HLA-Cw6 is one of this region's most strongly associated alleles affecting disease onset, course, severity, comorbidities, and treatment outcomes (Chen and Tsai, 2018). Although the exact role of HLA-C in psoriasis development remains unclear, there seems to be an interplay/relation between HLA-Cw6 status and immune dysregulation in psoriasis patients.

While genetic factors are well documented in psoriasis, several environmental triggers, such as mechanical skin trauma and inflammation, infections, drugs, smoking, excessive alcohol intake, mental stress and microbiota/diet, and epigenetic modifications, may induce, trigger or exacerbate the disease.

The mechanism through which external factors contribute to the irregular proliferation of keratinocytes and the progression to psoriatic lesions involves innate and adaptive immunity cells (Armstrong and Read, 2020). Briefly, after exposure to non-genetic triggers of psoriasis, damaged keratinocytes express antimicrobial peptides (AMPs), including cathelicidin (LL-37), β -defensins, and S100 proteins (psoriasin and Koebnerisin), self-DNA and pro-inflammatory cytokines. The most well-studied AMP is LL-37 which, when produced by damaged keratinocytes, forms aggregates with self-DNA and, along with secreted pro-inflammatory cytokines, results in the activation of plasmacytoid dendritic cells (pDCs) and natural killer cells (NK). Activated pDCs and NK cells secrete interferon-alpha (IFN- α), interferon-gamma (IFN- γ), and tumor necrosis factor-alpha (TNF- α), which activate myeloid dendritic cells (mDCs) to migrate in the lymph node. In turn, mDCs produce interleukin-12 (IL-12) and interleukin-23 (IL-23), resulting in the differentiation of naïve T cells to Th-1 and Th-17 cells, respectively. The differentiation step of naïve T cells into effector cells, mainly Th17 cells, is critical for disease maintenance. Activated T cells migrate from the lymph nodes to the skin microenvironment where Th17 cells secrete interleukin-22 (IL-22), interleukin-17 (IL-17) and TNF- α , and activated Th1 cells secrete TNF- α and IFN- γ . These secreted cytokines induce keratinocyte proliferation, differentiation and further production of antimicrobial peptides and pro-inflammatory cytokines in a feedback loop that causes psoriasis symptomatology. In established psoriasis, premature keratinocytes are abundant throughout the epidermis, causing parakeratosis and the scales along with increased levels of infiltrated immune cells in the epidermis (DCs, macrophages and T cells) and the dermis (mainly neutrophils and some T cells) (Nestle et al., 2009; Armstrong and Read, 2020; Ni and Lai, 2020).

The presence of autoantigens which trigger the expansion of autoreactive T cells has prompted researchers to investigate psoriasis as an autoimmune disease. Up to date, LL-37, ADAMTSL5, PLA2G4D and keratin 17 are the most well-studied autoantigens of psoriasis associated with the presence of autoreactive T cells. On the other hand, antibodies against the autoantigens anti-LL37 and ADAMTSL6 have been observed in the serum of patients with psoriatic arthritis and some patients with psoriasis, supporting the autoimmune nature of psoriasis (Frasca et al., 2018; Yuan et al., 2019; Ten Bergen et al., 2020). However, the lack of adequate data and the specific role of autoantibodies in the inflammatory cascade that initiate psoriasis have stalled the unwinding progression to the disease etiology.



3 Metabolic aspects of psoriasis

One of the most common comorbidities of psoriasis is metabolic syndrome (MetS), including related cardiometabolic disturbances such as insulin resistance (IR), obesity, diabetes and dyslipidemia. Increasing evidence suggests that patients with higher psoriasis area and severity index (PASI) score have more severe MetS phenotype indicating potential interconnection between psoriasis and MetS. Studies focusing on the overlapping mechanisms of psoriasis and metabolic diseases have yielded encouraging results for unraveling disease pathogenesis, prompting researchers to further study the metabolic aspects of psoriasis. As described in a recent review, endoplasmic reticulum stress, reactive oxygen species, gut dysbiosis and adipocytokines levels comprise the main factors linking psoriasis

pathogenesis with MetS (Hao et al., 2021). However, in a separate study, psoriasis severity was associated with insulin resistance independently of MetS. Insulin resistance is a metabolic disturbance occurring in obese but also lean-healthy individuals as an early indicator of a pre-diabetic state (Polc et al., 2018). This was also observed in psoriasis, where body mass index (BMI) and waist circumference did not affect IR association with disease severity (Eckel et al., 2015). However, patients with psoriasis are not monitored for insulin resistance and other metabolic complications by their physicians, preventing other comorbidities. Metabolic state profiling is a relatively new field in clinical practice due to the limited established biomarkers, yet it fills the gap in prevention, prediction, diagnosis of metabolic comorbidities and treatment response monitoring as part of precision medicine (Newgard, 2017).

3.1 Metabolic reprogramming in psoriasis

Immune cell infiltration and cytokine-driven aberrant keratinocyte overgrowth and differentiation are prominent features of psoriasis lesions. Both keratinocytes and immunocompetent cells can actively metabolize nutrients in their microenvironment (Nestle et al., 2009), suggesting increased cell nutritional requirements in psoriatic skin. As a result, proliferating epidermal and immune cells seem to undergo similar or specific metabolic rewiring to fuel the anabolic pathways and cytokine release (Kamleh et al., 2015) (Figure 1).

3.1.1 Derangements in cellular metabolism

Under normal conditions, keratinocytes use glucose to produce energy via the glycolysis pathway and largely depend on glucose transporter 1 (GLUT1) for glucose uptake. Upon activation, such as in psoriasis-associated hyperplasia, GLUT1 expression is upregulated to meet the proliferating keratinocytes' elevated metabolic and biosynthetic demands/needs (Cibrian et al., 2020a; Pålsson-McDermott and O'Neill, 2020). The levels of GLUT1 expression seem to correlate with the PASI score, promoting histological alterations, such as epidermal thickness, inflammatory infiltrate density, microvessel density, and Ki-67 expression (Nestle et al., 2009). Genetic or chemical targeting of GLUT1 in keratinocytes could decrease (imiquimod (IMQ)-induced) psoriasiform hyperplasia in animal models (Zhang et al., 2018; Cibrian et al., 2020a). In addition, (topical) pharmacological inhibition of GLUT1 could block inflammatory gene expression and significantly suppress inflammatory infiltration and cytokine secretion in skin biopsies from psoriasis patients, suggesting that infiltrating lymphocytes can also be targeted (Zhang et al., 2018; Cibrian et al., 2020a). Consistent with previous studies, this finding indicates that activated T cells rely on GLUT1 to expand and survive upon inflammation, as described in the following paragraphs (Macintyre et al., 2014). GLUT1 might thus serve as an attractive therapeutic target in hyperproliferative skin diseases, including psoriasis.

Given that T cells lead the way over other immunocompetent cell types in immune-related diseases, recent research has increasingly focused on T cell immunometabolism in the setting of inflammatory skin. T cells participate at various stages during psoriasis progression depending on the specific cell type, from naïve T cells to the activated helper T cells (Th1 and Th-17), the regulatory T cells, the cytotoxic and the tissue-resident memory T cells. Each cell type has a unique role, having distinct energy, differentiation, and gene expression requirements. The microenvironment regulates the above through complex metabolic networks. T cell activation, as in psoriasis, induces a drastic metabolic reprogramming necessary to cope with massive proliferation and effector subset differentiation. In this regard, glycolytic activity seems to be crucial for T cells not only as an energy source but also as a metabolic basis for anabolic biosynthesis. A detailed description of the metabolic reprogramming in T cells participating in skin inflammation is presented by von Meyenn et al. (2019). Briefly, effector T cells, including CD4⁺ and CD8⁺ T cells, largely depend on glycolytic pathways to meet their increased demands in energy and intermediate substrate requirements. Upon antigen stimulation, GLUT1 transporters are rapidly presented in the cell surface of

the previously naïve T cells to facilitate glucose uptake, which is the primary source for cell survival, proliferation and cytokine production. Activated T cells undergo aerobic glycolysis, mediated by the conversion of pyruvate to lactate in the presence of oxygen. As a result, cells generate significant amounts of intermediate metabolites used for cell proliferation and ATP molecules for cell survival and function through downstream metabolic cascades (Almeida et al., 2016). Modulation of glycolysis is being exploited as a T cell immunometabolic target to regulate the inflammatory response in psoriasis mediated by effector T cells and T-helper cells. T cell glycolysis was reported to be upregulated in experimental models of autoimmune diseases, whereas its inhibition has ameliorated disease outcomes in experimental autoimmune disease models (Gerriets et al., 2015; Yin et al., 2015).

Different from naïve or activated T cells, memory T cells' survival and function depend on oxidative phosphorylation (OXPHOS) due to the skin microenvironment characterized by reduced oxygen, glucose, and nutrient levels and increased levels of lipids. Thus, memory T cells, responsible for peripheral tissue surveillance, upregulate OXPHOS and fatty acids oxidation to produce energy for cell survival and *de novo* fatty acids and cholesterol synthesis for cell proliferation. Specifically for the skin tissue-resident memory T cells (skin TRM), energy is primarily produced through the catabolism of exogenous free fatty acids from cutaneous lipids. Furthermore, it has been proposed that the dependence of TRM cells' survival on lipids increases with time, presenting a novel therapeutic target in disease progression and relapsing. Besides GLUT1, increased expression of the amino acid transporters of the L-type amino acid transporter ((LAT) family has been found in the epidermis of patients with psoriasis. LAT1, the primary transporter of L-Leucine, is over-expressed in activated keratinocytes and immune cells, such as T and B cells, IL-17-secreting $\gamma\delta$ T cells, macrophages, and natural killer cells. Specific deficiency of LAT1 in activated lymphocytes seems to prevent the differentiation to Th1, Th2, and Th17 cell lineages mediated by activating the mechanistic target of rapamycin (mTOR). Also, LAT1 inhibition or deletion can decrease IL-23/1 β -induced proliferation and secretion of IL-17/22 in $\gamma\delta$ T cells, conferring protection against psoriasiform hyperplasia (Cibrian et al., 2020b).

LAT-2 and LAT-3 transporters, responsible for transporting several other amino acids, support LAT-1 function by forming heterodimers with CD-98. Inhibition of the LAT-1 transporter in the IMQ animal model did not suppress epidermal proliferation indicating the compensatory role for other transporters of the LAT family (Cibrian et al., 2020b).

Cationic Amino Acid Transporter-1 and -2 (CAT1 and CAT2), the main transporters of L-Arginine, are continuously expressed by keratinocytes, promoting the metabolism of L-arginine to nitric oxide (NO). NO is an essential physiological modulator of wound repair through its effect on cell proliferation, angiogenesis and inflammation, and its production is regulated by inducible NO synthase (iNOS) and arginase (Luo and Chen, 2005). Levels of L-arginine have decreased in the blood of patients with psoriasis, which might be associated with the increased levels of arginase in psoriatic lesions, indicating a role for CAT1 and CAT2 in psoriasis (Cibrian et al., 2020a).

Sodium neutral amino acid transporter 1 (SNAT1) and alanine serine cysteine transporter ASCT2 transporters are responsible for

the uptake of L-glutamine, L-alanine and L-serine, which can modulate cell differentiation and proliferation of T cells and cytokine secretion. The exact role of these transporters in inflammatory skin diseases, including psoriasis, remains to be elucidated. However, there is evidence that circulating amino acids levels are valuable markers for disease severity and response to treatment monitoring (Kamleh et al., 2015; Ottas et al., 2017).

3.1.2 Molecular mechanisms of psoriasis immunometabolism

Metabolic and nutrient sensing pathways can coordinate immune cells' and keratinocytes' activation and differentiation in psoriatic skin (Cibrian et al., 2020a). The phosphoinositide 3-kinase (PI3K)/Akt/mTOR cascade acts as a critical mediator of inflammation and master sensor of the metabolic status at the intracellular level (Zhang and Zhang, 2019; Pålsson-McDermott and O'Neill, 2020). mTOR, the master sensor of nutrients and growth factors, plays a central role between the extracellular nutrient status triggers and the promotion of cell differentiation and proliferation. It is a serine/threonine kinase forming the mTORC1 and mTORC2, which regulates the anabolic and catabolic cellular processes depending on the metabolic needs and available "food." Briefly, under starvation conditions, mTORC1 is inhibited, thus downregulating cell growth mechanisms, including protein synthesis and synthesis of lipids and nucleotides and glycolysis, while mechanisms of survival and maintenance are upregulated, including autophagy and protein degradation (UPS). On the other hand, mTORC1 downregulates cell proliferation and growth and migration (Cibrian et al., 2020a; Pålsson-McDermott and O'Neill, 2020). Several lines of evidence suggest that activated mTOR signaling seems to be involved in the pathogenesis of psoriasis through the upregulation of cell proliferation and secretion of inflammatory mediators (Patel et al., 2018; Cibrian et al., 2020a). Specifically, stimulation of mTOR is essential for T helper effector cell lineages by promoting the differentiation towards Th1, Th2, and Th17. Increased mTOR signaling has been found in proliferating $\gamma\delta$ T cells secreting IL-17 in response to innate stimuli such as IL-23 and IL-1 β . The mTOR pathway is also activated in psoriasis patients' Treg and peripheral blood mononuclear cells. In addition, upregulation of mTOR signaling in psoriatic skin may also play a role in T cells proliferation and function, defective differentiation of keratinocytes, and their secretion of pro-inflammatory mediators (Buerger et al., 2013; Bürger et al., 2017; Cibrian et al., 2020a). Usually, mTORC1 is activated in cells of the basal layer of healthy skin, promoting their differentiation and reducing their proliferative capacity, but it is deactivated in the keratinocytes of the epidermis. Continuous activation of mTORC1 in keratinocytes has been proposed as a critical mechanism of psoriasis development. Specifically, it was shown that exposure of keratinocytes to IL-1 β , IL-17A, IL-22 and TNF- α activates mTORC1 and the downstream targets, thus leading to proliferation increase and differentiation stall (Mitra et al., 2012; Buerger et al., 2017). The involvement of the Akt/mTOR pathway in the development of psoriatic plaques was further demonstrated by the increased secretion of IL-6, CXCL8, or VEGF by keratinocytes exposed to TNF, mediated by mTORC (Patel et al., 2018).

These mechanisms could explain the studies demonstrating a link between metabolic complications such as IR and obesity with psoriasis, high prevalence rates of cardiometabolic comorbidities in

psoriasis, and improvement of psoriasis skin lesions after dietary intervention (Ip and Kirchhof, 2017; Mahil et al., 2019). The molecular pathways underlying the causal relationship between inflammatory skin diseases, such as psoriasis, and insulin resistance include the presence of the insulin receptors and insulin growth factors receptors (IGFR) on keratinocytes and fibroblasts and their regulation by insulin levels. Evidence from patients with psoriasis demonstrates upregulation of the PI3K/Akt pathway in peripheral blood cells and reduced levels of the Akt downstream mediator, FOXO, in psoriatic lesions (Ochaion et al., 2009; Liu et al., 2011). According to the proposed mechanism, under IR conditions, the resulting hyperinsulinemia facilitates insulin binding to its receptor IRS and IGFR despite their low affinity promoting keratinocyte and fibroblast proliferation. Moreover, overexpression of the PI3K/Akt pathway leads to the translocation of the phosphorylated FOXO to the cytoplasm, thereby preventing it from exerting its role as a cell cycle regulator (Buerger, 2018). In addition, beyond its role in T cell proliferation and function, mTOR is upregulated in keratinocytes in response to the pro-inflammatory cytokines and growth factors, promoting cell proliferation and defective differentiation (Zhang and Zhang, 2019).

Overall, our improved understanding of skin and T cell immunometabolism, coupled with the interplay between metabolic and inflammatory pathways, has led to significant progress in biomarker discovery, paving the way for novel targeted treatments, which will be discussed in the following sections.

4 Metabolic biomarkers in psoriasis

Studies focusing on the metabolism of psoriasis have yielded insightful findings prompting researchers to investigate potential biomarkers that will deepen our knowledge of the complex relationship between metabolism and immune responses and serve as prognostic tools.

The field focused on the study of metabolism is metabolomics, which as part of the other -omics sciences such as genomics and proteomics, has multiple applications in basic research and biomarker discovery.

Metabolomics is the gold standard for the diagnosis of inborn metabolic errors. With the emergence of sensitive equipment and methodologies, subtle changes in metabolism can be detected, as those happening during inflammatory diseases. The unprecedented advantage of analyzing the metabolome is that metabolites are the end products of cellular processes in response to genetic and non-genetic factors. Specifically, metabolites can give the researcher or clinician information on the traits that have led to a specific phenotype of an individual or a group of people with the same phenotype (e.g., disease) shaped by the combination of genetic expression, environment, epigenetic modifications and all other kinds of influences. In fact, by analyzing metabolites, one can look directly at the phenotype and see how it is affected by a disease, drug, diet and other intermediate factors (e.g., microbiota). Therefore, metabolites open a new window in discovering predictive biomarkers due to their ability to "sense" metabolic abnormalities before they lead to severe phenotype and

TABLE 1 Metabolic biomarkers in psoriasis related to energy metabolism, inflammation and insulin resistance and the gut microbiome. FA, Fatty acids; SFA, Saturated fatty acids; UFA, Unsaturated fatty acids; BCAA, Branched-chain amino acids.

Metabolic pathway	Metabolic biomarker	Type of sample	Group	Interpretation	Potential clinical application	References
Energy metabolism	Reduced glucose, lactic acid, myoinositol, and increased choline	Psoriatic lesions	10 patients with psoriasis, lesions vs. uninvolved skin and corticosteroids treated vs. untreated/ 100 psoriatic patients vs. 100 healthy individuals	Glucose overconsumption and changes in related metabolites in the epidermis cover energy demands	Diagnostic, response to treatment/ Diagnostic, disease severity	Sitter et al. (2013) , Dutkiewicz et al. (2016)
	Increased lactic acid, 2-ketoglutaric acid, aspartic acid, glutamic acid and succinic acid	Peripheral blood	10 patients with psoriasis, 10 patients with psoriasis and psoriatic arthritis and 10 control/14 psoriasis patients and 15 healthy controls	Increased amino acid mobilization from the periphery to cover energy demands in the skin	Diagnostic / Diagnostic	Armstrong et al. (2014) , Dutkiewicz et al. (2016) , Kang et al. (2017)
	Lower citric acid, alanine, methyl succinic acid and succinic acid	Urine	1,210 patients and 100 controls (two patient subgroups were recruited representing extreme disease activity)	Perturbed TCA cycle and alanine glucose cycle	Diagnosis and monitoring of disease activity	Julià et al. (2016)
Inflammation and Insulin resistance	Decreased arachidonic acid (Increased arachidonic-derived metabolites in lesions)	Peripheral blood	12 patients with psoriasis vulgaris and 12 healthy volunteers/ epidermis specimens from 8 psoriasis patients (involved vs. uninvolved epidermis)	Pro-inflammatory state, insulin resistance	Diagnostic / Diagnostic	Hammarström et al. (1975) , Li et al. (2019)
	Increased dihomo-gamma-linolenic acid	Peripheral blood	Patients with ichthyosis vulgaris, acne vulgaris or psoriasis and healthy individuals		Diagnostic	GRATTAN et al. (1990)
	Decreased total omega-3 FA	Peripheral blood	85 patients with exacerbated plaque psoriasis and 32 healthy controls	Abnormal FAs profile associated with psoriasis severity	Disease severity	Mysliwiec et al. (2017)
	Increased SFA/UFA	Peripheral blood	85 patients with exacerbated plaque psoriasis and 32 healthy controls		Disease severity	Mysliwiec et al. (2017)
	Increased BCAA	Peripheral blood	14 patients with psoriasis and 15 healthy controls		Early diagnosis	Kang et al. (2017)
Gut microbiome	Increased phenol, p-cresol, 3-hydroxyisovalerate	Peripheral blood	50 healthy female volunteers (administered a prebiotic beverage to 19 healthy female volunteers)	Association with keratinization and epidermal differentiation	Diagnostic	Dawson et al. (2011) , Miyazaki et al. (2014) , Souto-Carneiro et al. (2020) , Chen et al. (2021a) , Yu et al. (2021)

disease symptoms. In addition, metabolomics is already employed in novel therapeutic strategies for psoriasis, aiming to shape immunometabolism and regulate uncontrolled immune responses ([Sarandi et al., 2021](#)).

We conducted a literature search for articles focused on metabolomics and psoriasis on MEDLINE PubMed. The detailed search strategy included the following keywords: (psoriasis) AND (metabolomics). We scrutinized journal articles, excluding review articles, book chapters, preprints, and articles not written in English

or without access to the full article. The search was not restricted in terms of metabolomics methodology used and sample type. Obtained results were scanned for metabolic biomarkers in human psoriasis samples categorized into the following groups 1) Glycolysis, 2) TCA cycle, 3) Aminoacid metabolism, 4) Lipids metabolism, 5) Microbiome. Metabolites categorized in other groups were not included. The categories were selected based on the key metabolic derangements in keratinocytes and T cells that dominate psoriasis progression. These categories were also used to

group the metabolism-based therapeutic targets of psoriasis in an attempt to obtain a better overview of the potential clinical application of psoriasis metabolic biomarkers. The following sections will discuss up-to-date findings on the metabolic biomarkers of key disturbed metabolic pathways in keratinocytes and T cell subpopulations (Table 1).

4.1 Glucose metabolism and TCA cycle

As described earlier, keratinocytes rely primarily on glucose breakdown to meet their energy demands, while local T cells employ glycolysis and OXPHOS for ATP production. Previous metabolomics studies have demonstrated reduced glucose and glycolysis-related downstream metabolites (lactic acid and myoinositol) in psoriatic lesions/skin, reflecting the metabolic changes and increased glucose uptake to cover the higher energy requirements. Notably, topical corticosteroid treatment restored glucose and myoinositol levels similar to the uninvolved skin site. Choline, responsible for the mobilization of lipids to produce energy, has also been found to increase in psoriatic lesions and to decrease in treated lesions (Sitter et al., 2013; Dutkiewicz et al., 2016). On the contrary, circulating lactate levels were higher in the serum of patients with psoriasis, together with metabolites from amino acid metabolism, including 2-ketoglutaric acid, aspartic acid, and glutamic acid (Lian et al., 2020). It has been suggested that these observations may indicate an increased mobilization of amino acids through the periphery to the inflammation site for the proliferative requirements of the skin and immune cells (Armstrong et al., 2014; Kang et al., 2017). Furthermore, metabolomic profiling of psoriasis has demonstrated a difference in the levels of metabolites participating in the TCA cycle, including citrate, methyl succinic acid and succinic acid and several essential amino acids for energy production and the generation of intermediate metabolites (Julià et al., 2016).

2-Ketoglutaric acid has been found to be higher in the serum of patients with psoriasis compared to healthy individuals but lower compared to psoriatic arthritis patients (Armstrong et al., 2014). 2-Ketoglutaric acid has a dual role as a TCA cycle intermediate and as a precursor of glutamate, which is further metabolized to proline for collagen synthesis. According to the researchers, increasing 2-ketoglutaric acid may be due to an increased need for glutamine, insulin resistance, and excess need for collagen synthesis. However, given the central role of this metabolite in multiple pathways, a causal relationship has not been established requiring additional markers.

4.2 Lipid metabolism

Skin is a lipid-rich and nutrient-scarce microenvironment that appears to be shaping the metabolic functions of T cells that migrate from the nutrient-rich lymphoid tissues. Even though we lack quantification studies on the differential levels of glucose, lipids and other nutrients in the skin, there is growing evidence that migrating T cells undergo metabolic adaptation within the skin. Specifically, it has been shown that skin TRM free fatty acids uptake is higher than that of peripheral T cells, either memory or effector

T cells, upregulating uptake and beta-oxidation mechanisms to meet their energy and substrate demands (Pan et al., 2017).

Peroxisome proliferator-activated receptor gamma (PPAR- γ or PPARG) is a nuclear receptor responsible for lipid uptake and storage. Studies have suggested that PPAR- γ exerts a central survival mechanism for TRM metabolic adaptation in the lipid-rich environment through the upregulation of the fatty-acid-binding protein 4/5 facilitating the transport of fatty acids (Pan et al., 2017). Interestingly, the abundance of several metabolites, including unsaturated fatty acids, regulate the PPAR- γ activity and has been associated with the suppression of keratinocytes growth, suggesting that a non-pharmacological regulation of lipids would serve as a metabolic target for skin diseases (Garner et al., 1995; Ramot et al., 2015).

Metabolism of free fatty acids is mediated by carnitine, an amine that functions as a transporter of long-chain fatty acids to mitochondria for beta-oxidation. Carnitine also acts as a scavenger contributing to the clearance of amino acid metabolism intermediates. The binding of fatty acids to carnitine is mediated by carnitine palmitoyl transferase-1 (CPT-1). CPT-1 pharmacological suppression resulted in reduced production and survival of the skin TRM (Pan et al., 2017).

Metabolic profiling of fatty acids in human biofluids has yielded encouraging results regarding biomarker discovery for psoriasis and its association with disease severity and type, which has been recently reviewed elsewhere (Koussioris et al., 2021; Sarandi et al., 2021). Overall, altered lipid metabolism in psoriasis has been associated with increased beta-oxidation, lipid synthesis, and downregulation of lipolysis (Lian et al., 2020). Many identified markers are associated with IR and inflammation, highlighting the interconnection between psoriasis and metabolic disorders. Specifically, arachidonic acid and dihomo-gamma linolenic acid levels, which have been found altered in several studies in psoriasis, are gaining increasing attention as they reflect IR and might have a predictive value for metabolic complications related to psoriasis (Hammarström et al., 1975; GRATTAN et al., 1990; Li et al., 2019; Tsoukalas et al., 2019). Of note, dysregulated patterns of arachidonic acid metabolism have been reported in several studies analyzing psoriatic lesions indicating a central role in the progression of topical inflammation and disease (Koussioris et al., 2021). On the other hand, circulating anti-inflammatory omega-3 fatty acids were found to be lower in patients with higher PASI score, and the ratio of saturated fatty acids to unsaturated fatty acids (SFA/UFA) was positively associated with disease duration (Myśliwiec et al., 2017). Longitudinal studies of healthy populations with present metabolic dysfunctions, such as IR but no disease, will validate the predictive value of such biomarkers in psoriasis and reinforce the role of metabolic reprogramming in psoriasis.

4.3 Amino acid metabolism

Psoriatic lesions are characterized by extensive acanthosis of the epidermis through the hyper-proliferation of the keratinocytes. It has been suggested that changes in amino acid levels in the skin or biofluid samples of patients with psoriasis may reflect the increased demands on amino acids for collagen synthesis, cell proliferation

and nucleic acids synthesis. Amino acid availability changes in the skin microenvironment can thus be a limiting factor for skin and immune cells through the mTOR pathway. In addition, branch chain amino acids (BCAA) (valine, leucine, isoleucine) and their alpha-ketoacids derivatives are emerging as potent biomarkers in psoriasis and would serve as early indicators of metabolic derangements for disease onset (Kang et al., 2017; Li et al., 2019; Zhao et al., 2019; Souto-Carneiro et al., 2020; Chen et al., 2021a). BCAA's association with psoriasis mainly lies in their involvement as activators of the mTOR pathway promoting IR, oxidation and inflammation. In addition, BCAA's increased levels may result in IR and metabolic disturbance through the continuous supply of the TCA cycle, causing mitochondrial overload, defective oxidation and insulin sensitivity reduction (Tsoukalas et al., 2021).

Other studies on circulating levels of amino acids have identified downstream metabolites of the glutamine/glutamate pathway, the urea cycle, and the metabolism of tryptophan and phenylalanine, which, according to researchers, are implicated in the development of psoriatic lesions (Koussioris et al., 2021).

4.4 Gut microbiome

The gut-skin axis has been at the center of interest for many skin diseases, including psoriasis. The human gut is colonized by bacteria and other microorganisms, which are indispensable for the host's homeostasis and health. Alterations in gut diversity and abundance have been linked to pathological conditions due to their central role in intestinal barrier maintenance, regulation of the immune response and protection from pathogens, production of essential nutrients such as biotin, and metabolites (short-chain fatty acids) through food digestion that fuels important metabolic pathways. Although the causal relationship between gut homeostasis disruption, known as dysbiosis, with psoriasis, is not fully established, intestine barrier permeability and epidermal differentiation seem to be key factors. The hypothesis described by Chen et al. (2020) suggests that gut dysbiosis due to diet, medication, and medical and family history leads to impaired integrity of the intestine barrier and abnormal production of microbial metabolites. Phenol, p-cresol and hippurate are endogenously produced by pathogenic bacteria and have been used as functional biomarkers of pathogens' overgrowth (Chen et al., 2021b). Exposure of antigens and metabolites from the gut to the circulation activates the immune response mediated by Th-17 cells, a dominant population in psoriasis, and suppression of the Tregs. In addition, phenol and p-cresol have been associated with impaired keratinization and disrupted epidermal differentiation (Dawson et al., 2011; Miyazaki et al., 2014). Conversely, 3-hydroxyisovalerate is a marker indicating the abundance of biotin-dependent bacteria, including certain *Lactobacillus* species that are beneficial to the host. In a previous human study, 3-hydroxyisovalerate was found to be significantly altered in patients with generalized pustular psoriasis (Yu et al., 2021). Overall, metabolomic studies investigating microbial metabolites in psoriasis are very scarce, and most studies use DNA-based microbiome analysis. However, neither DNA technique can capture the microbiome's metabolic function, which can be directly linked to its targets (metabolism,

immune response, etc.). Even though metagenomics has emerged as more sensitive to detecting the diversity of present microbiomes, according to recent study reviews, microbiome composition and not abundance are strongly associated with psoriasis, and future better-designed studies will validate existing findings (Sikora et al., 2020). Qualitative and quantitative analysis of the metabolites related to gut dysbiosis would open a new path in biomarker discovery of psoriasis through the involvement of gut microbiota and novel metabolic therapeutic targets.

5 Metabolic targets for psoriasis treatment

Current treatment approaches for psoriasis are mainly based on disease severity and the presence of psoriatic arthritis. In mild to moderate cases, treatment mainly includes topical anti-psoriatic agents, i.e., topical steroids, topical calcineurin inhibitors, vitamin D analogs, and retinoids, while, in severe cases, systemic, classical or biological therapies are usually required (Armstrong and Read, 2020).

Several therapies targeting immunometabolism exist, including pharmacological agents with known anti-inflammatory properties that target metabolism, such as metformin, dimethyl fumarate and methotrexate, reviewed by Pålsson-McDermott and O'Neill (2020). However, novel targeted therapies are emerging based on immune cells' and keratinocytes' different metabolic demands. The distinctive advantage of these therapeutic strategies lies in the selectivity of the drug against cells undergoing metabolic reprogramming, which leaves normal cells unaffected and preserves tissue homeostasis.

5.1 Glycolysis

A promising metabolic target of psoriasis is the dependence of activated keratinocytes and T cells on glucose and the upregulation of the Glut1 transporter. Pharmacological inhibition of Glut1 with the agent WZB117 resulted in the suppression of the inflammatory response in skin biopsies of patients with psoriasis and decreased hyperplasia in animal models of psoriasis (Zhang et al., 2018). In this direction, the glycolysis inhibitor 2-deoxy-D-glucose (2-DG) has been proposed as a potential therapeutic target in Th-17-dependent diseases, including psoriasis. Specifically, treatment with 2-DG reduced the skin thickness and improved the skin lesions in a psoriatic mouse model (Huang et al., 2019; Liu et al., 2021). In this regard, a low-glycemic diet has been suggested to improve psoriasis as a supportive treatment, especially in overweight patients (Ford et al., 2018). It has been previously shown that a very low carbohydrate ketogenic diet protocol improves the expansion of psoriatic lesions with the concurrent improvement of biochemical and inflammation markers in patients with psoriasis. The nutritional intervention resulted in the reprogramming of several metabolic pathways, to the levels of healthy control, with the most significant being dysmetabolism and amino acid metabolism possibly linked to keratinocytes hyperproliferation (Castaldo et al., 2021).

5.2 Amino acid metabolism

Additional metabolic targets of psoriasis include amino acids metabolic pathways involved in Th17 cell differentiation and activation, which are indispensable for disease progression. CB-839, a glutaminase inhibitor, was reported to inhibit Th17 proliferation and promote Th1 expansion without altering Tregs survival leading to Treg skewing phenotype. Glutaminase inhibition and subsequent deprivation of glutamate and aspartate promoted glycolysis and the contribution of glucose-derived production of amino acids, possibly contributing to the excess production of ROS (Johnson et al., 2018). Similarly, treatment with halofuginone, a plant-derived inhibitor of glutamyl-prolyl-tRNA synthetase, which is responsible for the attachment of glutamic acid to tRNA during protein synthesis, leads to amino acid starvation response. As a result, Th17 differentiation is ablated, which is a protective mechanism in mice with Th-17-driven experimental autoimmune disease (Sundrud et al., 2009). In addition to amino acid metabolism reprogramming, rapamycin-mediated inhibition of mTORC1 defines T-cells' differentiation and polarization, promoting a Treg-enriched phenotype and downregulation of Th17 expansion. Treatment with rapamycin has been reported to exert beneficial effects in patients using rapamycin-based topical therapy, validated in experimental animal models of psoriasis (Buerger, 2018). mTOR inhibition through a fasting diet has been shown to exert beneficial effects on multiple levels beyond weight loss, including restoring the Treg/Th17 balance through metabolic rewiring (Ford et al., 2018; de Cabo and Mattson, 2019). Specifically, in psoriasis, a positive correlation between fasting and disease activity decrease has been observed in an observational study (Damiani et al., 2019).

5.3 Lipid metabolism

Moreover, the dependency of TRM cells migrating from the periphery to the lipid-rich skin on lipid metabolism has emerged as a potential anti-psoriatic strategy. Specifically, these cells upregulate the uptake and breakdown of fatty acids to adjust to the skin microenvironment. Thus, inhibition of either of these mechanisms may prove beneficial. Specifically, treatment with etomoxir, a carnitine-palmitoyltransferase one inhibitor, significantly reduced the TRM population and improved the psoriatic phenotype (Pan et al., 2017). Furthermore, dietary interventions have also been regarded as essential strategies in the metabolic reprogramming of patients with psoriasis, given the negative impact of saturated fats-rich diets on disease severity (Herbert et al., 2018; Higashi et al., 2018). In addition, several reports on the overproduction of arachidonic acid-derived eicosanoids in psoriatic skin lesions (Koussioris et al., 2021). Hence, (dietary) supplementation with n-3 fatty acids might be a helpful adjuvant in psoriasis treatment.

5.4 Dysbiosis

Restoration of the intestinal microbiota as part of an anti-psoriatic treatment strategy has gained increasing attention.

Probiotics, prebiotics and synbiotics (the simultaneous administration of pro- and prebiotics) are some widely used methods to restore the balanced microbial community of beneficial and harmful living organisms in the gut. Some clinical studies report a beneficial effect of probiotics/prebiotics administration on disease severity assessed by PASI score and inflammation markers, including CRP and interleukin levels (Groeger et al., 2013; Navarro-López et al., 2019; Moludi et al., 2022). Besides the enrichment of beneficial microorganisms, limiting the expansion and activity of potentially harmful organisms that support the psoriatic pro-inflammatory state is crucial. Adherence to the Mediterranean diet, one of the most extensively studied diet-related anti-inflammatory strategies, has been reported to improve the psoriatic phenotype. However, the role of the gut microbiome is not clear. In this sense, several other diets have been reported to improve patients' quality of life with psoriasis depending on their comorbidities, such as a gluten-free diet when coeliac disease is present. Other diet-related anti-psoriatic strategies where the role of the gut microbiome has been explored include the administration of bioactive compounds such as polyphenols, omega-3 fatty acids and other natural compounds (Chung et al., 2022).

5.5 Vitamin D

Vitamin D is a widely used adjuvant therapy for psoriasis due to its known immunomodulatory effects but also through regulating the activity and proliferation of VDR-expressing keratinocytes. A growing number of studies showing a therapeutic effect of vitamin D treatment on psoriatic lesions and inflammatory responses were recently reviewed by Brozyna et al. However, some contradicting results stemming from differences in the study design hamper the establishment of vitamin D supplementation as part of the treatment of psoriasis. Among limitations, the most important is that the efficacy of vitamin D administration is assessed in clinical trials that are designed based on protocols that evaluate drug response, where the effect is immediate. In contrast with drugs, the impact of nutrient supplementation on disease activity requires more extended periods of treatment, the presence of other nutrients, called cofactors, and sufficient levels not only in the periphery but at a cellular level to exert its biological function (Scragg, 2018; Boucher, 2020; Tsoukalas and Sarandi, 2020). The VITAL randomized control trial showed that vitamin D and omega-3 supplementation for 5 years was associated with reduced autoimmune disease incidence, including psoriasis, with the most pronounced effect observed 2 years after the initiation of the intervention (Hahn et al., 2022). In addition, nutrient efficacy on disease activity needs to be tested in combination with immunomodulatory drug agents, especially in severe cases, and not as comparators since they target distinct yet complementary biological pathways. Beyond the beneficial effects on immune system response and keratinocyte activity, recent reports show that the administration of vitamin D restores gut microbiota balance, serving as a possible mode of action for its anti-psoriatic effects and, more importantly, the response variation observed in many patients (Singh et al., 2020). As a general remark, there is increasing evidence that the gut microbiome plays a significant role in disease progression and treatment

TABLE 2 Therapeutic opportunities for psoriasis targeting metabolic pathways through pharmacological agents and supportive dietary recommendations.

Metabolic pathway	Metabolic target	Pharmacological intervention	Cellular effect	Psoriatic phenotype effect	Supportive dietary intervention	References
Glucose metabolism	GLUT	WZB117	Glucose uptake inhibition	Decreased inflammation in human skin biopsies and reduced hyperplasia in mice	Low glycemic diet	Ford et al. (2018), Zhang et al. (2018), Castaldo et al. (2021)
		2-DG	Glycolysis inhibition	Skin thickness reduction and improved skin lesions in mice	Low glycemic diet	Ford et al. (2018), Huang et al. (2019), Castaldo et al. (2021), Liu et al. (2021)
Aminoacid metabolism	Glutaminase	CB-839	Glutamine metabolism inhibition	Restoration of Treg levels and decrease of pro-inflammatory Th17 population	—	Johnson et al. (2018)
	Glutamyl-prolyl-tRNA synthetase	Halofuginone	Amino acid starvation response	Ablation of Th-17 population in Th-17 autoimmune experimental model	—	Sundrud et al. (2009)
	mTORC1	Rapamycin	Inhibition of cellular proliferation and activity	Restoration of Treg levels and decrease of pro-inflammatory Th17 population having beneficial effects in mice	Fasting diet	Buerger (2018), Ford et al. (2018), de Cabo and Mattson (2019)
Lipid metabolism	Carnitine-palmitoyltransferase 1	Etomoxir	Inhibition of fatty acids oxidation	Reduction of TRM population with subsequent improvement of psoriatic phenotype	Low saturated and high omega-3 polyunsaturated fatty acids diet	Pan et al. (2017), Herbert et al. (2018), Higashi et al. (2018)
Gut Microbiome	Beneficial gut microbiota	Probiotics/Prebiotics	Restoration of the balance between beneficial and harmful microorganisms in the gut	Improved disease severity and inflammation markers decrease	Mediterranean Diet/ gluten-free diet (if coeliac disease coexists)	Groeger et al. (2013), Navarro-López et al. (2019), Moludi et al. (2022)

response (Yeh et al., 2019). Therefore, restoration of the microbial community can directly or indirectly benefit patients receiving therapy, while gut microbiome biomarkers may serve as predictive markers of treatment selection.

6 Combinatorial treatment of psoriasis

Psoriasis is a skin disease with many comorbidities, a high risk of relapse and significant deterioration of patients' quality of life. The impact of psoriasis on the quality of life of patients is comparable to that of cancer, cardiovascular disease and depression, while it is responsible for 5.6 million all-age disability-adjusted life-years (DALYs) according to the 2016 Global Burden of Disease Study report (Global, 2017). As a result, patient satisfaction, adverse effects and costs have increased the need for novel therapeutic targets. In addition, treatment efficacy is mainly evaluated by skin clearance. However, it has been suggested that patient-reported outcomes, such as the dermatology life quality index (DLQI), should be included in the standardized outcome measures of the intervention (Strober et al., 2019). However, this applies primarily in mild to moderate

severity cases that do not receive biological therapy because in severe cases under systemic treatment and well-tolerated disease progression, the satisfaction rate of patients and physicians are high (Florek et al., 2018). Yet, in severe psoriasis cases under systemic treatment, even though lesions might be significantly reduced, the metabolic complications of psoriasis and the high risk for other chronic diseases should not be overlooked. In cases with mild psoriasis where patients do not meet their goals or the lesions require long-term use of medications, patients seek nutritional-based interventions that have minimum adverse effects and can be integrated into their daily routine (Afach et al., 2021). Although the efficacy of nutritional strategies on disease activity has not been deciphered, there is growing evidence that metabolic rewiring would be a valuable tool against psoriasis progression and restoration of the healthy metabolic state (Cibrian et al., 2020a). However, accumulating lines of evidence and studies, including the present paper, indicate the crucial role of metabolic networks, including the metabolites, the enzymes and the cofactors on the crosstalk of immune and tissue cells driving psoriasis pathogenesis. Therefore, combining drug-based treatment to fine-tune the immune response and the systemic

metabolism with nutritional plans tailor-made to provide the nutrients required to counterbalance the metabolic deregulation of psoriasis would have significant benefits. Specifically, first-line treatment might include the management of excessive inflammatory-mediated symptomatology with systemic treatment (biological and/or metabolic) for the short term. Then, treatment would consist of diet, lifestyle changes and well-tolerated topical treatment to prevent disease relapse or manifestations of other systemic inflammation diseases, applicable for the long-term with minimum side-effects and economic burden for the patient and the healthcare system (Nestle et al., 2009). Table 2 presents therapeutic opportunities for psoriasis targeting metabolic pathways through pharmacological agents and supportive dietary recommendations based on available experimental data. Available study results on the efficacy of metabolic targeting of psoriasis can be grouped into four categories; Energy metabolism, Aminoacids metabolism, Lipids metabolism, and Gut microbiome. Targeting specific metabolic networks of affected cells in psoriasis to reprogram pro-inflammatory cells to their normal state is an attractive approach to increase efficacy and reduce relapse and side effects.

7 Discussion and concluding remarks

Psoriasis is an inflammatory disorder affecting mainly the skin. However, new evidence shows that multiple associated complications in distant tissues can develop into comorbidities such as CVD and metabolic syndrome. Psoriatic lesions are characterized by hyperplasia of the epidermis due to the hyperproliferation of keratinocytes and delayed apoptosis, originating from the additive effects of environmental and genetic factors and mediated by complex crosstalk between immune and skin cells. Distinct changes in the metabolism of immune cells, mainly activated T cells, tissue-residing memory cells, and keratinocytes, have been linked to the critical pathogenetic mechanisms of psoriasis, including activation, increased proliferation and differentiation of the involved cells. Dysfunctional apoptosis of keratinocytes plays a crucial role in epidermal hyperplasia, possibly mediated by abnormal cytokine secretion by the affected T cells (Wang et al., 2020). Anti-psoriatic treatments that target keratinocytes, such as UV radiation or vitamin D3, have been shown to increase apoptosis rates in the lesional epidermis providing the basis for further research in therapy (Fukuya et al., 2002). In terms of metabolic regulation of apoptotic pathways, lipids have been demonstrated to act as pro-apoptotic or anti-apoptotic agents in a cell-specific manner, possibly related to the beneficial effect of essential fatty acids supplementation to keratinocyte growth (Garner et al., 1995; Wójcik et al., 2020).

Our understanding of the intertwined processes of metabolism, cell function and immune responses in psoriasis is still growing. However, metabolic disruptions in energy production pathways, amino acids and lipids metabolism and dysbiosis seem to be common, prompting us to look for novel diagnostic and therapeutic tools. Although validation studies are required, up-to-

date studies have identified several metabolic biomarkers associated with the distinct metabolic fingerprint of psoriasis or associated metabolic complications such as IR. These metabolic pathways can also be targeted through drug inhibitors to limit the immune response and keratinocyte hyperproliferation, stalling disease progression. In addition, tailor-made nutritional plans to restore metabolic imbalances, thus protecting unaffected cells and promoting anti-inflammatory and resolution pathways, can contribute to the long-term control of psoriasis. However, metabolomic studies have several limitations, including the variability between studies due to the lack of a standardized method and study design that hampers reproducibility and interpretation of the findings. In addition, small sample size, different population characteristics and lack of validation datasets significantly stall the biomarker discovery process. The metabolic rewiring of cells that promote inflammation and psoriasis progression to their normal state to resolve inflammation is an exciting yet growing field, and future clinical trials are needed to investigate their application in human real life settings.

To conclude, monitoring metabolic fluctuations as part of the early diagnosis of metabolic comorbidities, prevention and treatment optimization has emerged as a powerful strategy for psoriasis and ongoing ventures report encouraging findings. With the use of metabolic biomarkers to close monitor the response to treatment and overall metabolic health, clinicians will be able to provide long-term therapy for psoriasis and prevention, early diagnosis and treatment of related comorbidities. Future studies in this direction should focus on longitudinal interventional studies to validate these biomarkers and large metabolomics studies to report differences across populations.

Author contributions

Conceptualization and design: ES, DT, and AT, Manuscript writing: ES, SK-K, and PS, Critical review and suggestions GE, MS, GR, ND, and AT, Supervision and editing of the final manuscript ES, SK-K, DT, and AT. All authors contributed to the article and approved the submitted version.

Conflict of interest

The authors declare that the research was conducted in the absence of any commercial or financial relationships that could be construed as a potential conflict of interest.

Publisher's note

All claims expressed in this article are solely those of the authors and do not necessarily represent those of their affiliated organizations, or those of the publisher, the editors and the reviewers. Any product that may be evaluated in this article, or claim that may be made by its manufacturer, is not guaranteed or endorsed by the publisher.

References

- Afach, S., Chaimani, A., Evrenoglou, T., Penso, L., Brouste, E., Sbidian, E., et al. (2021). Meta-analysis results do not reflect the real safety of biologics in psoriasis. *Br. J. Dermatol.* 184 (3), 415–424. doi:10.1111/bjd.19244
- Almeida, L., Lochner, M., Berod, L., and Sparwasser, T. (2016). Metabolic pathways in T cell activation and lineage differentiation. *Semin. Immunol.* 28 (5), 514–524. doi:10.1016/j.smim.2016.10.009
- Armstrong, A. W., Mehta, M. D., Schupp, C. W., Gondo, G. C., Bell, S. J., and Griffiths, C. E. M. (2021). Psoriasis prevalence in adults in the United States. *JAMA Dermatol.* 157 (8), 940–946. doi:10.1001/jamadermatol.2021.2007
- Armstrong, A. W., and Read, C. (2020). Pathophysiology, clinical presentation, and treatment of psoriasis: A review. *JAMA* 323 (19), 1945–1960. doi:10.1001/jama.2020.4006
- Armstrong, A. W., Wu, J., Johnson, M. A., Grapov, D., Azizi, B., Dhillon, J., et al. (2014). Metabolomics in psoriatic disease: Pilot study reveals metabolite differences in psoriasis and psoriatic arthritis. *F1000Research* 3 (5), 248. doi:10.12688/f1000research.4709.1
- Boucher, B. J. (2020). Why do so many trials of vitamin D supplementation fail? *Endocr. Connect.* 9 (9), R195–R206–R206. doi:10.1530/EC-20-0274
- Buerger, C. (2018). Epidermal mTORC1 signaling contributes to the pathogenesis of psoriasis and could serve as a therapeutic target. *Front. Immunol.* 9 (NOV), 1–7. doi:10.3389/fimmu.2018.02786
- Buerger, C., Malisiewicz, B., Eiser, A., Hardt, K., and Boehncke, W. H. (2013). Mammalian target of rapamycin and its downstream signalling components are activated in psoriatic skin. *Br. J. Dermatol.* 169 (1), 156–159. doi:10.1111/bjd.12271
- Buerger, C., Shirsath, N., Lang, V., Berard, A., Diehl, S., Kaufmann, R., et al. (2017). Inflammation dependent mTORC1 signaling interferes with the switch from keratinocyte proliferation to differentiation. *PLoS One* 12 (7), e0180853. doi:10.1371/journal.pone.0180853
- Bürger, C., Shirsath, N., Lang, V., Diehl, S., Kaufmann, R., Weigert, A., et al. (2017). Blocking mTOR signalling with rapamycin ameliorates imiquimod-induced psoriasis in mice. *Acta Derm. Venereol.* 97 (9), 1087–1094. doi:10.2340/00015555-2724
- Castaldo, G., Pagano, I., Grimaldi, M., Marino, C., Molettieri, P., Santoro, A., et al. (2021). Effect of very-low-calorie ketogenic diet on psoriasis patients: A nuclear magnetic resonance-based metabolomic study. *J. Proteome Res.* 20 (3), 1509–1521. doi:10.1021/acs.jproteome.0c00646
- Chen, C., Hou, G., Zeng, C., Ren, Y., Chen, X., and Peng, C. (2021a). Metabolomic profiling reveals amino acid and carnitine alterations as metabolic signatures in psoriasis. *Theranostics* 11 (2), 754–767. doi:10.7150/thno.51154
- Chen, G., Chen, Z.-M., Fan, X.-Y., Jin, Y.-L., Li, X., Wu, S.-R., et al. (2021b). Gut-brain-skin Axis in psoriasis: A review. *Dermatol Ther. (Heidelb)*. 11 (1), 25–38. doi:10.1007/s13555-020-00466-9
- Chen, L., Li, J., Zhu, W., Kuang, Y., Liu, T., Zhang, W., et al. (2020). Skin and gut microbiome in psoriasis: Gaining insight into the pathophysiology of it and finding novel therapeutic strategies. *Front. Microbiol.* 11, 589726. doi:10.3389/fmicb.2020.589726
- Chen, L., and Tsai, T.-F. (2018). HLA-Cw6 and psoriasis. *Br. J. Dermatol.* 178 (4), 854–862. doi:10.1111/bjd.16083
- Chung, M., Bartholomew, E., Yeroushalmi, S., Hakimi, M., Bhutani, T., and Liao, W. (2022). Dietary intervention and supplements in the management of psoriasis: Current perspectives. *PsoriasisAuckl. NZ* 12, 151–176. doi:10.2147/PTT.S328581
- Cibrian, D., Castillo-González, R., Fernández-Gallego, N., de la Fuente, H., Jorge, I., Saiz, M. L., et al. (2020b). Targeting L-type amino acid transporter 1 in innate and adaptive T cells efficiently controls skin inflammation. *J. Allergy Clin. Immunol.* 145 (1), 199–214. doi:10.1016/j.jaci.2019.09.025
- Cibrian, D., de la Fuente, H., and Sánchez-Madrid, F. (2020a). Metabolic pathways that control skin homeostasis and inflammation. *Trends Mol. Med.* 26 (11), 975–986. doi:10.1016/j.molmed.2020.04.004
- Damiani, G., Watad, A., Bridgewood, C., Pigatto, P. D. M., Pacifico, A., Malagoli, P., et al. (2019). The impact of ramadan fasting on the reduction of PASI score, in moderate-to-severe psoriatic patients: A real-life multicenter study. *Nutrients* 11 (2), 277. doi:10.3390/nu11020277
- Dawson, L. F., Donahue, E. H., Cartman, S. T., Barton, R. H., Bundy, J., McNerney, R., et al. (2011). The analysis of para-cresol production and tolerance in *Clostridium difficile* 027 and 012 strains. *BMC Microbiol.* 11, 86. doi:10.1186/1471-2180-11-86
- de Cabo, R., and Mattson, M. P. (2019). Effects of intermittent fasting on health, aging, and disease. *N. Engl. J. Med.* 381 (26), 2541–2551. doi:10.1056/NEJMr1905136
- Dutkiewicz, E. P., Hsieh, K.-T., Wang, Y.-S., Chiu, H.-Y., and Urban, P. L. (2016). Hydrogel micropatch and mass spectrometry-assisted screening for psoriasis-related skin metabolites. *Clin. Chem.* 62 (8), 1120–1128. doi:10.1373/clinchem.2016.256396
- Eckel, N., Mühlenbruch, K., Meidtnier, K., Boeing, H., Stefan, N., and Schulze, M. B. (2015). Characterization of metabolically unhealthy normal-weight individuals: Risk factors and their associations with type 2 diabetes. *Metabolism* 64 (8), 862–871. doi:10.1016/j.metabol.2015.03.009
- Florek, A. G., Wang, C. J., and Armstrong, A. W. (2018). Treatment preferences and treatment satisfaction among psoriasis patients: A systematic review. *Arch. Dermatol. Res.* 310 (4), 271–319. doi:10.1007/s00403-018-1808-x
- Ford, A. R., Siegel, M., Bagel, J., Cordoro, K. M., Garg, A., Gottlieb, A., et al. (2018). Dietary recommendations for adults with psoriasis or psoriatic arthritis from the medical board of the national psoriasis foundation: A systematic review. *JAMA dermatol.* 154 (8), 934–950. doi:10.1001/jamadermatol.2018.1412
- Frasca, L., Palazzo, R., Chimenti, M. S., Alivernini, S., Tolusso, B., Bui, L., et al. (2018). Anti-LL37 antibodies are present in psoriatic arthritis (PsA) patients: New biomarkers in PsA. *Front. Immunol.* 9, 1936. doi:10.3389/fimmu.2018.01936
- Fukuya, Y., Higaki, M., Higaki, Y., and Kawashima, M. (2002). Effect of vitamin D3 on the increased expression of Bcl-xL in psoriasis. *Arch. Dermatol. Res.* 293 (12), 620–625. doi:10.1007/s00403-001-0280-0
- Garner, W. L., Oyatsu, Y., Zuccaro, C., Rodriguez, J. L., Smith, D. J., and Marcelo, C. L. (1995). The effect of essential fatty acid supplementation on keratinocyte replication. *Prostagl. Leukot. Essent. Fat. Acids* 52 (5), 349–355. doi:10.1016/0952-3278(95)90037-3
- Gerriets, V. A., Kishton, R. J., Nichols, A. G., Macintyre, A. N., Inoue, M., Ilkayeva, O., et al. (2015). Metabolic programming and PDHK1 control CD4+ T cell subsets and inflammation. *J. Clin. Invest.* 125 (1), 194–207. doi:10.1172/JCI76012
- Global, regional (2017). Global, regional, and national disability-adjusted life-years (DALYs) for 333 diseases and injuries and healthy life expectancy (HALE) for 195 countries and territories, 1990–2016: A systematic analysis for the global burden of disease study 2016. *Lancet (London, Engl.)* 390 (10100), 1260–1344. doi:10.1016/S0140-6736(17)32130-X
- Grattan, C., Burton, J. L., Manku, M., Stewart, C., and Horrobin, D. F. (1990). Essential-fatty-acid metabolites in plasma phospholipids in patients with ichthyosis vulgaris, acne vulgaris and psoriasis. *Clin. Exp. Dermatol.* 15 (3), 174–176. doi:10.1111/j.1365-2230.1990.tb02066.x
- Groeger, D., O'Mahony, L., Murphy, E. F., Bourke, J. F., Dinan, T. G., Kiely, B., et al. (2013). Bifidobacterium infantis 35624 modulates host inflammatory processes beyond the gut. *Gut Microbes* 4 (4), 325–339. doi:10.4161/gmic.25487
- Hahn, J., Cook, N. R., Alexander, E. K., Friedman, S., Walter, J., Bubes, V., et al. (2022). Vitamin D and marine omega 3 fatty acid supplementation and incident autoimmune disease: VITAL randomized controlled trial. *BMJ* 376, e066452. doi:10.1136/bmj-2021-066452
- Hammarström, S., Hamberg, M., Samuelsson, B., Duell, E. A., Stawiski, M., and Voorhees, J. J. (1975). Increased concentrations of nonesterified arachidonic acid, 12L-hydroxy-5,8,10,14-eicosatetraenoic acid, prostaglandin E2, and prostaglandin F2alpha in epidermis of psoriasis. *Proc. Natl. Acad. Sci. U. S. A.* 72 (12), 5130–5134. doi:10.1073/pnas.72.12.5130
- Hao, Y., Zhu, Y., Zou, S., Zhou, P., Hu, Y., Zhao, Q., et al. (2021). Metabolic syndrome and psoriasis: Mechanisms and future directions. *Front. Immunol.* 12, 711060. doi:10.3389/fimmu.2021.711060
- Hawkes, J. E., Chan, T. C., and Krueger, J. G. (2017). Psoriasis pathogenesis and the development of novel targeted immune therapies. *J. Allergy Clin. Immunol.* 140 (3), 645–653. doi:10.1016/j.jaci.2017.07.004
- Herbert, D., Franz, S., Popkova, Y., Anderegg, U., Schiller, J., Schwede, K., et al. (2018). High-Fat diet exacerbates early psoriatic skin inflammation independent of obesity: Saturated fatty acids as key players. *J. Invest. Dermatol.* 138 (9), 1999–2009. doi:10.1016/j.jid.2018.03.1522
- Higashi, Y., Yamakuchi, M., Fukushima, T., Ibusuki, A., Hashiguchi, T., and Kanekura, T. (2018). High-fat diet exacerbates imiquimod-induced psoriasis-like dermatitis in mice. *Exp. Dermatol.* 27 (2), 178–184. doi:10.1111/exd.13484
- Hu, P., Wang, M., Gao, H., Zheng, A., Li, J., Mu, D., et al. (2021). The role of helper T cells in psoriasis. *Front. Immunol.* 12, 788940. doi:10.3389/fimmu.2021.788940
- Huang, X., Chen, J., Zeng, W., Wu, X., Chen, M., and Chen, X. (2019). Membrane-enriched solute carrier family 2 member 1 (SLC2A1/GLUT1) in psoriatic keratinocytes confers sensitivity to 2-deoxy-D-glucose (2-DG) treatment. *Exp. Dermatol.* 28 (2), 198–201. doi:10.1111/exd.13850
- Ip, W., and Kirchhof, M. G. (2017). Glycemic control in the treatment of psoriasis. *Dermatology* 233 (1), 23–29. doi:10.1159/000472149
- Johnson, M. O., Wolf, M. M., Madden, M. Z., Andrejeva, G., Sugiura, A., Contreras, D. C., et al. (2018). Distinct regulation of Th17 and Th1 cell differentiation by glutamine-dependent metabolism. *Cell.* 175 (7), 1780–1795. doi:10.1016/j.cell.2018.10.001
- Julia, A., Vinaixa, M., Domènech, E., Fernández-Nebro, A., Cañete, J. D., Ferrándiz, C., et al. (2016). Urine metabolome profiling of immune-mediated inflammatory diseases. *BMC Med.* 14 (1), 1–12.
- Kamleh, M. A., Snowden, S. G., Grapov, D., Blackburn, G. J., Watson, D. G., Xu, N., et al. (2015). LC-MS metabolomics of psoriasis patients reveals disease severity-dependent increases in circulating amino acids that are ameliorated by anti-TNFα treatment. *J. Proteome Res.* 14 (1), 557–566. doi:10.1021/pr500782g

- Kang, H., Li, X., Zhou, Q., Quan, C., Xue, F., Zheng, J., et al. (2017). Exploration of candidate biomarkers for human psoriasis based on gas chromatography-mass spectrometry serum metabolomics. *Br. J. Dermatol* 176 (3), 713–722. doi:10.1111/bjd.15008
- Koussioris, J., Looby, N., Anderson, M., Kulasingam, V., and Chandran, V. (2021). Metabolomics studies in psoriatic disease: A review. *Metabolites* 11 (6), 375. doi:10.3390/metabo11060375
- Lande, R., Gregorio, J., Facchinetti, V., Chatterjee, B., Wang, Y.-H., Homey, B., et al. (2007). Plasmacytoid dendritic cells sense self-DNA coupled with antimicrobial peptide. *Nature* 449 (7162), 564–569. doi:10.1038/nature06116
- Lee, H. J., HanDo, K., Park, H. E., Han, J. H., Bang, C. H., Park, Y. M., et al. (2021). Changes in metabolic syndrome and risk of psoriasis: A nationwide population-based study. *Sci. Rep.* 11 (1), 24043. doi:10.1038/s41598-021-03174-2
- Li, S.-S., Liu, Y., Li, H., Wang, L.-P., Xue, L.-F., Yin, G.-S., et al. (2019). Identification of psoriasis vulgaris biomarkers in human plasma by non-targeted metabolomics based on UPLC-Q-TOF/MS. *Eur. Rev. Med. Pharmacol. Sci.* 23 (9), 3940–3950. doi:10.26355/eurrev_201905_17823
- Lian, N., Shi, L.-Q., Hao, Z.-M., and Chen, M. (2020). Research progress and perspective in metabolism and metabolomics of psoriasis. *Chin. Med. J. Engl.* 133 (24), 2976–2986. doi:10.1097/CM9.0000000000001242
- Liu, Y., Luo, W., and Chen, S. (2011). Comparison of gene expression profiles reveals aberrant expression of FOXO1, Aurora A/B and EZH2 in lesional psoriatic skins. *Mol. Biol. Rep.* 38 (6), 4219–4224. doi:10.1007/s11033-010-0544-x
- Liu, Y.-Z., Xu, M.-Y., Dai, X.-Y., Yan, L., Li, L., Zhu, R.-Z., et al. (2021). Pyruvate kinase M2 mediates glycolysis contributes to psoriasis by promoting keratinocyte proliferation. *Front. Pharmacol.* 12, 765790. doi:10.3389/fphar.2021.765790
- Lowes, M. A., Kikuchi, T., Fuentes-Duculan, J., Cardinale, I., Zaba, L. C., Haider, A. S., et al. (2008). Psoriasis vulgaris lesions contain discrete populations of Th1 and Th17 T cells. *J. Invest. Dermatol* 128 (5), 1207–1211. doi:10.1038/sj.jid.5701213
- Luo, J., and Chen, A. F. (2005). Nitric oxide: A newly discovered function on wound healing. *Acta Pharmacol. Sin.* 26 (3), 259–264. doi:10.1111/j.1745-7254.2005.00058.x
- Macintyre, A. N., Gerriets, V. A., Nichols, A. G., Michalek, R. D., Rudolph, M. C., Deoliveira, D., et al. (2014). The glucose transporter Glut1 is selectively essential for CD4 T cell activation and effector function. *Cell. Metab.* 20 (1), 61–72. doi:10.1016/j.cmet.2014.05.004
- Mahil, S. K., McSweeney, S. M., Kloczko, E., McGowan, B., Barker, J. N., and Smith, C. H. (2019). Does weight loss reduce the severity and incidence of psoriasis or psoriatic arthritis? A critically appraised topic. *Br. J. Dermatol* 181 (5), 946–953. doi:10.1111/bjd.17741
- Mitra, A., Raychaudhuri, S. K., and Raychaudhuri, S. P. (2012). IL-22 induced cell proliferation is regulated by PI3K/Akt/mTOR signaling cascade. *Cytokine* 60 (1), 38–42. doi:10.1016/j.cyt.2012.06.316
- Miyazaki, K., Masuoka, N., Kano, M., and Iizuka, R. (2014). Bifidobacterium fermented milk and galacto-oligosaccharides lead to improved skin health by decreasing phenols production by gut microbiota. *Benef. Microbes* 5 (2), 121–128. doi:10.3920/BM2012.0066
- Moludi, J., Fathollahi, P., Khedmatgozar, H., Pourteymour Fard Tabrizi, F., Ghareaghaj Zare, A., Razmi, H., et al. (2022). Probiotics supplementation improves quality of life, clinical symptoms, and inflammatory status in patients with psoriasis. *J. Drugs Dermatol* 21 (6), 637–644. doi:10.36849/JDD.6237
- Myśliwiec, H., Baran, A., Harasim-Symbor, E., Myśliwiec, P., Milewska, A. J., Chabowski, A., et al. (2017). Serum fatty acid profile in psoriasis and its comorbidity. *Arch. Dermatol Res.* 309 (5), 371–380. doi:10.1007/s00403-017-1748-x
- National Psoriasis Foundation (2022). *Psoriasis statistics [internet]*. Available at: <https://www.psoriasis.org/psoriasis-statistics/>.
- Navarro-López, V., Martínez-Andrés, A., Ramírez-Boscá, A., Ruzafa-Costas, B., Núñez-Delegido, E., Carrión-Gutiérrez, M. A., et al. (2019). Efficacy and safety of oral administration of a mixture of probiotic strains in patients with psoriasis: A randomized controlled clinical trial. *Acta Derm. Venereol.* 99 (12), 1078–1084. doi:10.2340/00015555-3305
- Nestle, F. O., Kaplan, D. H., and BarkerPsoriasis, J. (2009). Psoriasis. *N. Engl. J. Med.* 361 (5), 496–509. doi:10.1056/NEJMra0804595
- Newgard, C. B. (2017). Metabolomics and metabolic diseases: Where do we stand? *Cell. Metab.* 25 (1), 43–56. doi:10.1016/j.cmet.2016.09.018
- Ni, X., and Lai, Y. (2020). Keratinocyte: A trigger or an executor of psoriasis? *J. Leukoc. Biol.* 108 (2), 485–491. doi:10.1002/JLB.5MR0120-439R
- Ochaion, A., Bar-Yehuda, S., Cohen, S., Barer, F., Patoka, R., Amital, H., et al. (2009). The anti-inflammatory target A(3) adenosine receptor is over-expressed in rheumatoid arthritis, psoriasis and Crohn's disease. *Cell. Immunol.* 258 (2), 115–122. doi:10.1016/j.cellimm.2009.03.020
- Ottas, A., Fishman, D., Okas, T. L., Kingo, K., and Soomets, U. (2017). The metabolic analysis of psoriasis identifies the associated metabolites while providing computational models for the monitoring of the disease. *Arch. Dermatol Res.* 309 (7), 519–528. doi:10.1007/s00403-017-1760-1
- Pålsson-McDermott, E. M., and O'Neill, L. A. J. (2020). Targeting immunometabolism as an anti-inflammatory strategy. *Cell. Res.* 30 (4), 300–314. doi:10.1038/s41422-020-0291-z
- Pan, Y., Tian, T., Park, C. O., Lofftus, S. Y., Mei, S., Liu, X., et al. (2017). Survival of tissue-resident memory T cells requires exogenous lipid uptake and metabolism. *Nature* 543 (7644), 252–256. doi:10.1038/nature21379
- Parisi, R., Iskandar, I. Y. K., Kontopantelis, E., Augustin, M., Griffiths, C. E. M., Ashcroft, D. M., et al. (2020). National, regional, and worldwide epidemiology of psoriasis: Systematic analysis and modelling study. *BMJ* 369, m1590. doi:10.1136/bmj.m1590
- Patel, A. B., Tsilioni, I., Weng, Z., and Theoharides, T. C. (2018). TNF stimulates IL-6, CXCL8 and VEGF secretion from human keratinocytes via activation of mTOR, inhibited by tetramethoxyluteolin. *Exp. Dermatol* 27 (2), 135–143. doi:10.1111/exd.13461
- Polic, M. V., Miskulin, M., Smolic, M., Kralik, K., Miskulin, I., Berkovic, M. C., et al. (2018). Psoriasis severity—A risk factor of insulin resistance independent of metabolic syndrome. *Int. J. Environ. Res. Public Health* 15 (7), 1486–1487. doi:10.3390/ijerph15071486
- Ramot, Y., Mastrofrancesco, A., Camera, E., Desreumaux, P., Paus, R., and Picardo, M. (2015). The role of ppar γ -mediated signalling in skin biology and pathology: New targets and opportunities for clinical dermatology. *Exp. Dermatol* 24 (4), 245–251. doi:10.1111/exd.12647
- Sarandi, E., Thanasoula, M., Anamaterou, C., Papakonstantinou, E., Geraci, F., Papamichael, M. M., et al. (2021). Metabolic profiling of organic and fatty acids in chronic and autoimmune diseases. *Adv. Clin. Chem.* 101, 169–229. doi:10.1016/bs.acc.2020.06.003
- Schön, M. P., and Erpenbeck, L. (2018). The interleukin-23/interleukin-17 Axis links adaptive and innate immunity in psoriasis. *Front. Immunol.* 9, 1323. doi:10.3389/fimmu.2018.01323
- Scragg, R. (2018). Limitations of vitamin D supplementation trials: Why observational studies will continue to help determine the role of vitamin D in health. *J. Steroid Biochem. Mol. Biol.* 177, 6–9. doi:10.1016/j.jsbmb.2017.06.006
- Sikora, M., Stec, A., Chrabaszcz, M., Knot, A., Waskiel-Burnat, A., Rakowska, A., et al. (2020). Gut microbiome in psoriasis: An updated review. *Pathog. (Basel, Switz.)* 9 (6), 463. doi:10.3390/pathogens9060463
- Singh, P., Rawat, A., Alwakeel, M., Sharif, E., and Al Khodor, S. (2020). The potential role of vitamin D supplementation as a gut microbiota modifier in healthy individuals. *Sci. Rep.* 10 (1), 21641. doi:10.1038/s41598-020-77806-4
- Sitter, B., Johnsson, M. K., Halgunset, J., and Bathen, T. F. (2013). Metabolic changes in psoriatic skin under topical corticosteroid treatment. *BMC Dermatol* 13, 8. doi:10.1186/1471-5945-13-8
- Souto-Carneiro, M., Tóth, L., Behnisch, R., Urbach, K., Klika, K. D., Carvalho, R. A., et al. (2020). Differences in the serum metabolome and lipidome identify potential biomarkers for seronegative rheumatoid arthritis versus psoriatic arthritis. *Ann. Rheum. Dis.* 79 (4), 499–506. doi:10.1136/annrheumdis-2019-216374
- Stern, R. S., Nijsten, T., Feldman, S. R., Margolis, D. J., and Rolstad, T. (2004). Psoriasis is common, carries a substantial burden even when not extensive, and is associated with widespread treatment dissatisfaction. *J. Invest. Dermatol. Symp. Proc.* 9 (2), 136–139. doi:10.1046/j.1087-0024.2003.09102.x
- Strober, B. E., van der Walt, J. M., Armstrong, A. W., Bourcier, M., Carvalho, A. V. E., Chouela, E., et al. (2019). Clinical goals and barriers to effective psoriasis care. *Dermatol Ther. (Heidelb.)* 9 (1), 5–18. doi:10.1007/s13555-018-0279-5
- Sugiyama, H., Gyulai, R., Toichi, E., Garacz, E., Shimada, S., Stevens, S. R., et al. (2005). Dysfunctional blood and target tissue CD4+CD25high regulatory T cells in psoriasis: Mechanism underlying unrestrained pathogenic effector T cell proliferation. *J. Immunol.* 174 (1), 164–173. doi:10.4049/jimmunol.174.1.164
- Sundrud, M. S., Koralov, S. B., Feuerer, M., Calado, D. P., Kozhaya, A. E., Rhule-Smith, A., et al. (2009). Halofuginone inhibits TH17 cell differentiation by activating the amino acid starvation response. *Science* 324 (5932), 1334–1338. doi:10.1126/science.1172638
- Takeshita, J., Grewal, S., Langan, S. M., Mehta, N. N., Ogdie, A., Van Voorhees, A. S., et al. (2017). Psoriasis and comorbid diseases: Epidemiology. *J. Am. Acad. Dermatol* 76 (3), 377–390. doi:10.1016/j.jaad.2016.07.064
- Ten Bergen, L. L., Petrovic, A., Aarebrot, A. K., and Appel, S. (2020). Current knowledge on autoantigens and autoantibodies in psoriasis. *Scand. J. Immunol.* 92 (4), e12945. doi:10.1111/sji.12945
- Tsoukalas, D., Fragoulakis, V., Sarandi, E., Docea, A. O., Papakonstantinou, E., Tsilimidos, G., et al. (2019). Targeted metabolomic analysis of serum fatty acids for the prediction of autoimmune diseases. *Front. Mol. Biosci.* 6, 120. doi:10.3389/fmolb.2019.00120
- Tsoukalas, D., Sarandi, E., and Georgaki, S. (2021). The snapshot of metabolic health in evaluating micronutrient status, the risk of infection and clinical outcome of COVID-19. *Clin. Nutr. ESPEN* 44, 173–187. doi:10.1016/j.clnesp.2021.06.011
- Tsoukalas, D., and Sarandi, E. (2020). Micronutrient deficiencies in patients with COVID-19: How metabolomics can contribute to their prevention and replenishment. *BMJ Nutr. Prev. Heal* 3, 419–420. doi:10.1136/bmjnp-2020-000169

- Vollmer, S., Menssen, A., Trommler, P., Schendel, D., and Prinz, J. C. (1994). T lymphocytes derived from skin lesions of patients with psoriasis vulgaris express a novel cytokine pattern that is distinct from that of T helper type 1 and T helper type 2 cells. *Eur. J. Immunol.* 24 (10), 2377–2382. doi:10.1002/eji.1830241018
- von Meyenn, L., Bertschi, N. L., and Schlapbach, C. (2019). Targeting T cell metabolism in inflammatory skin disease. *Front. Immunol.* 10, 2285. doi:10.3389/fimmu.2019.02285
- Wang, B., Han, D., Li, F., Hou, W., Wang, L., Meng, L., et al. (2020). Elevated IL-22 in psoriasis plays an anti-apoptotic role in keratinocytes through mediating Bcl-xL/Bax. *Apoptosis* 25 (9–10), 663–673. doi:10.1007/s10495-020-01623-3
- Wójcik, P., Żarković, N., Gegotek, A., and Skrzydlewska, E. (2020). Involvement of metabolic lipid mediators in the regulation of apoptosis. *Biomolecules* 10 (3), 402. doi:10.3390/biom10030402
- Yeh, N.-L., Hsu, C.-Y., Tsai, T.-F., and Chiu, H.-Y. (2019). Gut microbiome in psoriasis is perturbed differently during secukinumab and ustekinumab therapy and associated with response to treatment. *Clin. Drug Investig.* 39 (12), 1195–1203. doi:10.1007/s40261-019-00849-7
- Yin, Y., Choi, S.-C., Xu, Z., Perry, D. J., Seay, H., Croker, B. P., et al. (2015). Normalization of CD4+ T cell metabolism reverses lupus. *Sci. Transl. Med.* 7 (274), 274ra18. doi:10.1126/scitranslmed.aaa0835
- Yu, N., Peng, C., Chen, W., Sun, Z., Zheng, J., Zhang, S., et al. (2021). Circulating metabolomic signature in generalized pustular psoriasis blunts monocyte hyperinflammation by triggering amino acid response. *Front. Immunol.* 12, 739514. doi:10.3389/fimmu.2021.739514
- Yuan, Y., Qiu, J., Lin, Z.-T., Li, W., Haley, C., Mui, U. N., et al. (2019). Identification of novel autoantibodies associated with psoriatic arthritis. *Arthritis Rheumatol. Hob. NJ* 71 (6), 941–951. doi:10.1002/art.40830
- Zhang, M., and Zhang, X. (2019). The role of PI3K/AKT/FOXO signaling in psoriasis. *Arch. Dermatol. Res.* 311 (2), 83–91. doi:10.1007/s00403-018-1879-8
- Zhang, Z., Zi, Z., Lee, E. E., Zhao, J., Contreras, D. C., South, A. P., et al. (2018). Differential glucose requirement in skin homeostasis and injury identifies a therapeutic target for psoriasis. *Nat. Med.* 24 (5), 617–627. doi:10.1038/s41591-018-0003-0
- Zhao, Y., Jhamb, D., Shu, L., Arneson, D., Rajpal, D. K., and Yang, X. (2019). Multi-omics integration reveals molecular networks and regulators of psoriasis. *BMC Syst. Biol.* 13 (1), 8. doi:10.1186/s12918-018-0671-x
- Zhou, X., Chen, Y., Cui, L., Shi, Y., and Guo, C. (2022). Advances in the pathogenesis of psoriasis: From keratinocyte perspective. *Cell. Death Dis.* 13 (1), 81. doi:10.1038/s41419-022-04523-3



OPEN ACCESS

EDITED BY

Dimitris Tsoukalas,
Metabolomic Medicine, Greece

REVIEWED BY

Shumin Qin,
The Second Affiliated Hospital of
Guangzhou University of Chinese
Medicine, China
Rui Shi,
Dongfang Hospital, China

*CORRESPONDENCE

Zhi-ning Fan
✉ fanzhiningnmu@hotmail.com
Hai-yang Wang
✉ nanjingwhy@126.com

†These authors have contributed equally to
this work

RECEIVED 09 February 2023

ACCEPTED 19 May 2023

PUBLISHED 19 July 2023

CITATION

Wang Y, Zhuang H, Jiang X-h, Zou R-h,
Wang H-y and Fan Z-n (2023) Unveiling
the key genes, environmental toxins,
and drug exposures in modulating the
severity of ulcerative colitis: a
comprehensive analysis.
Front. Immunol. 14:1162458.
doi: 10.3389/fimmu.2023.1162458

COPYRIGHT

© 2023 Wang, Zhuang, Jiang, Zou, Wang
and Fan. This is an open-access article
distributed under the terms of the [Creative
Commons Attribution License \(CC BY\)](#). The
use, distribution or reproduction in other
forums is permitted, provided the original
author(s) and the copyright owner(s) are
credited and that the original publication in
this journal is cited, in accordance with
accepted academic practice. No use,
distribution or reproduction is permitted
which does not comply with these terms.

Unveiling the key genes, environmental toxins, and drug exposures in modulating the severity of ulcerative colitis: a comprehensive analysis

Yao Wang[†], Hao Zhuang[†], Xiao-han Jiang[†], Rui-han Zou,
Hai-yang Wang* and Zhi-ning Fan*

Digestive Endoscopy Department, Jiangsu Province Hospital, The First Affiliated Hospital with Nanjing
Medical University, Nanjing, China

Background: As yet, the genetic abnormalities involved in the exacerbation of
Ulcerative colitis (UC) have not been adequately explored based on
bioinformatic methods.

Materials and methods: The gene microarray data and clinical information were
downloaded from Gene Expression Omnibus (GEO) repository. The scale-free gene
co-expression networks were constructed by R package “WGCNA”. Gene
enrichment analysis was performed via Metascape database. Differential
expression analysis was performed using “Limma” R package. The “randomForest”
packages in R was used to construct the random forest model. Unsupervised
clustering analysis performed by “ConsensusClusterPlus” R package was utilized to
identify different subtypes of UC patients. Heat map was established using the R
package “pheatmap”. Diagnostic parameter capability was evaluated by ROC curve.
The “XSum” packages in R was used to screen out small-molecule drugs for the
exacerbation of UC based on cMap database. Molecular docking was performed
with Schrodinger molecular docking software.

Results: Via WGCNA, a total 77 high Mayo score-associated genes specific in UC
were identified. Subsequently, the 9 gene signatures of the exacerbation of UC
was screened out by random forest algorithm and Limma analysis, including
BGN, CHST15, CYR1, GPR137B, GPR4, ITGA5, LILRB1, SLFN11 and ST3GAL2. The
ROC curve suggested good predictive performance of the signatures for
exacerbation of UC in both the training set and the validation set. We
generated a novel genotyping scheme based on the 9 signatures. The
percentage of patients achieved remission after 4 weeks intravenous
corticosteroids (CS-IV) treatment was higher in cluster C1 than that in cluster
C2 (54% vs. 27%, Chi-square test, $p=0.02$). Energy metabolism-associated
signaling pathways were significantly up-regulated in cluster C1, including the
oxidative phosphorylation, pentose and glucuronate interconversions and citrate
cycle TCA cycle pathways. The cluster C2 had a significant higher level of CD4+ T
cells. The “XSum” algorithm revealed that Exisulind has a therapeutic potential for
UC. Exisulind showed a good binding affinity for GPR4, ST3GAL2 and LILRB1
protein with the docking glide scores of -7.400 kcal/mol, -7.191 kcal/mol and $-$

6.721 kcal/mol, respectively. We also provided a comprehensive review of the environmental toxins and drug exposures that potentially impact the progression of UC.

Conclusion: Using WGCNA and random forest algorithm, we identified 9 gene signatures of the exacerbation of UC. A novel genotyping scheme was constructed to predict the severity of UC and screen UC patients suitable for CS-IV treatment. Subsequently, we identified a small molecule drug (Exisulind) with potential therapeutic effects for UC. Thus, our study provided new ideas and materials for the personalized clinical treatment plans for patients with UC.

KEYWORDS

ulcerative colitis, microarray, biomarker, genomics, bioinformatics

Introduction

As a chronic relapsing bowel disease, Ulcerative colitis (UC) is characterized by intestinal inflammation, mucosal injury, and fibrosis (1). The most common symptoms of UC are bloody diarrhoea, weight loss and abdominal pain. UC has represented an increasing prevalence worldwide and carried a significant global disease burden in the past few years (2). Aggravating and relieving factors of UC remains undefined, yet multiple genetic and environmental factors have been demonstrated to participate in its severity and progression (3–6). With the rapid development of high-throughput sequencing, bioinformatic analysis of gene expression profiling has been widely applied to investigate molecular mechanisms and identify potential therapeutic targets (7–9). However, few studies have explored the underlying mechanisms and biomarkers of exacerbation and remission for UC based on bioinformatic methods.

In many high-quality studies, the severity of disease was scored using the Mayo score for UC (10–13). The Mayo score ranges from 0 to 12, with higher scores indicating more severe disease (14). The Mayo score consists of four items: stool frequency, rectal bleeding, findings of flexible proctosigmoidoscopy and the clinical assessment (15). Mayo score can also be used to assess the disease activity and efficacy of the therapeutic regimen for UC (13).

In this study, we aim to investigate the key gene alterations affecting the severity of UC based on Mayo score and bioinformatic analysis, contributing to the development of personalized clinical management and treatment regimens for UC. The workflow chart of our study was shown in [Supplementary Figure 1](#).

Materials and methods

Data acquisition

The microarray data and clinical information of UC patients were downloaded from the Gene Expression Omnibus (GEO)

(GSE109142, and GSE92415) (16). The GSE109142, and GSE92415 cohorts contained Mayo scores information for all samples. Sample sizes: GSE109142 (Normal, $n = 20$; UC, $n = 206$); GSE92415 (Normal, $n = 21$; UC, $n = 162$). The microarray data was download at <https://www.ncbi.nlm.nih.gov/geo/> on December 1, 2022. The GSE109142 cohort was used as the training set considering its relatively large sample size. The GSE92415 cohort was used as the validation set. Furthermore, another independent validation dataset (GSE73661) was then obtained from GEO database, in which 166 UC patients for whom mayo endoscopic score were available.

Weighted correlation network analysis

R package “WGCNA” was utilized to construct the co-expression networks based on the microarray data (17). As a soft-thresholding power, the primary role of β was to emphasize strong correlations between the genes and penalize weak correlations. The topological overlap matrix (TOM) was transformed from the adjacency after we chose the β based on the “pickSoftThreshold” algorithm which came with the “WGCNA” R package (18). Pearson’s correlation analysis was conducted to appraise the correlation between module eigengenes (MEs) and Mayo score. Subsequently, gene module with the highest pearson’s coefficient was considered as the module most relevant to the Mayo score (Mayo score-related module) in UC. We set the screening criteria as $|MM| > 0.8$ and $|GS| > 0.1$, and then we obtained the distinct hub genes in the Mayo score-related module (9). Specific schematic process of WGCNA can be found in [Supplementary Figure 2](#).

WGCNA was performed separately on GSE109142 and GSE92415 to determine Mayo score-related hub genes, respectively. The intersection of the hub genes from GSE109142 and GSE92415 was included in the next step of analysis and the results was visualized using the “VENNY 2.1” online tool (19) (<https://bioinfogp.cnb.csic.es/tools/venny/index.html>).

Gene enrichment analysis

The Metascape database was utilized to perform enrichment analyses (20). All other parameters set as default. Terms with a *p* value < 0.01, minimum count of 3, and an enrichment factor > 1.5 were utilized in the next step of the analysis. Using screening criteria of kappa scores = 4 and similarity > 0.3, Metascape was utilized to perform hierarchical clustering to partition enrichment terms into distinct clusters, and the terms with the minimum *p* value were selected as the representative terms.

Gene Set Enrichment Analysis (GSEA) software (version 3.0) (<http://software.broadinstitute.org/gsea/index.jsp>) was used to perform GSEA analysis and identify significantly enriched pathways in different group (21). In the GSEA runs, maximum gene set size was set to 5,000 and minimum gene set size was set to 5. FDR ≤ 0.25 were considered as statistically significant. The KEGG pathways (c2.cp.kegg.v7.4.symbols.gmt) were arranged according to the normalized enrichment scores (NES) (22). Top five significantly enriched KEGG pathways were shown.

Linear models for microarray data (Limma) analysis and random forest

Based on upper and lower quartiles of the set of Mayo scores in training set, UC patients were stratified to low-, moderate-, and high-Mayo score groups. Substantially, Limma analysis and random forest was used to screen the key gene signatures from the intersection of the hub genes (23). Differential gene expression analysis followed the Limma pipeline performed by R package “limma” (version 3.40.6). Differential expression genes (DEGs) were identified according to the filter criteria (|fold change| > 1.5, FDR < 0.05). The random forest algorithms was performed by the “randomForest” packages in R (24). The ‘randomForest’ package in R was used to grow a forest of 500 trees using the default settings. Based on the “randomForest” algorithms, we selected the top 10 genes with the highest importance for downstream analysis. The intersection of the results between Limma and random forest methods was identified as the key gene signatures.

Unsupervised hierarchical clustering

Unsupervised clustering was performed through R package “ConsensusClusterPlus”, using agglomerative pam clustering with a 1-pearson correlation distances and resampling 80% of the samples for 10 repetitions (25). The optimal number of clusters was determined using the empirical cumulative distribution function plot. We divided UC patients into different molecular patterns based on the expression matrix of key gene signatures obtain by Limma and random forest methods.

Identification of immune infiltration characterization of UC

The Immune Cell Abundance Identifier (ImmuCellAI) database was used to estimate the abundance of 24 types of immune cells in

GSE109142 by inputting microarray data (26). ImmuCellAI database is a online tool to estimate the abundance of the 24 immune cells, comprising of 18 T-cell subtypes and 6 other immune cells: B cell, NK cell, Monocyte cell, Macrophage cell, Neutrophil cell and DC cell.

Discovery of potential drugs by computational methods

A similarity scoring algorithm called eXtreme Sum (XSum) was performed to screen the candidate small molecule drugs based on the connectivity map (cMap) database (27). The DEGs between different immune infiltration subtypes were used as input file of “XSum” algorithm. Subsequently, a score was calculated for each small molecule drugs of cMap database by “XSum” algorithm. Lower score indicates greater potential to act as a therapeutic drug for reversing the immune infiltration condition.

RCSB Protein Data Bank (PDB) (www.rcsb.org/pdb/home/home.do) was used to obtain the crystal structures of proteins coded by the hub gene (28). Furthermore, the 3D structure of the small molecule drugs was download from PubChem (<https://www.ncbi.nlm.nih.gov/pccompound>) (29). The molecular docking process involved preparing the proteins and ligands, setting up a grid, and docking the compounds; these were conducted using the Schrodinger software (30). The best pose was choose based on the docking score and the rationality of molecular conformation.

Chemical-gene interaction analysis

To explore the interplay between environmental chemical toxicant exposure and the UC exacerbation, we conducted an analysis utilizing the meticulously curated research studies on the Comparative Toxicogenomic Database (CTD). In our analysis, we scrutinized environmental toxicants and drugs affecting the gene expression of all key genes previously identified. Our analysis is limited to human species only.

Real time quantitative PCR detection of GPR4, ST3GAL2, and LILRBgene expression

TRIzol reagent (Ambion, USA) was utilized for total RNA extraction, followed by reverse transcription of the extracted mRNA into cDNA using PrimeScriptTM RT Master Mix (Takara, Japan). RT-qPCR was performed to quantify the transcripts using ChamQ SYBR qPCR Master Mix (Vazyme, China). Through RT-qPCR, gene expression was detected and the relative expression levels of the genes were evaluated using the 2-ΔΔCT method. To serve as an internal reference, GAPDH was used and the experiment was repeated thrice to establish the average. The following primer sequences were utilized for the detection of GPR4, ST3GAL2, and LILRB1 expression levels:

The forward primer of GPR4 was 5'-CATCGTGCTGGTCTGCTT-3'.

The reverse primer of GPR4 was 5'-CACAGTTGAGGCTGGTGAA-3'.

The forward primer of ST3GAL2 was 5'-TTCACCTACTCGCACCACA-3'.

The reverse primer of ST3GAL2 was 5'-CGACAGGCACAGCTCTTG-3'.

The forward primer of LILRB1 was 5'-CCTTGTGGGCACTCCATT-3'.

The reverse primer of LILRB1 was 5'-ACGCATCTCGCATCTGG-3'.

Four patients with UC and four healthy controls who have signed informed consents were recruited from Jiangsu Provincial People's Hospital. Samples of inflamed intestinal tissue from UC patients and normal tissue were harvested from colonoscopy biopsy specimens of both patients and controls.

Statistical analyses

R software (version 4.0.4) was utilized for all statistical procedures. Continuous variables were compared with the Wilcoxon/Kruskal–Wallis test. Differences in proportion were tested by the chi-square test. A *p* value less than 0.05 was considered significant. Receiver operating characteristic (ROC) curve was constructed to assess the predictive efficacy (31). Dimensionality reduction was performed using principal component analysis (PCA), uniform Manifold Approximation and Projection (UMAP) t-distributed stochastic neighbor embedding (tSNE) (32–34).

Results

Mayo score-related gene module revealed by WGCNA

In GSE109142 cohort, the soft threshold for network construction was set to 22 (Supplementary Figures 3A, B). In WGCNA analysis, sample clustering was performed based on gene expression patterns to detect outliers (Supplementary Figure 3C). Then, 9 gene modules in GSE109142 cohort were identified (Supplementary Figures 3D, E; Supplementary Table 1). The MEs of modules were utilized to evaluate Pearson's correlation coefficients between the modules and Mayo score. Then, we identified the salmon module as the most tightly module linked with Mayo score in GSE109142 (Pearson's correlation $r = 0.40$, $p < 0.0001$; Figure 1A). There were 1131 genes included in the salmon module (Supplementary Figure 3E). Subsequently, we screened 398 distinct hub genes in the salmon module based on the criteria of $|MM| > 0.8$ and $|GS| > 0.1$ (Supplementary Table 2).

In GSE92415 cohort, the soft threshold for network construction was set to 12 (Supplementary Figures 4A, B). Sample clustering in GSE92415 was also performed and shown in Supplementary Figure 4C. A total 14 gene modules were identified (Supplementary Figures 4D, E; Supplementary Table 3). The dark red module was the most related module with Mayo score in GSE92415 (Pearson's correlation $r = 0.46$, $p < 0.0001$; Figure 1B). A total 375 hub genes were obtained in the dark red module (Supplementary Table 4).

By taking the intersection of the hub gene set in GSE109142 and GSE92415, a total 77 Mayo score-related genes were identified (Figure 2A). Top 20 enriched pathways of these Mayo score-related genes were revealed by Metascape analysis. These Mayo score-

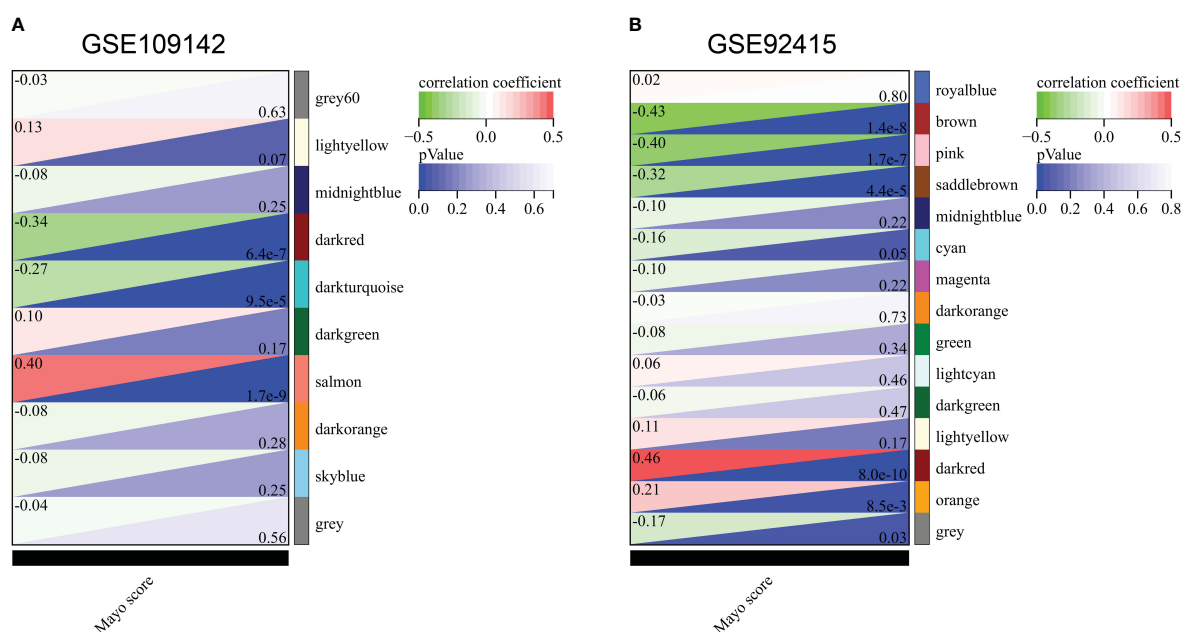


FIGURE 1
Correlation of gene co-expression modules with Mayo score in GSE109142 cohort (A) and GSE92415 cohort (B).

related genes were primarily involved in blood vessel development, immunomodulatory and inflammatory reactions (Figure 2B).

Key gene signatures of high-Mayo score patients revealed by Limma and random forest analysis

Limma and random forest analysis was used to identify the high-Mayo score related key gene signatures (HMGs) from the 77 Mayo score-related genes. A total 64 of 77 Mayo score-related genes were highly expressed in high-Mayo score patients. Besides, ten key genes were identified based random forest algorithm. Venn diagram showed the intersection of results of Limma and random forest analysis. Then, 9 HMGs were screened out, including BGN, CHST15, CYYR1, GPR137B, GPR4, ITGA5, LILRB1, SLFN11 and ST3GAL2 (Figure 3A).

All the HMGs were significantly up-regulated in the UC patients with high-Mayo scores and down-regulated in the UC patients with low-Mayo scores ($p < 0.001$; Figure 3B). In addition, the expression levels of these HMGs were significantly higher in the UC samples compared to normal colon mucosa tissue ($p < 0.0001$; Figure 3C). The PCA, UMAP and tSNE analysis grouped UC samples separately from the normal healthy controls suggesting that the HMGs was distinctive genomic signatures of the colon mucosa in UC. Furthermore, ROC analysis revealed that the overall characteristic portraits of HMGs can be an excellent predictive indicator in the diagnosis of UC (Supplementary Figure 5).

Validation of HMGs for UC patients with high Mayo scores

In validation set (GSE92415), Spearman correlation indicated that all the 9 HMGs were significantly positively correlated with the Mayo score, especially GPR4 ($\text{Rho}=0.520$; $p<0.0001$; Supplementary Figure 6A). The HMGs were significantly up-regulated in UC patients with high Mayo scores in GSE92415 ($p<0.01$; Supplementary Figure 6B). In addition, HMGs were significantly up-regulated in UC samples compared to normal colon mucosa tissue in GSE92415 ($p<0.0001$; Supplementary Figure 6C). ROC analysis suggested that HMGs can be a predictive indicator in the diagnosis of UC patients with high Mayo scores (Supplementary Figure 7).

In another independent validation dataset (GSE73661), the expression levels of HMGs were significantly higher in UC patients with higher mayo endoscopic scores (Supplementary Figure 8A). Lower expression levels of HMGs were observed in non-UC tissues compared to UC tissues (Supplementary Figure 8B). ROC analysis suggested a good diagnostic ability of HMGs for high mayo endoscopic score (2-3; Supplementary Figure 8C).

A novel typing scheme uncover the disease severity and treatment outcomes of UC

Unsupervised clustering was performed in GSE109142 using R Package “ConsensusCluster Plus” based on the 9 HMGs. The

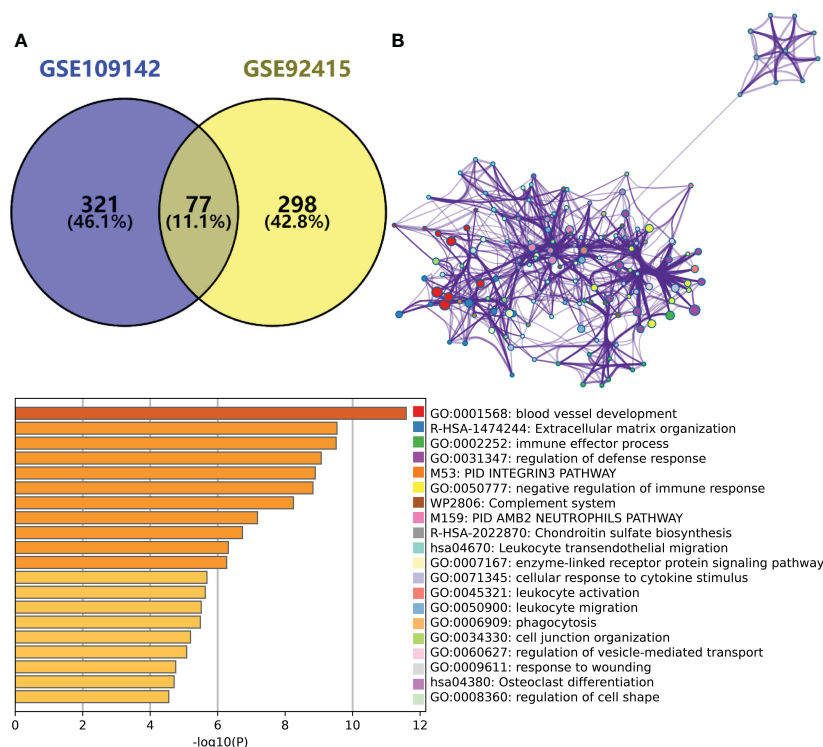


FIGURE 2

(A) Venn plot showing the intersection between the hub genes of GSE109142 cohort and GSE92415 cohort. (B) Metascape enrichment analysis results of the hub genes common to GSE109142 cohort and GSE92415 cohort (n=77).

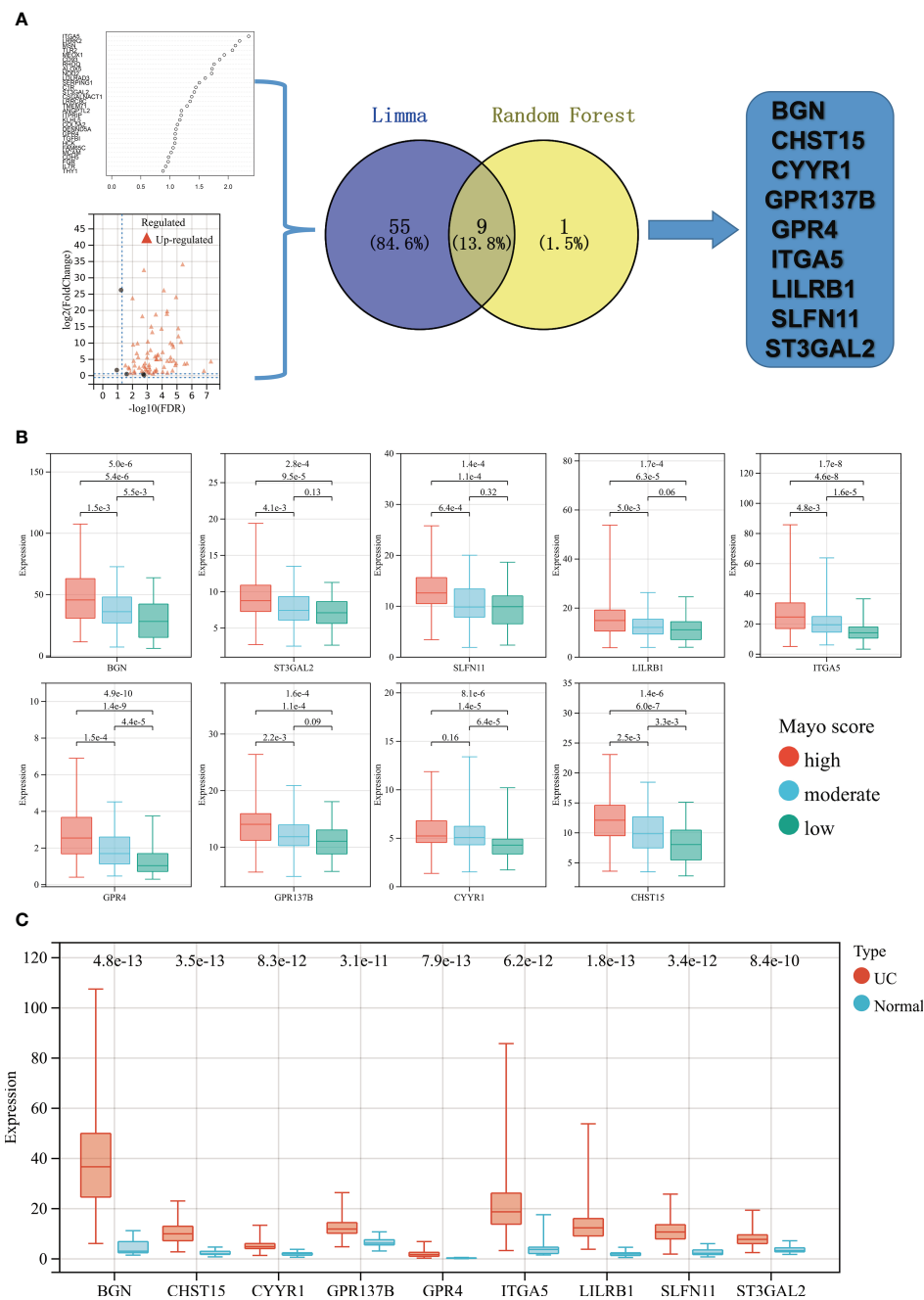


FIGURE 3

(A) Flowchart of HMGSs screening and selection process. (B) Based on upper and lower quartiles of the set of Mayo scores in GSE109142 cohort, UC patients were stratified to high- (red), moderate- (blue), and low- (green) Mayo score groups. Boxplots showing the expression levels of the 9 HMGSs across different Mayo score group. (C) Boxplots showing the expression levels of the 9 HMGSs in UC intestinal samples (red) and normal intestinal samples (blue).

optimal number of clusters was determined using the empirical CDF plot (Figures 4A, B). On the basis of the consensus scores, the CDF curve achieved the best partition efficiency when $k = 2$ (Figures 4C, D). We therefore divided the UC patients into different molecular subtypes (cluster C1 and cluster C2). The heatmap demonstrated the distinct gene expression patterns of HMGSs between the different clusters (Figure 4E). Expression level of HMGSs in cluster C2 were higher than those in the cluster C1. UC patients in cluster C2 had higher levels of Mayo

score, Pucai score and fecal calprotectin, suggesting a higher disease severity (Figures 5A–C). In GSE109142 cohort, 53 patients received 5-aminosalicylic acid (5ASA) treatment, 81 received oral corticosteroids (CS-Oral) treatment, 72 received intravenous corticosteroids (CS-IV) treatment. Symptoms were reassessed after 4 weeks of initial treatment. Chi-square test indicated that the proportion of patients with global symptom relief after initial treatment was higher in cluster C1 than that in cluster C2 (59% vs. 42%, $p=0.01$; Figure 5D). Additionally, patients of cluster C1 were

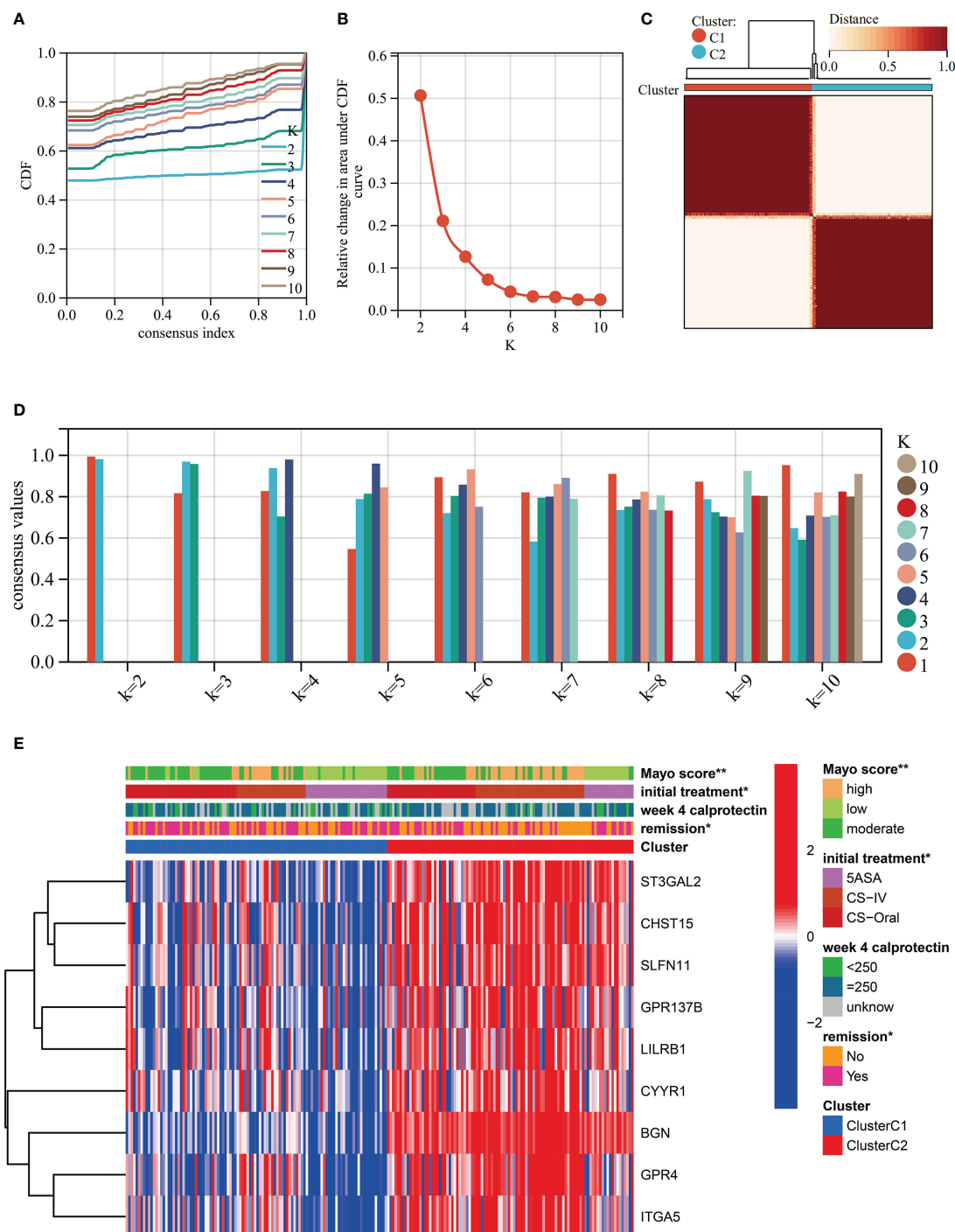


FIGURE 4

Unsupervised clustering performed in training dataset (GSE109142) based on the 9 HMGs. (A) Consensus clustering cumulative distribution function (CDF) for $k = 2-10$. (B) Relative change in the area under the CDF curve ($k = 2-10$). (C) Consensus clustering matrix for $k=2$. (D) Cluster consensus values for $k = 2-10$. (E) Heatmap for the normalized expression of the 9 HMGs.

more likely to derive benefit from CS-IV treatment (54% vs. 27%, $p=0.02$; Figure 5D). We carried out subsequent analyses to experimentally test whether our molecular typing scheme predicting CS-IV sensitivity is rooted in the variation of disease severity. We initially conducted ROC analysis and identified that disease severity index, Mayo score, lacks significant predictive capability towards CS-IV treatment responsiveness, with

AUC=0.44(95% CI: 0.30-0.57). Furthermore, we stratified all patients receiving CS-IV treatment into high-Mayo score and low-Mayo score groups according to the median value of Mayo score (10). Subsequently, chi-square test revealed no significant difference between the proportions of patients responding to CS-IV treatment in the high-Mayo score group and the low-Mayo score group ($p=0.4628$). Thus, we infer that the predictive ability of our

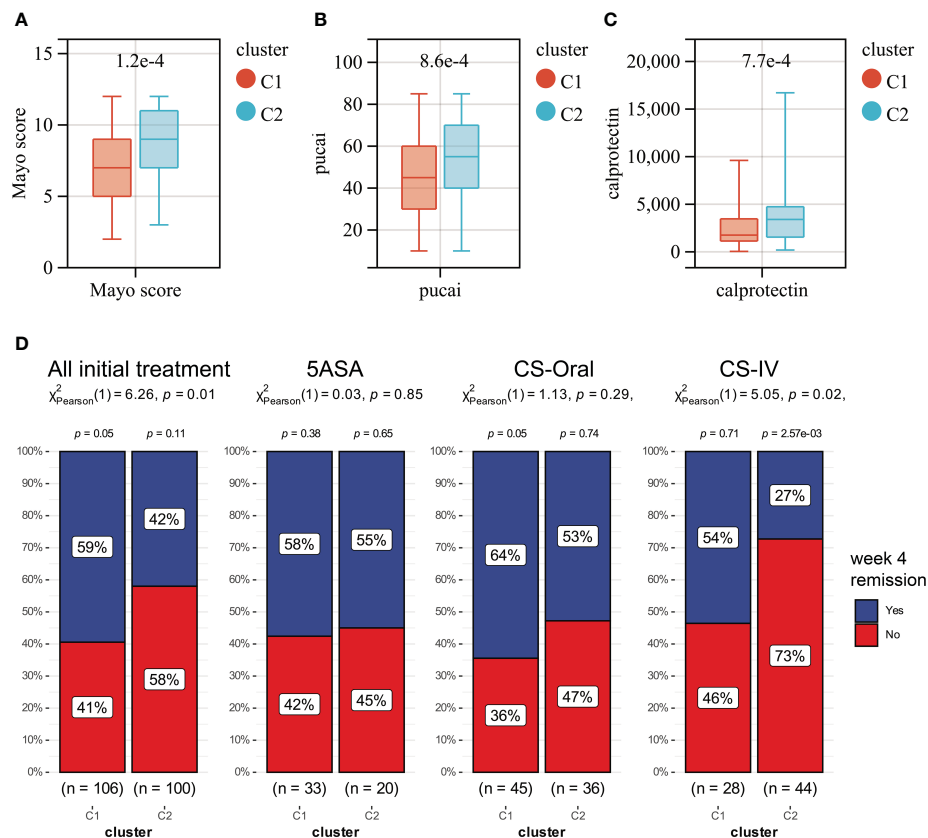


FIGURE 5

Boxplots showing the levels of Mayo score (A), Pucal score (B) and fecal calprotectin (C) in cluster C1 (red) and cluster C2 (blue). (D) The distribution of patients who responded or did not respond to different treatments in Clusters C1 and C2.

established molecular typing scheme for CS-IV treatment responsiveness is relatively independent of disease severity.

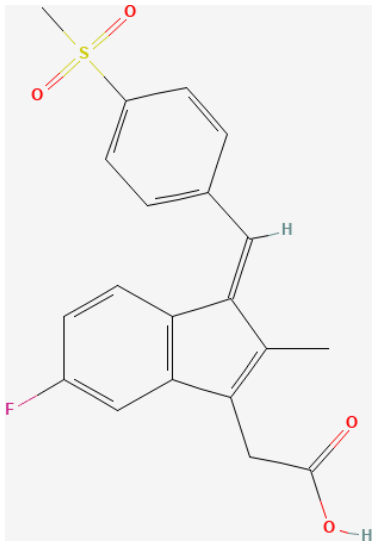
Further GSEA analysis was performed to investigate the reason for the difference of disease severity and treatment outcomes between cluster C1 and cluster C2. Several energy metabolism-associated signaling pathways were significantly up-regulated in cluster C1, including the oxidative phosphorylation, ascorbate and aldarate metabolism, Parkinson's disease, pentose and glucuronate interconversions and citrate cycle TCA cycle pathways (Supplementary Figure 9A). The cluster C2 was enriched in ECM receptor interaction, neuroactive ligand receptor interaction, cell adhesion molecules, hedgehog signaling pathway and basal cell carcinoma pathway (Supplementary Figure 9B). Furthermore, 15 of the 24 measured immune cell infiltration was significantly different between cluster C1 and cluster C2 (Supplementary Figure 9C; Supplementary Table 5). The most prominent difference is the higher number of infiltrating CD4⁺ T cells in cluster C2.

Discovery of potential drugs by computational methods

In our study, we input the top 1000 DEGs (500 up-regulated and 500 down-regulated genes) between high- and low-Mayo score group into the "XSum" algorithm to perform cMap analysis. Then,

cMap analysis revealed that Exisulind has the minimum XSum scores (Supplementary Table 6). Chemical structure formulae of Exisulind was shown in Table 1. Therefore, Exisulind was identified as the potential small molecular compounds to reverse the high Mayo score. In other words, Exisulind had the potential to attenuate the severity of UC and delay the disease progression. To further predict whether Exisulind could be a direct inhibitor for HMGs, molecular docking was performed based on the Schrodinger software. Exisulind showed best binding affinities for GPR4, ST3GAL2 and LILRB1 with the docking glide scores of -7.400 kcal/mol, -7.191 kcal/mol and -6.721 kcal/mol, respectively (Figures 6A–C). In the present study, we employed RT-qPCR to validate the gene expression levels of GPR4, ST3GAL2, and LILRB1 in the inflamed intestine of UC patients. Consistent with our previous findings, upregulation of GPR4, ST3GAL2, and LILRB1 was observed in the inflamed intestine of UC patients (n=4) compared to normal intestinal tissue (n=4), laying the foundation for considering them as potential therapeutic targets for UC (Supplementary Figure 10). Therefore, partial validation of Exisulind's potential for anti-UC activity was established by its favorable molecular docking poses with the above-mentioned three genes. The docking glide scores between Exisulind and CHST15, CYR1, ITGA5, SLFN11, GPR137B and BGN protein were -4.582 kcal/mol, -4.496 kcal/mol, -5.484 kcal/mol, -4.571 kcal/mol, -4.784 kcal/mol and -3.740 kcal/mol, respectively. In summary, Exisulind was a potential therapeutic agent for the treatment of UC.

TABLE 1 Chemical structure formulae of Exisulind.

Title	Description
PubChem CID	5472495
Structure	
Molecular Formula	C ₂₀ H ₁₇ FO ₄ S
Synonyms	Exisulind Sulindac sulfone Aptosyn 59973-80-7 Prevatec
Molecular Weight	372.4

Exploration of environmental toxin exposures with potential to impact the severity of UC

We explored all potential Environmental Toxin Exposures that may impact the expression levels of HMGs by leveraging the CTD database. Subsequently, we have acquired a total of 110 different types of Environmental Toxin Exposures that could affect the expression level or methylation state of HMGs, showing in Table 2. Thus, these Environmental Toxin Exposures have the potential to modulate the severity of UC, an effect that is mediated by the intermediary factors HMGs. Hence, avoiding exposure to these toxins might facilitate an improvement in therapeutic responsiveness among UC patients.

Moreover, we investigated the relationship between certain drugs and HMGs through the CTD database (Table 3). Therefore, the administration of these drugs may exacerbate or alleviate the severity of UC. Further studies may be warranted to elucidate the underlying mechanisms to optimize drug choice and dosages, ultimately promoting better outcomes in UC management.

As yet, the genetic abnormalities involved in the exacerbation of UC have not been adequately explored. The identification of these

genetic abnormalities may have great clinical implications in targeting UC treatment and hold the promise for achieving clinical disease remission of UC.

Based on multiple bioinformatic methods, we identified 9 gene signatures (HMGs) and one potential therapeutic small-molecule drug (Exisulind) of the exacerbation of UC. Verification in multiple datasets suggested that the 9 HMGs exhibit good diagnostic capacity in predicting the severity of UC. Furthermore, the 9 HMGs were also good biomarkers of UC. Thus, our research here provided a resource for future studies and highlighted 9 potential therapeutic targets. In addition, we generated a novel genotyping scheme based on the 9 HMGs and then found that UC patients in cluster C1 were susceptible to benefit from CS-IV treatment. A further GSEA enrichment analysis indicated that cluster C1 was indeed enriched in several energy metabolism-associated signaling pathways, including the oxidative phosphorylation, pentose and glucuronate interconversions and citrate cycle TCA cycle pathways. Corticosteroids plays an important role in regulating both energy metabolism and glucose homeostasis (35). The unique energy metabolism pattern of cluster C1 was most likely responsible for the sensitivity to corticosteroids therapy. Numerous studies have shown evidence supporting that cellular energy metabolism pathways are altered during the differentiation and activation of immune cells (36). In addition, metabolic products and intermediates also regulate the cellular function of several immune cells (37). Our study yielded similar result that cluster C1 had a remarkably distinct immune cell infiltration characterization

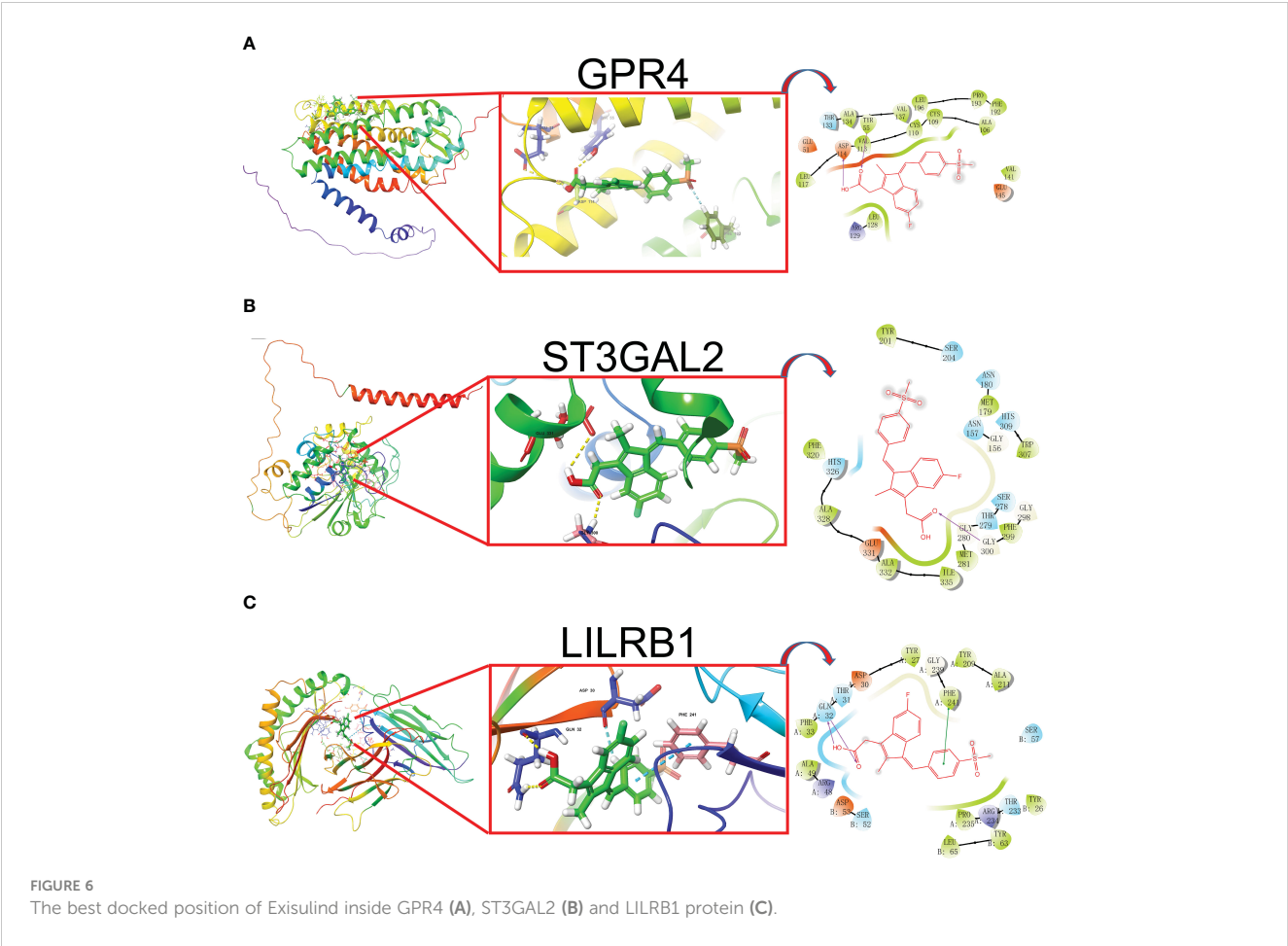


TABLE 2 The interaction between environmental toxin exposure and HMGSs

Chemical Name	Gene Symbol	Organism	Interaction	ReferencesPubMedID
Benzo(a)pyrene	GPR4	Homo sapiens	Benzo(a)pyrene affects the methylation of GPR4 promoter	27901495
Benzo(a)pyrene	GPR4	Homo sapiens	Benzo(a)pyrene results in decreased expression of GPR4 mRNA	22316170
Benzo(a)pyrene	GPR4	Homo sapiens	Benzo(a)pyrene results in increased methylation of GPR4 3' UTR	27901495
Benzo(a)pyrene	GPR4	Homo sapiens	Benzo(a)pyrene results in increased methylation of GPR4 5' UTR	27901495
bisphenol A	GPR4	Homo sapiens	bisphenol A results in decreased expression of GPR4 mRNA	31715268
butyraldehyde	GPR4	Homo sapiens	butyraldehyde results in increased expression of GPR4 mRNA	26079696
Cadmium	GPR4	Homo sapiens	Cadmium results in decreased expression of GPR4 mRNA	24376830
cobaltous chloride	GPR4	Homo sapiens	cobaltous chloride results in decreased expression of GPR4 mRNA	19320972
Nickel	GPR4	Homo sapiens	Nickel results in increased expression of GPR4 mRNA	25583101

(Continued)

TABLE 2 Continued

Chemical Name	Gene Symbol	Organism	Interaction	ReferencesPubMedID
nickel sulfate	GPR4	Homo sapiens	nickel sulfate results in decreased expression of GPR4 mRNA	22714537
Oxygen	GPR4	Homo sapiens	Oxygen deficiency results in increased expression of GPR4 protein	33161135
Smoke	GPR4	Homo sapiens	Smoke results in decreased expression of GPR4 mRNA	34520756
Sugars	GPR4	Homo sapiens	[Anti-Inflammatory Agents binds to and results in decreased activity of GPR4 protein] inhibits the reaction [[Biological Factors binds to Sugars] which results in increased expression of IL1B mRNA]	32370492
Sugars	GPR4	Homo sapiens	[Anti-Inflammatory Agents binds to and results in decreased activity of GPR4 protein] inhibits the reaction [[Biological Factors binds to Sugars] which results in increased expression of IL1B protein]	32370492
Sugars	GPR4	Homo sapiens	[Anti-Inflammatory Agents binds to and results in decreased activity of GPR4 protein] inhibits the reaction [[Biological Factors binds to Sugars] which results in increased expression of IL6 mRNA]	32370492
Sugars	GPR4	Homo sapiens	[Anti-Inflammatory Agents binds to and results in decreased activity of GPR4 protein] inhibits the reaction [[Biological Factors binds to Sugars] which results in increased expression of IL6 protein]	32370492
Sugars	GPR4	Homo sapiens	[Anti-Inflammatory Agents binds to and results in decreased activity of GPR4 protein] inhibits the reaction [[Biological Factors binds to Sugars] which results in increased expression of MMP13 mRNA]	32370492
Sugars	GPR4	Homo sapiens	[Anti-Inflammatory Agents binds to and results in decreased activity of GPR4 protein] inhibits the reaction [[Biological Factors binds to Sugars] which results in increased expression of MMP13 protein]	32370492
Sugars	GPR4	Homo sapiens	[Anti-Inflammatory Agents binds to and results in decreased activity of GPR4 protein] inhibits the reaction [[Biological Factors binds to Sugars] which results in increased expression of MMP3 mRNA]	32370492
Sugars	GPR4	Homo sapiens	[Anti-Inflammatory Agents binds to and results in decreased activity of GPR4 protein] inhibits the reaction [[Biological Factors binds to Sugars] which results in increased expression of MMP3 protein]	32370492
Sugars	GPR4	Homo sapiens	[Anti-Inflammatory Agents binds to and results in decreased activity of GPR4 protein] inhibits the reaction [[Biological Factors binds to Sugars] which results in increased expression of NOS2 mRNA]	32370492
Sugars	GPR4	Homo sapiens	[Anti-Inflammatory Agents binds to and results in decreased activity of GPR4 protein] inhibits the reaction [[Biological Factors binds to Sugars] which results in increased expression of NOS2 protein]	32370492
Sugars	GPR4	Homo sapiens	[Anti-Inflammatory Agents binds to and results in decreased activity of GPR4 protein] inhibits the reaction [[Biological Factors binds to Sugars] which results in increased expression of PTGS2 mRNA]	32370492
Sugars	GPR4	Homo sapiens	[Anti-Inflammatory Agents binds to and results in decreased activity of GPR4 protein] inhibits the reaction [[Biological Factors binds to Sugars] which results in increased expression of PTGS2 protein]	32370492

(Continued)

TABLE 2 Continued

Chemical Name	Gene Symbol	Organism	Interaction	ReferencesPubMedID
Sugars	GPR4	Homo sapiens	[Anti-Inflammatory Agents binds to and results in decreased activity of GPR4 protein] inhibits the reaction [[Biological Factors binds to Sugars] which results in increased expression of TNF mRNA]	32370492
Sugars	GPR4	Homo sapiens	[Anti-Inflammatory Agents binds to and results in decreased activity of GPR4 protein] inhibits the reaction [[Biological Factors binds to Sugars] which results in increased expression of TNF protein]	32370492
Sugars	GPR4	Homo sapiens	[Biological Factors binds to Sugars] which results in increased expression of GPR4 mRNA	32370492
Sugars	GPR4	Homo sapiens	[Biological Factors binds to Sugars] which results in increased expression of GPR4 protein	32370492
tert-Butylhydroperoxide	GPR4	Homo sapiens	tert-Butylhydroperoxide results in increased expression of GPR4 mRNA	15336504
4-(5-benzo(1,3)dioxol-5-yl-4-pyridin-2-yl-1H-imidazol-2-yl)benzamide	CYYR1	Homo sapiens	[NOG protein co-treated with methylmercuric chloride co-treated with dorsomorphin co-treated with 4-(5-benzo(1,3)dioxol-5-yl-4-pyridin-2-yl-1H-imidazol-2-yl)benzamide] results in increased expression of CYYR1 mRNA	27188386
Aflatoxin B1	CYYR1	Homo sapiens	Aflatoxin B1 results in decreased methylation of CYYR1 gene	27153756
Arsenic	CYYR1	Homo sapiens	[sodium arsenate results in increased abundance of Arsenic] which results in decreased expression of CYYR1 mRNA	32525701
arsenite	CYYR1	Homo sapiens	arsenite results in decreased expression of CYYR1 mRNA	23974009
Benzo(a)pyrene	CYYR1	Homo sapiens	Benzo(a)pyrene results in increased methylation of CYYR1 promoter	27901495
Cadmium	CYYR1	Homo sapiens	Cadmium results in decreased expression of CYYR1 mRNA	23369406
cobaltous chloride	CYYR1	Homo sapiens	cobaltous chloride results in decreased expression of CYYR1 mRNA	19320972
dorsomorphin	CYYR1	Homo sapiens	[NOG protein co-treated with methylmercuric chloride co-treated with dorsomorphin co-treated with 4-(5-benzo(1,3)dioxol-5-yl-4-pyridin-2-yl-1H-imidazol-2-yl)benzamide] results in increased expression of CYYR1 mRNA	27188386
Ethanol	CYYR1	Homo sapiens	Ethanol results in decreased expression of CYYR1 mRNA	23378141
methylmercuric chloride	CYYR1	Homo sapiens	methylmercuric chloride results in increased expression of CYYR1 mRNA	23179753 26272509
methylmercuric chloride	CYYR1	Homo sapiens	[NOG protein co-treated with methylmercuric chloride co-treated with dorsomorphin co-treated with 4-(5-benzo(1,3)dioxol-5-yl-4-pyridin-2-yl-1H-imidazol-2-yl)benzamide] results in increased expression of CYYR1 mRNA	27188386
Silicon Dioxide	CYYR1	Homo sapiens	Silicon Dioxide analog results in increased expression of CYYR1 mRNA	23806026
sodium arsenate	CYYR1	Homo sapiens	[sodium arsenate results in increased abundance of Arsenic] which results in decreased expression of CYYR1 mRNA	32525701
Tobacco Smoke Pollution	CYYR1	Homo sapiens	Tobacco Smoke Pollution results in decreased expression of CYYR1 mRNA	30291989 33660061
Aflatoxin B1	ST3GAL2	Homo sapiens	Aflatoxin B1 results in decreased methylation of ST3GAL2 intron	30157460

(Continued)

TABLE 2 Continued

Chemical Name	Gene Symbol	Organism	Interaction	ReferencesPubMedID
Arsenic	ST3GAL2	Homo sapiens	Arsenic affects the methylation of ST3GAL2 gene	25304211
Arsenic Trioxide	ST3GAL2	Homo sapiens	Arsenic Trioxide results in decreased expression of ST3GAL2 mRNA	20458559
Arsenic Trioxide	ST3GAL2	Homo sapiens	Arsenic Trioxide results in increased expression of ST3GAL2 mRNA	20458559
Benzo(a)pyrene	ST3GAL2	Homo sapiens	Benzo(a)pyrene results in increased methylation of ST3GAL2 5' UTR	27901495
Copper Sulfate	ST3GAL2	Homo sapiens	Copper Sulfate results in decreased expression of ST3GAL2 mRNA	19549813
Diazinon	ST3GAL2	Homo sapiens	Diazinon results in increased methylation of ST3GAL2 gene	22964155
dicrotophos	ST3GAL2	Homo sapiens	dicrotophos results in increased expression of ST3GAL2 mRNA	28302478
Methyl Methanesulfonate	ST3GAL2	Homo sapiens	Methyl Methanesulfonate results in decreased expression of ST3GAL2 mRNA	23649840
Smoke	ST3GAL2	Homo sapiens	Smoke results in decreased expression of ST3GAL2 mRNA	34520756
Tobacco Smoke Pollution	ST3GAL2	Homo sapiens	Tobacco Smoke Pollution results in decreased expression of ST3GAL2 mRNA	33660061
Vehicle Emissions	ST3GAL2	Homo sapiens	Vehicle Emissions results in decreased methylation of ST3GAL2 gene	25487561
1-Butanol	CHST15	Homo sapiens	[[Gasoline co-treated with 1-Butanol] results in increased abundance of [Particulate Matter co-treated with Polycyclic Aromatic Hydrocarbons]] which results in decreased expression of CHST15 mRNA	29432896
4-(4-((5-(4,5-dimethyl-2-nitrophenyl)-2-furanyl)methylene)-4,5-dihydro-3-methyl-5-oxo-1H-pyrazol-1-yl)benzoic acid	CHST15	Homo sapiens	4-(4-((5-(4,5-dimethyl-2-nitrophenyl)-2-furanyl)methylene)-4,5-dihydro-3-methyl-5-oxo-1H-pyrazol-1-yl)benzoic acid results in increased expression of CHST15 mRNA	26191083
4-(5-benzo(1,3)dioxol-5-yl-4-pyridin-2-yl-1H-imidazol-2-yl)benzamide	CHST15	Homo sapiens	[NOG protein co-treated with entinostat co-treated with dorsomorphin co-treated with 4-(5-benzo(1,3)dioxol-5-yl-4-pyridin-2-yl-1H-imidazol-2-yl)benzamide] results in increased expression of CHST15 mRNA	27188386
4-(5-benzo(1,3)dioxol-5-yl-4-pyridin-2-yl-1H-imidazol-2-yl)benzamide	CHST15	Homo sapiens	[NOG protein co-treated with Panobinostat co-treated with dorsomorphin co-treated with 4-(5-benzo(1,3)dioxol-5-yl-4-pyridin-2-yl-1H-imidazol-2-yl)benzamide] results in increased expression of CHST15 mRNA	27188386
4-(5-benzo(1,3)dioxol-5-yl-4-pyridin-2-yl-1H-imidazol-2-yl)benzamide	CHST15	Homo sapiens	[NOG protein co-treated with Phenylmercuric Acetate co-treated with dorsomorphin co-treated with 4-(5-benzo(1,3)dioxol-5-yl-4-pyridin-2-yl-1H-imidazol-2-yl)benzamide] results in increased expression of CHST15 mRNA	27188386
4-(5-benzo(1,3)dioxol-5-yl-4-pyridin-2-yl-1H-imidazol-2-yl)benzamide	CHST15	Homo sapiens	[NOG protein co-treated with trichostatin A co-treated with dorsomorphin co-treated with 4-(5-benzo(1,3)dioxol-5-yl-4-pyridin-2-yl-1H-imidazol-2-yl)benzamide] results in increased expression of CHST15 mRNA	27188386
4-(5-benzo(1,3)dioxol-5-yl-4-pyridin-2-yl-1H-imidazol-2-yl)benzamide	CHST15	Homo sapiens	[NOG protein co-treated with Valproic Acid co-treated with dorsomorphin co-treated with 4-(5-benzo(1,3)dioxol-5-yl-4-pyridin-2-yl-1H-imidazol-2-yl)benzamide] results in increased expression of CHST15 mRNA	27188386
7,8-Dihydro-7,8-dihydroxybenzo(a)pyrene 9,10-oxide	CHST15	Homo sapiens	7,8-Dihydro-7,8-dihydroxybenzo(a)pyrene 9,10-oxide results in decreased expression of CHST15 mRNA	19150397 20382639

(Continued)

TABLE 2 Continued

Chemical Name	Gene Symbol	Organism	Interaction	ReferencesPubMedID
7,8-Dihydro-7,8-dihydroxybenzo(a)pyrene 9,10-oxide	CHST15	Homo sapiens	7,8-Dihydro-7,8-dihydroxybenzo(a)pyrene 9,10-oxide results in increased expression of CHST15 mRNA	26238291
9,10-dihydro-9,10-dihydroxybenzo(a)pyrene	CHST15	Homo sapiens	9,10-dihydro-9,10-dihydroxybenzo(a)pyrene results in decreased expression of CHST15 mRNA	26238291
Air Pollutants, Occupational	CHST15	Homo sapiens	Air Pollutants, Occupational results in decreased expression of CHST15 mRNA	23195993
arsenite	CHST15	Homo sapiens	arsenite results in increased methylation of CHST15 promoter	23974009
Benzo(a)pyrene	CHST15	Homo sapiens	Benzo(a)pyrene affects the expression of CHST15 mRNA	22316170
Benzo(a)pyrene	CHST15	Homo sapiens	Benzo(a)pyrene affects the methylation of CHST15 intron	30157460
Benzo(a)pyrene	CHST15	Homo sapiens	Benzo(a)pyrene results in decreased expression of CHST15 mRNA	20106945 21632981 26238291
Benzo(a)pyrene	CHST15	Homo sapiens	Benzo(a)pyrene results in increased expression of CHST15 mRNA	32234424
bisphenol A	CHST15	Homo sapiens	bisphenol A affects the expression of CHST15 mRNA	30903817
bisphenol A	CHST15	Homo sapiens	[bisphenol A co-treated with Fulvestrant] results in increased methylation of CHST15 gene	31601247
bisphenol A	CHST15	Homo sapiens	bisphenol A results in decreased methylation of CHST15 gene	31601247
Copper Sulfate	CHST15	Homo sapiens	Copper Sulfate results in decreased expression of CHST15 mRNA	19549813
Diethylhexyl Phthalate	CHST15	Homo sapiens	Diethylhexyl Phthalate results in decreased expression of CHST15 mRNA	28412506
dorsomorphin	CHST15	Homo sapiens	[NOG protein co-treated with entinostat co-treated with dorsomorphin co-treated with 4-(5-benzo(1,3)dioxol-5-yl-4-pyridin-2-yl-1H-imidazol-2-yl)benzamide] results in increased expression of CHST15 mRNA	27188386
dorsomorphin	CHST15	Homo sapiens	[NOG protein co-treated with Panobinostat co-treated with dorsomorphin co-treated with 4-(5-benzo(1,3)dioxol-5-yl-4-pyridin-2-yl-1H-imidazol-2-yl)benzamide] results in increased expression of CHST15 mRNA	27188386
dorsomorphin	CHST15	Homo sapiens	[NOG protein co-treated with Phenylmercuric Acetate co-treated with dorsomorphin co-treated with 4-(5-benzo(1,3)dioxol-5-yl-4-pyridin-2-yl-1H-imidazol-2-yl)benzamide] results in increased expression of CHST15 mRNA	27188386
dorsomorphin	CHST15	Homo sapiens	[NOG protein co-treated with trichostatin A co-treated with dorsomorphin co-treated with 4-(5-benzo(1,3)dioxol-5-yl-4-pyridin-2-yl-1H-imidazol-2-yl)benzamide] results in increased expression of CHST15 mRNA	27188386
dorsomorphin	CHST15	Homo sapiens	[NOG protein co-treated with Valproic Acid co-treated with dorsomorphin co-treated with 4-(5-benzo(1,3)dioxol-5-yl-4-pyridin-2-yl-1H-imidazol-2-yl)benzamide] results in increased expression of CHST15 mRNA	27188386
Ethanol	CHST15	Homo sapiens	[[Gasoline co-treated with Ethanol] results in increased abundance of [Particulate Matter co-treated with Polycyclic Aromatic Hydrocarbons]] which results in decreased expression of CHST15 mRNA	29432896
Formaldehyde	CHST15	Homo sapiens	Formaldehyde results in decreased expression of CHST15 mRNA	20655997

(Continued)

TABLE 2 Continued

Chemical Name	Gene Symbol	Organism	Interaction	ReferencesPubMedID
Formaldehyde	CHST15	Homo sapiens	Formaldehyde results in increased expression of CHST15 mRNA	23649840
Gasoline	CHST15	Homo sapiens	[[Gasoline co-treated with 1-Butanol] results in increased abundance of [Particulate Matter co-treated with Polycyclic Aromatic Hydrocarbons]] which results in decreased expression of CHST15 mRNA	29432896
Gasoline	CHST15	Homo sapiens	[[Gasoline co-treated with Ethanol] results in increased abundance of [Particulate Matter co-treated with Polycyclic Aromatic Hydrocarbons]] which results in decreased expression of CHST15 mRNA	29432896
Gasoline	CHST15	Homo sapiens	[Gasoline results in increased abundance of [Particulate Matter co-treated with Polycyclic Aromatic Hydrocarbons]] which results in decreased expression of CHST15 mRNA	29432896
Hydrogen Peroxide	CHST15	Homo sapiens	Hydrogen Peroxide affects the expression of CHST15 mRNA	23410634
Mustard Gas	CHST15	Homo sapiens	Mustard Gas results in decreased expression of CHST15 mRNA	12884408
Nickel	CHST15	Homo sapiens	Nickel results in decreased expression of CHST15 mRNA	23195993
nickel sulfate	CHST15	Homo sapiens	nickel sulfate results in decreased expression of CHST15 mRNA	22714537
Particulate Matter	CHST15	Homo sapiens	[[Gasoline co-treated with 1-Butanol] results in increased abundance of [Particulate Matter co-treated with Polycyclic Aromatic Hydrocarbons]] which results in decreased expression of CHST15 mRNA	29432896
Particulate Matter	CHST15	Homo sapiens	[[Gasoline co-treated with Ethanol] results in increased abundance of [Particulate Matter co-treated with Polycyclic Aromatic Hydrocarbons]] which results in decreased expression of CHST15 mRNA	29432896
Particulate Matter	CHST15	Homo sapiens	[Gasoline results in increased abundance of [Particulate Matter co-treated with Polycyclic Aromatic Hydrocarbons]] which results in decreased expression of CHST15 mRNA	29432896
Phenylmercuric Acetate	CHST15	Homo sapiens	[NOG protein co-treated with Phenylmercuric Acetate co-treated with dorsomorphin co-treated with 4-(5-benzo(1,3)dioxol-5-yl-4-pyridin-2-yl-1H-imidazol-2-yl)benzamide] results in increased expression of CHST15 mRNA	27188386
Phenylmercuric Acetate	CHST15	Homo sapiens	Phenylmercuric Acetate results in increased expression of CHST15 mRNA	26272509
Polycyclic Aromatic Hydrocarbons	CHST15	Homo sapiens	[[Gasoline co-treated with 1-Butanol] results in increased abundance of [Particulate Matter co-treated with Polycyclic Aromatic Hydrocarbons]] which results in decreased expression of CHST15 mRNA	29432896
Polycyclic Aromatic Hydrocarbons	CHST15	Homo sapiens	[[Gasoline co-treated with Ethanol] results in increased abundance of [Particulate Matter co-treated with Polycyclic Aromatic Hydrocarbons]] which results in decreased expression of CHST15 mRNA	29432896
Polycyclic Aromatic Hydrocarbons	CHST15	Homo sapiens	[Gasoline results in increased abundance of [Particulate Matter co-treated with Polycyclic Aromatic Hydrocarbons]] which results in decreased expression of CHST15 mRNA	29432896
potassium chromate(VI)	CHST15	Homo sapiens	[potassium chromate(VI) co-treated with epigallocatechin gallate] results in decreased expression of CHST15 mRNA	22079256
potassium chromate(VI)	CHST15	Homo sapiens	potassium chromate(VI) results in decreased expression of CHST15 mRNA	22079256

(Continued)

TABLE 2 Continued

Chemical Name	Gene Symbol	Organism	Interaction	ReferencesPubMedID
Smoke	CHST15	Homo sapiens	Smoke results in decreased expression of CHST15 mRNA	34520756
tert-Butylhydroperoxide	CHST15	Homo sapiens	tert-Butylhydroperoxide affects the expression of CHST15 mRNA	23410634
Tetrachlorodibenzodioxin	CHST15	Homo sapiens	Tetrachlorodibenzodioxin results in decreased expression of CHST15 mRNA	20106945 21632981 26238291
Tobacco Smoke Pollution	CHST15	Homo sapiens	Tobacco Smoke Pollution results in decreased expression of CHST15 mRNA	28065790
Tobacco Smoke Pollution	CHST15	Homo sapiens	Tobacco Smoke Pollution results in increased expression of CHST15 mRNA	33660061
Triclosan	CHST15	Homo sapiens	Triclosan results in decreased expression of CHST15 mRNA	30510588
tris(1,3-dichloro-2-propyl) phosphate	CHST15	Homo sapiens	tris(1,3-dichloro-2-propyl)phosphate results in decreased expression of CHST15 mRNA	26179874
Urethane	CHST15	Homo sapiens	Urethane results in decreased expression of CHST15 mRNA	28818685
Vanadates	CHST15	Homo sapiens	Vanadates results in increased expression of CHST15 mRNA	22714537
4-(5-benzo(1,3)dioxol-5-yl-4-pyridin-2-yl-1H-imidazol-2-yl) benzamide	SLFN11	Homo sapiens	[NOG protein co-treated with Valproic Acid co-treated with dorsomorphin co-treated with 4-(5-benzo(1,3)dioxol-5-yl-4-pyridin-2-yl-1H-imidazol-2-yl)benzamide] results in increased expression of SLFN11 mRNA	27188386
7,8-Dihydro-7,8-dihydroxybenzo(a) pyrene 9,10-oxide	SLFN11	Homo sapiens	7,8-Dihydro-7,8-dihydroxybenzo(a)pyrene 9,10-oxide results in decreased expression of SLFN11 mRNA	20382639
Benzene	SLFN11	Homo sapiens	Benzene results in increased expression of SLFN11 mRNA	15929907
Benzo(a)pyrene	SLFN11	Homo sapiens	Benzo(a)pyrene affects the methylation of SLFN11 promoter	27901495
Benzo(a)pyrene	SLFN11	Homo sapiens	Benzo(a)pyrene results in decreased methylation of SLFN11 5' UTR	27901495
bisphenol A	SLFN11	Homo sapiens	bisphenol A results in decreased methylation of SLFN11 gene	31601247
cobaltous chloride	SLFN11	Homo sapiens	cobaltous chloride results in decreased expression of SLFN11 mRNA	19320972
Copper	SLFN11	Homo sapiens	[Disulfiram binds to Copper] which results in decreased expression of SLFN11 mRNA	24690739
dorsomorphin	SLFN11	Homo sapiens	[NOG protein co-treated with Valproic Acid co-treated with dorsomorphin co-treated with 4-(5-benzo(1,3)dioxol-5-yl-4-pyridin-2-yl-1H-imidazol-2-yl)benzamide] results in increased expression of SLFN11 mRNA	27188386
methylmercuric chloride	SLFN11	Homo sapiens	methylmercuric chloride results in increased expression of SLFN11 mRNA	28001369
Mustard Gas	SLFN11	Homo sapiens	Mustard Gas results in decreased expression of SLFN11 mRNA	25102026
Nickel	SLFN11	Homo sapiens	Nickel results in increased expression of SLFN11 mRNA	25583101
Polystyrenes	SLFN11	Homo sapiens	Polystyrenes results in increased expression of SLFN11 mRNA	25102311
potassium chromate(VI)	SLFN11	Homo sapiens	potassium chromate(VI) results in increased expression of SLFN11 mRNA	22714537

(Continued)

TABLE 2 Continued

Chemical Name	Gene Symbol	Organism	Interaction	ReferencesPubMedID
Tobacco Smoke Pollution	SLFN11	Homo sapiens	Tobacco Smoke Pollution results in decreased expression of SLFN11 mRNA	33660061
Vanadates	SLFN11	Homo sapiens	Vanadates results in decreased expression of SLFN11 mRNA	22714537
4-(4-((5-(4,5-dimethyl-2-nitrophenyl)-2-furanyl)methylene)-4,5-dihydro-3-methyl-5-oxo-1H-pyrazol-1-yl)benzoic acid	GPR137B	Homo sapiens	4-(4-((5-(4,5-dimethyl-2-nitrophenyl)-2-furanyl)methylene)-4,5-dihydro-3-methyl-5-oxo-1H-pyrazol-1-yl)benzoic acid results in increased expression of GPR137B mRNA	26191083
4-(5-benzo(1,3)dioxol-5-yl-4-pyridin-2-yl-1H-imidazol-2-yl)benzamide	GPR137B	Homo sapiens	[NOG protein co-treated with Phenylmercuric Acetate co-treated with dorsomorphin co-treated with 4-(5-benzo(1,3)dioxol-5-yl-4-pyridin-2-yl-1H-imidazol-2-yl)benzamide] results in increased expression of GPR137B mRNA	27188386
7,8-Dihydro-7,8-dihydroxybenzo(a)pyrene 9,10-oxide	GPR137B	Homo sapiens	7,8-Dihydro-7,8-dihydroxybenzo(a)pyrene 9,10-oxide results in increased expression of GPR137B mRNA	20382639
Aflatoxin B1	GPR137B	Homo sapiens	Aflatoxin B1 affects the methylation of GPR137B intron	30157460
Aflatoxin B1	GPR137B	Homo sapiens	Aflatoxin B1 results in decreased methylation of GPR137B gene	27153756
aflatoxin B2	GPR137B	Homo sapiens	aflatoxin B2 results in increased methylation of GPR137B intron	30157460
aristolochic acid I	GPR137B	Homo sapiens	aristolochic acid I results in decreased expression of GPR137B mRNA	33212167
Arsenic	GPR137B	Homo sapiens	Arsenic affects the methylation of GPR137B gene	25304211
Benzene	GPR137B	Homo sapiens	Benzene results in increased expression of GPR137B mRNA	19162166
Benzo(a)pyrene	GPR137B	Homo sapiens	Benzo(a)pyrene affects the methylation of GPR137B intron	30157460
Benzo(a)pyrene	GPR137B	Homo sapiens	Benzo(a)pyrene affects the methylation of GPR137B promoter	27901495
benzo(e)pyrene	GPR137B	Homo sapiens	benzo(e)pyrene results in increased methylation of GPR137B intron	30157460
bisphenol A	GPR137B	Homo sapiens	bisphenol A results in increased expression of GPR137B mRNA	29275510
Copper Sulfate	GPR137B	Homo sapiens	Copper Sulfate results in increased expression of GPR137B mRNA	19549813
dorsomorphin	GPR137B	Homo sapiens	[NOG protein co-treated with Phenylmercuric Acetate co-treated with dorsomorphin co-treated with 4-(5-benzo(1,3)dioxol-5-yl-4-pyridin-2-yl-1H-imidazol-2-yl)benzamide] results in increased expression of GPR137B mRNA	27188386
Fonofos	GPR137B	Homo sapiens	Fonofos results in decreased methylation of GPR137B promoter	22847954
Formaldehyde	GPR137B	Homo sapiens	Formaldehyde results in increased expression of GPR137B mRNA	23649840
Lead	GPR137B	Homo sapiens	Lead affects the expression of GPR137B mRNA	28903495
methylmercuric chloride	GPR137B	Homo sapiens	methylmercuric chloride results in increased expression of GPR137B mRNA	28001369
Methyl Methanesulfonate	GPR137B	Homo sapiens	Methyl Methanesulfonate results in increased expression of GPR137B mRNA	21527772

(Continued)

TABLE 2 Continued

Chemical Name	Gene Symbol	Organism	Interaction	ReferencesPubMedID
Parathion	GPR137B	Homo sapiens	Parathion results in decreased methylation of GPR137B promoter	22847954
Phenylmercuric Acetate	GPR137B	Homo sapiens	[NOG protein co-treated with Phenylmercuric Acetate co-treated with dorsomorphin co-treated with 4-(5-benzo(1,3)dioxol-5-yl-4-pyridin-2-yl-1H-imidazol-2-yl)benzamide] results in increased expression of GPR137B mRNA	27188386
Phenylmercuric Acetate	GPR137B	Homo sapiens	Phenylmercuric Acetate results in increased expression of GPR137B mRNA	26272509
Selenium	GPR137B	Homo sapiens	Selenium results in decreased expression of GPR137B mRNA	19244175
Silicon Dioxide	GPR137B	Homo sapiens	Silicon Dioxide analog results in increased expression of GPR137B mRNA	25895662
terbufos	GPR137B	Homo sapiens	terbufos results in decreased methylation of GPR137B promoter	22847954
Tobacco Smoke Pollution	GPR137B	Homo sapiens	Tobacco Smoke Pollution results in increased expression of GPR137B mRNA	28065790
tris(1,3-dichloro-2-propyl) phosphate	GPR137B	Homo sapiens	tris(1,3-dichloro-2-propyl)phosphate results in increased expression of GPR137B mRNA	26179874
Urethane	GPR137B	Homo sapiens	Urethane results in increased expression of GPR137B mRNA	28818685
vanadyl sulfate	GPR137B	Homo sapiens	vanadyl sulfate results in decreased expression of GPR137B mRNA	16330358
1-Methyl-3-isobutylxanthine	ITGA5	Homo sapiens	[INS protein co-treated with Dexamethasone co-treated with 1-Methyl-3-isobutylxanthine co-treated with Indomethacin co-treated with bis(4-hydroxyphenyl)sulfone] results in decreased expression of ITGA5 mRNA	28628672
1-Methyl-3-isobutylxanthine	ITGA5	Homo sapiens	[INS protein co-treated with Dexamethasone co-treated with 1-Methyl-3-isobutylxanthine co-treated with Indomethacin co-treated with bisphenol A] results in decreased expression of ITGA5 mRNA	28628672
1-Naphthylisothiocyanate	ITGA5	Homo sapiens	1-Naphthylisothiocyanate results in increased expression of [ITGB6 protein co-treated with ITGA5 protein]	21037076
1-Naphthylisothiocyanate	ITGA5	Homo sapiens	[1-Naphthylisothiocyanate results in increased expression of [ITGB6 protein co-treated with ITGA5 protein]] which results in increased activity of TGFβ1 protein	21037076
1-Naphthylisothiocyanate	ITGA5	Homo sapiens	F2R protein promotes the reaction [1-Naphthylisothiocyanate results in increased expression of [ITGB6 protein co-treated with ITGA5 protein]]	21037076
1-Naphthylisothiocyanate	ITGA5	Homo sapiens	F3 protein promotes the reaction [1-Naphthylisothiocyanate results in increased expression of [ITGB6 protein co-treated with ITGA5 protein]]	21037076
2-(4-morpholinyl)-8-phenyl-4H-1-benzopyran-4-one	ITGA5	Homo sapiens	2-(4-morpholinyl)-8-phenyl-4H-1-benzopyran-4-one inhibits the reaction [IGF1 protein results in increased expression of and affects the localization of [ITGA5 protein binds to ITGB3 protein]]	16465378
2-methoxy-N-(3-methyl-2-oxo-1,2,3,4-tetrahydroquinazolin-6-yl) benzenesulfonamide	ITGA5	Homo sapiens	2-methoxy-N-(3-methyl-2-oxo-1,2,3,4-tetrahydroquinazolin-6-yl) benzenesulfonamide inhibits the reaction [TGFβ1 protein results in increased expression of ITGA5 mRNA]	26644586
2-methoxy-N-(3-methyl-2-oxo-1,2,3,4-tetrahydroquinazolin-6-yl) benzenesulfonamide	ITGA5	Homo sapiens	2-methoxy-N-(3-methyl-2-oxo-1,2,3,4-tetrahydroquinazolin-6-yl) benzenesulfonamide results in decreased expression of ITGA5 mRNA	26644586
3-(6-methoxypyridin-3-yl)-3-(2-oxo-3-(3-(5,6,7,8-tetrahydro(1,8)	ITGA5	Homo sapiens	3-(6-methoxypyridin-3-yl)-3-(2-oxo-3-(3-(5,6,7,8-tetrahydro(1,8) naphthyridin-2-yl)propyl)imidazolidin-1-yl)propionic acid binds to [ITGA5 protein binds to ITGB3 protein]	14561098

(Continued)

TABLE 2 Continued

Chemical Name	Gene Symbol	Organism	Interaction	ReferencesPubMedID
naphthyridin-2-yl)propyl)imidazolidin-1-yl)propionic acid				
4-(4-((5-(4,5-dimethyl-2-nitrophenyl)-2-furanyl)methylene)-4,5-dihydro-3-methyl-5-oxo-1H-pyrazol-1-yl)benzoic acid	ITGA5	Homo sapiens	4-(4-((5-(4,5-dimethyl-2-nitrophenyl)-2-furanyl)methylene)-4,5-dihydro-3-methyl-5-oxo-1H-pyrazol-1-yl)benzoic acid results in increased expression of ITGA5 mRNA	26191083
4-hydroxy-2-nonenal	ITGA5	Homo sapiens	4-hydroxy-2-nonenal results in decreased expression of ITGA5 mRNA	12419474
Aluminum Oxide	ITGA5	Homo sapiens	[Aluminum Oxide co-treated with Magnesium] results in increased expression of ITGA5 protein	12209937
aristolochic acid I	ITGA5	Homo sapiens	aristolochic acid I results in increased expression of ITGA5 mRNA	33212167
Arsenic	ITGA5	Homo sapiens	[sodium arsenate results in increased abundance of Arsenic] which results in increased expression of ITGA5 mRNA	32525701
Atrazine	ITGA5	Homo sapiens	Atrazine inhibits the reaction [Tetradecanoylphorbol Acetate results in increased expression of ITGA5 mRNA]	24211529
Benomyl	ITGA5	Homo sapiens	Benomyl results in decreased expression of ITGA5 mRNA	25530041
Benzene	ITGA5	Homo sapiens	Benzene results in increased expression of ITGA5 mRNA	19162166
benzo(e)pyrene	ITGA5	Homo sapiens	benzo(e)pyrene results in increased methylation of ITGA5 intron	30157460
bisphenol A	ITGA5	Homo sapiens	[bisphenol A co-treated with Fulvestrant] results in increased methylation of ITGA5 gene	31601247
bisphenol A	ITGA5	Homo sapiens	bisphenol A results in decreased expression of ITGA5 mRNA	31715268 32981897
bisphenol A	ITGA5	Homo sapiens	bisphenol A results in decreased expression of ITGA5 protein	31675489 32981897
bisphenol A	ITGA5	Homo sapiens	[INS protein co-treated with Dexamethasone co-treated with 1-Methyl-3-isobutylxanthine co-treated with Indomethacin co-treated with bisphenol A] results in decreased expression of ITGA5 mRNA	28628672
bisphenol B	ITGA5	Homo sapiens	bisphenol B results in increased expression of ITGA5 protein	34186270
bisphenol F	ITGA5	Homo sapiens	bisphenol F results in increased expression of ITGA5 protein	34186270
Cadmium	ITGA5	Homo sapiens	[Cadmium Chloride results in increased abundance of Cadmium] which results in decreased expression of ITGA5 mRNA	29741670
Cadmium	ITGA5	Homo sapiens	Cadmium results in decreased expression of ITGA5 mRNA	20570719
Cadmium	ITGA5	Homo sapiens	Cadmium results in increased expression of ITGA5 mRNA	20570719
Cadmium Chloride	ITGA5	Homo sapiens	Cadmium Chloride results in decreased expression of ITGA5 mRNA	26472689
Cadmium Chloride	ITGA5	Homo sapiens	[Cadmium Chloride results in increased abundance of Cadmium] which results in decreased expression of ITGA5 mRNA	29741670
Cadmium Chloride	ITGA5	Homo sapiens	Cadmium Chloride results in increased expression of ITGA5 protein	28527916
carbendazim	ITGA5	Homo sapiens	carbendazim results in decreased expression of ITGA5 mRNA	25530041

(Continued)

TABLE 2 Continued

Chemical Name	Gene Symbol	Organism	Interaction	ReferencesPubMedID
Clioquinol	ITGA5	Homo sapiens	ITGA5 protein promotes the reaction [[Clioquinol binds to Copper] which results in increased phosphorylation of EGFR protein]	18346929
cobaltous chloride	ITGA5	Homo sapiens	cobaltous chloride results in increased expression of ITGA5 protein	16798617
Copper	ITGA5	Homo sapiens	[Chelating Agents binds to Copper] which results in increased expression of ITGA5 mRNA	30911355
Copper	ITGA5	Homo sapiens	ITGA5 protein promotes the reaction [[Clioquinol binds to Copper] which results in increased phosphorylation of EGFR protein]	18346929
Cosmetics	ITGA5	Homo sapiens	[Plasticizers co-treated with Cosmetics co-treated with Flame Retardants co-treated with perfluorooctanoic acid co-treated with Phytoestrogens] results in decreased expression of ITGA5 mRNA	33325755
DDT	ITGA5	Homo sapiens	DDT results in increased expression of ITGA5 mRNA	22902829
decabromobiphenyl ether	ITGA5	Homo sapiens	decabromobiphenyl ether results in decreased expression of ITGA5 protein	31675489
diallyl trisulfide	ITGA5	Homo sapiens	diallyl trisulfide results in decreased expression of ITGA5 protein	28741790
Dibutyl Phthalate	ITGA5	Homo sapiens	Dibutyl Phthalate results in increased expression of ITGA5 mRNA	34902519
Endosulfan	ITGA5	Homo sapiens	Endosulfan results in increased expression of ITGA5 mRNA	22902829
erucylphospho-N,N,N-trimethylpropylammonium	ITGA5	Homo sapiens	erucylphospho-N,N,N-trimethylpropylammonium results in increased expression of ITGA5 mRNA	29464035
Ethanol	ITGA5	Homo sapiens	Ethanol results in increased expression of ITGA5 mRNA	12720008
Flame Retardants	ITGA5	Homo sapiens	[Plasticizers co-treated with Cosmetics co-treated with Flame Retardants co-treated with perfluorooctanoic acid co-treated with Phytoestrogens] results in decreased expression of ITGA5 mRNA	33325755
glyphosate	ITGA5	Homo sapiens	glyphosate results in decreased expression of ITGA5 mRNA	31295307
Heptachlor	ITGA5	Homo sapiens	Heptachlor results in increased expression of ITGA5 mRNA	22902829
hexabrominated diphenyl ether 153	ITGA5	Homo sapiens	hexabrominated diphenyl ether 153 results in decreased expression of ITGA5 protein	31675489
Hydrogen Peroxide	ITGA5	Homo sapiens	Hydrogen Peroxide results in decreased expression of ITGA5 mRNA	12419474
Magnesium	ITGA5	Homo sapiens	[Aluminum Oxide co-treated with Magnesium] results in increased expression of ITGA5 protein	12209937
Ozone	ITGA5	Homo sapiens	[Aripiprazole co-treated with Ozone] results in increased expression of ITGA5 mRNA	31476115
Ozone	ITGA5	Homo sapiens	Ozone results in increased expression of ITGA5 mRNA	31476115
peracetylated N-azidoacetylmannosamine	ITGA5	Homo sapiens	peracetylated N-azidoacetylmannosamine results in decreased expression of ITGA5 mRNA	30181604
perfluoro-n-nonanoic acid	ITGA5	Homo sapiens	perfluoro-n-nonanoic acid results in increased expression of ITGA5 mRNA	32588087
perfluorooctanoic acid	ITGA5	Homo sapiens	[Plasticizers co-treated with Cosmetics co-treated with Flame Retardants co-treated with perfluorooctanoic acid co-treated with Phytoestrogens] results in decreased expression of ITGA5 mRNA	33325755

(Continued)

TABLE 2 Continued

Chemical Name	Gene Symbol	Organism	Interaction	ReferencesPubMedID
Plant Extracts	ITGA5	Homo sapiens	[Plant Extracts results in increased abundance of Cannabinoids] inhibits the reaction [TNF protein results in increased expression of ITGA5 mRNA]	31250491
Plasticizers	ITGA5	Homo sapiens	[Plasticizers co-treated with Cosmetics co-treated with Flame Retardants co-treated with perfluorooctanoic acid co-treated with Phytoestrogens] results in decreased expression of ITGA5 mRNA	33325755
potassium chromate(VI)	ITGA5	Homo sapiens	potassium chromate(VI) results in decreased expression of ITGA5 mRNA	22714537
quinoline	ITGA5	Homo sapiens	quinoline analog binds to and results in decreased activity of [ITGA5 protein binds to ITGB3 protein]	16984141
Silicon Dioxide	ITGA5	Homo sapiens	Silicon Dioxide analog results in increased expression of ITGA5 mRNA	25895662
Smoke	ITGA5	Homo sapiens	Smoke results in increased expression of ITGA5 mRNA	34520756
sodium arsenate	ITGA5	Homo sapiens	[sodium arsenate results in increased abundance of Arsenic] which results in increased expression of ITGA5 mRNA	32525701
sodium arsenite	ITGA5	Homo sapiens	sodium arsenite affects the methylation of ITGA5 gene	28589171
Sodium Selenite	ITGA5	Homo sapiens	Sodium Selenite results in increased expression of ITGA5 mRNA	18175754
tablysin-15, Tabanus yao	ITGA5	Homo sapiens	tablysin-15, Tabanus yao inhibits the reaction [VTN protein binds to [ITGA5 protein binds to ITGB3 protein]]	21475772
tert-Butylhydroperoxide	ITGA5	Homo sapiens	tert-Butylhydroperoxide results in decreased expression of ITGA5 mRNA	12419474
Tetrachlorodibenzodioxin	ITGA5	Homo sapiens	[Tetrachlorodibenzodioxin co-treated with 2-methyl-2H-pyrazole-3-carboxylic acid (2-methyl-4-o-tolylazophenyl)amide] results in decreased expression of ITGA5 mRNA	29704546
Tetrachlorodibenzodioxin	ITGA5	Homo sapiens	Tetrachlorodibenzodioxin results in increased expression of ITGA5 mRNA	16051281 22902829
Tetradecanoylphorbol Acetate	ITGA5	Homo sapiens	Atrazine inhibits the reaction [Tetradecanoylphorbol Acetate results in increased expression of ITGA5 mRNA]	24211529
Tetradecanoylphorbol Acetate	ITGA5	Homo sapiens	Tetradecanoylphorbol Acetate results in increased expression of ITGA5 mRNA	24211529
titanium dioxide	ITGA5	Homo sapiens	[Vitalium analog binds to titanium dioxide] which results in increased expression of ITGA5 mRNA	23825117
Tobacco Smoke Pollution	ITGA5	Homo sapiens	Tobacco Smoke Pollution affects the expression of ITGA5 protein	30291989
Tobacco Smoke Pollution	ITGA5	Homo sapiens	Tobacco Smoke Pollution results in increased expression of ITGA5 mRNA	27865774 33660061
tris(2-butoxyethyl) phosphate	ITGA5	Homo sapiens	tris(2-butoxyethyl) phosphate affects the expression of ITGA5 mRNA	29024780
Urethane	ITGA5	Homo sapiens	Urethane results in increased expression of ITGA5 mRNA	28818685
Vanadates	ITGA5	Homo sapiens	Vanadates results in increased expression of ITGA5 mRNA	22714537
Vitalium	ITGA5	Homo sapiens	[Vitalium analog binds to titanium dioxide] which results in increased expression of ITGA5 mRNA	23825117
4-(4-((5-(4,5-dimethyl-2-nitrophenyl)-2-furanyl)methylene)-4,5-dihydro-3-methyl-5-oxo-1H-pyrazol-1-yl)benzoic acid	LILRB1	Homo sapiens	4-(4-((5-(4,5-dimethyl-2-nitrophenyl)-2-furanyl)methylene)-4,5-dihydro-3-methyl-5-oxo-1H-pyrazol-1-yl)benzoic acid results in increased expression of LILRB1 mRNA	26191083

(Continued)

TABLE 2 Continued

Chemical Name	Gene Symbol	Organism	Interaction	ReferencesPubMedID
4,5-dihydro-3-methyl-5-oxo-1H-pyrazol-1-yl)benzoic acid				
Aflatoxin B1	LILRB1	Homo sapiens	Aflatoxin B1 affects the expression of LILRB1 protein	20106945
Aflatoxin B1	LILRB1	Homo sapiens	Aflatoxin B1 results in decreased expression of LILRB1 mRNA	21632981
Aflatoxin B1	LILRB1	Homo sapiens	Aflatoxin B1 results in increased methylation of LILRB1 gene	27153756
Air Pollutants, Occupational	LILRB1	Homo sapiens	Air Pollutants, Occupational results in decreased expression of LILRB1 mRNA	23195993
Arsenic	LILRB1	Homo sapiens	Arsenic affects the methylation of LILRB1 gene	25304211
Arsenic Trioxide	LILRB1	Homo sapiens	Arsenic Trioxide results in decreased expression of LILRB1 mRNA	27829220
Arsenic Trioxide	LILRB1	Homo sapiens	Arsenic Trioxide results in increased expression of LILRB1 mRNA	22072212
Asbestos, Crocidolite	LILRB1	Homo sapiens	Asbestos, Crocidolite results in decreased expression of LILRB1 mRNA	29523930
Benzo(a)pyrene	LILRB1	Homo sapiens	Benzo(a)pyrene results in decreased expression of LILRB1 mRNA	21632981
Benzo(a)pyrene	LILRB1	Homo sapiens	Benzo(a)pyrene results in decreased methylation of LILRB1 5' UTR	27901495
benzo(e)pyrene	LILRB1	Homo sapiens	benzo(e)pyrene results in increased methylation of LILRB1 intron	30157460
cobaltous chloride	LILRB1	Homo sapiens	cobaltous chloride results in increased expression of LILRB1 mRNA	23052192
erucylphospho-N,N,N-trimethylpropylammonium	LILRB1	Homo sapiens	erucylphospho-N,N,N-trimethylpropylammonium results in increased expression of LILRB1 mRNA	29464035
Ethyl Methanesulfonate	LILRB1	Homo sapiens	Ethyl Methanesulfonate results in decreased expression of LILRB1 mRNA	23649840
Hydrogen Peroxide	LILRB1	Homo sapiens	Hydrogen Peroxide affects the expression of LILRB1 mRNA	21179406
Methyl Methanesulfonate	LILRB1	Homo sapiens	Methyl Methanesulfonate results in decreased expression of LILRB1 mRNA	23649840
Nickel	LILRB1	Homo sapiens	Nickel results in decreased expression of LILRB1 mRNA	23195993
Nickel	LILRB1	Homo sapiens	Nickel results in increased expression of LILRB1 mRNA	24768652 25583101
sodium bichromate	LILRB1	Homo sapiens	sodium bichromate results in decreased expression of LILRB1 mRNA	17685462
Tetrachlorodibenzodioxin	LILRB1	Homo sapiens	Tetrachlorodibenzodioxin results in decreased expression of LILRB1 mRNA	20106945 21632981
Zinc	LILRB1	Homo sapiens	Zinc deficiency results in increased expression of LILRB1 mRNA	22171008
2,2',4,4'-tetrabromodiphenyl ether	BGN	Homo sapiens	2,2',4,4'-tetrabromodiphenyl ether results in decreased expression of BGN protein	31675489
2,4,6-tribromophenol	BGN	Homo sapiens	2,4,6-tribromophenol results in decreased expression of BGN mRNA	31675489

(Continued)

TABLE 2 Continued

Chemical Name	Gene Symbol	Organism	Interaction	ReferencesPubMedID
4-(4-((5-(4,5-dimethyl-2-nitrophenyl)-2-furanyl)methylene)-4,5-dihydro-3-methyl-5-oxo-1H-pyrazol-1-yl)benzoic acid	BGN	Homo sapiens	4-(4-((5-(4,5-dimethyl-2-nitrophenyl)-2-furanyl)methylene)-4,5-dihydro-3-methyl-5-oxo-1H-pyrazol-1-yl)benzoic acid results in increased expression of BGN mRNA	26191083
4-(5-benzo(1,3)dioxol-5-yl-4-pyridin-2-yl-1H-imidazol-2-yl)benzamide	BGN	Homo sapiens	[NOG protein co-treated with Phenylmercuric Acetate co-treated with dorsomorphin co-treated with 4-(5-benzo(1,3)dioxol-5-yl-4-pyridin-2-yl-1H-imidazol-2-yl)benzamide] results in increased expression of BGN mRNA	27188386
4-(5-benzo(1,3)dioxol-5-yl-4-pyridin-2-yl-1H-imidazol-2-yl)benzamide	BGN	Homo sapiens	[NOG protein co-treated with trichostatin A co-treated with dorsomorphin co-treated with 4-(5-benzo(1,3)dioxol-5-yl-4-pyridin-2-yl-1H-imidazol-2-yl)benzamide] results in increased expression of BGN mRNA	27188386
4-(5-benzo(1,3)dioxol-5-yl-4-pyridin-2-yl-1H-imidazol-2-yl)benzamide	BGN	Homo sapiens	[NOG protein co-treated with Valproic Acid co-treated with dorsomorphin co-treated with 4-(5-benzo(1,3)dioxol-5-yl-4-pyridin-2-yl-1H-imidazol-2-yl)benzamide] results in increased expression of BGN mRNA	27188386
4-hydroxy-2-nonenal	BGN	Homo sapiens	[[BGN mRNA alternative form binds to OTUB1 protein] which binds to and results in decreased ubiquitination of and results in increased stability of SLC7A11 protein] which results in decreased abundance of 4-hydroxy-2-nonenal	35234341
Aflatoxin B1	BGN	Homo sapiens	Aflatoxin B1 results in decreased methylation of BGN intron	30157460
aflatoxin B2	BGN	Homo sapiens	aflatoxin B2 results in increased methylation of BGN intron	30157460
Aluminum Oxide	BGN	Homo sapiens	Aluminum Oxide results in increased expression of BGN mRNA	19464052
aristolochic acid I	BGN	Homo sapiens	aristolochic acid I results in decreased expression of BGN mRNA	33212167
Asbestos, Crocidolite	BGN	Homo sapiens	Asbestos, Crocidolite results in increased expression of BGN protein	29553831
Benzo(a)pyrene	BGN	Homo sapiens	Benzo(a)pyrene affects the methylation of BGN intron	30157460
Benzo(a)pyrene	BGN	Homo sapiens	Benzo(a)pyrene affects the methylation of BGN promoter	27901495
Benzo(a)pyrene	BGN	Homo sapiens	Benzo(a)pyrene results in increased methylation of BGN 5' UTR	27901495
benzo(e)pyrene	BGN	Homo sapiens	benzo(e)pyrene results in increased methylation of BGN intron	30157460
Cadmium	BGN	Homo sapiens	[Cadmium Chloride results in increased abundance of Cadmium] which results in decreased expression of BGN mRNA	29741670 35301059
Cadmium Chloride	BGN	Homo sapiens	[Cadmium Chloride results in increased abundance of Cadmium] which results in decreased expression of BGN mRNA	29741670 35301059
Chromium	BGN	Homo sapiens	Chromium results in decreased expression of BGN mRNA	21437242
cobaltous chloride	BGN	Homo sapiens	cobaltous chloride results in decreased secretion of BGN protein	22079246
Diazinon	BGN	Homo sapiens	Diazinon results in increased methylation of BGN gene	22964155
dorsomorphin	BGN	Homo sapiens	[NOG protein co-treated with Phenylmercuric Acetate co-treated with dorsomorphin co-treated with 4-(5-benzo(1,3)dioxol-5-yl-4-pyridin-2-yl-1H-imidazol-2-yl)benzamide] results in increased expression of BGN mRNA	27188386

(Continued)

TABLE 2 Continued

Chemical Name	Gene Symbol	Organism	Interaction	ReferencesPubMedID
dorsomorphin	BGN	Homo sapiens	[NOG protein co-treated with trichostatin A co-treated with dorsomorphin co-treated with 4-(5-benzo(1,3)dioxol-5-yl-4-pyridin-2-yl-1H-imidazol-2-yl)benzamide] results in increased expression of BGN mRNA	27188386
dorsomorphin	BGN	Homo sapiens	[NOG protein co-treated with Valproic Acid co-treated with dorsomorphin co-treated with 4-(5-benzo(1,3)dioxol-5-yl-4-pyridin-2-yl-1H-imidazol-2-yl)benzamide] results in increased expression of BGN mRNA	27188386
Ethanol	BGN	Homo sapiens	[[Gasoline co-treated with Ethanol] results in increased abundance of [Particulate Matter co-treated with Polycyclic Aromatic Hydrocarbons]] which results in decreased expression of BGN mRNA	29432896
Ferrous Compounds	BGN	Homo sapiens	[[BGN mRNA alternative form binds to OTUB1 protein] which binds to and results in decreased ubiquitination of and results in increased stability of SLC7A11 protein] which results in decreased abundance of Ferrous Compounds	35234341
Gasoline	BGN	Homo sapiens	[[Gasoline co-treated with Ethanol] results in increased abundance of [Particulate Matter co-treated with Polycyclic Aromatic Hydrocarbons]] which results in decreased expression of BGN mRNA	29432896
Lactic Acid	BGN	Homo sapiens	Lactic Acid affects the expression of BGN mRNA	30851411
Malondialdehyde	BGN	Homo sapiens	[[BGN mRNA alternative form binds to OTUB1 protein] which binds to and results in decreased ubiquitination of and results in increased stability of SLC7A11 protein] which results in decreased abundance of Malondialdehyde	35234341
Oxygen	BGN	Homo sapiens	Oxygen deficiency results in increased expression of BGN mRNA	26516004
Particulate Matter	BGN	Homo sapiens	[[Gasoline co-treated with Ethanol] results in increased abundance of [Particulate Matter co-treated with Polycyclic Aromatic Hydrocarbons]] which results in decreased expression of BGN mRNA	29432896
Phenylmercuric Acetate	BGN	Homo sapiens	[NOG protein co-treated with Phenylmercuric Acetate co-treated with dorsomorphin co-treated with 4-(5-benzo(1,3)dioxol-5-yl-4-pyridin-2-yl-1H-imidazol-2-yl)benzamide] results in increased expression of BGN mRNA	27188386
Phenylmercuric Acetate	BGN	Homo sapiens	Phenylmercuric Acetate results in increased expression of BGN mRNA	26272509
Plant Extracts	BGN	Homo sapiens	[Plant Extracts co-treated with Resveratrol] results in decreased expression of BGN mRNA	23557933
Polycyclic Aromatic Hydrocarbons	BGN	Homo sapiens	[[Gasoline co-treated with Ethanol] results in increased abundance of [Particulate Matter co-treated with Polycyclic Aromatic Hydrocarbons]] which results in decreased expression of BGN mRNA	29432896
potassium chromate(VI)	BGN	Homo sapiens	potassium chromate(VI) results in decreased expression of BGN mRNA	22714537
Tetrachlorodibenzodioxin	BGN	Homo sapiens	Tetrachlorodibenzodioxin affects the expression of BGN mRNA	22574217
Tobacco Smoke Pollution	BGN	Homo sapiens	Tobacco Smoke Pollution affects the expression of BGN protein	30291989
Tobacco Smoke Pollution	BGN	Homo sapiens	Tobacco Smoke Pollution results in decreased expression of BGN mRNA	33660061
tris(2-butoxyethyl) phosphate	BGN	Homo sapiens	tris(2-butoxyethyl) phosphate affects the expression of BGN mRNA	29024780

(Continued)

TABLE 2 Continued

Chemical Name	Gene Symbol	Organism	Interaction	ReferencesPubMedID
Uranium	BGN	Homo sapiens	Uranium affects the expression of BGN mRNA	15672453
uranyl acetate	BGN	Homo sapiens	uranyl acetate affects the expression of BGN mRNA	15672453

TABLE 3 The interaction between drug exposure and HMGSs

Chemical Name	Gene Symbol	Organism	Interaction	References PubMedID
Acetaminophen	GPR4	Homo sapiens	Acetaminophen results in decreased expression of GPR4 mRNA	22230336
Acetaminophen	GPR4	Homo sapiens	Acetaminophen results in increased expression of GPR4 mRNA	26690555
Anti-Inflammatory Agents	GPR4	Homo sapiens	Anti-Inflammatory Agents binds to and results in decreased activity of GPR4 protein	32370492
Anti-Inflammatory Agents	GPR4	Homo sapiens	[Anti-Inflammatory Agents binds to and results in decreased activity of GPR4 protein] inhibits the reaction [[Biological Factors binds to Sugars] which results in increased expression of IL1B mRNA]	32370492
Anti-Inflammatory Agents	GPR4	Homo sapiens	[Anti-Inflammatory Agents binds to and results in decreased activity of GPR4 protein] inhibits the reaction [[Biological Factors binds to Sugars] which results in increased expression of IL1B protein]	32370492
Anti-Inflammatory Agents	GPR4	Homo sapiens	[Anti-Inflammatory Agents binds to and results in decreased activity of GPR4 protein] inhibits the reaction [[Biological Factors binds to Sugars] which results in increased expression of IL6 mRNA]	32370492
Anti-Inflammatory Agents	GPR4	Homo sapiens	[Anti-Inflammatory Agents binds to and results in decreased activity of GPR4 protein] inhibits the reaction [[Biological Factors binds to Sugars] which results in increased expression of IL6 protein]	32370492
Anti-Inflammatory Agents	GPR4	Homo sapiens	[Anti-Inflammatory Agents binds to and results in decreased activity of GPR4 protein] inhibits the reaction [[Biological Factors binds to Sugars] which results in increased expression of MMP13 mRNA]	32370492
Anti-Inflammatory Agents	GPR4	Homo sapiens	[Anti-Inflammatory Agents binds to and results in decreased activity of GPR4 protein] inhibits the reaction [[Biological Factors binds to Sugars] which results in increased expression of MMP13 protein]	32370492
Anti-Inflammatory Agents	GPR4	Homo sapiens	[Anti-Inflammatory Agents binds to and results in decreased activity of GPR4 protein] inhibits the reaction [[Biological Factors binds to Sugars] which results in increased expression of MMP3 mRNA]	32370492
Anti-Inflammatory Agents	GPR4	Homo sapiens	[Anti-Inflammatory Agents binds to and results in decreased activity of GPR4 protein] inhibits the reaction [[Biological Factors binds to Sugars] which results in increased expression of MMP3 protein]	32370492
Anti-Inflammatory Agents	GPR4	Homo sapiens	[Anti-Inflammatory Agents binds to and results in decreased activity of GPR4 protein] inhibits the reaction [[Biological Factors binds to Sugars] which results in increased expression of NOS2 mRNA]	32370492
Anti-Inflammatory Agents	GPR4	Homo sapiens	[Anti-Inflammatory Agents binds to and results in decreased activity of GPR4 protein] inhibits the reaction [[Biological Factors binds to Sugars] which results in increased expression of NOS2 protein]	32370492
Anti-Inflammatory Agents	GPR4	Homo sapiens	[Anti-Inflammatory Agents binds to and results in decreased activity of GPR4 protein] inhibits the reaction [[Biological Factors binds to Sugars] which results in increased expression of PTGS2 mRNA]	32370492

(Continued)

TABLE 3 Continued

Chemical Name	Gene Symbol	Organism	Interaction	References PubMedID
Anti-Inflammatory Agents	GPR4	Homo sapiens	[Anti-Inflammatory Agents binds to and results in decreased activity of GPR4 protein] inhibits the reaction [[Biological Factors binds to Sugars] which results in increased expression of PTGS2 protein]	32370492
Anti-Inflammatory Agents	GPR4	Homo sapiens	[Anti-Inflammatory Agents binds to and results in decreased activity of GPR4 protein] inhibits the reaction [[Biological Factors binds to Sugars] which results in increased expression of TNF mRNA]	32370492
Anti-Inflammatory Agents	GPR4	Homo sapiens	[Anti-Inflammatory Agents binds to and results in decreased activity of GPR4 protein] inhibits the reaction [[Biological Factors binds to Sugars] which results in increased expression of TNF protein]	32370492
Antirheumatic Agents	GPR4	Homo sapiens	Antirheumatic Agents results in decreased expression of GPR4 mRNA	24449571
Biological Factors	GPR4	Homo sapiens	[Anti-Inflammatory Agents binds to and results in decreased activity of GPR4 protein] inhibits the reaction [[Biological Factors binds to Sugars] which results in increased expression of IL1B mRNA]	32370492
Biological Factors	GPR4	Homo sapiens	[Anti-Inflammatory Agents binds to and results in decreased activity of GPR4 protein] inhibits the reaction [[Biological Factors binds to Sugars] which results in increased expression of IL1B protein]	32370492
Biological Factors	GPR4	Homo sapiens	[Anti-Inflammatory Agents binds to and results in decreased activity of GPR4 protein] inhibits the reaction [[Biological Factors binds to Sugars] which results in increased expression of IL6 mRNA]	32370492
Biological Factors	GPR4	Homo sapiens	[Anti-Inflammatory Agents binds to and results in decreased activity of GPR4 protein] inhibits the reaction [[Biological Factors binds to Sugars] which results in increased expression of IL6 protein]	32370492
Biological Factors	GPR4	Homo sapiens	[Anti-Inflammatory Agents binds to and results in decreased activity of GPR4 protein] inhibits the reaction [[Biological Factors binds to Sugars] which results in increased expression of MMP13 mRNA]	32370492
Biological Factors	GPR4	Homo sapiens	[Anti-Inflammatory Agents binds to and results in decreased activity of GPR4 protein] inhibits the reaction [[Biological Factors binds to Sugars] which results in increased expression of MMP13 protein]	32370492
Biological Factors	GPR4	Homo sapiens	[Anti-Inflammatory Agents binds to and results in decreased activity of GPR4 protein] inhibits the reaction [[Biological Factors binds to Sugars] which results in increased expression of MMP3 mRNA]	32370492
Biological Factors	GPR4	Homo sapiens	[Anti-Inflammatory Agents binds to and results in decreased activity of GPR4 protein] inhibits the reaction [[Biological Factors binds to Sugars] which results in increased expression of MMP3 protein]	32370492
Biological Factors	GPR4	Homo sapiens	[Anti-Inflammatory Agents binds to and results in decreased activity of GPR4 protein] inhibits the reaction [[Biological Factors binds to Sugars] which results in increased expression of NOS2 mRNA]	32370492
Biological Factors	GPR4	Homo sapiens	[Anti-Inflammatory Agents binds to and results in decreased activity of GPR4 protein] inhibits the reaction [[Biological Factors binds to Sugars] which results in increased expression of NOS2 protein]	32370492
Biological Factors	GPR4	Homo sapiens	[Anti-Inflammatory Agents binds to and results in decreased activity of GPR4 protein] inhibits the reaction [[Biological Factors binds to Sugars] which results in increased expression of PTGS2 mRNA]	32370492
Biological Factors	GPR4	Homo sapiens	[Anti-Inflammatory Agents binds to and results in decreased activity of GPR4 protein] inhibits the reaction [[Biological Factors binds to Sugars] which results in increased expression of PTGS2 protein]	32370492
Biological Factors	GPR4	Homo sapiens	[Anti-Inflammatory Agents binds to and results in decreased activity of GPR4 protein] inhibits the reaction [[Biological Factors binds to Sugars] which results in increased expression of TNF mRNA]	32370492
Biological Factors	GPR4	Homo sapiens	[Anti-Inflammatory Agents binds to and results in decreased activity of GPR4 protein] inhibits the reaction [[Biological Factors binds to Sugars] which results in increased expression of TNF protein]	32370492

(Continued)

TABLE 3 Continued

Chemical Name	Gene Symbol	Organism	Interaction	References PubMedID
Biological Factors	GPR4	Homo sapiens	[Biological Factors binds to Sugars] which results in increased expression of GPR4 mRNA	32370492
Biological Factors	GPR4	Homo sapiens	[Biological Factors binds to Sugars] which results in increased expression of GPR4 protein	32370492
Estradiol	GPR4	Homo sapiens	[Estradiol co-treated with TGFβ1 protein] results in increased expression of GPR4 mRNA	30165855
Lysophosphatidylcholines	GPR4	Homo sapiens	GPR4 protein promotes the reaction [Lysophosphatidylcholines results in increased expression of CASP3 protein]	34293432
Lysophosphatidylcholines	GPR4	Homo sapiens	GPR4 protein promotes the reaction [Lysophosphatidylcholines results in increased expression of IL18 protein]	34293432
Lysophosphatidylcholines	GPR4	Homo sapiens	GPR4 protein promotes the reaction [Lysophosphatidylcholines results in increased expression of IL1B protein]	34293432
Lysophosphatidylcholines	GPR4	Homo sapiens	GPR4 protein promotes the reaction [Lysophosphatidylcholines results in increased expression of IL33 protein]	34293432
Lysophosphatidylcholines	GPR4	Homo sapiens	GPR4 protein promotes the reaction [Lysophosphatidylcholines results in increased expression of NLRP3 protein]	34293432
Lysophosphatidylcholines	GPR4	Homo sapiens	Lysophosphatidylcholines results in increased expression of GPR4 mRNA	34293432
Lysophosphatidylcholines	GPR4	Homo sapiens	Lysophosphatidylcholines results in increased expression of GPR4 protein	34293432
Methotrexate	GPR4	Homo sapiens	Methotrexate results in decreased expression of GPR4 mRNA	24449571
quercitrin	GPR4	Homo sapiens	quercitrin results in increased expression of GPR4 mRNA	25193878
SCH772984	GPR4	Homo sapiens	SCH772984 inhibits the reaction [GPR4 protein affects the phosphorylation of MAPK1 protein]	33161135
SCH772984	GPR4	Homo sapiens	SCH772984 inhibits the reaction [GPR4 protein affects the phosphorylation of MAPK3 protein]	33161135
Valproic Acid	GPR4	Homo sapiens	Valproic Acid affects the expression of GPR4 mRNA	25979313
Valproic Acid	GPR4	Homo sapiens	Valproic Acid results in increased methylation of GPR4 gene	29154799
Acetaminophen	CYYR1	Homo sapiens	Acetaminophen results in increased expression of CYYR1 mRNA	29067470
bis(4-hydroxyphenyl) sulfone	CYYR1	Homo sapiens	bis(4-hydroxyphenyl)sulfone results in increased methylation of CYYR1 gene	31601247
Sunitinib	CYYR1	Homo sapiens	Sunitinib results in decreased expression of CYYR1 mRNA	31533062
Testosterone	CYYR1	Homo sapiens	Testosterone results in decreased expression of CYYR1 mRNA	33359661
Valproic Acid	CYYR1	Homo sapiens	Valproic Acid affects the expression of CYYR1 mRNA	25979313
Valproic Acid	CYYR1	Homo sapiens	Valproic Acid results in decreased expression of CYYR1 mRNA	23179753 25192806 28001369
abrine	ST3GAL2	Homo sapiens	abrine results in decreased expression of ST3GAL2 mRNA	31054353
Cannabidiol	ST3GAL2	Homo sapiens	Cannabidiol results in decreased expression of ST3GAL2 mRNA	33244087

(Continued)

TABLE 3 Continued

Chemical Name	Gene Symbol	Organism	Interaction	References PubMedID
Doxorubicin	ST3GAL2	Homo sapiens	Doxorubicin results in decreased expression of ST3GAL2 mRNA	29803840
Estradiol	ST3GAL2	Homo sapiens	Estradiol results in increased expression of ST3GAL2 mRNA	19429434
GSK-J4	ST3GAL2	Homo sapiens	GSK-J4 results in decreased expression of ST3GAL2 mRNA	29301935
Raloxifene Hydrochloride	ST3GAL2	Homo sapiens	Raloxifene Hydrochloride results in increased expression of ST3GAL2 mRNA	19429434
Sunitinib	ST3GAL2	Homo sapiens	Sunitinib results in decreased expression of ST3GAL2 mRNA	31533062
Tamoxifen	ST3GAL2	Homo sapiens	Tamoxifen results in increased expression of ST3GAL2 mRNA	19429434
Tretinoin	ST3GAL2	Homo sapiens	Tretinoin results in increased expression of ST3GAL2 mRNA	33167477
Valproic Acid	ST3GAL2	Homo sapiens	Valproic Acid affects the expression of ST3GAL2 mRNA	25979313
Ampicillin	CHST15	Homo sapiens	Ampicillin results in increased expression of CHST15 mRNA	21632981
Antirheumatic Agents	CHST15	Homo sapiens	Antirheumatic Agents results in decreased expression of CHST15 mRNA	24449571
belinostat	CHST15	Homo sapiens	belinostat results in increased expression of CHST15 mRNA	27188386
Biological Factors	CHST15	Homo sapiens	Biological Factors results in increased expression of CHST15 mRNA	32739440
Carbamazepine	CHST15	Homo sapiens	Carbamazepine affects the expression of CHST15 mRNA	25979313
CGP 52608	CHST15	Homo sapiens	CGP 52608 promotes the reaction [RORA protein binds to CHST15 gene]	28238834
Cyclosporine	CHST15	Homo sapiens	Cyclosporine results in decreased expression of CHST15 mRNA	25562108
Doxorubicin	CHST15	Homo sapiens	Doxorubicin results in decreased expression of CHST15 mRNA	29803840
entinostat	CHST15	Homo sapiens	entinostat results in increased expression of CHST15 mRNA	26272509
entinostat	CHST15	Homo sapiens	[NOG protein co-treated with entinostat co-treated with dorsomorphin co-treated with 4-(5-benzo(1,3)dioxol-5-yl-4-pyridin-2-yl-1H-imidazol-2-yl)benzamide] results in increased expression of CHST15 mRNA	27188386
epigallocatechin gallate	CHST15	Homo sapiens	[potassium chromate(VI) co-treated with epigallocatechin gallate] results in decreased expression of CHST15 mRNA	22079256
Estradiol	CHST15	Homo sapiens	[Estradiol co-treated with Progesterone] results in decreased expression of CHST15 mRNA	20660070
Estradiol	CHST15	Homo sapiens	[Estradiol co-treated with TGFB1 protein] results in increased expression of CHST15 mRNA	30165855
Fulvestrant	CHST15	Homo sapiens	[bisphenol A co-treated with Fulvestrant] results in increased methylation of CHST15 gene	31601247
ICG 001	CHST15	Homo sapiens	ICG 001 results in increased expression of CHST15 mRNA	26191083
Leflunomide	CHST15	Homo sapiens	Leflunomide results in increased expression of CHST15 mRNA	28988120

(Continued)

TABLE 3 Continued

Chemical Name	Gene Symbol	Organism	Interaction	References PubMedID
Lipopolysaccharides	CHST15	Homo sapiens	[S-(1,2-dichlorovinyl)cysteine co-treated with Lipopolysaccharides] results in decreased expression of CHST15 mRNA	35811015
Methotrexate	CHST15	Homo sapiens	Methotrexate results in decreased expression of CHST15 mRNA	24449571
Oxyquinoline	CHST15	Homo sapiens	Oxyquinoline results in increased expression of CHST15 mRNA	21632981
Panobinostat	CHST15	Homo sapiens	[NOG protein co-treated with Panobinostat co-treated with dorsomorphin co-treated with 4-(5-benzo(1,3)dioxol-5-yl-4-pyridin-2-yl-1H-imidazol-2-yl)benzamide] results in increased expression of CHST15 mRNA	27188386
Panobinostat	CHST15	Homo sapiens	Panobinostat results in increased expression of CHST15 mRNA	26272509
Progesterone	CHST15	Homo sapiens	[Estradiol co-treated with Progesterone] results in decreased expression of CHST15 mRNA	20660070
Quercetin	CHST15	Homo sapiens	Quercetin results in decreased expression of CHST15 mRNA	21632981
S-(1,2-dichlorovinyl) cysteine	CHST15	Homo sapiens	[S-(1,2-dichlorovinyl)cysteine co-treated with Lipopolysaccharides] results in decreased expression of CHST15 mRNA	35811015
sulforaphane	CHST15	Homo sapiens	sulforaphane results in increased expression of CHST15 mRNA	31838189
Thapsigargin	CHST15	Homo sapiens	Thapsigargin results in increased expression of CHST15 mRNA	22378314
Tretinoin	CHST15	Homo sapiens	Tretinoin results in decreased expression of CHST15 mRNA	23724009
Tretinoin	CHST15	Homo sapiens	Tretinoin results in increased expression of CHST15 mRNA	18052213 21934132 33167477
trichostatin A	CHST15	Homo sapiens	[NOG protein co-treated with trichostatin A co-treated with dorsomorphin co-treated with 4-(5-benzo(1,3)dioxol-5-yl-4-pyridin-2-yl-1H-imidazol-2-yl)benzamide] results in increased expression of CHST15 mRNA	27188386
trichostatin A	CHST15	Homo sapiens	trichostatin A results in increased expression of CHST15 mRNA	24935251 26272509
Valproic Acid	CHST15	Homo sapiens	[NOG protein co-treated with Valproic Acid co-treated with dorsomorphin co-treated with 4-(5-benzo(1,3)dioxol-5-yl-4-pyridin-2-yl-1H-imidazol-2-yl)benzamide] results in increased expression of CHST15 mRNA	27188386
Valproic Acid	CHST15	Homo sapiens	Valproic Acid affects the expression of CHST15 mRNA	25979313
Valproic Acid	CHST15	Homo sapiens	Valproic Acid results in increased expression of CHST15 mRNA	19101580 23179753 24383497 24935251 26272509 27188386 28001369
Vitamin K 3	CHST15	Homo sapiens	Vitamin K 3 affects the expression of CHST15 mRNA	23410634
Vorinostat	CHST15	Homo sapiens	Vorinostat results in increased expression of CHST15 mRNA	27188386
abrine	SLFN11	Homo sapiens	abrine results in decreased expression of SLFN11 mRNA	31054353
Calcitriol	SLFN11	Homo sapiens	Calcitriol results in increased expression of SLFN11 mRNA	16002434
Cytarabine	SLFN11	Homo sapiens	Cytarabine results in increased expression of SLFN11 mRNA	21198554

(Continued)

TABLE 3 Continued

Chemical Name	Gene Symbol	Organism	Interaction	References PubMedID
Dasatinib	SLFN11	Homo sapiens	Dasatinib results in decreased expression of SLFN11 mRNA	20579391
Disulfiram	SLFN11	Homo sapiens	[Disulfiram binds to Copper] which results in decreased expression of SLFN11 mRNA	24690739
Doxorubicin	SLFN11	Homo sapiens	Doxorubicin results in decreased expression of SLFN11 mRNA	29803840
entinostat	SLFN11	Homo sapiens	entinostat results in increased expression of SLFN11 mRNA	27188386
Enzyme Inhibitors	SLFN11	Homo sapiens	[Enzyme Inhibitors results in decreased activity of OGA protein] which results in increased O-linked glycosylation of SLFN11 protein	23301498
GSK-J4	SLFN11	Homo sapiens	GSK-J4 results in decreased expression of SLFN11 mRNA	29301935
incobotulinumtoxinA	SLFN11	Homo sapiens	incobotulinumtoxinA results in increased expression of SLFN11 mRNA	29522793
jinfukang	SLFN11	Homo sapiens	jinfukang results in increased expression of SLFN11 mRNA	27392435
Ribonucleotides	SLFN11	Homo sapiens	SLFN11 protein binds to Ribonucleotides	30528433
Temozolomide	SLFN11	Homo sapiens	Temozolomide results in increased expression of SLFN11 mRNA	31758290
trichostatin A	SLFN11	Homo sapiens	trichostatin A results in increased expression of SLFN11 mRNA	24935251
Valproic Acid	SLFN11	Homo sapiens	[NOG protein co-treated with Valproic Acid co-treated with dorsomorphin co-treated with 4-(5-benzo(1,3)dioxol-5-yl-4-pyridin-2-yl-1H-imidazol-2-yl)benzamide] results in increased expression of SLFN11 mRNA	27188386
Valproic Acid	SLFN11	Homo sapiens	Valproic Acid affects the expression of SLFN11 mRNA	25979313
Valproic Acid	SLFN11	Homo sapiens	Valproic Acid results in increased expression of SLFN11 mRNA	23179753 24383497 26272509 27188386 28001369
Vorinostat	SLFN11	Homo sapiens	Vorinostat results in increased expression of SLFN11 mRNA	27188386
abrine	GPR137B	Homo sapiens	abrine results in decreased expression of GPR137B mRNA	31054353
Antirheumatic Agents	GPR137B	Homo sapiens	Antirheumatic Agents results in decreased expression of GPR137B mRNA	24449571
Azathioprine	GPR137B	Homo sapiens	Azathioprine results in increased expression of GPR137B mRNA	22623647
Calcitriol	GPR137B	Homo sapiens	Calcitriol results in increased expression of GPR137B mRNA	21592394
Calcitriol	GPR137B	Homo sapiens	[Testosterone co-treated with Calcitriol] results in increased expression of GPR137B mRNA	21592394
CGP 52608	GPR137B	Homo sapiens	CGP 52608 promotes the reaction [RORA protein binds to GPR137B gene]	28238834
Coumestrol	GPR137B	Homo sapiens	Coumestrol results in decreased expression of GPR137B mRNA	19167446
Cyclophosphamide	GPR137B	Homo sapiens	Cyclophosphamide results in increased expression of GPR137B mRNA	21527772

(Continued)

TABLE 3 Continued

Chemical Name	Gene Symbol	Organism	Interaction	References PubMedID
Cyclosporine	GPR137B	Homo sapiens	Cyclosporine affects the expression of GPR137B mRNA	20106945
Cyclosporine	GPR137B	Homo sapiens	Cyclosporine results in increased expression of GPR137B mRNA	21632981 25562108
Dactinomycin	GPR137B	Homo sapiens	Dactinomycin results in increased expression of GPR137B mRNA	21527772
Demecolcine	GPR137B	Homo sapiens	Demecolcine results in increased expression of GPR137B mRNA	23649840
Doxorubicin	GPR137B	Homo sapiens	Doxorubicin results in decreased expression of GPR137B mRNA	29803840
Estradiol	GPR137B	Homo sapiens	Estradiol results in decreased expression of GPR137B mRNA	31614463
gardiquimod	GPR137B	Homo sapiens	gardiquimod results in increased expression of GPR137B mRNA	28003376
gardiquimod	GPR137B	Homo sapiens	Protein Kinase Inhibitors inhibits the reaction [gardiquimod results in increased expression of GPR137B mRNA]	28003376
GSK-J4	GPR137B	Homo sapiens	GSK-J4 results in increased expression of GPR137B mRNA	29301935
ICG 001	GPR137B	Homo sapiens	ICG 001 results in increased expression of GPR137B mRNA	26191083
Methapyrilene	GPR137B	Homo sapiens	Methapyrilene results in increased methylation of GPR137B intron	30157460
Protein Kinase Inhibitors	GPR137B	Homo sapiens	Protein Kinase Inhibitors inhibits the reaction [gardiquimod results in increased expression of GPR137B mRNA]	28003376
quercitrin	GPR137B	Homo sapiens	quercitrin results in increased expression of GPR137B mRNA	25193878
Temozolomide	GPR137B	Homo sapiens	Temozolomide results in increased expression of GPR137B mRNA	31758290
Testosterone	GPR137B	Homo sapiens	[Testosterone co-treated with Calcitriol] results in increased expression of GPR137B mRNA	21592394
Testosterone	GPR137B	Homo sapiens	Testosterone results in increased expression of GPR137B mRNA	21592394 33359661
Thapsigargin	GPR137B	Homo sapiens	Thapsigargin results in decreased expression of GPR137B mRNA	29453283
Tretinoin	GPR137B	Homo sapiens	Tretinoin results in increased expression of GPR137B mRNA	16249480 33167477
trichostatin A	GPR137B	Homo sapiens	trichostatin A results in increased expression of GPR137B mRNA	24935251
Tunicamycin	GPR137B	Homo sapiens	Tunicamycin results in decreased expression of GPR137B mRNA	29453283
Valproic Acid	GPR137B	Homo sapiens	Valproic Acid affects the expression of GPR137B mRNA	25979313
Valproic Acid	GPR137B	Homo sapiens	Valproic Acid results in increased expression of GPR137B mRNA	23179753 24935251 27188386 29154799
Vincristine	GPR137B	Homo sapiens	Vincristine results in increased expression of GPR137B mRNA	23649840
2-methyl-2H-pyrazole-3-carboxylic acid (2-methyl-4-o-tolylazophenyl)amide	ITGA5	Homo sapiens	[Tetrachlorodibenzodioxin co-treated with 2-methyl-2H-pyrazole-3-carboxylic acid (2-methyl-4-o-tolylazophenyl)amide] results in decreased expression of ITGA5 mRNA	29704546

(Continued)

TABLE 3 Continued

Chemical Name	Gene Symbol	Organism	Interaction	References PubMedID
abrine	ITGA5	Homo sapiens	abrine results in increased expression of ITGA5 mRNA	31054353
Acetone	ITGA5	Homo sapiens	Acetone results in increased expression of ITGA5 mRNA	12720008
AL-10 compound	ITGA5	Homo sapiens	AL-10 compound results in decreased metabolism of ITGA5 protein	20112294
arginyl-glycyl-aspartic acid	ITGA5	Homo sapiens	arginyl-glycyl-aspartic acid inhibits the reaction [Resveratrol binds to [ITGA5 protein binds to ITGB3 protein]]	16790523
Aripiprazole	ITGA5	Homo sapiens	[Aripiprazole co-treated with Ozone] results in increased expression of ITGA5 mRNA	31476115
Aspirin	ITGA5	Homo sapiens	Aspirin results in decreased expression of ITGA5 mRNA	15928584
beta-Naphthoflavone	ITGA5	Homo sapiens	beta-Naphthoflavone results in decreased expression of ITGA5 mRNA	32858204
bis(4-hydroxyphenyl)sulfone	ITGA5	Homo sapiens	bis(4-hydroxyphenyl)sulfone results in increased expression of ITGA5 protein	34186270
bis(4-hydroxyphenyl)sulfone	ITGA5	Homo sapiens	[INS protein co-treated with Dexamethasone co-treated with 1-Methyl-3-isobutylxanthine co-treated with Indomethacin co-treated with bis(4-hydroxyphenyl)sulfone] results in decreased expression of ITGA5 mRNA	28628672
bleomycetin	ITGA5	Homo sapiens	bleomycetin results in increased expression of ITGA5 mRNA	21040473
Bromodeoxyuridine	ITGA5	Homo sapiens	Bromodeoxyuridine results in increased expression of ITGA5 mRNA	7519154
Bromodeoxyuridine	ITGA5	Homo sapiens	Bromodeoxyuridine results in increased expression of ITGA5 protein	7519154
Cannabidiol	ITGA5	Homo sapiens	Cannabidiol inhibits the reaction [TNF protein results in increased expression of ITGA5 mRNA]	31250491
Cannabinoids	ITGA5	Homo sapiens	[Plant Extracts results in increased abundance of Cannabinoids] inhibits the reaction [TNF protein results in increased expression of ITGA5 mRNA]	31250491
CGP 52608	ITGA5	Homo sapiens	CGP 52608 promotes the reaction [RORA protein binds to ITGA5 gene]	28238834
Chelating Agents	ITGA5	Homo sapiens	[Chelating Agents binds to Copper] which results in increased expression of ITGA5 mRNA	30911355
Cisplatin	ITGA5	Homo sapiens	Cisplatin affects the expression of ITGA5 mRNA	23300844
Decitabine	ITGA5	Homo sapiens	Decitabine affects the expression of ITGA5 mRNA	23300844
Dexamethasone	ITGA5	Homo sapiens	[INS protein co-treated with Dexamethasone co-treated with 1-Methyl-3-isobutylxanthine co-treated with Indomethacin co-treated with bis(4-hydroxyphenyl)sulfone] results in decreased expression of ITGA5 mRNA	28628672
Dexamethasone	ITGA5	Homo sapiens	[INS protein co-treated with Dexamethasone co-treated with 1-Methyl-3-isobutylxanthine co-treated with Indomethacin co-treated with bisphenol A] results in decreased expression of ITGA5 mRNA	28628672
Diazepam	ITGA5	Homo sapiens	Diazepam results in increased expression of ITGA5 mRNA	19114084
Doxorubicin	ITGA5	Homo sapiens	Doxorubicin results in decreased expression of ITGA5 mRNA	29803840
Estradiol	ITGA5	Homo sapiens	[Estradiol co-treated with TGFBI protein] results in increased expression of ITGA5 mRNA	30165855

(Continued)

TABLE 3 Continued

Chemical Name	Gene Symbol	Organism	Interaction	References PubMedID
Estradiol	ITGA5	Homo sapiens	[Progesterone co-treated with Estradiol] results in increased expression of ITGA5 mRNA	20226447
Folic Acid	ITGA5	Homo sapiens	Folic Acid affects the expression of ITGA5 mRNA	16361273
Fulvestrant	ITGA5	Homo sapiens	[bisphenol A co-treated with Fulvestrant] results in increased methylation of ITGA5 gene	31601247
Glucose	ITGA5	Homo sapiens	Glucose results in decreased expression of ITGA5 mRNA	31655124
GSK1210151A	ITGA5	Homo sapiens	GSK1210151A inhibits the reaction [TGFB1 protein results in increased expression of ITGA5 mRNA]	26644586
GSK1210151A	ITGA5	Homo sapiens	GSK1210151A results in decreased expression of ITGA5 mRNA	26644586
Hydrocortisone	ITGA5	Homo sapiens	Hydrocortisone results in increased expression of ITGA5 mRNA	21267416
ICG 001	ITGA5	Homo sapiens	ICG 001 results in increased expression of ITGA5 mRNA	26191083
Indomethacin	ITGA5	Homo sapiens	[INS protein co-treated with Dexamethasone co-treated with 1-Methyl-3-isobutylxanthine co-treated with Indomethacin co-treated with bis(4-hydroxyphenyl)sulfone] results in decreased expression of ITGA5 mRNA	28628672
Indomethacin	ITGA5	Homo sapiens	[INS protein co-treated with Dexamethasone co-treated with 1-Methyl-3-isobutylxanthine co-treated with Indomethacin co-treated with bisphenol A] results in decreased expression of ITGA5 mRNA	28628672
Ivermectin	ITGA5	Homo sapiens	Ivermectin results in decreased expression of ITGA5 protein	32959892
(+)-JQ1 compound	ITGA5	Homo sapiens	(+)-JQ1 compound inhibits the reaction [TGFB1 protein results in increased expression of ITGA5 mRNA]	26644586
(+)-JQ1 compound	ITGA5	Homo sapiens	(+)-JQ1 compound results in decreased expression of ITGA5 mRNA	26644586
Leuprolide	ITGA5	Homo sapiens	Leuprolide inhibits the reaction [IGF1 protein results in increased expression of and affects the localization of [ITGA5 protein binds to ITGB3 protein]]	17143537
Methapyrilene	ITGA5	Homo sapiens	Methapyrilene results in increased methylation of ITGA5 intron	30157460
Methotrexate	ITGA5	Homo sapiens	Methotrexate results in increased expression of ITGA5 mRNA	17400583
Phytoestrogens	ITGA5	Homo sapiens	[Plasticizers co-treated with Cosmetics co-treated with Flame Retardants co-treated with perfluorooctanoic acid co-treated with Phytoestrogens] results in decreased expression of ITGA5 mRNA	33325755
Progesterone	ITGA5	Homo sapiens	[Progesterone co-treated with Estradiol] results in increased expression of ITGA5 mRNA	20226447
Progesterone	ITGA5	Homo sapiens	Progesterone results in increased expression of ITGA5 mRNA	20226447 21795739
Quercetin	ITGA5	Homo sapiens	Quercetin results in increased expression of ITGA5 mRNA	30152185
Resveratrol	ITGA5	Homo sapiens	arginyl-glycyl-aspartic acid inhibits the reaction [Resveratrol binds to [ITGA5 protein binds to ITGB3 protein]]	16790523
Resveratrol	ITGA5	Homo sapiens	[ITGA5 protein binds to ITGB3 protein] promotes the reaction [Resveratrol results in increased phosphorylation of MAPK1 protein]	16790523
Resveratrol	ITGA5	Homo sapiens	[ITGA5 protein binds to ITGB3 protein] promotes the reaction [Resveratrol results in increased phosphorylation of MAPK3 protein]	16790523

(Continued)

TABLE 3 Continued

Chemical Name	Gene Symbol	Organism	Interaction	References PubMedID
Resveratrol	ITGA5	Homo sapiens	[ITGA5 protein binds to ITGB3 protein] promotes the reaction [Resveratrol results in increased phosphorylation of TP53 protein]	16790523
Resveratrol	ITGA5	Homo sapiens	Resveratrol binds to [ITGA5 protein binds to ITGB3 protein]	16790523
Resveratrol	ITGA5	Homo sapiens	Resveratrol results in decreased expression of ITGA5 protein	18089832
Rosiglitazone	ITGA5	Homo sapiens	Rosiglitazone results in increased expression of ITGA5 protein	19467017
Rosiglitazone	ITGA5	Homo sapiens	Tretinoin promotes the reaction [Rosiglitazone results in increased expression of ITGA5 protein]	19467017
Sunitinib	ITGA5	Homo sapiens	Sunitinib results in increased expression of ITGA5 mRNA	31533062
Temozolomide	ITGA5	Homo sapiens	Temozolomide results in decreased expression of ITGA5 mRNA	31758290
Tetracycline	ITGA5	Homo sapiens	Tetracycline results in increased expression of ITGA5 mRNA	28882639
Topotecan	ITGA5	Homo sapiens	ITGA5 protein affects the susceptibility to Topotecan	16217747
Tretinoin	ITGA5	Homo sapiens	Tretinoin promotes the reaction [Rosiglitazone results in increased expression of ITGA5 protein]	19467017
Troglitazone	ITGA5	Homo sapiens	Troglitazone results in increased expression of ITGA5 mRNA	19140230
Valproic Acid	ITGA5	Homo sapiens	CEBPA protein affects the reaction [Valproic Acid results in decreased expression of ITGA5 mRNA]	32623605
Valproic Acid	ITGA5	Homo sapiens	Valproic Acid results in decreased expression of ITGA5 mRNA	29154799 32623605
Antirheumatic Agents	LILRB1	Homo sapiens	Antirheumatic Agents results in decreased expression of LILRB1 mRNA	24449571
Catechin	LILRB1	Homo sapiens	[Catechin co-treated with Grape Seed Proanthocyanidins] results in decreased expression of LILRB1 mRNA	24763279
Grape Seed Proanthocyanidins	LILRB1	Homo sapiens	[Catechin co-treated with Grape Seed Proanthocyanidins] results in decreased expression of LILRB1 mRNA	24763279
Levonorgestrel	LILRB1	Homo sapiens	[testosterone undecanoate co-treated with Levonorgestrel] results in increased expression of LILRB1 mRNA	19074003
Lipopolysaccharides	LILRB1	Homo sapiens	[S-(1,2-dichlorovinyl)cysteine affects the susceptibility to Lipopolysaccharides] which results in increased expression of LILRB1 mRNA	35811015
Lipopolysaccharides	LILRB1	Homo sapiens	[S-(1,2-dichlorovinyl)cysteine co-treated with Lipopolysaccharides] results in decreased expression of LILRB1 mRNA	35811015
Methapyrilene	LILRB1	Homo sapiens	Methapyrilene results in increased methylation of LILRB1 intron	30157460
Methotrexate	LILRB1	Homo sapiens	Methotrexate results in decreased expression of LILRB1 mRNA	17400583
S-(1,2-dichlorovinyl) cysteine	LILRB1	Homo sapiens	[S-(1,2-dichlorovinyl)cysteine affects the susceptibility to Lipopolysaccharides] which results in increased expression of LILRB1 mRNA	35811015
S-(1,2-dichlorovinyl) cysteine	LILRB1	Homo sapiens	[S-(1,2-dichlorovinyl)cysteine co-treated with Lipopolysaccharides] results in decreased expression of LILRB1 mRNA	35811015
S-(1,2-dichlorovinyl) cysteine	LILRB1	Homo sapiens	S-(1,2-dichlorovinyl)cysteine results in decreased expression of LILRB1 mRNA	35811015

(Continued)

TABLE 3 Continued

Chemical Name	Gene Symbol	Organism	Interaction	References PubMedID
testosterone undecanoate	LILRB1	Homo sapiens	[testosterone undecanoate co-treated with Levonorgestrel] results in increased expression of LILRB1 mRNA	19074003
testosterone undecanoate	LILRB1	Homo sapiens	testosterone undecanoate results in increased expression of LILRB1 mRNA	19074003
Valproic Acid	LILRB1	Homo sapiens	Valproic Acid results in increased methylation of LILRB1 gene	29154799
Vincristine	LILRB1	Homo sapiens	Vincristine results in decreased expression of LILRB1 mRNA	23649840
Acetaminophen	BGN	Homo sapiens	Acetaminophen results in increased expression of BGN mRNA	22230336
Antineoplastic Agents, Immunological	BGN	Homo sapiens	[Antineoplastic Agents, Immunological results in decreased susceptibility to Antineoplastic Agents, Immunological] which results in increased expression of BGN mRNA alternative form	35234341
Antineoplastic Agents, Immunological	BGN	Homo sapiens	BGN mRNA alternative form results in decreased susceptibility to Antineoplastic Agents, Immunological	35234341
Antineoplastic Agents, Immunological	BGN	Homo sapiens	erastin inhibits the reaction [[Antineoplastic Agents, Immunological results in decreased susceptibility to Antineoplastic Agents, Immunological] which results in increased expression of BGN mRNA alternative form]	35234341
beta-Naphthoflavone	BGN	Homo sapiens	beta-Naphthoflavone results in decreased expression of BGN mRNA	32858204
Cisplatin	BGN	Homo sapiens	Cisplatin affects the expression of BGN mRNA	23300844
Dasatinib	BGN	Homo sapiens	Dasatinib results in increased expression of BGN mRNA	20579391
Decitabine	BGN	Homo sapiens	Decitabine affects the expression of BGN mRNA	23300844
Dexamethasone	BGN	Homo sapiens	Dexamethasone results in decreased expression of BGN mRNA	25047013
Diazepam	BGN	Homo sapiens	Diazepam results in increased expression of BGN mRNA	19114084
Doxorubicin	BGN	Homo sapiens	Doxorubicin affects the expression of BGN protein	29385562
Doxorubicin	BGN	Homo sapiens	Doxorubicin results in increased expression of BGN mRNA	29803840
erastin	BGN	Homo sapiens	BGN mRNA alternative form inhibits the reaction [erastin results in decreased expression of MKI67 protein]	35234341
erastin	BGN	Homo sapiens	erastin inhibits the reaction [[Antineoplastic Agents, Immunological results in decreased susceptibility to Antineoplastic Agents, Immunological] which results in increased expression of BGN mRNA alternative form]	35234341
erastin	BGN	Homo sapiens	erastin results in decreased expression of BGN mRNA alternative form	35234341
Estradiol	BGN	Homo sapiens	[Estradiol co-treated with TGFB1 protein] results in increased expression of BGN mRNA	30165855
Estradiol	BGN	Homo sapiens	Estradiol results in increased expression of BGN mRNA	19429434 21185374
Glutathione	BGN	Homo sapiens	[[BGN mRNA alternative form binds to OTUB1 protein] which binds to and results in decreased ubiquitination of and results in increased stability of SLC7A11 protein] which results in increased chemical synthesis of Glutathione	35234341
ICG 001	BGN	Homo sapiens	ICG 001 results in increased expression of BGN mRNA	26191083

(Continued)

TABLE 3 Continued

Chemical Name	Gene Symbol	Organism	Interaction	References PubMedID
Isotretinoin	BGN	Homo sapiens	Isotretinoin results in increased expression of BGN mRNA	20436886
Methapyrilene	BGN	Homo sapiens	Methapyrilene results in increased methylation of BGN intron	30157460
Paclitaxel	BGN	Homo sapiens	BGN protein affects the susceptibility to Paclitaxel	16217747
Raloxifene Hydrochloride	BGN	Homo sapiens	Raloxifene Hydrochloride results in increased expression of BGN mRNA	19429434
Resveratrol	BGN	Homo sapiens	[Plant Extracts co-treated with Resveratrol] results in decreased expression of BGN mRNA	23557933
Temozolomide	BGN	Homo sapiens	Temozolomide results in increased expression of BGN mRNA	31758290
trichostatin A	BGN	Homo sapiens	[NOG protein co-treated with trichostatin A co-treated with dorsomorphin co-treated with 4-(5-benzo(1,3)dioxol-5-yl-4-pyridin-2-yl-1H-imidazol-2-yl)benzamide] results in increased expression of BGN mRNA	27188386
trichostatin A	BGN	Homo sapiens	trichostatin A results in increased expression of BGN mRNA	24935251 26272509
Valproic Acid	BGN	Homo sapiens	[NOG protein co-treated with Valproic Acid co-treated with dorsomorphin co-treated with 4-(5-benzo(1,3)dioxol-5-yl-4-pyridin-2-yl-1H-imidazol-2-yl)benzamide] results in increased expression of BGN mRNA	27188386
Valproic Acid	BGN	Homo sapiens	Valproic Acid results in decreased expression of BGN mRNA	29154799
Valproic Acid	BGN	Homo sapiens	Valproic Acid results in increased expression of BGN mRNA	23179753 26272509
Valproic Acid	BGN	Homo sapiens	Valproic Acid results in increased methylation of BGN gene	29154799

compared to cluster C2. The cluster C2 had a significant higher level of CD4+ T cells. CD4+ T cells have been reported as a major initiators in the disease process of UC (38). Blockade and depletion of CD4+ T cells are an effective means of treatments for IBD (39). Therefore, a higher degree of CD4+ T cells in cluster C2 may contributed to the higher disease severity. Overall, our study provided a convenient and valuable tool to predict severity of UC and screen UC patients suitable for CS-IV treatment. Intravenous administration of corticosteroids can achieve therapeutic effects with reduced oral administration dosages, and can alleviate adverse reactions associated with oral corticosteroids such as gastrointestinal discomfort. Additionally, it is worth noting that most UC patients that receive corticosteroid therapy *via* the intravenous route have a higher degree of disease severity. It is worth noting that a majority of UC patients who receive corticosteroid administration *via* the intravenous route have a higher degree of disease severity. Thus, our molecular typing scheme may be specific only to the severe UC patient population in predicting therapeutic responsiveness.

Exisulind, or what is also termed “Sulindac sulfone”, is a metabolite of sulindac and is also a non-steroidal anti-inflammatory drug (NSAID). NSAIDs have generally been considered to be related to an increased risk of mucosal ulceration. But a high-quality meta-analyze showed that NSAIDs did not elicit exacerbations and serious complications of the IBD (40). By the

way, the anti-tumor application of Exisulind has already been explored in Phase I or Phase II clinical trials, suggesting that Exisulind is well tolerated with relatively few adverse effects (41–44). Although Exisulind has only weak anti-inflammatory effect, extensive experimental data have proved that Exisulind have a therapeutic potential to prevent and cure many diseases of the colon. The mTORC1 pathway has been reported to modulate the regulation and differentiation of immune cells, and then ameliorate colitis (45). It is worthy to mention that Exisulin has been shown to inhibit the mTORC1 pathway by directly targeting voltage-dependent anion channel 1 and 2 (46). Regulation of the mTORC1 pathway may be one of the underlying mechanisms responsible for the therapeutic effectiveness of Exisulind.

Additionally, our molecular docking results suggested that GPR4 is the protein with the highest docking score with Exisulind. Thus, GPR4 protein might be another potential targets of Exisulind in UC. As a pro-inflammatory G protein-coupled receptor (GPCR), GPR4 showed a higher expression level in vascular endothelial cells (47–49). GPR4 has a significant role in regulating endothelium-blood cell interaction and leukocyte infiltration. In addition, GPR4 exhibits capability to regulate vascular permeability and tissue edema under inflammatory conditions (50–52). Numerous experimental animal studies

revealed that GPR4 is involved in the development and progression of UC. GPR4 played a protective role in dextran sulfate sodium-induced acute colitis mouse model (53–55). Therefore, the inhibition of GPR4 could be a underlying mechanism responsible for the therapeutic effects of Exisulind on UC.

We present a comprehensive review aimed at investigating the effect of environmental toxins exposure on HMGs expression levels - a phenomenon that may play a potential role in influencing the severity of UC. It is noteworthy to mention that this effect is not limited solely to environmental toxins as some drug exposure may trigger similar effects. Our objective is to shed light on the crucial interplay between external factors and HMGs, and its clinical implications in the context of UC pathogenesis. Our research provides novel insights and resources that can facilitate a more comprehensive examination of the complex relationship between UC progression and environmental toxin exposure. Consequently, these findings can potentially inform novel perspectives for guiding clinical treatment strategies for UC patients, thereby improving the standard of care for this condition.

This study provided new ideas and materials for the personalized clinical treatment plans for patients with UC, although some limitations to the present study need to be considered. First of all, this research only included a bioinformatics analysis, lacking further experimental verification as a solid foundation. Secondly, one of the limitations of our study is that this research is a retrospective study rather than a prospectively trial. Our identification of potential therapeutic agents for UC was based on computational methods, thus necessitating further *in vitro* and *in vivo* experimental validation and exploration of underlying mechanisms. Therefore, future follow-up studies with prospective clinical trials and mechanistic exploration are required for corroboration of our findings.

Conclusion

In summary, we explored the genetic abnormalities involved in the exacerbation of UC based on microarray technology. By combining WGCNA and random forest algorithm, we identified 9 gene signatures (HMGs) of the exacerbation of UC. Then a novel genotyping scheme was generated based on the 9 HMGs, dividing patients into two subtypes (cluster C1 and cluster C2). Patients in cluster C1 were susceptible to benefit from CS-IV treatment. Subsequently, we identified a small molecule drug (Exisulind) with potential therapeutic effects for UC. We also provided a comprehensive review of the environmental toxins and drug exposures that potentially impact the progression of UC. Thus, our research contributed to the development of personalized clinical management and treatment regimens for UC.

Data availability statement

Publicly available datasets were analyzed in this study. This data can be found in Gene Expression Omnibus (GEO) database

(<https://www.ncbi.nlm.nih.gov/geo/>). The accession numbers can be found in the article/Supplementary Material.

Ethics statement

The studies involving human subjects were evaluated and authorized by the Ethics Committees of the Jiangsu Province Hospital. Participants in the study provided written, informed consent to participate in this study. Consent was obtained in writing from individuals for the use of any potentially discernible data or images in this article.

Author contributions

Conceptualization, YW; Formal analysis, YW and R-HZ; Methodology, HZ and YW; Project administration, Z-NF; Supervision, H-YW; Writing - original draft, YW; Writing - review and editing, Z-NF and HW; Sample collection and PCR, X-HJ. All authors have contributed to this article and have approved the final version submitted.

Funding

This research was funded by the Nanjing Municipal Science and Technology Plan Project (202205052), the GSKY20220109 Scientific Research Project of Gu Su College, Nanjing Medical University, the Nanjing Municipal Science and Technology Plan Project (202110014), the Social Development Program of Jiangsu Provincial Department of Science and Technology (BE2022704), and the National Natural Science Foundation of China (82000621).

Acknowledgments

We thank particularly Dr. Sonia Zebaze Dongmo (E-mail: zebazedongmosonia@163.com) for carefully reading the manuscript and editing the language.

Conflict of interest

The authors declare that the research was conducted in the absence of any commercial or financial relationships that could be construed as a potential conflict of interest.

Publisher's note

All claims expressed in this article are solely those of the authors and do not necessarily represent those of their affiliated organizations, or those of the publisher, the editors and the reviewers. Any product that may be evaluated in this article, or claim that may be made by its manufacturer, is not guaranteed or endorsed by the publisher.

Supplementary material

The Supplementary Material for this article can be found online at: <https://www.frontiersin.org/articles/10.3389/fimmu.2023.1162458/full#supplementary-material>

SUPPLEMENTARY FIGURE 1

Flowchart illustrating the workflow of this study.

SUPPLEMENTARY FIGURE 2

Flow chart of the WGCNA analysis pipeline.

SUPPLEMENTARY FIGURE 3

Determination of soft-threshold power in the WGCNA in GSE109142 cohort. (A) Analysis of the scale-free index for various soft-threshold powers (β). (B) Analysis of the mean connectivity for various soft-threshold powers. (C) Clustering dendrogram of UC patients in the GSE109142 cohort. Identification of modules closely associated with Mayo score. (D) Dendrogram of all differentially expressed genes clustered based on the measurement of dissimilarity (1-TOM). The color band shows the results obtained from the automatic single-block analysis. (E) Number of genes in each module.

SUPPLEMENTARY FIGURE 4

Determination of soft-threshold power in the WGCNA in GSE92415 cohort. (A) Analysis of the scale-free index for various soft-threshold powers (β). (B) Analysis of the mean connectivity for various soft-threshold powers. (C) Clustering dendrogram of UC patients in the GSE92415 cohort. Identification of modules closely associated with Mayo score. (D) Dendrogram of all differentially expressed genes clustered based on the measurement of dissimilarity (1-TOM). The color band shows the results obtained from the automatic single-block analysis. (E) Number of genes in each module.

SUPPLEMENTARY FIGURE 5

PCA, UMAP and tSNE cluster representation of the 9 HMGs expression patterns. ROC curve of first principal component, second principal

component and the sum of first and second principal component for differentiating UC from normal samples.

SUPPLEMENTARY FIGURE 6

(A) Correlations between Mayo score and HMGs assessed by Spearman correlation in GSE92415 cohort. (B) Based on upper and lower quartiles of the set of Mayo scores in GSE92415 cohort, UC patients were stratified to high- (red), moderate- (blue), and low- (green) Mayo score groups. Boxplots showing the expression levels of the 9 HMGs across different Mayo score group. (C) Boxplots showing the expression levels of HMGs in UC intestinal samples (red) and normal intestinal samples (blue).

SUPPLEMENTARY FIGURE 7

ROC curve illustrating the potential of HMGs to differentiate between UC patients with high- and low- Mayo scores in GSE92415 cohort.

SUPPLEMENTARY FIGURE 8

Independent dataset (GSE73661) verification results. (A) Boxplots showing the expression levels of the HMGs in the UC patient groups with different Mayo endoscopic scores. (B) Boxplots showing the expression levels of HMGs in UC intestinal samples (red) and normal intestinal samples (blue). (C) ROC curve illustrating the potential of HMGs to differentiate between UC patients with high- and low- Mayo endoscopic scores in GSE73661 cohort.

SUPPLEMENTARY FIGURE 9

GSEA enrichment analysis results in GSE109142 cohort. The top five most enriched KEGG pathways in cluster C1 (A) and Cluster C2 (B) were shown. (C) Box-plot highlighting the differences in immune cell infiltration between the cluster C1 (red) and Cluster C2 (blue).

SUPPLEMENTARY FIGURE 10

Experimental verification of gene expression levels of GPR4, ST3GAL2, and LILRB1 using qRT-PCR.

SUPPLEMENTARY TABLE 5

The immune cell infiltration of each UC patient of GSE109142 cohort evaluated by ImmuCellAI database.

References

- Ordás I, Eckmann L, Talamini M, Baumgart DC, Sandborn WJ. Ulcerative colitis. *Lancet* (2012) 380:1606–19. doi: 10.1016/S0140-6736(12)60150-0
- Lu PD, Zhao YH. Targeting NF-κB pathway for treating ulcerative colitis: comprehensive regulatory characteristics of Chinese medicines. *Chin Med* (2020) 15:15. doi: 10.1186/s13020-020-0296-z
- Zeng B, Shi S, Ashworth G, Dong C, Liu J, Xing F. ILC3 function as a double-edged sword in inflammatory bowel diseases. *Cell Death Dis* (2019) 10:315. doi: 10.1038/s41419-019-1540-2
- Gogokhia L, Buhre K, Bell R, Hoffman B, Brown DG, Hanke-Gogokhia C, et al. Expansion of bacteriophages is linked to aggravated intestinal inflammation and colitis. *Cell Host Microbe* (2019) 25:285–299.e8. doi: 10.1016/j.chom.2019.01.008
- Yang L, Wu G, Wu Q, Peng L, Yuan L. METTL3 overexpression aggravates LPS-induced cellular inflammation in mouse intestinal epithelial cells and DSS-induced IBD in mice. *Cell Death Discovery* (2022) 8:62. doi: 10.1038/s41420-022-00849-1
- Shi YJ, Hu SJ, Zhao QQ, Liu XS, Liu C, Wang H. Toll-like receptor 4 (TLR4) deficiency aggravates dextran sulfate sodium (DSS)-induced intestinal injury by down-regulating IL6, CCL2 and CSF3. *Ann Transl Med* (2019) 7:713. doi: 10.21037/atm.2019.12.28
- Wang Y, Wang Z, Sun J, Qian Y. Identification of HCC subtypes with different prognosis and metabolic patterns based on mitophagy. *Front Cell Dev Biol* (2021) 9:799507. doi: 10.3389/fcell.2021.799507
- Wang Y, Sun J, Yang Y, Zebaze Dongmo S, Qian Y, Wang Z. Identification and development of subtypes with poor prognosis in gastric cancer based on both hypoxia and immune cell infiltration. *Int J Gen Med* (2021) 14:9379–99. doi: 10.2147/IJGM.S326647
- Chen H, Zhang J, Sun X, Wang Y, Qian Y. Mitophagy-mediated molecular subtypes depict the hallmarks of the tumour metabolism and guide precision chemotherapy in pancreatic adenocarcinoma. *Front Cell Dev Biol* (2022) 10:901207. doi: 10.3389/fcell.2022.901207
- Guerrero-Alba R, Valdez-Morales EE, Jimenez-Vargas NN, Lopez-Lopez C, Jaramillo-Polanco J, Okamoto T, et al. Stress activates pronociceptive endogenous opioid signalling in DRG neurons during chronic colitis. *Gut* (2017) 66:2121–31. doi: 10.1136/gutjnl-2016-311456
- Gottlieb K, Requa J, Karnes W, Chandra Gudivada R, Shen J, Rael E, et al. Central reading of ulcerative colitis clinical trial videos using neural networks. *Gastroenterology* (2021) 160:710–719.e2. doi: 10.1053/j.gastro.2020.10.024
- Mohammed Vashist N, Samaan M, Mosli MH, Parker CE, MacDonald JK, Nelson SA, et al. Endoscopic scoring indices for evaluation of disease activity in ulcerative colitis. *Cochrane Database Syst Rev* (2018) 1:CD011450. doi: 10.1002/14651858.CD011450.pub2
- Rutgeerts P, Sandborn WJ, Feagan BG, Reinisch W, Olson A, Johans J, et al. Infliximab for induction and maintenance therapy for ulcerative colitis. *N Engl J Med* (2005) 353:2462–76. doi: 10.1056/NEJMoa050516
- Yang S, Park JS, Hwang SH, Cho KH, Na HS, Choi J, et al. Metformin-inducible small heterodimer partner interacting leucine zipper protein ameliorates intestinal inflammation. *Front Immunol* (2021) 12:652709. doi: 10.3389/fimmu.2021.652709
- Colombel JF, Rutgeerts P, Reinisch W, Esser D, Wang Y, Lang Y, et al. Early mucosal healing with infliximab is associated with improved long-term clinical outcomes in ulcerative colitis. *Gastroenterology* (2011) 141:1194–201. doi: 10.1053/j.gastro.2011.06.054
- Clough E, Barrett T. The gene expression omnibus database. *Methods Mol Biol* (2016) 1418:93–110. doi: 10.1007/978-1-4939-3578-9_5
- Langfelder P, Horvath S. WGCNA: an R package for weighted correlation network analysis. *BMC Bioinf* (2008) 9:559. doi: 10.1186/1471-2105-9-559
- Wang F, Wang B, Long J, Wang F, Wu P. Identification of candidate target genes for endometrial cancer, such as ANO1, using weighted gene co-expression network analysis. *Exp Ther Med* (2019) 17:298–306. doi: 10.3892/etm.2018.6965
- Wang Z, Li X, Chen H, Han L, Ji X, Wang Q, et al. Decreased HLF expression predicts poor survival in lung adenocarcinoma. *Med Sci Monit* (2021) 27:e2929333. doi: 10.12659/MSM.929333

20. Zhou Y, Zhou B, Pache L, Chang M, Khodabakhshi AH, Tanaseichuk O, et al. Metascape provides a biologist-oriented resource for the analysis of systems-level datasets. *Nat Commun* (2019) 10:1523. doi: 10.1038/s41467-019-09234-6
21. Subramanian A, Tamayo P, Mootha VK, Mukherjee S, Ebert BL, Gillette MA, et al. Gene set enrichment analysis: a knowledge-based approach for interpreting genome-wide expression profiles. *Proc Natl Acad Sci USA* (2005) 102:15545–50. doi: 10.1073/pnas.0506580102
22. Kanehisa M, Furumichi M, Tanabe M, Sato Y, Morishima K. KEGG: new perspectives on genomes, pathways, diseases and drugs. *Nucleic Acids Res* (2017) 45: D353–61. doi: 10.1093/nar/gkw1092
23. Ritchie ME, Phipson B, Wu D, Hu Y, Law CW, Shi W, Smyth, G.K. limma powers differential expression analyses for RNA-sequencing and microarray studies. *Nucleic Acids Res* (2015) 43:e47. doi: 10.1093/nar/gkv007
24. Alderden J, Pepper GA, Wilson A, Whitney JD, Richardson S, Butcher R, et al. Predicting pressure injury in critical care patients: a machine-learning model. *Am J Crit Care* (2018) 27:461–8. doi: 10.4037/ajcc.2018525
25. Wilkerson MD, Hayes DN. ConsensusClusterPlus: a class discovery tool with confidence assessments and item tracking. *Bioinformatics* (2010) 26:1572–3. doi: 10.1093/bioinformatics/btq170
26. Miao YR, Zhang Q, Lei Q, Luo M, Xie GY, Wang H, et al. ImmCellAI: a unique method for comprehensive T-cell subsets abundance prediction and its application in cancer immunotherapy. *Advanced Sci (Weinheim Baden-Wurttemberg Germany)* (2020) 7:1902880. doi: 10.1002/adv.201902880
27. Cheng J, Yang L, Kumar V, Agarwal P. Systematic evaluation of connectivity map for disease indications. *Genome Med* (2014) 6:540. doi: 10.1186/s13073-014-0095-1
28. Berman HM, Westbrook J, Feng Z, Gilliland G, Bhat TN, Weissig H, et al. The protein data bank. *Nucleic Acids Res* (2000) 28:235–42. doi: 10.1093/nar/28.1.235
29. Kim S, Chen J, Cheng T, Gindulyte A, He J, He S, et al. PubChem in 2021: new data content and improved web interfaces. *Nucleic Acids Res* (2021) 49:D1388–95. doi: 10.1093/nar/gkaa971
30. Bhachoo J, Beuming T. Investigating protein-peptide interactions using the Schrödinger computational suite. *Methods Mol Biol* (2017) 1561:235–54. doi: 10.1007/978-1-4939-6798-8_14
31. Mandrekar JN. Receiver operating characteristic curve in diagnostic test assessment. *J Thorac Oncol* (2010) 5:1315–6. doi: 10.1097/JTO.0b013e3181ec173d
32. Ben Salem K, Ben Abdelaziz A. Principal component analysis (PCA). *Tunis Med* (2021) 99:383–9.
33. Vermeulen M, Smith K, Eremin K, Rayner G, Walton M. Application of uniform manifold approximation and projection (UMAP) in spectral imaging of artworks. *Spectrochim Acta A Mol Biomol Spectrosc* (2021) 252:119547. doi: 10.1016/j.saa.2021.119547
34. Cheng Y, Wang X, Xia Y. Supervised t-distributed stochastic neighbor embedding for data visualization and classification. *INFORMS J ON COMPUTING* (2021) 33:419–835. doi: 10.1287/ijoc.2020.0961
35. Vegiopoulos A, Herzig S. Glucocorticoids, metabolism and metabolic diseases. *Mol Cell Endocrinol* (2007) 275:43–61. doi: 10.1016/j.mce.2007.05.015
36. Eleftheriadis T, Pissas G, Yiannaki E, Markala D, Arampatzis S, Antoniadi G, et al. Inhibition of indoleamine 2,3-dioxygenase in mixed lymphocyte reaction affects glucose influx and enzymes involved in aerobic glycolysis and glutaminolysis in alloreactive T-cells. *Hum Immunol* (2013) 74:1501–9. doi: 10.1016/j.humimm.2013.08.268
37. Hosomi K, Kunisawa J. Diversity of energy metabolism in immune responses regulated by micro-organisms and dietary nutrition. *Int Immunol* (2020) 32:447–54. doi: 10.1093/intimm/dxaa020
38. Imam T, Park S, Kaplan MH, Olson MR. Effector T helper cell subsets in inflammatory bowel diseases. *Front Immunol* (2018) 9:1212. doi: 10.3389/fimmu.2018.01212
39. Stronkhorst A, Radema S, Yong SL, Bijl H, ten Berge IJ, Tytgat GN, et al. CD4 antibody treatment in patients with active Crohn's disease: a phase 1 dose finding study. *Gut* (1997) 40:320–7. doi: 10.1136/gut.40.3.320
40. Moninuola OO, Milligan W, Lochhead P, Khalili H. Systematic review with meta-analysis: association between acetaminophen and nonsteroidal anti-inflammatory drugs (NSAIDs) and risk of Crohn's disease and ulcerative colitis exacerbation. *Aliment. Pharmacol Ther* (2018) 47:1428–39. doi: 10.1111/apt.14606
41. Dawson NA, Halabi S, Ou SS, Biggs DD, Kessinger A, Vogelzang N, et al. A phase II study of estramustine, docetaxel, and exisulind in patients with hormone-refractory prostate cancer: results of cancer and leukemia group b trial 90004. *Clin Genitourin Cancer*. (2008) 6:110–6. doi: 10.3816/CGC.2008.n.017
42. Attia S, Traynor AM, Kim K, Merchant JJ, Hoang T, Ahuja HG, et al. Phase I/II study of vinorelbine and exisulind as first-line treatment of advanced non-small cell lung cancer in patients at least 70 years old: a wisconsin oncology network study. *J Thorac Oncol* (2008) 3:1018–25. doi: 10.1097/JTO.0b013e3181834fa1
43. Weiss GJ, Vokes EE, Bunn PA Jr., Magree L, Rusk J, Albert D, et al. Docetaxel and exisulind in previously treated non-small cell lung cancer (NSCLC) patients: a multicenter, phase II clinical trial. *J Thorac Oncol* (2007) 2:933–8. doi: 10.1097/JTO.0b013e3181462051
44. Sinibaldi VJ, Elza-Brown K, Schmidt J, Eisenberger MA, Rosenbaum E, Denmeade SR, et al. Phase II evaluation of docetaxel plus exisulind in patients with androgen independent prostate carcinoma. *Am J Clin Oncol* (2006) 29:395–8. doi: 10.1097/01.coc.0000225411.95479.b4
45. Wu X, Dou Y, Yang Y, Bian D, Luo J, Tong B, et al. Arctigenin exerts anti-colitis efficacy through inhibiting the differentiation of Th1 and Th17 cells via an mTORC1-dependent pathway. *Biochem Pharmacol* (2015) 96:323–36. doi: 10.1016/j.bcp.2015.06.008
46. Aono Y, Horinaka M, Iizumi Y, Watanabe M, Taniguchi T, Yasuda S, et al. Sulindac sulfone inhibits the mTORC1 pathway in colon cancer cells by directly targeting voltage-dependent anion channel 1 and 2. *Biochem Biophys Res Commun* (2018) 505:1203–10. doi: 10.1016/j.bbrc.2018.10.050
47. Chen A, Dong L, Leffler NR, Asch AS, Witte ON, Yang LV. Activation of GPR4 by acidosis increases endothelial cell adhesion through the cAMP/Epac pathway. *PLoS One* (2011) 6:e27586. doi: 10.1371/journal.pone.0027586
48. Dong L, Li Z, Leffler NR, Asch AS, Chi JT, Yang LV. Acidosis activation of the proton-sensing GPR4 receptor stimulates vascular endothelial inflammatory responses revealed by transcriptome analysis. *PLoS One* (2013) 8:e61991. doi: 10.1371/journal.pone.0061991
49. Dong L, Krewson EA, Yang LV. Acidosis activates endoplasmic reticulum stress pathways through GPR4 in human vascular endothelial cells. *Int J Mol Sci* (2017) 18:278. doi: 10.3390/ijms18020278
50. Yang LV, Oppelt KA, Thomassen MJ, Marie MA, Nik Akhtar S, McCallen JD. Can GPR4 be a potential therapeutic target for COVID-19. *Front Med (Lausanne)* (2020) 7:626796. doi: 10.3389/fmed.2020.626796
51. Velcicky J, Miltz W, Oberhauser B, Orain D, Vaupel A, Weigand K, et al. Development of selective, orally active GPR4 antagonists with modulatory effects on nociception, inflammation, and angiogenesis. *J Med Chem* (2017) 60:3672–83. doi: 10.1021/acs.jmedchem.6b01703
52. Krewson EA, Sanderlin EJ, Marie MA, Akhtar SN, Velcicky J, Loetscher P, et al. The proton-sensing GPR4 receptor regulates paracellular gap formation and permeability of vascular endothelial cells. *iScience* (2020) 23:100848. doi: 10.1016/j.isci.2020.100848
53. Sanderlin EJ, Leffler NR, Lertpiriyapong K, Cai Q, Hong H, Bakthavachalu V, et al. GPR4 deficiency alleviates intestinal inflammation in a mouse model of acute experimental colitis. *Biochim Biophys Acta Mol Basis Dis* (2017) 1863:569–84. doi: 10.1016/j.bbadis.2016.12.005
54. Sanderlin EJ, Marie M, Velcicky J, Loetscher P, Yang LV. Pharmacological inhibition of GPR4 remedies intestinal inflammation in a mouse colitis model. *Eur J Pharmacol* (2019) 852:218–30. doi: 10.1016/j.ejphar.2019.03.038
55. Wang Y, de Vallière C, Imenez Silva PH, Leonardi I, Gruber S, Gerstgrasser A, et al. The proton-activated receptor GPR4 modulates intestinal inflammation. *J Crohn's colitis*. (2018) 12:355–68. doi: 10.1093/ecco-jcc/jjx147



OPEN ACCESS

EDITED BY

Aristidis M. Tsatsakis,
University of Crete, Greece

REVIEWED BY

Rohit Saluja,
All India Institute of Medical Sciences,
India

*CORRESPONDENCE

Chao-Chun Yang,
✉ yangcc@mail.ncku.edu.tw

RECEIVED 29 March 2023

ACCEPTED 29 June 2023

PUBLISHED 21 July 2023

CITATION

Cruz CJG and Yang C-C (2023), Clinical application of serum biomarkers for detecting and monitoring of chronic plaque psoriasis.
Front. Mol. Biosci. 10:1196323.
doi: 10.3389/fmolb.2023.1196323

COPYRIGHT

© 2023 Cruz and Yang. This is an open-access article distributed under the terms of the [Creative Commons Attribution License \(CC BY\)](#). The use, distribution or reproduction in other forums is permitted, provided the original author(s) and the copyright owner(s) are credited and that the original publication in this journal is cited, in accordance with accepted academic practice. No use, distribution or reproduction is permitted which does not comply with these terms.

Clinical application of serum biomarkers for detecting and monitoring of chronic plaque psoriasis

Criselda Jean G. Cruz^{1,2} and Chao-Chun Yang^{1,2*}

¹Department of Dermatology, National Cheng Kung University Hospital, College of Medicine, National Cheng Kung University, Tainan, Taiwan, ²International Center for Wound Repair and Regeneration, National Cheng Kung University, Tainan, Taiwan

Psoriasis, a chronic, multisystemic inflammatory disease affecting millions of people globally, manifests as erythematous, thick, scaly plaques on the skin. Clinical evaluation remains to be the benchmark for diagnosis and monitoring of this debilitating disease. With current advancements in targeted molecular therapy for psoriasis such as biologics, molecular detection methods may also help guide clinical decisions and therapeutic strategies through quantification of circulating biomarkers, which could reflect the underlying pathogenic events happening at a certain point of the disease course. In this review, we will discuss how biomarkers are detected in serum samples using enzyme-linked immunosorbent assay (ELISA). This review will feature candidate biomarkers supported by clinical data for psoriasis including, but not limited to, cytokines, chemokines, adipokines, and antimicrobial peptides. A better understanding of the common method used for biomarker detection would enable physicians to interpret and correlate laboratory results with the disease pathogenesis and clinical outcomes, e.g., severity assessment and/or therapeutic response. With better health outcomes as the main goal, the utility of such information to evaluate and even predict treatment response would be a major step closer towards patient-tailored management.

KEYWORDS

psoriasis, ELISA, biomarkers, biologics, interleukins, skin inflammation

1 Introduction

Psoriasis is a chronic, immune-mediated condition manifesting as thick, raised, scaly plaques ([World Health Organization, 2016](#)). Psoriasis vulgaris or chronic plaque psoriasis constitutes 90% of all diagnosed psoriasis cases, some presenting with other systemic comorbidities, e.g., psoriatic arthritis, cardiovascular diseases, diabetes mellitus, cancer, and depression, thereby causing serious debilitation in one's quality of life ([Di Meglio et al., 2014](#); [World Health Organization, 2016](#); [Rendon and Schäkel, 2019](#)).

Onset and exacerbation of psoriasis is multifactorial, including genetic and environmental factors ([Armstrong and Read, 2020](#)). Its complex inflammatory processes involve members of the adaptive immune system. Excessive activation of myeloid dendritic cells occurs due to the cytokines secreted by plasmacytoid dendritic cells (pDC), keratinocytes, macrophages, and T cells, resulting in the secretion of interleukin (IL)-12 and IL-23 ([Alwan and Nestle, 2015](#)). IL-12 drives naive T cells to differentiate into T_H1 cells, which secretes interferon-gamma (IFN- γ) and tumor necrosis factor-alpha (TNF- α). IL-23 plays a critical role for T_H17- and T_H22-mediated

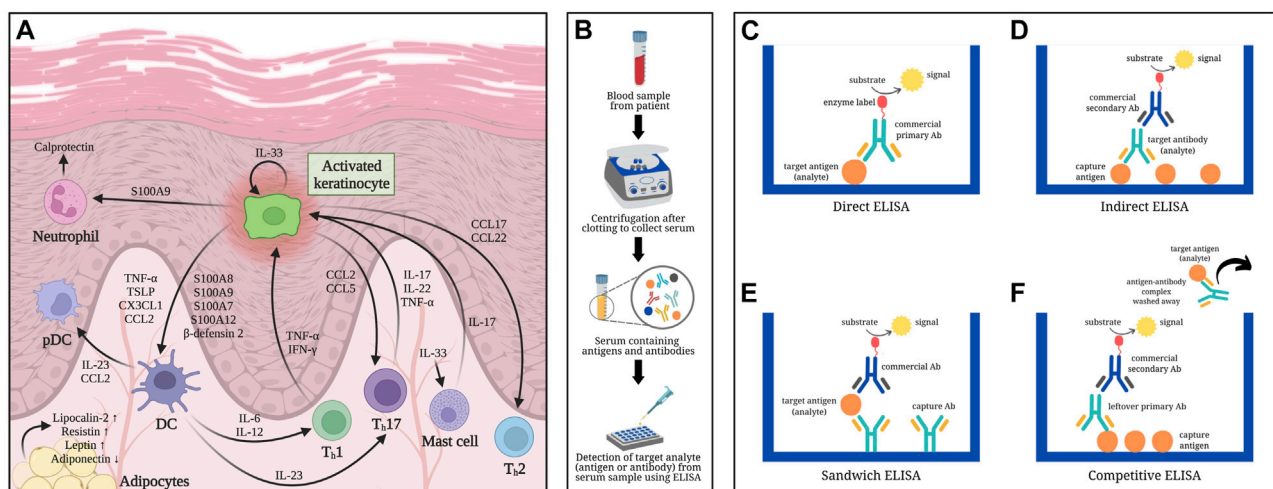


FIGURE 1

Overview of psoriasis-related serum biomarkers determined using ELISA-based methods: **(A)** Involvement of serum biomarkers in the pathogenesis of psoriasis. **(B)** Schematic diagram of serum collection from blood samples: Whole blood from a patient is allowed to clot first then centrifuged to separate the serum from clotted blood cells. **(C)** Direct ELISA: Antigens (analyte) from serum are immobilized onto a polystyrene microtiter plate followed by a blocking step (i.e., using bovine serum albumin) to cover any remaining plastic surface prior to adding the commercial enzyme-linked antibody (Ab) that would specifically bind to the antigens being measured. Signal emitted is directly proportional to the quantity of analytes. **(D)** Indirect ELISA: The microtiter plate is first coated with capture antigens, which would bind the antibodies (analyte) referred to as primary antibody from the serum sample. An enzyme-labeled secondary antibody (usually commercially obtained), which is host-specific to the primary antibody, is then added to detect the analytes captured onto the microtiter plate, hence emitting a signal proportional to the amount of analyte. **(E)** Sandwich ELISA: Capture antibodies specific to the analyte (antigen) are immobilized onto the wells of a microtiter plate, followed by the addition of the serum sample containing the antigens of interest. Once the antigens bind to the capture antibodies, a second antibody specific to a different epitope region of the analyte is added into the wells. The second antibody may or may not be labeled; in the latter case, an enzyme-conjugated third antibody, which is specific to the constant (Fc) region of the second antibody, would be included and act as the reporting antibody. The signal detected is directly correlated to the amount of antigens detected in the sample. **(F)** Competitive ELISA: Antigens are initially pre-coated onto the wells of a microtiter plate. The sample containing antigens to be measured are preincubated with primary antibodies to create mobile antibody-antigen complexes before adding the sample mixture onto the antigen-coated microtiter plates. Antigens, when present in high amounts, would result in fewer unbound primary antibodies. After washing off the sample mixture containing the mobile antibody-antigen complexes, any free primary antibodies would be captured by the immobilized antigens in the microtiter plate. A secondary antibody against the Fc region of the primary antibody is then added to report how much of it remained in the microtiter plate. Low signal detected in competitive ELISA implies that high amount of antigens were present in the sample, resulting in less unbound primary antibodies that could bind with the capture antigens on the microtiter plate.

cytokine release, i.e., T_H17 secretes IL-17, IL-22, and TNF- α , while T_H22 produces IL-22 (Armstrong and Read, 2020). Overall, these inflammatory signals lead to the skin and systemic manifestations in psoriasis, e.g., keratinocyte proliferation, immune cells infiltrating skin lesions, vasodilation, and angiogenesis (Nestle et al., 2009; Armstrong and Read, 2020).

Skin biopsy is an invasive procedure seldom used in diagnosing psoriasis (Greaves and Weinstein, 1995). Less invasive diagnostics offer the advantage of clinching the diagnosis while allowing repetitive measurements when warranted. Circulating proteins, also referred to as biomarkers, can be quantified through less invasive procedures and can indicate disease activity and progression, i.e., significant deviation from normal levels likely reflects an abnormal process occurring within the body (Molteni and Reali, 2012; Aronson and Ferner, 2017).

Biomarker studies for psoriasis aim to seek for reliable yet minimally invasive indicators of disease status and/or treatment response. Although psoriasis is often clinically diagnosed, biomarkers may serve as an aid for clinicians in quantitatively monitoring disease activity and therapeutic response. In this review, we discussed serum protein biomarkers that have been clinically correlated with psoriasis, as summarized in Figure 1A and Table 1. Immunoassay methods were also briefly discussed in

the context of serum biomarker detection. In doing so, we hope to provide clinicians with the fundamentals of immunoassays to facilitate better interpretation of immunoassay results and develop personalized and effective therapeutic strategies.

2 Principles of protein-based immunoassay for serum biomarker detection

Biomarker detection may require a few drops of blood by finger prick method to a few milliliters by venipuncture (Paul and Veenstra, 2022). Serum can be separated from other blood components by centrifugation after allowing blood to coagulate (Figure 1B). Antibody-based techniques, e.g., enzyme-linked immunosorbent assay (ELISA), have high sensitivity and specificity in detecting proteins from serum. ELISA utilizes the specific binding between proteins and antibodies in producing a measurable signal (Alhajj and Farhana, 2023).

Regarded as the gold standard for immunoassays, ELISA was first described in 1972 as a simple yet sensitive analytical technique for antibody quantification, detecting less than 1 ng/mL of antibody

TABLE 1 Serum biomarkers for psoriasis in correlation with disease severity and/or treatment response.

Serum biomarker	Serum level: Psoriasis vs. healthy	Correlates with severity? ^a	Reflects treatment response? ^a	References
IL-6	up	Y	Y (adalimumab, infliximab)	Arican et al. (2005), Shibata et al. (2009), Muramatsu et al. (2017), Michalak-Stoma et al. (2022)
IL-12	up	Y	Y (etanercept)	Arican et al. (2005), Takahashi et al. (2010), Brito-Luna et al. (2016), Lu et al. (2016)
IL-17	up	Y	Y (etanercept)	Arican et al. (2005), Caproni et al. (2009), Takahashi et al. (2010), Yilmaz et al. (2012), Nassar et al. (2022)
IL-22	up	Y	Y (etanercept, guselkumab, ustekinumab)	Boniface et al. (2007), Caproni et al. (2009), Lo et al. (2010), Shimauchi et al. (2013), Dudakov et al. (2015), Gordon et al. (2019), Wawrzycki et al. (2019), Philipp et al. (2020)
IL-33	up	N		Balato et al. (2012), Mitsui et al. (2016), Li et al. (2017), Borsky et al. (2020)
IFN- γ	up	N		Jacob et al. (2003), Arican et al. (2005), Moustafa et al. (2009), Takahashi et al. (2010), Kurtovic and Halilovic (2018)
TNF- α	up	N		Arican et al. (2005), Takahashi et al. (2010), Kyriakou et al. (2014), Ovcina-Kurtovic and Kasumagic-Halilovic (2022)
TSLP	up	Y		El-Ghareeb et al. (2019)
HMGB1	up	N		Bergmann et al. (2016), Strohbuecker et al. (2019), Borsky et al. (2020)
IL-10	no difference			Dowlathshahi et al. (2013), Bai et al. (2018)
CX3CL1	up	Y		Congjun et al. (2015)
TARC/CCL17	up	N		Purzycka-Bohdan et al. (2022)
CCL2	up	N		Purzycka-Bohdan et al. (2022)
CCL3	up	N		Purzycka-Bohdan et al. (2022)
CCL5	up	N		Purzycka-Bohdan et al. (2022)
CCL18	up	N		Purzycka-Bohdan et al. (2022)
CCL22	up	N		Purzycka-Bohdan et al. (2022)
Lipocalin-2	up (acute types)	Y		Nguyen and Nguyen (2022)
Resistin	up	Y		Bai et al. (2018), Seth et al. (2020)
Adiponectin	down	N		Shibata et al. (2009), Oh et al. (2014)
Leptin	up	Y		Cerman et al. (2008), Zhu et al. (2013), Oh et al. (2014)
Calprotectin	up	Y	Y (methotrexate)	Hamza et al. (2019), Scali et al. (2022), Li et al. (2023)
S100A8	up	Y		Benoit et al. (2006), Matsunaga et al. (2021)
S100A9	up	Y		Benoit et al. (2006), Matsunaga et al. (2021)
S100A7	up	Y		Wilsmann-Theis et al. (2016)
S100A12	up	Y		Wilsmann-Theis et al. (2016)
β -defensin 2	up	Y	Y (secukinumab, tofacitinib)	Jin et al. (2017), Morita et al. (2020)
FGL1	down	Y		Sun et al. (2022)
OAS2	up	Y		Zhou et al. (2020)

^aY: yes, N: no.

(Engvall and Perlmann, 1972). The quantifiable signal results from an enzyme-substrate reaction indicating that the analyte is present and binds the reporting antibody conjugated with the enzyme

(Figures 1C–F). Different types of ELISA (direct, indirect, sandwich, and competitive) mainly vary in the number of steps involved.

Direct ELISA is a straightforward manner of immunoassay (Figure 1C), wherein the antigens (analyte) from serum acts as capture molecules for its specific reporting enzyme-linked antibody (Aydin, 2015; Alhajj and Farhana, 2023). Indirect ELISA enables detection of antibody from serum when captured by immobilized antigens followed by the addition of an enzyme-labeled secondary antibody (Figure 1D) (Aydin, 2015; Alhajj and Farhana, 2023). Sandwich ELISA, as the name implies, involves two antibodies that capture the antigen of interest in between (Figure 1E). Commonly used for biomarker detection, sandwich ELISA has specific primary antibodies immobilized instead of directly coating the microtiter plate with analytes, thereby increasing its specificity while reducing nonspecific binding (Aydin, 2015; Alhajj and Farhana, 2023). Competitive ELISA is another platform that allows detection of antigens or biomarkers (Figure 1F). It is often useful when the analyte is small and difficult to be “sandwiched” in between antibodies (Gan and Patel, 2013; Aydin, 2015; Alhajj and Farhana, 2023).

Other techniques for biomarker detection include mass spectrometry, flow cytometry, and protein microarrays; however, these are not readily accessible in clinical settings hence were excluded in this review. ELISA is a well-established method that is feasible in most laboratories as commercial kits are often readily available. Given its high sensitivity and specificity, sandwich ELISA is most commonly used in biomarker assays (Del Campo et al., 2015). The subsequent section discusses psoriasis-related protein biomarkers, most of which were studied using sandwich-type ELISA.

3 Serum biomarkers for psoriasis

Candidate serum biomarkers for psoriasis discussed in this review include cytokines, chemokines, adipokines, and antimicrobial peptides, as summarized in Table 1.

3.1 Cytokines and chemokines

During inflammation, cytokines and chemokines are secreted by various immune cells to mediate signaling pathways and recruit effector cells towards the affected sites, hence may serve as candidate biomarkers for long-term inflammatory diseases such as psoriasis.

3.1.1 IL-6

With its implications on epidermal and dermal growth and differentiation, IL-6 is being explored as a dendritic cell (DC)-produced inflammatory marker as it induces T cell conversion to T_H17, which in effect produces other inflammatory cytokines (Goodman et al., 2009; Pietrzak et al., 2020; Kutsuna et al., 2022). Baseline IL-6 levels in serum of psoriasis patients were found to be significantly elevated compared to healthy individuals (Arican et al., 2005; Shibata et al., 2009; Michalak-Stoma et al., 2022). Moreover, a significant correlation was noted between serum IL-6 and PASI scores in psoriasis vulgaris patients (Muramatsu et al., 2017). Therapeutic response was also reflected by significant decrease in serum IL-6 levels after treatment with biologics such as adalimumab and infliximab.

3.1.2 IL-12

IL-12 plays a role in T-cell-mediated immunity and is considered as one of the key cytokines responsible for formation and persistence of psoriatic plaques (Ergen and Yusuf, 2018). Patients with plaque psoriasis exhibited elevated serum IL-12, which also correlates with PASI scores (Arican et al., 2005; Takahashi et al., 2010; Brito-Luna et al., 2016). In addition, patients who were classified as non-responders to a 24-week treatment of etanercept were noted to have lower baseline IL-12 serum levels than the responders, hence may be suggestive of IL-12 as a potential biomarker or predictor for clinical response to etanercept, which is a TNF-inhibitor used to treat psoriasis (Lu et al., 2016). Moreover, serum IL-12 level could potentially serve as an indicator for clinical response to etanercept with 50% sensitivity and 96% specificity. In this study, clinical response was defined by a reduction of 75% in the PASI score after treatment.

3.1.3 IL-17

Produced by various immune cells such as T_H17, neutrophils, and mast cells, IL-17 is a key cytokine responsible for keratinocyte proliferation and production of other cytokines and antimicrobial peptides in psoriasis (Veldhoen et al., 2006; Lin et al., 2011; Keijsers et al., 2014; Dyring-Andersen et al., 2017). Serum IL-17 concentration was higher in individuals with chronic plaque psoriasis than in healthy controls (Takahashi et al., 2010; Nassar et al., 2022). IL-17 in serum also correlated with severity in psoriasis patients (Arican et al., 2005; Takahashi et al., 2010; Yilmaz et al., 2012). It has been reported that IL-17 levels in serum decreased after treatment with etanercept, suggesting that IL-17 is a potential biomarker for both disease severity and therapeutic response monitoring (Caproni et al., 2009).

3.1.4 IL-22

Described as a proinflammatory cytokine produced by CD4 memory T cells (e.g., T_H1, T_H17, T_H22), IL-22, a member of the IL-10 family, have been found to be significantly elevated in patients with psoriasis compared to healthy controls (Boniface et al., 2007; Lo et al., 2010; Shimauchi et al., 2013; Dudakov et al., 2015; Gordon et al., 2019; Wawrzynski et al., 2019). These studies also demonstrated that IL-22 levels exhibit a positive correlation with disease severity based on PASI scores, making it a potential cytokine suitable for monitoring psoriasis activity. IL-22 may also be a biomarker indicating treatment response due to the notable decrease in serum IL-22 levels after treatment with either etanercept, guselkumab (anti-IL-23) or ustekinumab (anti-IL-12/23) (Caproni et al., 2009; Gordon et al., 2019; Philipp et al., 2020).

3.1.5 IL-33

Regarded as both cytokine and damage-associated molecular pattern, IL-33 is released upon keratinocyte damage in psoriasis then activates inflammatory pathways in an autocrine manner (De la Fuente et al., 2015; Zeng et al., 2021). IL-33 secreted by endothelial cells could activate mast cells, which then initiate inflammation in unaffected psoriatic skin (Theoharides et al., 2010). Studies have reported that IL-33 levels are elevated in the serum of psoriasis patients than the healthy controls, although no correlation found between IL-33 levels and PASI scores (Mitsui et al., 2016; Li et al., 2017; Borsky et al., 2020). Despite having reported to be increased in other skin conditions such as vitiligo and atopic dermatitis (Tamagawa-Mineoka et al., 2014; Vaccaro et al., 2016), IL-33 elevation was significantly higher in psoriatic than in AD lesions, hence lesional

IL-33 seem to correlate strongly with psoriasis in a localized manner (Balato et al., 2012).

3.1.6 IFN- γ

IFN- γ is a T_H1 -derived cytokine that mediates downstream processes favoring keratinocyte proliferation, a key occurrence in psoriasis pathogenesis (Nickoloff and Nestle, 2004). Although there was no overall significant correlation to disease type or severity in terms of PASI score, elevated IFN- γ serum concentration has been associated with active psoriasis in multiple studies (Jacob et al., 2003; Arican et al., 2005; Moustafa et al., 2009; Takahashi et al., 2010; Kurtovic and Halilovic, 2018). Altogether, increased IFN- γ likely indicates presence of psoriasis, though might not be suitable in terms of assessing disease severity due to conflicting reports regarding its correlation with PASI scores.

3.1.7 TNF- α

TNF- α is another key proinflammatory cytokine that promotes immune cell migration towards the skin resulting in keratinocyte proliferation, which is one of the hallmark manifestations of psoriasis (Conrad and Gilliet, 2018; Ogawa et al., 2018; Ovcina-Kurtovic and Kasumagic-Halilovic, 2022). In psoriasis, affected keratinocytes produce excessive TNF- α , hence activating dendritic cells to produce IL-12 and IL-23. These cytokines promote T cell differentiation into T_H1 and T_H17 , which produce more TNF- α and other proinflammatory cytokines such as IL-17 and IFN- γ , leading to the pathologic manifestations of psoriasis, i.e., keratinocyte hyperproliferation, acanthosis, parakeratosis, and hypogranulosis (Conrad and Gilliet, 2018; Ogawa et al., 2018). Serum TNF- α was found to be significantly higher in those with psoriasis than those without (Arican et al., 2005; Takahashi et al., 2010; Kyriakou et al., 2014; Ovcina-Kurtovic and Kasumagic-Halilovic, 2022); however, majority of these studies report that its correlation with PASI scores was not significant.

3.1.8 Thymic stromal lymphopoietin (TSLP)

TSLP is a proallergic keratinocyte-derived cytokine, which has been described to induce dendritic cell maturation and IL-23 production in psoriasis pathogenesis (Volpe et al., 2014). Serum TSLP has been reported to be elevated in psoriasis patients with a significant correlation to disease severity (El-Ghareeb et al., 2019). TSLP may be a potential indicator for early detection and diagnosis of active psoriasis.

3.1.9 High-mobility group box 1 (HMGB1)

Previous studies found that HMGB1, a proinflammatory cytokine, was significantly increased in sera of psoriasis patients compared to healthy controls (Bergmann et al., 2016; Strohbuecker et al., 2019; Borsky et al., 2020); however, its relationship with disease severity is yet to be established.

3.1.10 IL-10

Despite being an anti-inflammatory cytokine expected to be downregulated in the presence of psoriasis, no significant difference has been noted in the baseline serum IL-10 levels between patients with psoriasis and healthy individuals (Dowlathshahi et al., 2013; Bai et al., 2018). In attempt to quantify serum IL-10 concentrations in psoriasis patients, multiple cytokine analysis approach was applied by Michalak-Stoma et al. (2022); however, signal intensities for IL-10 were

insufficient for quantification, implying that this anti-inflammatory cytokine may not be an ideal serum biomarker for psoriasis.

3.1.11 Fractalkine (CX3CL1)

Fractalkine, a membrane-bound chemokine, was significantly elevated in the serum of psoriasis patients compared to healthy individuals (Congjun et al., 2015). In the same study, the positive correlation between CX3CL1 serum levels and PASI scores was also demonstrated, suggesting the potential utility of this biomarker to assess disease severity.

3.1.12 Thymus and activation-regulated chemokine (TARC/CCL17) and other chemokines

Thymus and activation-regulated chemokine or CCL17 serum levels were significantly higher in patients with chronic plaque psoriasis compared to that of the healthy controls (Purzycka-Bohdan et al., 2022). Moreover, serum TARC correlated positively with pruritus assessed using the visual analog scale, but no overall significant correlation was seen between serum TARC and PASI scores. Other chemokines, namely, CCL2/MCP-1, CCL3/MIP-1 α , CCL5/RANTES, CCL18/PARC and CCL22/MDC, although not significantly correlated with disease severity, were also found to be elevated in patients with chronic plaque psoriasis.

3.2 Adipokines

Adipose-tissue derived mediators called adipokines have been linked with metabolic disturbances and chronic inflammation including psoriasis. Immune dysregulation in psoriasis leads to secretion of adipokines into the bloodstream, hence such molecules potentially reflect disease activity (Śluczawska-Głabowska et al., 2023).

3.2.1 Lipocalin-2

Detected in blood samples through ELISA, lipocalin-2 is an adipokine that has been correlated with disease severity in psoriasis patients. In a study of 62 patients with psoriasis, the BSA and PASI scores in cases of psoriatic erythroderma and psoriasis vulgaris, as well as the severity score of generalized pustular psoriasis, were all noted to have positive correlation with lipocalin-2 levels (Nguyen and Nguyen, 2022). Furthermore, lipocalin-2 levels were significantly higher in patients with acute types of psoriasis than in chronic types, indicating the potential of this adipokine as a biomarker for psoriasis accompanied with acute inflammation.

3.2.2 Resistin

Resistin is a pro-inflammatory adipokine involved in TNF- α -related pathways in psoriasis (Nakajima et al., 2013; Müge et al., 2019). Serum resistin concentrations were significantly higher in psoriasis patients than that of healthy individuals (Bai et al., 2018). A correlation between serum resistin and PASI score was also reported, in which more severe cases of psoriasis had higher resistin levels than those with lower PASI scores (Seth et al., 2020).

3.2.3 Adiponectin

Psoriasis patients exhibited lower serum adiponectin levels relative to the healthy controls (Shibata et al., 2009; Oh et al., 2014), indicating

that adiponectin's supposedly anti-inflammatory role is downregulated in psoriasis. Furthermore, no significant correlation was noted between adiponectin levels in serum of patients and their PASI scores.

3.2.4 Leptin

Leptin, an energy-regulating secretory hormone from adipose tissue, has been associated with proinflammatory cytokine induction (Cerman et al., 2008). Serum leptin levels were found to be elevated in psoriasis patients compared to healthy controls and positively correlates with PASI scores (Cerman et al., 2008; Zhu et al., 2013; Oh et al., 2014).

3.3 Antimicrobial peptides

3.3.1 S100 proteins

Calprotectin is an antimicrobial peptide and calcium-binding soluble protein secreted by monocytes and neutrophils during inflammation (Voganatsi et al., 2001). Regarded as a potential novel biomarker for psoriasis, serum calprotectin was significantly higher and correlates positively with PASI scores in psoriatic patients than healthy controls (Scali et al., 2022; Li et al., 2023). Both PASI scores and serum calprotectin levels significantly decreased after 3-month methotrexate therapy of patients with psoriasis vulgaris, demonstrating its potential as a prognostic marker for treatment response (Hamza et al., 2019). Furthermore, calprotectin might indicate disease relapse as serum levels were noted to be significantly higher in relapsed cases compared to nonrelapsed cases of psoriasis.

Calcium-binding S100 proteins A8 (S100A8) and A9 (S100A9) levels were significantly increased in both serum and stratum corneum of psoriasis patients while also positively correlating with PASI scores (Benoit et al., 2006; Matsunaga et al., 2021), demonstrating the capability of these proteins in reflecting disease severity. Additionally, serum S100A7 (psoriasin) and S100A12 (calgranulin-c) were found to be elevated in psoriasis patients, with the latter being regarded as the most promising S100 protein biomarker thus far in terms of correlating with severity of psoriasis (Wilschmann-Theis et al., 2016).

3.3.2 β -defensin 2 (BD-2)

Inflammation drives the expression of BD-2 from keratinocytes (Cieřlik et al., 2021). Baseline serum BD-2 levels were higher in patients with active psoriasis than healthy controls (Morita et al., 2020). Furthermore, serum BD-2 positively correlated with PASI score and was found to decrease after treatment with secukinumab, an anti-IL-17A drug. A similar trend was reported upon treatment with tofacitinib, a JAK-inhibitor (Jin et al., 2017). Serum BD-2 levels could potentially reflect psoriasis severity and treatment response to secukinumab or tofacitinib, although warranting further studies.

3.4 Other potential novel protein biomarkers

3.4.1 Fibrinogen-like protein 1 (FGL1)

FGL1, a 68-kD protein from the fibrinogen family, was found to be significantly lower in the serum of psoriasis patients than healthy controls (Sun et al., 2022). Despite this observation, PASI scores of patients with psoriasis remained positively correlated with serum FGL1 concentration.

3.4.2 2-5-Oligoadenylate synthase 2 (OAS2)

OAS2 is a potential novel biomarker identified from proteomic profiles of psoriasis patients, who exhibited significantly higher OAS2 serum levels than healthy controls (Zhou et al., 2020). The reported positive correlation between PASI score and OAS2 levels suggests that OAS2 potentially reflects disease severity. Moreover, OAS2 was shown to differentiate those with low PASI scores ($\text{PASI} \leq 10$) from healthy controls.

4 Discussion: future prospects and clinical application

Quantification of biomarkers from a small amount of blood or serum sample obtained via minimally invasive approaches offers plenty of advantages, including the willingness and increased compliance of patients, emphasizing the importance of biomarker identification and assays. One promising approach is by integrating high throughput technologies such as proteomics analysis as demonstrated in the discovery of OAS2 as a candidate biomarker for psoriasis (Zhou et al., 2020).

Establishing reliable biomarkers for psoriasis involves several stages. First is to identify detectable biomarkers that reflect key clinical outcomes (e.g., disease severity and treatment response). Validation studies, wherein biomarkers are assayed and correlated with the patients' clinical manifestations, is preferably conducted in a larger cohort to better establish the correlation. Determining a biomarker's correlation to the disease status (whether positive or negative), its cut-off values, sensitivity, and specificity provides useful information that can support a physician's clinical decision-making and management of psoriasis patients.

Author contributions

Conceptualization: CC and C-CY; Writing—original draft: CC and C-CY; Writing—review and editing: CC and C-CY. All authors contributed to the article and approved the submitted version.

Funding

This research was supported in part by the National Science and Technology Council (NSTC), Taiwan (grant number NSTC 111-2314-B-006-101).

Acknowledgments

Figures were created with [BioRender.com](https://www.biorender.com).

Conflict of interest

The authors declare that the research was conducted in the absence of any commercial or financial relationships that could be construed as a potential conflict of interest.

Publisher's note

All claims expressed in this article are solely those of the authors and do not necessarily represent those of their affiliated

References

- Alhajj, M., and Farhana, A. (2023). "Enzyme linked immunosorbent assay," in *StatPearls* (Island: StatPearls Publishing).
- Alwan, W., and Nestle, F. O. (2015). Pathogenesis and treatment of psoriasis: Exploiting pathophysiological pathways for precision medicine. *Clin. Exp. Rheumatol.* 33 (5), S2–S6.
- Arican, O., Aral, M., Sasmaz, S., and Ciragil, P. (2005). Serum levels of TNF- α , IFN- γ , IL-6, IL-8, IL-12, IL-17, and IL-18 in patients with active psoriasis and correlation with disease severity. *Mediat. Inflamm.* 2005, 273–279. doi:10.1155/MI.2005.273
- Armstrong, A. W., and Read, C. (2020). Pathophysiology, clinical presentation, and treatment of psoriasis: A review. *Jama* 323 (19), 1945–1960. doi:10.1001/jama.2020.4006
- Aronson, J. K., and Ferner, R. E. (2017). Biomarkers-A general review. *Curr. Protoc. Pharmacol.* 76, 9.23.1–9.23.17. doi:10.1002/cpph.19
- Aydin, S. (2015). A short history, principles, and types of ELISA, and our laboratory experience with peptide/protein analyses using ELISA. *Peptides* 72, 4–15. doi:10.1016/j.peptides.2015.04.012
- Bai, F., Zheng, W., Dong, Y., Wang, J., Garstka, M. A., Li, R., et al. (2018). Serum levels of adipokines and cytokines in psoriasis patients: A systematic review and meta-analysis. *Oncotarget* 9 (1), 1266–1278. doi:10.18632/oncotarget.22260
- Balato, A., Lembo, S., Mattii, M., Schiattarella, M., Marino, R., De Paulis, A., et al. (2012). IL-33 is secreted by psoriatic keratinocytes and induces pro-inflammatory cytokines via keratinocyte and mast cell activation. *Exp. Dermatol.* 21 (11), 892–894. doi:10.1111/exd.12027
- Benoit, S., Toksoy, A., Ahlmann, M., Schmidt, M., Sunderkötter, C., Foell, D., et al. (2006). Elevated serum levels of calcium-binding S100 proteins A8 and A9 reflect disease activity and abnormal differentiation of keratinocytes in psoriasis. *Br. J. Dermatol.* 155 (1), 62–66. doi:10.1111/j.1365-2133.2006.07198.x
- Bergmann, C., Strohbuecker, L., Lotfi, R., Sucker, A., Joosten, I., Koenen, H., et al. (2016). High mobility group box 1 is increased in the sera of psoriatic patients with disease progression. *J. Eur. Acad. Dermatol. Venereol.* 30 (3), 435–441. doi:10.1111/jdv.13564
- Boniface, K., Guignouard, E., Pedretti, N., Garcia, M., Delwail, A., Bernard, F. X., et al. (2007). A role for T cell-derived interleukin 22 in psoriatic skin inflammation. *Clin. Exp. Immunol.* 150 (3), 407–415. doi:10.1111/j.1365-2249.2007.03511.x
- Borsky, P., Fiala, Z., Andrys, C., Beranek, M., Hamakova, K., Malkova, A., et al. (2020). Alarmins HMGB1, IL-33, S100A7, and S100A12 in psoriasis vulgaris. *Mediat. Inflamm.* 2020, 8465083. doi:10.1155/2020/8465083
- Brito-Luna, M. J., Villanueva-Quintero, D. G., Sandoval-Talamantes, A. K., Fafutis-Morris, M., Graciano-Machuca, O., Sanchez-Hernandez, P. E., et al. (2016). Correlation of IL-12, IL-22, and IL-23 in patients with psoriasis and metabolic syndrome. Preliminary report. *Prelim. Rep. Cytokine* 85, 130–136. doi:10.1016/j.cyto.2016.06.020
- Caproni, M., Antiga, E., Melani, L., Volpi, W., Del Bianco, E., and Fabbri, P. (2009). Serum levels of IL-17 and IL-22 are reduced by etanercept, but not by acitretin, in patients with psoriasis: A randomized-controlled trial. *J. Clin. Immunol.* 29 (2), 210–214. doi:10.1007/s10875-008-9233-0
- Cerman, A. A., Bozkurt, S., Sav, A., Tulunay, A., Elbaşı, M. O., and Ergun, T. (2008). Serum leptin levels, skin leptin and leptin receptor expression in psoriasis. *Br. J. Dermatol.* 159 (4), 820–826. doi:10.1111/j.1365-2133.2008.08742.x
- Cieslik, M., Bagińska, N., Górski, A., and Jończyk-Matysiak, E. (2021). Human β -defensin 2 and its postulated role in modulation of the immune response. *Cells* 10 (11), 2991. doi:10.3390/cells10112991
- Congjun, J., Yanmei, Z., Huiling, J., Zhen, Y., and Shuo, L. (2015). Elevated local and serum cx3cl1(fractalkine) expression and its association with disease severity in patients with psoriasis. *Ann. Clin. Lab. Sci.* 45 (5), 556–561.
- Conrad, C., and Gilliet, M. (2018). Psoriasis: From pathogenesis to targeted therapies. *Clin. Rev. Allergy & Immunol.* 54 (1), 102–113. doi:10.1007/s12016-018-8668-1
- De la Fuente, M., MacDonald, T. T., and Hermoso, M. A. (2015). The IL-33/ST2 axis: Role in health and disease. *Cytokine & Growth Factor Rev.* 26 (6), 615–623. doi:10.1016/j.cytogfr.2015.07.017
- Del Campo, M., Jongbloed, W., Twaalfhoven, H. A., Veerhuis, R., Blankenstein, M. A., and Teunissen, C. E. (2015). Facilitating the validation of novel protein biomarkers for dementia: An optimal workflow for the development of sandwich immunoassays. *Front. Neurol.* 6, 202. doi:10.3389/fneur.2015.00202
- Di Meglio, P., Villanova, F., and Nestle, F. O. (2014). Psoriasis. *Cold Spring Harb. Perspect. Med.* 4 (8), a015354. doi:10.1101/cshperspect.a015354
- Dowlathshahi, E. A., van der Voort, E. A., Arends, L. R., and Nijsten, T. (2013). Markers of systemic inflammation in psoriasis: A systematic review and meta-analysis. *Br. J. Dermatol.* 169 (2), 266–282. doi:10.1111/bjd.12355
- Dudakov, J. A., Hanash, A. M., and van den Brink, M. R. (2015). Interleukin-22: Immunobiology and pathology. *Annu. Rev. Immunol.* 33, 747–785. doi:10.1146/annurev-immunol-032414-112123
- Dyring-Andersen, B., Honoré, T. V., Madelung, A., Bzorek, M., Simonsen, S., Clemmensen, S. N., et al. (2017). Interleukin (IL)-17A and IL-22-producing neutrophils in psoriatic skin. *Br. J. Dermatol.* 177 (6), e321–e322. doi:10.1111/bjd.15533
- El-Ghareeb, M. I., Helmy, A., Al Kazzaz, S., and Samir, H. (2019). Serum TSLP is a potential biomarker of psoriasis vulgaris activity. *Psoriasis (Auckl)* 9, 59–63. doi:10.2147/ptt.S212774
- Engvall, E., and Perlmann, P. (1972). Enzyme-linked immunosorbent assay, elisa. *J. Immunol.* 109 (1), 129–135. doi:10.4049/jimmunol.109.1.129
- Ergen, E. N., and Yusuf, N. (2018). Inhibition of interleukin-12 and/or interleukin-23 for the treatment of psoriasis: What is the evidence for an effect on malignancy? *Exp. Dermatol.* 27 (7), 737–747. doi:10.1111/exd.13676
- Gan, S. D., and Patel, K. R. (2013). Enzyme immunoassay and enzyme-linked immunosorbent assay. *J. Invest. Dermatol.* 133 (9), e12. doi:10.1038/jid.2013.287
- Goodman, W. A., Levine, A. D., Massari, J. V., Sugiyama, H., McCormick, T. S., and Cooper, K. D. (2009). IL-6 signaling in psoriasis prevents immune suppression by regulatory T cells. *J. Immunol.* 183 (5), 3170–3176. doi:10.4049/jimmunol.0803721
- Gordon, K. B., Armstrong, A. W., Foley, P., Song, M., Shen, Y. K., Li, S., et al. (2019). Guselkumab efficacy after withdrawal is associated with suppression of serum IL-23-regulated IL-17 and IL-22 in psoriasis: VOYAGE 2 study. *J. Invest. Dermatol.* 139 (12), 2437–2446.e1. doi:10.1016/j.jid.2019.05.016
- Greaves, M. W., and Weinstein, G. D. (1995). Treatment of psoriasis. *N. Engl. J. Med.* 332 (9), 581–588. doi:10.1056/nejm199503023320907
- Hamza, A., Hassan, E., Donia, H., and Maamon, Y. (2019). Serum calprotectin as a predictive biomarker in the treatment of psoriasis vulgaris with methotrexate. *J. Egypt. Women's Dermatologic Soc.* 16 (2), 112–118. doi:10.4103/jewd.Jewd_12_19
- Jacob, S. E., Nassiri, M., Kerdel, F. A., and Vencek, V. (2003). Simultaneous measurement of multiple Th1 and Th2 serum cytokines in psoriasis and correlation with disease severity. *Mediat. Inflamm.* 12 (5), 309–313. doi:10.1080/09629350310001619753
- Jin, T., Sun, Z., Chen, X., Wang, Y., Li, R., Ji, S., et al. (2017). Serum human beta-defensin-2 is a possible biomarker for monitoring response to JAK inhibitor in psoriasis patients. *Dermatology* 233 (2–3), 164–169. doi:10.1159/000475809
- Keijsers, R., Hendriks, A. G. M., van Erp, P. E. J., van Cranenbroek, B., van de Kerkhof, P. C. M., Koenen, H., et al. (2014). *In vivo* induction of cutaneous inflammation results in the accumulation of extracellular trap-forming neutrophils expressing ROR γ t and IL-17. *J. Invest. Dermatol.* 134 (5), 1276–1284. doi:10.1038/jid.2013.526
- Kurtovic, N. O., and Halilovic, E. K. (2018). Serum concentrations of interferon gamma (IFN- γ) in patients with psoriasis: Correlation with clinical type and severity of the disease. *Med. Arch.* 72 (6), 410–413. doi:10.5455/medarh.2018.72.410-413
- Kutsuna, T., Hino, K., Hasegawa, H., Watamori, K., Kidani, T., Imai, H., et al. (2022). Psoriatic arthritis successfully treated with second-line anti-interleukin-6 treatment: A case report and review of the literature. *J. Med. Case Rep.* 16 (1), 402. doi:10.1186/s13256-022-03624-z
- Kyriakou, A., Patsatsi, A., Vyzantiadis, T. A., and Sotiriadis, D. (2014). Serum levels of TNF- α , IL-12/23p40, and IL-17 in plaque psoriasis and their correlation with disease severity. *J. Immunol. Res.* 2014, 467541. doi:10.1155/2014/467541
- Li, B., Li, G., Song, Z., and Zhang, Z. (2023). Serum calprotectin as a promising inflammatory biomarker in psoriatic arthritis: A 1-year longitudinal study. *Rheumatol. Ther.* 10 (1), 149–160. doi:10.1007/s40744-022-00501-5
- Li, J., Liu, L., Rui, W., Li, X., Xuan, D., Zheng, S., et al. (2017). New interleukins in psoriasis and psoriatic arthritis patients: The possible roles of interleukin-33 to interleukin-38 in disease activities and bone erosions. *Dermatology* 233 (1), 37–46. doi:10.1159/000471798
- Lin, A. M., Rubin, C. J., Khandpur, R., Wang, J. Y., Riblett, M., Yalavarthi, S., et al. (2011). Mast cells and neutrophils release IL-17 through extracellular trap formation in psoriasis. *J. Immunol.* 187 (1), 490–500. doi:10.4049/jimmunol.1100123

- Lo, Y. H., Torii, K., Saito, C., Furuhashi, T., Maeda, A., and Morita, A. (2010). Serum IL-22 correlates with psoriatic severity and serum IL-6 correlates with susceptibility to phototherapy. *J. Dermatol. Sci.* 58 (3), 225–227. doi:10.1016/j.jdermsci.2010.03.018
- Lu, J., Tang, S., Xie, S., Yi, X., Yu, N., Gao, Y., et al. (2016). The potential of IL-12 in predicting clinical response to etanercept treatment in patients with psoriasis. *Int. J. Clin. Exp. Med.* 9 (12), 23519–23524.
- Matsunaga, Y., Hashimoto, Y., and Ishiko, A. (2021). Stratum corneum levels of calprotectin proteins S100A8/A9 correlate with disease activity in psoriasis patients. *J. Dermatol.* 48 (10), 1518–1525. doi:10.1111/1346-8138.16032
- Michalak-Stoma, A., Bartosińska, J., Racziewicz, D., Kowal, M., Kozak, J., Gujski, M., et al. (2022). Multiple cytokine analysis of Th1/Th2/Th9/Th17/Th22/treg cytokine pathway for individual immune profile assessment in patients with psoriasis. *Med. Sci. Monit.* 28, e938277. doi:10.12659/msm.938277
- Mitsui, A., Tada, Y., Takahashi, T., Shibata, S., Kamata, M., Miyagaki, T., et al. (2016). Serum IL-33 levels are increased in patients with psoriasis. *Clin. Exp. Dermatol.* 41 (2), 183–189. doi:10.1111/ced.12670
- Molteni, S., and Reali, E. (2012). *Biomarkers in the pathogenesis, diagnosis, and treatment of psoriasis*. Psoriasis: Targets and Therapy, 55–66.
- Morita, A., Tani, Y., Matsumoto, K., Yamaguchi, M., Teshima, R., and Ohtsuki, M. (2020). Assessment of serum biomarkers in patients with plaque psoriasis on secukinumab. *J. Dermatol.* 47 (5), 452–457. doi:10.1111/1346-8138.15278
- Moustafa, Y. M., Abdel Aal, I., Mohamed, E., Abdel Baky, A., and Taher, S. (2009). Assessment of serum interferon gamma and interleukin-4 in psoriasis vulgaris. *Egypt. J. Med. Microbiol.* 18 (3), 45–48.
- Müge, A. E., Nilsel, İ., and Şehri, E. (2019). Association of leptin, resistin, and high-molecular-weight adiponectin levels with psoriasis area and severity index scores, obesity, and insulin resistance in psoriasis patients. *Dermatol. Sin.* 37 (1), 33–39. doi:10.4103/ds.ds_9_18
- Muramatsu, S., Kubo, R., Nishida, E., and Morita, A. (2017). Serum interleukin-6 levels in response to biologic treatment in patients with psoriasis. *Mod. Rheumatol.* 27 (1), 137–141. doi:10.3109/14397595.2016.1174328
- Nakajima, H., Nakajima, K., Tarutani, M., and Sano, S. (2013). Clear association between serum levels of adipokines and T-helper 17-related cytokines in patients with psoriasis. *Clin. Exp. Dermatol.* 38 (1), 66–70. doi:10.1111/j.1365-2230.2012.04465.x
- Nassar, A. A., Bakr, N. M., Elyousefi, E. H. I., Elkholy, B. M., and Fawzy, M. M. (2022). Serum immunoglobulin E and interleukin-17 levels in patients with chronic plaque psoriasis: A case-control study. *J. Cosmet. Dermatol.* 21 (11), 6377–6384. doi:10.1111/jocd.15299
- Nestle, F. O., Kaplan, D. H., and Barker, J. (2009). Psoriasis. *N. Engl. J. Med.* 361 (5), 496–509. doi:10.1056/NEJMra0804595
- Nguyen, C. T. H., and Nguyen, O. P. T. (2022). Increased plasma lipocalin-2 levels correlate with disease severity and may be a marker of acute inflammatory response in patients with psoriasis. *Dermatol. Rep.* 14 (4), 9469. doi:10.4081/dr.2022.9469
- Nickoloff, B. J., and Nestle, F. O. (2004). Recent insights into the immunopathogenesis of psoriasis provide new therapeutic opportunities. *J. Clin. Invest.* 113 (12), 1664–1675. doi:10.1172/jci22147
- Ogawa, E., Sato, Y., Minagawa, A., and Okuyama, R. (2018). Pathogenesis of psoriasis and development of treatment. *J. Dermatology* 45 (3), 264–272. doi:10.1111/1346-8138.14139
- Oh, Y. J., Lim, H. K., Choi, J. H., Lee, J. W., and Kim, N. I. (2014). Serum leptin and adiponectin levels in Korean patients with psoriasis. *J. Korean Med. Sci.* 29 (5), 729–734. doi:10.3346/jkms.2014.29.5.729
- Ovcina-Kurtovic, N., and Kasumagic-Halilovic, E. (2022). Serum levels of tumor necrosis factor - alpha in patients with psoriasis. *Mater Sociomed.* 34 (1), 40–43. doi:10.5455/msm.2022.33.40-43
- Paul, J., and Veenstra, T. D. (2022). Separation of serum and plasma proteins for in-depth proteomic analysis. *Separations* 9 (4), 89. doi:10.3390/separations9040089
- Philipp, S., Menter, A., Nikkels, A. F., Barber, K., Landells, I., Eichenfield, L. F., et al. (2020). Ustekinumab for the treatment of moderate-to-severe plaque psoriasis in paediatric patients (≥6 to < 12 years of age): Efficacy, safety, pharmacokinetic and biomarker results from the open-label CADMUS jr study. *Br. J. Dermatol.* 183 (4), 664–672. doi:10.1111/bjd.19018
- Pietrzak, A., Chabros, P., Grywalska, E., Pietrzak, D., Kandzierski, G., Wawrzynski, B. O., et al. (2020). Serum concentration of interleukin 6 is related to inflammation and dyslipidemia in patients with psoriasis. *Postępy Dermatol. Alergol.* 37 (1), 41–45. doi:10.5114/ada.2018.78028
- Purzycka-Bohdan, D., Nedoszytko, B., Zabłotna, M., Gleń, J., Szczekowska-Dobosz, A., and Nowicki, R. J. (2022). Chemokine profile in psoriasis patients in correlation with disease severity and pruritus. *Int. J. Mol. Sci.* 23 (21), 13330. doi:10.3390/ijms232113330
- Rendon, A., and Schäkel, K. (2019). Psoriasis pathogenesis and treatment. *Int. J. Mol. Sci.* 20 (6), 1475. doi:10.3390/ijms20061475
- Scali, E., Dastoli, S., Procopio, A. C., Ricca, D., Mazzei, V., Cinaglia, P., et al. (2022). Evaluation of serum calprotectin as novel biomarker in psoriatic patients: A prospective pilot study. *Minerva Med.* 113 (5), 833–837. doi:10.23736/s0026-4806.22.08041-7
- Seth, D., Ehler, A. N., Golden, J. B., Damiani, G., McCormick, T. S., Cameron, M. J., et al. (2020). Interaction of resistin and systolic blood pressure in psoriasis severity. *J. Invest. Dermatol.* 140 (6), 1279–1282.e1. doi:10.1016/j.jid.2019.07.727
- Shibata, S., Saeki, H., Tada, Y., Karakawa, M., Komine, M., and Tamaki, K. (2009). Serum high molecular weight adiponectin levels are decreased in psoriasis patients. *J. Dermatol. Sci.* 55 (1), 62–63. doi:10.1016/j.jdermsci.2009.02.009
- Shimauchi, T., Hirakawa, S., Suzuki, T., Yasuma, A., Majima, Y., Tatsuno, K., et al. (2013). Serum interleukin-22 and vascular endothelial growth factor serve as sensitive biomarkers but not as predictors of therapeutic response to biologics in patients with psoriasis. *J. Dermatol.* 40 (10), 805–812. doi:10.1111/1346-8138.12248
- Sluczanska-Glabowska, S., Stanisiewska, M., Marchlewicz, M., Duchnik, E., Luczkowska, K., Safranow, K., et al. (2023). Adiponectin, leptin and resistin in patients with psoriasis. *J. Clin. Med.* 12 (2), 663. doi:10.3390/jcm12020663
- Strohbecker, L., Koenen, H., van Rijssen, E., van Cranenbroek, B., Fasse, E., Joosten, I., et al. (2019). Increased dermal expression of chromatin-associated protein HMGB1 and concomitant T-cell expression of the DNA RAGE in patients with psoriasis vulgaris. *Psoriasis (Auckl)* 9, 7–17. doi:10.2147/ptt.S190507
- Sun, X., Liu, L., Chen, S., Wang, J., Cai, X., Song, J., et al. (2022). Fibrinogen-like protein 1 as a novel biomarker of psoriasis severity. *J. Inflamm. Res.* 15, 4637–4647. doi:10.2147/jir.S378953
- Takahashi, H., Tsuji, H., Hashimoto, Y., Ishida-Yamamoto, A., and Iizuka, H. (2010). Serum cytokines and growth factor levels in Japanese patients with psoriasis. *Clin. Exp. Dermatology* 35 (6), 645–649. doi:10.1111/j.1365-2230.2009.03704.x
- Tamagawa-Mineoka, R., Okuzawa, Y., Masuda, K., and Katoh, N. (2014). Increased serum levels of interleukin 33 in patients with atopic dermatitis. *J. Am. Acad. Dermatology* 70 (5), 882–888. doi:10.1016/j.jaad.2014.01.867
- Theoharides, T. C., Zhang, B., Kempuraj, D., Tegen, M., Vasiadi, M., Angelidou, A., et al. (2010). IL-33 augments substance P-induced VEGF secretion from human mast cells and is increased in psoriatic skin. *Proc. Natl. Acad. Sci.* 107 (9), 4448–4453. doi:10.1073/pnas.100803107
- Vaccaro, M., Cicero, F., Mannucci, C., Calapai, G., Spataro, G., Barbuza, O., et al. (2016). IL-33 circulating serum levels are increased in patients with non-segmental generalized vitiligo. *Arch. Dermatol. Res.* 308 (7), 527–530. doi:10.1007/s00403-016-1675-2
- Veldhoen, M., Hocking, R. J., Atkins, C. J., Locksley, R. M., and Stockinger, B. (2006). TGFβ in the context of an inflammatory cytokine milieu supports de novo differentiation of IL-17-producing T cells. *Immunity* 24 (2), 179–189. doi:10.1016/j.immuni.2006.01.001
- Voganatsi, A., Panyutich, A., Miyasaki, K. T., and Murthy, R. K. (2001). Mechanism of extracellular release of human neutrophil calprotectin complex. *J. Leukoc. Biol.* 70 (1), 130–134. doi:10.1189/jlb.70.1.130
- Volpe, E., Pattarini, L., Martinez-Cingolani, C., Meller, S., Donnadiu, M. H., Bogiatzi, S. I., et al. (2014). Thymic stromal lymphopoietin links keratinocytes and dendritic cell-derived IL-23 in patients with psoriasis. *J. Allergy Clin. Immunol.* 134 (2), 373–381. doi:10.1016/j.jaci.2014.04.022
- Wawrzynski, B., Pietrzak, A., Grywalska, E., Krasowska, D., Chodorowska, G., and Roliński, J. (2019). Interleukin-22 and its correlation with disease activity in plaque psoriasis. *Arch. Immunol. Ther. Exp. Warsz.* 67 (2), 103–108. doi:10.1007/s00005-018-0527-5
- Wilsman-Theis, D., Wagenpfeil, J., Holzinger, D., Roth, J., Koch, S., Schnautz, S., et al. (2016). Among the S100 proteins, S100A12 is the most significant marker for psoriasis disease activity. *J. Eur. Acad. Dermatol. Venereol.* 30 (7), 1165–1170. doi:10.1111/jdv.13269
- World Health Organization (2016). *Global report on psoriasis*. Brazil: World Health Organization.
- Yilmaz, S. B., Cicek, N., Coskun, M., Yegin, O., and Alpsoy, E. (2012). Serum and tissue levels of IL-17 in different clinical subtypes of psoriasis. *Arch. Dermatol. Res.* 304 (6), 465–469. doi:10.1007/s00403-012-1229-1
- Zeng, F., Chen, H., Chen, L., Mao, J., Cai, S., Xiao, Y., et al. (2021). An autocrine circuit of IL-33 in keratinocytes is involved in the progression of psoriasis. *J. Invest. Dermatol.* 141 (3), 596–606.e7. doi:10.1016/j.jid.2020.07.027
- Zhou, Y., Wang, P., Yan, B. X., Chen, X. Y., Landeck, L., Wang, Z. Y., et al. (2020). Quantitative proteomic profile of psoriatic epidermis identifies OAS2 as a novel biomarker for disease activity. *Front. Immunol.* 11, 1432. doi:10.3389/fimmu.2020.01432
- Zhu, K. J., Zhang, C., Li, M., Zhu, C. Y., Shi, G., and Fan, Y. M. (2013). Leptin levels in patients with psoriasis: A meta-analysis. *Clin. Exp. Dermatol.* 38 (5), 478–483. doi:10.1111/ced.12171



OPEN ACCESS

EDITED BY

Dimitris Tsoukalas,
Metabolomic Medicine, Greece

REVIEWED BY

Haitao Wang,
National Cancer Institute (NIH),
United States
Evangelia Sarandi,
University of Crete, Greece

*CORRESPONDENCE

Dongyi He,
✉ dongyihe@medmail.com.cn

[†]These authors have contributed equally
to this work

RECEIVED 08 April 2023

ACCEPTED 07 November 2023

PUBLISHED 17 November 2023

CITATION

Zhao J, Wei K, Shi Y, Jiang P, Xu L,
Chang C, Xu L, Zheng Y, Shan Y, Liu J, Li L,
Guo S, Schrodi SJ, Wang R and He D
(2023), Identification of immunological
characterization and Anoikis-related
molecular clusters in rheumatoid arthritis.
Front. Mol. Biosci. 10:1202371.
doi: 10.3389/fmolb.2023.1202371

COPYRIGHT

© 2023 Zhao, Wei, Shi, Jiang, Xu, Chang,
Xu, Zheng, Shan, Liu, Li, Guo, Schrodi,
Wang and He. This is an open-access
article distributed under the terms of the
[Creative Commons Attribution License](#)
(CC BY). The use, distribution or
reproduction in other forums is
permitted, provided the original author(s)
and the copyright owner(s) are credited
and that the original publication in this
journal is cited, in accordance with
accepted academic practice. No use,
distribution or reproduction is permitted
which does not comply with these terms.

Identification of immunological characterization and Anoikis-related molecular clusters in rheumatoid arthritis

Jianan Zhao^{1,2,3†}, Kai Wei^{1,2,3†}, Yiming Shi^{1,2,3}, Ping Jiang^{1,2,3},
Lingxia Xu^{1,2,3}, Cen Chang^{1,2,3}, Linshuai Xu^{1,2,3}, Yixin Zheng^{1,2,3},
Yu Shan^{1,2,3}, Jia Liu^{1,3,4}, Li Li^{1,3,4}, Shicheng Guo^{5,6},
Steven J. Schrodi^{5,6}, Rongsheng Wang^{1,2,3} and Dongyi He^{1,2,4,3*}

¹Department of Rheumatology, Shanghai Guanghua Hospital, Shanghai University of Traditional Chinese Medicine, Shanghai, China, ²Guanghua Clinical Medical College, Shanghai University of Traditional Chinese Medicine, Shanghai, China, ³Institute of Arthritis Research in Integrative Medicine, Shanghai Academy of Traditional Chinese Medicine, Shanghai, China, ⁴Arthritis Institute of Integrated Traditional and Western Medicine, Shanghai Chinese Medicine Research Institute, Shanghai, China, ⁵Computation and Informatics in Biology and Medicine, University of Wisconsin-Madison, Madison, WI United States, ⁶Department of Medical Genetics, School of Medicine and Public Health, University of Wisconsin-Madison, Madison, WI, United States

Objective: To investigate the potential association between Anoikis-related genes, which are responsible for preventing abnormal cellular proliferation, and rheumatoid arthritis (RA).

Methods: Datasets GSE89408, GSE198520, and GSE97165 were obtained from the GEO with 282 RA patients and 28 healthy controls. We performed differential analysis of all genes and *HLA* genes. We performed a protein-protein interaction network analysis and identified hub genes based on *STRING* and cytoscape. Consistent clustering was performed with subgrouping of the disease. SsgSEA were used to calculate immune cell infiltration. Spearman's correlation analysis was employed to identify correlations. Enrichment scores of the GO and KEGG were calculated with the ssGSEA algorithm. The WGCNA and the *DGIdb* database were used to mine hub genes' interactions with drugs.

Results: There were 26 differentially expressed Anoikis-related genes ($FDR = 0.05$, $\log_2FC = 1$) and *HLA* genes exhibited differential expression ($P < 0.05$) between the disease and control groups. Protein-protein interaction was observed among differentially expressed genes, and the correlation between *PIM2* and *RAC2* was found to be the highest; There were significant differences in the degree of immune cell infiltration between most of the immune cell types in the disease group and normal controls ($P < 0.05$). Anoikis-related genes were highly correlated with *HLA* genes. Based on the expression of Anoikis-related genes, RA patients were divided into two disease subtypes (cluster1 and cluster2). There were 59 differentially expressed Anoikis-related genes found, which exhibited significant differences in functional enrichment, immune cell infiltration degree, and *HLA* gene expression ($P < 0.05$). Cluster2 had significantly higher levels in all aspects than cluster1 did. The co-expression network analysis showed that cluster1 had 51 hub differentially expressed genes and cluster2 had 72 hub

differentially expressed genes. Among them, three hub genes of cluster1 were interconnected with 187 drugs, and five hub genes of cluster2 were interconnected with 57 drugs.

Conclusion: Our study identified a link between Anoikis-related genes and RA, and two distinct subtypes of RA were determined based on Anoikis-related gene expression. Notably, cluster2 may represent a more severe state of RA.

KEYWORDS

rheumatoid arthritis, anoikis-related molecular clusters, anoikis, cell death, immunological characterization

1 Introduction

Rheumatoid arthritis (RA) is a chronic autoimmune disease that triggers inflammation in the joints, leading to potential long-term joint damage and disability. Notably, RA can also extend beyond the joints to affect vital organs such as the lungs, heart, blood vessels, skin, and eyes. It is estimated that approximately 0.5% of the adult population worldwide are affected by RA, with a higher incidence rate observed in women compared to men. While individuals of all ages can be affected by this condition, the peak age of onset is typically between 50 and 59 years (Smith and Berman, 2022). The current therapeutic interventions for RA consist of disease-modifying antirheumatic drugs (DMARDs), nonsteroidal anti-inflammatory drugs (NSAIDs), and biologics. While analgesics and NSAIDs can alleviate pain and stiffness associated with RA, their efficacy is often limited, and NSAIDs may involve the risk of gastrointestinal and cardiac toxicity (Zhao et al., 2022a). Although DMARDs, which constitute the primary treatment for RA, can be administered in combination, their multiple adverse effects include hepatotoxicity, hematometabolic disorders, nausea, and interstitial lung disease. Biological agents such as anti-tumor necrosis factor (TNF)- α antibodies have demonstrated efficacy in treating RA; however, their clinical use carries the risk of infusion and injection site infections, and their efficacy may vary depending on the patient's individual needs (Zhao et al., 2022a). The introduction of these novel therapies has improved the clinical management of RA patients (Zhao et al., 2022a). Nevertheless, due to the complex and heterogeneous nature of the pathogenesis of RA, a substantial portion of patients exhibit an inadequate clinical response, highlighting the need for targeted development of innovative therapeutics.

The term “Anoikis” was first introduced in 1990 (Frisch and Francis, 1994). It is a crucial mechanism for preventing the continued growth of developmentally abnormal cells or attachment to inappropriate matrix when there is no interaction with the extracellular matrix (Taddei et al., 2012). The loss of extracellular matrix attachment disrupts integrin connections, leading to rapid endothelial cell death (Meredith et al., 1993). Anoikis mainly occurs through two pathways: intrinsic and extrinsic pathways. Intrinsic pathway involves mitochondria as a critical organelle, and the key events are mitochondrial permeabilization and regulation of Bcl-2 protein family. The extrinsic pathway involves cell surface death receptor proteins, such as Fas or TNFR, which gradually forms a death-inducing signaling complex and activate downstream caspase 8, eventually leading to Anoikis (Gilmore, 2005). Tumor cells are considered an essential condition in the tumor metastasis process due to their insensitivity to Anoikis, which is called Anoikis

resistance. The current understanding suggests that the primary mechanisms behind Anoikis resistance include alterations in integrin expression patterns, excessive expression of extracellular matrix, activation of survival signals induced by oxidative stress, hypoxic microenvironments, and expression of key molecules such as Twist, HGF/Met, EphA2 receptors, and TrkB (Taddei et al., 2012).

There are multiple types of cells in RA that collectively contribute to the abnormal pathological features of RA. RA FLS exhibit multiple tumor-like characteristics and survive and proliferate excessively in tumor-like microenvironments. The abnormal proliferation of RA FLS is partially attributed to the inhibition of cell apoptosis (Bartok and Firestein, 2010; Bottini and Firestein, 2013). RA FLS exhibits characteristics of invasive growth and has been observed in experiments to not rely on wall attachment for growth (Lafyatis et al., 1989). Studies have reported that RA FLS increases its resistance to Anoikis and promotes abnormal pathological characteristics through upregulation of *CTFG* mediated by *ADAM15/YAP1* (Janczi et al., 2023). Additionally, the hypoxic microenvironment in RA joints is also an important cause of Anoikis resistance in RA FLS (Taddei et al., 2012; Zhao et al., 2022b). The relationship between other immune cells in RA and Anoikis resistance remains unclear, therefore in this article, we aim to provide theoretical references for the development of clinical diagnosis and treatment plans by analyzing the potential connection between Anoikis-related genes and RA.

2 Materials and methods

2.1 Data source and processing

The GSE89408, GSE198520, and GSE97165 datasets were downloaded from the GEO database (GEO Accession viewer (nih.gov)). The samples from GSE89408, GSE198520, and GSE97165 are all derived from synovial biopsy tissue samples obtained from individuals with or without RA. Raw counts data from the downloaded datasets were converted into fpkm data and $\log_2(\text{fpkm}+1)$ was applied, as shown in Table 1. For annotation, the downloaded GEO dataset was annotated based on the GENCODE (V38) gtf annotation file, and coding genes were extracted. Probe IDs were converted to gene symbols, duplicates were removed, and batch effect was removed before merging the data. Subsequent analyses were based on the merged data. An anoikis-related gene set was selected from the MSigDB (V7.4) database (GSEA | MSigDB (gsea-msigdb.org)). The complete analysis workflow is shown in Supplementary Figure S1.

TABLE 1 Sample information.

	Rheumatoid arthritis	Normal	Data processing	Follow-up processing
GSE198520	92	0	Counts to fpkm	log2 (fpkm+1)
GSE89408	152	28	Counts to fpkm	log2 (fpkm+1)
GSE97165	38	0	Counts to fpkm	log2 (fpkm+1)

2.2 Gene difference analysis

To identify differentially expressed genes between disease and control groups, the expression profile data from the merged dataset and the disease/control groupings were used. Differential analysis on all genes was performed using the R package limma, and volcano plots, and heat maps were generated for Anokis-related genes. Limma is based on a linear model and employs weighted least squares to estimate differential gene expression. It corrects for multiple testing issues using Bayesian methods. Genes were considered downregulated if the false discovery rate (FDR) < 0.05 and \log_2FC < 1, and upregulated if the FDR < 0.05 and \log_2FC > 1. The R package RCircos was used to generate a chromosome position diagram of differentially expressed Anokis-related genes to determine their positions on the chromosome. The gene re-annotation file was downloaded from GENCODE (https://ftp.ebi.ac.uk/pub/databases/genocode/Genocode_human/release_38/genocode.v38.annotation.gff3.gz), which provided information for all differentially expressed genes. The String database was used to construct a PPI network based on differentially expressed Anokis-related genes. Spearman correlation analysis was performed on the differentially expressed Anokis-related genes between two scenarios: all samples and disease samples. Using Spearman's correlation analysis, we evaluated the correlation between differentially expressed Anokis-related genes across all and disease samples. When $p < 0.05$ is obtained, a statistically significant correlation between the two variables is recognized. Additionally, we analyzed the differential expression of *HLA* genes between the disease and control groups, along with the Spearman correlation analysis between Anokis-related genes and *HLA* genes.

2.3 Analysis of immune infiltration

We used ssGSEA to quantify immune cell infiltration. Immune response gene set enrichment scores were calculated and analyzed for differences between subgroups with immune response gene sets obtained from the immport database (<https://www.immport.org/shared/genelists>), consisting of 17 immune response gene sets. Additionally, we evaluated the Spearman correlation between Anokis-related genes and immune response gene set enrichment scores.

2.4 Consistency clustering and disease subtyping

We performed consensus clustering using the R package ConsensusClusterPlus based on Anokis-related differentially expressed genes and disease sample data to identify molecular

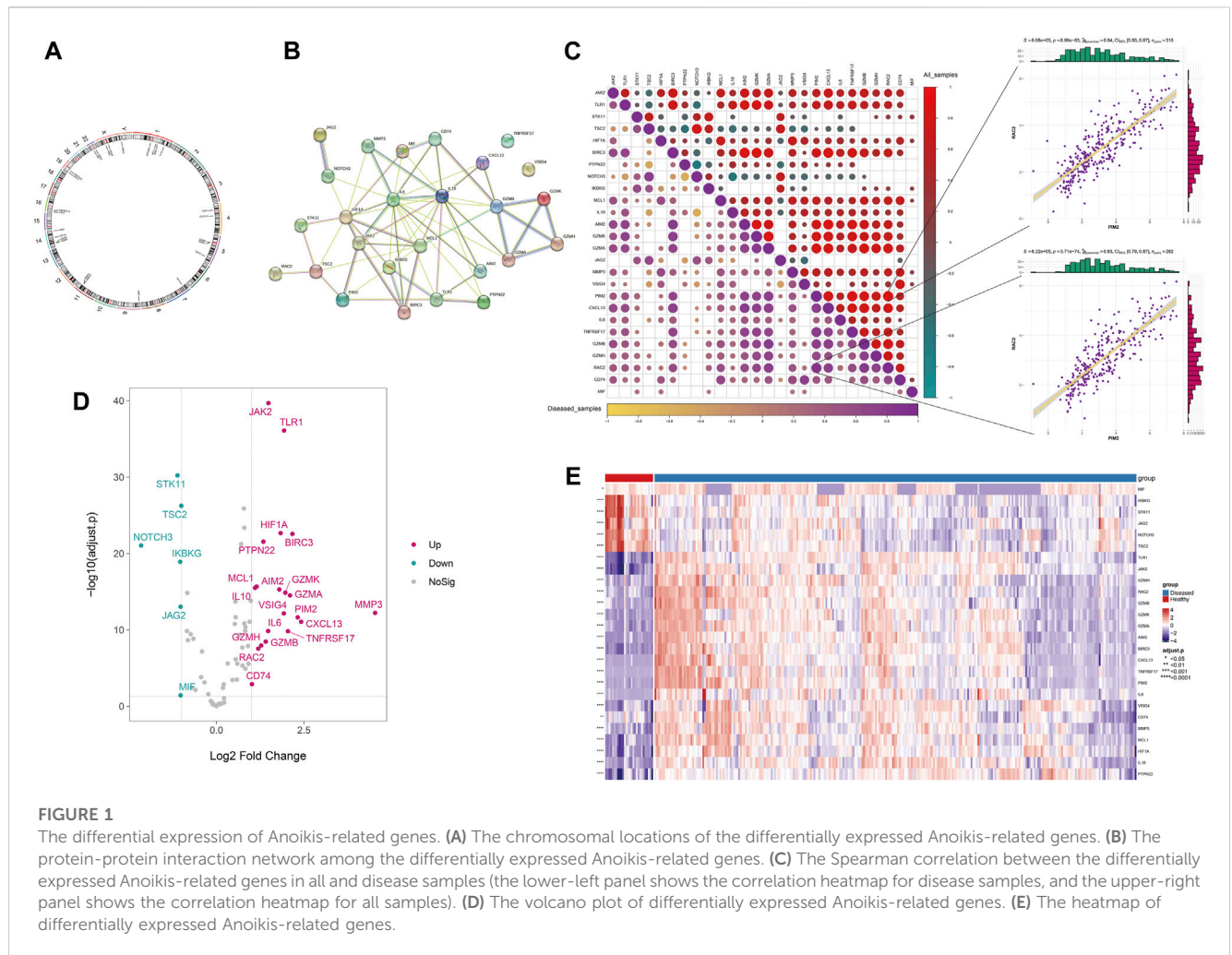
subtypes based on the optimal clustering K value. The distance metric used for clustering was km, and the clustering method was euclidean; 1,000 repetitions were performed to ensure the stability of the classification. We performed PCA clustering analysis on the disease expression data to show the aggregation status between different subgroups. Based on the subtypes, we analyzed the expression differences of Anokis-related genes between subtypes and generated heat maps and box plots to visualize the differential expression of Anokis-related genes.

2.5 Functional enrichment differences

We calculated the enrichment scores of GO and KEGG pathways using the ssGSEA algorithm from the R package GSVA. We analyzed the enrichment differences of GO and KEGG pathways among the groups and plotted heatmaps.

2.6 WGCNA analysis

WGCNA analysis was performed using the R package WGCNA. First, a similarity matrix was constructed based on the gene expression data. The gene expression similarity matrix was then transformed into an adjacency matrix, with β as the soft threshold, and the network type was signed. The adjacency matrix was then transformed into a topological overlap measure (TOM) matrix, which described the degree of association between genes. The module membership (MM), which measured the identity of a gene in a module, was evaluated based on the Pearson correlation between the gene's expression profile across all samples and the expression profile of the feature vector gene ME. Finally, gene significance (GS) was calculated to measure the correlation between genes and external information. We identified differentially expressed genes between subtypes and intersected them with hub genes selected by WGCNA to construct a PPI network. Hub gene enrichment in different clusters through further GO and KEGG analysis, with a significance threshold set at $FDR < 0.05$ to determine statistically significant enrichment results. Subsequently, we validated differential gene expression across different clusters using RNA-seq expression data from clinical synovial tissue samples recruited from the Guanghua Hospital Precision Medicine Research Cohort, including 9 RA patients and 15 osteoarthritis (OA) patients (Zhang et al., 2022). Hub nodes in the PPI network were identified using cytoscape, and gene degree was used to filter hub genes. Genes with high degree of association were considered hub key genes. We then used the DGIdb database v4.2.0 (<https://www.dgldb.org/>) to query for drug interactions with these hub genes and presented the interaction relationships using a Sankey diagram.



2.7 Statistical analysis

For differential significance analysis, Wilcoxon test was used for comparisons between two groups unless otherwise specified, and Kruskal–Wallis test was used for comparisons between more than two groups. R version 4.1.2 was used for statistical analysis. In the figures, ns indicates $P > 0.05$, * indicates $P < 0.05$, ** $P < 0.01$, *** $P < 0.001$, and **** indicates $P < 0.0001$.

3 Results

3.1 Landscape of anoiakis-related genes in the disease

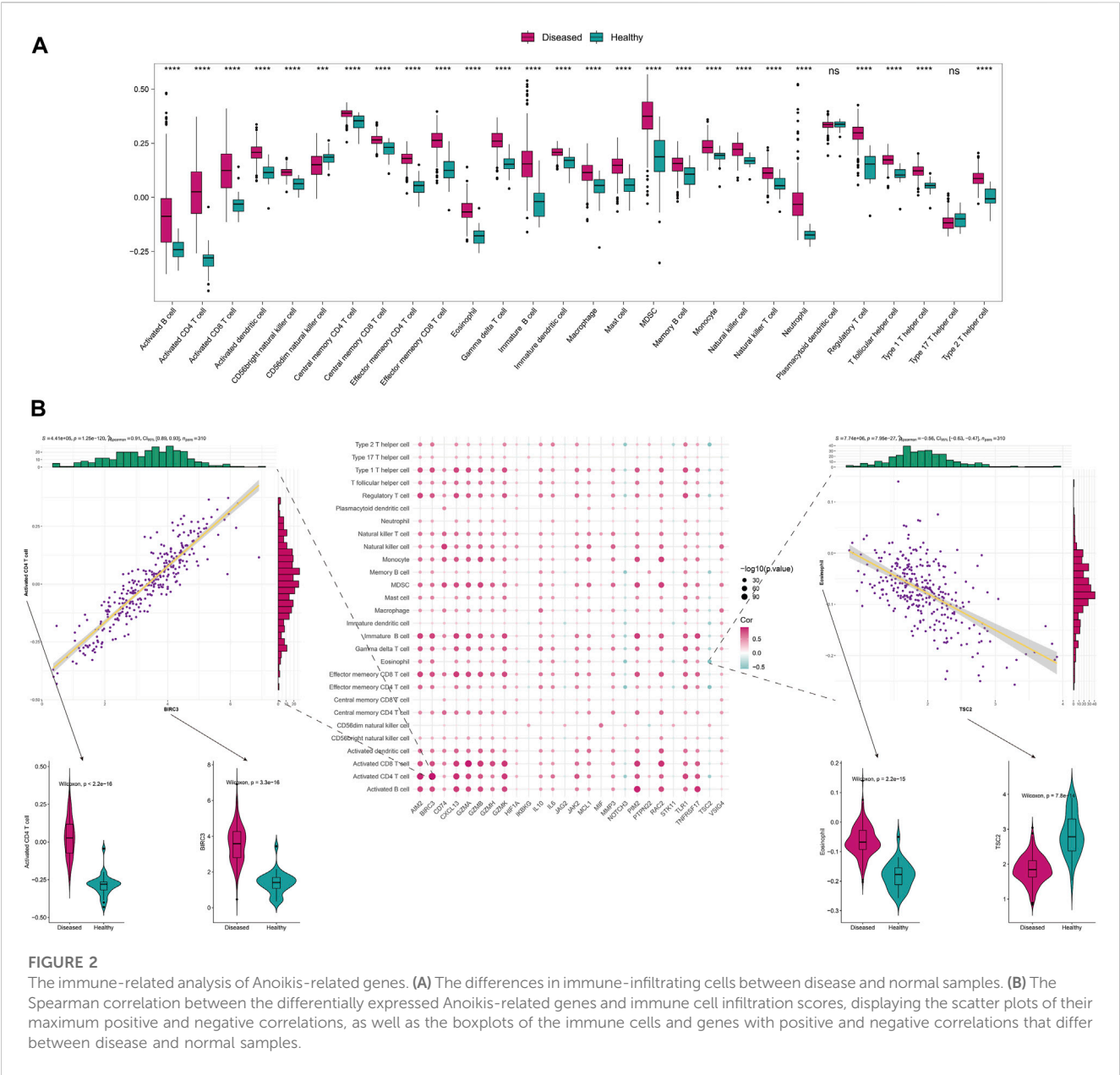
Based on the integrated expression data, differential analysis was performed between disease and normal samples. The results showed that 26 Anoiakis-related genes were differentially expressed between disease and normal samples ($P < 0.05$), with 20 upregulated and 6 downregulated genes (Figure 1D,E), and their chromosomal locations were shown in Figure 1A. The protein interaction network of differentially expressed Anoiakis genes revealed that *IL6*, *MMP3*, *HIF1A*, *IKBKG*, *IL10*, *MCL1*, *JAK2*, and others had a higher degree of connectivity (Figure 1B). The results of the expression correlation

analysis among differentially expressed genes (disease samples, all samples) showed that the correlations between *PIM2* and *RAC2* were the highest in all samples and disease samples ($r = 0.84$ and 0.83 , $P = 8.99 \times 10^{-83}$ and 3.71×10^{-74} , respectively) (Figure 1C).

3.2 Anoiakis-related genes are involved in disease immune regulation

To further explore the correlation with immune status, we quantified different immune cell subtypes using ssGSEA based on the integrated data and compared the differences in infiltration levels between groups using the rank-sum test. The box plots of the infiltration scores of different immune cells between disease and normal samples showed that most of the immune cells, such as activated B cell, activated CD4+T cell, activated CD8+T cell, and activated dendritic cell, were significantly different between disease and normal groups ($P < 0.05$) (Figure 2A).

We also analyzed the correlation between Anoiakis-related differentially expressed genes and immune-infiltrating cells. The two points with the highest positive and negative correlations were selected. Notably, significant positive correlation was observed between *BIRC3* and activated CD4+T cell ($r = 0.91$, $P = 1.25 \times 10^{-120}$), while significant negative correlation was observed between *TSC2* and Eosinophil ($r = -0.56$, $P = 7.95 \times 10^{-27}$) (Figure 2B). Furthermore, we analyzed



the correlation between Ankois-related gene expression and *HLA* gene. Interestingly, most of the *HLA* genes were differentially expressed between the disease and normal groups ($P < 0.05$). Among them, *CD74* and *NOTCH3* were the genes with highest positive and negative correlations with *HLA-DRB1/DMB*, respectively ($r = 0.82$, $P = 8.44 \times 10^{-78}$ and $r = -0.40$, $P = 4.91 \times 10^{-13}$) (Supplementary Figure S2).

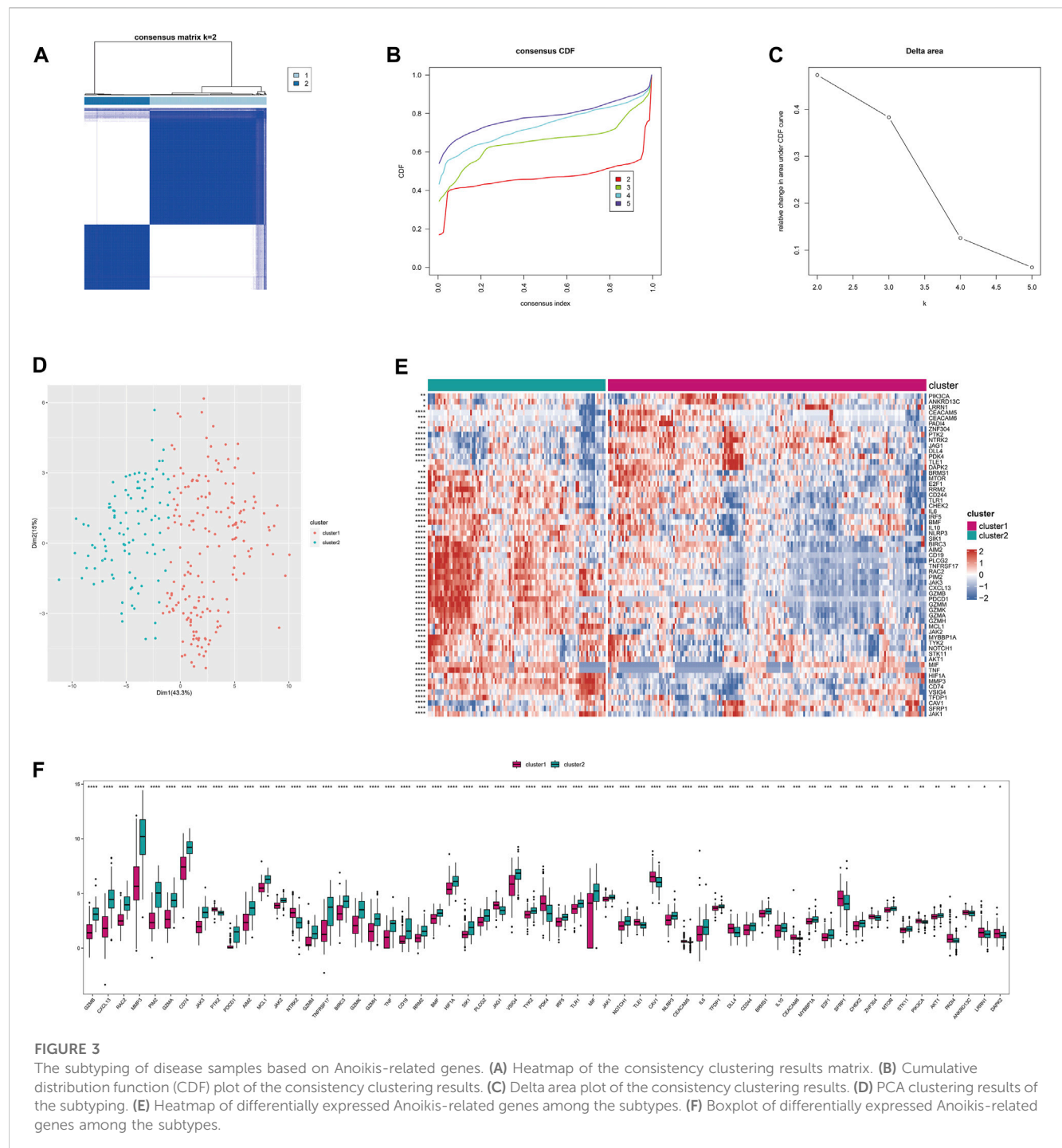
3.3 The expression of ankois-related genes stratifies the disease into biologically distinct subtypes

This stratification can be used to reflect similar disease states and help implement personalized treatments. Based on the Ankois-related differentially expressed genes (26 genes) between RA and normal groups, consistent clustering was performed on the integrated

rheumatoid arthritis dataset to identify sample subgroups with similar expression patterns and molecular subtypes based on the optimal clustering K. Here, we identified the 2 subtypes with the most gradual decrease in CDF as the optimal clustering number (Figures 3A–D). Differential analysis was performed on the Ankois-related genes between subtypes, and 59 differentially expressed Ankois-related genes ($P < 0.05$) were identified. Heatmaps and boxplots were used to visualize the differentially expressed Ankois-related genes between subgroups. (Figures 3E,F).

3.4 There were functional enrichment differences between different subgroups

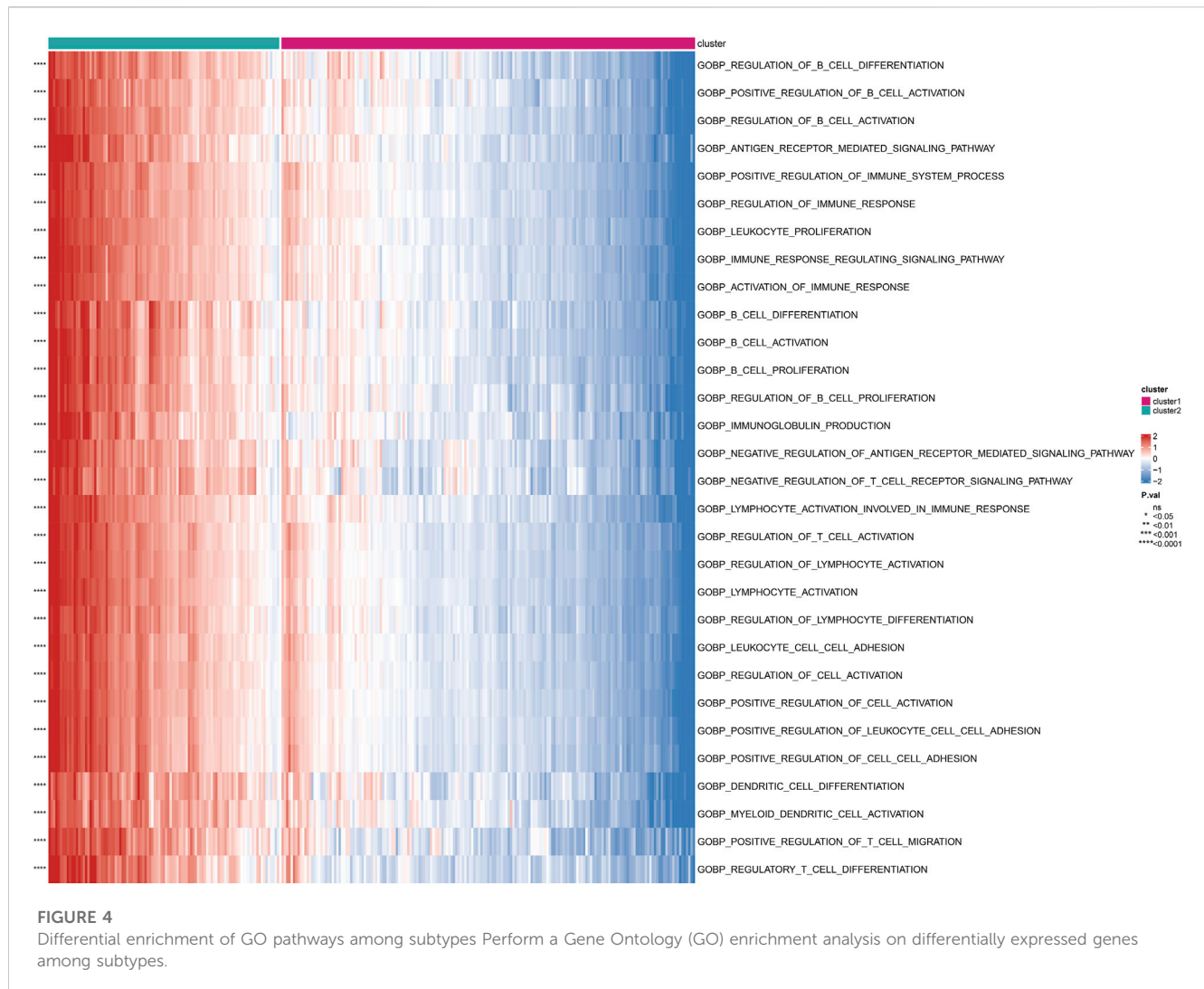
Based on the subgrouping, we calculated the enrichment scores of GO and KEGG pathways between different subgroups, analyzed



the enrichment score differences of GO and KEGG pathways between subgroups, and visualized them in heatmaps. Many pathways of GO and KEGG showed significant differences in enrichment scores between subgroups ($P < 0.05$). The top 30 GO processes were mainly related to the proliferation, adhesion, and differentiation reactions of lymphocyte T cells, B cells, and immune cells. The top 30 KEGG pathways also included autoimmune diseases, multiple immune cell receptor pathways, cell apoptosis, and cell adhesion. The enrichment scores of these GO and KEGG pathways in Cluster 2 were significantly higher than those in Cluster 1 ($P < 0.05$) (Figure 4; Figure 5).

3.5 The subtypes had different immune characteristics

Based on the integrated rheumatoid arthritis data, ssGSEA was used to quantify different immune cell subtypes, and the differences in infiltration levels between subgroups were compared using the rank-sum test. The boxplots of infiltration scores of different immune cells between subgroups showed that most of the immune infiltrations, such as activated B cell, activated CD4+T cell, activated CD8 +T cell, and activated dendritic cell, were significantly different between subgroups ($P < 0.05$), and the

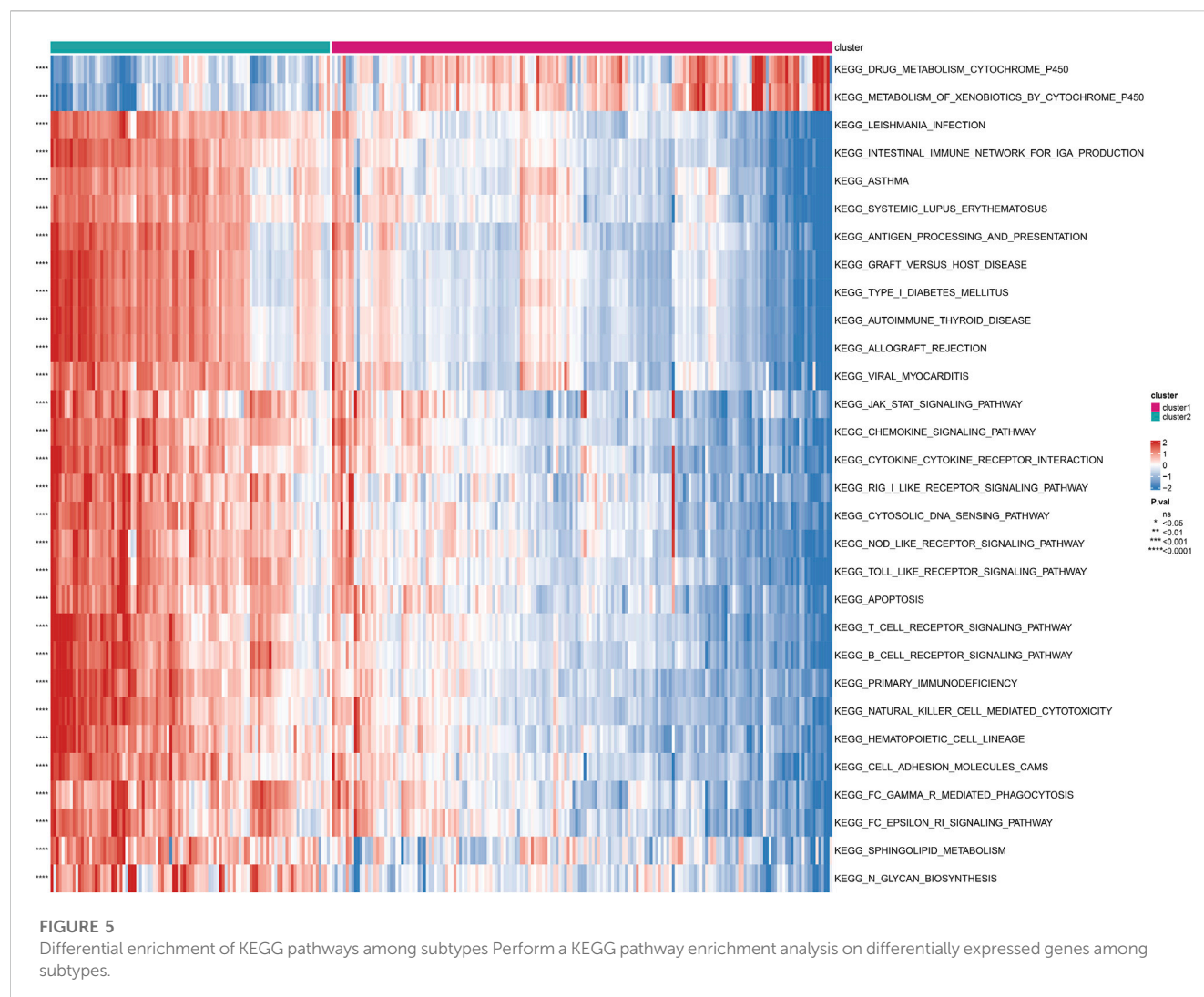


immune cell infiltrations in Cluster 2 were significantly higher than those in Cluster 1 ($P < 0.05$) (Figure 6A). We also compared the immune response gene sets between subgroups and found that most immune response gene sets, such as antigen processing and presentation, antimicrobials, and BCR signaling pathway, were significantly different between subgroups, and the immune response gene sets in Cluster 2 were significantly higher than those in Cluster 1 ($P < 0.05$) (Figure 6). In addition, we compared the expression of *HLA* genes between subgroups and found that 19 *HLA* genes were significantly different between subgroups, with the expression of *HLA* genes in Cluster 2 being significantly higher than that in Cluster 1 ($P < 0.05$) (Figure 6).

3.6 Identification of key molecules based on co-expression network analysis

Based on the subgrouping, the R package limma was used to calculate the differentially expressed genes between subgroups, and 1,295 differentially expressed genes were identified ($FDR < 0.05$ and $|\log_2FC| > 0.585$). Based on the merged data of rheumatoid arthritis, the R package WGCNA was used to construct a weight co-expression

network. First, the data was filtered with the method set to “ward.D2”. Studies have shown that the co-expression network complies with the scale-free network, where the logarithm of the number of nodes with a connectivity of k ($\log(k)$) is negatively correlated with the logarithm of the probability of the node appearing ($\log(P(k))$) and the correlation coefficient is greater than 0.85. To ensure that the network is a scale-free network, the optimal $\beta = 10$ was selected (Figure 7). Next, the expression matrix was transformed into an adjacency matrix and then into a topological matrix. Based on TOM, the average-linkage hierarchical clustering method was used to cluster genes and the standard of mixed dynamic tree cut was set, with each gene module having a minimum number of 30 genes. After determining the gene modules using the dynamic tree cut method, the eigengenes for each module were calculated and the modules were subjected to cluster analysis with a height set to 0.25. Modules that were close in distance were merged into new modules. The Pearson correlation coefficient between the ME of each module and the sample phenotype features was calculated, with a higher value indicating greater importance. In Figure 7E, rows represent the eigengenes of each module, columns represent the sample phenotype features, with red indicating positive correlation and blue indicating negative correlation. The higher the color



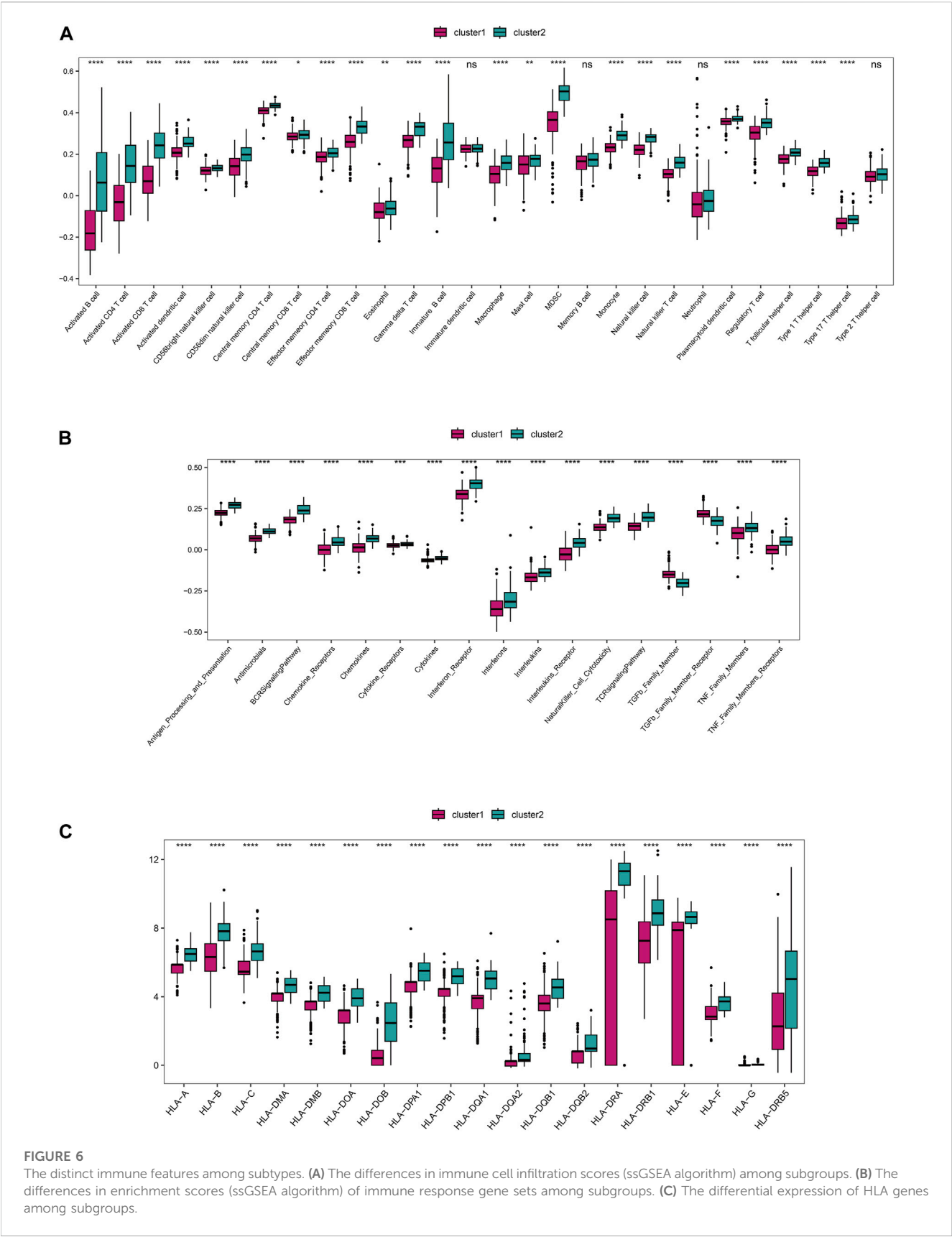
intensity, the higher the correlation. Based on cluster1, the magenta module with the highest positive correlation was selected, and based on cluster2, the red module with the highest positive correlation was selected. Using module membership (MM) > 0.6 and gene significance (GS) > 0.5, 72 and 200 core genes were respectively screened from the two modules (Figures 7F–G). These genes were intersected with the differentially expressed genes between the subtypes mentioned above, resulting in 51 hub cluster1 differential genes and 172 hub cluster2 differential genes (Figure 7).

To further elucidate biological functions of hub genes within distinct clusters, we use GO and KEGG enrichment analyses. The enrichment results revealed that cluster 1 was primarily associated with cellular components such as the basal cortex, collagen-containing extracellular matrix, cell leading edge, and basal part of the cell ($FDR < 0.05$). Additionally, it showed significant involvement in signaling pathways like the Hippo signaling pathway across multiple species ($FDR < 0.05$). Cluster 2 exhibited significant enrichment in biological processes, including lymphocyte differentiation, mononuclear cell differentiation, and T cell differentiation ($FDR < 0.05$). In terms of cellular components, it was associated with the immunological synapse, plasma membrane signaling receptor complex, and

phagocytic vesicle ($FDR < 0.05$). Moreover, molecular functions related to cytokine receptor activity, cytokine binding, and immune receptor activity were enriched ($FDR < 0.05$). Cluster 2 also demonstrated significant involvement in signaling pathways such as Th17 cell differentiation, Natural killer cell-mediated cytotoxicity, and the TNF signaling pathway ($FDR < 0.05$) (Supplementary Figure S3). We further validated 42 differential genes from 51 hub cluster 1 and 153 differential genes from 172 hub cluster 2, showing significant differential expression ($FDR < 0.05$) in synovial tissues of both RA and OA (Table 2) (Supplementary Table S1).

3.7 Potential treatment strategies

We constructed PPI networks for the 51 cluster1 hub differential genes and the 172 cluster2 hub differential genes, respectively (Figure 8). Cytoscape was used to identify hub nodes (key genes selected by degree for each cluster) in the PPI networks, which were then used for gene-drug interactions. The top 6 genes with the highest degree (top 4 genes with degree of 2–5) were selected as key genes for gene-drug interactions in cluster1. Next, we mined gene-drug interaction relationships based on the DGIdb database v4.2.0



(<https://www.dgidb.org/>), displaying unique gene-drug interactions with 3 genes and 187 drugs, and a Sankey diagram was drawn to illustrate the interactions (Figure 9). Similarly, the top 6 genes with the highest degree (top 6 genes with degree of 43–63) were selected as key genes for gene-drug interactions in cluster2. Gene-drug interaction relationships were mined based on the DGIdb

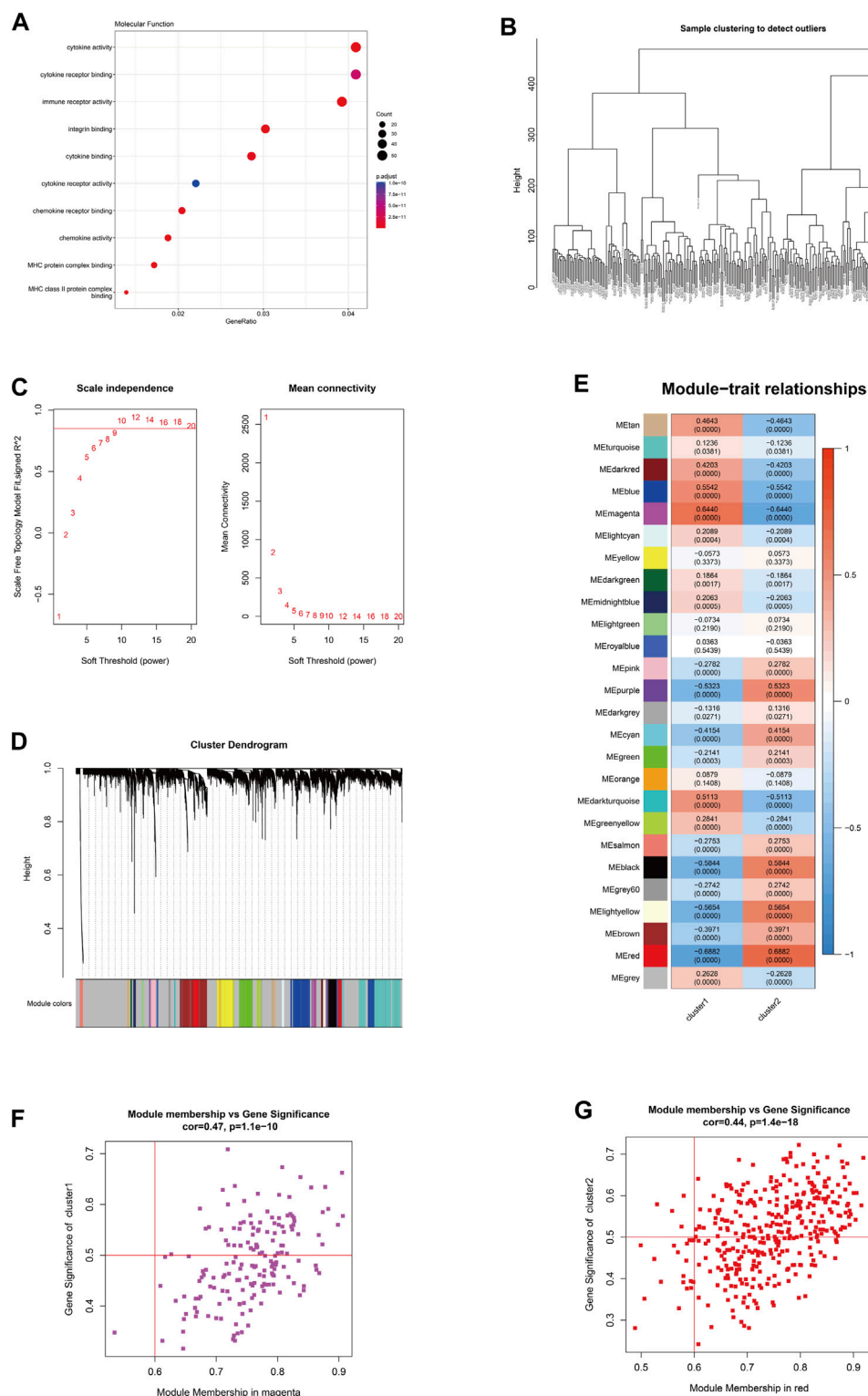


FIGURE 7

The hub gene selection using WGCNA. **(A)** The molecular functions of differentially expressed genes among subtypes according to GO enrichment analysis. **(B)** The hierarchical clustering tree of WGCNA training samples. **(C)** The different soft thresholds and the corresponding scale-free fitting indices (scale-free R^2) where the x-axis represents the different soft thresholds and the y-axis represents the corresponding scale-free fitting indices. **(D)** Gene hierarchical clustering dendrogram and modules constructed by WGCNA, where the gray nodes in the color bar indicate genes not assigned to any module, and the remaining colors represent the built modules. **(E)** Heatmap showing the module-trait correlation. **(F)** The magenta module with the highest positive correlation in cluster 1. **(G)** The red module with the highest positive correlation in cluster 2.

TABLE 2 The information on hub key genes and their interacting drugs.

	Cluster1	Cluster2
Number of hub genes	72	200
Number of hub differential genes	51	172
Key drug interaction genes	6	6
Number of genes detected by DGIDB	3	5
Number of drug interactions	187	57

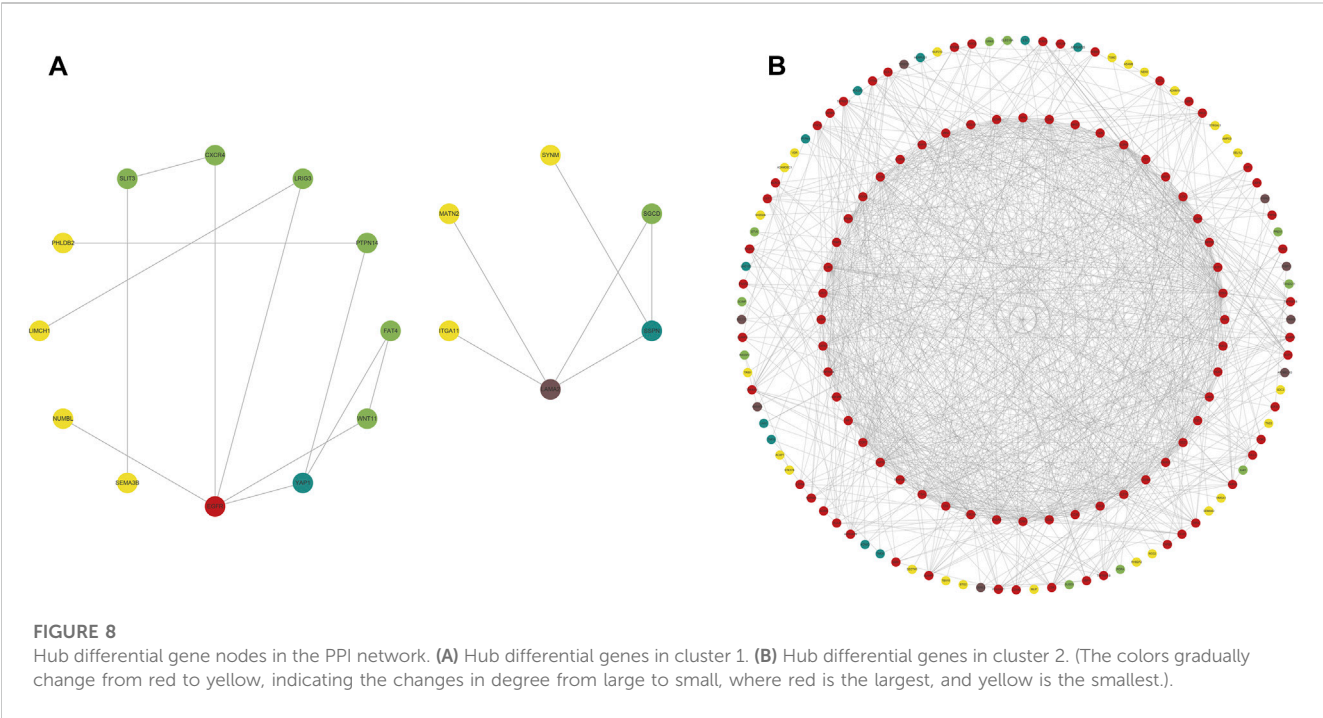
database v4.2.0 (<https://www.dgldb.org/>), displaying unique gene-drug interactions with 5 genes and 57 drugs, and a Sankey diagram was drawn to illustrate the interactions (Figure 10).

4 Discussion

Rheumatoid arthritis (RA) is a self-immune disease that seriously endangers the physical and mental health of patients, and can involve multiple systems in the body and have various complications. The existing first-line therapies are not sufficient to achieve clinical cure for all patients, and some patients may experience adverse reactions due to the complexity of the pathogenesis. Therefore, a thorough understanding and research on the pathogenic mechanisms of RA is of great significance for the development of clinical strategies for RA. Anoikis, as an important mechanism of cell death, may play a role in RA through mechanisms that promote cell death, particularly in cases where fibroblast-like synoviocytes (FLS) exhibit resistance to anoikis, which may lead to RA disease progression.

Firstly, we analyzed the differential expression of anoikis-associated genes between disease and normal samples and

conducted protein interaction analysis, revealing that IL6, MMP3, HIF1A, IKBKG, IL10, MCL1, JAK2, and other genes may interact with each other. The *IL-6/JAK2/STAT3/VEGF* pathway is also a key pathway for promoting FLS proliferation and angiogenesis in RA (Cheng et al., 2020), where IL-6 can promote MMP3 secretion leading to bone destruction (Takeuchi et al., 2021). Several biologics have been used for the treatment of IL6-related autoimmune diseases, such as Tocilizumab, Siltuximab, and Sarilumab. These medications are biologic agents that target the IL6 signaling pathway and have been clinically used for treating various autoimmune diseases associated with IL6, including rheumatoid arthritis, systemic sclerosis, giant cell arteritis, and juvenile idiopathic arthritis. They work by blocking the IL6 signaling pathway through targeting the IL-6 receptor or binding directly to IL-6, thus inhibiting inflammation and immune reaction to alleviate disease symptoms and control disease progression. HIF1A has also been reported to be associated with angiogenesis and inflammation in RA (Brouwer et al., 2009), where TNF can induce glucose metabolism transition of FLS through *GLUT1* and *HIF1A* (Koedderitzsch et al., 2021). *IKBKG* and *MCL1* belong to the crucial part of pro-survival pathway proteins, which may contribute to the resistance of FLS to anoikis-apoptosis and promote proliferation (Jiao et al., 2018). Additionally, we found that *RAC2* and *PIM2* had the highest correlation in disease samples and all samples. *RAC2* is significantly upregulated in the inducible nitric oxide synthase (iNOS) regulated NO production process in RA synovium (Dey et al., 2016); whereas, our previous unpublished results showed that overexpression of *PIM2* may promote inflammation by promoting synovial proliferation. The high correlation between *RAC2* and *PIM2* may be reflected in the synergistic regulation of FLS proliferation. The differential expression of these genes may represent a pattern of regulating FLS proliferation, inflammation, and bone destruction.



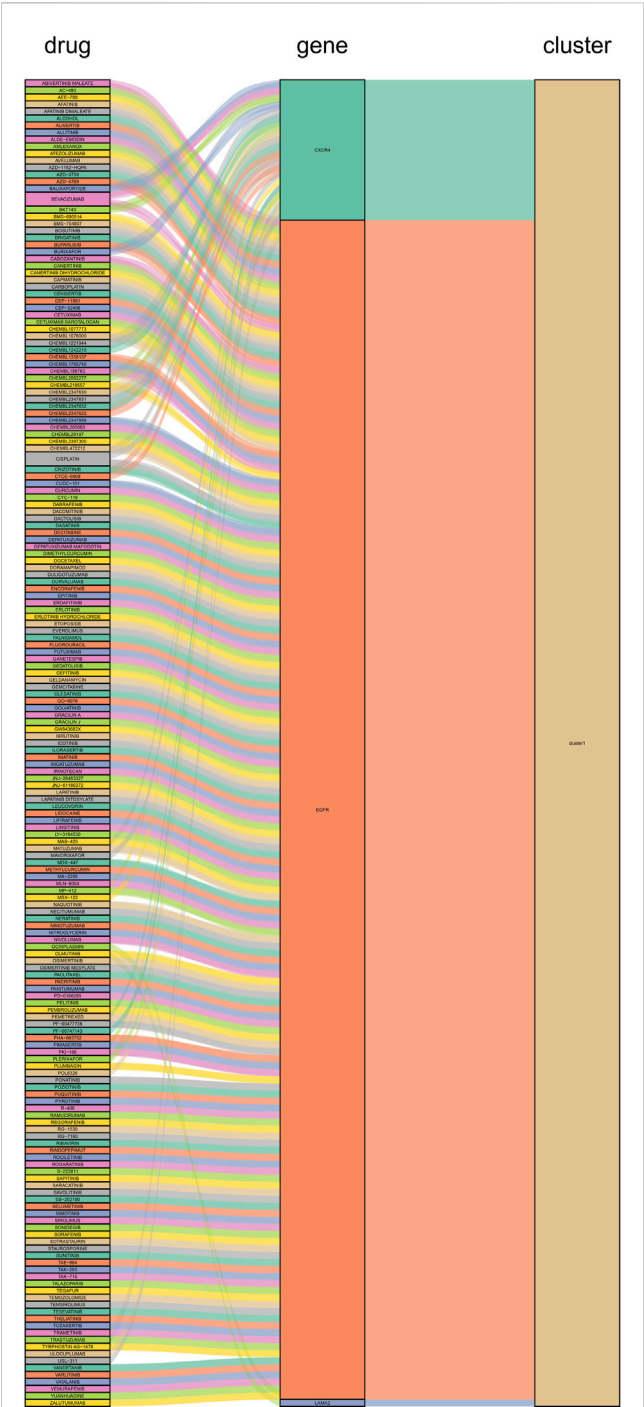


FIGURE 9 Interactions between cluster 1 hub differential genes and drugs. Utilize hub genes identified by Cluster 1 and perform an analysis of the interaction between the hub genes and drugs based on a drug database, followed by displaying the results.

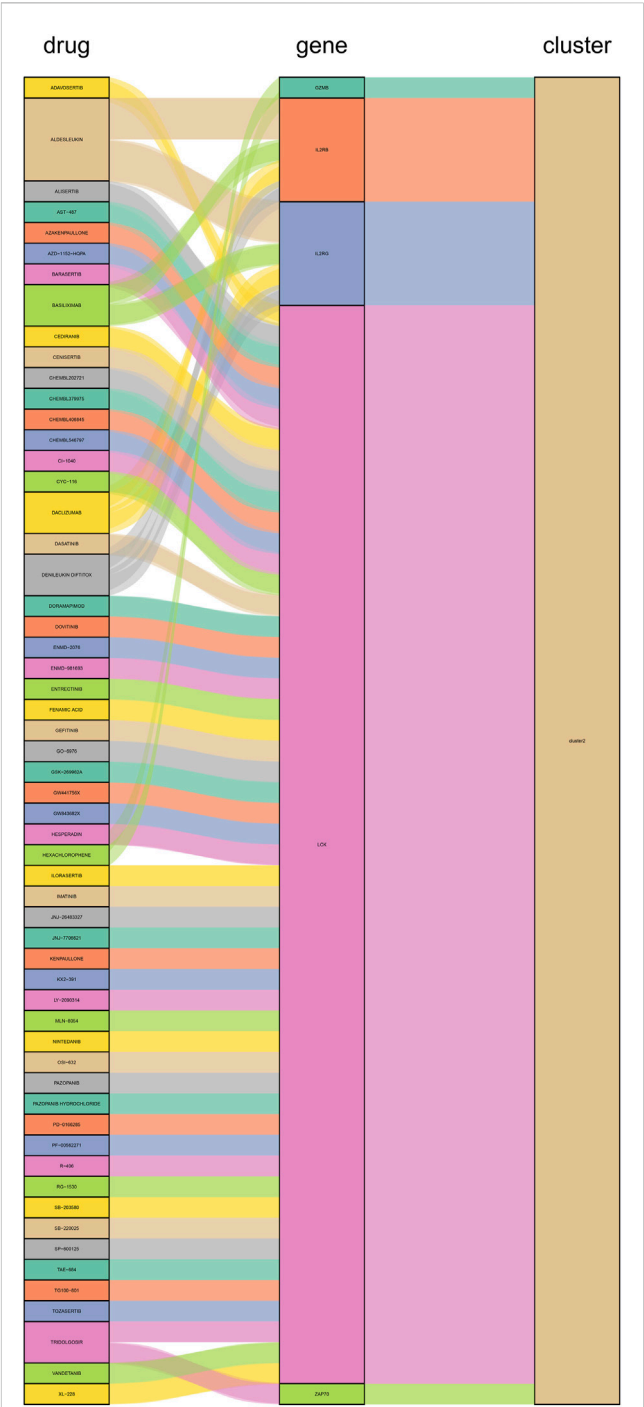


FIGURE 10 Interactions between cluster 2 hub differential genes and drugs. Utilize hub genes identified by Cluster 2 and perform an analysis of the interaction between the hub genes and drugs based on a drug database, followed by displaying the results.

In order to further explore the correlation between these genes and immunity, we conducted immune infiltration analysis, and found that most immune cells, including activated B cell, activated CD4+T cell, activated CD8+T cell, and activated dendritic cell, showed significant differences between disease and normal groups. As a type of autoimmune disease, RA involves

various immune cells infiltrating in the local joint microenvironment, which together promote the progression of RA (Zhao et al., 2021; Zhao et al., 2022c). We further analyzed the correlation between Anokis-related differentially expressed genes and immune infiltration cells, among which the correlation between *BIRC3* and *TSC2* with activated CD4+T cell and Eosinophil

was the highest positive or negative correlation relationship. BIRC3 is a survival-promoting protein and a downstream target of ATF6a. It significantly increases in the RA synovium and CIA animal model, and its positive expression correlation with activated CD4⁺ T cells may imply that BIRC3 positively promotes the survival of autoimmune T cells (Ge et al., 2022). Although Eosinophil is considered to induce inflammation in asthma, it may have a suppressive effect on inflammation in RA by increasing the differentiation of anti-inflammatory macrophages (Chen et al., 2016; Andreev et al., 2021). The relationship between TSC2 and Eosinophil and RA has not been studied in detail. TSC2 mainly participates in the mTOR-mediated cellular autophagy pathway, and further studies are needed to investigate the relationship among them (Miao et al., 2019).

The estimated heritability of RA patients is 40%–60%, of which 10%–40% is contributed by *HLA* genes. *HLA* genes exhibit high variability, both in terms of the classical locus of *HLA* class I and class II genes. These genes translate proteins that process antigen peptides and present them to other cells of the immune system. *HLA* class I genes mainly include *HLA-A*, *HLA-B*, and *HLA-C*, while *HLA* class II genes mainly include *HLA-DRB1*, *HLA-DQB1*, and *HLA-DPB1* (Ali and Vito, 2016). Therefore, we further analyzed the differential expression of *HLA* genes and their correlation with Anokis-related genes. We found that most *HLA* genes showed differential expression between the normal and disease groups, mainly including *HLA-A/B/DMA/DMB/DOA/DPA1/DPB1/DQA1/DQA2/DQB1/DQB2/DRA/DRB1/F/DRB5*. In addition, *CD74* and *NOTCH3* exhibited the highest positive or negative correlation with *HLA-DRB1/DMB*, respectively. *CD74* is a membrane protein mainly distributed on the surface of immune cells, which transduces signals by binding to MIF (Sánchez-Zuno et al., 2021), while *HLA-DRB1* shares epitope sequences that mainly encode antigen presentation proteins and contribute to ACPA-positive RA (Kampstra and Toes, 2017). The positive correlation between the two may reflect the degree of immune cell-mediated autoimmune inflammation. *NOTCH3* and *NOTCH* target genes are significantly upregulated in FLS, and in animal models, inhibition of *NOTCH3* or blocking *NOTCH* signaling can reduce inflammation and prevent joint damage in inflammatory arthritis (Wei et al., 2020). *HLA-DMA0103* and *HLA-DMB0104* alleles are considered to be biomarkers reflecting the severity of RA disease (Morel et al., 2004), but further experimental evidence is needed to confirm the negative correlation between *NOTCH3* and *HLA-DMB*.

The use of differential genes for disease typing is beneficial for individualized treatment. Based on the 26 differential genes associated with Anokis, we further divided the disease group into two clusters (cluster 1 and cluster 2). Functional enrichment, immune infiltration, and *HLA* genotyping analyses were then conducted. We found that most immune cells showed significantly differential expression between the two clusters, with the majority of immune cells exhibiting significantly higher scores in cluster 2 than in cluster 1. Consistently, most immune response gene sets, such as antigen processing and presentation, antimicrobials, and BCR signaling pathway, as well as *HLA* gene expression, were significantly higher in cluster 2 than in cluster 1, with statistical differences. In summary, this may indicate that cluster 2 has a more severe inflammatory response and disease severity.

Subsequently, we conducted WGCNA analysis, which is a system biology method that uses gene expression data to construct an unscaled network. We first found a large number of differential genes between the two clusters, and GO enrichment analysis showed that the major

pathological factors of RA were mainly related to cytokines and cytokine receptors. Through WGCNA analysis and intersecting with the aforementioned differential genes, we obtained 51 hub cluster 1 differential genes and 172 hub cluster 2 differential genes. Based on these cluster-specific differentially expressed genes, we initially conducted GO and KEGG enrichment analyses to further elucidate their biological functions. Cluster 1 was notably associated with the Hippo signaling pathway, a crucial factor influencing RA FLS behavior. Within this pathway, the tyrosine phosphatase PTPN14 has been reported to enhance the pathological manifestations of RA FLS by forming a complex with YAP (Bottini et al., 2019). Cluster 2's enrichment results revealed associations with a multitude of lymphocytes and related signaling pathways. Lymphocytes, including T cells, are pivotal effector cells in RA inflammation and its subsequent progression. Subsequently, we conducted additional validation of the identified cluster genes in synovial tissue from both RA and OA patients. This validation process included 42 hub genes from cluster 1 and 153 hub genes from cluster 2. These genes were identified as significant differential hub genes in OA or HC and RA respectively, marking them as pivotal genes distinguishing the two clusters. These genes represent important directions for our future research, warranting further elucidation of their functionality and underlying mechanisms. We further analyzed protein-protein interactions and mined core hub genes. We also explored the interactions between these hub genes and drugs based on the *DGIdb* database. We identified three hub genes that interact with drugs in cluster 1, namely, *CXCR4*, *EGFR*, and *LAMA2*, and five hub genes that interact with drugs in cluster 2, namely, *GZMB*, *IL2RB*, *IL2RG*, *LCK*, and *ZAP70*. *CXCR4* is aberrantly expressed in multiple immune cell populations in RA and has multiple functions, including promoting FLS proliferation, facilitating T cell migration, promoting the differentiation of inflammatory macrophages, and promoting inflammation, angiogenesis, and bone destruction processes (Zhao et al., 2022a). *EGFR* has long been considered a potential therapeutic target for RA, as its activation primarily promotes synoviocyte proliferation and cytokine production, and *EGFR* activation is also an important mechanism by which cells resist apoptosis, which may contribute to FLS overproliferation (Yuan et al., 2013). *LAMA2* is primarily associated with congenital muscular dystrophies (CMD) (Barraza-Flores et al., 2020). *LAMA2* is a major component of the basement membrane and an extracellular protein that mediates cellular adhesion, migration, and other functions through its interactions with other extracellular matrix molecules. As there is a lack of direct research on the relationship between *LAMA2* and RA, further experimental studies are needed to establish a link between the two. Given that *LAMA2*'s physiological functions, it may affect the proliferation and migration of multiple cells, including FLS, via apoptosis resistance. *GZMB* is mainly associated with inflammation and matrix degradation and is the strongest apoptotic activity of the granzyme family members, with caspase-like abilities. In RA, *GZMB* is abnormally expressed in multiple immune and non-immune cells, which may contribute to bone destruction through mechanisms such as matrix degradation (Zheng et al., 2023a). Studies have shown that *GZMB* can increase tissue-destructive effects by inducing apoptosis, contributing to the pathological characteristics of RA (Buzza et al., 2005). *IL2RB* is a subunit of the IL-2 receptor that mainly participates in T cell-mediated immune responses and is associated with early bone erosion in RA as a susceptibility gene (Ruyssen-Witrand et al., 2014). The protein

encoded by IL2RG is an important signaling component of many interleukin receptors, including interleukin-2, -4, -7, and -21, and may participate in multiple signaling pathways in RA. *LCK* and *ZAP70* mainly participate in the development and activation of lymphocyte T and B cells, promoting the abnormal immune state in RA. *LCK* can bind to cell surface receptors (including CD4 and CD8) and other signaling molecules (Hu et al., 2022), while mutations in *ZAP70* change the sensitivity of developing T cells to thymic positive/negative selection by altering self-peptide/MHC complexes, change the self-reactive TCR repertoire to include dominant arthritis-specific ones, and affect thymic development and the production of self-immune inhibitory regulatory T cells (Treg) (Takeuchi et al., 2020).

Finally, we discussed the relevance between key hub genes in the two clusters and potential drug efficacy. In cluster 1, the major drug-related genes included *CXCR4*, *EGFR*, and *LAMA2*. Targeting the inhibition of *CXCR4* and *EGFR* may be crucial directions to suppress the aberrant pathological behavior of RA FLS and angiogenesis. For example, BEVACIZUMAB can counteract angiogenesis by inhibiting VEGF (Mitsubishi et al., 2015), while *CXCR4* antagonists exhibit stronger anti-angiogenic effects (Gravina et al., 2017). OLMUTINIB is also an *EGFR* inhibitor (Roskoski, 2019), and given the biological functions associated with *LAMA2*, it suggests that targeting *LAMA2* and *EGFR* may hold therapeutic value for RA. In cluster 2, the major drug-related genes included *GZMB*, *IL2RB*, *IL2RG*, *LCK*, and *ZAP70*. The connection between the *GZMB* family and RA has been progressively elucidated (Zheng et al., 2023b). DACLIZUMAB is a specific IL2 receptor-targeting drug, which is related to *GZMB*, *IL2RB*, and *IL2RG*, and research indicates its therapeutic potential in the experimental arthritis model induced by CIA (Brok et al., 2001). It is possible that innovative treatments for RA targeting IL2 may emerge in the future. As for *LCK* and *ZAP70*, as previously mentioned, they are primarily associated with lymphocytes, and numerous drugs target these genes, potentially impacting various lymphocytes. This naturally affects the abnormal inflammation and bone destruction in RA, although further exploration is needed to determine if targeting *LCK* and *ZAP70* for drug development is a viable approach.

In summary, our analysis revealed that the hub genes in cluster 1 mainly function in the excessive proliferation of FLS in early RA and the autoimmune cell migration process, while the hub genes in cluster 2 mainly function in the excessive activation of autoimmune cells and bone destruction processes in later stages of RA. Compared to cluster 1, cluster 2 represents a more severe RA state. Moreover, these key hub genes in the clusters are also associated with some clinical drugs, including common clinical drugs for RA, which can provide guidance for the clinical treatment and target development of RA.

Data availability statement

The original contributions presented in the study are included in the article/Supplementary Material, further inquiries can be directed to the corresponding author.

Ethics statement

All research participants gave their informed permission and the Guanghua hospital ethics committee authorized it (No. 2018-K-12). The studies were conducted in accordance with the local legislation and institutional requirements. Written informed consent for participation was not required from the participants or the participants' legal guardians/next of kin in accordance with the national legislation and institutional requirements.

Author contributions

JZ and YS is responsible for the collection, collation, and writing of the original manuscript. KW, PJ, LX, CC, LX, YZ, JL, LL, SG, SS and RW for the collection, collation of the original data. DH are responsible for the concept development, revision, and manuscript review. All authors contributed to the article and approved the submitted version.

Funding

This work was funded by the National Natural Science Funds of China (82074234 and 82071756), Shanghai Chinese Medicine Development Office, National Administration of Traditional Chinese Medicine, Regional Chinese Medicine (Specialist) Diagnosis and Treatment Center Construction Project-Rheumatology, State Administration of Traditional Chinese Medicine, Shanghai Municipal Health Commission, East China Region-based Chinese and Western Medicine Joint Disease Specialist Alliance, and Shanghai DH Famous Chinese Medicine Studio Construction Project (SHGZS-202220).

Conflict of interest

The authors declare that the research was conducted in the absence of any commercial or financial relationships that could be construed as a potential conflict of interest.

Publisher's note

All claims expressed in this article are solely those of the authors and do not necessarily represent those of their affiliated organizations, or those of the publisher, the editors and the reviewers. Any product that may be evaluated in this article, or claim that may be made by its manufacturer, is not guaranteed or endorsed by the publisher.

Supplementary material

The Supplementary Material for this article can be found online at: <https://www.frontiersin.org/articles/10.3389/fmolb.2023.1202371/full#supplementary-material>

SUPPLEMENTARY FIGURE S1

Flowchart of analysis process. Download relevant datasets from GEO, and perform batch effect removal analysis to obtain corresponding RA and HC samples, then conduct subsequent analysis on the merged sample data.

SUPPLEMENTARY FIGURE S2

The differential analysis of HLA genes in Anokis-related genes. A: The differences in HLA gene expression between disease and normal samples. B: The Spearman correlation between differentially expressed Anokis-related genes and HLA gene expression, displaying the scatter plots of their maximum positive and negative correlations and the boxplots of the positive and negative correlations of Anokis-related genes and HLA genes that differ between disease and normal samples.

SUPPLEMENTARY FIGURE S3

GO and KEGG for hub genes in cluster 1 and cluster 2 A: GO results for hub genes in cluster 1. B: KEGG results for hub genes in cluster 1. C: GO results for hub genes in cluster 2. D: KEGG results for hub genes in cluster 2.

SUPPLEMENTARY TABLE S1

Validations for hub genes in cluster 1 and cluster 2. The expression of hub genes in cluster 1 and cluster 2 was analyzed in clinical synovial tissue samples collected from the Guanghua Hospital Precision Medicine Research Cohort, which includes 9 rheumatoid arthritis (RA) patients and 15 osteoarthritis (OA) patients, and significant differences were observed (FDR <0.05).

References

- Ali, A., and Vito, S. (2016). Genetic markers as therapeutic target in rheumatoid arthritis: a game changer in clinical therapy? *Rheumatol. Int.* 36 (11), 1601–1607. doi:10.1007/s00296-016-3563-7
- Andreev, D., Liu, M., Kachler, K., Llerins Perez, M., Kirchner, P., Kölle, J., et al. (2021). Regulatory eosinophils induce the resolution of experimental arthritis and appear in remission state of human rheumatoid arthritis. *Ann. Rheum. Dis.* 80 (4), 451–468. doi:10.1136/annrheumdis-2020-218902
- Barraza-Flores, P., Hermann, H. J., Bates, C. R., Allen, T. G., Grunert, T. T., and Burkin, D. J. (2020). Human laminin-111 and laminin-211 protein therapy prevents muscle disease progression in an immunodeficient mouse model of LAMA2-CMD. *Skelet. Muscle* 10 (1), 18. doi:10.1186/s13395-020-00235-4
- Bartok, B., and Firestein, G. S. (2010). Fibroblast-like synoviocytes: key effector cells in rheumatoid arthritis. *Immunol. Rev.* 233 (1), 233–255. doi:10.1111/j.0105-2896.2009.00859.x
- Bottini, A., Wu, D. J., Ai, R., Le Roux, M., Bartok, B., Bombardieri, M., et al. (2019). PTPN14 phosphatase and YAP promote TGF β signalling in rheumatoid synoviocytes. *Ann. Rheum. Dis.* 78 (5), 600–609. doi:10.1136/annrheumdis-2018-213799
- Bottini, N., and Firestein, G. S. (2013). Duality of fibroblast-like synoviocytes in RA: passive responders and imprinted aggressors. *Nat. Rev. Rheumatol.* 9 (1), 24–33. doi:10.1038/nrrheum.2012.190
- Brok, H. P., Tekoppele, J. M., Hakimi, J., Kerwin, J. A., Nijenhuis, E. M., De Groot, C. W., et al. (2001). Prophylactic and therapeutic effects of a humanized monoclonal antibody against the IL-2 receptor (DACLIZUMAB) on collagen-induced arthritis (CIA) in rhesus monkeys. *Clin. Exp. Immunol.* 124 (1), 134–141. doi:10.1046/j.1365-2249.2001.01487.x
- Brouwer, E., Gouw, A. S., Posthumus, M. D., van Leeuwen, M. A., Boerboom, A. L., Bijzet, J., et al. (2009). Hypoxia inducible factor-1- α (HIF-1 α) is related to both angiogenesis and inflammation in rheumatoid arthritis. *Clin. Exp. Rheumatol.* 27 (6), 945–951.
- Buzza, M. S., Zamurs, L., Sun, J., Bird, C. H., Smith, A. I., Trapani, J. A., et al. (2005). Extracellular matrix remodeling by human granzyme B via cleavage of vitronectin, fibronectin, and laminin. *J. Biol. Chem.* 280 (25), 23549–23558. doi:10.1074/jbc.M412001200
- Chen, Z., Andreev, D., Oeser, K., Krljanac, B., Hueber, A., Kleyer, A., et al. (2016). Th2 and eosinophil responses suppress inflammatory arthritis. *Nat. Commun.* 7, 11596. doi:10.1038/ncomms11596
- Cheng, W. X., Huang, H., Chen, J. H., Zhang, T. T., Zhu, G. Y., Zheng, Z. T., et al. (2020). Genistein inhibits angiogenesis developed during rheumatoid arthritis through the IL-6/JAK2/STAT3/VEGF signalling pathway. *J. Orthop. Transl.* 22, 92–100. doi:10.1016/j.jot.2019.07.007
- Dey, P., Panga, V., and Raghunathan, S. (2016). A cytokine signalling network for the regulation of inducible nitric oxide synthase expression in rheumatoid arthritis. *PLoS One* 11 (9), e0161306. doi:10.1371/journal.pone.0161306
- Frisch, S. M., and Francis, H. (1994). Disruption of epithelial cell-matrix interactions induces apoptosis. *J. Cell Biol.* 124 (4), 619–626. doi:10.1083/jcb.124.4.619
- Ge, L., Wang, T., Shi, D., Geng, Y., Fan, H., Zhang, R., et al. (2022). ATF6 α contributes to rheumatoid arthritis by inducing inflammatory cytokine production and apoptosis resistance. *Front. Immunol.* 13, 965708. doi:10.3389/fimmu.2022.965708
- Gilmore, A. P. (2005). *Anoikis. Cell Death Differ.* 12, 1473–1477. doi:10.1038/sj.cdd.4401723
- Gravina, G. L., Mancini, A., Marampon, F., Colapietro, A., Delle Monache, S., Sferra, R., et al. (2017). The brain-penetrating CXCR4 antagonist, PRX177561, increases the antitumor effects of bevacizumab and sunitinib in preclinical models of human glioblastoma. *J. Hematol. Oncol.* 10 (1), 5. doi:10.1186/s13045-016-0377-8
- Hu, X. X., Zhang, A. J., Pan, W. W., Xin, Q. L., Chen, J. Y., Zhang, L. L., et al. (2022). An IgD-Fc-Ig fusion protein restrains the activation of T and B cells by inhibiting IgD-IgDR-Lck signaling in rheumatoid arthritis. *Acta Pharmacol. Sin.* 43 (2), 387–400. doi:10.1038/s41401-021-00665-w
- Janczi, T., Fehrl, Y., Kinne, R. W., Böhm, B., and Burkhardt, H. (2023). The role of YAP1 target gene CTGF in the anoikis resistance of rheumatoid arthritis synovial fibroblasts. *Rheumatol. Oxf.* 62 (2), 850–860. doi:10.1093/rheumatology/keac354
- Jiao, Y., Ding, H., Huang, S., Liu, Y., Sun, X., Wei, W., et al. (2018). Bcl-XL and Mcl-1 upregulation by calreticulin promotes apoptosis resistance of fibroblast-like synoviocytes via activation of PI3K/Akt and STAT3 pathways in rheumatoid arthritis. *Clin. Exp. Rheumatol.* 36 (5), 841–849.
- Kampstra, A. S. B., and Toes, R. E. M. (2017). HLA class II and rheumatoid arthritis: the bumpy road of revelation. *Immunogenetics* 69 (8–9), 597–603. doi:10.1007/s00251-017-0987-5
- Koedderitzsch, K., Keszina, E., Li, L., Herrmann, M., and Biesemann, N. (2021). TNF induces glycolytic shift in fibroblast like synoviocytes via GLUT1 and HIF1A. *Sci. Rep.* 11 (1), 19385. doi:10.1038/s41598-021-98651-z
- Lafyatis, R., Remmers, E. F., Roberts, A. B., Yocum, D. E., Sporn, M. B., and Wilder, R. L. (1989). Anchorage-independent growth of synoviocytes from arthritic and normal joints. Stimulation by exogenous platelet-derived growth factor and inhibition by transforming growth factor-beta and retinoids. *J. Clin. Invest.* 83 (4), 1267–1276. doi:10.1172/JCI114011
- Meredith, J. E., Jr., Fazeli, B., and Schwartz, M. A. (1993). The extracellular matrix as a cell survival factor. *Mol. Biol. Cell* 4 (9), 953–961. doi:10.1091/mbc.4.9.953
- Miao, Y., Lv, Q., Qiao, S., Yang, L., Tao, Y., Yan, W., et al. (2019). Alpinetin improves intestinal barrier homeostasis via regulating AhR/suv39h1/TSC2/mTORC1/autophagy pathway. *Toxicol. Appl. Pharmacol.* 384, 114772. doi:10.1016/j.taap.2019.114772
- Mitsushashi, A., Goto, H., Saijo, A., Trung, V. T., Aono, Y., Ogino, H., et al. (2015). Fibrocyte-like cells mediate acquired resistance to anti-angiogenic therapy with bevacizumab. *Nat. Commun.* 6, 8792. doi:10.1038/ncomms9792
- Morel, J., Roch-Bras, F., Molinari, N., Sany, J., Eliaou, J. F., and Combe, B. (2004). HLA-DMA*0103 and HLA-DMB*0104 alleles as novel prognostic factors in rheumatoid arthritis. *Ann. Rheum. Dis.* 63 (12), 1581–1586. doi:10.1136/ard.2003.012294
- Roskoski, R., Jr. (2019). Small molecule inhibitors targeting the EGFR/ErbB family of protein-tyrosine kinases in human cancers. *Pharmacol. Res.* 139, 395–411. doi:10.1016/j.phrs.2018.11.014
- Ruyssen-Witrand, A., Lukas, C., Nigon, D., Dawidowicz, K., Morel, J., Sibilia, J., et al. (2014). Association of IL-2RA and IL-2RB genes with erosive status in early rheumatoid arthritis patients (ESPOIR and RMP cohorts). *Jt. Bone Spine* 81 (3), 228–234. doi:10.1016/j.jbspin.2013.10.002
- Sánchez-Zuno, G. A., Bucala, R., Hernández-Bello, J., Román-Fernández, I. V., García-Chagollán, M., Nicoletti, F., et al. (2021). Canonical (CD74/CD44) and non-canonical (CXCR2, 4 and 7) MIF receptors are differentially expressed in rheumatoid arthritis patients evaluated by DAS28-ESR. *J. Clin. Med.* 11 (1), 120. doi:10.3390/jcm11010120
- Smith, M. H., and Berman, J. R. (2022). What is rheumatoid arthritis? *Jama* 327 (12), 1194. doi:10.1001/jama.2022.0786
- Taddei, M. L., Giannoni, E., Fiaschi, T., and Chiarugi, P. (2012). Anoikis: an emerging hallmark in health and diseases. *J. Pathol.* 226 (2), 380–393. doi:10.1002/path.3000
- Takeuchi, T., Yoshida, H., and Tanaka, S. (2021). Role of interleukin-6 in bone destruction and bone repair in rheumatoid arthritis. *Autoimmun. Rev.* 20 (9), 102884. doi:10.1016/j.autrev.2021.102884
- Takeuchi, Y., Hirota, K., and Sakaguchi, S. (2020). Impaired T cell receptor signaling and development of T cell-mediated autoimmune arthritis. *Immunol. Rev.* 294 (1), 164–176. doi:10.1111/imr.12841
- Wei, K., Korsunsky, I., Marshall, J. L., Gao, A., Watts, G. F. M., Major, T., et al. (2020). Notch signalling drives synovial fibroblast identity and arthritis pathology. *Nature* 582 (7811), 259–264. doi:10.1038/s41586-020-2222-z

Yuan, F. L., Li, X., Lu, W. G., Sun, J. M., Jiang, D. L., and Xu, R. S. (2013). Epidermal growth factor receptor (EGFR) as a therapeutic target in rheumatoid arthritis. *Clin. Rheumatol.* 32 (3), 289–292. doi:10.1007/s10067-012-2119-9

Zhang, R., Jin, Y., Chang, C., Xu, L., Bian, Y., Shen, Y., et al. (2022). RNA-Seq and network analysis reveal unique chemokine activity signatures in the synovial tissue of patients with rheumatoid arthritis. *Front. Med.* 9, 799440. doi:10.3389/fmed.2022.799440

Zhao, J., Guo, S., Schrodi, S. J., and He, D. (2021). Molecular and cellular heterogeneity in rheumatoid arthritis: mechanisms and clinical implications. *Front. Immunol.* 12, 790122. doi:10.3389/fimmu.2021.790122

Zhao, J., Guo, S., Schrodi, S. J., and He, D. (2022b). Cuproptosis and cuproptosis-related genes in rheumatoid arthritis: implication, prospects, and perspectives. *Front. Immunol.* 13, 930278. doi:10.3389/fimmu.2022.930278

Zhao, J., Guo, S., Schrodi, S. J., and He, D. (2022c). Absent in melanoma 2 (AIM2) in rheumatoid arthritis: novel molecular insights and implications. *Cell Mol. Biol. Lett.* 27 (1), 108. doi:10.1186/s11658-022-00402-z

Zhao, J., Wei, K., Jiang, P., Chang, C., Xu, L., Xu, L., et al. (2022a). G-Protein-Coupled receptors in rheumatoid arthritis: recent insights into mechanisms and functional roles. *Front. Immunol.* 13, 907733. doi:10.3389/fimmu.2022.907733

Zheng, Y., Zhao, J., Shan, Y., Guo, S., Schrodi, S. J., and He, D. (2023a). Role of the granzyme family in rheumatoid arthritis: current Insights and future perspectives. *Front. Immunol.* 14, 1137918. doi:10.3389/fimmu.2023.1137918

Zheng, Y., Zhao, J., Shan, Y., Guo, S., Schrodi, S. J., and He, D. (2023b). Role of the granzyme family in rheumatoid arthritis: current Insights and future perspectives. *Front. Immunol.* 14, 1137918. doi:10.3389/fimmu.2023.1137918



OPEN ACCESS

EDITED BY

Evangelia Sarandi,
University of Crete, Greece

REVIEWED BY

Marc S. Horwitz,
University of British Columbia, Canada
Hong Zan,
Prellis Biologics, United States

*CORRESPONDENCE

Elias A. Rahal,
✉ er00@aub.edu.lb

RECEIVED 20 June 2023

ACCEPTED 20 March 2024

PUBLISHED 04 April 2024

CITATION

Shehab M, Hussein H, Fadlallah S and Rahal EA (2024), An IL-17A-centric response to Epstein-Barr virus DNA mediated by dendritic Cell-T cell interactions.
Front. Mol. Biosci. 11:1243366.
doi: 10.3389/fmolb.2024.1243366

COPYRIGHT

© 2024 Shehab, Hussein, Fadlallah and Rahal. This is an open-access article distributed under the terms of the [Creative Commons Attribution License \(CC BY\)](#). The use, distribution or reproduction in other forums is permitted, provided the original author(s) and the copyright owner(s) are credited and that the original publication in this journal is cited, in accordance with accepted academic practice. No use, distribution or reproduction is permitted which does not comply with these terms.

An IL-17A-centric response to Epstein-Barr virus DNA mediated by dendritic Cell-T cell interactions

Marwa Shehab¹, Hadi Hussein^{1,2}, Sukayna Fadlallah^{1,2} and Elias A. Rahal^{1,2*}

¹Department of Experimental Pathology, Immunology and Microbiology, American University of Beirut, Beirut, Lebanon, ²Center for Infectious Diseases Research, American University of Beirut, Beirut, Lebanon

Introduction: The Epstein-Barr virus has been associated with a considerable number of autoimmune diseases. We have previously demonstrated that EBV DNA enhances the production of IL-17A, a pro-inflammatory cytokine, via endosomal Toll-like receptor signalling.

Methods: We used RNA-seq to analyze the transcriptional profile of mouse immune cells treated with EBV DNA.

Results: We observed that EBV DNA upregulates an IL-17A-centric network of mediators. Ensemble Gene Set Enrichment Analysis (EGSEA) showed enriched expression of sets involved in inflammatory responses including IFN γ and TNF- α -associated pathways as well as proinflammatory diseases. On the other hand, while macrophages and B cells were somewhat able to induce an IL-17A response from T cells to EBV DNA, they were less potent than dendritic cells. EBV virions were also capable of eliciting the production of inflammatory mediators from dendritic cell-T cell cultures largely mirroring responses to the viral DNA.

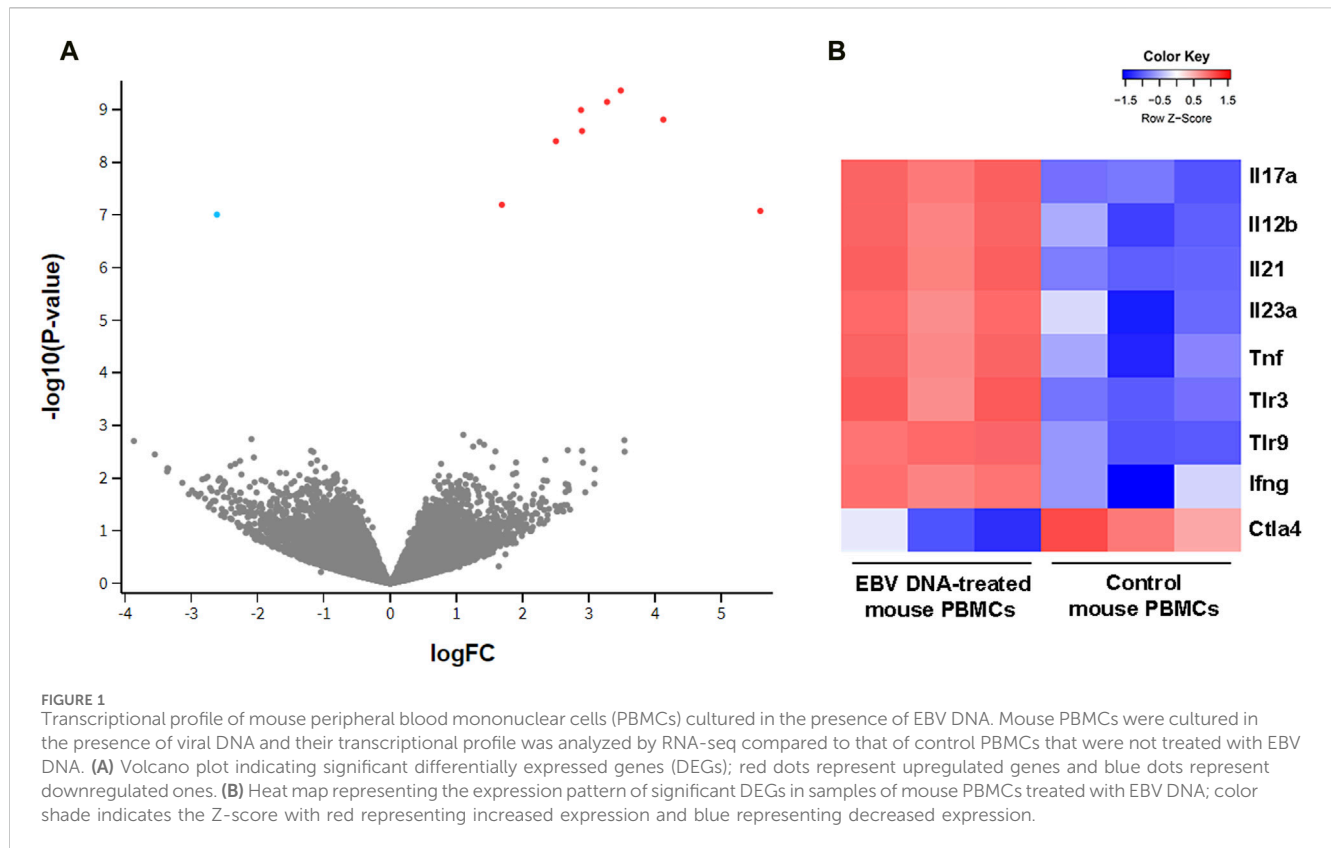
Conclusions: Given the wide prevalence of EBV in the population, our analyses reveal a network of mediators and cell types that may serve as therapeutic targets in a large proportion of people affected by autoimmune diseases.

KEYWORDS

Epstein–Barr virus, IL-17A, Th17, endosomal toll like receptors, inflammation, autoimmunity, TLR3, TLR9

1 Introduction

The Epstein-Barr virus (EBV) is known to be a potent modulator of immune processes. This virus establishes a lifelong latent infection with frequent reactivations in the host (Lunemann et al., 2007). Due to its ubiquitous nature, frequent reactivation potential and immune response modulation, EBV is thought to be involved in several autoimmune diseases. The general consensus is that EBV acts as an inflammatory trigger providing innate and adaptive activation signals (Iwakiri, 2014). EBV has been associated with autoimmune diseases including systemic lupus erythematosus (SLE) (James et al., 1997), rheumatoid arthritis (RA) (Lotz and Roudier, 1989), Sjorgen's syndrome (SS) (Fox et al., 1987), and multiple sclerosis (MS) (Ascherio and Munger, 2010).



Ninety-nine percent of young SLE patients are seropositive for EBV compared to 70% of age-matched controls (James et al., 1997). Moreover, increased levels of IgA antibodies against the EBV viral capsid antigen (VCA) were detected in sera of SLE patients (Chen et al., 2005). On the other hand, several sero-epidemiological investigations reported a higher incidence of MS in EBV infected patients (Lunemann et al., 2007) and some studies have described increased titers of antibodies against EBV antigens in RA patient sera (Shirodaria et al., 1987). Higher levels of Epstein-Barr nuclear antigen 1 (EBNA-1) antibodies have also been observed in SLE, MS and RA patients (Petersen et al., 1990; Lunemann et al., 2008; Draborg et al., 2012).

An increase in latently infected memory B cells is believed to underlie an elevated EBV genome load in SLE patients compared to healthy controls (Kang et al., 2004; Gross et al., 2005; Larsen et al., 2011). Furthermore, there is a direct association between the number of EBV infected B cells and SLE disease activity (Gross et al., 2005). A high EBV load has also been observed in RA patients (Tosato et al., 1984; Blaschke et al., 2000; Balandraud et al., 2003; Lunemann et al., 2008). In MS patients, inconsistent data regarding the EBV viral load has been reported; Wandinger et al. (2000) detected higher levels of EBV DNA in patient sera during disease exacerbation periods and Wagner et al. (2004) described an association between EBV DNA in plasma and an increased risk of MS. Other studies did not detect any differences in EBV DNA levels between blood samples from MS patients and controls (Lunemann et al., 2006; Lindsey et al., 2009; Lucas et al., 2011).

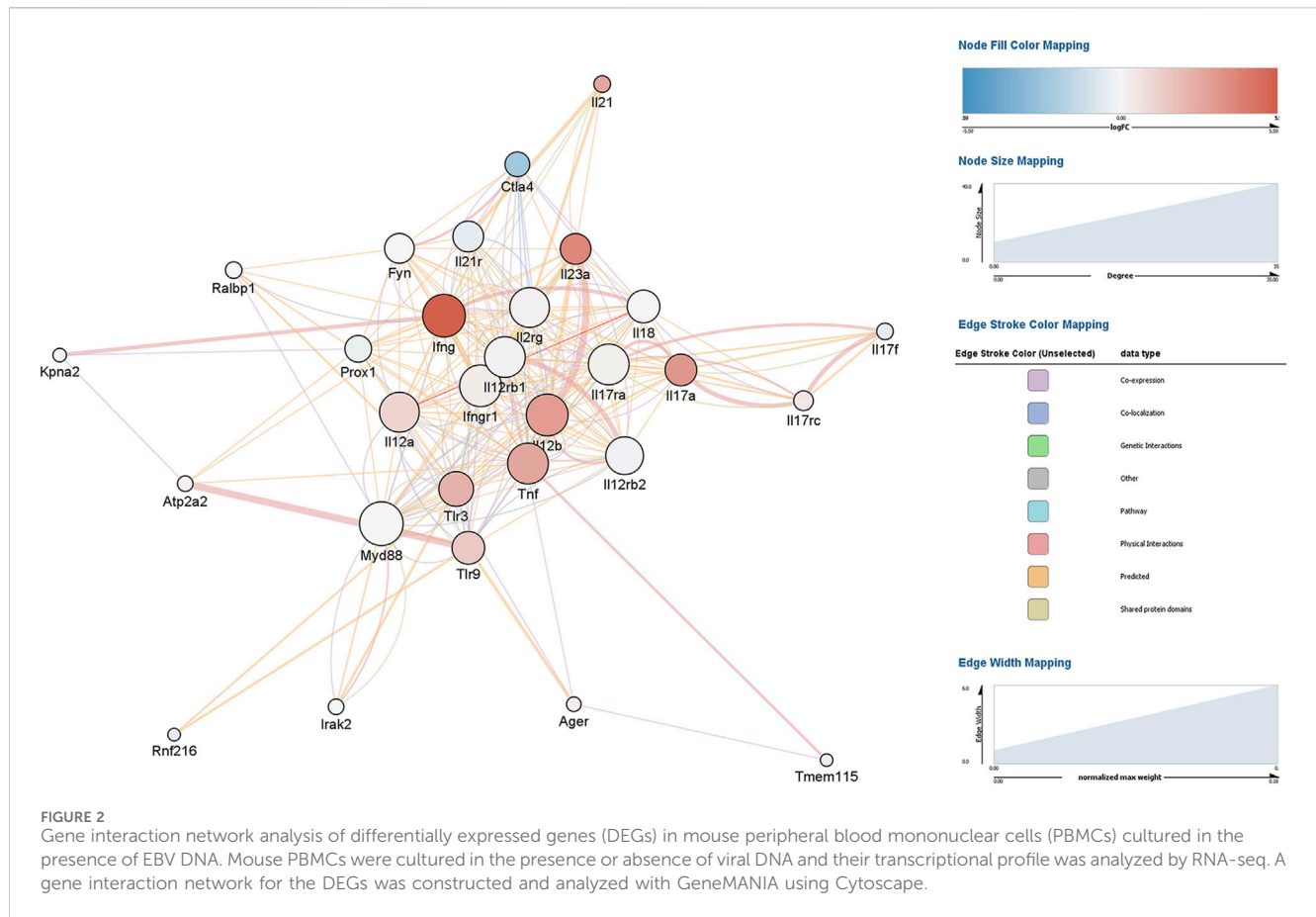
Given that EBV DNA is rich in immunostimulatory CpG motifs (Kieff et al., 1982; Fiola et al., 2010), we previously assessed its contribution to autoimmune disease and proinflammatory pathways. We observed not only increased levels of EBV DNA in blood from RA

patients, but also a correlation between EBV DNA levels and those of IL-17A, a proinflammatory mediator produced by T helper 17 (Th17) cells and highly associated with autoimmune processes (Salloum et al., 2018). Administration of EBV DNA to mice and treatment of mouse peripheral blood mononuclear cells with the viral DNA also enhanced the production of IL-17A via endosomal Toll-like receptor (TLR) signalling (Rahal et al., 2015; Shehab et al., 2019). In the study at hand, we sought to examine the network of mediators involved as well as to determine the cell types that play a role in this response.

2 Methods

2.1 RNA-seq and transcriptional profile analyses

To assess the effect of EBV DNA on the transcriptional profile of mouse PBMCs, RNA-seq was used. Study protocols were approved by the Animal Care and Use Committee (IACUC) at the American University of Beirut (AUB). BALB/c mouse PBMCs were isolated from 4 to 6 week old female mouse blood using Histopaque® (Sigma-Aldrich, Saint Louis, Missouri) and then were cultured in a 96-well plate whereby each well contained 25×10^4 PBMCs in 250 μ L of the RPMI 1640 culture medium (Lonza, Basel, Switzerland) supplemented with 10% FBS (Sigma-Aldrich, Saint Louis, Missouri) and 1% penicillin-streptomycin (Lonza, Basel, Switzerland). Cells were cultured for 12 h at 37°C with 5% CO₂ in the presence or absence of 9×10^3 copies of EBV DNA. Triplicates of each treatment were performed. Cells were then collected and total RNA was extracted using Qiazol



(Qiagen, Hilden, Germany) according to the manufacturer's instructions. The isolated RNA was subsequently sequenced by Macrogen Inc. (Seoul, Korea) using the NovaSeq 6000 S4 Reagent Kit and an Illumina NovaSeq 6000 System (Illumina Inc., San Diego, CA, United States). Reads were trimmed with Trimmomatic and the trimmed reads were mapped to the *Mus musculus* mm10 reference genome using HISAT2; featureCounts was then used to assign sequence reads to genomic features and Limma-Voom was subsequently employed for differential expression (DE) analysis.

To visualize and analyse functional association network interactions involving the DEGs, GeneMANIA (Warde-Farley et al., 2010) using Cytoscape v3.8.2 was employed setting the max resultant genes to 20 and max resultant attributes to 10. Gene set enrichment (GSE) was conducted using EGSEA (Alhamdoosh et al., 2017) which combines data from 12 enrichment algorithms allowing analyses across multiple gene set collections. EGSEA v1.10.0 and EGSEAdat v1.10.0 were used with the Wilkinson *p*-value combining method employed for this analysis.

2.2 Isolation of immune cell-populations and flow cytometry analyses

Four to 6 week-old female BALB/c mice were used to isolate immune cell populations. For isolation of DCs, B cells and T cells,

mouse spleens were each digested in 10 mL of a digestion mix consisting of 10 mg/mL collagenase IV (Roche) and 10 mg/mL DNaseI (Sigma-Aldrich, Saint Louis, Missouri) for 1 h at 37°C with gentle shaking. Splenocytes were then passed through Corning® 70 µm cell strainers and washed with 1X PBS (Sigma-Aldrich, Saint Louis, Missouri). Cells obtained per spleen were then incubated with 5 mL of RBC lysis buffer (Qiagen, Hilden, Germany) for 10 min at room temperature. After two additional washes with 1X PBS, cells were incubated in T25 flasks in complete RPMI for 24 h at 37°C in 5% CO₂. Cells were subsequently washed with 1X PBS and enumerated using a TC20™ Automated Cell Counter (Bio-Rad). To isolate elicited macrophages from peritoneal compartments, mice were each injected with 2.5 mL of 3% Brewer's Thioglycolate medium (Scharlau, Barcelona, Spain) in the peritoneal cavity. After 4 days, mice were sacrificed and a small incision along the mouse midline was introduced with sterile scissors. The intact peritoneal wall was exposed and about 10 mL of cold sterile 1X PBS per mouse was injected in the cavity. The compartment was massaged for 5 min and the peritoneal fluid was then aspirated and centrifuged at 400 g for 10 min at 4°C. After two washes with 1X PBS, cells were resuspended in DMEM/F12-10 medium (Lonza, Basel, Switzerland) supplemented with 10% FBS (Sigma-Aldrich, Saint Louis, Missouri) and 1% penicillin-streptomycin (Lonza, Basel, Switzerland) and enumerated. A total of 10⁷ cells per well were cultured in 6-well plates in 2 mL of DMEM/F12-10 medium (Lonza, Basel, Switzerland) supplemented with 10% FBS and 1%

TABLE 1 Node characteristics of the EBV DNA gene response network identified with GeneMANIA ranked by degree.

Gene name	Degree	Log score	Neighborhood connectivity	Score	Stress	Topological coefficient
Myd88	33	−4.088	15.529	0.017	184	0.555
Ifng	32	−0.610	14.350	0.543	226	0.513
Ifngr1	31	−2.984	17.063	0.051	46	0.609
Il12b	31	−0.350	16.500	0.705	76	0.589
Il12rb1	30	−3.029	15.882	0.048	100	0.567
Il17ra	30	−3.211	15.263	0.040	218	0.545
Tnf	30	−0.550	14.571	0.577	242	0.538
Il2rg	29	−3.854	16.056	0.021	96	0.573
Il12a	29	−4.250	15.368	0.014	174	0.549
Il12rb2	27	−3.790	16.882	0.023	54	0.603
Tlr3	24	−0.394	14.824	0.675	256	0.529
Tlr9	22	−0.541	14.077	0.582	124	0.521
Il18	22	−3.659	16.059	0.026	132	0.574
Il17a	21	−0.524	15.529	0.592	176	0.555
Il23a	20	−0.325	16.786	0.723	40	0.646
Il21r	20	−3.256	15.615	0.039	62	0.558
Fyn	19	−4.307	16.063	0.013	74	0.574
Prox1	16	−4.182	15.600	0.015	96	0.557
Ctla4	14	−0.384	17.727	0.681	10	0.682
Il17rc	9	−2.618	14.000	0.073	4	0.700
Il21	6	−0.314	16.800	0.731	6	0.730
Il17f	6	−3.602	13.333	0.027	0	0.702
Ralbp1	6	−4.209	18.200	0.015	2	0.728
Irak2	5	−3.978	17.000	0.019	0	0.895
Atp2a2	5	−2.468	14.400	0.085	14	0.576
Ager	4	−3.813	12.750	0.022	10	0.568
Kpna2	3	−3.543	13.333	0.029	0	0.606
Tmem115	2	−4.035	12.500	0.018	4	0.575
Rnf216	2	−3.618	15.000	0.027	0	0.714

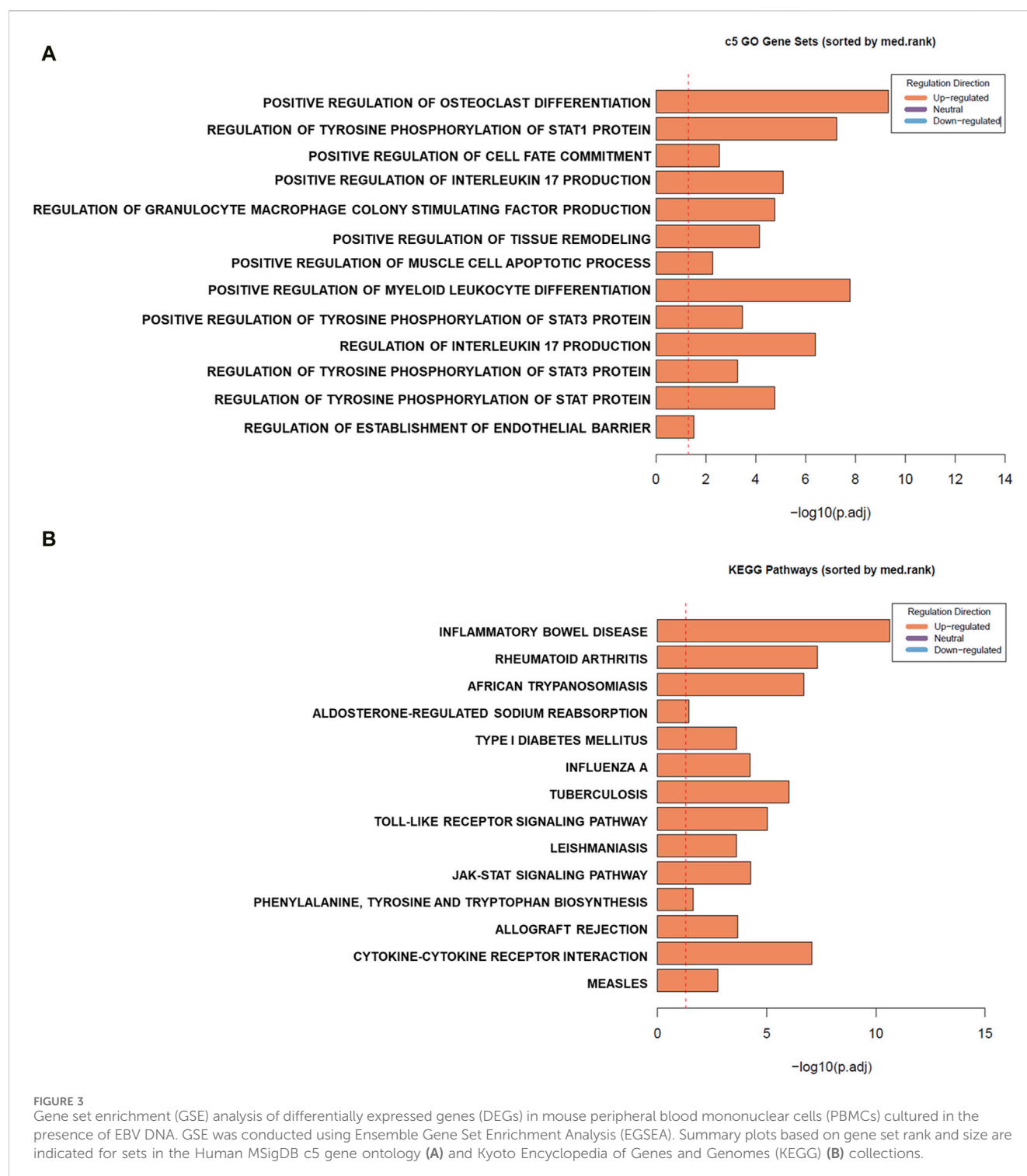
penicillin-streptomycin (Lonza, Basel, Switzerland) then incubated overnight at 37°C in 5% CO₂.

To isolate T cells, B cells, DCs, and macrophages, Fluorescence Activated Cell Sorting (FACS) was performed using a BD FACSAria™ II-SORP (BD Biosciences, San Jose, CA). For total leukocytes, an anti-mouse CD45 labelled with APC/Cy7 (BioLegend Inc. San Diego, CA) was employed. Then, for total T cells, an anti-mouse CD3 labelled with Alexa Fluor® 647 (BioLegend Inc. San Diego, CA) was used. For B cells, PE-labelled anti-CD19 (BioLegend Inc. San Diego, CA) was employed and an anti-CD11c labelled with Brilliant Violet 421™ (BioLegend Inc. San Diego, CA) was used to collect pan DCs including plasmacytoid and myeloid DCs. The antibodies used for sorting of macrophages from

the peritoneal exudate included anti-mouse CD11b and F4/80 labelled with PE and Brilliant Violet 421™ (BioLegend Inc. San Diego, CA) respectively.

2.3 Cell cultures and treatments

Isolated mouse B cells, DCs and macrophages were cultured each alone or with T cells in 96-well plates. Each APC population was co-cultured with T cells at a ratio of 1:10 which was found to be an optimal ratio in preliminary experiments for DCs. A similar ratio was then used for the other APC types to allow potency comparisons



across cell types assessed. Thus, 15,000 of each APC type was cultured with 150,000 T cells per well in a total volume of 250 μ L of complete RPMI. Mouse PBMCs (25×10^4 per well) were also examined. Cells were either left untreated or cultured in the presence of 9×10^3 copies of EBV DNA or 9×10^3 EBV virions. The viral DNA was isolated from a P3HR-1 strain of EBV, which was also the strain used for testing the effects of the EBV viral particles. *S. epidermidis* DNA (1.7pg, equivalent to the weight of 9×10^3 copies of EBV DNA) was used as a non-viral control DNA. Transcriptional analyses were

conducted after 12 h of culture while supernatant levels of mediators were assayed 24 h after incubation.

For flow cytometry analysis of IL-17A positive cells, 25×10^4 PBMCs were treated with 9×10^3 copies of EBV DNA, 1.7 pg of *S. epidermidis* DNA, or mock treated (with culture medium). After 24 h of incubation cells were stained with anti-mouse CD3 labelled with Alexa Fluor® 647 (BioLegend Inc. San Diego, CA) and anti-mouse IL-17A labelled with Brilliant Violet 605™ (BioLegend Inc. San Diego, CA) then analyzed by flow cytometry.

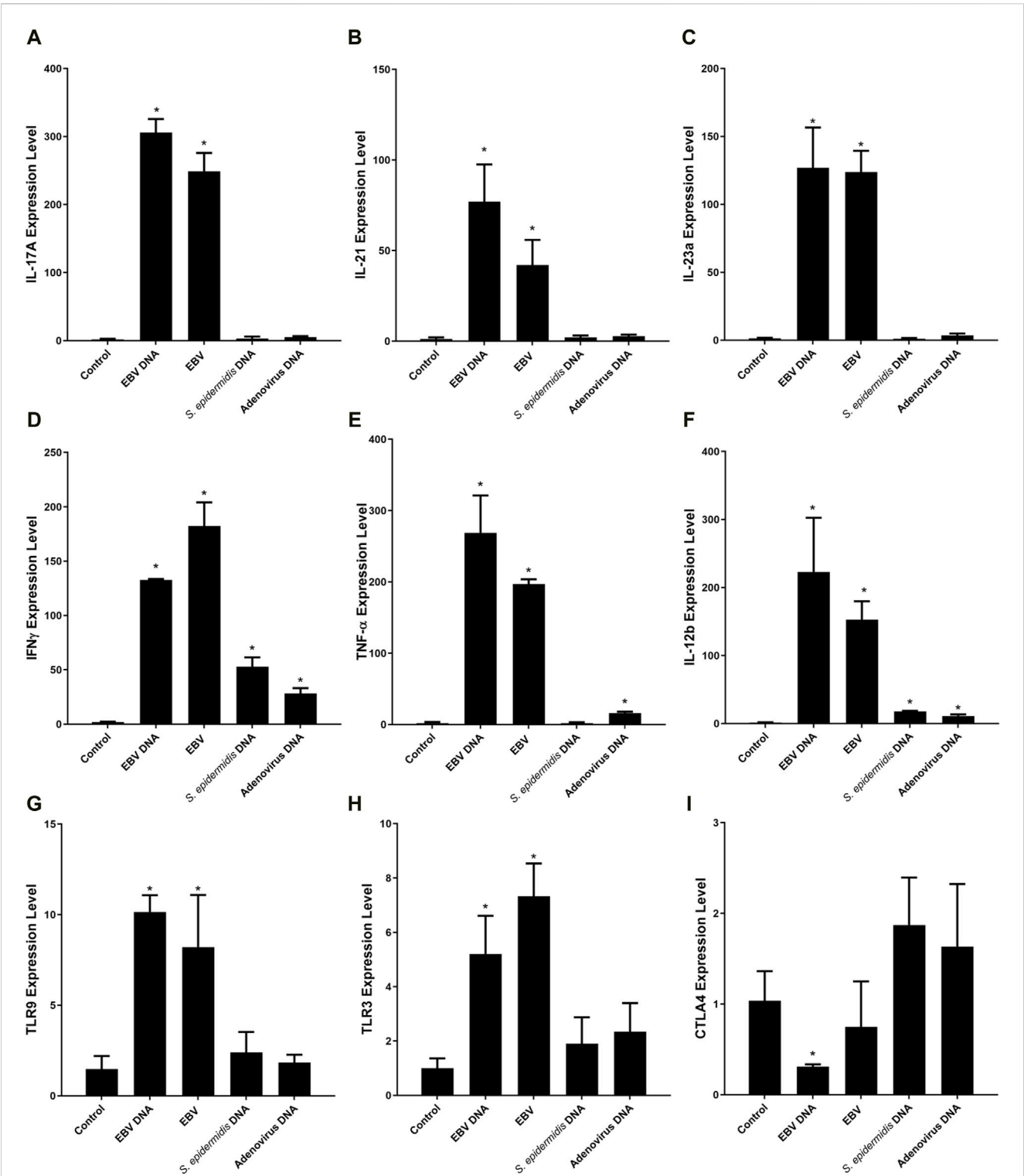
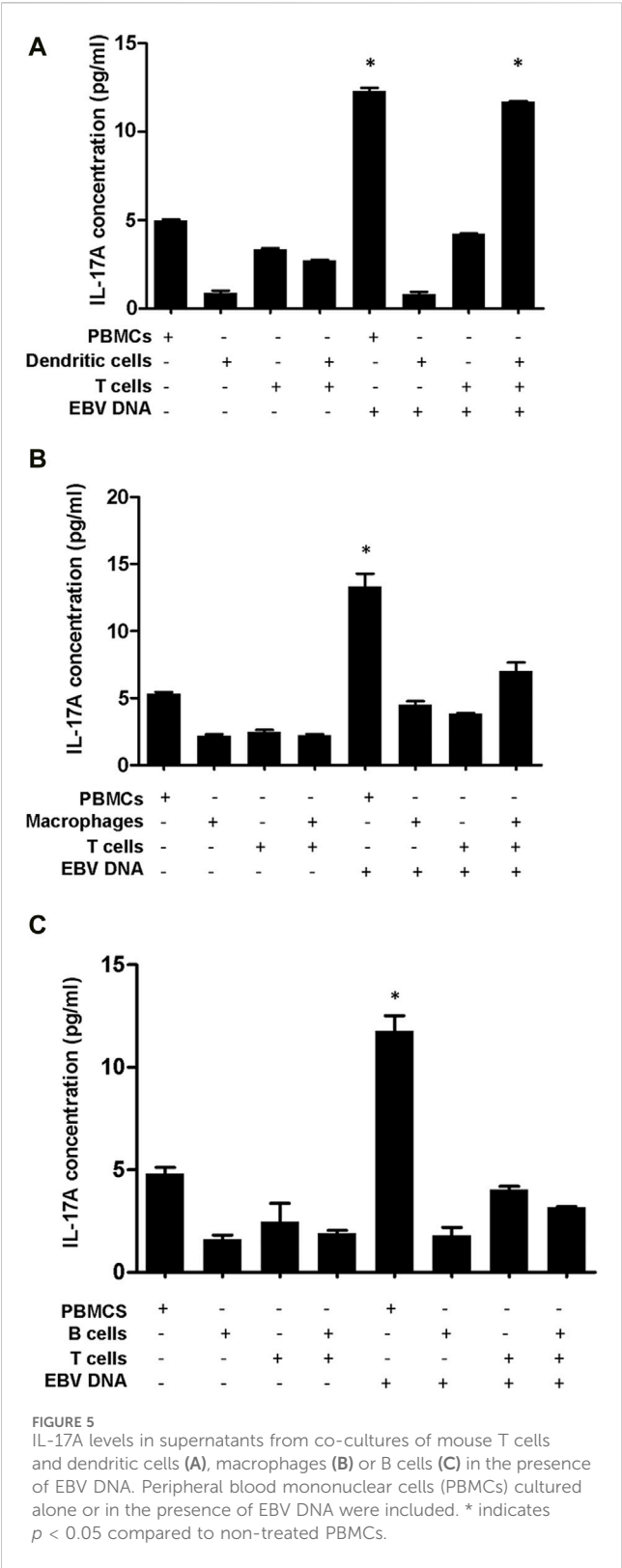


FIGURE 4 Relative expression of IL-17A (A), IL-21 (B), IL-23a (C), IFN γ (D), TNF- α (E), IL-12b (F), TLR9 (G), TLR3 (H) and CTLA4 (I) in mouse peripheral blood mononuclear cells (PBMCs) cultured with EBV DNA. Mouse PBMCs were cultured in the presence or absence of viral DNA and relative expression levels were assessed with real-time PCR. The effects of bacterial control DNA from *S. epidermidis* and viral control DNA from human adenovirus type 1 C were assessed as well. * indicates $p < 0.05$ compared to non-treated PBMCs.



2.4 Enzyme-linked immunosorbent assay (ELISA)

Mouse IL-17A, IFN γ and TNF- α ELISA Kits (Abcam, Cambridge, United Kingdom) were used to determine culture

supernatant levels of these mediators. Kits were used as per the manufacturer's instructions.

2.5 Real-time PCR

To determine the relative expression of the IL-17A, IL-21, IL-23a, IFN γ , TNF- α , IL-12b, TLR9, TLR3, and CTLA4 genes, total RNA was isolated using Qiazol (Qiagen, Hilden, Germany) according to the manufacturer's instructions. cDNA was synthesized employing the QuantiTect Reverse Transcription Kit (Qiagen, Hilden, Germany) and then real time RT-PCR was carried out using iTaq Universal SYBR Green Supermix (Bio-Rad) and employing the Bio-Rad CFX96 Real Time PCR Detection System (Bio-Rad). β -actin expression was used for expression normalization per sample. Previously published primers for IL-21 (Pesce et al., 2006), IL-23a (Teng et al., 2014), IL-12b (Sun et al., 2017), IL-17A, IFN γ , TNF- α , TLR9, TLR3, CTLA4, and β -actin (Andari et al., 2021) were used; primers were obtained from Macrogen Inc.

2.6 Statistical analysis

Statistical analyses for ELISA and real-time PCR were performed using GraphPad Prism. Means were compared using the two-tailed paired Student's t-test. p -values less than 0.05 were considered statistically significant.

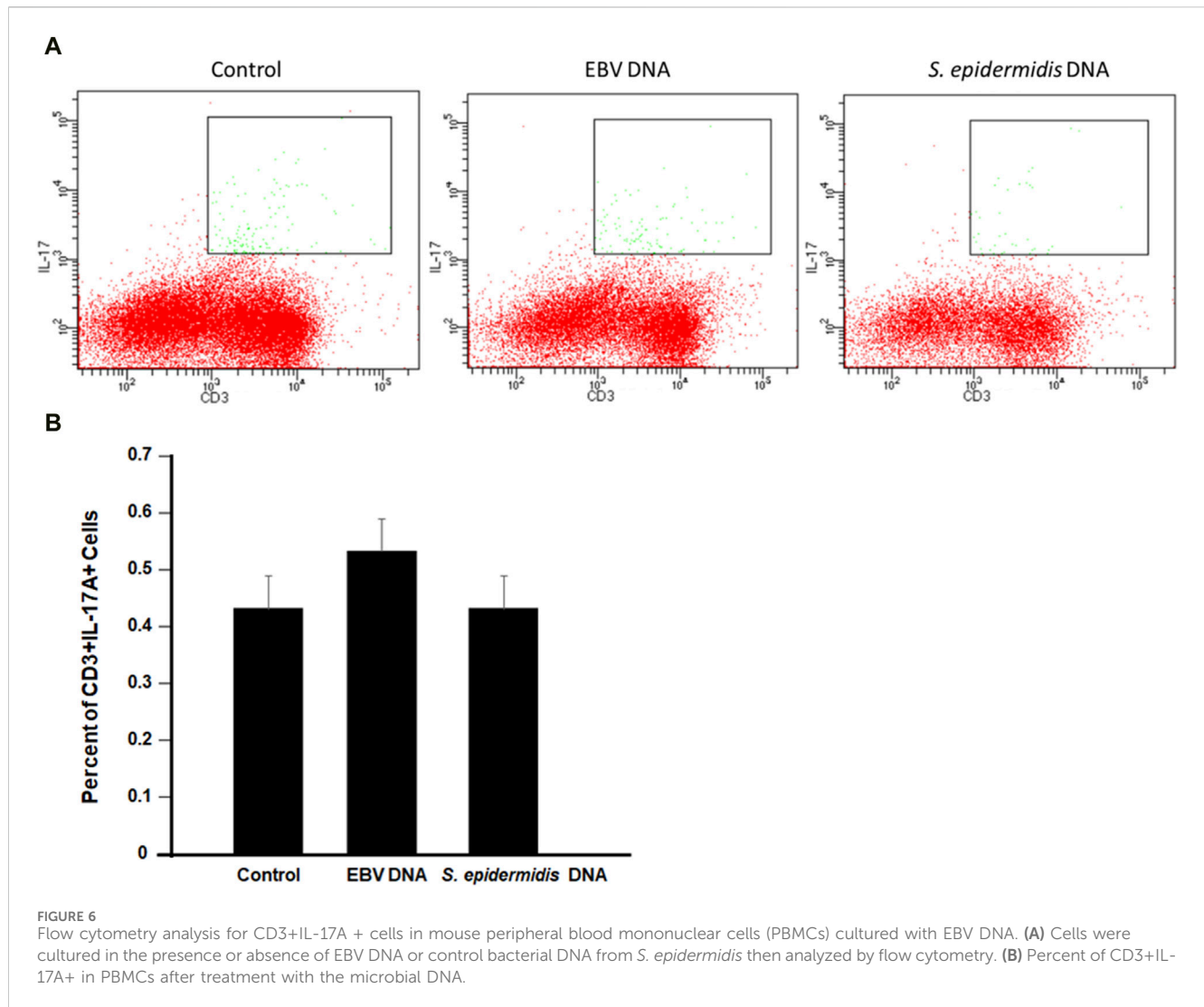
3 Results

3.1 Transcriptional profile of EBV DNA-treated mouse peripheral blood mononuclear cells

To examine the effect of EBV DNA on the transcriptional profile of mouse peripheral blood mononuclear cells (PBMCs), cells were cultured in the presence or absence of the viral DNA then subjected to RNA extraction followed by RNA-seq. Analysis of differentially-expressed genes (DEGs) revealed a total of nine genes whose expression was significantly altered by the EBV DNA treatment. The expression of eight genes, including IL-17A, IFN γ , IL-21 and TNF- α , was significantly increased in the EBV DNA-treated group and one gene, CTLA4, showed a significant decrease in expression. Figure 1A is a volcano plot representing gene expression comparisons and Figure 1B is a heat map of the DEGs.

Constructing an interaction gene network with GeneMANIA using Cytoscape to predict interactions between DEGs and other genes resulted in a network of 29 genes and 264 interaction edges (Figure 2). Node degrees were calculated to identify hub genes in the network; this analysis indicated that MyD88 followed closely by IFN γ were hub genes with the highest degree of connectivity in this module (Table 1).

To assess the enrichment of gene sets detected to be differentially expressed in mouse PBMCs across human gene sets, Ensemble Gene Set Enrichment Analysis (EGSEA) was conducted (Figure 3) first using the Human MSigDB c5 gene ontology collection. We observed enrichment of gene sets involved mainly in inflammatory pathways



such as those involved in positive regulation of IL-17 production, regulation of granulocyte macrophage colony stimulating factor production, positive regulation of myeloid leukocyte differentiation, and positive regulation of tissue remodelling. On the other hand, analysis using the Kyoto Encyclopedia of Genes and Genomes (KEGG) collections revealed enrichment of gene sets involved in proinflammatory diseases such as inflammatory bowel disease, rheumatoid arthritis, and type 1 diabetes mellitus, all of which are diseases associated with EBV infections.

To validate the RNA-seq differential expression signature observed, the expression of all 9 DEGs was assessed in PBMCs treated with EBV DNA (Figure 4). Results paralleled the RNA-seq observations with enhanced expression of IL-17A, IL-21, IL-23a, IFN γ , TNF- α , IL-12b, TLR9 and TLR3 but a decreased expression of CTLA4. Culturing PBMCs with the virus itself also resulted in a similar expression pattern. Treatment with control bacterial DNA from *S. epidermidis* was able to enhance the expression of IFN γ and IL-12b, albeit not to the extent induced by EBV DNA; the bacterial DNA was not able to increase the expression of the other genes assessed. To examine the effects of another mammalian DNA virus, we assessed those of human adenovirus type 1 subgroup C; this viral

DNA was also not able to replicate the expressional signature of EBV DNA. It was able to enhance the expression of IFN γ , TNF- α and IL-12b but to a much lesser extent compared to EBV DNA and it was not able to increase the expression of the other genes. This indicates that this IL-17A-centric signature is not induced by just any type of DNA and is likely more unique to EBV, and possibly to other herpesviruses as well.

3.2 Dendritic cell-T cell interactions drive the IL-17A-centric response to EBV DNA

Analysis of the proinflammatory network of genes triggered by EBV DNA indicated IL-17A to be one of the most highly upregulated genes with MyD88 seemingly a hub gene in this interaction network. With MyD88 being an adapter protein integral to TLR signalling, the role we observed for endosomal TLRs in the response to EBV DNA and the types of cytokines observed to be upregulated, T cell stimulation by innate immune responses to the viral DNA was a likely scenario. Hence, we sought to determine whether professional antigen presenting cells (APCs)

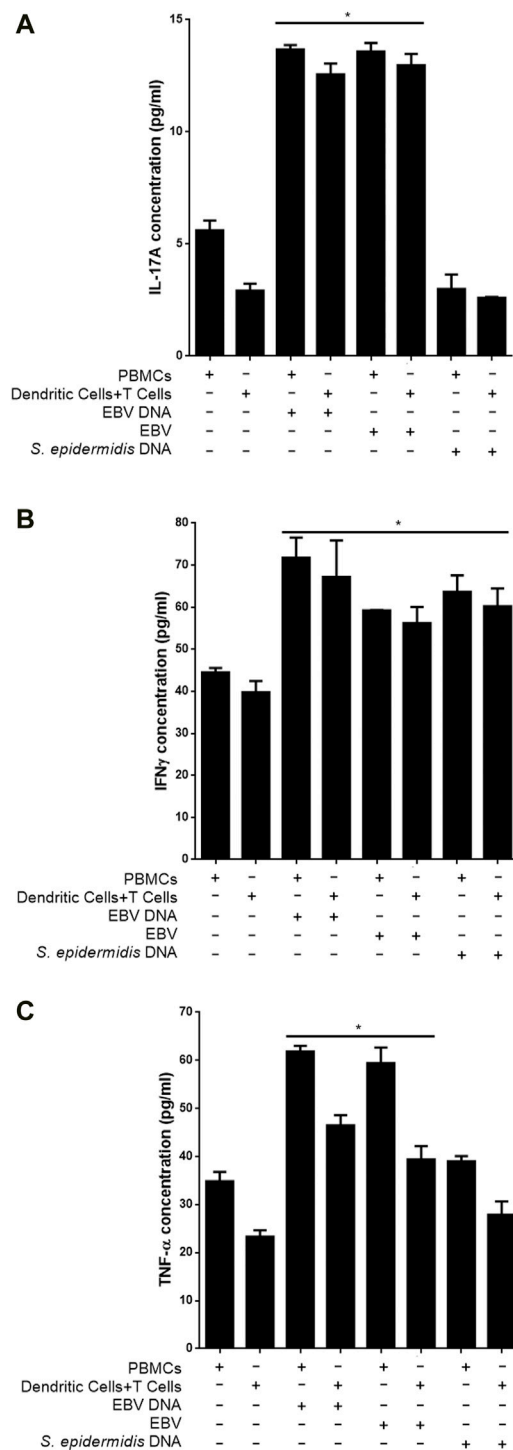


FIGURE 7
Proinflammatory mediator levels in supernatants from co-cultures of mouse T cells and dendritic cells in the presence of EBV. Cells were cultured with EBV, its DNA or with bacterial control DNA from *S. epidermidis*. Responses from mouse Peripheral blood mononuclear cells (PBMCs) were also assessed. Levels of IL-17A (A), IFNγ (B) and TNF-α (C) were assessed in supernatants. * indicates $p < 0.05$ compared to respective non-treated cells.

mediate such a stimulation. Therefore, we examined the three types of professional APCs, B cells, dendritic cells (DCs) and macrophages; these cells were cultured alone or with T cells in

the presence or absence of EBV DNA. This was followed by IL-17A level assessment in culture supernatants.

IL-17A levels were found to be significantly increased by 4.28 folds ($p = 0.0001$) in supernatants from mouse DCs and T cells co-cultured in the presence of EBV DNA compared to co-cultures of DCs and T cells without EBV DNA (Figure 5A). This co-culture of DCs and T cells with EBV DNA had a level similar to that of PBMCs cultured with EBV DNA; this PBMC control culture showed a 2.46-fold increase ($p = 0.0006$) in IL-17A levels compared to PBMCs cultured in the absence of the viral DNA. Mouse peritoneal elicited macrophages co-cultured with T cells showed a 3.12-fold increase in IL-17A levels upon treatment with EBV DNA compared to elicited macrophages and T cells co-cultured without EBV DNA ($p = 0.0095$) (Figure 5B). However, this increased level was 47.5% less than that observed in supernatants from PBMCs cultured in the presence of EBV DNA and hence not significant when compared to it ($p = 0.0715$). On the other hand, B cells co-cultured with T cells in the presence of EBV DNA resulted in some increase in IL-17A levels compared to a co-culture of these cell populations in the absence of EBV DNA; however, the level was 73% less than that of PBMCs treated with EBV DNA (Figure 5C). This indicates that DCs are the most potent in inducing an IL-17A response from T cells in the presence of EBV DNA.

To examine whether the increased production of IL-17A upon EBV treatment of mouse immune cells was due to enhanced differentiation of T cells into Th17 cells, PBMCs were treated with EBV DNA, *S. epidermidis* DNA or mock treated with culture medium. Cells were subsequently analyzed by flow cytometry (Figure 6). We observed no marked differences between the different treatments which indicates that there is increased production of IL-17A from the EBV DNA-stimulated cells rather than enhanced differentiation into Th17 cells.

3.3 EBV virions trigger an IL-17A proinflammatory response from dendritic cell-T cell cultures

To examine whether EBV particles are capable of triggering IL-17A production from DC and T cell co-cultures similar to the viral DNA, mouse cells were cultured with the viral particles. Subsequently, IL-17A levels were determined in culture supernatants (Figure 7A). We observed a 4.43-fold ($p = 0.0017$) increase in IL-17A levels from supernatants of DCs and T cells co-cultured in the presence of EBV compared to a co-culture of these cells in the absence of the virus. An increase of 2.42 folds ($p = 0.0026$) in IL-17A levels was also observed when PBMCs were cultured with the virus. Hence, the IL-17A response to the virus itself largely paralleled that to the viral DNA. On the other hand, control bacterial DNA from *S. epidermidis* was incapable of enhancing the production of IL-17A from PBMCs or DC-T cell co-cultures.

We also assessed whether other proinflammatory mediators observed to be triggered by EBV DNA were also triggered by the virus itself. Hence, IFNγ (Figure 7B) and TNF-α (Figure 7C) levels were examined in culture supernatants. A 41.43% increase in the level of IFNγ ($p = 0.0383$) was detected in supernatants from DC and T cell co-cultures in the presence of the virus compared to cells

grown in the absence of the virus; PBMCs, on the other hand, showed a 32.92% ($p = 0.0024$) increase in IL-17A levels when cultured with EBV. EBV DNA was similarly capable of significantly increasing IFN γ from these cell types. Worth noting, is that unlike its inability to enhance production of IL-17A from PBMCs or DC-T cell co-cultures, *S. epidermidis* DNA was able to significantly increase IFN γ levels from these cells. Levels of TNF- α were also significantly elevated upon culturing PBMCs or DCs and T cells with the virus; similar observations were made in cultures of these cells with EBV DNA but not with *S. epidermidis* DNA.

4 Discussion

Infection with EBV has often been associated with autoimmune diseases including RA, SLE, MS, SS, mixed connective tissue disease, dermatomyositis/polymyositis and systemic sclerosis (Draborg et al., 2013). Various mechanisms have been proposed for how EBV infection potentiates autoimmune diseases. For example, multiple human nuclear antigens share epitope similarities with the EBV protein EBNA-1 and antibodies directed against EBNA-1 have been shown to cross react with double stranded DNA (Yadav et al., 2011) and with Ro, a component of several human ribonucleoprotein complexes (McClain et al., 2005). EBNA-1 was also shown to harbor epitopes that share similarities with myelin basic protein, the implicated autoantigen in multiple sclerosis, and with La antigen, which may trigger Sjögren's syndrome, in addition to Sm (the small nuclear ribonucleoprotein) which may play a role in SLE (Poole et al., 2006; Kakalacheva et al., 2011; Carter, 2012). On the other hand, persistent inflammatory responses in infectious mononucleosis, caused by EBV, have been also been suggested to accidentally result in the activation of auto-reactive lymphocytes hence resulting in autoimmunity (Lossius et al., 2012).

We have previously observed that EBV DNA, which is rich in immunostimulatory CpG motifs, enhances the production of IL-17A from mouse cells via endosomal TLR signaling (Shehab et al., 2019). IL-17A is a pro-inflammatory mediator that is prominently associated with autoimmunity. IL-17A is mostly produced by Th17 T-lymphocytes (Huber et al., 2013; Li et al., 2013). This cytokine was shown to increase T cell proliferation, antibody production from B cells and IL-1 and TNF- α secretion from macrophages (Bettelli et al., 2007; Iwakura et al., 2008). Furthermore, IL-17A can promote the release of myeloperoxidase from neutrophils (Zelante et al., 2007) and enhance expression of major histocompatibility complex II (MHC II) molecules on DCs (Banwell et al., 2007). In addition, IL-17A stimulates the release of IL-6 as well as IL-8 from keratinocytes and enhances the expression of these two cytokines by epithelial cells (Bettelli et al., 2007; Iwakura et al., 2008). Additionally, IL-17A is involved in neutrophil proliferation, maturation and chemotaxis processes. By stimulating the expression of inflammatory factors such as IL-6, IL-8, TNF- α and granulocyte-macrophage colony-stimulating factor (GM-CSF), chemokines like KC, MCP-1 and MIP-2 and matrix metalloproteases, IL-17A appears involved in enhancing tissue inflammation (Bettelli et al., 2007; Costa et al., 2010). IL-17A also triggers the expression of antimicrobial peptides such as β -defensin 2 (Liang et al., 2006). In *Candida albicans* infections IL-17A acts on epithelial cells inducing them to produce IL-8, a chemotactic factor for neutrophils which then counteract this fungal infection. In mice with a knocked out IL-17A

receptor, a high fungal burden and a low survival rate were observed (Aggarwal and Gurney, 2002; Huang et al., 2004; Zelante et al., 2007). Contrary to its potentially beneficial effects in counteracting bacterial and fungal infections, IL-17A is believed to be involved in the pathogenesis of various autoimmune diseases. Mice with IL-17A or IL-17A receptor deficiency are less predisposed to experimental autoimmune encephalomyelitis (EAE) induction; these mice develop milder symptoms compared to non-deficient mice (Li et al., 2013; Qu et al., 2013). In autoimmune diseases, IL-17A seems to be often associated with another cytokine, a Th17 inducer, IL-23. Mice deficient in IL-23 or in IL-23 receptor are also not susceptible to EAE induction (Cua et al., 2003; McGeachy et al., 2009; Qu et al., 2013). IL-23 is essential for the survival and expansion of Th17 (Langrish et al., 2005; Bettelli et al., 2007; Burgler et al., 2009; McGeachy et al., 2009; Torchinsky et al., 2009; Qu et al., 2013). The differentiation of naïve T cells to Th17 requires RAR-related orphan receptor gamma (thymus) (ROR γ T), IFN-regulatory factor 4 (IRF4), aryl hydrocarbon receptor (AHR) and STAT3 in addition to TNF- α and IL-6 (Iwakura et al., 2008; Burgler et al., 2009; Costa et al., 2010; Qu et al., 2013). On the other hand, Th17 differentiation is negatively regulated by IFN- γ , IL-4, IL-2, type I IFN, IL-27 (Iwakura et al., 2008) and retinoic acid (Mucida et al., 2007). Although Th17 cells are known for their production of IL-17A, these cells can also express IL-22, IL-21, GM-CSF and potentially TNF- α and IL-1 β (Qu et al., 2013). Hence, the network of proinflammatory mediators we detected to be involved in the response to EBV DNA involves ones that are associated with mediating IL-17A responses or that play a role in its regulation. On the other hand, we observed the downregulation of CTLA4 which is an immunoregulatory marker that suppresses T cell responses (Walker, 2013).

On the other hand, we observed upregulation of TLR3 and 9 with MyD88 detected to be a hub gene in our network analyses. TLRs are receptors that recognize pathogen-associated molecular patterns (PAMPs) and MyD88 is an adaptor protein that relays TLR signaling to downstream mediators. The TLR-MyD88 pathway has been implicated in autoimmune diseases (Devarapu and Anders, 2018; Zheng et al., 2019). Various pattern recognition receptors (PRRs) have been documented to respond to viral DNA; prominent among these are the Toll-like receptors (TLRs), but multiple other cellular receptors are potentially capable of detecting viral nucleic acids and these include DAI, RIG-I and AIM2 among many others [34]. We did not observe these to be transcriptionally upregulated in response to EBV DNA.

Expression of TLR9, the main TLR to respond to CpG rich DNA, in plasmacytoid DCs (pDCs) is the highest among other TLRs. Similarly, B cells and monocytic cells express TLR9; however, when compared to pDCs, they have lower TLR9 expression levels (Hornung et al., 2002). TLR9 was shown to be restricted to pDCs and not expressed in monocyte-derived DCs and CD11c+ DCs (Jarrossay et al., 2001; Kadowaki et al., 2001; Krug et al., 2001). In mouse secondary lymphoid tissues there are various DC types including CD11chi subsets like CD8 α +, CD4+, the double-negative DCs, and the pDCs which are CD11clow (Vremec et al., 2000; Bjorck, 2001; Nakano et al., 2001). Endosomal TLRs are expressed by all these DC subsets with no significant differences between conventional CD11chi DCs and pDCs. In the study at hand, murine splenic DCs were sorted according to presence of the CD11c marker since we aimed at collecting all DC subsets. Splenic DCs co-cultured with T cell populations mirrored murine PBMC responses

to EBV DNA. Hence, the high level of endosomal TLR expression by DCs likely underlies the potency of these cells to induce an IL-17A response from T-cells. While elicited peritoneal macrophages and splenic B cells were somewhat able to induce a response to EBV DNA, they were less potent in inducing T-cells to produce prominent levels of IL-17A.

On the other hand, our EGSEA analyses predict possible involvement of EBV DNA in IBD. We previously used a *Drosophila melanogaster* model to assess immune responses to EBV DNA (Sherri et al., 2018) and observed that this viral DNA enhances gut inflammatory responses in the fly model (Madi et al., 2021). We also observed enhanced IMD signaling in these flies; the IMD pathway is comparable to TNF receptor signaling in mammalian symptoms. We have similarly reported that EBV DNA exacerbates colitis in a mouse model of IBD (Andari et al., 2021). Hence, the roles played by this viral DNA in exacerbating or triggering inflammatory processes in IBD as well as other proinflammatory disease is worth further investigation.

Owing to the persistent nature of an EBV infection and its ability to cause recurrent infections, viral DNA that is shed would contribute to autoimmune processes on a more or less consistent basis. The EBV DNA cellular sensors along with downstream mediators and cells involved in the proinflammatory response unveiled by our study may serve as therapeutic targets in autoimmune and proinflammatory diseases. Very few studies have attempted to assess the burden of the more than 80 known autoimmune diseases. Conservative estimates in the United States indicate that 5%–8% of the population have an autoimmune disease (Autoimmune Diseases Coordinating Committee, 2002). With more than 90% of the population being EBV seropositive, such therapeutic targets may be useful for the majority of people affected by an autoimmune disease.

Data availability statement

The RNAseq raw data discussed in this publication have been deposited in NCBI's Gene Expression Omnibus (Edgar et al., 2002) and are accessible through GEO Series accession number GSE171757 (<https://www.ncbi.nlm.nih.gov/geo/query/acc.cgi?acc=GSE171757>). All other data is available from the authors upon reasonable request.

References

- Aggarwal, S., and Gurney, A. L. (2002). IL-17: prototype member of an emerging cytokine family. *J. Leukoc. Biol.* 71 (1), 1–8. doi:10.1189/jlb.71.1.1
- Alhamdoosh, M., Ng, M., Wilson, N. J., Sheridan, J. M., Huynh, H., Wilson, M. J., et al. (2017). Combining multiple tools outperforms individual methods in gene set enrichment analyses. *Bioinformatics* 33 (3), 414–424. doi:10.1093/bioinformatics/btw623
- Andari, S., Hussein, H., Fadlallah, S., Jurjus, A. R., Shirinian, M., Hashash, J. G., et al. (2021). Epstein-Barr virus DNA exacerbates colitis symptoms in a mouse model of inflammatory bowel disease. *Viruses* 13 (7), 1272. doi:10.3390/v13071272
- Ascherio, A., and Munger, K. L. (2010). Epstein-barr virus infection and multiple sclerosis: a review. *J. Neuroimmune Pharmacol.* 5 (3), 271–277. doi:10.1007/s11481-010-9201-3
- Autoimmune Diseases Coordinating Committee (2002). "Autoimmune diseases research plan," in *Autoimmune diseases coordinating committee. U.S. Department of health and human services* (United States: National Institutes of Health NIH Publication).
- Balandraud, N., Meynard, J. B., Auger, I., Sovran, H., Mugnier, B., Reviron, D., et al. (2003). Epstein-Barr virus load in the peripheral blood of patients with rheumatoid arthritis: accurate quantification using real-time polymerase chain reaction. *Arthritis Rheum.* 48 (5), 1223–1228. doi:10.1002/art.10933
- Banwell, B., Krupp, L., Kennedy, J., Tellier, R., Tenenbaum, S., Ness, J., et al. (2007). Clinical features and viral serologies in children with multiple sclerosis: a multinational observational study. *Lancet Neurol.* 6 (9), 773–781. doi:10.1016/S1474-4422(07)70196-5
- Bettelli, E., Oukka, M., and Kuchroo, V. K. (2007). T(H)-17 cells in the circle of immunity and autoimmunity. *Nat. Immunol.* 8 (4), 345–350. doi:10.1038/ni0407-345
- Bjorck, P. (2001). Isolation and characterization of plasmacytoid dendritic cells from Flt3 ligand and granulocyte-macrophage colony-stimulating factor-treated mice. *Blood* 98 (13), 3520–3526. doi:10.1182/blood.v98.13.3520
- Blaschke, S., Schwarz, G., Moneke, D., Binder, L., Muller, G., and Reuss-Borst, M. (2000). Epstein-Barr virus infection in peripheral blood mononuclear cells, synovial fluid cells, and synovial membranes of patients with rheumatoid arthritis. *J. Rheumatol.* 27 (4), 866–873.

Ethics statement

The animal study was approved by the Animal Care and Use Committee (IACUC) at the American University of Beirut (AUB). The study was conducted in accordance with the local legislation and institutional requirements.

Author contributions

MS: Data curation, Formal analysis, Methodology, Investigation, Writing—original draft. HH: Data curation, Investigation. SF: Data curation, Investigation. ER: Formal analysis, Funding acquisition, Methodology, Investigation, Project administration, Resources, Supervision, Validation, Writing—review and editing. All authors contributed to the article and approved the submitted version.

Funding

This study was funded by a grant from the Medical Practice Plan (MPP) at the American University of Beirut. The funder did not have any contribution to study design, data collection and analysis, decision to publish, or preparation of the manuscript.

Conflict of interest

The authors declare that the research was conducted in the absence of any commercial or financial relationships that could be construed as a potential conflict of interest.

Publisher's note

All claims expressed in this article are solely those of the authors and do not necessarily represent those of their affiliated organizations, or those of the publisher, the editors and the reviewers. Any product that may be evaluated in this article, or claim that may be made by its manufacturer, is not guaranteed or endorsed by the publisher.

- Burgler, S., Ouaked, N., Bassin, C., Basinski, T. M., Mantel, P. Y., Siegmund, K., et al. (2009). Differentiation and functional analysis of human T(H)17 cells. *J. Allergy Clin. Immunol.* 123 (3), 588–595. doi:10.1016/j.jaci.2008.12.017
- Carter, C. J. (2012). Epstein-Barr and other viral mimicry of autoantigens, myelin and vitamin D-related proteins and of EIF2B, the cause of vanishing white matter disease: massive mimicry of multiple sclerosis relevant proteins by the *Synechococcus* phage. *Immunopharmacol. Immunotoxicol.* 34 (1), 21–35. doi:10.3109/08923973.2011.572262
- Chen, C. J., Lin, K. H., Lin, S. C., Tsai, W. C., Yen, J. H., Chang, S. J., et al. (2005). High prevalence of immunoglobulin A antibody against Epstein-Barr virus capsid antigen in adult patients with lupus with disease flare: case control studies. *J. Rheumatol.* 32 (1), 44–47.
- Costa, V. S., Mattana, T. C., and da Silva, M. E. (2010). Unregulated IL-23/IL-17 immune response in autoimmune diseases. *Diabetes Res. Clin. Pract.* 88 (3), 222–226. doi:10.1016/j.diabres.2010.03.014
- Cua, D. J., Sherlock, J., Chen, Y., Murphy, C. A., Joyce, B., Seymour, B., et al. (2003). Interleukin-23 rather than interleukin-12 is the critical cytokine for autoimmune inflammation of the brain. *Nature* 421 (6924), 744–748. doi:10.1038/nature01355
- Devarapu, S. K., and Anders, H. J. (2018). Toll-like receptors in lupus nephritis. *J. Biomed. Sci.* 25 (1), 35. doi:10.1186/s12929-018-0436-2
- Draborg, A. H., Duus, K., and Houen, G. (2012). Epstein-Barr virus and systemic lupus erythematosus. *Clin. Dev. Immunol.* 2012, 370516. doi:10.1155/2012/370516
- Draborg, A. H., Duus, K., and Houen, G. (2013). Epstein-Barr virus in systemic autoimmune diseases. *Clin. Dev. Immunol.* 2013, 535738. doi:10.1155/2013/535738
- Edgar, R., Domrachev, M., and Lash, A. E. (2002). Gene Expression Omnibus: NCBI gene expression and hybridization array data repository. *Nucleic Acids Res.* 30 (1), 207–210. doi:10.1093/nar/30.1.207
- Fiola, S., Gosselin, D., Takada, K., and Gosselin, J. (2010). TLR9 contributes to the recognition of EBV by primary monocytes and plasmacytoid dendritic cells. *J. Immunol.* 185 (6), 3620–3631. doi:10.4049/jimmunol.0903736
- Fox, R. I., Chilton, T., Scott, S., Benton, L., Howell, F. V., and Vaughan, J. H. (1987). Potential role of Epstein-Barr virus in Sjogren's syndrome. *Rheum. Dis. Clin. North Am.* 13 (2), 275–292. doi:10.1016/s0889-857x(21)00847-4
- Gross, A. J., Hochberg, D., Rand, W. M., and Thorley-Lawson, D. A. (2005). EBV and systemic lupus erythematosus: a new perspective. *J. Immunol.* 174 (11), 6599–6607. doi:10.4049/jimmunol.174.11.6599
- Hornung, V., Rothenfusser, S., Britsch, S., Krug, A., Jahrsdorfer, B., Giese, T., et al. (2002). Quantitative expression of toll-like receptor 1-10 mRNA in cellular subsets of human peripheral blood mononuclear cells and sensitivity to CpG oligodeoxynucleotides. *J. Immunol.* 168 (9), 4531–4537. doi:10.4049/jimmunol.168.9.4531
- Huang, W., Na, L., Fidel, P. L., and Schwarzenberger, P. (2004). Requirement of interleukin-17A for systemic anti-Candida albicans host defense in mice. *J. Infect. Dis.* 190 (3), 624–631. doi:10.1086/422329
- Huber, M., Heink, S., Pagenstecher, A., Reinhard, K., Ritter, J., Visekruna, A., et al. (2013). IL-17A secretion by CD8+ T cells supports Th17-mediated autoimmune encephalomyelitis. *J. Clin. Invest.* 123 (1), 247–260. doi:10.1172/JCI63681
- Iwakiri, D. (2014). Epstein-Barr virus-encoded RNAs: key molecules in viral pathogenesis. *Cancers (Basel)* 6 (3), 1615–1630. doi:10.3390/cancers6031615
- Iwakura, Y., Nakae, S., Saijo, S., and Ishigame, H. (2008). The roles of IL-17A in inflammatory immune responses and host defense against pathogens. *Immunol. Rev.* 226, 57–79. doi:10.1111/j.1600-065X.2008.00699.x
- James, J. A., Kaufman, K. M., Farris, A. D., Taylor-Albert, E., Lehman, T. J., and Harley, J. B. (1997). An increased prevalence of Epstein-Barr virus infection in young patients suggests a possible etiology for systemic lupus erythematosus. *J. Clin. Invest.* 100 (12), 3019–3026. doi:10.1172/JCI119856
- Jarrossay, D., Napolitani, G., Colonna, M., Sallusto, F., and Lanzavecchia, A. (2001). Specialization and complementarity in microbial molecule recognition by human myeloid and plasmacytoid dendritic cells. *Eur. J. Immunol.* 31 (11), 3388–3393. doi:10.1002/1521-4141(200111)31:11<3388::aid-immu3388>3.0.co;2-q
- Kadowaki, N., Ho, S., Antonenko, S., Malefyt, R. W., Kastelein, R. A., Bazan, F., et al. (2001). Subsets of human dendritic cell precursors express different toll-like receptors and respond to different microbial antigens. *J. Exp. Med.* 194 (6), 863–869. doi:10.1084/jem.194.6.863
- Kakalacheva, K., Munz, C., and Lunemann, J. D. (2011). Viral triggers of multiple sclerosis. *Biochim. Biophys. Acta* 1812 (2), 132–140. doi:10.1016/j.bbdis.2010.06.012
- Kang, I., Quan, T., Nolasco, H., Park, S. H., Hong, M. S., Crouch, J., et al. (2004). Defective control of latent Epstein-Barr virus infection in systemic lupus erythematosus. *J. Immunol.* 172 (2), 1287–1294. doi:10.4049/jimmunol.172.2.1287
- Kieff, E., Dambaugh, T., Heller, M., King, W., Cheung, A., van Santen, V., et al. (1982). The biology and chemistry of Epstein-Barr virus. *J. Infect. Dis.* 146 (4), 506–517. doi:10.1093/infdis/146.4.506
- Krug, A., Towarowski, A., Britsch, S., Rothenfusser, S., Hornung, V., Bals, R., et al. (2001). Toll-like receptor expression reveals CpG DNA as a unique microbial stimulus for plasmacytoid dendritic cells which synergizes with CD40 ligand to induce high amounts of IL-12. *Eur. J. Immunol.* 31 (10), 3026–3037. doi:10.1002/1521-4141(200110)31:10<3026::aid-immu3026>3.0.co;2-h
- Langrish, C. L., Chen, Y., Blumenschein, W. M., Mattson, J., Basham, B., Sedgwick, J. D., et al. (2005). IL-23 drives a pathogenic T cell population that induces autoimmune inflammation. *J. Exp. Med.* 201 (2), 233–240. doi:10.1084/jem.20041257
- Larsen, M., Sauce, D., Deback, C., Arnaud, L., Mathian, A., Miyara, M., et al. (2011). Exhausted cytotoxic control of Epstein-Barr virus in human lupus. *PLoS Pathog.* 7 (10), e1002328. doi:10.1371/journal.ppat.1002328
- Li, Z., Li, K., Zhu, L., Kan, Q., Yan, Y., Kumar, P., et al. (2013). Inhibitory effect of IL-17 on neural stem cell proliferation and neural cell differentiation. *BMC Immunol.* 14, 20. doi:10.1186/1471-2172-14-20
- Liang, S. C., Tan, X. Y., Luxenberg, D. P., Karim, R., Dunussi-Joannopoulos, K., Collins, M., et al. (2006). Interleukin (IL)-22 and IL-17 are coexpressed by Th17 cells and cooperatively enhance expression of antimicrobial peptides. *J. Exp. Med.* 203 (10), 2271–2279. doi:10.1084/jem.20061308
- Lindsey, J. W., Hatfield, L. M., Crawford, M. P., and Patel, S. (2009). Quantitative PCR for Epstein-Barr virus DNA and RNA in multiple sclerosis. *Mult. Scler.* 15 (2), 153–158. doi:10.1177/1352458508097920
- Lossius, A., Johansen, J. N., Torkildsen, O., Vartdal, F., and Holmoy, T. (2012). Epstein-Barr virus in systemic lupus erythematosus, rheumatoid arthritis and multiple sclerosis-association and causation. *Viruses* 4 (12), 3701–3730. doi:10.3390/v4123701
- Lotz, M., and Roudier, J. (1989). Epstein-Barr virus and rheumatoid arthritis: cellular and molecular aspects. *Rheumatol. Int.* 9 (3–5), 147–152. doi:10.1007/BF00271872
- Lucas, R. M., Hughes, A. M., Lay, M. L., Ponsonby, A. L., Dwyer, D. E., Taylor, B. V., et al. (2011). Epstein-Barr virus and multiple sclerosis. *J. Neurol. Neurosurg. Psychiatry* 82 (10), 1142–1148. doi:10.1136/jnnp-2011-300174
- Lunemann, J. D., Edwards, N., Muraro, P. A., Hayashi, S., Cohen, J. I., Munz, C., et al. (2006). Increased frequency and broadened specificity of latent EBV nuclear antigen-1-specific T cells in multiple sclerosis. *Brain* 129 (6), 1493–1506. doi:10.1093/brain/awl067
- Lunemann, J. D., Huppke, P., Roberts, S., Bruck, W., Gartner, J., and Munz, C. (2008). Broadened and elevated humoral immune response to EBNA1 in pediatric multiple sclerosis. *Neurology* 71 (13), 1033–1035. doi:10.1212/01.wnl.0000326576.91097.87
- Lunemann, J. D., Kamradt, T., Martin, R., and Munz, C. (2007). Epstein-barr virus: environmental trigger of multiple sclerosis? *J. Virol.* 81 (13), 6777–6784. doi:10.1128/JVI.00153-07
- Madi, J. R., Outa, A. A., Ghannam, M., Hussein, H. M., Shehab, M., Hasan, Z., et al. (2021). *Drosophila melanogaster* as a model system to assess the effect of Epstein-Barr virus DNA on inflammatory gut diseases. *Front. Immunol.* 12, 586930. doi:10.3389/fimmu.2021.586930
- McClain, M. T., Heinlen, L. D., Dennis, G. J., Roebuck, J., Harley, J. B., and James, J. A. (2005). Early events in lupus humoral autoimmunity suggest initiation through molecular mimicry. *Nat. Med.* 11 (1), 85–89. doi:10.1038/nm1167
- McGeachy, M. J., Chen, Y., Tato, C. M., Laurence, A., Joyce-Shaikh, B., Blumenschein, W. M., et al. (2009). The interleukin 23 receptor is essential for the terminal differentiation of interleukin 17-producing effector T helper cells *in vivo*. *Nat. Immunol.* 10 (3), 314–324. doi:10.1038/ni.1698
- Mucida, D., Park, Y., Kim, G., Turovskaya, O., Scott, I., Kronenberg, M., et al. (2007). Reciprocal TH17 and regulatory T cell differentiation mediated by retinoic acid. *Science* 317 (5835), 256–260. doi:10.1126/science.1145697
- Nakano, H., Yanagita, M., and Gunn, M. D. (2001). CD11c(+)B220(+)Gr-1(+) cells in mouse lymph nodes and spleen display characteristics of plasmacytoid dendritic cells. *J. Exp. Med.* 194 (8), 1171–1178. doi:10.1084/jem.194.8.1171
- Pesce, J., Kaviratne, M., Ramalingam, T. R., Thompson, R. W., Urban, J. F., Jr., Cheever, A. W., et al. (2006). The IL-21 receptor augments Th2 effector function and alternative macrophage activation. *J. Clin. Invest.* 116 (7), 2044–2055. doi:10.1172/JCI27727
- Petersen, J., Rhodes, G., Roudier, J., and Vaughan, J. H. (1990). Altered immune response to glycine-rich sequences of Epstein-Barr nuclear antigen-1 in patients with rheumatoid arthritis and systemic lupus erythematosus. *Arthritis Rheum.* 33 (7), 993–1000. doi:10.1002/art.1780330711
- Poole, B. D., Scofield, R. H., Harley, J. B., and James, J. A. (2006). Epstein-Barr virus and molecular mimicry in systemic lupus erythematosus. *Autoimmunity* 39 (1), 63–70. doi:10.1080/08916930500484849
- Qu, N., Xu, M., Mizoguchi, I., Furusawa, J., Kaneko, K., Watanabe, K., et al. (2013). Pivotal roles of T-helper 17-related cytokines, IL-17, IL-22, and IL-23, in inflammatory diseases. *Clin. Dev. Immunol.* 2013, 968549. doi:10.1155/2013/968549
- Rahal, E. A., Hajjar, H., Rajeh, M., Yamout, B., and Abdelnoor, A. M. (2015). Epstein-Barr virus and human herpes virus 6 type A DNA enhance IL-17 production in mice. *Viral Immunol.* 28 (5), 297–302. doi:10.1089/vim.2014.0129
- Salloum, N., Hussein, H. M., Jammaz, R., Jiche, S., Uthman, I. W., Abdelnoor, A. M., et al. (2018). Epstein-Barr virus DNA modulates regulatory T-cell programming in addition to enhancing interleukin-17A production via Toll-like receptor 9. *PLoS One* 13 (7), e0200546. doi:10.1371/journal.pone.0200546
- Shehab, M., Sherri, N., Hussein, H., Salloum, N., and Rahal, E. A. (2019). Endosomal toll-like receptors mediate enhancement of interleukin-17a production triggered by Epstein-Barr virus DNA in mice. *J. Virol.* 93 (20), e00987-19. doi:10.1128/JVI.00987-19

- Sherri, N., Salloum, N., Mouawad, C., Haidar-Ahmad, N., Shirinian, M., and Rahal, E. A. (2018). Epstein-Barr virus DNA enhances dipterin expression and increases hemocyte numbers in *Drosophila melanogaster* via the immune deficiency pathway. *Front. Microbiol.* 9, 1268. doi:10.3389/fmicb.2018.01268
- Shirodaria, P. V., Haire, M., Fleming, E., Merrett, J. D., Hawkins, S. A., and Roberts, S. D. (1987). Viral antibody titers. Comparison in patients with multiple sclerosis and rheumatoid arthritis. *Arch. Neurol.* 44 (12), 1237–1241. doi:10.1001/archneur.1987.00520240019006
- Sun, J., Huang, P., Liang, J., Li, J., Shen, M., She, X., et al. (2017). Cooperation of Rel family members in regulating A β 1-40-mediated pro-inflammatory cytokine secretion by retinal pigment epithelial cells. *Cell Death Dis.* 8 (10), e3115. doi:10.1038/cddis.2017.502
- Teng, X., Hu, Z., Wei, X., Wang, Z., Guan, T., Liu, N., et al. (2014). IL-37 ameliorates the inflammatory process in psoriasis by suppressing proinflammatory cytokine production. *J. Immunol.* 192 (4), 1815–1823. doi:10.4049/jimmunol.1300047
- Torchinsky, M. B., Garaude, J., Martin, A. P., and Blander, J. M. (2009). Innate immune recognition of infected apoptotic cells directs T(H)17 cell differentiation. *Nature* 458 (7234), 78–82. doi:10.1038/nature07781
- Tosato, G., Steinberg, A. D., Yarchoan, R., Heilman, C. A., Pike, S. E., De Seau, V., et al. (1984). Abnormally elevated frequency of Epstein-Barr virus-infected B cells in the blood of patients with rheumatoid arthritis. *J. Clin. Invest.* 73 (6), 1789–1795. doi:10.1172/JCI111388
- Vremec, D., Pooley, J., Hochrein, H., Wu, L., and Shortman, K. (2000). CD4 and CD8 expression by dendritic cell subtypes in mouse thymus and spleen. *J. Immunol.* 164 (6), 2978–2986. doi:10.4049/jimmunol.164.6.2978
- Wagner, H. J., Munger, K. L., and Ascherio, A. (2004). Plasma viral load of Epstein-Barr virus and risk of multiple sclerosis. *Eur. J. Neurol.* 11 (12), 833–834. doi:10.1111/j.1468-1331.2004.00871.x
- Walker, L. S. (2013). Treg and CTLA-4: two intertwining pathways to immune tolerance. *J. Autoimmun.* 45, 49–57. doi:10.1016/j.jaut.2013.06.006
- Wandinger, K., Jabs, W., Siekhaus, A., Bubel, S., Trillenber, P., Wagner, H., et al. (2000). Association between clinical disease activity and Epstein-Barr virus reactivation in MS. *Neurology* 55 (2), 178–184. doi:10.1212/wnl.55.2.178
- Warde-Farley, D., Donaldson, S. L., Comes, O., Zuberi, K., Badrawi, R., Chao, P., et al. (2010). The GeneMANIA prediction server: biological network integration for gene prioritization and predicting gene function. *Nucleic Acids Res.* 38, W214–W220. doi:10.1093/nar/gkq537
- Yadav, P., Tran, H., Ebegebe, R., Gottlieb, P., Wei, H., Lewis, R. H., et al. (2011). Antibodies elicited in response to EBNA-1 may cross-react with dsDNA. *PLoS One* 6 (1), e14488. doi:10.1371/journal.pone.0014488
- Zelante, T., De Luca, A., Bonifazi, P., Montagnoli, C., Bozza, S., Moretti, S., et al. (2007). IL-23 and the Th17 pathway promote inflammation and impair antifungal immune resistance. *Eur. J. Immunol.* 37 (10), 2695–2706. doi:10.1002/eji.200737409
- Zheng, C., Chen, J., Chu, F., Zhu, J., and Jin, T. (2019). Inflammatory role of TLR-MyD88 signaling in multiple sclerosis. *Front. Mol. Neurosci.* 12, 314. doi:10.3389/fnmol.2019.00314



OPEN ACCESS

EDITED BY

Evangelia Sarandi,
University of Crete, Greece

REVIEWED BY

Robert Cody Sharp,
University of Florida, United States
Dongjun Chung,
The Ohio State University, United States

*CORRESPONDENCE

Guanghua Chen
✉ chgh20031103@163.com

RECEIVED 22 December 2023

ACCEPTED 31 May 2024

PUBLISHED 13 June 2024

CITATION

Cao G, Luo Q, Wu Y and Chen G (2024)
Inflammatory bowel disease and rheumatoid
arthritis share a common genetic structure.
Front. Immunol. 15:1359857.
doi: 10.3389/fimmu.2024.1359857

COPYRIGHT

© 2024 Cao, Luo, Wu and Chen. This is an
open-access article distributed under the terms
of the [Creative Commons Attribution License](#)
(CC BY). The use, distribution or reproduction
in other forums is permitted, provided the
original author(s) and the copyright owner(s)
are credited and that the original publication
in this journal is cited, in accordance with
accepted academic practice. No use,
distribution or reproduction is permitted
which does not comply with these terms.

Inflammatory bowel disease and rheumatoid arthritis share a common genetic structure

Guoling Cao¹, Qinghua Luo², Yunxiang Wu³
and Guanghua Chen^{3*}

¹Department of Anorectal Surgery, The People's Hospital of Cangnan, Wenzhou, China, ²Clinical Medical College, Jiangxi University of Chinese Medicine, Nanchang, China, ³Department of Anorectal Surgery, Affiliated Hospital of Jiangxi University of Chinese Medicine, Nanchang, China

Background: The comorbidity rate of inflammatory bowel disease (IBD) and rheumatoid arthritis (RA) is high; nevertheless, the reasons behind this high rate remain unclear. Their similar genetic makeup probably contributes to this comorbidity.

Methods: Based on data obtained from the genome-wide association study of IBD and RA, we first assessed an overall genetic association by performing the linkage disequilibrium score regression (LDSC) analysis. Further, a local correlation analysis was performed by estimating the heritability in summary statistics. Next, the causality between the two diseases was analyzed by two-sample Mendelian randomization (MR). A genetic overlap was analyzed by the conditional/conjoint false discovery rate (cond/conjFDR) method. LDSC with specific expression of gene analysis was performed to identify related tissues between the two diseases. Finally, GWAS multi-trait analysis (MTAG) was also carried out.

Results: IBD and RA are correlated at the genomic level, both overall and locally. The MR results suggested that IBD induced RA. We identified 20 shared loci between IBD and RA on the basis of a conjFDR of <0.01. Additionally, we identified two tissues, namely spleen and small intestine terminal ileum, which were commonly associated with both IBD and RA.

Conclusion: Herein, we proved the presence of a polygenic overlap between the genetic makeup of IBD and RA and provided new insights into the genetic architecture and mechanisms underlying the high comorbidity between these two diseases.

KEYWORDS

rheumatoid arthritis, inflammatory bowel disease, genetic risk loci, genetic structure, GWAS, gut joint axis

1 Introduction

Inflammatory bowel disease (IBD) is a common, chronic, nonspecific, immunologic clinical disease of the gastrointestinal tract (1). Clinically, the condition is generally categorized as either Crohn's disease (CD) or ulcerative colitis (UC). There are distinct differences between UC and CD. UC typically presents with continuous mucosal inflammatory lesions extending from the rectum to the proximal colon, whereas CD can affect any segment of the gastrointestinal tract and is characterized by transmural inflammation and cobblestone-like changes (2). Patients with IBD commonly experience abdominal pain, increased stool frequency, weight loss, and multiple extra-intestinal symptoms (3, 4). Over the last few decades, the number of people suffering from the disease has increased significantly in Western countries (5). Almost 60,000 cases of IBD were reported worldwide in 2017 (6). Clinically, IBD is associated with several immune-mediated diseases including rheumatoid arthritis (RA) (7). RA is the most common chronic autoimmune disease of the synovial joints (8) and is characterized by intra-articular manifestations, such as the swelling of and deformity in the joints, and extra-articular manifestations, including rheumatoid nodules, vasculitis, pleural effusions, and accelerated atherosclerosis (9). Both IBD and RA are multifactorial diseases influenced by environmental factors. Risk factors for RA include exposure to tobacco smoke, occupational dust, high sodium diet, and excessive red meat consumption (10). Microorganisms such as mycoplasma, Epstein-Barr virus (EBV), porphyromonas, Proteus mirabilis, and Mycobacterium avium paratuberculosis (MAP) have been implicated in the pathogenesis of RA (11, 12). Similarly, IBD is affected by smoking, psychological stressors, pollutants in the air and water, dietary habits, and bacterial and viral infections (13–15).

IBD and RA analysis at the genetic level may reveal potential associations between them. TNF-like ligand 1A (TL1A), a common genetic risk locus between IBD and RA, competitively binds to death receptor 3 (DR3) or decoy receptor 3 (DcR3), stimulates downstream signaling pathways, and affects the regulation of effector cell proliferation, activation, and apoptosis and the production of cytokines and chemokines, which eventually affect IBD and RA progression (16, 17). Additionally, polymorphisms in the interferon regulatory factor 5 (IRF5) and TNF receptor superfamily member 14 (TNFRSF14) motifs can predispose the susceptibility of IBD and RA (18–21). Presently, detailed studies on mining shared genetic risk loci between IBD and RA are lacking; therefore, herein, we focused on identifying risk loci for these comorbidities.

Existing genome-wide association studies (GWAS) are developing rapidly over time, and GWAS on IBD and RA can help elucidate the underlying genetic mechanisms. While conducting common genetic structure analysis of complex diseases, it is not advisable to simply take the GWAS sites shared by two diseases. The reason is their genetic risk architecture is generally dependent on common genetic variants having small effect sizes, which can easily lead to false-negative results (22). Nevertheless, this error can be avoided by employing some novel genetic statistics methods and the genetic architecture of both diseases can be effectively studied (23–25). To better understand

the common genetic structure between IBD and RA, we employed such methods.

In the present study, we first analyzed overall and local genetic correlations; a linkage disequilibrium score regression (LDSC) analysis was performed for the former (26), whereas estimated heritability in summary statistics (HESS) was performed for the latter (27). Subsequently, Mendelian randomization (MR) was used for analyzing causal correlations (28). Additionally, we investigated the potential genetic correlation between IBD and RA regarding a multigene overlap by following the conditional/conjoint false discovery rate (cond/conjFDR) method, which helped identify concordant genetic risk variant loci (29). The LDSC with specific expression of gene (LDSC-SEG) approach was used to identify tissues related to the two diseases (30). Finally, GWAS multitrait analysis (MTAG) was performed for the two diseases (31). We hope that the present study will help better understand shared genetic structures and molecular mechanisms between IBD and RA.

2 Methods and materials

2.1 GWAS data

Data on IBD was collected from the IEU GWAS database (<https://gwas.mrcieu.ac.uk/>), and GWAS summary statistics for IBD (ID: ebi-a-GCST004131), CD (ID: ebi-a-GCST004132) and UC (ID: ebi-a-GCST004133) were obtained from the European Bioinformatics Institute (EBI) database (32). Among them, IBD data includes a total of 59957 samples, including 25042 patients and 34915 healthy controls; The data of CD includes a total of 40266 samples, including 12194 patients and 28072 healthy controls; UC's data includes a total of 45975 samples, including 12366 patients and 33609 healthy controls. The latest summary-level statistics for RA were obtained from the FinnGen GWAS results (<https://r10.finnngen.fi/>) (33), which comprised a total of 12,555 patients with RA and 240,862 controls. All the participants were of European ancestry. We also selected the RA data (ID: ukb-b-9125) from the IEU database for validation. The flow chart of the present study is presented in Figure 1.

2.2 Genetic correlation analysis

LDSC (version 1.0.1) calculates the genetic correlation between two shapes to show the average degree of the sharing of genetic effects between the pairs of traits (30). Genetic correlation (r_g), the most important objective of the present study, ranges from -1 to 1 , with the “ $-$ ” sign denoting a negative correlation and the “ $+$ ” sign denoting a positive correlation. Per the LDSC manual, the first step is to convert all GWAS summary statistics into the LDSC format with the help of the default parameters of `munge_sumstats.py` provided in the package. The second step is to calculate genetic correlations using the `-rg`, `-ref-ld-chr`, and `-w-ld-chr` parameters in `ldsc.py`. The precalculated LD scores passed to the `-ref-ld-chr` and `-w-ld-chr` parameters can be downloaded from <https://alkesgroup.broadinstitute.org/LDSCORE/>. Moreover, information

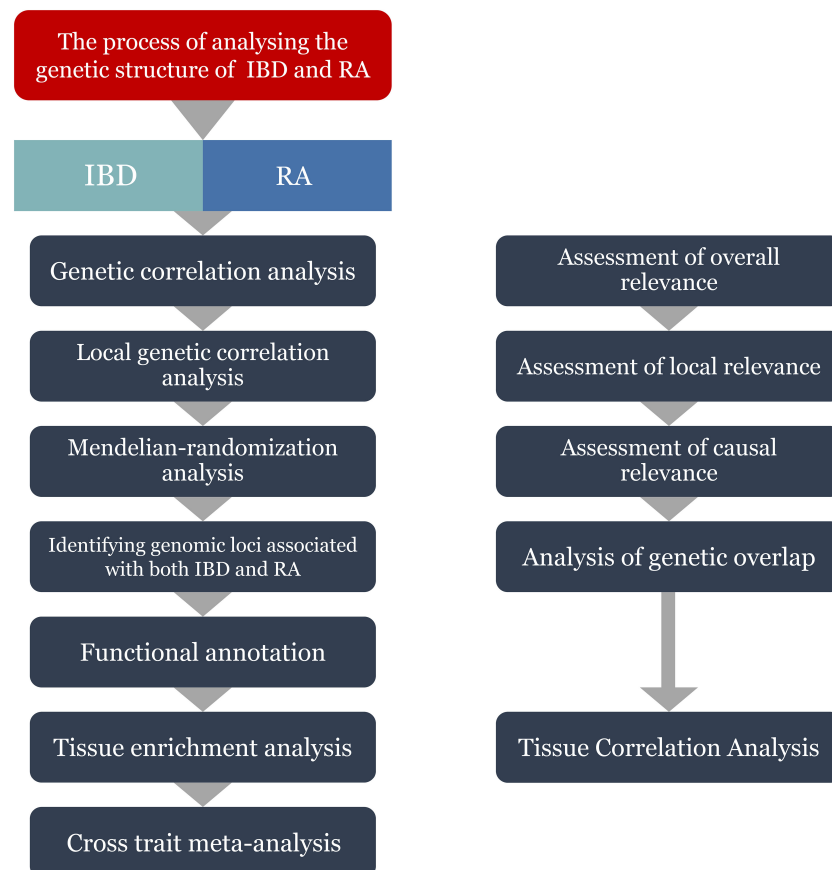


FIGURE 1

Flowchart of the study. IBD, inflammatory bowel disease; RA, Rheumatoid arthritis.

on European pedigrees from the 1000 Genomes Project (34), which was consistent with the European pedigrees of the GWAS samples, was used as a reference panel for chain imbalance.

2.3 Local genetic correlation analysis

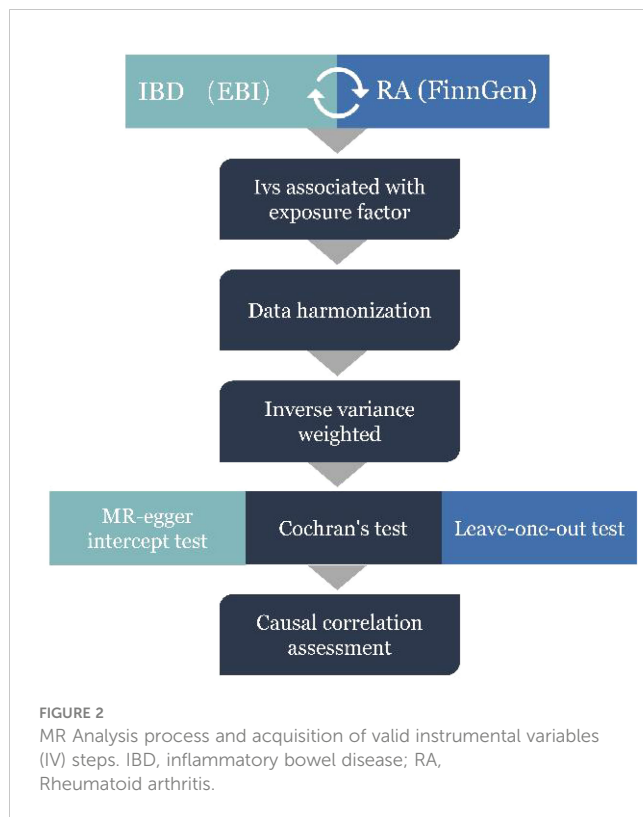
In the local genetic correlation analysis, we investigated 1703 gene segments that were delineated and that should be independent of prespecified LDs. HESS, a novel computational tool, calculates local SNP heritability and measures the degree of similarity between the pairs of traits driven by genetic variation (27). However, the HESS results should be corrected using the Bonferroni method, for which a correlation was considered statistically significant at $P < 0.05/1703 = 2.94E-05$.

2.4 MR analysis

The specific procedure followed for the MR analysis is presented in Figure 2. First, according to the correlation assumption of MR, we set the P-value to be less than 5×10^{-8} to obtain single nucleotide polymorphisms (SNPs) that are closely related to exposure. Second, LD was excluded by setting the r^2 value

to 0.001 and kilobase pairs (kb) to 10 000 (35). Additionally, we manually input all exposure-related SNPs into Phenoscanner (<http://www.phenoscanner.medschl.cam.ac.uk/>) to check for any confounding variables related to outcomes. If confounding variables were present, the corresponding SNPs were deleted to satisfy the assumption that IVs is independent of confounding factors and outcomes.

Pleiotropy, heterogeneity, and sensitivity are important tools for the quality control of the MR analysis results. Based on the results of two polyvalence assessments, MR-Egger regression (36) and MR-PRESSO test (37), we identified abnormal SNPs, which were rejected. The results of inverse variance weighted (IVW) and MR Egger methods, including Cochran's Q statistic and the corresponding P-value, where the P-value is the weighing of the presence and absence of heterogeneity ($P < 0.05$ denoting no heterogeneity), showed heterogeneity. The leave-one-out method eliminates each SNP in turn to calculate the combined effect of the remaining SNPs in order to determine whether the SNP exerts an unfavorable main effect on the overall causal relationship (38). Additionally, we analyzed the eligibility of the included SNPs by calculating the F-value ($F = \beta^2/SE^2$), where β is the effect value of the allele, and SE is the standard error (39). An F-value greater than 10 suggested the eligibility and absence of weak instrumental variables and vice versa (40).



TwosampleMR was used for the MR analysis, and IVW was selected as the stochastic model; this is the most critical method for evaluating analysis results. IVW evaluates the average causal effect between two traits, and the evaluation includes calculating the Wald ratio estimates for each SNP (41). The entire MR analysis is bidirectional.

2.5 Identifying shared genomic loci between IBD and RA

The empirical Bayesian statistical framework of condFDR and conjFDR analyses was used to identify shared genetic risk loci for IBD and RA (42). First, conditional quantile–quantile (Q–Q) plots were generated, which showed overlapping SNP associations among different traits. The conditional Q–Q plot analysis sets SNPs against secondary traits as a reference and evaluates all SNPs against the primary traits. Second, condFDR was used as a reference to reorder the test statistics of the primary trait (e.g., IBD) on the basis of the strength of the association with the secondary trait (e.g., RA) to enhance the feasibility of SNP identification (29). Next, the primary and secondary traits were inverted to perform a reverse condFDR analysis. The loci of the primary and secondary traits were considered significant at $\text{condFDR} \leq 0.01$. Finally, the maximum value of condFDR was set as the value of conjFDR to ensure that the FDR associated with the two traits was more accurate. The entire analysis was performed by directly eliminating SNPs around the major histocompatibility complex expansion region, which improved the accuracy of the FDR

estimates (43). The detailed procedure for the conjFDR analysis is available at <https://github.com/precimed/pleiofdr>.

2.6 Functional annotation

FUMA (44), an online analysis website (available at <https://fuma.ctglab.nl/>), allows for the positional mapping and functional annotation of new, shared, and specific locus. We considered candidate SNPs with $\text{conjFDR} < 0.05$ and $\text{LD } r^2 < 0.6$ with each other as independent significant SNPs. Among them, those SNPs with $\text{LD } r^2 < 0.1$ were designated as lead SNPs. All the candidate SNPs in $\text{LD } r^2 \geq 0.6$ with a lead SNP demarcated the boundaries of a genomic locus. We merged loci separated by less than 250 kb. Therefore, any candidate SNP located within the boundaries of a genomic locus was defined to belong to a single independent genomic locus. We also employed the Combined Annotation Dependent Depletion (CADD), a framework that objectively integrates diverse annotations into a unified quantitative score, which is pivotal in evaluating functional, deleterious, and pathogenic genetic variations. A CADD score exceeding 12.37 signifies harmfulness (45).

We investigated pathway enrichment for the mapped genes. Gene ontology (GO) annotation and Kyoto Encyclopedia of Genes and Genomes (KEGG) pathway enrichment analyses were performed to identify common trends related to the function of differentially expressed genes (46), which was achieved by performing GO annotations of genes from the R package *org.Hs.eg.db* (version 3.1.0). The genes were mapped to the background set, and the enrichment analysis was performed using the R package *clusterProfiler* (version 3.14.3). The minimum gene set included 5 entities and the maximum gene set included 5000 entities, and the P-value and FDR value were set to less than 0.05 and less than 0.1, respectively. For this, the enrichment analysis tool of the Sangerbox platform (<http://vip.sangerbox.com/>) was used (47).

2.7 Tissue enrichment analysis

The LDSC–SEG analysis was performed by considering the tissue gene expression data as a reference and combining the GWAS data of both IBD and RA to identify tissues associated with IBD and RA (30). In this analysis, the t-statistic of each gene expressed in different tissues was calculated, the t-statistic scores of all genes were ranked in ascending order, and the top 10% of the genes were considered as the gene set corresponding to the lesion tissue. Further, the gene sets were divided into strong and weak specific expression gene sets per their intensity. In each gene set, a 100-kb window was set between the front and back of the transcribed region of each gene in order to establish the annotation information of the tissue genome. Finally, GWAS summary statistics were performed to assess the role of focused genome annotation in trait heritability. GTEx (v8) offers insights into 53 distinct tissue types, encompassing data on SNP mutations linked to quantitative traits of gene expression across various tissues (48). S-LDSC

provides preprocessed reference comparison panels for 53 tissues of the GTEx project in this version, which allows researchers to more conveniently evaluate the correlation between tissues and traits. We downloaded and used pre-calculated GTEx project gene expression data as genomic annotations for each tissue to reveal the potential tissue origins of the comorbidity inheritance between IBD and RA. The detailed procedure of the LDSC-SEG analysis is available at <https://github.com/bulik/ldsc/wiki/Cell-type-specific-analyse>.

2.8 Cross-trait meta-analysis

Utilizing Python 3.11.5, we conducted a GWAS multi-trait analysis (MTAG) between IBD and RA to ascertain the risk SNPs significantly associated with both traits (31). MTAG facilitates the joint analysis of GWAS statistical summaries for different traits without potential sample overlap between studies. It is predicated on the establishment of a variance-covariance matrix with shared effect sizes across traits (31). The GWAS derived from MTAG analysis between the two traits was submitted to the FUMA (44) online analysis platform for identification of the associated genetic risk loci.

3 Results

3.1 Genetic correlation

The LDSC analysis results showed 2380 SNPs that were significantly correlated to IBD and 773 SNPs that were significantly correlated to RA. 2076 and 1042 on the CD and UC side, respectively. Excluding the intercept, the probability of inheritance for IBD was 31.3%, whereas that for RA was 2.73%, and a positive correlation was observed between the two ($r_g = 0.1279$, $P = 0.0191$). The correlation of RA with CD ($r_g = 0.1242$, $P = 0.0347$) was also positive, but there was no significant association in terms of UC ($r_g = 0.1006$, $P = 0.0756$). The results of the validation were consistent with the above performance (Table 1).

The local genetic correlation mapping analysis indicated a local genetic overlap between IBD and RA, and the specific site was on two chromosomes, 6 and 12. CD aspects are expressed on chromosomes 1 and 12 and UC on chromosome 6 (Figures 3A-C). Localized

correlations in ukb-b-9125 are enriched on chromosomes 1 and 6 (Supplementary Figures 1A-C).

3.2 MR

In the MR analysis of IBD on RA orientation, 81 SNPs were studied. The IVW results showed a positive causal effect of IBD on RA risk ($P = 0.0039$). The leave-one-out analyses showed no potentially affecting SNP-driven causal associations, indicating the reliability of the present results (Figure 4). Additionally, MR-PRESSO showed no horizontal multidirectionality ($P = 0.3873$). The reverse MR analysis showed no significant causal effect of RA on IBD. There was no causal relationship between IBD subtypes and RA (Supplementary Table 1). There were too few reverse dependent instrumental variables, and only positive MR was performed for IBD and ukb-b-9125, with results suggesting no causality (Supplementary Table 1). The F-values for all instrumental variables were greater than 10, which suggested the absence of a bias in the weak instrumental variables (Supplementary Table 1).

3.3 conjFDR analysis to identify shared genomic loci between IBD and RA

The conditional Q-Q plots for IBD and RA showed that when the association significance of one disease increased, the other disease significantly shifted to the left from the expected zero line, which suggested the presence of genetic enrichment and a shared genetic background between IBD (including CD and UC) and RA (Figures 5A-F). The same conclusion was reached with respect to ukb-b-9125 (Supplementary Figures 2A-F). The ConjFDR analysis showed that all genes between the two traits overlapped in a way that the overlapping improved the qualitative confidence and guaranteed that the identified loci belonged to both diseases. At $\text{conjFDR} < 0.01$, there were 20 genetic risk loci shared by IBD GWAS and RA GWAS (Figure 6A; Supplementary Table 2), of which 17 showed the same direction of effect (Supplementary Table 2). For CD and UC, the genetic risk loci were 21 and 13, respectively, of which 16 and 13 showed the same direction of effect (Figures 6B, C; Supplementary Tables 3, 4). Ukb-b-9125 had

TABLE 1 Genetic correlation of RA and IBD(including CD and UC).

Trait1	Trait2	H2(trait1)	H2(trait2)	Rg	Se	P
IBD	RA	0.3130	0.0273	0.1279	0.0546	0.0191
CD	RA	0.4457	0.0273	0.1242	0.0588	0.0347
UC	RA	0.2387	0.0273	0.1006	0.0566	0.0756
IBD	ukb-b-9125	0.3130	0.0045	0.2468	0.0921	0.0074
CD	ukb-b-9125	0.4457	0.0045	0.2450	0.0865	0.0046
UC	ukb-b-9125	0.2387	0.0045	0.1707	0.1092	0.1181

H2: Represents the observed genetic contribution, the larger the better. Rg: Correlation between two traits, r_g ranges from -1 to 1, and the closer the value is to 1 or -1, the stronger the correlation is (plus or minus represents positive and negative correlation). Se: standard error of genetic correlation. P: the statistically significant association is defined to be p.

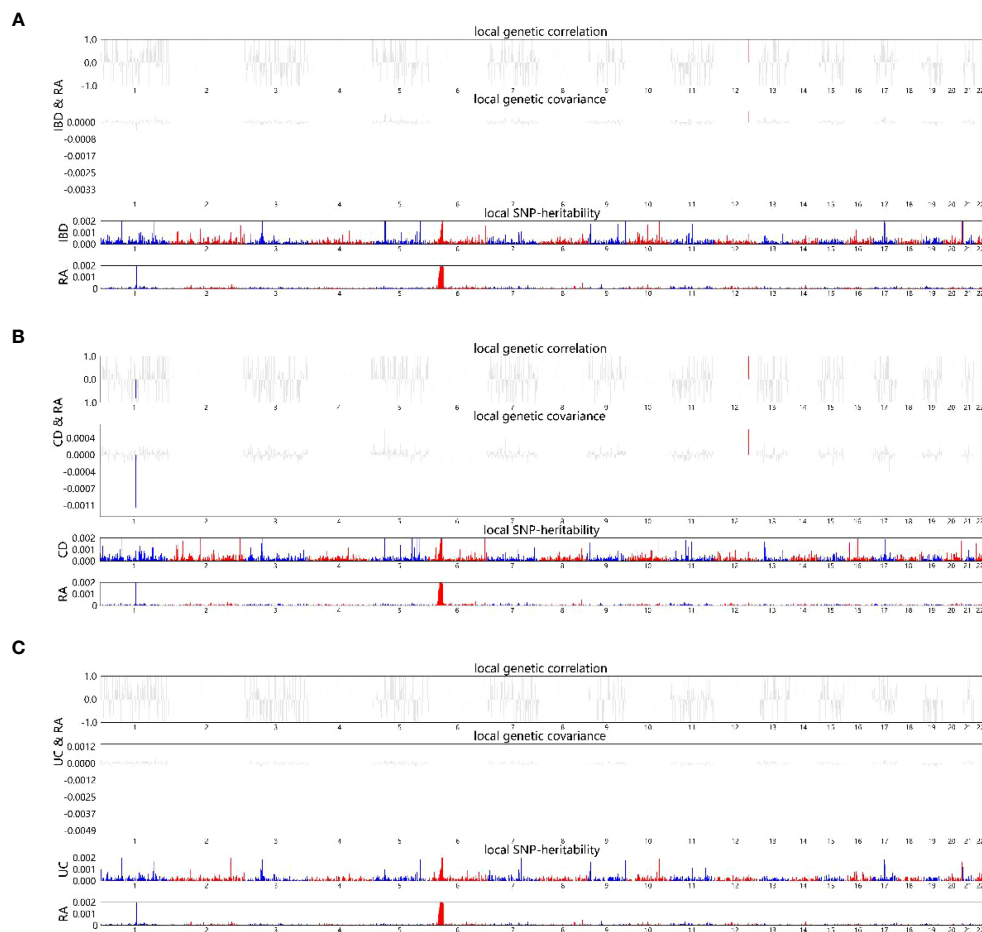


FIGURE 3

HESS analysis of RA and IBD, CD and UC. The top and middle sections of each subgraph represent local genetic correlations and covariances, respectively, and the colored bars represent loci with significant local genetic correlations and covariances. The bottom portion represents the local snp heritability of an individual trait, and the colored bars represent loci with significant local snp heritability. (A) Local genetic correlation between IBD and RA. (B) Local genetic correlation between CD and RA. (C) Local genetic correlation between UC and RA. RA, Rheumatoid arthritis; IBD, inflammatory bowel disease; CD, Crohn's disease; UC, ulcerative colitis.

fewer genetically risk loci between ukb-b-9125 and IBD, CD, and UC, corresponding to 1, 3, and 0, respectively (Supplementary Figures 3A-C).

3.4 Functional annotations

At $\text{concFDR} < 0.01$, a total of 92 mapping genes (Supplementary Table 5) and 1575 candidate SNPs were obtained for IBD and RA, which mainly corresponded to ncRNA_intronic ($n = 544$, 34.8%), intronic ($n = 530$, 34.0%), and intergenic ($n = 327$, 20.9%) functions (Supplementary Table 6). Among the 20 genetic risk loci, the functional attributes intronic, intergenic, ncRNA_intronic, downstream, and ncRNA_exoni corresponded to 9, 5, 3, 2, and 1 SNPs, respectively (Supplementary Table 2). Among these 20 genetic risk loci, the combined annotation-dependent depletion value of the SNP rs353341 exceeded the threshold of 12.37, which indicated that it was deleterious (45). There are 2061 and 1311 candidate SNPs for CD

and UC, respectively (Supplementary Tables 7, 8). For mapping genes, there are 103 for CD and 67 for UC (Supplementary Tables 9, 10).

The GO annotation and KEGG pathway enrichment analyses were performed on the 92 mapped genes in IBD, and the results showed that in terms of biological processes, the top three aspects of gene enrichment were signaling regulation, protein metabolism regulation, and cellular response to cytokine stimulus (Figure 7A). In terms of cellular components, the cytosol, membrane raft, and membrane microdomain were the main directions of gene enrichment (Figure 7B). In terms of molecular functions, genes were mainly enriched for protein kinase binding and kinase binding (Figure 7C). Conversely, the notable pathways analyzed by KEGG were Epstein-Barr virus (EBV) infection, Janus kinase signal transducer and activator of transcription (JAK-STAT) signaling pathway, and Th1 and Th2 cell differentiation (Figure 7D). The results of the enrichment analysis for CD and UC can be seen in Supplementary Figures 4, 5.

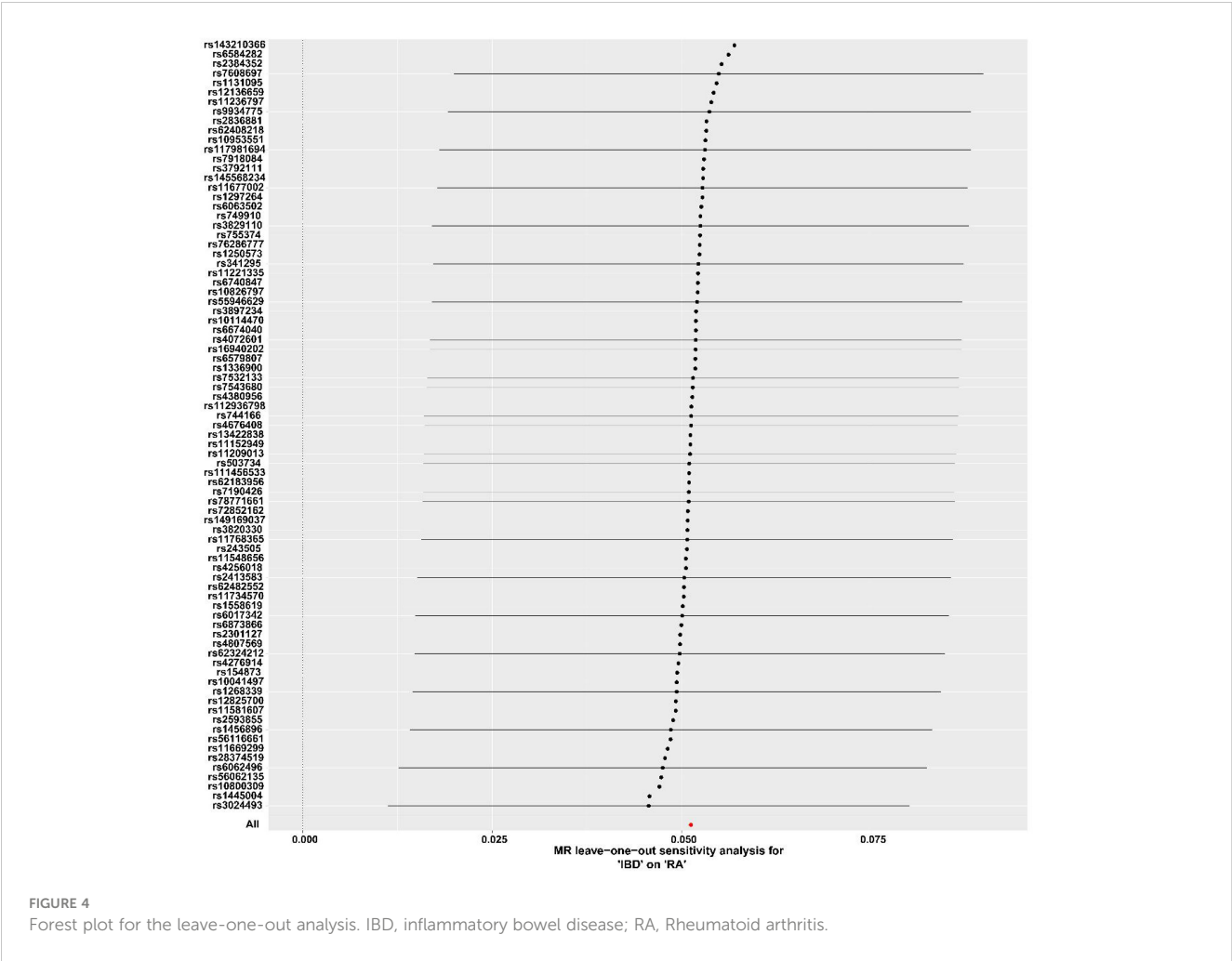


FIGURE 4 Forest plot for the leave-one-out analysis. IBD, inflammatory bowel disease; RA, Rheumatoid arthritis.

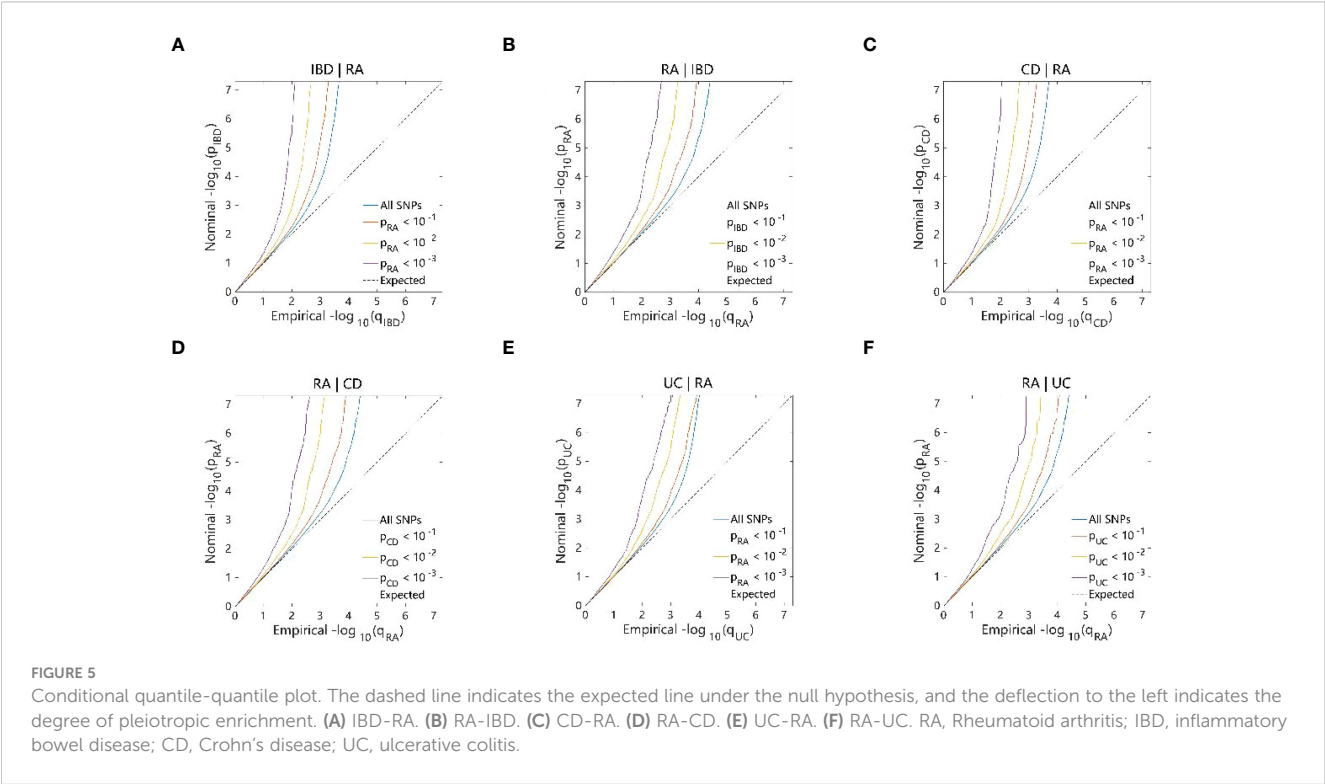


FIGURE 5 Conditional quantile-quantile plot. The dashed line indicates the expected line under the null hypothesis, and the deflection to the left indicates the degree of pleiotropic enrichment. (A) IBD-RA. (B) RA-IBD. (C) CD-RA. (D) RA-CD. (E) UC-RA. (F) RA-UC. RA, Rheumatoid arthritis; IBD, inflammatory bowel disease; CD, Crohn's disease; UC, ulcerative colitis.

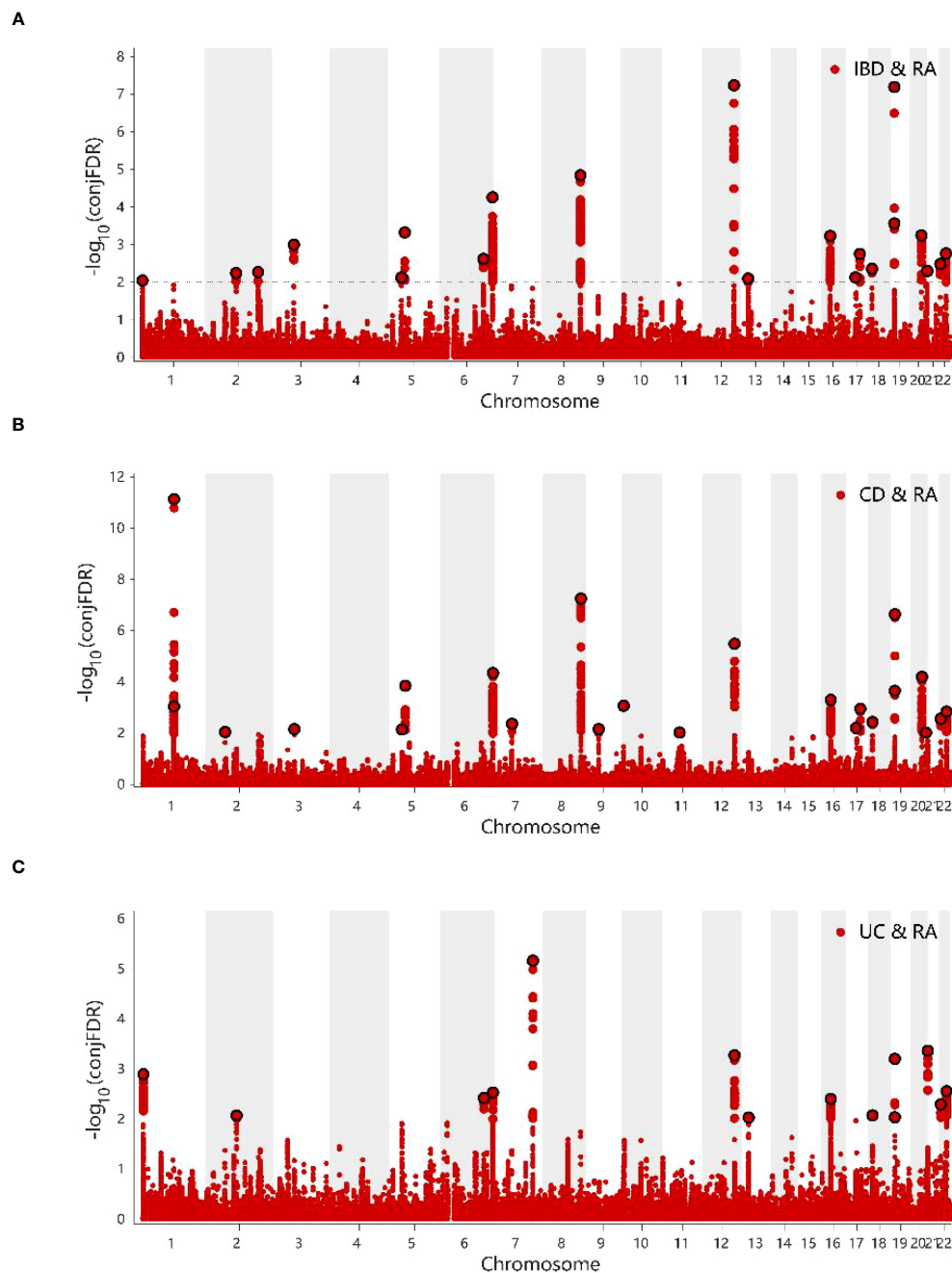


FIGURE 6

(A) ConjFDR Manhattan plot of IBD and RA. (B) ConjFDR Manhattan plot of CD and RA. (C) ConjFDR Manhattan plot of UC and RA. The shared risk loci between RA and IBD, CD and UC were marked. The statistically significant causality is defined to be $\text{conjFDR} < 0.01$. RA, Rheumatoid arthritis; IBD, inflammatory bowel disease; CD, Crohn's disease; UC, ulcerative colitis.

3.5 Trait-related tissue

Based on the tissue expression data from GTEx, we performed additional LDSC-SEG analyses to identify disease-associated tissues. At $P < 0.05$, IBD was associated with the whole blood, lung, spleen, small intestine terminal ileum, EBV-transformed lymphocytes, adipose visceral (omentum), nerve tibial, transverse colon, sun-exposed skin (lower leg), and uterus (Figure 8A; Supplementary Table 11). Tissues that showed a significant correlation with RA were the spleen, whole blood, EBV-

transformed lymphocytes, and small intestine terminal ileum (Figure 8B; Supplementary Table 12). Crohn's disease is closely associated with whole blood, spleen, lungs, terminal ileum of the small intestine, EBV-transforming lymphocytes, fatty viscera (omentum), fallopian tubes, and uterus (Figures 8C; Supplementary Table 13). Tissues significantly associated with UC include the lung, terminal ileum of the small intestine, whole blood, spleen, transverse colon, tibial nerve and bladder (Figures 8D; Supplementary Table 14). LDSC-SEG results for ukb-b-9125 indicated significant associations with spleen tissue as

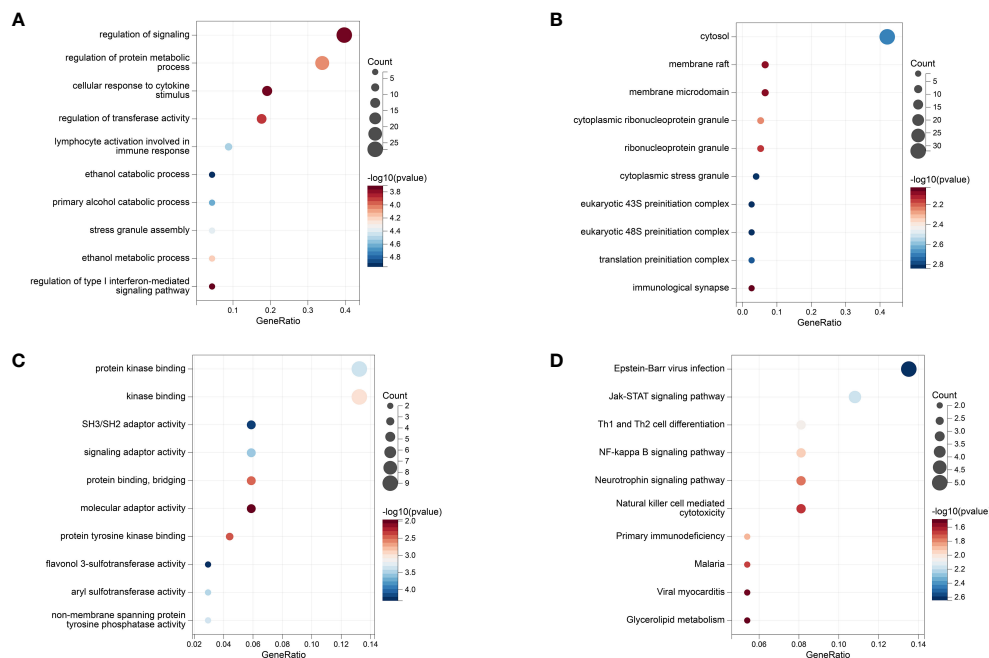


FIGURE 7

The Results of Enrichment analysis. (A) GO enrichment analysis at biological process. (B) GO enrichment analysis at molecular function. (C) GO enrichment analysis at cell composition. (D) KEGG analysis.

well as the terminal ileum of the small intestine; also showing significant association with bladder and mammary gland tissue (Figures 8E; Supplementary Table 15). The spleen and small intestine terminal ileum were common to both diseases, which suggested that IBD and RA might have a common tissue origin. The relevant specific analyses and their results are presented in Supplementary Tables 11–15.

3.6 MTAG

After performing MTAG analysis and Fuma annotation for both IBD and RA, a total of 94 genetic risk loci were identified (Supplementary Table 16). The conjfdr and MTAG analysis revealed the intersection of five genes (FOXP1, RP11-95M15.1, RP11-89M16.1, PTPN2, and UBE2L3) (Supplementary Figure 6A). For CD, we found 80 genetic risk loci (Supplementary Table 17), with the corresponding intersection genes being AC020743.4, RP11-89M16.1, PTPN2, and UBE2L3 (Supplementary Figure 6B). Upon analyzing UC, only 49 genetic risk loci were identified (Supplementary Table 18), with the intersection genes being RP11-95M15.1 and IRF5 from the two analyses (Supplementary Figure 6C).

4 Discussion

In the present study, the results of LDSC and HESS suggested a genetic correlation between IBD and RA, at both the overall and local levels. Subsequently, we performed a conjFDR analysis at the

SNP level to mine novel genetic variants associated with the two shapes of IBD and RA. Finally, considering tissue genetic data as a reference, we performed an LDSC-SEG analysis to obtain two common tissue sources, namely the spleen and small intestine terminal ileum and provided favorable histologic evidence. The present results showed the genetic association between IBD and RA and provided insights into the possible regulatory functions of the shared genetic factors. Nevertheless, the functions need further investigation.

Several existing cross-sectional observational studies have suggested an association between IBD and RA (49–51). Other prospective studies have reported that IBD can increase the risk of RA (52, 53). A meta-analysis of the association between IBD and RA showed that IBD increased RA prevalence (54). These previous results are in line with the present MR results. Additionally, the potential genetic overlap between IBD and RA provided some genetic evidence to support these results. A US retrospective study found that CD patients were more likely to develop RA than UC (55). The findings of a meta-analysis on the risk of rheumatoid arthritis in inflammatory bowel disease have confirmed this (54). The CD and UC are commonly characterized as Th1-dominant and Th2-dominant, respectively (56, 57), while RA is often classified as a Th1-driven disease (58). Therefore, there is a closer relationship between CD and RA. In the overall genetic correlation analysis, we observed that RA was significant with CD and not with UC. A study published by Afroz et al. mentions that the expression of HLA-DOB is significantly upregulated *in vivo* in RA patients (59). The human leukocyte antigen HLA-DOB plays an important role in viral infections by influencing multiple alleles involved in antigen presentation (60, 61). In addition, a previous

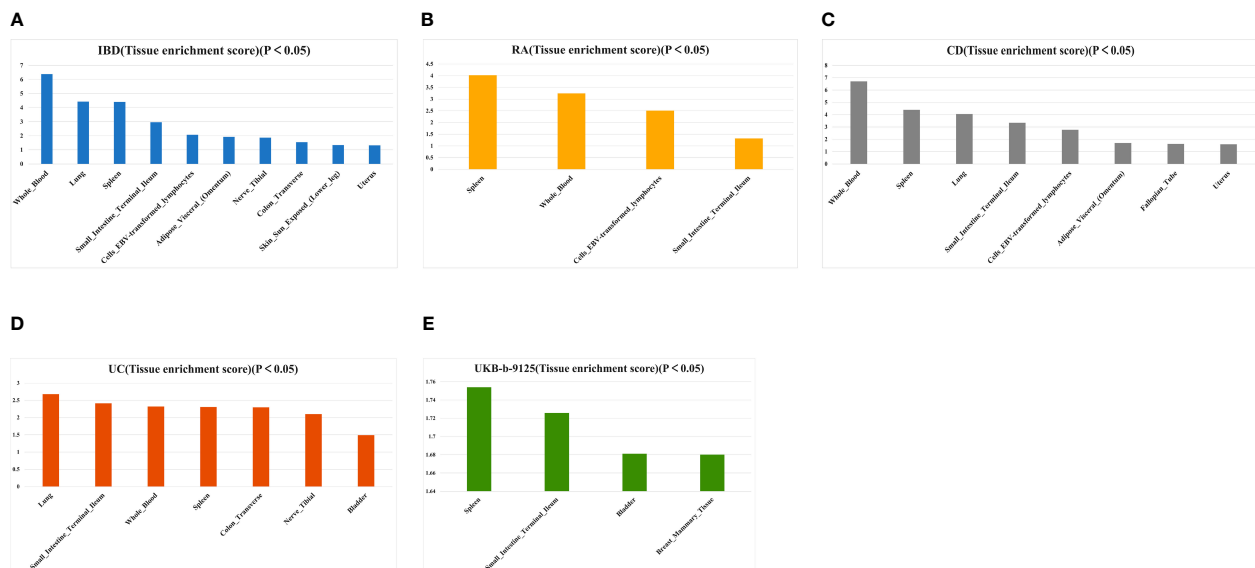


FIGURE 8

Tissues enrichment results of IBD (A), AS (B), CD (C), UC (D), and ukb-b-9125 (E) using gene expression data of 53 tissues from GTEx. RA, Rheumatoid arthritis; IBD, inflammatory bowel disease; CD, Crohn's disease; UC, ulcerative colitis.

analysis of the colonic transcriptome found that HLA-DOB was significantly upregulated in patients with CD, but not in patients with UC (62). From the above, it is clear that HLA-DOB expression and the virus-induced autoimmunity it generates might be the mechanism for the pathogenesis of RA combined with CD. This also provides an explanation for the discordant genetic effects of RA on CD and UC observed in our study.

The gut–joint axis is emerging as a new research hotspot in the biomedical field; however, the action mechanism of the gut–joint axis is poorly understood. A recent study published in *Nature Communications* has reported that patients with newly-onset RA show increased serum connexin levels and decreased intestinal tight junction protein levels. In a mouse model for arthritis, the gut produced inflammatory lesions that developed earlier than did arthritis, and targeting intestinal mucosal proteins alleviated arthritis symptoms (63). The gut–joint axis is associated with the activation of the innate immune system of the host, in which gut microbe-related factors, including short-chain fatty acids, bile acids, and tryptophan and its metabolites, and intestinal flora play a crucial role (64). IBD and RA are immune-mediated diseases, and they interact with each other to form the gut–joint axis, and the overlapping genetic structure may be the potential basis for their action mechanisms.

The results of KEGG-enriched pathways is very interesting. EBV infection disrupts cellular immunity, and its presence increases IBD and RA incidences (65, 66). JAK–STAT signaling is an essential pathway in immunology, which is generally activated, phosphorylated, and dimerized by the phosphorylation of intracellular JAK, which further activates STAT. Then, the proteins migrate to the nucleus as homo/heterodimers to bind to specific DNA-binding sites and eventually participate in the

immunological processes of IBD and RA (67–69). The first-generation JAK inhibitor, tofacitinib, is being considered for IBD and RA treatment (70).

Based on *conjdr* and MTAG analysis, the genes that warrant attention are ubiquitin-conjugating enzyme E2 L3 (UBE2L3) and interferon regulatory factor 5 (IRF5). The former is a significant gene associated with both IBD and CD, while the latter is a significant gene unique to UC. *Conjdr* suggests that they demonstrate a positive association ($Z > 0$) between the two diseases and serve as their susceptibility genes. UBE2L3 encodes a ubiquitin-conjugating enzyme, which regulates interferon and TLR7/9 signaling pathways (71). According to two GWAS studies, UBE4L3 was a possible new risk gene for IBD as it played an important role in intestinal pathogenesis (72, 73). Variation in the UBE2L3 region is a critical locus for altered immune mechanisms in RA (74, 75). Studies have reported a correlation between IRF5 and UC. In a clinical trial investigating thalidomide's efficacy in treating UC, it was found that thalidomide effectively modulated M1 macrophage polarization by targeting IRF5, ultimately leading to an amelioration of inflammation (76). Yang et al. conducted immunohistochemistry, western blotting, and quantitative real-time polymerase chain reaction analyses on peripheral blood and mucosal samples from IBD patients, revealing elevated levels of IRF5 expression significantly correlated with disease activity. This suggests that IRF5 could serve as a potential therapeutic target for UC (18). Furthermore, research indicates that the association between IRF5 and UC extends beyond the European population to include the Han population (77).

The LDSC–SEG analysis indicated that the spleen was associated with both diseases. As the largest secondary lymphoid

organ in the body, the spleen exhibits diverse immune functions and plays a role in hematopoiesis and erythrocyte clearance (78). A study has shown the use of spleen-targeted H2S donor-loaded liposomes for effective immunotherapy against IBD (79). Additionally, splenic sympathetic overactivity drives inflammation and disease progression in immune disorders, such as IBD and RA, via the G-coupled protein receptor kinase pathway (80).

In the present study, we used powerful statistical inference methods, such as conjFDR, to examine the directional association of all overlapping genetic variants; this examination was independent of genetic correlation and improved qualitative confidence. Nevertheless, the study has some limitations. First, our study was conducted on the European population; thus, the present conclusions might not apply to other populations. Second, the identified lead SNPs may be associated with other disease-causing SNPs, and some genetic and environmental risk factors, such as rare variants and infections, may confound the present results. Finally, the validation of an independent cohort was not performed because the present study was based on the methodological aspects of computer simulation with publicly available GWAS data.

5 Conclusion

In conclusion, we obtained evidence for a shared genetic architecture between IBD and RA by targeting large-scale GWAS pooled data and using diverse genomic approaches. Furthermore, we found local and overall genetic correlations and causal associations between IBD and RA by mining genetic risk loci and tissues that were common to both. The present findings provide valuable insights into the shared genetic architecture between IBD and RA, providing necessary information for devising treatment strategies for IBD and RA.

Data availability statement

The original contributions presented in the study are included in the article/**Supplementary Material**. Further inquiries can be directed to the corresponding author.

References

- Ashton JJ, Beattie RM. Personalised therapy for inflammatory bowel disease. *Lancet*. (2019) 393:1672–4. doi: 10.1016/S0140-6736(18)33125-8
- Flynn S, Eisenstein S. Inflammatory bowel disease presentation and diagnosis. *Surg Clin North Am*. (2019) 99:1051–62. doi: 10.1016/j.suc.2019.08.001
- He R, Zhao S, Cui M, Chen Y, Ma J, Li J, et al. Cutaneous manifestations of inflammatory bowel disease: basic characteristics, therapy, and potential pathophysiological associations. *Front Immunol*. (2023) 14:1234535. doi: 10.3389/fimmu.2023.1234535
- Romano L, Pellegrino R, Arcaniolo D, Gravina AG, Miranda A, Priadko K, et al. Lower urinary tract symptoms in patients with inflammatory bowel diseases: A cross-sectional observational study. *Dig Liver Dis*. (2023) 56:628–34. doi: 10.1016/j.dld.2023.10.010. S1590-8658(23)00998-2.
- Kaplan GG. The global burden of IBD: from 2015 to 2025. *Nat Rev Gastroenterol Hepatol*. (2015) 12:720–7. doi: 10.1038/nrgastro.2015.150
- GBD 2017 Inflammatory Bowel Disease Collaborators. The global, regional, and national burden of inflammatory bowel disease in 195 countries and territories, 1990–2017: a systematic analysis for the Global Burden of Disease Study 2017. *Lancet Gastroenterol Hepatol*. (2020) 5:17–30. doi: 10.1016/S2468-1253(19)30333-4
- Colia R, Corrado A, Cantatore FP. Rheumatologic and extraintestinal manifestations of inflammatory bowel diseases. *Ann Med*. (2016) 48:577–85. doi: 10.1080/07853890.2016.1195011
- Gibofsky A. Epidemiology, pathophysiology, and diagnosis of rheumatoid arthritis: A Synopsis. *Am J Manag Care*. (2014) 20:S128–135.

Author contributions

QL: Writing – original draft, Visualization. GCa: Writing – original draft, Methodology, Formal analysis, Data curation, Conceptualization. YW: Writing – original draft, Visualization. GCh: Writing – review & editing, Supervision.

Funding

The author(s) declare that no financial support was received for the research, authorship, and/or publication of this article.

Acknowledgments

The authors thank Bullet Edits Limited for the linguistic editing and proofreading of the manuscript.

Conflict of interest

The authors declare that the research was conducted in the absence of any commercial or financial relationships that could be construed as a potential conflict of interest.

Publisher's note

All claims expressed in this article are solely those of the authors and do not necessarily represent those of their affiliated organizations, or those of the publisher, the editors and the reviewers. Any product that may be evaluated in this article, or claim that may be made by its manufacturer, is not guaranteed or endorsed by the publisher.

Supplementary material

The Supplementary Material for this article can be found online at: <https://www.frontiersin.org/articles/10.3389/fimmu.2024.1359857/full#supplementary-material>

9. Smolen JS, Aletaha D, McInnes IB. Rheumatoid arthritis. *Lancet*. (2016) 388:2023–38. doi: 10.1016/S0140-6736(16)30173-8
10. Deane KD, Demoruelle MK, Kelmenson LB, Kuhn KA, Norris JM, Holers VM. Genetic and environmental risk factors for rheumatoid arthritis. *Best Pract Res Clin Rheumatol*. (2017) 31:3–18. doi: 10.1016/j.berh.2017.08.003
11. Sharp RC, Beg SA, Naser SA. Polymorphisms in protein tyrosine phosphatase non-receptor type 2 and 22 (PTPN2/22) are linked to hyper-proliferative T-cells and susceptibility to mycobacteria in rheumatoid arthritis. *Front Cell Infect Microbiol*. (2018) 8:11. doi: 10.3389/fcimb.2018.00011
12. Li S, Yu Y, Yue Y, Zhang Z, Su K. Microbial infection and rheumatoid arthritis. *J Clin Cell Immunol*. (2013) 4:174. doi: 10.4172/2155-9899.1000174
13. Sharp RC, Beg SA, Naser SA. Role of PTPN2/22 polymorphisms in pathophysiology of Crohn's disease. *World J Gastroenterol*. (2018) 24:657–70. doi: 10.3748/wjg.v24.i6.657
14. Abegunde AT, Muhammad BH, Bhatti O, Ali T. Environmental risk factors for inflammatory bowel diseases: Evidence based literature review. *World J Gastroenterol*. (2016) 22:6296–317. doi: 10.3748/wjg.v22.i27.6296
15. Zhang L, Liu F, Xue J, Lee SA, Liu L, Riordan SM. Bacterial species associated with human inflammatory bowel disease and their pathogenic mechanisms. *Front Microbiol*. (2022) 13:801892. doi: 10.3389/fmicb.2022.801892
16. Xu W-D, Li R, Huang A-F. Role of TL1A in inflammatory autoimmune diseases: A comprehensive review. *Front Immunol*. (2022) 13:891328. doi: 10.3389/fimmu.2022.891328
17. Aiba Y, Nakamura M. The role of TL1A and DR3 in autoimmune and inflammatory diseases. *Mediators Inflammation*. (2013) 2013:258164. doi: 10.1155/2013/258164
18. Yang Y, Zhang C, Jing D, He H, Li X, Wang Y, et al. IRF5 acts as a potential therapeutic marker in inflammatory bowel diseases. *Inflammation Bowel Dis*. (2021) 27:407–17. doi: 10.1093/ibd/izaa200
19. Said NM, Ezzeldin N, Said D, Ebaid AM, Atef DM, Atef RM. HLA-DRB1, IRF5, and CD28 gene polymorphisms in Egyptian patients with rheumatoid arthritis: susceptibility and disease activity. *Genes Immun*. (2021) 22:93–100. doi: 10.1038/s41435-021-00134-8
20. Shui J-W, Kronenberg M. HVEM is a TNF receptor with multiple regulatory roles in the mucosal immune system. *Immune Netw*. (2014) 14:67–72. doi: 10.4110/in.2014.14.2.67
21. Huang H, Huang S-C, Hua D-J, Sun Q-Q, Cen H, Xin X-F. Interaction analysis between BLK rs13277113 polymorphism and BANK1 rs3733197 polymorphism, MMEL1/TNFRSF14 rs3890745 polymorphism in determining susceptibility to rheumatoid arthritis. *Autoimmunity*. (2017) 50:403–8. doi: 10.1080/08916934.2017.1377191
22. Boyle EA, Li YI, Pritchard JK. An expanded view of complex traits: from polygenic to omnigenic. *Cell*. (2017) 169:1177–86. doi: 10.1016/j.cell.2017.05.038
23. Fominykh V, Shadrin AA, Jaholkowski PP, Bahrami S, Athanasios L, Wightman DP, et al. Shared genetic loci between Alzheimer's disease and multiple sclerosis: Crossroads between neurodegeneration and immune system. *Neurobiol Dis*. (2023) 183:106174. doi: 10.1016/j.nbd.2023.106174
24. Hope S, Shadrin AA, Lin A, Bahrami S, Rødevand L, Frei O, et al. Bidirectional genetic overlap between autism spectrum disorder and cognitive traits. *Transl Psychiatry*. (2023) 13:295. doi: 10.1038/s41398-023-02563-7
25. Shang M-Y, Wu Y, Zhang C-Y, Qi H-X, Zhang Q, Huo J-H, et al. Bidirectional genetic overlap between bipolar disorder and intelligence. *BMC Med*. (2022) 20:464. doi: 10.1186/s12916-022-02668-8
26. Bulik-Sullivan B, Finucane HK, Anttila V, Gusev A, Day FR, Loh P-R, et al. Psychiatric Genomics Consortium, Genetic Consortium for Anorexia Nervosa of the Wellcome Trust Case Control Consortium 3, Duncan L, et al. An atlas of genetic correlations across human diseases and traits. *Nat Genet*. (2015) 47:1236–41. doi: 10.1038/ng.3406
27. Shi H, Mancuso N, Spendlove S, Pasaniuc B. Local genetic correlation gives insights into the shared genetic architecture of complex traits. *Am J Hum Genet*. (2017) 101:737–51. doi: 10.1016/j.ajhg.2017.09.022
28. Didelez V, Sheehan N. Mendelian randomization as an instrumental variable approach to causal inference. *Stat Methods Med Res*. (2007) 16:309–30. doi: 10.1177/0962280206077743
29. Smeland OB, Frei O, Shadrin A, O'Connell K, Fan C-C, Bahrami S, et al. Discovery of shared genomic loci using the conditional false discovery rate approach. *Hum Genet*. (2020) 139:85–94. doi: 10.1007/s00439-019-02060-2
30. Bulik-Sullivan BK, Loh P-R, Finucane HK, Ripke S, Yang J. Schizophrenia Working Group of the Psychiatric Genomics Consortium, Patterson N, Daly MJ, Price AL, Neale BM. LD Score regression distinguishes confounding from polygenicity in genome-wide association studies. *Nat Genet*. (2015) 47:291–5. doi: 10.1038/ng.3211
31. Turley P, Walters RK, Maghazian O, Okbay A, Lee JJ, Fontana MA, et al. Multi-trait analysis of genome-wide association summary statistics using MTAG. *Nat Genet*. (2018) 50:229–37. doi: 10.1038/s41588-017-0009-4
32. de Lange KM, Moutsianas L, Lee JC, Lamb CA, Luo Y, Kennedy NA, et al. Genome-wide association study implicates immune activation of multiple integrin genes in inflammatory bowel disease. *Nat Genet*. (2017) 49:256–61. doi: 10.1038/ng.3760
33. Kurki MI, Karjalainen J, Palta P, Sipilä TP, Kristiansson K, Donner KM, et al. FinnGen provides genetic insights from a well-phenotyped isolated population. *Nature*. (2023) 613:508–18. doi: 10.1038/s41586-022-05473-8
34. 1000 Genomes Project Consortium, Auton A, Brooks LD, Durbin RM, Garrison EP, Kang HM, et al. A global reference for human genetic variation. *Nature*. (2015) 526:68–74. doi: 10.1038/nature15393
35. Hemani G, Zheng J, Elsworth B, Wade KH, Haberland V, Baird D, et al. The MR-Base platform supports systematic causal inference across the human phenotype. *Elife*. (2018) 7:e34408. doi: 10.7554/eLife.34408
36. Burgess S, Thompson SG. Interpreting findings from Mendelian randomization using the MR-Egger method. *Eur J Epidemiol*. (2017) 32:377–89. doi: 10.1007/s10654-017-0255-x
37. Verbanck M, Chen C-Y, Neale B, Do R. Detection of widespread horizontal pleiotropy in causal relationships inferred from Mendelian randomization between complex traits and diseases. *Nat Genet*. (2018) 50:693–8. doi: 10.1038/s41588-018-0099-7
38. Gronau QF, Wagenmakers E-J. Limitations of Bayesian leave-one-out cross-validation for model selection. *Comput Brain Behav*. (2019) 2:1–11. doi: 10.1007/s42113-018-0011-7
39. Bowden J, Del Greco MF, Minelli C, Davey Smith G, Sheehan NA, Thompson JR. Assessing the suitability of summary data for two-sample Mendelian randomization analyses using MR-Egger regression: the role of the I² statistic. *Int J Epidemiol*. (2016) 45:1961–74. doi: 10.1093/ije/dyw220
40. Burgess S, Thompson SG. CRPCHD Genetics Collaboration. Avoiding bias from weak instruments in Mendelian randomization studies. *Int J Epidemiol*. (2011) 40:755–64. doi: 10.1093/ije/dyr036
41. Burgess S, Butterworth A, Thompson SG. Mendelian randomization analysis with multiple genetic variants using summarized data. *Genet Epidemiol*. (2013) 37:658–65. doi: 10.1002/gepi.21758
42. Solovieff N, Cotsapas C, Lee PH, Purcell SM, Smoller JW. Pleiotropy in complex traits: challenges and strategies. *Nat Rev Genet*. (2013) 14:483–95. doi: 10.1038/nrg3461
43. Schwartzman A, Lin X. The effect of correlation in false discovery rate estimation. *Biometrika*. (2011) 98:199–214. doi: 10.1093/biomet/asq075
44. Watanabe K, Taskesen E, van Bochoven A, Posthuma D. Functional mapping and annotation of genetic associations with FUMA. *Nat Commun*. (2017) 8:1826. doi: 10.1038/s41467-017-01261-5
45. Kircher M, Witten DM, Jain P, O'Roak BJ, Cooper GM, Shendure J. A general framework for estimating the relative pathogenicity of human genetic variants. *Nat Genet*. (2014) 46:310–5. doi: 10.1038/ng.2892
46. Dennis G, Sherman BT, Hosack DA, Yang J, Gao W, Lane HC, et al. DAVID: database for annotation, visualization, and integrated discovery. *Genome Biol*. (2003) 4:P3. doi: 10.1186/gb-2003-4-5-p3
47. Shen W, Song Z, Zhong X, Huang M, Shen D, Gao P, et al. Sangerbox: A comprehensive, interaction-friendly clinical bioinformatics analysis platform. *iMeta*. (2022) 1:e36. doi: 10.1002/imt2.36
48. Finucane HK, Reshef YA, Anttila V, Slowikowski K, Gusev A, Byrnes A, et al. Heritability enrichment of specifically expressed genes identifies disease-relevant tissues and cell types. *Nat Genet*. (2018) 50:621–9. doi: 10.1038/s41588-018-0081-4
49. Cohen R, Robinson D, Paramore C, Fraeman K, Renahan K, Bala M. Autoimmune disease comorbidity among inflammatory bowel disease patients in the United States, 2001–2002. *Inflammation Bowel Dis*. (2008) 14:738–43. doi: 10.1002/ibd.20406
50. Halling ML, Kjeldsen J, Knudsen T, Nielsen J, Hansen LK. Patients with inflammatory bowel disease have increased risk of autoimmune and inflammatory diseases. *World J Gastroenterol*. (2017) 23:6137–46. doi: 10.3748/wjg.v23.i33.6137
51. Yang BR, Choi N-K, Kim M-S, Chun J, Joo SH, Kim H, et al. Prevalence of extraintestinal manifestations in Korean inflammatory bowel disease patients. *PLoS One*. (2018) 13:e0200363. doi: 10.1371/journal.pone.0200363
52. Park S-W, Kim TJ, Lee JY, Kim ER, Hong SN, Chang DK, et al. Comorbid immune-mediated diseases in inflammatory bowel disease: a nation-wide population-based study. *Aliment Pharmacol Ther*. (2019) 49:165–72. doi: 10.1111/apt.15076
53. Burisch J, Jess T, Egeberg A. Incidence of immune-mediated inflammatory diseases among patients with inflammatory bowel diseases in Denmark. *Clin Gastroenterol Hepatol*. (2019) 17:2704–12.e3. doi: 10.1016/j.cgh.2019.03.040
54. Chen Y, Chen L, Xing C, Deng G, Zeng F, Xie T, et al. The risk of rheumatoid arthritis among patients with inflammatory bowel disease: a systematic review and meta-analysis. *BMC Gastroenterol*. (2020) 20:192. doi: 10.1186/s12876-020-01339-3
55. Martinez EC, Vilchez E, Ng WL, Gautam SS, Gavilanes D, Joseph M, et al. INFLAMMATORY BOWEL DISEASE AND RHEUMATOID ARTHRITIS. *Gastroenterology*. (2024) 166:S37–8. doi: 10.1053/j.gastro.2023.11.110
56. Parronchi P, Romagnani P, Annunziato F, Sampognaro S, Becchio A, Giannarini L, et al. Type 1 T-helper cell predominance and interleukin-12 expression in the gut of patients with Crohn's disease. *Am J Pathol*. (1997) 150:823–32.
57. Heller F, Florian P, Bojarski C, Richter J, Christ M, Hillenbrand B, et al. Interleukin-13 is the key effector Th2 cytokine in ulcerative colitis that affects epithelial tight junctions, apoptosis, and cell restitution. *Gastroenterology*. (2005) 129:550–64. doi: 10.1016/j.gastro.2005.05.002

58. Firestein GS. Evolving concepts of rheumatoid arthritis. *Nature*. (2003) 423:356–61. doi: 10.1038/nature01661
59. Afroz S, Giddaluru J, Vishwakarma S, Naz S, Khan AA, Khan N. A comprehensive gene expression meta-analysis identifies novel immune signatures in rheumatoid arthritis patients. *Front Immunol*. (2017) 8:74. doi: 10.3389/fimmu.2017.00074
60. Denzin LK, Khan AA, Viridis F, Wilks J, Kane M, Beilinson HA, et al. Neutralizing antibody responses to viral infections are linked to the non-classical MHC class II gene H2-Ob. *Immunity*. (2017) 47:310–22.e7. doi: 10.1016/j.immuni.2017.07.013
61. Han J, Chen C, Wang C, Qin N, Huang M, Ma Z, et al. Transcriptome-wide association study for persistent hepatitis B virus infection and related hepatocellular carcinoma. *Liver Int*. (2020) 40:2117–27. doi: 10.1111/liv.14577
62. Yang L, Tang S, Baker SS, Arijis I, Liu W, Alkhouri R, et al. Difference in pathomechanism between Crohn's disease and ulcerative colitis revealed by colon transcriptome. *Inflammation Bowel Dis*. (2019) 25:722–31. doi: 10.1093/ibd/izy359
63. Tajik N, Frech M, Schulz O, Schäfer F, Lucas S, Azizov V, et al. Targeting zonulin and intestinal epithelial barrier function to prevent onset of arthritis. *Nat Commun*. (2020) 11:1995. doi: 10.1038/s41467-020-15831-7
64. Xu X, Wang M, Wang Z, Chen Q, Chen X, Xu Y, et al. The bridge of the gut-joint axis: Gut microbial metabolites in rheumatoid arthritis. *Front Immunol*. (2022) 13:1007610. doi: 10.3389/fimmu.2022.1007610
65. Wei H-T, Xue X-W, Ling Q, Wang P-Y, Zhou W-X. Positive correlation between latent Epstein-Barr virus infection and severity of illness in inflammatory bowel disease patients. *World J Gastrointest Surg*. (2023) 15:420–9. doi: 10.4240/wjgs.v15.i3.420
66. Miljanovic D, Cirkovic A, Jermic I, Basaric M, Lazarevic I, Grk M, et al. Markers of Epstein-Barr virus infection in association with the onset and poor control of rheumatoid arthritis: A prospective cohort study. *Microorganisms*. (2023) 11:1958. doi: 10.3390/microorganisms11081958
67. Hu X, Li J, Fu M, Zhao X, Wang W. The JAK/STAT signaling pathway: from bench to clinic. *Signal Transduct Target Ther*. (2021) 6:402. doi: 10.1038/s41392-021-00791-1
68. Salas A, Hernandez-Rocha C, Duijvestein M, Faubion W, McGovern D, Vermeire S, et al. JAK-STAT pathway targeting for the treatment of inflammatory bowel disease. *Nat Rev Gastroenterol Hepatol*. (2020) 17:323–37. doi: 10.1038/s41575-020-0273-0
69. Hu L, Liu R, Zhang L. Advance in bone destruction participated by JAK/STAT in rheumatoid arthritis and therapeutic effect of JAK/STAT inhibitors. *Int Immunopharmacol*. (2022) 111:109095. doi: 10.1016/j.intimp.2022.109095
70. Shah RJ, Banerjee S, Raychaudhuri S, Raychaudhuri SP. JAK-STAT inhibitors in Immune mediated diseases: An Overview. *IJDVL*. (2023) 89:691–9. doi: 10.25259/IJDVL_1152_2022
71. Mauro D, Manou-Stathopoulou S, Rivellese F, Sciacca E, Goldmann K, Tsang V, et al. UBE2L3 regulates TLR7-induced B cell autoreactivity in Systemic Lupus Erythematosus. *J Autoimmun*. (2023) 136:103023. doi: 10.1016/j.jaut.2023.103023
72. Fransen K, Visschedijk MC, van Sommeren S, Fu JY, Franke L, Festen EAM, et al. Analysis of SNPs with an effect on gene expression identifies UBE2L3 and BCL3 as potential new risk genes for Crohn's disease. *Hum Mol Genet*. (2010) 19:3482–8. doi: 10.1093/hmg/ddq264
73. Kabachiev B, Silverberg MS. Expression quantitative trait loci analysis identifies associations between genotype and gene expression in human intestine. *Gastroenterology*. (2013) 144:1488–1496. doi: 10.1053/j.gastro.2013.03.001
74. Zernakova A, Stahl EA, Trynka G, Raychaudhuri S, Festen EA, Franke L, et al. Meta-analysis of genome-wide association studies in celiac disease and rheumatoid arthritis identifies fourteen non-HLA shared loci. *PLoS Genet*. (2011) 7:e1002004. doi: 10.1371/journal.pgen.1002004
75. Orozco G, Eyre S, Hinks A, Bowes J, Morgan AW, Wilson AG, et al. Study of the common genetic background for rheumatoid arthritis and systemic lupus erythematosus. *Ann Rheum Dis*. (2011) 70:463–8. doi: 10.1136/ard.2010.137174
76. Lu J, Liu D, Tan Y, Li R, Wang X, Deng F. Thalidomide attenuates colitis and is associated with the suppression of M1 macrophage polarization by targeting the transcription factor IRF5. *Dig Dis Sci*. (2021) 66:3803–12. doi: 10.1007/s10620-021-07067-2
77. Li P, Lv H, Yang H, Qian J-M. IRF5, but not TLR4, DEFB1, or VDR, is associated with the risk of ulcerative colitis in a Han Chinese population. *Scand J Gastroenterol*. (2013) 48:1145–51. doi: 10.3109/00365521.2013.828775
78. Lewis SM, Williams A, Eisenbarth SC. Structure-function of the immune system in the spleen. *Sci Immunol*. (2019) 4:eaau6085. doi: 10.1126/sciimmunol.aau6085
79. Oh C, Lee W, Park J, Choi J, Lee S, Li S, et al. Development of spleen targeting H2S donor loaded liposome for the effective systemic immunomodulation and treatment of inflammatory bowel disease. *ACS Nano*. (2023) 17:4327–45. doi: 10.1021/acsnano.2c08898
80. Bellinger DL, Lorton D. Sympathetic nerve hyperactivity in the spleen: causal for nonpathogenic-driven chronic immune-mediated inflammatory diseases (IMIDs)? *Int J Mol Sci*. (2018) 19:1188. doi: 10.3390/ijms19041188



OPEN ACCESS

EDITED BY

Evangelia Sarandi,
University of Crete, Greece

REVIEWED BY

Ting Lei,
Zhejiang University, China
Zewu Zhu,
Central South University, China
Saeed Mohammadi,
Golestan University of Medical Sciences, Iran

*CORRESPONDENCE

Yuan Ma

✉ mayuan_xmu@163.com

Chenyang Li

✉ lichenyang_xmu@163.com

†These authors have contributed equally to this work

RECEIVED 21 February 2024

ACCEPTED 30 October 2024

PUBLISHED 22 November 2024

CITATION

Ren Z, He L, Wang J, Shu L, Li C and Ma Y (2024) The harmful effect of ankylosing spondylitis on diabetes mellitus: new evidence from the Mendelian randomization analysis. *Front. Endocrinol.* 15:1369466. doi: 10.3389/fendo.2024.1369466

COPYRIGHT

© 2024 Ren, He, Wang, Shu, Li and Ma. This is an open-access article distributed under the terms of the [Creative Commons Attribution License \(CC BY\)](#). The use, distribution or reproduction in other forums is permitted, provided the original author(s) and the copyright owner(s) are credited and that the original publication in this journal is cited, in accordance with accepted academic practice. No use, distribution or reproduction is permitted which does not comply with these terms.

The harmful effect of ankylosing spondylitis on diabetes mellitus: new evidence from the Mendelian randomization analysis

Zheng Ren^{1†}, Liang He^{2†}, Jing Wang^{1†}, Li Shu¹,
Chenyang Li^{3*} and Yuan Ma^{1*}

¹Xinjiang Institute of Spinal Surgery, Sixth Affiliated Hospital of Xinjiang Medical University, Urumqi, China, ²Institute of General Surgery, Wulumuqi General Hospital of People's Liberation Army (PLA), Urumqi, China, ³Micro Operation of the Third People's Hospital of Xinjiang Uygur Autonomous Region, Urumqi, China

Background: While observational research has highlighted a possible link between ankylosing spondylitis (AS) and type 2 diabetes (T2DM), the quality of evidence remains limited, and the causal relationship is yet to be established. This study aims to explore the causal link between AS and T2DM, as well as its impact on traits related to glucose metabolism.

Method: To infer a causal relationship between AS and various diabetes-related traits, including type 1 diabetes (T1DM), T2DM, blood glucose levels, fasting glucose, glycated hemoglobin, and fasting insulin, we employed Mendelian randomization (MR) analysis. We sourced GWAS summary data for both exposure and outcome variables from the IEU OpenGWAS database, GWAS Catalog, and FinnGen database. To synthesize the results of the MR analyses, we applied meta-analysis techniques using either a fixed or random effects model. For identifying and excluding instrumental variants (IVs) that exhibit horizontal pleiotropy with the outcomes, we utilized the MR-PRESSO method. Sensitivity analyses were conducted using the MR-Egger method, along with Q and I² tests, to ensure the robustness of our findings.

Results: Our analysis revealed a significant association between AS and an increased risk of T1DM with an odds ratio (OR) of 1.5754 (95% CI: 1.2935 to 1.9187) and T2DM with an OR of 1.0519 (95% CI: 1.0059 to 1.1001). Additionally, AS was associated with elevated levels of fasting glucose (beta coefficient = 0.0165, 95% CI: 0.0029 to 0.0301) and blood glucose (beta coefficient = 0.0280, 95% CI: 0.0086 to 0.0474), alongside a decrease in fasting insulin levels (beta coefficient = -0.0190, 95% CI: -0.0330 to -0.0050).

Conclusion: Our findings collectively underscore the detrimental impact of AS on the development of diabetes, highlighting the critical influence of autoimmune disorders in diabetes onset. This provides profound insights into the pathogenesis of diabetes from an immunological standpoint.

KEYWORDS

ankylosing spondylitis, type 1 and 2 diabetes mellitus, glucose metabolism, Mendelian randomization, meta-analysis

Introduction

Ankylosing spondylitis (AS) is classified as an autoimmune condition characterized by chronic inflammation and is often considered a type of spondyloarthritis (SpA) (1). Typically, individuals with AS experience progressive back pain and impairment of axial joints, notably the hips, though peripheral joints may also be affected (2). Beyond joint issues, AS patients frequently contend with extra-articular symptoms such as uveitis, psoriasis, and inflammatory bowel disease (IBD), which accompany the disease's progression (3). Epidemiological data indicate that AS predominantly emerges around the age of 30, with notable gender disparities in incidence rates and symptomatology (4). For instance, females with AS tend to encounter more severe active phases and fatigue more rapidly compared to males (5). Despite advances in early detection and diagnosis, treating AS remains a considerable challenge due to the complex and not fully understood pathophysiology of the disease (6). The development of AS is influenced by a multifaceted interplay of genetic, environmental, and immunological factors (7). Disruptions in both the innate and adaptive immune systems, triggered by genetic and environmental factors, are crucial in AS's pathology (8). Growing evidence indicates that the immune dysregulation seen in patients with ankylosing spondylitis (AS) not only impacts joint health but also disrupts the balance of other bodily systems, thereby increasing the risk of various conditions, including inflammatory bowel disease (IBD), myelodysplastic syndrome, and cardiovascular mortality (9–11). Furthermore, the alterations in glucose metabolism associated with ankylosing spondylitis underscore the complexity of this condition beyond its inflammatory symptoms. Understanding these metabolic changes is essential for developing targeted therapies and enhancing patient management strategies (12).

As of now, over 400 million individuals worldwide have been diagnosed with diabetes, and projections suggest this number could rise to 642 million by 2040, representing a significant and growing global public health challenge (13). Diabetes, a chronic condition marked by disturbances in energy metabolism, can be broadly categorized into type 1 diabetes mellitus (T1DM), type 2 diabetes mellitus (T2DM), and other subtypes based on the underlying

mechanisms involved (13). T1DM primarily results from autoimmune-mediated damage to the pancreas (14), whereas type 2 diabetes mellitus (T2DM) is often linked to metabolic disturbances related to obesity and unhealthy dietary habits (15). Recent research has highlighted the significant impact of immune system dysregulation in the development of T2DM (16). For instance, studies have indicated that chronic activation of IL-1, a key player in the innate immune response, can adversely affect the development of type 2 diabetes. This is due to elevated levels of IL-1 β , which are known to provoke inflammation and impair the function of β -cells (17). Similarly, Biondi and colleagues have documented that thyroid malfunctions stemming from immune disturbances are linked to a heightened risk of diabetes (18). These research findings enhance our comprehension of diabetes' pathogenesis through the lens of immune-related conditions, indicating a possible connection between autoimmune diseases and diabetes.

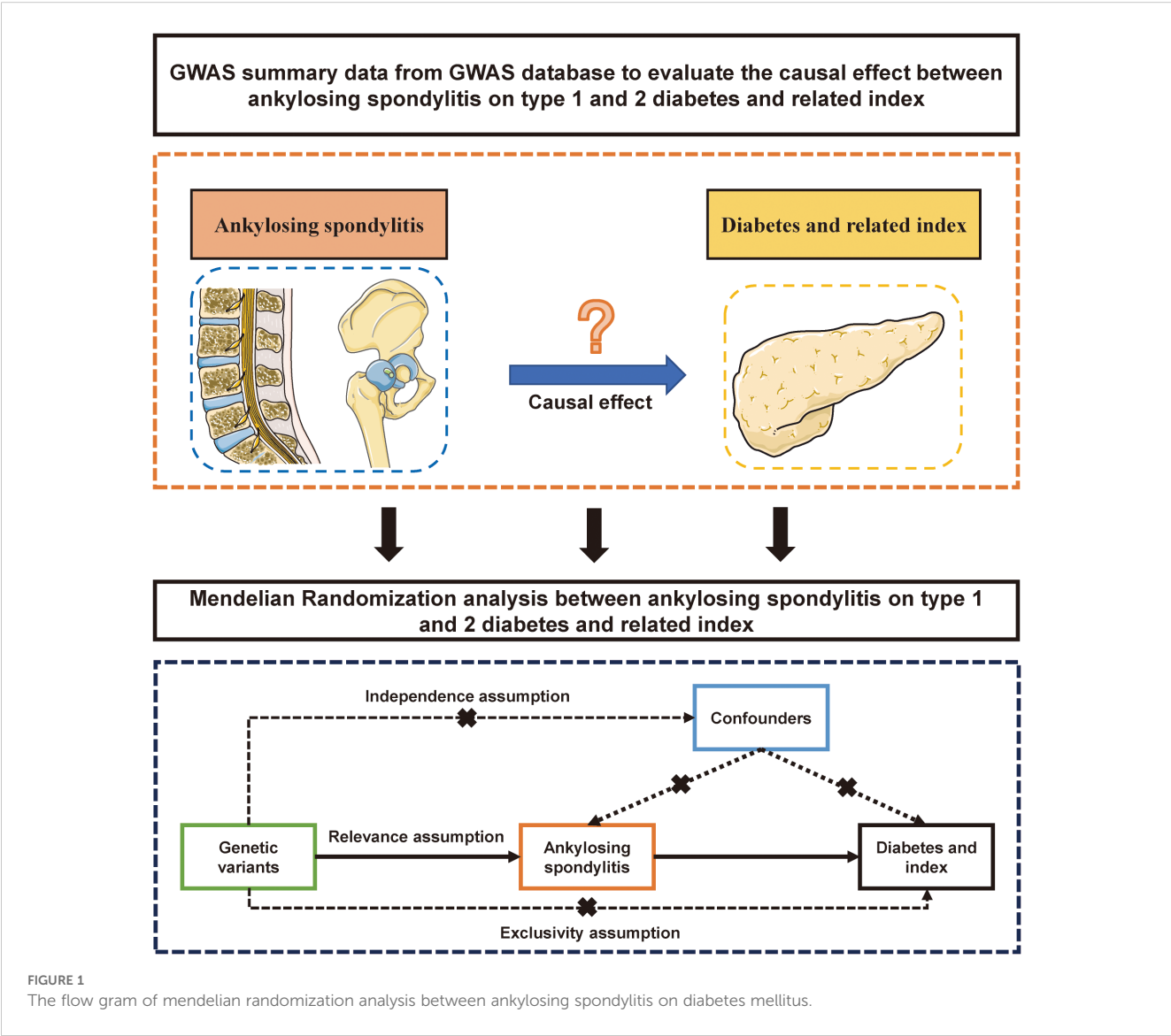
Therefore, the detrimental impact of ankylosing spondylitis (AS) on various bodily systems has sparked our curiosity in examining if AS influences diabetes or glucose metabolism in any way. Notably, two observational studies have highlighted a positive correlation between AS and T2DM (19, 20). Nonetheless, the evidence provided by these observational studies is of a low level, and the presence of unforeseen confounding factors could distort their results. Moreover, determining a causal relationship between AS and diabetes based solely on observational data is challenging. Recently, Mendelian randomization (MR) analysis has emerged as a powerful method for exploring the causal links between exposures and outcomes, offering a more reliable approach to understanding these associations (21). In MR analysis, instrumental variables (IVs), which consist of a collection of single nucleotide polymorphisms (SNPs), are used to mimic the exposure condition. This approach is analogous to randomly allocating individuals to either a treatment or control group, as is done in randomized controlled trials (RCTs) (22). Moreover, MR has the advantage over traditional observational epidemiological studies in that it can significantly reduce the impact of confounding factors, thereby diminishing the biases typically associated with observational research (23). MR serves as a valuable tool for

understanding the complex interplay between autoimmune diseases and various conditions, including metabolic disorders like sarcopenia (24, 25), bronchiectasis (26), and COVID-19 (27). Additionally, variants in TLR genes have been linked to several autoimmune conditions, including type 1 diabetes (T1D), Graves' disease, rheumatoid arthritis, systemic lupus erythematosus (SLE), and multiple sclerosis. These SNPs can disrupt essential signaling pathways, contributing to increased susceptibility to autoimmune disorders (28). The insights gained from these studies underscore the importance of genetic factors in determining disease risk and may inform future research directions aimed at developing targeted interventions for individuals with autoimmune disorders. In our research, we utilized a two-sample MR approach to examine the causal link between AS and diabetes. To our knowledge, this is the inaugural study to explore the causal relationship between AS and diabetes using MR analysis, potentially offering crucial insights into the mechanisms underlying diabetes.

Data and methods

Study design

This research aims to uncover the causal relationship between AS and diabetes, including its related traits, through a two-sample MR analysis. Compared to traditional clinical studies, MR utilizes instrumental variables to assess causal relationships between two factors. For topics where conducting clinical research is particularly challenging, MR studies offer a unique advantage as pioneering exploratory tools. Thus, we considered AS as the exposure and outcomes such as T1DM and T2DM, fasting glucose, fasting insulin, blood glucose, and glycated hemoglobin. Genetic instrumental variables (IVs) were selected to represent AS exposure. In cases where multiple datasets were analyzed using MR, a meta-analysis was conducted to aggregate the results of the MR studies. A detailed schematic flowchart outlining the study's methodology is presented in Figure 1.



Source of GWAS summary dataset

For this study, we utilized the most extensive genome-wide association study (GWAS) summary data available for both the exposure and outcomes, drawing from previous GWAS research. **Table 1** illustrates that the exposure GWAS summary data focused on AS, with an IEU GWAS ID of ebi-a-GCST005529 (Ncase=9069) (29). The outcome GWAS summary datasets covered diabetes and its related traits, sourced from the IEU GWAS database (<https://gwas.mrcieu.ac.uk/>), the FinnGen database (https://www.finnngen.fi/en/access_results), and the UK Biobank database (<http://www.nealelab.is/faq>). These outcome datasets include T1DM, T2DM, blood glucose, fasting glucose, fasting insulin, and

glycated hemoglobin, with sample sizes ranging from six thousand to three hundred thousand. To minimize the potential for ethnic stratification bias, our analysis was restricted to the European population. Further details and the summary data used in our study are provided in **Table 1**.

SNP selection and two-sample Mendelian randomization analysis

We employed the inverse variance weighted (IVW) method, augmented with multiplicative random effects, to assess the causal influence of AS on diabetes and related metabolic traits. Single

TABLE 1 The datasets used in this study from IEU GWAS database and GWAS Catalog database.

Explore or outcomes	PMID	IEUID or GWASID	Ncase	Ncontrol
Explore				
Ankylosing spondylitis	23749187	ebi-a-GCST005529	9,069	13578
Outcomes				
T2D	30054458	ebi-a-GCST006867	61,714	593952
	32499647	ebi-a-GCST010118	77,418	356,122
	29632382	ebi-a-GCST007515	48,286	250,671
	29358691	ebi-a-GCST005413	12,931	57,196
	22885922	ieu-a-24	34,840	114,981
	24509480	ieu-a-23	26,488	83,964
		FinnGen_R9_T2D	57698	308252
T1D	25751624	ebi-a-GCST005536	6,683	12,173
	32005708	ebi-a-GCST010681	9,266	15,574
	33830302	ebi-a-GCST90000529	7,467	10,218
		finn-b-T1D_WIDE	6,729	182,573
Blood glucose	22581228	ebi-a-GCST005186	58,074	
	20081858	ebi-a-GCST000568	46,186	
	25625282	ebi-a-GCST007858	33,231	
Fasting glucose	34059833	ebi-a-GCST90002232	200,622	
	22885924	ieu-b-114	133,010	
	22581228	ieu-b-113	58,074	
Fasting insulin	34059833	ebi-a-GCST90002238	151,013	
	22885924	ieu-b-116	108,557	
	22581228	ieu-b-115	51,750	
	20081858	ebi-a-GCST000571	38,238	
	25625282	ebi-a-GCST007857	30,825	
	31217584	ebi-a-GCST008033	12,687	
Glycated hemoglobin	34059833	ebi-a-GCST90002244	146,806	
		ukb-d-30750_irnt	344182	

T1D, Type 1 diabetes; T2D, Type 2 diabetes.

nucleotide polymorphisms (SNPs) from GWAS summary data served as the genetic instruments for MR analysis. It is crucial that three key assumptions are met before proceeding with MR analysis: 1) The genetic instruments must be significantly associated with the exposure, meaning the SNPs chosen for AS must have a p-value less than 5×10^{-8} , indicating a strong association with the exposure. 2) The selected SNPs should not have a strong association with the outcomes (diabetes and diabetes-related traits) independent of the exposure, with p-values for these outcomes being greater than 5×10^{-5} . 3) The genetic instruments must influence the outcomes solely through their effect on the exposure, ensuring that the identified SNPs impact diabetes and its related traits only via AS. To adhere to these principles, we implemented several strategies for selecting SNPs: 1) We applied an LD clustering algorithm (30) with parameters set to $P \leq 5 \times 10^{-8}$ and $r^2 = 0.001$ to exclude SNPs that may introduce bias due to linkage disequilibrium (LD), thereby minimizing complex LD effects. 2) We restricted the gene windows of SNPs to 100 kb to enhance the precision of our analysis. 3) To mitigate the risk of pleiotropy, which could skew results, we excluded SNPs if five or more were related to the exposure. 4) We calculated the F-value to evaluate the strength of the association between the IVs and both AS and the diabetes-related traits. A standard F-value of more than 20 was used to identify robustly associated SNPs, ensuring the efficacy of the genetic instruments. These meticulous screening methods for SNPs ensure the integrity and reliability of our MR analysis, following the formula provided in reference (31).

$$F = R^2(n - 1 - k)/(1 - R^2)k \quad (1)$$

Where R^2 is represented as instrumental variance, the variate n represents the sample size. The k represented the number of IVs.

When only a single SNP was identified, the Wald ratio method was employed to estimate the causal effect of this specific situation. For instances where the number of SNPs fell between 1 and 3, we implemented a fixed effect model to analyze the data. Conversely, when the number of selected SNPs was 3 or more, we adopted a random effects model alongside the IVW method for MR analysis. The odds ratio (OR) and 95% confidence intervals (CI) were calculated to assess the strength and precision of the causal relationship, with a p-value of less than 0.05 indicating statistical significance. For analyses involving four or more SNPs, the MR-PRESSO test was applied to detect and correct for horizontal pleiotropy, which occurs when genetic variants influence multiple traits in a manner not mediated through the trait of interest. Additionally, to ensure the robustness and reliability of our findings, sensitivity analyses were conducted. These analyses help confirm that the observed associations are not driven by pleiotropic effects of the selected genetic instruments and that the MR results are consistent under different statistical models.

Meta-analysis

To obtain accurate results, we used two types of meta-analysis models in our study: fixed-effect and random-effect models. The

choice of model depended on the similarity of the datasets. We used the fixed-effect model when the studies were similar, assuming a consistent effect size across all studies. Conversely, we used the random-effect model when there was significant variability among the studies, accounting for differences both within and between studies. This approach ensures that our conclusions are robust and consider variations in study populations and designs. Our meta-analysis followed the PRISMA guideline (32). Related studies used specific search terms for retrieval from PubMed, Embase, Cochrane Library: ("spondylitis, ankylosing"[MeSH Terms] OR ("spondylitis"[All Fields] AND "ankylosing"[All Fields]) OR "ankylosing spondylitis"[All Fields] OR ("ankylosing"[All Fields] AND "spondylitis"[All Fields])) AND ("diabetes mellitus"[MeSH Terms] OR ("diabetes"[All Fields] AND "mellitus"[All Fields]) OR "diabetes mellitus"[All Fields]).

Sensitivity analysis

To ensure the robustness and validity of the MR analysis investigating the impact of AS on diabetes and its related metabolic traits, we employed a comprehensive suite of statistical tests, including MR-PRESSO, Egger-intercept test, Cochrane's Q-test, heterogeneity I², and the leave-one-out sensitivity analysis. The MR-PRESSO test was specifically utilized to identify and adjust for any horizontal pleiotropy within our MR findings, initiating a global test for pleiotropy whenever the p-value fell below 0.05. Subsequent to this analysis, SNPs implicated in horizontal pleiotropy were excluded unless their removal resulted in the absence of SNPs for analysis. The Egger-intercept test was then applied to further probe for pleiotropic effects within the MR framework, with a p-value greater than 0.05 indicating an absence of pleiotropic bias. Additionally, Cochrane's Q-test and the calculation of heterogeneity I² were conducted to evaluate the variance in effect sizes across different studies, highlighting significant heterogeneity with p-values less than 0.05 and quantifying it in percentage terms through I². Finally, the leave-one-out sensitivity analysis was performed to test the influence of individual SNPs on the overall MR results, ensuring the stability and reliability of the causal inference by sequentially removing each SNP and recalculating the MR estimates. These analyses were conducted using the R statistical software, supplemented by various packages tailored for Mendelian randomization studies, thereby providing a thorough and reliable assessment of the causal relationship between AS and diabetes-related outcomes.

Ethical statement

The GWAS summary data utilized in this research were obtained from a public database, originally sourced from published studies. These studies had previously received ethical approval from their respective institutional ethics committees, including the completion of informed consent procedures. Consequently, our study did not require further ethical clearance.

Results

Effect of AS on T1DM

Table 1 provides a summary of the baseline GWAS data on type 1 diabetes, including four datasets that encompass 30,175 individuals with AS and 220,538 controls. Figure 2 illustrates the results from the MR analysis conducted using the IVW method, which revealed a consistently positive association between AS and the risk of T1DM across all datasets. Given the lack of significant heterogeneity among the results from the four MR analyses ($I^2 = 0\%$, $p=0.94$), a fixed-effect model was applied to aggregate the findings. The pooled results from the meta-analysis demonstrated that AS significantly elevates the risk of developing T1DM ($OR=1.5754$, $95\%CI: 1.2935 - 1.9187$). Additionally, the MR-Egger, Weighted median, and Weighted mode methods were employed for further analysis (Table 2), all indicating a significantly positive correlation between AS and T1DM across the datasets. Although the MR-Egger method suggested a positive trend, significant heterogeneity was identified in the datasets related to T1DM, prompting the use of the IVW method with multiplicative random effects for MR analysis (detailed in Table 3). The analysis also highlighted SNPs indicative of horizontal pleiotropy with the outcomes (Table 4). Following the identification of these SNPs, they were excluded, and the MR analysis was refined accordingly.

Effect of AS on T2DM

The analysis incorporated seven GWAS summary datasets related to type 2 diabetes, comprising 319,375 patients and 1,765,138 controls. Figure 2 demonstrates that a significantly positive correlation between AS and T2DM was identified in one of the datasets, with an odds ratio (OR) of 1.0910 and a 95%

confidence interval (CI) from 1.0144 to 1.1734. Meanwhile, five datasets displayed a positive association that did not reach statistical significance. Notably, one dataset revealed a non-significant negative correlation between AS and T2DM ($OR= 0.92$, $95\%CI: 0.7928 - 1.0677$). Given the lack of heterogeneity among the datasets ($I^2 = 0$, $p=0.49$), a fixed-effect model was applied to aggregate the results. The pooled analysis from the meta-analysis showed a significantly positive link between AS and T2DM ($OR=1.0519$, $95\%CI: 1.0059 - 1.1001$). Subsequent heterogeneity testing indicated the presence of significant heterogeneity in certain datasets. Consequently, the IVW method with multiplicative random effects was employed for the MR analysis. Additionally, MR-PRESSO analysis was conducted to investigate any SNPs indicative of horizontal pleiotropy with the outcomes, which were then excluded from further analysis as detailed in the subsequent study.

Effect of AS on blood glucose, fasting glucose, and glycated hemoglobin

Our analysis further explored the causal relationship between AS and levels of blood glucose and fasting glucose. According to Figure 3, the analysis included three GWAS summary datasets related to blood glucose, encompassing a total of 137,491 participants. Within these datasets, a significantly positive correlation with blood glucose was noted in one dataset ($\beta = 0.0506$, $95\%CI: 0.0084 - 0.0928$). The remaining two datasets suggested a positive relationship between AS and blood glucose, although these findings did not achieve statistical significance. Owing to the lack of heterogeneity among the datasets, a fixed-effect model was applied to consolidate the MR analysis results. This pooled analysis revealed a significant positive impact of AS on blood glucose levels ($\beta = 0.0280$, $95\% CI: 0.0086 - 0.0470$). Furthermore, alternative analytical approaches including MR-

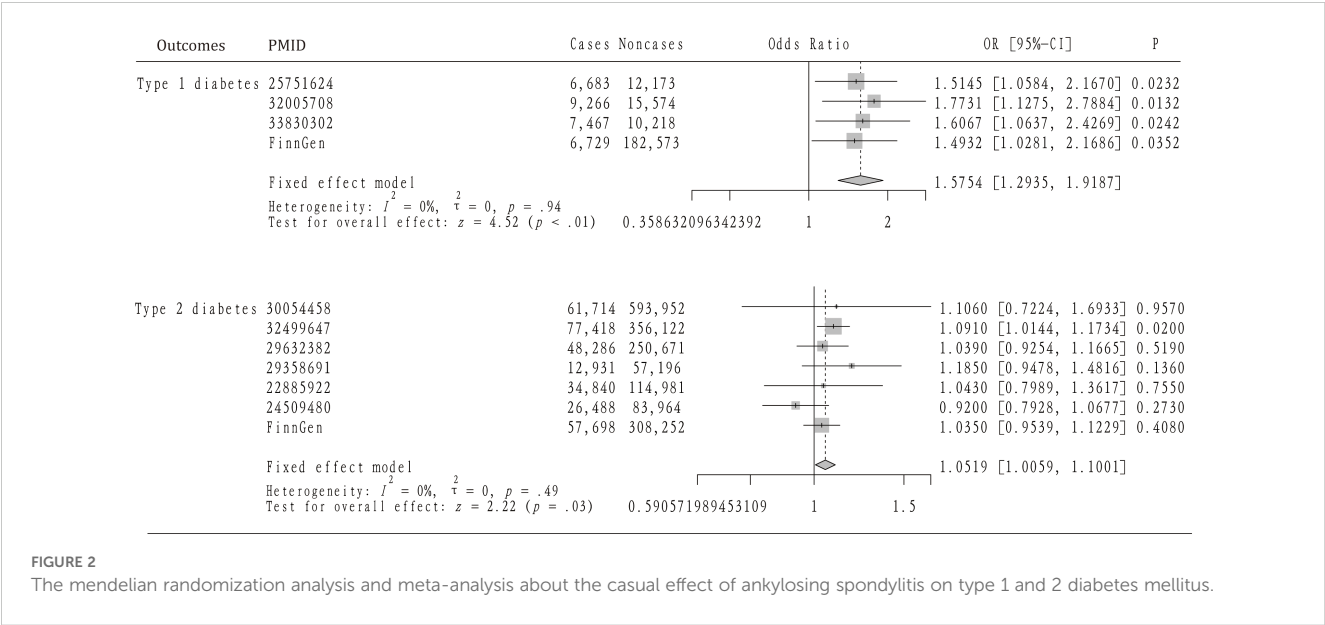


TABLE 2 The Mendelian Randomization analysis between ankylosing spondylitis on diabetes and diabetes-related clinical index based on MR-Egger, Weighted median, and Weighted mode methods.

Exposure	Outcome	Sources	N_SNP	MR-Egger						Weighted median						Weighted mode					
				beta	se	Pval	OR	lower95% CI	upper95% CI	beta	se	Pval	OR	lower95% CI	upper95% CI	beta	se	Pval	OR	lower95% CI	upper95% CI
Ankylosing spondylitis	T1D	ebi-a-GCST005536	17	0.760	0.486	0.139	2.137	0.825	5.536	0.589	0.199	0.003	1.802	1.220	2.663	0.664	0.278	0.030	1.943	1.126	3.350
		ebi-a-GCST010681	20	1.015	0.541	0.077	2.759	0.956	7.966	0.600	0.251	0.017	1.822	1.115	2.977	1.124	0.396	0.011	3.077	1.415	6.689
		ebi-a-GCST90000529	20	1.054	0.478	0.041	2.869	1.124	7.323	0.540	0.214	0.012	1.717	1.129	2.610	0.632	0.226	0.012	1.882	1.207	2.933
		finn-b-T1D_WIDE	20	1.162	0.542	0.046	3.197	1.105	9.249	0.662	0.217	0.002	1.939	1.266	2.970	0.768	0.266	0.009	2.156	1.280	3.631
	T2D	ebi-a-GCST006867	16	0.023	0.064	0.720	1.023	0.904	1.159	0.041	0.045	0.355	1.042	0.955	1.137	0.045	0.046	0.348	1.046	0.955	1.146
		ebi-a-GCST010118	21	0.139	0.062	0.039	1.149	1.017	1.299	0.128	0.041	0.002	1.137	1.049	1.233	0.111	0.039	0.010	1.117	1.034	1.206
		ebi-a-GCST007515	4	-0.032	0.102	0.784	0.969	0.793	1.183	0.039	0.041	0.339	1.040	0.960	1.126	0.038	0.044	0.450	1.039	0.953	1.133
		ebi-a-GCST005413	24	0.202	0.275	0.470	1.224	0.714	2.096	0.167	0.156	0.283	1.182	0.871	1.605	-0.117	0.239	0.629	0.889	0.557	1.421
		ieu-a-23	20	-0.171	0.130	0.204	0.842	0.653	1.087	-0.139	0.085	0.099	0.870	0.737	1.027	-0.139	0.078	0.090	0.870	0.747	1.014
		ieu-a-24	7	-0.238	0.135	0.138	0.788	0.605	1.027	-0.033	0.076	0.662	0.967	0.833	1.123	-0.030	0.072	0.690	0.970	0.842	1.118
		FinnGen_R9_T2D	22	0.020	0.072	0.780	1.021	0.886	1.176	0.020	0.042	0.638	1.020	0.940	1.107	0.016	0.045	0.722	1.016	0.931	1.109
	Fasting insulin	ebi-a-GCST90002238	25	-0.027	0.023	0.250	0.973	0.930	1.018	-0.032	0.013	0.011	0.968	0.944	0.993	-0.029	0.013	0.039	0.972	0.947	0.997
		ieu-b-115	19	-0.012	0.030	0.690	0.988	0.931	1.048	-0.029	0.020	0.143	0.972	0.935	1.010	-0.022	0.020	0.279	0.978	0.941	1.017
		ieu-b-116	5	-0.033	0.019	0.175	0.967	0.932	1.004	-0.021	0.013	0.106	0.979	0.955	1.004	-0.022	0.013	0.171	0.978	0.954	1.004
		ebi-a-GCST000571	19	-0.017	0.037	0.648	0.983	0.915	1.057	-0.040	0.024	0.100	0.961	0.917	1.008	-0.027	0.025	0.296	0.974	0.927	1.022
		ebi-a-GCST007857	4	0.004	0.040	0.934	1.004	0.928	1.086	0.015	0.023	0.533	1.015	0.969	1.062	0.014	0.023	0.578	1.014	0.970	1.061
		ebi-a-GCST008033	25	-0.046	0.079	0.568	0.955	0.818	1.116	-0.043	0.062	0.486	0.958	0.849	1.081	-0.044	0.059	0.461	0.957	0.852	1.074
	Glycated hemoglobin	ebi-a-GCST90002244	22	-0.008	0.013	0.537	0.992	0.966	1.018	-0.006	0.008	0.451	0.994	0.978	1.010	-0.005	0.008	0.508	0.995	0.979	1.010
		ukb-d-30750_irmt	17	0.105	0.053	0.067	1.111	1.001	1.232	0.061	0.024	0.011	1.063	1.014	1.114	0.059	0.027	0.045	1.061	1.006	1.120
	Blood glucose	ebi-a-GCST005186	19	0.019	0.024	0.450	1.019	0.972	1.068	0.024	0.019	0.201	1.024	0.987	1.062	0.021	0.018	0.248	1.022	0.986	1.058
			19	-0.003	0.029	0.928	0.997	0.943	1.055	0.015	0.022	0.483	1.015	0.973	1.060	0.013	0.020	0.532	1.013	0.973	1.054

(Continued)

TABLE 2 Continued

Exposure	Outcome	Sources	N_SNP	MR-Egger						Weighted median						Weighted mode					
				beta	se	Pval	OR	lower95% CI	upper95% CI	beta	se	Pval	OR	lower95% CI	upper95% CI	beta	se	Pval	OR	lower95% CI	upper95% CI
T1D, Type 1 diabetes; T2D, Type 2 diabetes.	Fasting glucose	ebi-a-GCST000568	4																		
		ebi-a-GCST007858		0.050	0.038	0.317	1.051	0.976	1.132	0.050	0.022	0.025	1.051	1.006	1.097	0.052	0.024	0.116	1.054	1.005	1.104
		ebi-a-GCST90002232	24	0.014	0.018	0.428	1.014	0.980	1.050	0.008	0.012	0.476	1.008	0.985	1.032	0.012	0.012	0.299	1.012	0.990	1.036
		ieu-b-114	4	0.012	0.020	0.612	1.012	0.973	1.053	0.014	0.013	0.277	1.014	0.989	1.041	0.014	0.014	0.378	1.015	0.987	1.043
		ieu-b-113	19	0.019	0.024	0.450	1.019	0.972	1.068	0.024	0.019	0.204	1.024	0.987	1.062	0.021	0.017	0.219	1.022	0.989	1.056

Egger, Weighted median, and Weighted mode methods did not identify a significant link between AS and blood glucose. Heterogeneity assessments also confirmed the absence of heterogeneity across the studies (Table 3).

Figure 3 also highlights the inclusion of three GWAS summary datasets related to fasting glucose for analysis, involving a total of 391,706 participants. Across all datasets, a positive correlation between AS and fasting glucose levels was noted, although these observations did not reach statistical significance. Given the uniformity of the MR analysis results, indicating no heterogeneity, a fixed-effect model was implemented for the meta-analysis. This analysis revealed that AS has a modest but positive impact on fasting glucose levels (OR=0.0165, 95%CI: 0.0029 – 0.0301). Furthermore, while not reaching statistical significance, MR analyses employing MR-Egger, Weighted median, and Weighted mode methodologies similarly suggested a positive relationship between AS and fasting glucose. Heterogeneity tests confirmed the lack of significant heterogeneity (Table 3), and MR-PRESSO analysis did not identify any SNPs indicative of horizontal pleiotropy with the outcomes. In addition, two datasets were analyzed concerning glycated hemoglobin, totaling 490,988 participants. Analysis of the UK Biobank (UKB) dataset indicated a significant increase in glycated hemoglobin levels attributable to AS (beta = 0.0566, 95%CI: 0.0151 – 0.0981), a finding not replicated in the second dataset. Due to detected heterogeneity, a random-effects model was utilized to aggregate MR analysis results, which did not establish a significant overall association. The presence of heterogeneity prompted the use of the IVW method with multiplicative random effects for further analysis. Additionally, any SNPs identified as exhibiting horizontal pleiotropy with outcomes were excluded from the MR analysis (Table 4).

Effect of AS on fasting insulin

Figure 3 details the inclusion of six datasets for analyzing the potential causal relationship between AS and fasting insulin levels, with a collective participation of 393,070 individuals. Among these, a single dataset indicated a positive correlation between AS and fasting insulin, though this did not achieve statistical significance. Conversely, the remaining five datasets exhibited a negative correlation between AS and fasting insulin, again without reaching statistical significance. Owing to the consistent results across the datasets, indicating no significant heterogeneity, a fixed-effect model was employed for the meta-analysis. This analysis suggested that AS might significantly reduce fasting insulin levels (OR=-0.0190, 95%CI: -0.1662, -0.0134). Significant heterogeneity was observed in only one dataset, leading to the application of the IVW method with multiplicative random effects for further MR analysis. The MR-PRESSO analysis did not identify any SNPs indicative of horizontal pleiotropy with respect to fasting insulin levels. Scatter plots illustrating the impact of ankylosing spondylitis on diabetes and its related traits can be found in Supplementary Figures S1, 2.

TABLE 3 The sensitivity analysis between ankylosing spondylitis on diabetes and diabetes-related clinical index by MR-PRESSO, Egger intercept, Q-test, and heterogeneity I2 methods.

Exposure	Outcome	Sources	N_SNP	MR-PRESSO				Egger_intercept	Pval	Q_statistics	Pval	Heterogeneity_I ^{2%}
				beta	se	Pval	GlobalTest_Pval					
Ankylosing spondylitis	T1D	ebi-a-GCST005536	17	0.415	0.183	0.037	0.009	-0.014	0.455	32.865	0.008	51
		ebi-a-GCST010681	20	0.573	0.231	0.023	0.001	-0.020	0.377	46.800	0.000	59
		ebi-a-GCST90000529	20	0.474	0.210	0.036	0.001	-0.026	0.196	45.325	0.001	58
		finn-b-T1D_WIDE	20	0.401	0.190	0.049	0.026	-0.028	0.152	32.953	0.024	42
	T2D	ebi-a-GCST006867	16	0.029	0.037	0.451	0.492	0.000	0.917	15.356	0.426	2
		ebi-a-GCST010118	21	0.087	0.037	0.030	0.159	-0.003	0.313	27.718	0.116	28
		ebi-a-GCST007515	4	0.038	0.059	0.565	0.443	0.008	0.480	6.613	0.085	55
		ebi-a-GCST005413	24	0.170	0.114	0.149	0.091	-0.001	0.899	32.034	0.099	28
		ieu-a-23	20	-0.083	0.076	0.287	0.170	0.006	0.412	26.344	0.121	28
		ieu-a-24	7	0.042	0.136	0.766	0.242	0.029	0.036	20.529	0.002	71
		FinnGen_R9_T2D	22	0.034	0.041	0.418	0.017	0.001	0.814	39.234	0.009	46
	Fasting insulin	ebi-a-GCST90002238	25	-0.023	0.013	0.092	0.004	0.000	0.829	48.580	0.002	51
		ieu-b-115	19	-0.030	0.018	0.115	0.102	-0.001	0.473	26.548	0.088	32
		ieu-b-116	5	-0.016	0.011	0.213	0.485	0.002	0.295	2.795	0.593	0
		ebi-a-GCST000571	19	-0.027	0.022	0.222	0.143	-0.001	0.731	25.781	0.105	30
		ebi-a-GCST007857	4	0.023	0.016	0.230	0.542	0.002	0.610	1.412	0.703	0
		ebi-a-GCST008033	25	-0.076	0.046	0.108	0.419	-0.002	0.640	25.217	0.394	5
	Glycated hemoglobin	ebi-a-GCST90002244	22	0.002	0.008	0.839	0.060	0.001	0.362	34.267	0.034	39
		ukb-d-30750_irmt	17	0.057	0.021	0.017	0.046	-0.002	0.338	27.173	0.040	41
	Blood glucose	ebi-a-GCST005186	19	0.025	0.014	0.094	0.624	0.000	0.745	16.837	0.534	0
		ebi-a-GCST000568	19	0.018	0.017	0.304	0.621	0.001	0.383	16.933	0.528	0
		ebi-a-GCST007858	4	0.051	0.015	0.047	0.719	0.000	0.986	1.548	0.671	0
	Fasting glucose	ebi-a-GCST90002232	24	0.014	0.010	0.188	0.112	0.000	0.963	33.185	0.078	31
		ieu-b-114	4	0.015	0.008	0.159	0.881	0.000	0.885	1.141	0.767	0
		ieu-b-113	19	0.025	0.014	0.094	0.643	0.000	0.745	16.837	0.534	0

T1D, Type 1 diabetes; T2D, Type 2 diabetes.

TABLE 4 Genetic instrumental variables detected by the MR-PRESSO method to show pleiotropy with ankylosing spondylitis on type 2 diabetes and glycated hemoglobin.

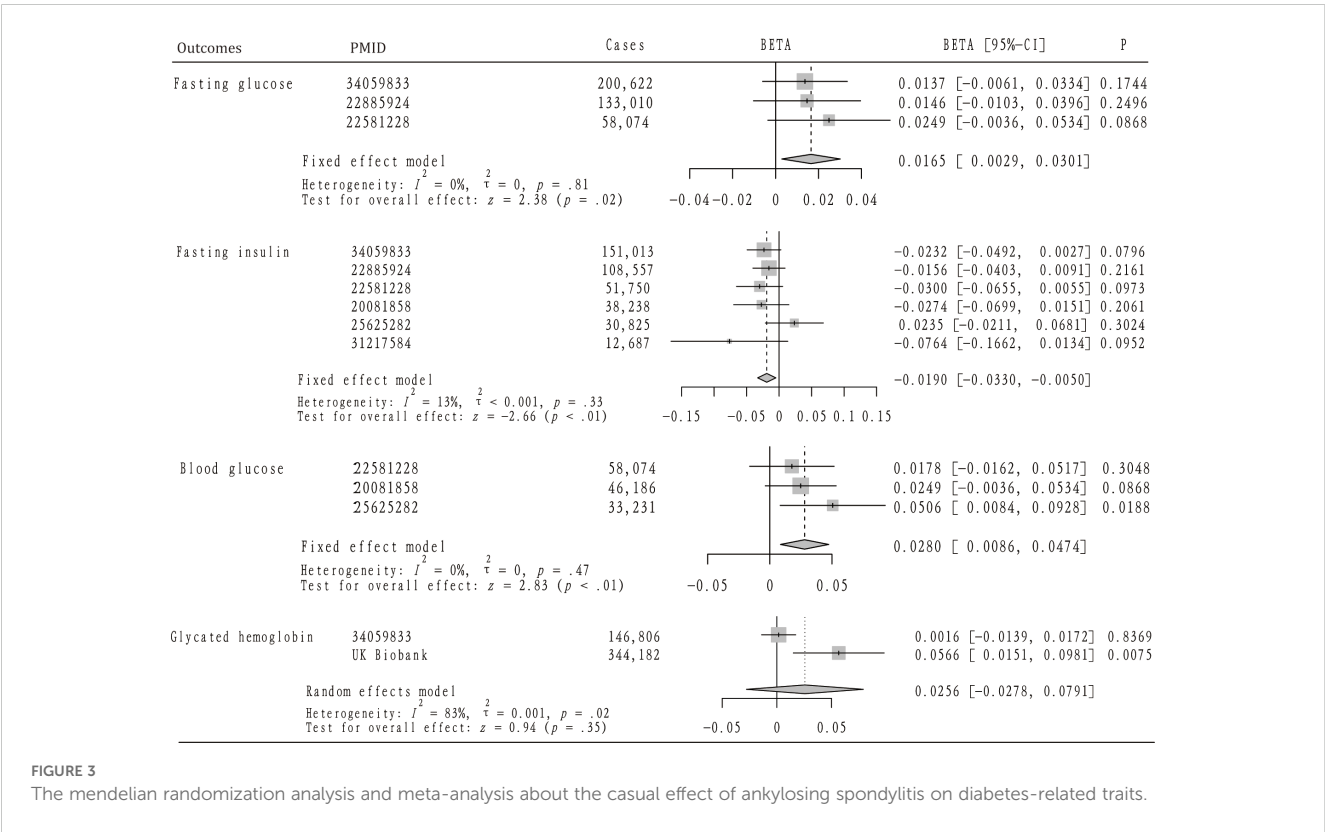
Explore	Outcome	Dataset	SNP	Chr	Pos	EA	NEA	Beta	Se	Pval
Ankylosing spondylitis	Type 2 diabetes	ebi-a-GCST005413	rs2596501	6	31321211	T	C	-0.152336	0.00419401	1E-200
	Type 2 diabetes	ebi-a-GCST010118	rs11190133	10	101278725	T	C	-0.0338671	0.00449401	4.84E-14
	Type 2 diabetes	finngen_R9_T2D	rs4129267	1	154426264	T	C	-0.0307685	0.00422605	3.32E-13
	Type 2 diabetes	ieu-a-26	rs1128905	9	139253839	C	T	-0.0237165	0.00409459	6.95E-09
	Type 2 diabetes	ieu-a-976	rs1128905	9	139253839	C	T	-0.0237165	0.00409459	6.95E-09
	Glycated hemoglobin	ukb-d-30750_irnt	rs1860545	12	6446777	A	G	-0.027474	0.00435378	2.78E-10
	Glycated hemoglobin	ukb-d-30750_irnt	rs2596501	6	31321211	T	C	-0.152336	0.00419401	1E-200
	Glycated hemoglobin	ukb-d-30750_raw	rs11065898	12	111862575	T	C	0.0262524	0.00480641	4.71E-08
	Glycated hemoglobin	ukb-d-30750_raw	rs9901869	17	45575206	A	G	0.0319036	0.00408853	6.04E-15

Discussion

Our analysis revealed a significant association between ankylosing spondylitis (AS) and an increased risk of type 1 diabetes mellitus (T1DM) and type 2 diabetes mellitus (T2DM). AS was linked to elevated fasting glucose and blood glucose levels, along with a decrease in fasting insulin levels. The study identified a causal relationship between AS and T2DM, as well as an impact on glucose metabolism traits.

Spondyloarthritis (SpA) encompasses a group of related but clinically varied diseases (33). Ankylosing spondylitis (AS) emerges

as the most common and severe form of SpA, predominantly targeting the axial skeleton, especially the sacroiliac joints (4). Characterized by inflammatory back pain, AS leads to significant discomfort and functional impairment in the spine and sacroiliac joints, thereby diminishing the quality of life for those affected and imposing a considerable societal and individual burden (34). AS is a condition that should be on the radar for diagnosis among young people presenting with back pain, particularly in young men (35). The early detection of AS poses a challenge but is of paramount importance. The disease is a complex immune-mediated condition with a pathophysiology that remains largely elusive (7). Historical



research dating back to 1973 has established a connection between the inheritance of the HLA-B27 allele and AS (36). In recent years, the IL-17A/IL-23 inflammatory axis has gained significant attention (37). Despite the complexity of its etiology, autoimmune mechanisms are believed to play a critical role in the development of AS.

Diabetes can be broadly categorized into the following main types: (1) Type 1 diabetes, (2) Type 2 diabetes, (3) Gestational diabetes mellitus (GDM), and (4) Specific types of diabetes resulting from other causes (38). T1DM is recognized as an autoimmune condition that necessitates lifelong insulin therapy upon diagnosis (39), and it predominantly affects children and adolescents (40). The underlying causes of T1DM are multifaceted and not fully understood (41), with prevailing research indicating that the disease primarily stems from the immune-mediated destruction of insulin-producing β -cells in the pancreas (42). The onset of diabetes is thought to result from a complex interaction of environmental factors, microbiota, genetics, metabolism, and immune responses that differ among individuals (43). Recent studies have pinpointed several genes within the MHC as key loci associated with susceptibility to diabetes (44), highlighting the role of immune mechanisms in the pathogenesis of T1DM.

In recent years, research interest in autoimmune diseases has surged, with both ankylosing spondylitis (AS) and diabetes being recognized within this category. This has led to a growing curiosity about the potential connection between these two conditions. Numerous studies suggest that individuals with AS are at an increased risk of developing diabetes. For instance, research indicates that people diagnosed with AS are more prone to diabetes than those without the condition (45). Additionally, the incidence of diabetes mellitus in the AS population was found to be 1.21 times higher compared to those without AS (19). Specifically, Chen et al. found that AS was associated with an increased risk of type 2 diabetes among the Asian population, with the AS group experiencing a 1.17 times higher incidence of T2DM compared to the non-AS group (20). A cross-sectional study also revealed that 13.64% of AS patients were diagnosed with diabetes mellitus (46). However, it's important to note that these studies primarily establish an association rather than a direct causative link between AS and diabetes mellitus.

Our research delves into the relationship between AS and diabetes mellitus by employing two-sample MR analysis. Our findings corroborate previous observational studies by demonstrating that AS is associated with an increased risk of both T1DM and T2DM. Additionally, our study uncovers that AS contributes to elevated fasting blood glucose levels and reduced insulin levels. Notably, our analysis suggests an increase in HbA1c levels associated with AS, although this finding did not reach statistical significance. Fasting glucose, fasting insulin, blood glucose, and glycated hemoglobin may be key biomarkers that may reveal important relationships with AS. Elevated fasting glucose and blood glucose levels in AS patients can indicate insulin resistance and impaired glucose metabolism, linking AS to an increased risk of type 2 diabetes. Similarly, altered fasting insulin levels may reflect the body's response to inflammation associated with AS, potentially

contributing to metabolic disturbances. HbA1c serves as a measure of average blood glucose over time; higher levels in AS patients could signify chronic hyperglycemia and a greater risk for diabetes. Monitoring these metabolic parameters is crucial for managing the health of individuals with AS and addressing potential metabolic complications. To the best of our knowledge, this is the first study to establish a causal link between AS and disruptions in glucose metabolism leading to diabetes mellitus, advancing beyond the mere observational associations reported by prior research. However, the underlying mechanisms of interaction between AS and diabetes mellitus demand further exploration. I propose several hypotheses centered around immunological mechanisms to guide future inquiries into this relationship.

The programmed death 1 (PD-1) pathway, including its ligands PD-L1 and PD-L2, is crucial for the inhibitory signaling of T cells. Disruptions in this pathway can lead to autoimmune diseases, such as AS and T1DM (47). For instance, research indicates that AS patients exhibit notably lower levels of PD-1+CD3+ and PD-1+CD4+ T cells (48). In animal models, specifically the L1C transgenic NOD mice that express higher levels of PD-L1, a reduced occurrence of spontaneous diabetes has been observed, suggesting a protective role of PD-L1 against diabetes (49). Dysfunctions in PD-1 and PD-L1 have been associated with increased infiltration of Th1 cells into the pancreatic islets (50), exacerbating the risk of diabetes by promoting a Th1-dominated (IFN- γ) pancreatic environment (51). Additionally, a meta-analysis highlighted the significance of PD1.5 and PD1.9 polymorphisms in both AS and T1DM (52). Thus, our investigation supports the hypothesis that PD-1 pathway abnormalities contribute to the development of both AS and type 1 diabetes, revealing a potential immunological link between these conditions.

Osteopontin (OPN) serves as a crucial regulator within both innate and adaptive immune responses, acting as a versatile cytokine and adhesion molecule (53). Studies have shown that individuals with ankylosing spondylitis (AS) exhibit elevated levels of OPN compared to healthy controls (54). Furthermore, genetic variations in the OPN gene have been linked to an increased risk of AS among the Han Chinese population (55). Similarly, elevated serum levels of OPN have been observed in adults diagnosed with T1DM (56). While the specific contributions of OPN to the pathophysiology of AS and T1D warrant further exploration, its role has been more thoroughly investigated in other autoimmune conditions, particularly rheumatoid arthritis. This indicates that OPN is a significant factor in the landscape of autoimmune diseases, although the exact mechanisms through which it operates remain to be fully elucidated.

Reactive oxygen species (ROS), produced as byproducts of metabolic activities, are implicated in numerous biological processes, such as inflammation, cancer, and aging (57). There is a growing body of research focusing on the relationship between AS and oxidative stress. Specifically, the underlying mechanisms of AS might involve an elevation in oxidative agents coupled with a reduction in the body's antioxidant defense capabilities (58). Markers of oxidative stress have been found to be higher in patients with AS (59). There is evidence suggesting that oxidative

stress contributes to the development of insulin resistance (60, 61). Insulin resistance is a condition where the body's cells become less responsive to insulin, impacting the uptake, metabolism, or storage of glucose, and has been associated with AS (62). Previous research indicates that levels of tumor necrosis factor (TNF), interleukin (IL)-1, and IL-6 are elevated in AS and contribute to the onset of insulin resistance (63). Given that insulin resistance is a key factor in the development of diabetes, it is plausible to consider whether oxidative stress, along with the elevated release of IL-1, IL-6, and TNF in AS, could lead to insulin resistance, thereby playing a role in the development of diabetes.

TNF is a critical factor in the pathogenesis of ankylosing spondylitis (AS), leading to the development of TNF-targeting therapies for its treatment (64). These TNF pathways are central to the immune-mediated inflammatory response seen in AS (65). However, treatments that target TNF have been observed to affect metabolic processes, including those involved in glucose metabolism (66). Research by Sidiropoulos indicated that anti-TNF therapy might promote insulin resistance and reduce the activity of glucose transporter protein 4 (67). Conversely, anti-TNF treatment has been associated with a decrease in plasma glucose levels through enhanced insulin sensitivity (68). Furthermore, the risk of diabetes mellitus in AS patients appears to be lower when anti-TNF therapy is combined with hydroxychloroquine (HCQ) (69). This body of research underscores the complex impact of anti-TNF treatments on glucose metabolism, suggesting a potential link between AS management strategies and the development of diabetes.

Recent research has placed the gut microbiome at the forefront of investigations into human autoimmune diseases. The 'epithelial barrier theory,' as proposed by Akdis, suggests that microbial dysbiosis and translocation can activate the immune system, leading to inflammatory conditions (70). Metagenomic studies have identified significant changes in the pro-inflammatory gut microbiota of individuals with ankylosing spondylitis (AS), indicating an alteration in the gut microbiota of patients who have not undergone treatment (71). These patients also exhibit dysbiosis, which affects intestinal epithelial and vascular barriers, and an increase in blood zonulin levels, suggesting compromised intestinal barrier function (63). It is estimated that intestinal mucosal inflammation occurs in approximately 70% of individuals with AS (72). The influence of HLA-B27 on the gut microbiota composition in AS has been noted as significant, echoing findings in type 1 diabetes, where distinct microbial compositions have been observed compared to healthy individuals (73). Previous research has identified significant variations in the microbial composition of people with type 1 diabetes compared to healthy controls (74). In cases of diabetes, a breach in the intestinal barrier's integrity has been linked to T cell-mediated autoimmunity against islet cells (75). Specifically, enteric bacterial infections compromising the intestinal barrier can activate diabetogenic CD8(+) T cells, leading to insulinitis (76). The Zonulin family peptide, a key regulator of intestinal tight junctions, is implicated in the development of a permeable intestinal barrier, dysbiosis, and inflammation (77). This evidence underscores the potential role of gut microbiome imbalance in the development of diabetes in individuals with AS.

Our study offers several advantages. Notably, it is among the first to leverage MR analysis to elucidate a causal link between AS and diabetes, with large-scale GWAS providing a refined understanding of their association. The use of MR analysis helps circumvent common pitfalls such as confounders and reverse causation, enhancing the reliability of our findings. However, the study is not without its limitations. A significant constraint is the lack of sex-specific analysis, which is critical given the varied prevalence of autoimmune diseases between genders. Future studies incorporating gender-specific MR analyses could offer more nuanced insights. Additionally, our research focused on European populations, limited by the availability of GWAS data, making our findings less generalizable to other ethnicities. Despite using various methods to assess heterogeneity, the possibility of residual heterogeneity remains. MR heterogeneity, stemming from factors like population differences and study design, must be addressed to improve result accuracy and credibility. Consequently, we cannot definitively conclude whether AS has a direct or indirect association with T1DM or T2DM. Further multivariable MR and mediation analyses are needed to clarify these relationships. In summary, our results lend support to a possible causal relationship between AS and diabetes mellitus. While MR analyses mitigate certain biases and errors, the limitations noted necessitate further investigations into the underlying mechanisms by which AS may contribute to the development of diabetes.

Conclusion

This study discovered, via MR analysis, that AS elevates the risk of both T1DM and T2DM. Additionally, our findings indicate that AS is associated with higher fasting and blood glucose levels, alongside a reduction in fasting insulin. Collectively, these outcomes highlight the detrimental impact of AS on diabetes development, underscoring the critical role of autoimmune disorders in diabetes pathogenesis. This research significantly contributes to our understanding of the immunological mechanisms underlying diabetes development.

Data availability statement

The original contributions presented in the study are included in the article/[Supplementary Material](#). Further inquiries can be directed to the corresponding authors.

Ethics statement

The data in this article come from FinnGen, UK-biobank, IEU OpenGWAS project, Biobank Japan Project, and GWAS Catalog databases. No Ethics approval and consent to participate is needed. The studies were conducted in accordance with the local legislation and institutional requirements. Written informed consent for participation in this study was provided by the participants' legal guardians/next of kin.

Author contributions

ZR: Writing – original draft, Project administration, Methodology, Investigation, Formal analysis, Data curation, Conceptualization. LH: Writing – review & editing, Data curation, Methodology, Supervision, Visualization, Validation. JW: Writing – original draft, Methodology, Investigation, Formal analysis, Data curation. LS: Writing – review & editing, Visualization, Validation, Supervision, Software, Resources, Project administration, Formal analysis. CL: Writing – original draft, Software, Project administration, Investigation, Formal analysis. YM: Writing – review & editing, Visualization, Validation, Supervision, Resources, Project administration, Methodology, Funding acquisition.

Funding

The author(s) declare financial support was received for the research, authorship, and/or publication of this article. This study was supported by the National Natural Science Foundation of China (Grant Nos. 82260446, 81360280, and 81760411).

References

1. Mauro D, Thomas R, Guggino G, Lories R, Brown MA, Ciccio F. Ankylosing spondylitis: an autoimmune or autoinflammatory disease? *Nat Rev Rheumatol*. (2021) 17:387–404. doi: 10.1038/s41584-021-00625-y
2. Ritchlin C, Adamopoulos IE. Axial spondyloarthritis: new advances in diagnosis and management. *Bmj*. (2021) 372:m4447. doi: 10.1136/bmj.m4447
3. Sieper J, Braun J, Dougados M, Baeten D. Axial spondyloarthritis. *Nat Rev Dis Primers*. (2015) 1:15013. doi: 10.1038/nrdp.2015.13
4. Smith JA. Update on ankylosing spondylitis: current concepts in pathogenesis. *Curr Allergy Asthma Rep*. (2015) 15:489. doi: 10.1007/s11882-014-0489-6
5. Landi M, Maldonado-Ficco H, Perez-Alamino R, Maldonado-Cocco JA, Citera G, Arturi P, et al. Gender differences among patients with primary ankylosing spondylitis and spondylitis associated with psoriasis and inflammatory bowel disease in an iberoamerican spondyloarthritis cohort. *Med (Baltimore)*. (2016) 95:e5652. doi: 10.1097/MD.00000000000005652
6. Yang H, Chen Y, Xu W, Shao M, Deng J, Xu S, et al. Epigenetics of ankylosing spondylitis: Recent developments. *Int J Rheum Dis*. (2021) 24:487–93. doi: 10.1111/1756-185X.14080
7. Simone D, Al Mossawi MH, Bowness P. Progress in our understanding of the pathogenesis of ankylosing spondylitis. *Rheumatol (Oxford)*. (2018) 57:vi4–9. doi: 10.1093/rheumatology/key001
8. Chen CW, Wei JC, Gu J, Yu D. Editorial: advances in pathogenesis, etiology, and therapies for ankylosing spondylitis. *Front Immunol*. (2021) 12:822582. doi: 10.3389/fimmu.2021.822582
9. Zhu W, He X, Cheng K, Zhang L, Chen D, Wang X, et al. Ankylosing spondylitis: etiology, pathogenesis, and treatments. *Bone Res*. (2019) 7:22. doi: 10.1038/s41413-019-0057-8
10. Xu GH, Lin J, Chen WQ. Concurrent ankylosing spondylitis and myelodysplastic syndrome: A case report. *World J Clin cases*. (2022) 10:1929–36. doi: 10.12998/wjcc.v10.i6.1929
11. Rezaeiemanesh A, Abdolmaleki M, Abdolmohammadi K, Aghaei H, Pakdel FD, Fatahi Y, et al. Immune cells involved in the pathogenesis of ankylosing spondylitis. *BioMed Pharmacother*. (2018) 100:198–204. doi: 10.1016/j.biopha.2018.01.108
12. Ou J, Xiao M, Huang Y, Tu L, Chen Z, Cao S, et al. Serum metabolomics signatures associated with ankylosing spondylitis and TNF inhibitor therapy. *Front Immunol*. (2021) 12:630791. doi: 10.3389/fimmu.2021.630791
13. Ogurtsova K, da Rocha Fernandes JD, Huang Y, Linnenkamp U, Guariguata L, Cho NH, et al. IDF Diabetes Atlas: Global estimates for the prevalence of diabetes for 2015 and 2040. *Diabetes Res Clin Pract*. (2017) 128:40–50. doi: 10.1016/j.diabres.2017.03.024
14. Katsarou A, Gudbjörnsdóttir S, Rawshani A, Dabelea D, Bonifacio E, Anderson BJ, et al. Type 1 diabetes mellitus. *Nat Rev Dis Primers*. (2017) 3:17016. doi: 10.1038/nrdp.2017.16
15. Chatterjee S, Khunti K, Davies MJ. Type 2 diabetes. *Lancet*. (2017) 389:2239–51. doi: 10.1016/S0140-6736(17)30058-2
16. Donath MY, Dinarello CA, Mandrup-Poulsen T. Targeting innate immune mediators in type 1 and type 2 diabetes. *Nat Rev Immunol*. (2019) 19:734–46. doi: 10.1038/s41577-019-0213-9
17. Dror E, Dalmas E, Meier DT, Wueest S, Thévenet J, Thienel C, et al. Postprandial macrophage-derived IL-1 β stimulates insulin, and both synergistically promote glucose disposal and inflammation. *Nat Immunol*. (2017) 18:283–92. doi: 10.1038/ni.3659
18. Biondi B, Kahaly GJ, Robertson RP. Thyroid dysfunction and diabetes mellitus: two closely associated disorders. *Endocr Rev*. (2019) 40:789–824. doi: 10.1210/er.2018-00163
19. Liao KF, Kuo YH, Lai SW. Diabetes mellitus in ankylosing spondylitis. *Ann Rheum Dis*. (2021) 80:e134. doi: 10.1136/annrheumdis-2019-216221
20. Chen HH, Yeh SY, Chen HY, Lin CL, Sung FC, Kao CH. Ankylosing spondylitis and other inflammatory spondyloarthritis increase the risk of developing type 2 diabetes in an Asian population. *Rheumatol Int*. (2014) 34:265–70. doi: 10.1007/s00296-013-2927-5
21. Sekula P, Del Greco MF, Pattaro C, Köttgen A. Mendelian randomization as an approach to assess causality using observational data. *J Am Soc Nephrol*. (2016) 27:3253–65. doi: 10.1681/ASN.2016010098
22. Hemani G, Zheng J, Elsworth B, Wade KH, Haberland V, Baird D, et al. The MR-Base platform supports systematic causal inference across the human phenotype. *Elife*. (2018) 7:e34408. doi: 10.7554/eLife.34408
23. Davey Smith G, Hemani G. Mendelian randomization: genetic anchors for causal inference in epidemiological studies. *Hum Mol Genet*. (2014) 23:R89–98. doi: 10.1093/hmg/ddu328
24. Su Q, Jin C, Yang Y, Wang J, Wang J, Zeng H, et al. Association between autoimmune diseases and sarcopenia: A two-sample mendelian randomization study. *Clin Epidemiol*. (2023) 15:901–10. doi: 10.2147/CLEP.S416778
25. Sun D, Ma R, Wang J, Wang Y, Ye Q. The causal relationship between sarcoidosis and autoimmune diseases: a bidirectional Mendelian randomization study in FinnGen. *Front Immunol*. (2024) 15:1325127. doi: 10.3389/fimmu.2024.1325127
26. Su Y, Zhang Y, Chai Y, Xu J. Autoimmune diseases and their genetic link to bronchiectasis: insights from a genetic correlation and Mendelian randomization study. *Front Immunol*. (2024) 15:1343480. doi: 10.3389/fimmu.2024.1343480
27. Li S, Yuan S, Schooling CM, Larsson SC. A Mendelian randomization study of genetic predisposition to autoimmune diseases and COVID-19. *Sci Rep*. (2022) 12:17703. doi: 10.1038/s41598-022-22711-1
28. Zhang Y, Liu J, Wang C, Liu J, Lu W. Toll-like receptors gene polymorphisms in autoimmune disease. *Front Immunol*. (2021) 12:672346. doi: 10.3389/fimmu.2021.672346

Conflict of interest

The authors declare that the research was conducted without any commercial or financial relationships that could be construed as a potential conflict of interest.

Publisher's note

All claims expressed in this article are solely those of the authors and do not necessarily represent those of their affiliated organizations, or those of the publisher, the editors and the reviewers. Any product that may be evaluated in this article, or claim that may be made by its manufacturer, is not guaranteed or endorsed by the publisher.

Supplementary material

The Supplementary Material for this article can be found online at: <https://www.frontiersin.org/articles/10.3389/fendo.2024.1369466/full#supplementary-material>

29. Cortes A, Hadler J, Pointon JP, Robinson PC, Karaderi T, Leo P, et al. Identification of multiple risk variants for ankylosing spondylitis through high-density genotyping of immune-related loci. *Nat Genet.* (2013) 45:730–8. doi: 10.1038/ng.2667
30. Cheng Q, Yang Y, Shi X, Yeung KF, Yang C, Peng H, et al. MR-LDP: a two-sample Mendelian randomization for GWAS summary statistics accounting for linkage disequilibrium and horizontal pleiotropy. *NAR Genom Bioinform.* (2020) 2:lqaa028. doi: 10.1093/nargab/lqaa028
31. Pierce BL, Ahsan H, Vanderweele TJ. Power and instrument strength requirements for Mendelian randomization studies using multiple genetic variants. *Int J Epidemiol.* (2011) 40:740–52. doi: 10.1093/ije/dyq151
32. Adu Y, Ring D, Teunis T. Randomized controlled trials studying nonoperative treatments of osteoarthritis often use misleading and uninformative control groups: A systematic review. *Clin Orthop Relat Res.* (2024). doi: 10.1097/CORR.0000000000003273
33. Dougados M, Baeten D. Spondyloarthritis. *Lancet.* (2011) 377:2127–37. doi: 10.1016/S0140-6736(11)60071-8
34. Burgos-Varga R, Wei JC, Rahman MU, Akkoc N, Haq SA, Hammoudeh M, et al. The prevalence and clinical characteristics of nonradiographic axial spondyloarthritis among patients with inflammatory back pain in rheumatology practices: a multinational, multicenter study. *Arthritis Res Ther.* (2016) 18:132. doi: 10.1186/s13075-016-1027-9
35. Escalante A. Ankylosing spondylitis. A common cause of low back pain. *Postgrad Med.* (1993) 94:153–60. doi: 10.1080/00325481.1993.11945685
36. Schlosstein L, Terasaki PI, Bluestone R, Pearson CM. High association of an HLA-A antigen, W27, with ankylosing spondylitis. *N Engl J Med.* (1973) 288:704–6. doi: 10.1056/NEJM197304052881403
37. McGeachy MJ, Chen Y, Tato CM, Laurence A, Joyce-Shaikh B, Blumenschein WM, et al. The interleukin 23 receptor is essential for the terminal differentiation of interleukin 17-producing effector T helper cells in vivo. *Nat Immunol.* (2009) 10:314–24. doi: 10.1038/ni.1698
38. (2) Classification and diagnosis of diabetes. *Diabetes Care.* (2015) 38 Suppl:S8–s16. doi: 10.2337/dc15-S005
39. Bluestone JA, Herold K, Eisenbarth G. Genetics, pathogenesis and clinical interventions in type 1 diabetes. *Nature.* (2010) 464:1293–300. doi: 10.1038/nature08933
40. Harjutsalo V, Sjöberg L, Tuomilehto J. Time trends in the incidence of type 1 diabetes in Finnish children: a cohort study. *Lancet.* (2008) 371:1777–82. doi: 10.1016/S0140-6736(08)60765-5
41. Ni Q, Pham NB, Meng WS, Zhu G, Chen X. Advances in immunotherapy of type I diabetes. *Adv Drug Deliv Rev.* (2019) 139:83–91. doi: 10.1016/j.addr.2018.12.003
42. Anderson MS, Bluestone JA. The NOD mouse: a model of immune dysregulation. *Annu Rev Immunol.* (2005) 23:447–85. doi: 10.1146/annurev.immunol.23.021704.115643
43. DiMeglio LA, Evans-Molina C, Oram RA. Type 1 diabetes. *Lancet.* (2018) 391:2449–62. doi: 10.1016/S0140-6736(18)31320-5
44. Mordes JP, Bortell R, Doukas J, Rigby M, Whalen B, Zipris D, et al. The BB/Wor rat and the balance hypothesis of autoimmunity. *Diabetes Metab Rev.* (1996) 12:103–9. doi: 10.1002/(SICI)1099-0895(199607)12:2<103::AID-DMR157>3.0.CO;2-2
45. Wang S, Tsou HK, Chiou JY, Wang YH, Zhang Z, Wei JC. Increased risk of inflammatory bowel disease among patients with ankylosing spondylitis: A 13-year population-based cohort study. *Front Immunol.* (2020) 11:578732. doi: 10.3389/fimmu.2020.578732
46. Kang JH, Chen YH, Lin HC. Comorbidity profiles among patients with ankylosing spondylitis: a nationwide population-based study. *Ann Rheum Dis.* (2010) 69:1165–8. doi: 10.1136/ard.2009.116178
47. Zamani MR, Aslani S, Salmaneinejad A, Javan MR, Rezaei N. PD-1/PD-L and autoimmunity: A growing relationship. *Cell Immunol.* (2016) 310:27–41. doi: 10.1016/j.cellimm.2016.09.009
48. Chen MH, Chen WS, Lee HT, Tsai CY, Chou CT. Inverse correlation of programmed death 1 (PD-1) expression in T cells to the spinal radiologic changes in Taiwanese patients with ankylosing spondylitis. *Clin Rheumatol.* (2011) 30:1181–7. doi: 10.1007/s10067-011-1721-6
49. Wang CJ, Chou FC, Chu CH, Wu JC, Lin SH, Chang DM, et al. Protective role of programmed death 1 ligand 1 (PD-L1) in nonobese diabetic mice: the paradox in transgenic models. *Diabetes.* (2008) 57:1861–9. doi: 10.2337/db07-1260
50. Wang J, Yoshida T, Nakaki F, Hiai H, Okazaki T, Honjo T. Establishment of NOD-Pdcd1^{-/-} mice as an efficient animal model of type I diabetes. *Proc Natl Acad Sci USA.* (2005) 102:11823–8. doi: 10.1073/pnas.0505497102
51. Hill NJ, Van Gunst K, Sarvetnick N. Th1 and Th2 pancreatic inflammation differentially affects homing of islet-reactive CD4 cells in nonobese diabetic mice. *J Immunol.* (2003) 170:1649–58. doi: 10.4049/jimmunol.170.4.1649
52. Lee YH, Bae SC, Kim JH, Song GG. Meta-analysis of genetic polymorphisms in programmed cell death 1. Associations with rheumatoid arthritis, ankylosing spondylitis, and type 1 diabetes susceptibility. *Z Rheumatol.* (2015) 74:230–9. doi: 10.1007/s00393-014-1415-y
53. Xu C, Wu Y, Liu N. Osteopontin in autoimmune disorders: current knowledge and future perspective. *Inflammopharmacology.* (2022) 30:385–96. doi: 10.1007/s10787-022-00932-0
54. Choi ST, Kim JH, Kang EJ, Lee SW, Park MC, Park YB, et al. Osteopontin might be involved in bone remodeling rather than in inflammation in ankylosing spondylitis. *Rheumatol (Oxford).* (2008) 47:1775–9. doi: 10.1093/rheumatology/ken385
55. Li J, Cai Y, Wang Z, Deng A, Yang G. Polymorphisms in the osteopontin are associated with susceptibility to ankylosing spondylitis in a han chinese population. *BioMed Res Int.* (2018) p:3458439. doi: 10.1155/2018/3458439
56. Barchetta I, Alessandri C, Bertocchini L, Cimini FA, Taverniti L, Di Franco M, et al. Increased circulating osteopontin levels in adult patients with type 1 diabetes mellitus and association with dysmetabolic profile. *Eur J Endocrinol.* (2016) 174:187–92. doi: 10.1530/EJE-15-0791
57. Kawahito S, Kitahata H, Oshita S. Problems associated with glucose toxicity: role of hyperglycemia-induced oxidative stress. *World J Gastroenterol.* (2009) 15:4137–42. doi: 10.3748/wjg.15.4137
58. Karakoc M, Altindag O, Keles H, Soran N, Selek S. Serum oxidative-antioxidative status in patients with ankylosing spondylitis. *Rheumatol Int.* (2007) 27:1131–4. doi: 10.1007/s00296-007-0352-3
59. Ye G, Xie Z, Zeng H, Wang P, Li J, Zheng G, et al. Oxidative stress-mediated mitochondrial dysfunction facilitates mesenchymal stem cell senescence in ankylosing spondylitis. *Cell Death Dis.* (2020) 11:775. doi: 10.1038/s41419-020-02993-x
60. Rudich A, Tirosh A, Potashnik R, Hemi R, Kanety H, Bashan N. Prolonged oxidative stress impairs insulin-induced GLUT4 translocation in 3T3-L1 adipocytes. *Diabetes.* (1998) 47:1562–9. doi: 10.2337/diabetes.47.10.1562
61. Dokken BB, Saengsirisuwan V, Kim JS, Teachey MK, Henriksen EJ. Oxidative stress-induced insulin resistance in rat skeletal muscle: role of glycogen synthase kinase-3. *Am J Physiol Endocrinol Metab.* (2008) 294:E615–21. doi: 10.1152/ajpendo.00578.2007
62. Khodabandehloo H, Gorgani-Firuzjaee S, Panahi G, Meshkani R. Molecular and cellular mechanisms linking inflammation to insulin resistance and β -cell dysfunction. *Transl Res.* (2016) 167:228–56. doi: 10.1016/j.trsl.2015.08.011
63. Wang CR, Tsai HW. Anti- and non-tumor necrosis factor- α -targeted therapies effects on insulin resistance in rheumatoid arthritis, psoriatic arthritis and ankylosing spondylitis. *World J Diabetes.* (2021) 12:238–60. doi: 10.4239/wjcd.v12.i3.238
64. Li J, Zhang Z, Wu X, Zhou J, Meng D, Zhu P. Risk of adverse events after anti-TNF treatment for inflammatory rheumatological disease. A meta-analysis. *Front Pharmacol.* (2021) 12:746396. doi: 10.3389/fphar.2021.746396
65. Brown MA, Kenna T, Wordsworth BP. Genetics of ankylosing spondylitis—insights into pathogenesis. *Nat Rev Rheumatol.* (2016) 12:81–91. doi: 10.1038/nrrheum.2015.133
66. da Silva BS, Bonfá E, de Moraes JC, Saad CG, Ribeiro AR, Gonçalves CR, et al. Effects of anti-TNF therapy on glucose metabolism in patients with ankylosing spondylitis, psoriatic arthritis or juvenile idiopathic arthritis. *Biologicals.* (2010) 38:567–9. doi: 10.1016/j.biologicals.2010.05.003
67. Sidiropoulos PI, Karvounaris SA, Boumpas DT. Metabolic syndrome in rheumatic diseases: epidemiology, pathophysiology, and clinical implications. *Arthritis Res Ther.* (2008) 10:207. doi: 10.1186/ar2397
68. Gonzalez-Gay MA, De Matias JM, Gonzalez-Juanatey C, Garcia-Porrúa C, Sanchez-Andrade A, Martin J, et al. Anti-tumor necrosis factor- α blockade improves insulin resistance in patients with rheumatoid arthritis. *Clin Exp Rheumatol.* (2006) 24:83–6.
69. Chen HH, Chen DY, Lin CC, Chen YM, Lai KL, Lin CH. Association between use of disease-modifying antirheumatic drugs and diabetes in patients with ankylosing spondylitis, rheumatoid arthritis, or psoriasis/psoriatic arthritis: a nationwide, population-based cohort study of 84,989 patients. *Ther Clin Risk Manag.* (2017) 13:583–92. doi: 10.2147/TCRM.S130666
70. Akdis CA. Does the epithelial barrier hypothesis explain the increase in allergy, autoimmunity and other chronic conditions? *Nat Rev Immunol.* (2021) 21:739–51. doi: 10.1038/s41577-021-00538-7
71. Zhou C, Zhao H, Xiao XY, Chen BD, Guo RJ, Wang Q, et al. Metagenomic profiling of the pro-inflammatory gut microbiota in ankylosing spondylitis. *J Autoimmun.* (2020) 107:102360. doi: 10.1016/j.jaut.2019.102360
72. Costello ME, Ciccia F, Willner D, Warrington N, Robinson PC, Gardiner B, et al. Brief report: intestinal dysbiosis in ankylosing spondylitis. *Arthritis Rheumatol.* (2015) 67:686–91. doi: 10.1002/art.38967
73. Asquith M, Sternes PR, Costello ME, Karstens L, Diamond S, Martin TM, et al. HLA alleles associated with risk of ankylosing spondylitis and rheumatoid arthritis influence the gut microbiome. *Arthritis Rheumatol.* (2019) 71:1642–50. doi: 10.1002/art.v71.10
74. Zhou H, Sun L, Zhang S, Zhao X, Gang X, Wang G. Evaluating the causal role of gut microbiota in type 1 diabetes and its possible pathogenic mechanisms. *Front Endocrinol (Lausanne).* (2020) 11:125. doi: 10.3389/fendo.2020.00125
75. Watts T, Berti I, Sapone A, Gerarduzzi T, Not T, Ziegle R, et al. Role of the intestinal tight junction modulator zonulin in the pathogenesis of type I diabetes in BB diabetic-prone rats. *Proc Natl Acad Sci USA.* (2005) 102:2916–21. doi: 10.1073/pnas.0500178102
76. Lee AS, Gibson DL, Zhang Y, Sham HP, Vallance BA, Dutz JP. Gut barrier disruption by an enteric bacterial pathogen accelerates insulinitis in NOD mice. *Diabetologia.* (2010) 53:741–8. doi: 10.1007/s00125-009-1626-y
77. Tajik N, Frech M, Schulz O, Schälter F, Lucas S, Azizov V, et al. Targeting zonulin and intestinal epithelial barrier function to prevent onset of arthritis. *Nat Commun.* (2020) 11:1995. doi: 10.1038/s41467-020-15831-7

Frontiers in Molecular Biosciences

Explores biological processes in living organisms
on a molecular scale

Focuses on the molecular mechanisms
underpinning and regulating biological processes
in organisms across all branches of life.

Discover the latest Research Topics

[See more →](#)

Frontiers

Avenue du Tribunal-Fédéral 34
1005 Lausanne, Switzerland
frontiersin.org

Contact us

+41 (0)21 510 17 00
frontiersin.org/about/contact



Frontiers in Molecular Biosciences

